IMPROVING COMPRESSION AFTER IMPACT RESPONSE COMPOSITE LAMINATES THROUGH PLY LEVEL HYBRIDIZATION WITH THIN PLIES AND UNSYMMETRICAL DESIGNS

Aravind Sasikumar

Universitat de Girona

DOCTORAL THESIS

Improving compression after impact response of composite laminates through ply level hybridization with thin plies and unsymmetrical designs

ARAVIND SASIKUMAR

AMADE
ANALYSIS AND ADVANCED MATERIALS
FOR STRUCTURAL DESIGN

2019

Universitat de Girona

Doctoral Thesis

Improving compression after impact response of composite laminates through ply level hybridization with thin plies and unsymmetrical designs

Aravind Sasikumar

2019

Doctoral Program in Technology

Advisors:

Dr. Daniel Trias Mansilla
Universitat de Girona

Dr. Josep Costa Balanzat
Universitat de Girona

Thesis submitted for the degree of Doctor of Philosophy

Aravind Sasikumar

Improving compression after impact response of composite laminates through ply level hybridization with thin plies and unsymmetrical designs

Doctoral Thesis, 2019

Doctoral Program in Technology

Advisors: Dr. Daniel Trias Mansilla and Dr. Josep Costa Balanzat

Universitat de Girona

AMADE Research Group

Escola Politècnica Superior

Dept. d'Enginyeria Mecànica i de la Construcció Industrial

Carrer Universitat de Girona, 4. Campus de Montilivi

17003 Girona

To my dear family...

Dream is not that which you see while sleeping,
it is something that does not let you sleep.

— APJ Abdul Kalam
(Scientist and Former President of India)

Acknowledgement

No gratitude is enough when it comes to thanking my family, my beloved parents and my sister, the reason why I am here writing this thesis. I awe it all to you.

I am extremely grateful to my thesis advisor Dr. Daniel Trias for the warm welcome he offered when I first reached Girona, for the continuous support provided right from the word 'GO'. I owe my sincere gratitude to my co-advisor Dr. Josep Costa, through his years of experience in the field of composites, and his keen eye for finding solutions, every meeting ended on a happy note. I would also like to thank the other professors at AMADE: Dr. Emilio González and Dr. Pere Maimí for helping me with the numerical doubts, Dr. Norbert Blanco for his support to perform C-scan inspections, Dr. Jordi Renart, Dr. Albert Turon and Dr. Joan Andreu for always lending their helping hand in tough situations. I would also like to express my sincere gratitude to Dr. Peter Linde who has played a major role in the completion of this thesis through his constant support in efficiently leading the Airnet project.

I would like to thank all the members at the AMADE research laboratory, Dr. Daniel Piedrafita, Ivan Recio, Albert Tena, Tiina Uotila, who have helped immensely in successfully completing the experimental campaign. This section is never complete if I don't thank my dear colleagues at the AMADE group, who created a very lively environment in the room. They were the source of inspiration and there are many memorable moments that I could take away from the last three years of my PhD life. Thanks to my ex-colleagues at AMADE: Gerard, Albert Soto, Adrian Ortega, Magda, Laura, Yi, Ahmed and Emara for the warm welcome they gave me when I first entered the PhD room. Countless gratitude to my present colleagues at AMADE group: Jordi, Santi, Adria, Jose, Sergio, Juan Jose, Javi, Julen, Younes, Said, Ivan and Oriol, for making it feel like another home. A special thanks to all my dear flatmates (Yi, Lina, Julen, Joey, Sergio, Claudia, Juan Jose) who I had in the last three years, for never making me miss my family and home in India. Thanks to some wonderful people I have met here: Lina, Yi, Patricia, Jordi and Mia who had made a

great influence in my life and will always be close to me. I also thank Prof. Pedro Camanho and his colleagues, Rodrigo Tavares and Carolina Furtado, from University of Porto for the valuable and productive discussions during the Airnet project.

Preface

The work contained in this Ph.D. thesis was conducted at the AMADE research group (Department of Mechanical Engineering and Industrial Construction, University of Girona, Spain). The thesis was carried out with the financial support from FI-DGR predoctoral Grants 2016 FI-B 00571, 2017 FI-B1 00089 and 2018 FI-B2 00118 from the Generalitat de Catalunya. The author also acknowledges the financial support from the Spanish Ministerio de Economía, Industria y Competitividad (MINECO) for the grant coded MAT2015-69491-C3-1-R supported by FEDER/EU.

A major part of the thesis is dedicated to the AIRNET project that was led by Airbus, Germany under Dr. Peter Linde, in collaboration with the INEGI research group (University of Porto), University of Dayton Research Institute (UDRI) and AMADE research group (University of Girona).

List of Publications

The present Ph.D. thesis has been prepared as a compendium of peer-reviewed journal papers, according to the regulations of the Universitat de Girona. The thesis is comprised of the following papers:

- **A. Sasikumar**, J. Costa, D. Trias, E.V. González, S.M. Garcia-Rodríguez, P. Maimí. Unsymmetrical stacking sequences as a novel approach to tailor damage resistance under out-of-plane impact loading. ***Composites Science and Technology***, 125–135 (2019) 173. doi: doi.org/10.1016/j.compscitech.2019.02.002.

  ISSN: 0266-3538, Impact Factor: 5.160, ranked 1/26 in the category of *Materials Science, Composites* (1st quartile)[1].

- **A. Sasikumar**, J. Costa, D. Trias, S.M. Garcia-Rodríguez. On how unsymmetrical laminate designs with tailored ply clusters affect the compression after impact strength of composite laminates. ***Composite Structures***, 111958 (2020) 238. doi: doi.org/10.1016/j.compstruct.2020.111958.

  ISSN: 0263-8223, Impact Factor: 4.829 and ranked 6/25 in the category of *Materials Science, Composites* (1st quartile)[2].

- **A. Sasikumar**, D. Trias, J. Costa, N. Blanco, J. Orr, P. Linde. Effect of ply thickness and ply level hybridization on the compression after impact strength of thin laminates. ***Composites Part A: Applied Science and Manufacturing***, 232–243 (2019) 121. doi: doi.org/10.1016/j.compositesa.2019.03.022.

  ISSN: 1359-835X, Impact Factor: 4.514, ranked 4/26 in the category of *Materials*

[1] According to the 2017 Journal Citation Reports
[2] According to the 2018 Journal Citation Reports

Science, Composites, ranked 2/46 in the category of *Engineering, Manufacturing* (1st quartile)[1].

- **A. Sasikumar**, D. Trias, J. Costa, N. Blanco, J. Orr, P. Linde. Impact and compression after impact response in thin laminates of spread-tow woven and non-crimp fabrics. ***Composite Structures***, 432–445 (2019) 215. doi: doi.org/10.1016/j.compstruct.2019.02.054.

  ISSN: 0263-8223, Impact Factor: 4.101 and ranked 5/26 in the category of *Materials Science, Composites* (1st quartile)[1].

- **A. Sasikumar**, D. Trias, J. Costa, V. Singery, P. Linde. Mitigating the weak impact response of thin-ply based thin laminates through an unsymmetrical laminate design incorporating intermediate grade plies. ***Composite Structures***, 93-104 (2019) 220. doi: doi.org/10.1016/j.compstruct.2019.03.069.

  ISSN: 0263-8223, Impact Factor: 4.101, ranked 5/26 in the category of *Materials Science, Composites* (1st quartile)[1].

- **A. Sasikumar**, J. Costa, D. Trias, J. LLobet, I. R. Cozár, A. Turon, P. Linde. A virtual testing based search for optimum compression after impact strength in thin laminates using ply-thickness hybridization and unsymmetrical designs. ***Composites Science and Technology***, 108188 (2020) 196. doi: doi.org/10.1016/j.compscitech.2020.108188.

  ISSN: 1359-835X, Impact Factor: 6.309, ranked 2/25 in the category of *Materials Science, Composites*, ranked 2/46 in the category of *Engineering, Manufacturing* (1st quartile)[2].

Other publications that have been derived from this thesis but do not belong to this thesis, and are not included in this document are listed below:

- S.M. Garcia-Rodríguez, J. Costa, V. Singery, P. Maimí, **A. Sasikumar**. On how matrix cracks induce delamination under out-of-plane shear and the associated in-situ effect. Submitted for publication in *Composites Part A: Applied Science and Manufacturing*.
  ISSN: 0266-3538, Impact Factor: 4.514, ranked 4/26 in the category of *Mate-*

rials Science, Composites (1st quartile)[1].

Conferences

- **A. Sasikumar**, D. Trias, S.M. García-Rodríguez, J. Costa. Experimental study to understand the effect of delamination position on impact damage tolerance using unsymmetrical laminates. 18th European Conference on Composite Materials (ECCM18 2018). Athens (Greece).
  International Conference. Poster presentation.

- **A. Sasikumar**, D. Trias, P. Linde, J. Costa. Experimental study on the impact and compression after impact response of thin composite laminates: Effect of fabric architecture and ply thickness. 21st International Conference on Composite Structures (ICCS21 2018). Bologna (Italy).
  International Conference. Oral presentation.

- **A. Sasikumar**, D. Trias, S.M. García-Rodríguez, J. Costa. Unsymmetrical laminates: Impact and compression after impact response. 55th Annual Technical Meeting of the Society of Engineering Science (SES 2018). Madrid (Spain).
  International Conference. Oral presentation.

- **A. Sasikumar**, D. Trias, J. Costa, P. Linde. Improving the weak impact resistance and tolerance of thin ply based thin laminates using novel unsymmetrical laminate design. 9th International Conference on Composites Testing and Model Identification (Comptest 2019). Luleå (Sweden).
  International Conference. Oral presentation.

- S.M. García-Rodríguez, J. Costa, V. Singery, **A. Sasikumar**. A 3D tomographic investigation to elucidate how thin-ply laminates improve the interlaminar shear strength and the effect of toughening the interfaces with veils. 10th European Solid Mechanics Conference (ESMC 2018). Bologna (Italy).

- S.M. García-Rodríguez, J. Costa, **A. Sasikumar**, V. Singery. On how ply thickness affects the short-beam response of thin non-crimp fabric laminates: X-ray tomographic investigation. 55th Annual Technical Meeting of the Society of Engineering Science (SES 2018). Madrid (Spain).

- S.M. García-Rodríguez, A. Barbera, **A. Sasikumar**, M. Ruiz, I. Boada, D. Trias, J. Costa. The effect ply-thickness has on the non-crimp fabric laminate impact response: X-ray tomography investigation. XIIth Congreso Nacional de Materiales Compuestos (MATCOMP 2017). San Sebastián (Spain).

- S.M. García-Rodríguez, J. Costa, V. Singery, **A. Sasikumar**. On the in-situ effect under transverse shear and the associated thin ply laminate impact response. (Comptest 2019). Luleå (Sweden).

Declaration

Universitat de Girona

Dr. Daniel Trias Mansilla, Associate Professor at Universitat de Girona,

and

Dr. Josep Costa Balanzat, Full professor at Universitat de Girona,

hereby CERTIFY that

The work entitled *Improving compression after impact response of composite laminates through ply level hybridization with thin plies and unsymmetrical designs*, submitted for the doctoral degree by Aravind Sasikumar, has been conducted under our supervision.

Girona, May 2019.

Daniel Trias Mansilla
Universitat de Girona

Josep Costa Balanzat
Universitat de Girona

List of Figures

List of Tables

Contents

Abstract

The unrelenting search the aeronautic industries have to produce lightweight and efficient new-generation aircraft has substantially increased the use of composite materials in the recent decades. Despite the weight savings and the structural strength offered, composite materials are vulnerable to out-of-plane loads which are characterized as low velocity impact loads. The alarming reduction in strength caused by these impact loads, particularly on the compression after impact (CAI) strength, has forced aircraft manufacturers to use highly conservative knock-down factors. As such, there has been a demand to push the boundaries of impact damage tolerance of composite structures through material reinforcement methods and laminate stacking sequence design approaches. On the other hand, in an attempt to go even lighter, the aircraft industry has recently moved to thin structures and the response thin laminates have towards impact and post-impact loads is still unclear. To exploit the potential of laminate designs, the present thesis proposes novel stacking sequences with the aim to improve the compression after impact strength of aerospace graded thick and thin composite laminates.

The first part of the thesis questions the conventional laminate mid-plane symmetry constraint and proposes unsymmetrical laminates, with no coupling responses, for impact loads that are also unsymmetrical. By means of experiment tests (low velocity impact, quasi-static indentation and compression after impact), damage evaluation (C-scan and micro computed X-ray tomography) and numerical methods, we demonstrate that impact damage can be tailored to occur at pre-determined through-the-thickness laminate locations using unsymmetrical designs with tailored ply clusters. Furthermore, by using X-ray tomographic inspections, the impact damage and the damage tolerances of the proposed unsymmetrical laminates are compared with a standard symmetric baseline laminate. The improved CAI strength of one of the unsymmetrical design reveals that symmetric laminates are not the optimal solution for impact load cases and pinpoints the feasibility of moving to unsymmetrical designs.

The next segment of the thesis studies the response of thin laminates (< 2 mm) towards impact and post-impact loads, with the main aim of assessing the damage tolerance capability thin plies have. The extensive experimental study used different material architectures: uni-directional tapes, woven fabrics and non-crimp fabrics, all made out of the same fibre-resin material system. Different ply grades were also included for each material to assess the ply thickness effect on impact response. Experimental results evidenced the vulnerability of thin-ply based thin laminates through extensive fibre damage that drastically reduce the CAI strength compared to intermediate ply grades. In addition, textile fabrics offer a promising prospect in terms of damage tolerance and economical manufacturing over their uni-directional counterparts.

In the quest to improve the weak response of thin-ply based thin laminates, we re-defined the potentials of laminate design to introduce hybrid laminates, where different ply grades are used in the laminate. Substantial improvements at zero added costs inspired us to propose a laminate design combining ply hybridization and unsymmetrical design with non-crimp fabric thin laminates. The novel design delays and reduces the fibre damage, resulting in a significant improvement in CAI strength over its thin-ply baseline counterpart. Finally, we made use of virtual numerical tests to propose numerous improved damage tolerant thin laminates (both symmetric and unsymmetric) using a ply hybridization technique. This thesis demonstrates the potential of using laminate design approach as an efficient and economic method towards improving damage tolerance.

Resum

Un dels grans objectius de la indústria aeronàutica en les darreres dècades ha estat el desenvolupament d'aeronaus més lleugeres i més eficients, de manera que en aquest període s'ha incrementat considerablement l'ús de materials compòsits. Aquests ofereixen una elevada resistència amb un pes molt reduït però són molt vulnerables a càrregues fora del pla, com les que es poden donar en forma d'impacte a baixa velocitat. Aquest tipus d'impacte produeix una alarmant reducció de la resistència del material, especialment la resistència a compressió després d'impacte (denominada en anglès CAI, per Compression After Impact). El risc que suposa aquest tipus de càrregues fa que els dissenyadors apliquin factors de reducció elevats a les propietats del material com a mesura de seguretat. Queda clar doncs que existeix encara una necessitat de millorar la tolerància al dany per impacte amb el disseny de la seqüència d'apilat del laminat. D'altra banda, dins aquest procès de reducció del pes, la indústria aeronàutica ha començat a explorar l'ús d'structures primes, tot i que la seva resposta a impactes encara no és del tot coneguda. En aquest àmbit, la present tesi doctoral es planteja la millora de la resistència a la compresió després d'imapcte (CAI) de laminats gruixuts i prims, emprant seqüències de laminat innovadores que explotin al màxim el potencial del material.

A la primera part de la tesi es qüestiona l'ús convenicional de laminats simètrics respecte al seu pla mig i es proposen dissenys assimètrics per a millorar el comportament a càrregues respecte impacte, que són assimètriques per naturalesa. Els dissenys assimètrics que es proposen eviten els acoblaments flexió-elongació. Mitjançant assaigs experimentals i virtuals es demostra que pot dissenyar-se un laminat de manera que el dany per impacte quedi confinat en posicions predeterminades del seu gruix. Adicionalment es compara el dany per impacte i la tolerància al dany dels laminats proposats amb les d'un laminat simètric estàndard, usant tomografia de raigs X. Les millores obtinguydes en resistència a compressió després d'impacte mostren com els laminats simètrics no són la millor opció y obren el camı'i a explorar els dissenys assimètrics.

Cambiant lleugerament el focus d'atenció, la següent par de la tesi estudia la resposta de laminats prims (gruix igual o inferior a 2 mm) a càrregues d'impacte i post-impacte,

amb l'objectiu d'analitzar la tolerància al dany de les làmines primes. Es realitza una extensa campanya experimental que considera diferents arquitectures de laminat que van des de la cinta unidireccional a woven fabrics y a los non-crimp fabrics, incloent capes de diferents capes de diferents gramatges en cada material. Els resultats experimentals mostren la vulnerabilitat dels laminats prims constutuïts únicament per làmines primes, degut al massiu dany de la fibra que redueix dràsticament la resistència a compressió després d'impacte. S'observa també que els teixits presenten un comportament prometedor amb respecte a la toleranacia al dany i a la reducció dels costos de fabriació, en comparació amb els seus equivalents unidireccionals.

Finalment, amb l'objectiu de millorar la mala resposta a impacte dels laminats prims constutuïts únicament per làmines primes, s'exploren els laminats híbrids, en que s'utilitzen làmines de diferent gruix (i gramatge) en el mateix laminat. Els resultats mostren millores substancials sense costos adicionals, si s'usa en el disseny dels laminats prims la combinació de hibridització i assimetria. Aquests dissenys innovadors retarden i redueixen el dany en la fibra, produint d'aquesta manera una millora significativa de la resistència a compressió amb respecte del laminat prim de partida. Finalment, mitjançant assaigs virtuals es proposa un laminat òptim (per a ambdós casos simètric i assimètric) amb respecte a la tolerància al dany per impacte. Queda així demostrat el potencial del disseny del laminat com a un mètode eficient i economicament viable per a assolir materials amb millor tolerància al dany.

Resumen

La gran determinación de la industria aeronáutica por producir una nueva generación de aeronaves ligeras y más eficientes ha conducido a incrementar el uso de materiales compuestos en las últimas décadas. Aunque éstos ofrecen ahorro de peso manteniendo elevados valores de resistencia, los materiales compuestos son vulnerables a cargas fuera del plano como las que pueden recibirse en forma de impactos a baja velocidad. Este tipo de impactos produce una alarmante reducción de la resistencia, en concreto de la resistencia después de impacto (denominada en inglés CAI, por Compression After Impact). El riesgo que conlleva de este tipo de cargas hace que los diseñadores apliquen elevados factores de reducción de las propiedades del material como medida de seguridad. Por esta razón, existe una clara necesidad de mejorar la tolerancia al daño por impacto mediante el diseño de la secuencia de apilado del laminado. Por otro lado, dentro del proceso de reducción del peso, la industria aeronáutica ha comenzado a explorar el uso de estructuras delgadas, aunque su respuesta a los impactos y posibles cargas posteriores a éstos no esté aún clara. En este ámbito, la presente tesis doctoral se plantea la mejora de la resistencia a compresión después de impacto (CAI) de laminados gruesos y delgados, mediante la introducción de secuencias de laminado innovadoras que expriman al máximo el potencial del material.

En la primera parte de la tesis se cuestiona el uso convencional de laminados simétricos respecto a su plano medio y se proponen diseños asimétricos para mejorar el comportamiento a cargas de impacto que también son asimétricas por naturaleza. Los diseños asimétricos que se consideran evitan los acoplamientos flexión-elongación. Se demuestra mediante ensayos experimentales y virtuales que puede diseñarse el laminado de manera que el daño por impacto quede confinado en predeterminadas posiciones de su espesor. Además, se compara el daño por impacto y tolerancia al daño de los laminados propuestos y un laminado simétrico estándar mediante tomografia de rayos X. Las mejoras obtenidas en la resistencia a compresión después de impacto muestran como los laminados simétricos no son la mejor opción y abren el camino a explorar los diseños asimétricos.

Cambiando un poco el foco de atención, la siguiente parte de la tesis estudia la

respuesta de laminados delgados (espesor inferior o igual a 2 mm) a cargas de impacto y post-impacto, con el objectivo de analizar la tolerancia al daño de las láminas delgadas. Se realiza una extensa campaña experimental que considera diferentes arquitecturas que van de la cinta unidireccional a los woven fabrics y a los non-crimp fabrics, incluyendo capas de distintos gramajes en cada material. Los resultados experimentales muestran la vulnerabilidad de los laminados delgados construidos a base de láminas delgadas, debido al masivo daño de la fibra que reduce drásticamente la resistencia a compresión después de impacto. Se observa también que los tejidos presentan un comportamiento prometedor con respecto a la tolerancia al daño y a la reducción de costes de fabricación, en comparación con sus equivalentes unidireccionales.

Finalmente, con el objetivo de mejorar la mala respuesta a impacto de los laminados delgados construidos con láminas delgadas se exploran los laminados híbridos, donde se emplean láminas de distinto espesor (y gramaje) en el mismo laminado. Los resultados muestran mejoras substanciales sin costes adicionales si se usa en el diseño de los laminados delgados non-crimp fabric la combinación de híbridación y asimetría. Estos diseños innovadores retrasan y reducen el daño en la fibra, produciendo así una mejora significativa de la resitencia a compresión con respecto al laminado delgado de partida. Finalmente, se emplea el ensayo virtual para proponer un laminado óptimo (para ambos casos simétrico y asimétrico) con respecto a la tolerancia al daño por impacto. Queda así demostrado el potencial del diseño del laminado como un método eficiente y economicamente viable para alcanzar materiales con mejor tolerancia al daño.

1 Introduction

1.1 Contextual Background

The word *composite* signifies a combination of many constituents, and similarly in the framework of materials science, a composite material refers to a heterogeneous mixture composed of different materials. Dated back to the 4000 BC, the same concept is used in the current decades to produce lightweight structures. Generally termed as advanced composites, long fibres (for e.g., carbon or glass) along with a polymer matrix makes way for a composite material that possesses improved material characteristics with respect to the individual constituents. By placing fibres at different orientations, polymer matrix composites can be tailored to have improved strength in the preferred directions, unlike metallic counterparts.

Focussing mainly on the aeronautic industries, the application of a specific material is determined by the cost and weight factors. Despite a 50% increase in the production costs of composite materials [1] over aluminium (the traditionally used material in the pre-composite phase), the wide application of composites is attributed to the weight savings along with the zero compromise on the specific strength properties. This weight reduction has resulted directly in reduced fuel consumption which indirectly accounts to reduced flight costs and lesser emissions from the airplanes. Therefore, the usage of composites in aircrafts has increased tremendously in the last five decades moving from a 5% to 50% of composites accounting to the total structural weight (as in Fig. 1.1). A substantial 15% weight saving was possible with the application of composite materials in modern day aircrafts and each kg of mass in a plane is equated to 5000 € in fuel costs ever year [2], hence highlighting the importance in weight savings through composites.

1.2 Impact loads and the threats followed

Even though composite materials have made a breakthrough in the field of aviation materials, the complexities associated with their response to different loading cases are still being researched on. Composites materials do not exhibit a sudden and

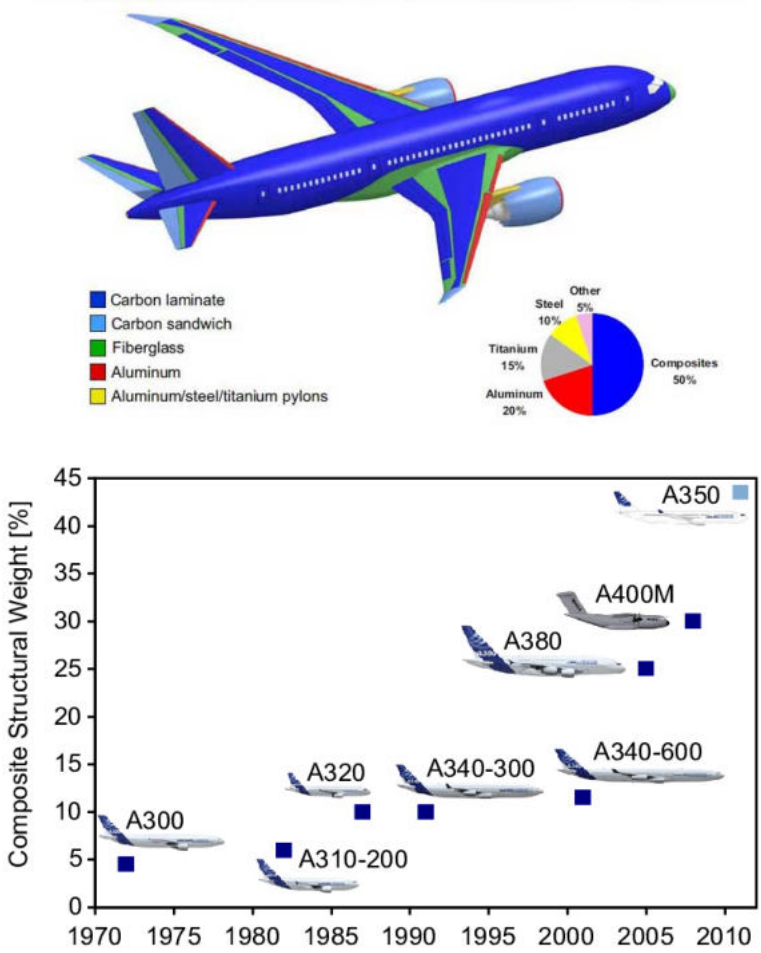

Fig. 1.1.: The evolution of the use of composite materials in airplanes in the last 5 decades (Images adapted from [3, 4] and the aircraft presented at the top is a Boeing 787).

complete loss of stiffness, instead they undergo a progressive damage evolution with the interaction of different damage forms. One of the critical loading cases is the impact loads experienced by aerospace structures during the long run of the flight. Impact on an exposed aerospace structure can be experienced in various forms: a tool drop during a maintenance inspection, runway debris impact, bird strike during take-off and landing, ground accidents, aircraft crash. While all these come under the category of impact loads, they can be categorized into low, intermediate and high velocity impact regimes depending on the velocity and mass of the impactor [5]. Low velocity impacts (LVI) are characterized as less than 10 m/s and are experienced in

the form of tool drops on aircrafts during scheduled maintenance services. At this instance it is obvious to question: why to worry about a tool drop damage of low velocity when compared to high velocity impacts that could be catastrophic?

Reports suggest that most accidents on aircrafts happen on the ground and not in the air [2]. This refers to ground vehicles hitting aircrafts and impacts on aircraft parts during maintenance inspections mainly attributed to tool drops. While the accidents that occur in the air are well documented, those that occur in ground are seldom reported. For a comprehensive understanding of the possible consequences of a low velocity impact, let's review a real life scenario.

Consider that an aircraft enters a maintenance inspection after 400-600 flight hours. During the maintenance activity, a technician accidentally drops a tool on the top of the wing as illustrated in the Fig. 1.2. Despite the fact that this 'low velocity impact' leaves no visible damage on the surface of the wing, there is damage created within the laminate in terms of cracks and delamination which goes unnoticed (represented in the figure as A). The aircraft returns back to operation and with each flight cycle, the aircraft wing experiences different loads, mainly compression at the top of the wing due to the bending associated with the lift created. The impact induced damage grows with flight hours, which may or may not leave a trace at the outer surfaces of the impacted site (represented by B in the figure). With increased flight hours and consequent loading, the damage grows extensively until a point where the laminate might fail suddenly because of the compressive load (represented as C in the figure).

The above scenario can now be reviewed in terms of the reduction in the residual strength and impact damage detectability with increasing flight hours. During a low velocity impact, the damage is generally visible from the non-impacted side before it is evident from the impacted side. Since in an aircraft, the non-impacted side is generally inaccessible (inside the wing box or fuselage), the damage can be detected only from the impacted side in the form of impact dent depth. Literature reports that a permanent indentation of 0.5 mm deep could be detected with a probability of 90% in a detailed visual inspection [8]. Fig. 1.3 presents the reduction in the compression strength and the increase in the size of the impact dent depth with increasing flight hours. Three different instants in time namely, A, B and C (as explained in Fig. 1.2) are studied to understand the threats of LVI damage. At A, the laminate exhibits

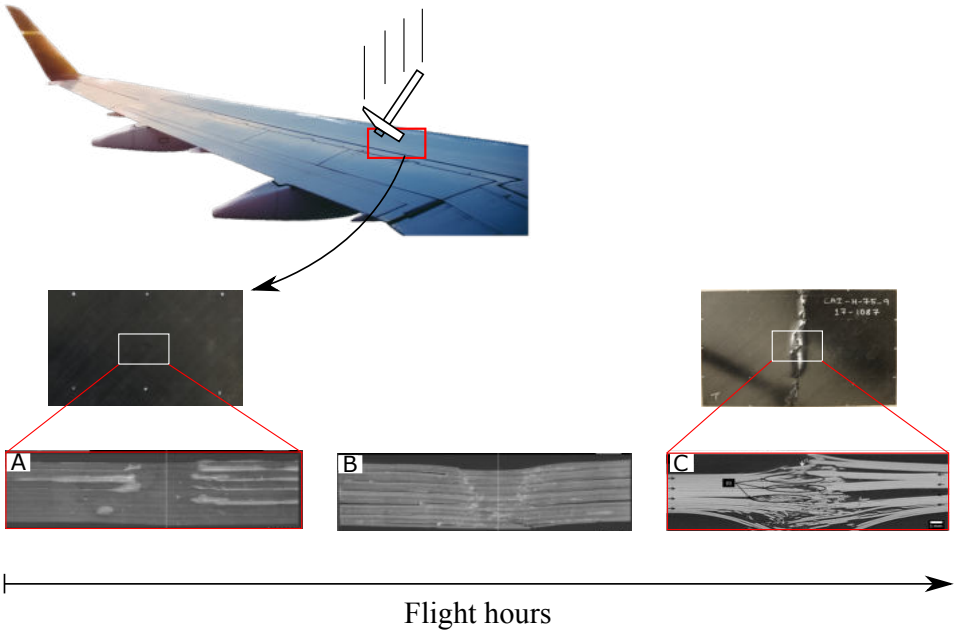

Fig. 1.2.: Scenario of a tool drop accident on an aircraft wing followed by the evolution of the barely visible damage with respect to the flight hours. (Note the damage scans [6, 7] used are just for understanding and do not represent real structure scan).

internal damage but with no traces of visible damage (an impact dent depth of less than 0.5 mm). Nevertheless there is already a considerable reduction in the compression strength compared to the pristine strength. With increased loading, at B, the impact induced damage has propagated, leading to a major reduction in the residual strength. At the same time, the laminate exhibits 0.5 mm dent depth which can be detected through detailed inspection. This is referred to as barely visible impact damage (BVID). At C, the laminate breaks down completely, thereby losing the load carrying capability. If a maintenance activity is not scheduled between B and C, the LVI damage created by a tool drop would result in a structural collapse.

At this stage, the concepts of damage resistance and damage tolerance can be introduced. Impact damage resistance refers to the capability of the laminate to resist the damage initiation or growth from the impact loads, whereas damage tolerance concept is explained as: '*The damage tolerance evaluation of the structure is intended to ensure that should serious fatigue, corrosion or accidental damage occur within the operational life of the airplane, the remaining structure can withstand*

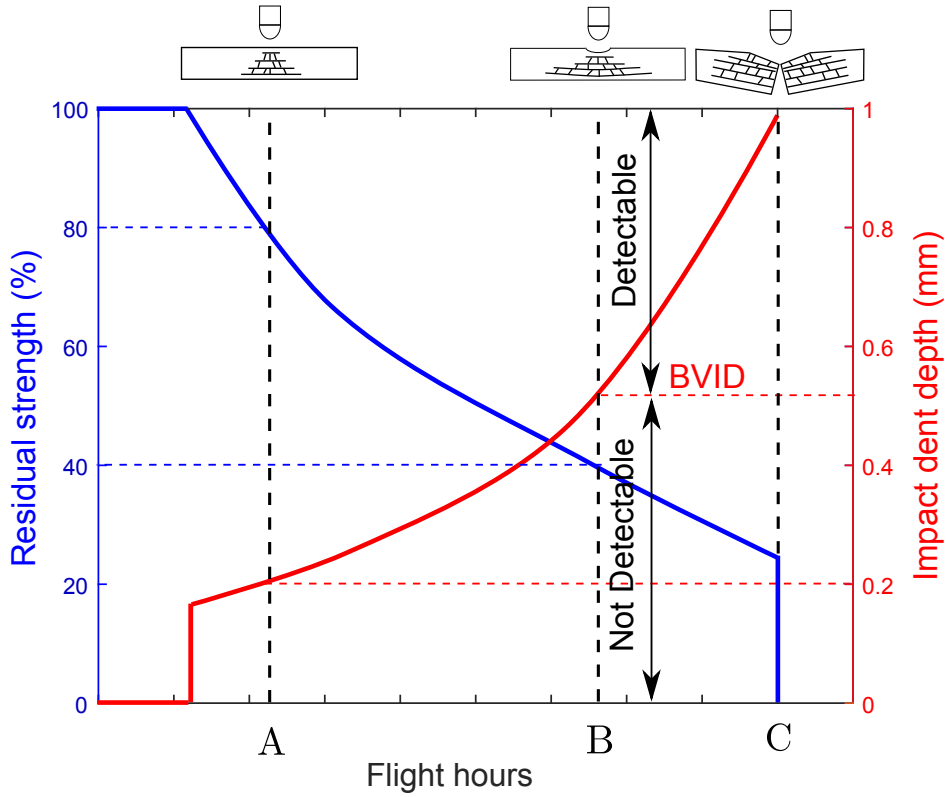

Fig. 1.3.: Residual strength reduction and impact damage detectability as a function of increasing flight hours.

reasonable loads without failure or excessive structural deformation until the damage is detected', by the American certification [8].

While increasing the number of inspections than what is followed now can help to detect the damage, but this is practically not feasible due to the direct and indirect costs associated with it. One of the other solutions is to push the boundaries of aeronautical structural design towards a more damage tolerant design. An increased compression after impact strength ensures that the structure with the impact damage could still stay in operation for a longer period of flight cycles carrying the operational loads, thus increasing the chances of a repair before a complete structural collapse. Lack of proper understanding of the impact damage evolution and its effect on strength reduction has forced the airplane manufacturers to use high conservative knock down factors. This has led to unwanted weight addition that depreciates the

advantages of composites and their light weight design over metallic counterparts. This situation demands for an extension of the damage tolerance boundaries of these composite structures.

In another context, aircraft industries have moved to thinner structures (less than 2 mm), especially in the fuselage and wing skins, as a move towards weight savings. Despite the application of thin structures, the response of thin laminates towards impact and post-impact loads is still in its early stages of research. Recent research has reported different critical damage mechanisms with thin laminates compared to the standard thick laminates under impact loads.

1.3 Motivation

In the quest to improve the damage tolerance, numerous researchers modified the material system such as using tougher resins, introducing interface toughening agents, varying the fibre architectures etc. Despite the substantial improvements in CAI strength, the added costs and the detrimental collateral effects to the material micro-structure have been the downside of this material reinforcement method. On the other hand, laminate design, referred to as modifying the laminate stacking sequence through tailoring the location, orientation and thickness of the ply, has also been reported to substantially improve the damage tolerance [9, 10]. Despite the economic feasibility and the easiness, laminate design has not been exploited to the full potential to finding optimum impact damage tolerant designs.

Recently, using non-conventional laminate designs, researchers have demonstrated the possibility to control the extent and location of impact damage within a composite laminate [11–13]. In the thickness direction of the laminate, impact loading is an unsymmetrical loading case that induces unsymmetrical damage modes. Despite the novelty in laminate designs, the conventional mid-plane laminate symmetry constraint is still unarguable to avoid coupling responses such as warpage during manufacturing. One of the main motivations of this thesis is to move out of the symmetry constraint box and to look for unsymmetrical laminate designs to improve the damage tolerance.

Further, in the context of thin laminates only a handful of research works are devoted to the impact response of thin laminates, compared to the extensive research available

on thick laminates. The impact response of a thin laminate is completely different from that of a thick laminate, and hence the conclusions derived from thick laminates cannot be extrapolated to thin ones. Thin plies have the potential to delay and suppress certain damage modes which have resulted in improved damage tolerance compared to other ply grades. But moving to thin laminates, will thin plies offer the same improvement as in the case of thick laminates ? or will their brittle characteristic be an issue when used in thin laminates ?

Following the demand to cut down the manufacturing costs, industries are considering textile fabrics as a replacement for uni-directional (UD) tapes. While the advantages in terms of layup costs of fabrics over UD tapes is quite promising, their potential to improve the CAI strength over conventional UD tapes, especially with thin laminates, is still questionable. Hence the aspect of thin laminates, the following questions have to answered: (a) what is the response of thin laminates to impact loads? (b) how does ply thickness affect the damage evolution and CAI strength of thin laminates? (c) Can textile fabrics be a potential substitute to uni-directional tapes to improve the damage tolerance?

1.4 Objective

The main objective of the thesis is to push the boundaries of laminate design to propose novel stacking sequences as an efficient and economical way to improve the impact damage tolerance of thick and thin composite laminates made of aerospace grade material.

This main objective is addressed through three sub-objectives:

Objective-1: To explore the possibilities of unsymmetrical laminates towards impact loads, in an effort to tailor the impact damage to happen at pre-determined through-the-thickness laminate locations.

Objective-2: To investigate ply thickness effects and fabric architecture on the impact and post-impact behaviour of laminates with reduced thickness (thin laminates) compared to the ones considered in the standard tests.

Objective-3: To make use of experimental and virtual testing to optimize the

CAI strength of laminates with an unsymmetrical and/or ply hybrid stacking sequences.

1.5 Thesis Layout

This thesis is written as a compendium of articles which are included as chapters within the thesis. Chapter 2 provides a brief literature review of the various building blocks of the research line of the thesis, that helps to identify the gaps found in literature. Chapter 3 details the experimental and numerical methodologies with details on the different materials used in the thesis. Each sub-objective put forward above is fulfilled through different papers. The first sub-objective is accomplished through Paper A and Paper B, where we demonstrate the feasibility to move away from the symmetry constraint and still offer improved damage tolerance over symmetric laminates. Paper C and D fulfils second sub-objective of studying the response of different ply grades and material systems based on thin laminates against impact and compression after impact loads. The final sub-objective is fulfilled by Paper C, E and F, where efficient and economic laminate design strategies are proposed to improve the compression after strength. An illustration of the objectives and the associated papers is presented in Fig. 1.4. Chapters 3 to 8 present the six generated papers and all are preceded by the motivation to each paper followed by a synopsis. This helps to elucidate the coherence of the papers and to maintain the narrative flow to the reader. Chapter 10 provides a complete discussion of the thesis, providing answers to the questions raised in the objectives section. Chapter 11 presents the concluding remarks followed by prospective ideas for future work in the same line of research.

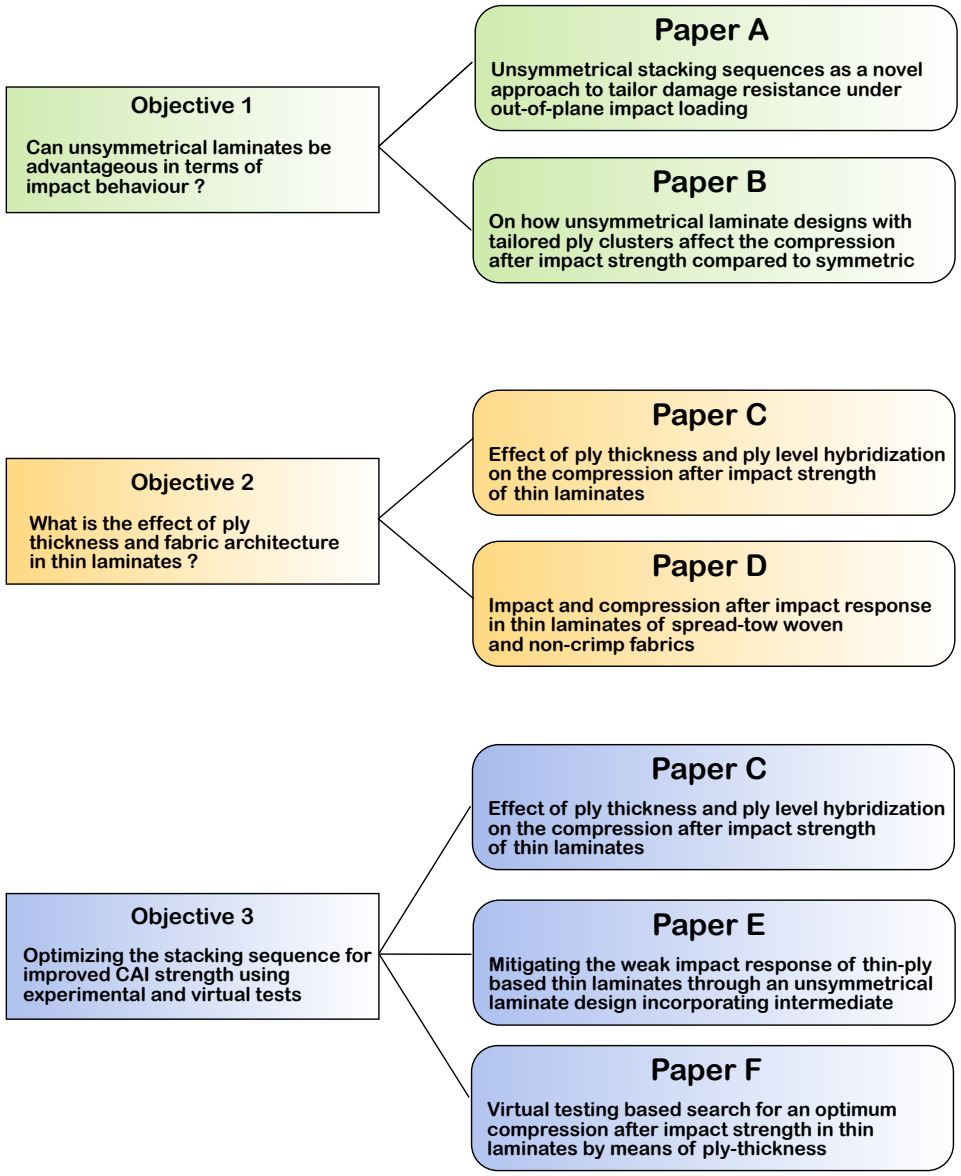

Fig. 1.4.: Illustration of the objectives and the papers addressing them.

Literature Review

2

2.1 Damage morphology

2.1.1 Low velocity impact

LVI is a complex loading case due to the interaction of different damage mechanisms namely matrix cracks, delamination and fibre failure [5]. Impact damage triggers different types of matrix cracks within the laminate depending on the location in the laminate and the load this region encounters. Fig. 2.1 illustrates a shear matrix crack (see (a)) and a tensile matrix crack (see (b)) that have been formed due to the shear and tensile stresses, respectively. These cracks grow through the ply to reach an interface to form a delamination. A majority of the energy is dissipated through delamination in an impact scenario and hence constitutes to a dominant damage mode. The main source of delamination is the high interlaminar stresses in combination with the low through-the-thickness strength of composite laminates. Cracks are a form of discontinuity that induces a delamination damage mainly in the form of tensile crack induced delamination at the non-impacted laminate surface and through shear crack induced delaminations at the sub-laminates close to impacted side and at the mid-plane [14]. Multiple delaminations link up through cracks in the through-the-thickness direction, normally reported as a spiral staircase pattern [15, 16].

In the impact framework, high interlaminar stresses can be encountered at the interfaces of clustered plies, at the interfaces with high mismatch angles steering to delamination. When more than one ply of the same orientation are blocked/clustered together, the adjacent interface experiences a higher bending stiffness mismatch [18] due to the increased thickness of the ply, leading to high interlaminar stresses. Similarly in the case of higher mismatch angles (for eg. [0°/90°] interface), the increased bending stiffness mismatch between the 0° and 90° ply introduces interlaminar shear stresses making way for delamination initiation. Following matrix cracks and delamination, fibre failure is also reported to occur at higher velocities. Fibre damage is typically observed at the zone under the impactor, and at the non-impacted site

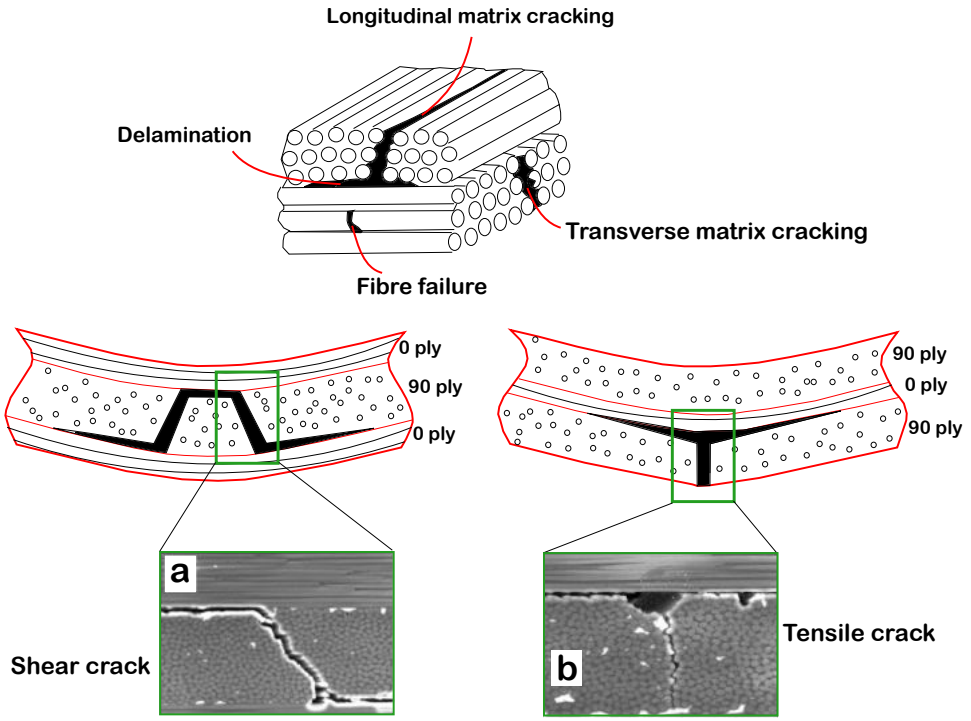

Fig. 2.1.: Illustration of different types of cracks and the corresponding delaminations induced (Image adapted from [17]).

due to tensile loads. Fibre failure, unlike delaminations, does not distribute in the through-the-thickness laminate direction in standard laminates.

2.1.1.1 Unsymmetrical through-the-thickness damage nature

With respect to the through-the-thickness direction, impact loading is an unsymmetrical loading scenario that creates unsymmetrical damage within the laminate [5, 6]. Fig. 2.2 reviews the different damage modes in a symmetric laminate, where there are tensile cracks at the bottom ply, shear cracks at the top sub-laminate, delaminations induced from these cracks mainly observed at the mid-plane and at the bottom sub-laminate. In addition, an undamaged cone (reported in [19]) right under the impactor is observed, where the cracks and delamination are seen to be formed from the boundaries of this cone. During an impact, the laminate experiences complex stress states in the thickness direction, varying from high local compressive stresses right under the impactor, tensile stresses at the non-impacted side due to bending,

shear stresses at the vicinity of the impactor and at the mid-plane. Despite this fact, laminate symmetry is strictly followed, where the top sub-laminate is mirrored to form the bottom sub-laminate, and hence providing the same layup to both the sides where only one side of the laminate is directly exposed to impact load.

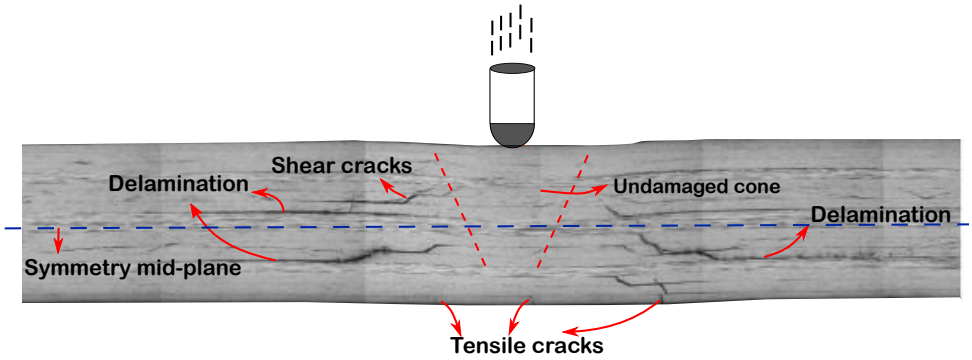

Fig. 2.2.: Illustrating the unsymmetrical impact damage modes in a symmetric laminate (Image adapted from [20]).

2.1.2 Compression after impact

Numerous theories have reported different damage morphologies during a compression after impact (CAI) test of an impacted specimen. With the already existing impact damage in the laminate and further its propagation and interaction with new damage modes under compression loading makes compression after impact one of the most complex loads to apprehend the underlying failure mechanisms. Impact induced delaminations tend to split the laminate into sub-laminates under compression loading. The thickness of the split sub-laminates depends on the through-the-thickness location of the impact induced delaminations.

The split sub-laminates has a reduced bending stiffness, thereby experiences buckling more easily. Buckling triggers the propagation of the existing delaminations and can grow up to the laminate edges to cause final failure.

Another phenomenon reported along with the impact induced delamination propagation is the local compressive failure of 0° plies, which are the load bearing plies in compression loading. During laminate splitting, there is load redistribution to the different sub-laminates which can induce fibre damage. In [8, 21], kink band formation in the 0° plies was reported to be the reason behind the final failure . In

agreement to this, Soutis et al. [22] mentioned that fibre micro-buckling in the 0° plies, along with the initiation and propagation of matrix cracking and delamination in the off-axis plies in the lateral length of the specimen also led to CAI failure.

Bull et al. [7] performed ex-situ micro-focus computed tomography during CAI loading to understand the interaction of damage modes and the failure sequence leading to failure. Delamination propagated into the undamaged cone under the impactor driven by the out-of-plane deflection of the sub-laminates, followed by the growth of pre-existing 0° fibre fracture. Bouvet et al. [8, 23] explained the CAI failure as given in Fig. 2.3, where under CAI, there is propagation of delaminations and propagation of compressive fibre fracture which was already induced during impact. A plane cut longitudinally through the impact centre shows the laminate buckling due to the delaminations, and also the extension of delamination.

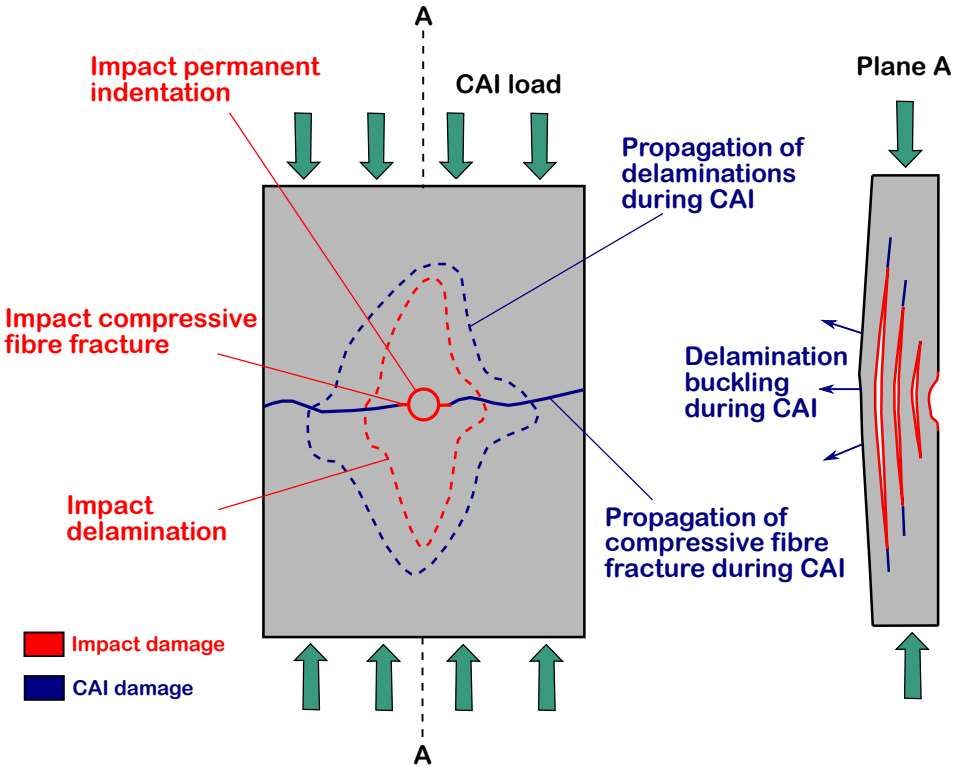

Fig. 2.3.: Representation of the impact damage and its propagation during CAI (Image adapted from [8]).

2.1.2.1 Correlating impact resistance to impact tolerance

With CAI strength looked upon as a critical parameter by airplane manufacturers, researchers studied the effect of different impact damage resistance parameters on CAI strength. Impact damage resistance is evaluated through several parameters such as delamination threshold load, maximum peak force, projected delamination area, dissipated energy and impact dent depth that are obtained from experimental impact test and post inspection. Comparing these parameters to CAI strength, researchers tried to find an effective global resistance parameter that could be best correlated to CAI strength.

Bull et al. [7] reported that an increase in projected damage area clearly resulted in the loss of residual compressive strength, whereas Sebaey et al. [9, 13] commented that projected damage area is misleading as a laminate with higher damage area offered higher CAI strength in some cases. Similar contradictory conclusions [9, 24] were seen when correlating peak load and delamination threshold load to CAI strength. In view of the unclear conclusions, researchers studied the effect of various delamination parameters such as through-the-thickness delamination location, orientation, size and the buckling modes under compression on the CAI strength. Using analytical and numerical analyses, different researchers [25, 26] studied the effect of the position of one embedded delamination on the CAI strength. They reported that the buckling load increased significantly as the position of the delamination approached the laminate mid-plane due to the change in the buckling mode from a local to a global one. A similar conclusion was reported by Butler et al. [26] using an analytical model. They stated that deep sited delaminations were safe as they opened under compressive loading and would not grow to cause failure. Despite these interesting conclusions, in a real impact scenario the effect on CAI strength could be completely different due to the development of many more complex damage forms.

2.2 Improving damage resistance and tolerance

Since LVI loads reduce the load carrying capacity of the laminate by upto 50% [5, 27], large safety margins were considered by the aircraft manufacturers with the composite structures. Large safety factors obviously increases the weight and costs, which substantially reduces the expected competitiveness compared to metallic

counterparts. This demanded the necessity to look for alternative methods to improve the impact resistance of the laminates and also the damage tolerance. The different methods available in the literature can be generally classified into (a) modifying the material system or termed as material reinforcement and (b) laminate design approach. While the former deals with modifying the fibre or resin material system or adding a modifying agent to enhance the toughness of the composite, the latter is dedicated to exploiting the laminate stacking sequence combinations in a way to tailor the damage resistance and tolerance.

2.2.1 Material reinforcement

2.2.1.1 Interlaminar toughening through interleaving

Interlaminar toughening involves incorporating an additional modifier to toughen the interface with the intention to improve the interlaminar fracture toughness of composites. The different forms of modifier material found in literature are co-mingled fibres [28], thermoplastic films [29], particles or non-woven veils [30, 31]. Irrespective of the different modifying agents added, the global mechanism behind improving the interface fracture toughness remains the same: to improve the impact resistance through delamination arresting. Out of the above mentioned methods, interleaving the interfaces with a non-woven veils was reported as a cost-effective (a 7% increase in the cost of materials) method along with the added advantage of easily incorporating into any manufacturing process. Interleaving veils was found to reinforce the interface during fracture through thermoplastic fibre bridging and the strong interaction between the resin and the thermoplastic fibres. Studies reported that laminates with veils increased the mode I and II fracture toughness, thereby arresting the damage propagation during impact. Laminate toughened with veils exhibited reduced damage area and contradictory conclusions of increase [32] and reduction in the residual CAI strength [33]. Despite this, some studies [34] reported a reduction in the in-plane properties, tensile and flexural modulus due to the reduction in the fibre volume fraction caused due to the veil incorporation. Fig. 2.4 (a) shows a mode I fracture surface of a polyamide veil interleaved laminate with veil fibres.

2.2.1.2 Z pinning and through-the-thickness reinforcement

The technique of Z-pinning revolves around the idea of introducing discrete pins in the through-the-thickness direction of the laminate, where the pins bind the laminate together [35, 36]. Aimed to increase the delamination and impact damage tolerance, z-pins increase the fracture toughness using the bridging force created by pin-laminate friction and thus hindering the crack growth [37]. A substantial reduction in the delamination damage area by up to 50% was reported when comparing the impact results of pinned and unpinned laminates [38]. In addition, pinned laminates also improved the mode I and II fracture toughnesses with the added benefit of transforming a crack propagation fro unstable to stable process. Following the improved impact resistance, the post-impact properties are improved due to the suppression in the delamination damage and the higher buckling resistance provided by the bridging action of the z-pins. Despite the extraordinary improvement, z-pinning has the disadvantage of: (a) insignificant effect below a threshold impact energy; (b) the change in the micro-structure created due to the insertion of the pins and (c) tedious and expensive insertion process. Z-pins induce fibre crimping, breakage and resin rich regions, which directly compromise the in-plane laminate properties. Fig. 2.4 (b) displays the micro-images of two types of Z-pins used to reinforce the laminate's through-the-thickness direction.

2.2.1.3 Bio-inspired designs

Using a bio-inspired approach, the laminate micro-structure was engineered to enhance the damage tolerance. Bullegas et al. [39] placed patterns of micro-cuts in the micro-structure of thin-ply CFRP laminates with the aim to increase the damage resistance. Through patterns of aligned micro-cuts in the 0° plies in a cross ply laminate, a formed crack was forced to steer from its original path to follow the micro-cuts, to increase the energy dissipation. In a following work [40], micro-cuts repeated in the form of shark-teeth (Fig. 2.4 (c)) were made across the load carrying fibres in an impact sample aiming to enhance the impact damage tolerance. Results from the low velocity impact penetration tests reported that the engineered laminate delayed the load drop (by 26%) to higher applied displacements with higher amount of energy dissipated before the load drop. The authors report that the engineered micro-cuts locally tailored the stiffness of the laminate. Despite the improvements,

reports on the cost-efficiency in the extra manufacturing step or other adverse effects of these micro-cuts were not discussed.

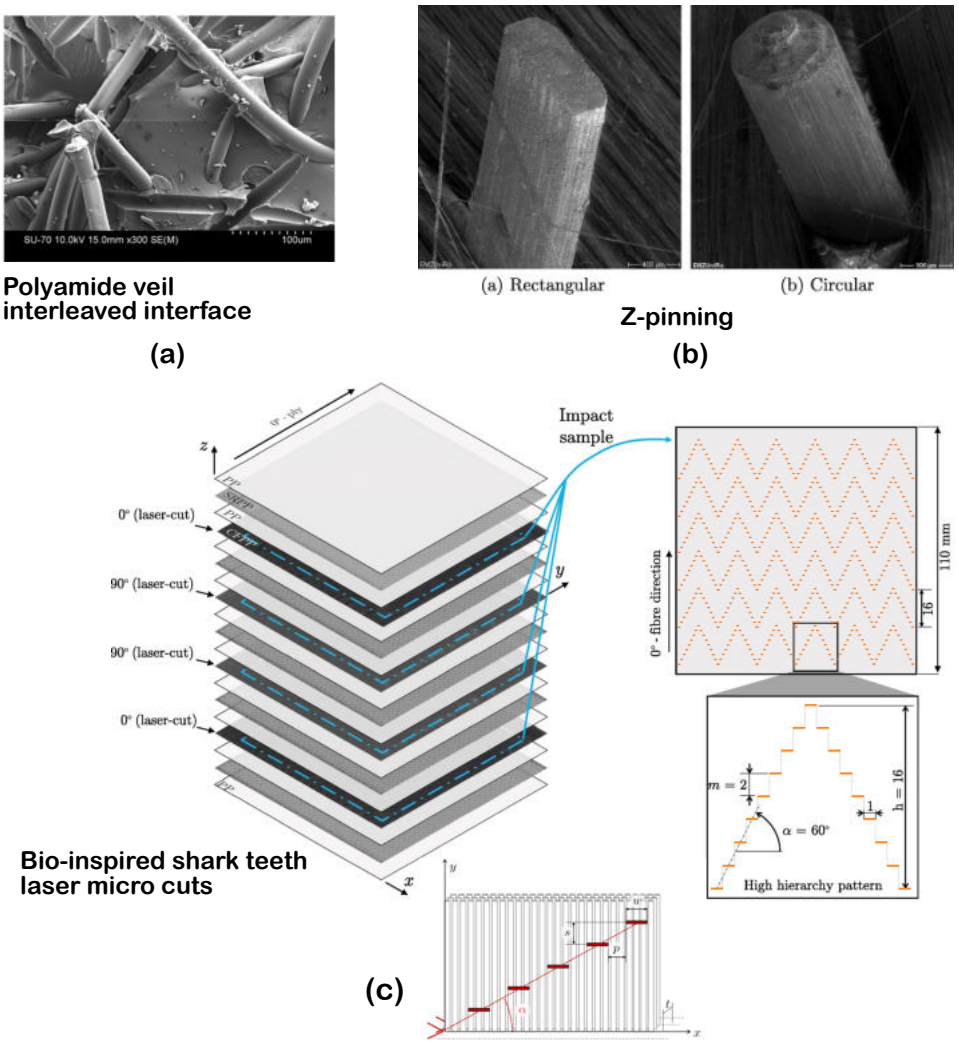

Fig. 2.4.: Different material reinforcement techniques in the literature to improve the damage resistance (Image adapted from [39, 40]).

In summary, all the material reinforcement methods explained above aim to resist delamination and matrix cracking by improving the fracture toughness. With improved resistance, a subsequent improvement in damage tolerance is demonstrated, despite the limitations of added costs and the changes in the micro-structure created by the reinforcements that impairs other properties.

2.2.2 Laminate design approach

Laminate design approach is dedicated to the tailoring of the stacking sequence through the orientation, the through-the-thickness location and the thickness of each ply with the objective to improve the laminate response according to the load encountered. Since this approach does not indulge in changing the composite material system or adding any reinforcing agent, it is one of the most economically effective methods. Despite the cost effectiveness, laminate design has not been used to the full potential to improve the impact resistance or tolerance, quite evident when compared to the magnitude of research available on its counterpart material reinforcement techniques.

Few researchers studied the effect of stacking sequence under LVI and reported that the impact damage, energy dissipated and CAI strength are influenced by the stacking sequence and pointed out the room for improvement [11, 12, 17, 41, 42]. One of the pioneering studies from Hitchen et al. [41] commented that between different laminates studied experimentally, a considerable difference in the dissipated energy and delamination area was observed, which led to different CAI strength values. The authors concluded that the delamination damage parameters (area, shape and the location), which are a function of the stacking sequence, strongly influenced the CAI strength. Hongkarnjanakul et al. [43] performed LVI and CAI tests on 7 different quasi-isotropic stacking sequences, with the baseline laminate $[0_2/45_2/90_2/-45_2]$ and other 6 more laminates formed by rotating and switching the location of the plies. The impact damage area and contour differed between the laminates, but no solid conclusion was obtained from the analysis of the CAI strength results.

2.2.2.1 Tailoring damage using dispersed ply orientations

Irrespective of the different stacking sequences used, all laminates were limited to the conventional ply orientations of 0°, ± 45 and 90°. With the advancement in the manufacturing techniques such as automated fibre placement and tape-laying technologies, Lopes et al. [44] redesigned the traditional stacking sequences with aim to improve the impact response by incorporating ply orientations that could vary in the 0°- 90° range with intervals of 5°, likely referred in the literature as dispersed ply orientations. Since the design space was considerably large, a Genetic Algorithm was used to find dispersed stacking sequences with certain conditions to have a proper

comparison with the traditional baseline laminate. A traditional laminate and two dispersed laminates were experimentally tested under LVI and CAI for a wide range of impact energies from 5 J to 50 J. The authors concluded that despite the use of non-conventional ply orientations, the results did not show any clear improvements over the baseline in terms of impact resistance and tolerance. Nevertheless, they suggested that the dispersed plies when combined with new constraints to tailor delamination damage at different locations could improve the damage tolerance.

Following the work of Lopes [44, 45], Sebaey et al. tailored delamination damage using ply clustering [9] and varied mismatch angled interfaces [13]. Clustered plies and high mismatch angled (MMA) interfaces facilitate delamination damage due high interlaminar shear stresses at the interfaces. The authors found dispersed laminates using Ant Colony Optimization methods, where two dispersed laminates studied the effect of local ply clustering and the other two laminates the effect mismatch angle at the interfaces have on CAI strength. The dispersed laminates substantially improved the CAI strength over a baseline (made of conventional ply orientations), and the key findings of the studies were: (a) laminate stacking sequences can be tailored to improve the CAI strength (b) local clustering of plies helps to localize delamination damage at particular locations which thereby improve the CAI strength by up to 30% over the baseline (c) a smaller mismatch angle between the plies (between 10° to 30°) helps to improve the CAI strength over larger mismatch angles. These conclusions opened the doors towards using laminate design strategy combined with an optimization method to look for improved impact damage tolerant laminates.

As a continuation, Liv et al. [11] demonstrated that impact damage can be pre-determined to happen at the desired locations using judicious laminate designing. The idea of the work was to force the delaminations to occur at the laminate surfaces using higher mismatch angles and thereby keep the central sub-laminate delaminations free to efficiently carry the compression load. Even though the design successfully forced the delaminations at the outer sub-laminates, it did not improve the CAI strength over the baseline. Table 2.1 details the baselines and the corresponding improvement or reduction in the CAI strength of the dispersed laminates from the above-mentioned works.

Tab. 2.1.: Non-conventional dispersed laminates and the improvement in CAI strengths

Source	Baseline laminate	Non-conventional laminates	Improvement in CAI strength (Impact energy)
Lopes et al. [44]	$[\pm 45/90/0/45/0_4/-45/0_2]_S$	$[\pm 45/0/70/-70/0/15/10/-10/-15/15/-15]_S$	7% (30 J)
		$[\pm 45/80/5/20/-20/10/-80/-10/-5/15/-15]_S$	−15% (30 J)
Sebaey et al. [9, 13]	$[45/0/-45/90]_{3S}$	$[0_2/55/65/80/-50/50/-80/-60/-50/20/-15]_S$	30% (30 J)
		$[10/35/65/85/65/35/5/-25/-35/-45/-55/-80]_S$	27% (30 J)
Liv et al. [11]	$[90/-45/0/45]_{3S}$	$[90/\pm 45/75/-60/60/-75/-30/-15/0/15/30/45]_S$	−15% (20 J)

2.2.2.2 Ply level hybridization

The progress in the application of composites led to the possibility of having different ply grades ranging from thick plies (around 250-300 gsm) to intermediate plies (100-200 gsm) to thin plies (30-100 gsm). Moving away from the conventional method of using only one ply grade throughout the laminate, few researchers [46, 47] recently demonstrated that ply hybridization (mixing plies of different thicknesses in the laminate) can improve the damage resistance. Furtado et al. [46] performed selective ply hybridization, where thin off-axis plies (67 gsm) were combined with 0° plies of the intermediate ply grade (134 gsm), that improved the notched response of the laminate. Arteiro et al. [47] performed similar study with a laminate with blocked 0° plies was compared with a laminate with dispersed 0° plies to compare the unnotched tension, compression and bearing responses. They reported that thicker 0° plies had a negligible effect on the unnotched tension and compression results. But a significant improvement was seen with tensile notched strength and bearing response. By means of mixing different ply grades in the laminate, both the above works demonstrated that the damage mechanisms and failure modes can be controlled in multi-directional laminates. The brittle failure nature of thin plies is improved with the addition of the thicker plies resulting in a globally enhanced laminate response.

In the aspect of impact and CAI response, Sebaey et al. [48] proposed hybrid laminates in attempt to improve the CAI strength. They studied the effect of mixing thick and thin fabric layers on the impact and CAI response. Three laminates were studied: a baseline made of thick fabric (330 gsm) layers and two hybrid laminates made of thick and thin fabric (85 gsm) layers. While the first hybrid laminate was designed with thicker plies at the specimen surface and the thin plies placed at the mid-plane, the second laminate had thick fabric layers surrounded by thin plies. Fig.

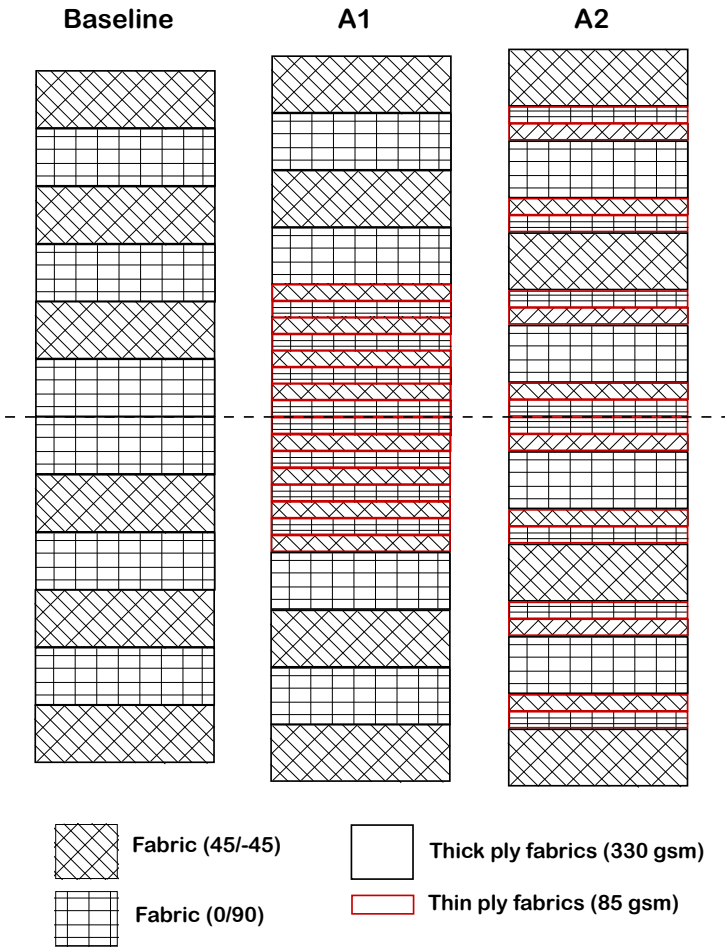

Fig. 2.5.: Baseline and the proposed laminates mad by mixing thick and thin ply fabrics (Image adapted from [48]).

2.5 illustrates the three laminates namely baseline, A1 and A2. CAI results from different impact energies revealed that thin plies blocked at the laminate middle (A1) had insignificant effect on the CAI strength compared to the baseline, whereas the laminate A2 improved the CAI strength by a maximum of 15%.

2.2.2.3 Moving to unsymmetrical laminate designs

Baker et al. [49] came up with the idea of using non-symmetric laminates over symmetric laminates as a solution towards impact load cases. They used a surrogate sub-laminate buckling model [50] to calculate the compression after impact strength

of fully orthotropic composite laminates including symmetric, anti-symmetric and non-symmetric laminates. The authors proposed unsymmetric laminates with no elastic coupling response to be compared against the symmetric laminates for the threshold stress levels obtained from the numerical buckling analysis. The main highlight of the work was to assess the benefits of non-symmetric laminates in terms of damage tolerance. The authors concluded that non-symmetric laminates can be a feasible solution despite they did not show any significant improvement over symmetric laminates in terms of threshold stresses from the damage tolerance point of view.

Recently, Wagih et al. [51] proposed and tested unsymmetrical laminates (with non-zero but low values of extensional-bending coupling matrix [B]) under quasi-static out-of-plane loading. By means of ply clustering and varying mismatch angles at different locations in the laminate, they designed different unsymmetrical laminate configurations with the aim to increase the load carrying capacity. Despite the insignificant global improvement in the damage resistance between the proposed unsymmetrical and symmetric baselines and the lack of impact damage tolerance study, the paper showed the prospects of moving to non-conventional laminate designs.

2.3 Thin plies

One of the last revolutions in the composite field was the introduction of thin plies that was aimed at pushing the boundaries of polymer composites to improve the structural integrity. Thin plies are referred to as those plies whose fibre areal weight is less than 125 gsm, and were keenly researched on after understanding the significant ply thickness effect on suppressing certain damage modes. Crossman et al. [52, 53] studied the thickness effect towards initiation and growth of transverse cracks and edge delaminations both analytically and experimentally. The results concluded that dispersing the plies instead of grouping (using thin plies) would lead to the suppression of the micro cracking and delaminations. There have been efforts to produce thin plies below 0.125 mm, but they resulted in being a very expensive and slow process which was also accompanied by damaging the fibres. The challenge of increased manufacturing costs demanded new faster and cheaper production methods to manufacture thin plies.

2.3.1 Tow-spreading manufacturing

Spread-tow manufacturing method emerged as a result of the increasing demands for a cost effective production of thin plies. Spread tow refers to the practice of spreading a fibre tow into thinner and flatter tows, i.e., basically from a 5 mm wide tape to a 25 mm wide tape [54]. Sihn et al. [55] used spread tow technology where conventional thick fibre tows were spread using continuous airflow provided by an air duct system. Fig. 2.6 illustrates the spread tow process where the thick fibre tows enter the spreading unit. The constant airflow along with vacuum makes the fibres sag downwards thereby losing the tension between the fibres and helping to spread (as shown in Fig. 2.6). The wider the tow is spread, the thinner the tow becomes. The low velocity of the airflow ensures that the fibres are not damaged.

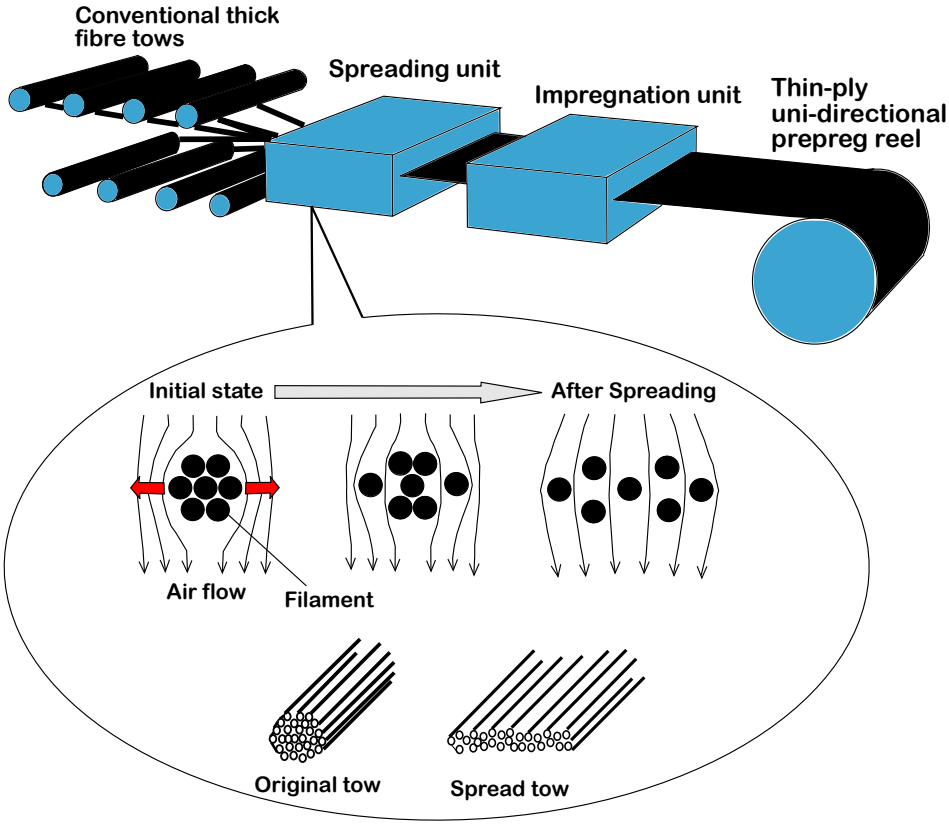

Fig. 2.6.: Illustration of the spread-two manufacturing process where the thick fibre tows are spread to thinner and flatter fibres (Image adapted from [55, 56]).

2.3.2 Potential benefits

Thin plies offered a broad range of potential benefits both in terms of structural response and design effectiveness. The prime motivation of the movement towards thin plies is to allow the production of thinner and lightweight structures along with the enhanced strength and damage resistance possible with the increased design space. Fig. 2.8 illustrates various advantages in a nutshell ranging from the ability to delay damage modes, increased out-of-plane response and an enhanced design space.

2.3.2.1 In-situ effect and delayed damage onset

Ply thickness has a significant effect on the onset of ply failure, namely matrix cracking and delamination [57]. The transverse tensile strength and shear strength are a function of the ply thickness, the location of the ply and the orientation of the adjacent plies. Therefore, when a ply is embedded in multi-directional laminate, it exhibits a higher strength than what is measured from uni-directional coupon tests. This effect is known as in-situ effect and it helps to delay damage modes such as transverse cracking and fibre kinking. Using fracture mechanics based models, Camanho et al. [58] demonstrated the increase in the transverse tensile and compressive strengths (Yt and Yc), and in-plane and out-of-plane shear strengths (Sl and St) as the ply thickness decreased (Fig. 2.8). Guillamet et al. [59] compared the delayed evolution of damage modes in thin-ply laminates when compared to standard-ply laminates (Fig. 2.8), where matrix cracking and matrix crack induced delamination are significantly delayed in thin plies. The same authors [60] monitored the onset of transverse cracks, matrix crack induced delaminations and free edge delaminations and concluded that thin plies clearly delayed or suppressed the studied damage modes, in agreement with the in-situ effect theories.

2.3.2.2 Improved out-of-plane response and CAI strength

During an out-of-plane loading, delamination is a critical damage phenomenon that significantly impairs the residual strength of the structure. With the ability to delay critical damage modes, thin plies were subjected to out-of-plane tests to assess their similar superiority under load cases like impacts. Sihn et al. [55] performed a wide experimental campaign to support the capability of thin plies in delaying or suppressing the initial damage. Along with un-notched tension, open hole tension,

they performed compression after impact tests, resulting in an increased ultimate strength for thin plies. Similarly, Yokozeki et al. [61] performed similar study on thin py laminates, and reported a 16% increase in compressive strength for non-hole compression tests, and a 8% increase in the CAI strength. It was worth noting that the delamination area was recorded to be the same for both thin and thick ply laminates, but the thin ply laminates produced narrow delaminations, and possessed superior resistance against delamination growth.

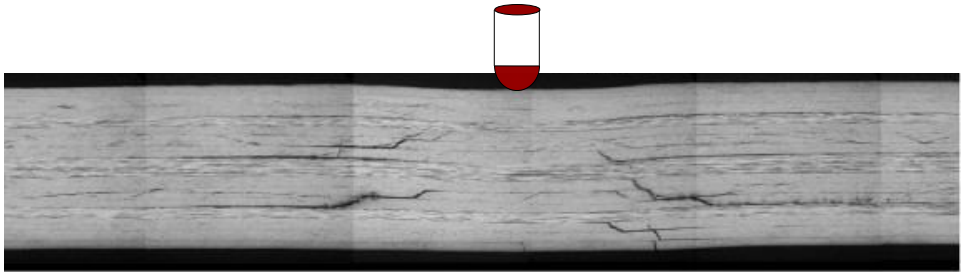

(a) Standard ply laminate

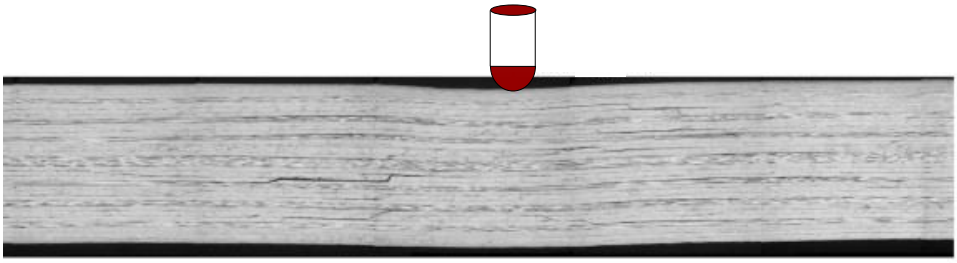

(b) Thin ply laminate

Fig. 2.7.: Damage comparison between a standard ply and thin ply laminate indented at the same deflection level (Image adapted from [20]).

Yokozeki et al. [20] performed quasi-static indentation (QSI) tests to study the difference in damage modes between thick and thin plies. Fig. 2.7 (a) and (b) compares the damage between a standard ply and thin ply laminate for the same deflection level of 3.5 mm, respectively. Through-the-thickness delaminations and matrix cracks at the non-impacted surface were noticed for the standard plies, where as the same was seen suppressed for thin plies. Due to the suppression of these damages, thin plies exhibited an earlier fibre breakage at a deflection of 3.5 mm

against a 4.5 mm deflection for the thick ply laminates. Saito et al. [62] performed low velocity impacts to understand the different damage mechanisms in a thin ply CFRP laminate, where thin ply laminate was formed of $[45/0-45/90]_{12s}$ consisting of 96 plies of 38 μm thick compared to $[45/0/-45/90]_{3s}$ of 24 plies of 147 μm thick. The delamination area was 16% higher for thin ply laminates compared to thick ply laminates, but the thin ply laminates improved the CAI strength by 23%.

2.3.2.3 Homogeneous micro-structure and enlarged design space

Amacher et al. [63] compared the microstructure between thick (300 gsm), intermediate (100 gsm) and thin (30 gsm) ply laminates, where a relatively inhomogeneous microstructure with varying fibre volume fractions was seen with the thick ply laminate. As the ply thickness reduced, the microstructure was more homogeneous (Fig. 2.8) with lesser resin rich areas. Further, with a constant laminate thickness, thin plies provide the possibility to use a larger number of ply orientations compared to thick plies. This leads to an enlarged design space which helps to have more laminate configurations and to achieve an optimal solution. Moreover, a large number of plies homogenises the laminate with the possibility to have continuous layup without following the symmetry constraint [57]. As the number of sub-laminate repetition increases, the values of the extensional-bending coupling matrix reduces dramatically to ensure there are no coupling responses like warping.

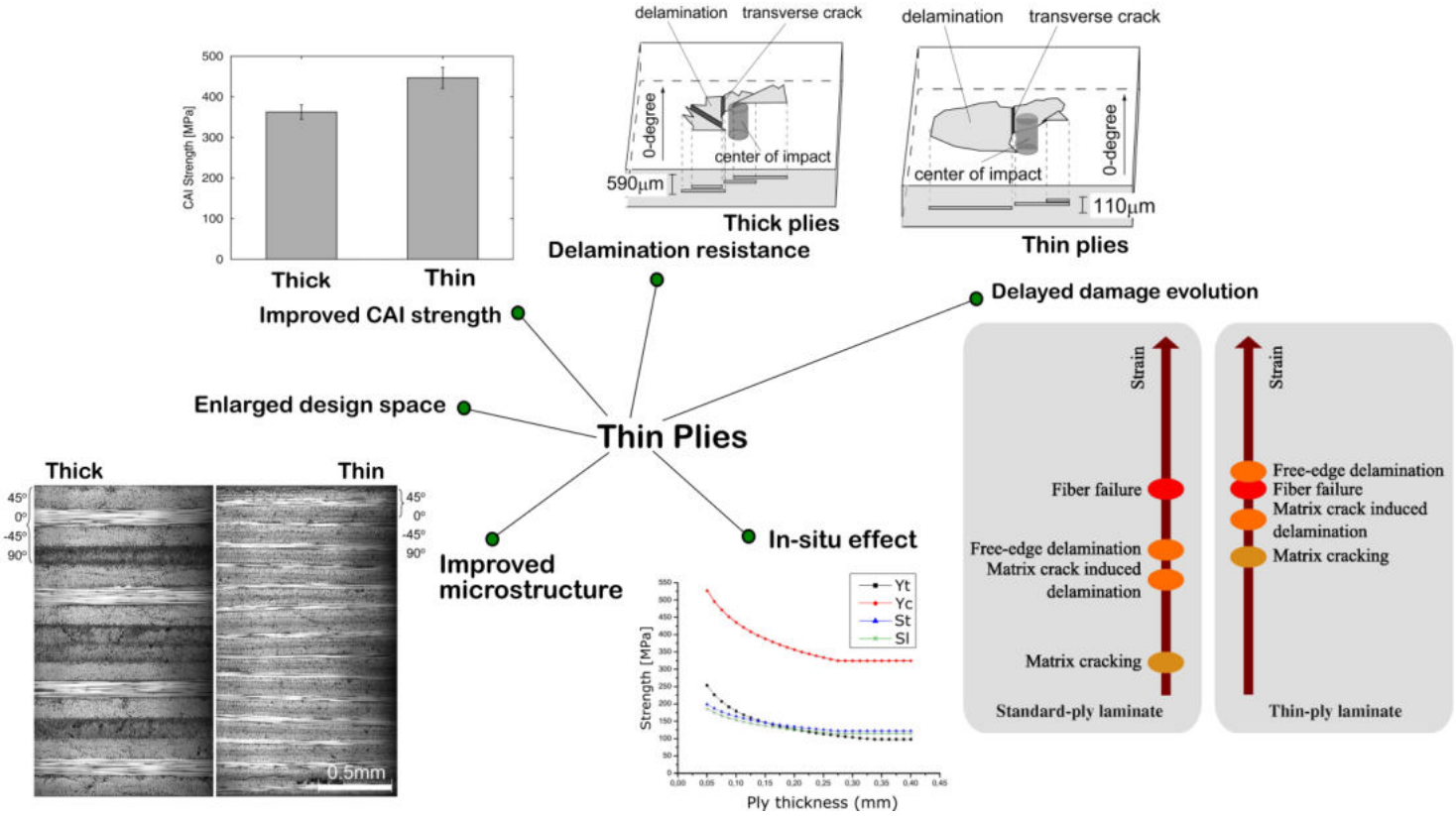

Fig. 2.8.: Several potential benefits of thin plies (Sub-images adapted from [54, 59, 62])

2.4 Moving from thick to thin laminates: a manufacturer's demand

Even though impact and post impact responses have been researched for many decades, bulk of the studies were using standard or thick laminates with a thickness of 4-5 mm (as recommended in the ASTM standard [64]). Over the years, aircraft manufacturers, in the quest towards lighter structures, have reduced the thickness of many primary aircraft components which include the fuselage and the wing skins, to less than 2 mm. A reduction in the laminate thickness means the impact response may be completely different, where the induced damage modes and their sequences are modified, when compared to thick laminates. The high reduction in the laminate's bending stiffness accounts to new responses, where the different conclusions reported for the impact and CAI response of thick laminates may not correlate well with thin laminates. Hence, this demanded the need to study the impact and CAI damage morphology for thin laminates and further the effect of different ply grades on the impact responses. Despite the application of thin laminates in modern aircrafts, only a handful of works have studied their CAI response.

2.4.1 Change in damage morphology

A thin laminate undergoes comparatively higher bending due to the reduced bending stiffness of the laminate. In thick laminates, as explained in the previous section, high localized contact stresses cause matrix cracks on the impacted surface. Impact damage progresses downwards to the non-impacted side, referred to as the pine tree pattern in the literature [5]. In the case of thin laminates, due to the high bending stresses, transverse matrix cracks start at the plies closest to the non-impacted side and cracks and delaminations propagate towards the laminate top, referred to as reverse pine tree pattern.

Fig. 2.9 qualitatively compares the force-deflection impact responses of a thick (4.4 mm) and thin laminate (1.6 mm). Note that the curves are not for quantitative comparison as the laminate thicknesses and the impacted energies (12 J and 10.5 J) are completely different. In view of the reduced thickness, the thin laminate showed high deflection levels (maximum d= 7 mm) whereas the thick laminate exhibited a maximum deflection of d= 3 mm. The force-deflection response curve of a laminate

is the sum of the bending and membrane stretching stiffnesses of the laminate. At higher laminate deflections, the laminate membrane-stretching behaviour is dominant over the bending response. The first load drop seen with thick laminates is referred to as the delamination threshold load. With thin laminates this load drop is coincident with the maximum peak force [65] and is reported to be due to fibre damage than delamination.

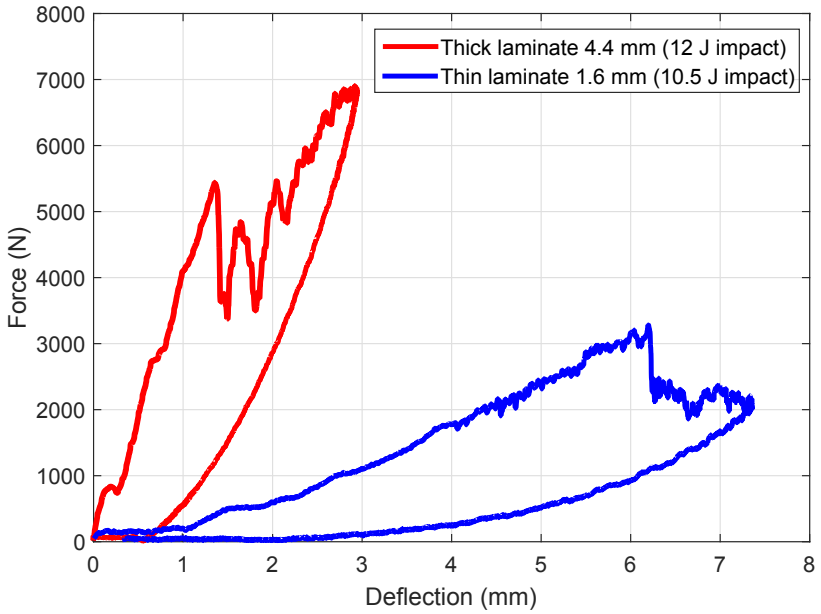

Fig. 2.9.: Qualitative (and not quantitative) comparison of the force-deflection responses of a thick and thin laminate impacted at 12 and 10.5 J, respectively.

One of the first works on thin laminates, Sanchez et al. [66] studied the damage tolerance of thin laminates (1.6 - 2.2 mm) of uni-directional tapes (quasi-isotropic and cross ply) and woven fabrics. Additionally they designed a new device for the compression after impact tests to avoid the invalid buckling failure of thin laminates. Following this work, Remacha et al. [67] came up with a new efficient design for the CAI testing of thin laminates to ensure the final failure is due to the propagation of the impact damage. Garcia et al. [68] studied the effect fabric thickness has on impact and CAI strength of thin laminates (2.15 mm) using non-crimp fabrics and demonstrated the sequence of failure events. Thin (67 gsm) and standard grade plies were utilised and it was concluded that a higher magnitude of fibre failure at

the non-impacted laminate face was observed with thin plies. This was reduced in the case of standard ply laminates and led to a 20% increase in the CAI strength. From the very few works on the impact response of thin laminates, a clear lack of a comprehensive study on the impact and CAI response, effect of ply thickness and material systems on the CAI strength with thin laminates (less than 2 mm) is evident.

2.5 Textile fabrics as an economic solution

Textile fabrics emerged as a promising aspect in the field of composites to meet the growing demands of enhanced damage resistance and tolerance and improved out-of-plane properties. In addition, the airline industries were constantly pushing to cut down the manufacturing costs. In this aspect, textile fabrics could be an excellent substitute for UD tapes, specially due to their faster deposition rates and reduced labour time. Textile fabrics differ from the UD tapes in that the fibre tows are either woven, stitched, braided or knitted with the aim to improve the mechanical performance and the economic feasibility.

2.5.1 Spread tow woven and non-crimp fabrics

Out of the different reinforcement architectures, woven fabrics and non-crimp fabrics have gained attention within the aerospace industries due to the potential benefits offered over the uni-directional tapes. Fig. 2.10 presents the uni-directional tapes, woven fabrics and non-crimp fabrics, where the fabrics differ in the two different reinforcement architecture. UD tows are woven together to make a woven fabric, whereas UD layers are stitched together to form non-crimp fabrics.

In the evolution of composite materials, woven fabrics made of standard ply grades came in as a substitute to UD tapes due to the increased fracture toughness associated with fabrics and the reduced costs due to faster layup [69, 70]. Research reported that the woven architecture substantially increased the interlaminar fracture toughness thereby resisting the delamination compared to UD tapes [71, 72]. But the high waviness in the fibres caused a reduction in the in-plane properties. At this instance, non-crimp fabrics came up with the solution to this waviness, as in non-crim fabrics two UD layers are stitched together using a polyester yarn which ensures there is no crimping/waviness in the fibres. Nevertheless, stitching was reported to induce resin rich areas that are weak zones for damage initiation. Recently, with the introduction

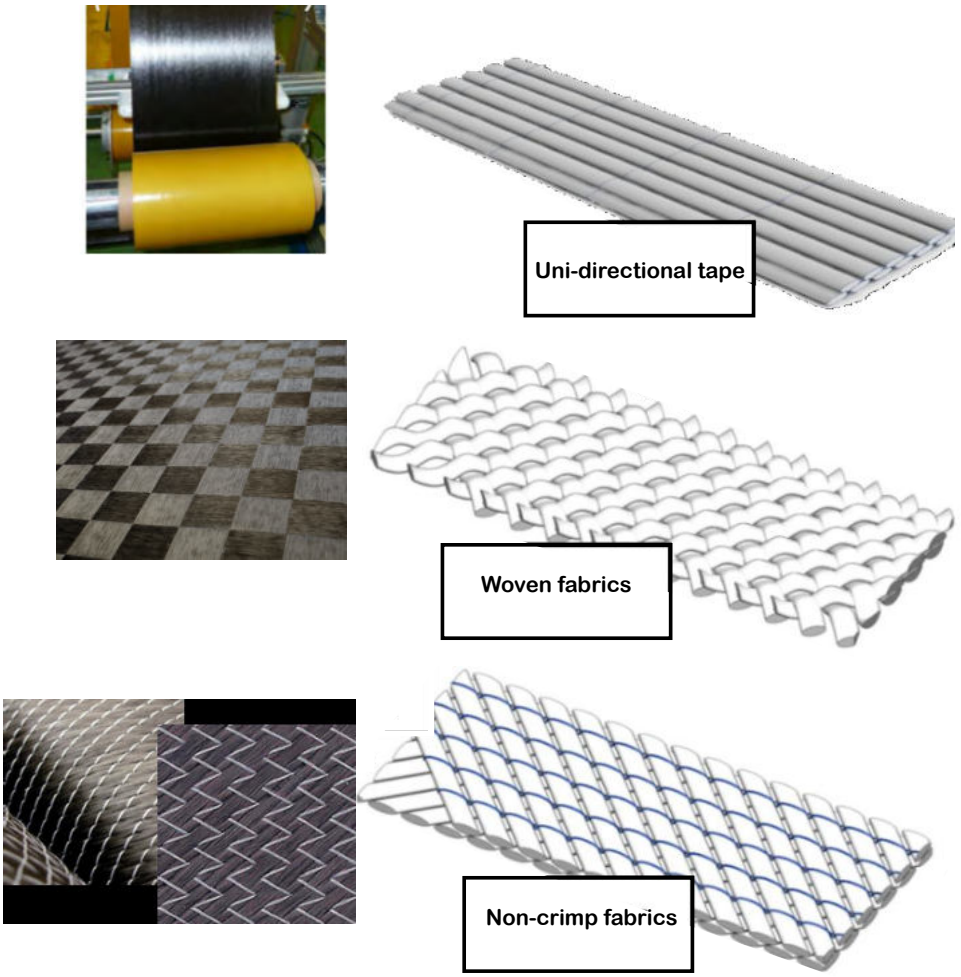

Fig. 2.10.: Comparing the material architecture between uni-directional tapes, woven fabrics and non-crimp fabrics.

of spread tow manufacturing, thin plies were used to manufacture these types of fabrics which substantially reduced the problems addressed above by reducing the waviness and reported only a slight reduction in the in-plane properties compared to UD tapes [73].

Since the fabrics are available from the manufacturers in layers of two or three, this substantially reduces the laying up time. Depending on the length to width ratio, a bi-axial non-crimp fabric offers 5 to 7 times faster layup for one-axis layup compared to UD tapes using automated tape laying [74]. Despite the cost savings, fabrics have

a disadvantage of reduced the design space, where the bi-angle layers are fixed and always go together in a stacking sequence, where as UD tapes are flexible to have any orientation per layer. For eg., a bi-axial NCF is available as [0°/45°] layer, which can be rotated and flipped to form other bi-angle layers, but impossible to form a [0°/90°] fabric layer.

2.5.2 Improved structural response

Vallons et al. [72] compared the interlaminar fracture toughness and the impact damage resistance of carbon non-crimp fabrics and twill weave fabrics. Thick grade plies (270 gsm for non-crimp fabrics and 190 gsm for woven fabrics) were utilised to study the impact response for 2.1 mm thick laminates. Comparatively, non-crimp fabrics showed lower mode II interlaminar fracture toughness over woven fabrics and also a lower impact damage resistance in terms of increased energy dissipation and damage area. Sanchez et al. [66] compared quasi-isotropic UD tapes with woven fabrics in terms of impact and compression after impact responses using thin laminates ranging from 1.6 to 2.2 mm. Woven fabrics showed improved CAI strengths over the UD tapes and the authors attributed this to the reinforcement architecture that helps to control the damage propagation. The cost benefits of fabrics over UD tapes is very evident from the literature, but the improved performance of fabrics over UD, especially in terms of impact and post impact loading, is not yet clearly known. In the framework of thin laminates, there is a clear lack of understanding whether the textile fabrics hold an upper hand over the UD tapes.

2.6 Virtual numerical testing

Low-cost virtual testing, using non-linear finite element analyses, is replacing many expensive experimental tests. The constitutive behaviour of a material can be modelled with intrinsic details to predict complex loading conditions of composite structures. Numerous works on simulating impact and compression after impact of composite laminates at the meso-scale level have been reported. Within the several FEM frameworks, continuum damage mechanics (CDM) combined with cohesive zone models (CDM) based models are the most widely used to model LVI and sequential CAI tests.

Some of the pioneering works [45, 75–78] demonstrated the ability to accurately

predict the LVI response, damage evolution and the CAI strength. Majority of the works aimed to improve the accuracy in the agreement with the experimental results and reduce the computational costs. They also studied the influence of the modelling strategies with different finite element types and cohesive interaction technologies on the virtual results. Only a handful of works virtually studied the effect of stacking sequences in an attempt to find the optimum laminates in terms of impact damage resistance or tolerance.

Hongkarnjanakul et al. [43] studied 12 stacking sequences to understand their effect on the low velocity impact response using a discrete 3D numerical model that was presented and validated in [19]. Abir et al. [79] numerically simulated the impact and compression after impact response of nine different laminates to study the effect ply blocking and buckling mechanisms have on the CAI strength. They reported that a change in stacking sequence can influence the delamination size and shape during impact which has an effect on the laminate buckling modes during compression loading. Laminate with a global buckling mode improved the CAI strength over the other laminates studied using an advanced FEM analysis. Dubary et al. [80] demonstrated that numerical tools [81] can be used to search for optimum damage tolerant laminates, where they explored 18 quasi-isotropic and symmetric stacking sequences and compared the results to that of a ply blocked baseline. Using a discrete ply model, they first validated the impact and CAI results of three stacking sequences with the experimental results. Further, a laminate design optimization was performed where the evolution of CAI stresses against the permanent indentation was studied. Finally, they concluded that a clear rule was not deducted to determine an optimum impact damage tolerant laminate, and suggested that it is necessary to experimentally validate the virtually obtained optimum laminate.

3 Methodology

3.1 Materials and specimens

The experimental campaigns performed in the thesis employed different fibre-resin composite materials varying in different ply grades, material architectures and resulting in different laminate thicknesses. Table 3.1 details the different fibre-resin material systems used, type of prepreg material architectures, ply and laminate thickness and the corresponding papers in which the respective materials were used. Paper A and B dealt with standard thick laminates (4.4 mm) made using uni-directional (UD) prepreg tapes using intermediate ply grades. The remaining papers performed studies with thin laminates (< 2 mm) made using the same fibre-resin system T700/M21 but with different material architectures such as: Uni-directional tapes (Paper-C), non-crimp fabrics (Paper D and E) and woven fabrics (Paper D). Different ply grades ranging from thick to intermediate to thin plies were utilised.

Tab. 3.1.: Details of the different material systems used in the thesis

Fibre/resin system	Material architecture	Ply thickness (mm)	Ply grade (gsm)	Laminate thickness (mm)	Corresponding Paper
IM7/8552	Uni-directional	0.182	Intermediate (190)	4.36	Paper-A
IM7/M21	Uni-directional	0.184	Intermediate (190)	4.41	Paper-B
T700/M21	Uni-directional	0.262	Thick (268)	1.83	Paper-C
		0.131	Intermediate (134)	1.70	
		0.075	Thin (75)	1.58	
T700/M21	Non-crimp fabrics	0.134	Intermediate (134)	1.61	Paper-D & E
		0.067	Thin (67)	1.61	
T700/M21	Woven fabrics	0.12	Intermediate (120)	1.68	Paper-D
		0.08	Thin (80)	1.76	

All the laminates were manufactured using standard autoclave procedures at different enterprises: Airborne Composites Sl, Girona, Spain (Paper A and E), INTA Madrid, Spain (Paper-B), University of Dayton Research Institute, Ohio, US (Paper C, D).

3.2 Experimental tests

3.2.1 Low velocity impact

Low velocity impact tests were performed at the AMADE research laboratory in accordance to the ASTM D7136 [64]. Impact tests were performed on 150 x 100 mm specimens using a CEAST Fractovis Plus instrumented drop-weight tower. The impact tower features a striker-mass carriage system, guiding bars, load cell instrumented impactor, an anti-rebound catcher device activated by pneumatic systems and the specimen clamping system. The pneumatic controlled anti-rebound system ensures that there are no repeated impacts on the specimen. Depending on the target impact energy, the mass of the striker system can be modified with a maximum mass of 5 kg. The steel impactor has a 16 mm diameter hemispherical tip with a mass of 0.7 kg.

Fig. 3.1 illustrates an exploded view of the impactor setup featuring the impactor, specimen, the base plate with the cut-out, where the specimen is placed using the guide pins to ensure that an impact is performed at the centre of the specimen. The specimen is clamped using four rubber pads into the base with a clamping force of 3000 N. Prior to placing the specimen, the impact energy needs to be inputted which is a function of the mass of the impactor system and the height from which the impactor is dropped. Once the mass is set, the drop height is adjusted to obtain the required impact energy. Fig. 3.2 presents the impact specimen showing the dimensions, impact point, the supported area and the foot-print of the rubber pads on the specimen.

Once the impact is performed, the data acquisition provides the impact response curves in terms of impact force-time, force-deflection and energy-time. This data can be post processed to obtain different impact resistance parameters such as: maximum peak force, dissipated energy, delamination threshold load (identified by the first significant load drop in the case of standard laminates). Photos of the impacted and non-impacted sides of the specimens are also taken to study the visible damage.

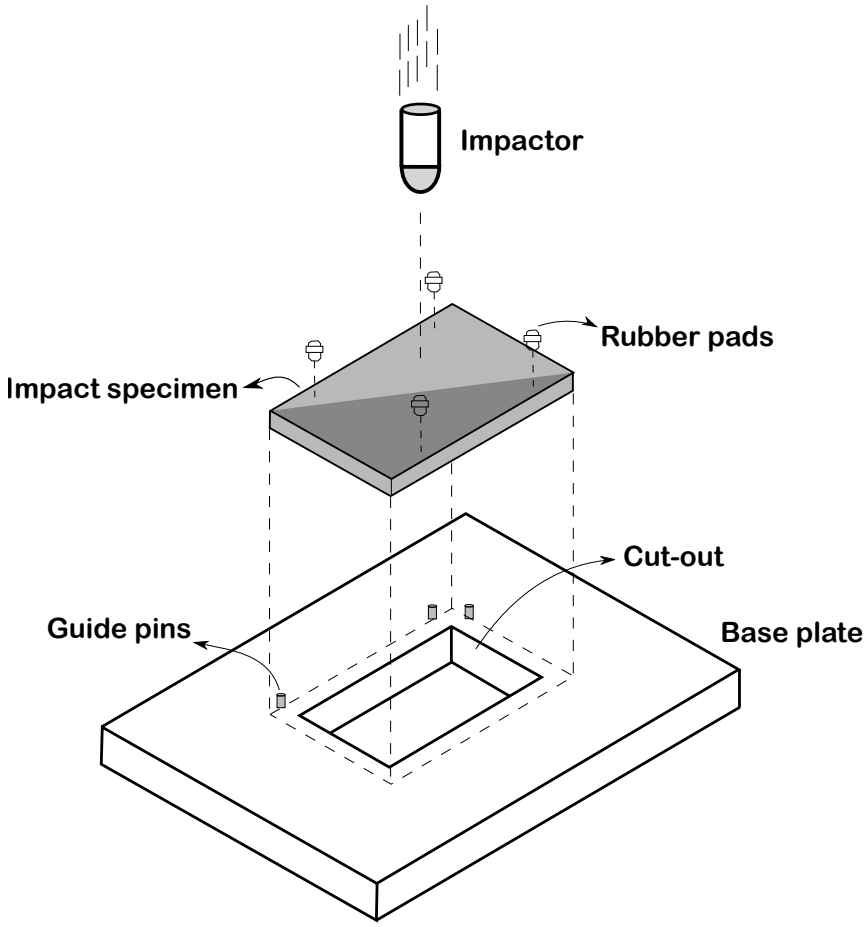

Fig. 3.1.: Exploded view of the impact setup featuring the impactor, specimen, base plate and the clamping system.

3.2.2 Quasi-static indentation

Quasi-static indentation (QSI) tests are an alternative to low velocity impact tests, due to the similarity in the loading responses and the damage characteristics [82–84]. Even though an impact scenario is dynamic in nature, a LVI loading has a high contact time that is long enough to allow the impact waves to get reflected multiple times from the specimen boundaries and hence the resulting response is considered as a purely static loading [42, 85, 86]. Compared to an impact loading, QSI tests can be interrupted amidst loading for damage inspection providing further insight into the damage evolution.

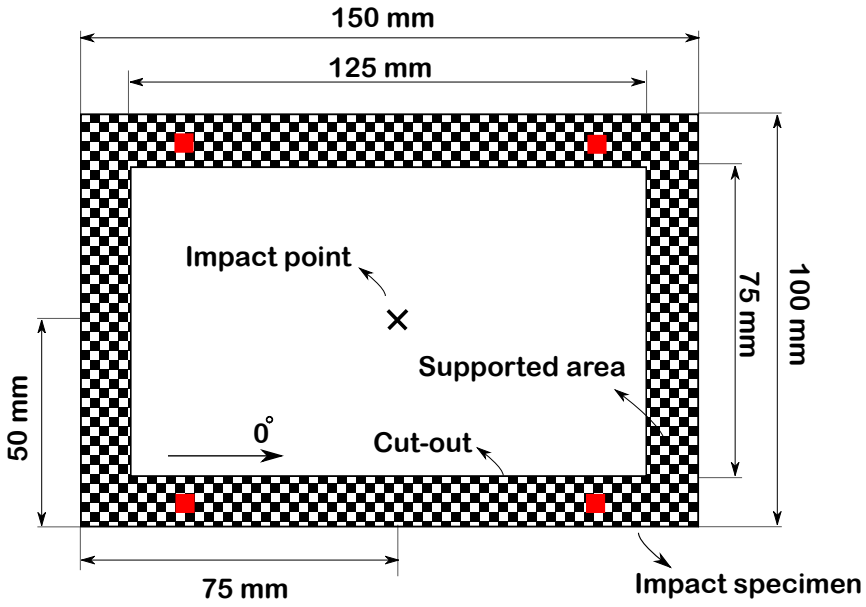

Fig. 3.2.: Top view of the impact specimen presenting the supported area, impact point, footprint of the clamping rubber pads and the associated dimensions (Image adapted from [42]).

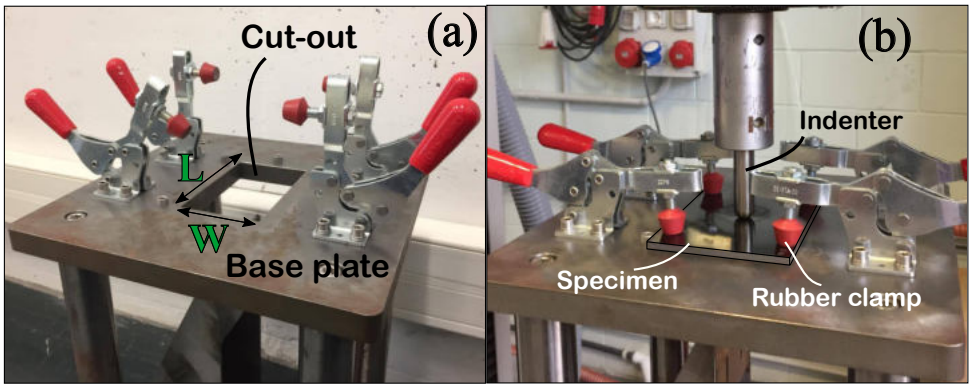

Fig. 3.3.: QSI fixture showing (a) cut-out region, clamping system and the base plate, (b) clamped specimen being indented.

QSI tests were performed using an MTS INSIGHT 50 testing machine with a 50 kN load cell replicating the same boundary conditions as the impact test. Fig. 3.3 (a) shows the QSI fixture characterising the cut-out region where the specimen is placed, rubber clamping system and the base plate, whereas Fig. 3.3 (b) presents the clamped specimen being indented. Displacement controlled indentation was performed on the

specimens at a rate of 1 mm/min using the same indenter configuration as of the LVI.

3.2.3 Plain compression

In this thesis, two different test methods were used to determine the plain compression strength of a laminate. We utilized the combined loading compression (CLC) in accordance to the ASTM D6641/D6641M-14 (for Paper B) and open-hole compression (OHC) tests following ASTM D6484/D6484M-14 [87] (for Paper C, D and E). While the former test was performed at the AMADE research laboratory at Girona, Spain, the latter was performed at INEGI faculty at Porto, Portugal.

CLC fixture characterizes four steel blocks fastened together in pairs and the specimen is clamped between the pairs of blocks by using four screws. 140 x 12.7 mm specimens were tabbed with glass fibre reinforced polymer (GFRP) to avoid end crushing during loading. Fig. 3.4 (a) illustrates the four steel blocks with the specimen clamped in the middle. Fig. 3.4 (b) presents the same test fixture without the upper block to show the composite specimen with GFRP tabs. It must be made sure that the specimen ends must be parallel to each other and the specimen is level with the bottom surface of the fixture. The whole assembly is loaded between flat platens, and the force applied to the fixture blocks must be transferred eventually to the specimen's central gauge section as shear forces. The combination of shear loading and end loading compared to the pre end loading or pure shear loading helps to introduce stress into the gauge section in a much gentler way, thereby providing a valid failure and less scattering.

Following the standards, OHC fixture was designed specially to prevent the buckling of the specimens to obtain the open hole compression strength of composite laminates. OHC tests use rather longer specimens of 305 x 30 mm dimensions. Fig. 3.5 illustrates a part of the whole fixture where the open hole specimen is clamped between two long steel bars that ensures no buckling. Both the above mentioned compression tests were performed at a cross head displacement rate of 1 mm/min.

3.2.4 Compression after impact test

To assess the damage tolerance of a laminate, compression after impact tests were performed complying with the ASTM D7137/D7137M-15 [88]. An MTS INSIGHT 300 machine with a 300 kN load cell with a cross head displacement loading rate

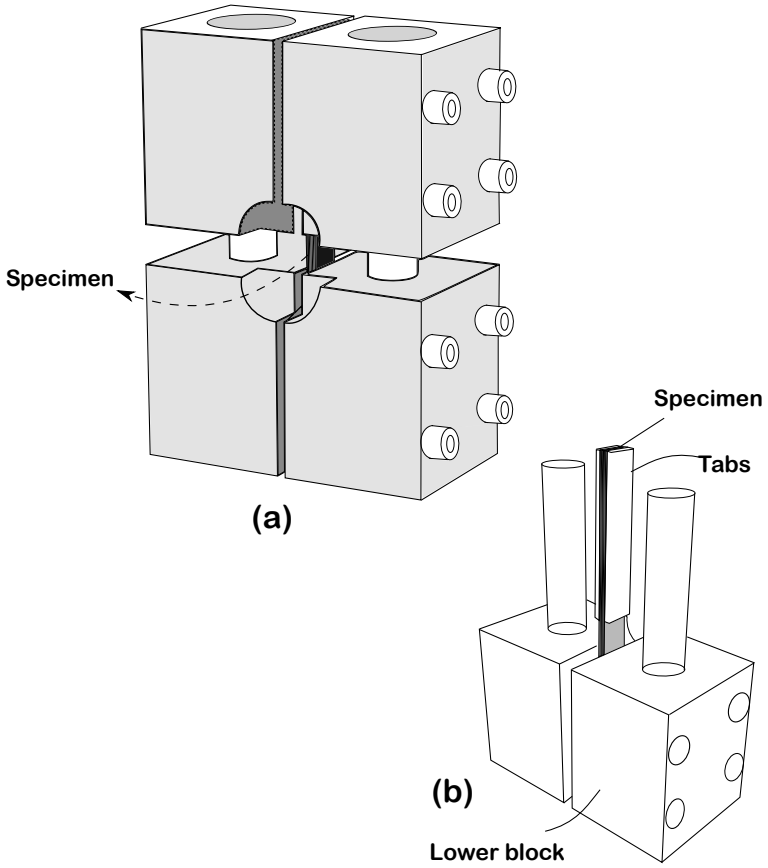

Fig. 3.4.: The combined loading compression (CLC) test fixture with (a) four steel blocks and (b) the tabbed specimen clamped at the middle.

of 1 mm/min was used. Fig. 3.6 (a) presents the CAI fixture used at the AMADE research laboratory, which follows the assembly suggested in AITM1-0010. The specimen is placed at the middle (not visible in Fig. 3.6) and the front and back support pieces are tightened using 12 bolts with a torque of 0.5 Nmm to touch the specimen. Fig. 3.6 (b) illustrates the front view of the setup, showing the different pieces that build up the CAI fixture support. The four edges of the specimen are clamped with the side plates as seen in Fig. 3.6 (b). Displacement controlled load is applied to the top plate, and it is extremely important for the specimen edges to have good tolerance and be parallel to the loading. The test is stopped when the specimen fails and a compressive failure through the impact damage is noted as a valid failure mode. The ultimate compressive failure load is marked and the

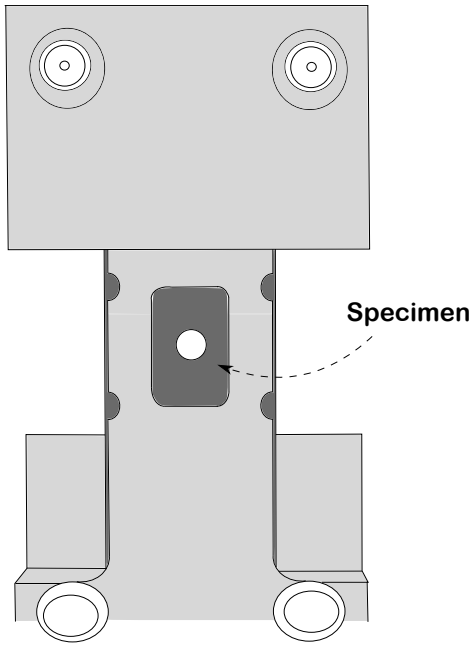

Fig. 3.5.: Illustration of a part of the open-hole compression fixture where the specimen is clamped between the steel blocks, leaving the gauge section unclamped.

compression after impact strength is calculated by dividing the failure load with the load bearing area of the specimen (specimen width multiplied by laminate thickness). The difference in the CAI strength and the plain compression strength gives the reduction in the compressive residual strength caused by the impact damage. To study the out-of-plane displacements of the specimen during compression loading and thereby understand the buckling modes, linear variable differential transformers (LVDT) are used. LVDTs are placed one on each side of the specimen touching the impact point. The out-of-plane displacements of the specimen's impact and non-impacted sides are recorded during the whole loading to understand the way the specimen buckled to cause final failure.

Moving to thin laminates, in addition to the above explained CAI fixture, a non-standard anti-buckling support fixture was added to avoid the premature buckling of thin laminates. Thin laminates were reported to fail by buckling instabilities and not by compression at the impacted region, thereby not providing the real CAI strength of the laminate. Fig. 3.7 displays the additional fixture proposed by Remacha et al. [67]

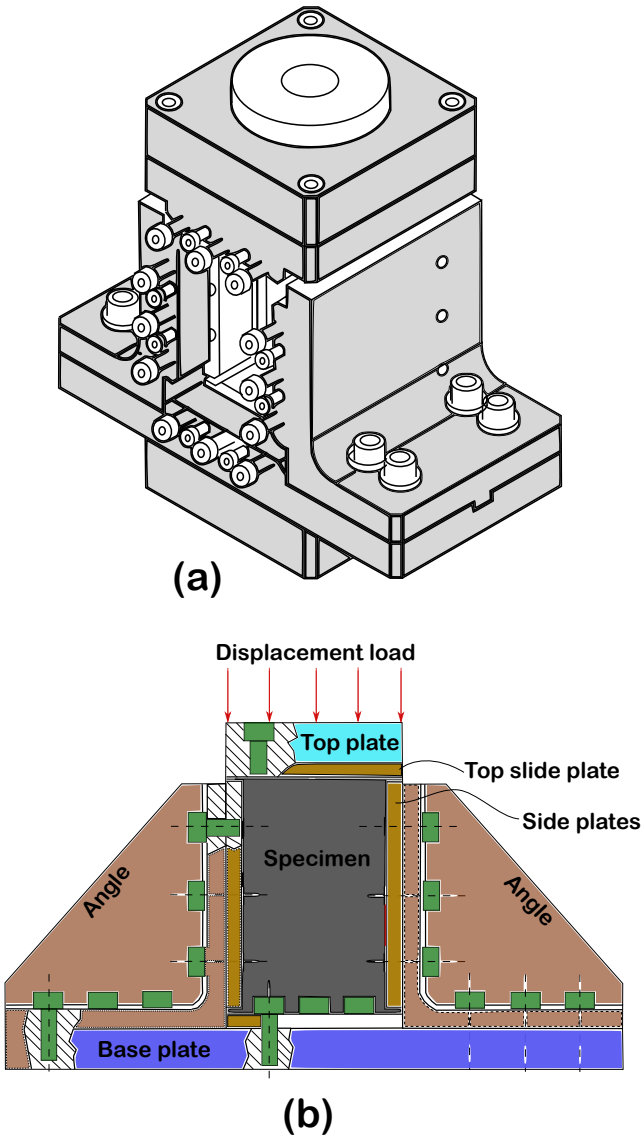

Fig. 3.6.: Sketch of the compression after impact support fixture presenting (a) the side view of the fixture used at AMADE research lab and (b) front view showing the specimen and the load application (Image adapted from [42]).

which is made of three anti-buckling ribs which delay the buckling of the laminate and thereby ensuring a compression failure. These extra supporting plates are clamped onto the CAI setup with a pre-defined torque value of 5 Nmm. A rectangular window of 52 x 42 mm with the impact point as the centre is left free of the vertical ribs to

allow for the impact damage to propagate during compression loading and cause final failure. Even though the extra fixture claims a valid compression failure, the fixture restricts the use of LVDTs or digital image correlation (DIC) techniques to study the buckling modes or displacement fields, as the fixture completely covers the specimen from both the sides.

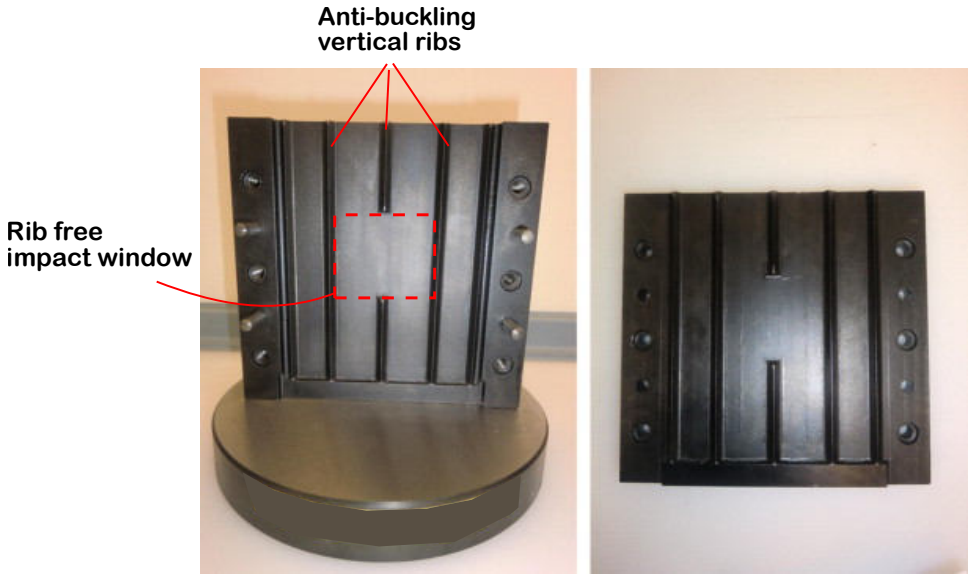

Fig. 3.7.: Additional anti-buckling device used for compression after impact tests of thin laminates (Image taken from [67]).

3.3 Damage inspection methods

3.3.1 Permanent indentation

Immediately after impact, the indentation depth of the impacted specimen is measured using a Mitutoyo digital depth gauge. The impacted specimen is placed on a steel frame and two indentation measurements are made at the impacted location, one by placing the gauge arms parallel to the length direction of the specimen and other to the width direction of the specimen. An average of these values provides the measure of the indentation depth of the specimen, an important parameter in analysing the damage detectability in a composite laminate.

3.3.2 Ultrasonic C-scan

Ultrasonic C-scan inspection is one of the primary and effective ways to assess the impact damage in the laminate. This non-destructive inspection method emits ultrasonic waves from a piezoelectric probe in the through-the-thickness direction of the specimen and these waves are reflected back to the probe when there is an interface such as the top of the specimen, internal defects such as delaminations. Fig. 3.8 presents the various components of the inspection system. The specimen or panel to be inspected is placed submerged inside a water tank. An OLYMPUS OMNI MX system featuring a piezoelectric probe of 5 MHz scans the specimens. The probe is also placed inside water, so that water acts as a couplant to facilitate the transmission of waves into the specimen. Scanning parameters such as the area of the specimen to be scanned, the scanning speed is fed into the Robotnik Software and the automated robotic arm scans the specimen. Depending on the attenuation in the reflected waves and the time of reception, C-scan results provide the extent and the through-the-thickness location of the damage. Note that only delamination damage can be detected in a C-scan inspection. Despite its fast practical use, C-scan inspection has the drawback of larger delaminations masking the underlying ones, hence it demands to perform the scans from both sides of the specimen.

In this thesis, all the impacted specimens were subjected to C-scan inspection. With QSI tests, the loading of the specimen was stopped and the specimen was subjected to C-scan inspection. Further the same specimen was subjected to higher indenter displacement levels followed by the same inspection process. The loading is normally interrupted when a load drop or a change in stiffness of the force-displacement response or an acoustic emission was noticed. Comparing the C-scan images of pre and post load drop helps to identify the particular delamination responsible for the load drop. This was performed in Papers A, D and E, where the complete damage evolution was studied with the added advantage of not using up specimens. Fig. 3.9 illustrates the sequence of QSI test interrupted by C-scan performed on a single specimen. This

3.3.3 X-Ray micro computed tomography

One step further, micro-computed X-ray tomography (μCT) resolves the shortcomings of the C-scan inspection. It uses X-rays to provide details of the damage modes

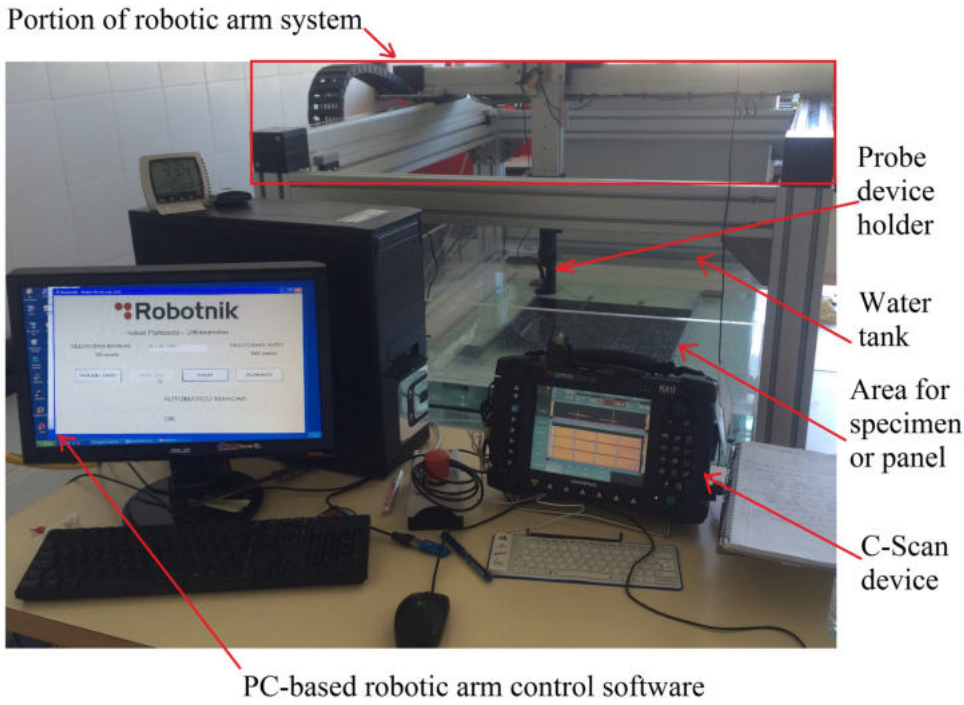

Fig. 3.8.: Ultrasonic C-scan inspection technique showing the robotic arm, water pool with the composite panel submerged and the scanning device (Image adapted from [12]).

at the micro-scale. AMADE laboratory uses an inspection unit that comprises of an X-ray source (of 20 W power and a focal spot of 5 microns), and detector of 2400 x 2400 pixel. Fig. 3.10 presents the X-ray source, the detector, the guide rail between the X-ray source and the detector, specimen holder and the specimen placed in line with the source and detector. The source and the detector were manufactured by HAMAMATSU and assembled by Novadep Scientific Instruments.

Prior to inspection, the impact specimens were cut into strips of 30 mm in width (with impact point as centre), making sure that the whole impact damage area is within this cut strip, which was determined by C-scan inspection. Using laminate strips (150 x 30 mm) instead of the impact specimens (150 x 100 mm) was to minimize the unwanted X-ray absorption perpendicular to the axis rotation. The specimen is placed accordingly in between the source and the detector to inspect the desired field of view. μCT inspection was performed only for Paper B, and the respective scanning parameters are provided in the following Table 3.2.

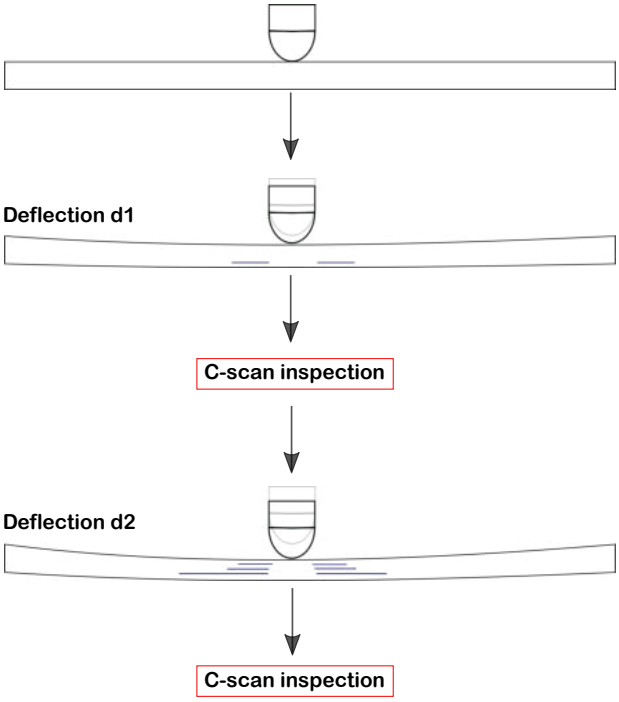

Fig. 3.9.: Sequence of quasi-static tests interrupted for C-scan inspection performed on a single specimen.

Tab. 3.2.: X-ray tomography inspection parameters

Scan parameters	Value
Voltage (kV)	50
Current (μA)	175
No. of projections	1400
No. of integrations per projection	3
Effective pixel size (μm)	10
Field of view (mm)	22
Inspection time per specimen (h)	2.5

The μCT slices obtained were post-processed in Matlab [89], where the images were filtered and segmented. The segmented pixels were categorized according to their distance from the impacted side which helps to allocate the damage to its respective ply or interface. These images were rendered in 3D using Starviewer software, finally providing a 3D representation of the impact damage featuring matrix cracks, delaminations and fibre failure, where the main damage form delamination is

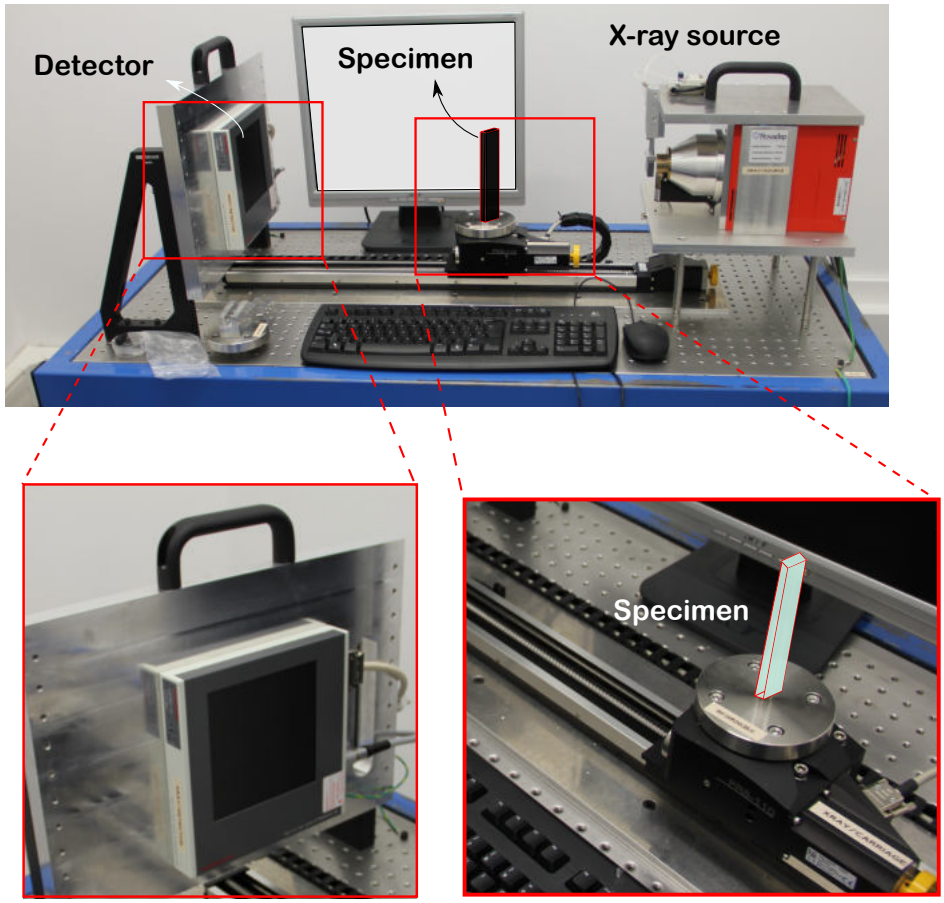

Fig. 3.10.: X-ray tomography experimental setup at the AMADE research laboratory, displaying the X-ray source, specimen and the detector in detail (Image adapted from [12]).

presented in colours representing different interfaces.

3.4 Experimental sequence

The whole experimental sequence can be divided into three blocks: impact damage resistance, damage inspection and the impact damage tolerance. Fig. 3.11 briefs the above three blocks and the experiments conducted in each one of them. At first, low velocity impacts are performed on the specimen to obtain the impact response curves and the damage resistance parameters. Then the specimen is subjected to C-scan

or X-ray tomography inspection where the former provides the extension and the projected delamination area, where as the latter provides a comprehensive insight into the damage modes.

Fig. 3.11 illustrates a cross sectional view of a μCT slice displaying the different damage modes and also the post-processed 3D rendered image with damage ascribed to different sub-laminates. Post inspection, the specimen is subjected to compression after impact to assess the damage tolerance characterised by the compression after impact value. In parallel to impact tests, quasi-static indentation tests are also performed with the main objective of understanding the damage sequence. QSI testing followed by damage inspection and further testing can be performed on the same specimen and this step can be repeated until the whole damage evolution is obtained.

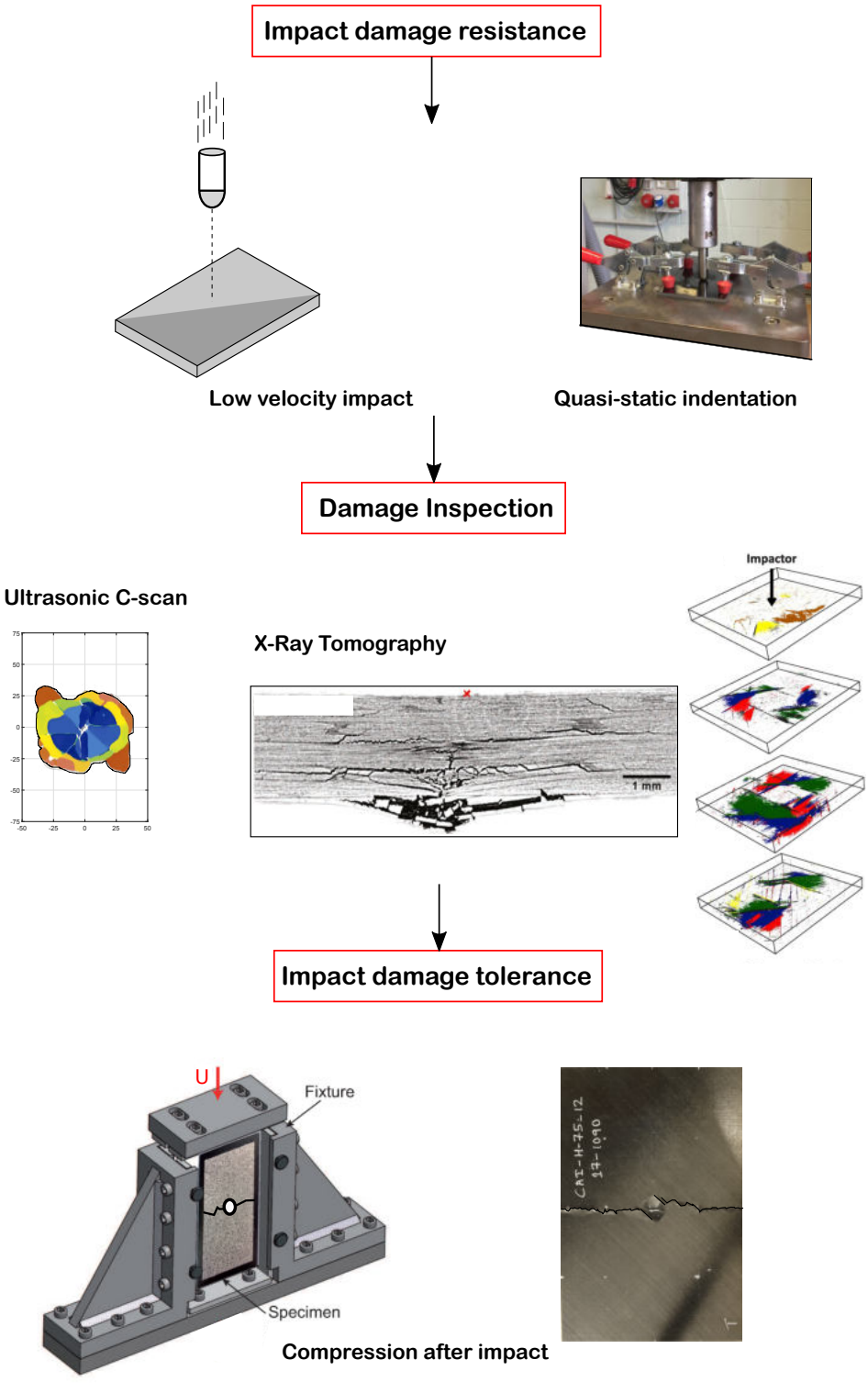

Fig. 3.11.: Flowchart of the experimental sequence followed in the thesis (Sub-images adapted from [68]).

3.5 Numerical modeling

The thesis simulates impact and compression after impact tests with the aim to provide more insight into the impact damage evolution (Paper A) and to propose improved damage tolerant stacking sequences (Paper F). An in-house numerical model (featuring constitutive models and modelling strategies developed at AMADE research group) is used in the thesis. A brief overview of the numerical model featuring constitutive damage models, numerical modelling strategy, virtual test setups and other details are provided here.

3.5.1 Virtual test setup

The virtual impact setup is modelled such that it replicates the experimental drop weight tower setup as per the ASTM standards [64]. Fig. 3.12 (a) illustrates the virtual setup, where a 16 mm in diameter hemispherical impactor is modelled using rigid elements (R3D4), and the laminate is clamped during the impact event using four rubber clamps which are also modelled using rigid elements. The 150 x 100 mm specimen is placed on a base plate of dimensions 125 x 75 mm. The base support and the rubber clamps are constrained in all degrees of freedom. Depending on the impact energy, the impactor is assigned an initial velocity in the out-of-plane direction. The mesh is refined under the impactor for a window of 75 x 75 mm (for Paper A) and 35 x 35 mm (for Paper F), while a coarse mesh of 4 mm (Paper A) and 3 mm (Paper F) is applied to the remaining area.

The compression after impact virtual setup is sketched in Fig 3.13, where (a) and (b) refer to the CAI assembly for thick and thin laminates, respectively. The specimen fixture assembly is placed between plates and displacement controlled loading is applied at the top. A pre-defined set of nodes are restrained in the out-of plane, lateral movement at the knife edges and side clamping zones of the specimen. In the case of thin laminates, additional anti-buckling ribs are modelled at the centre of the specimen which assures there is no buckling failure of the thin laminates. A rectangular window at the centre of the specimen is left free of the anti-buckling ribs with the aim to allow the impact damage to propagate during compression loading. The CAI simulation is performed using the RESTART command in Abaqus/Explicit, where the impact assembly and results are imported. The rigid parts (impactor, base plate and rubber clamps) are moved away before starting the CAI simulation.

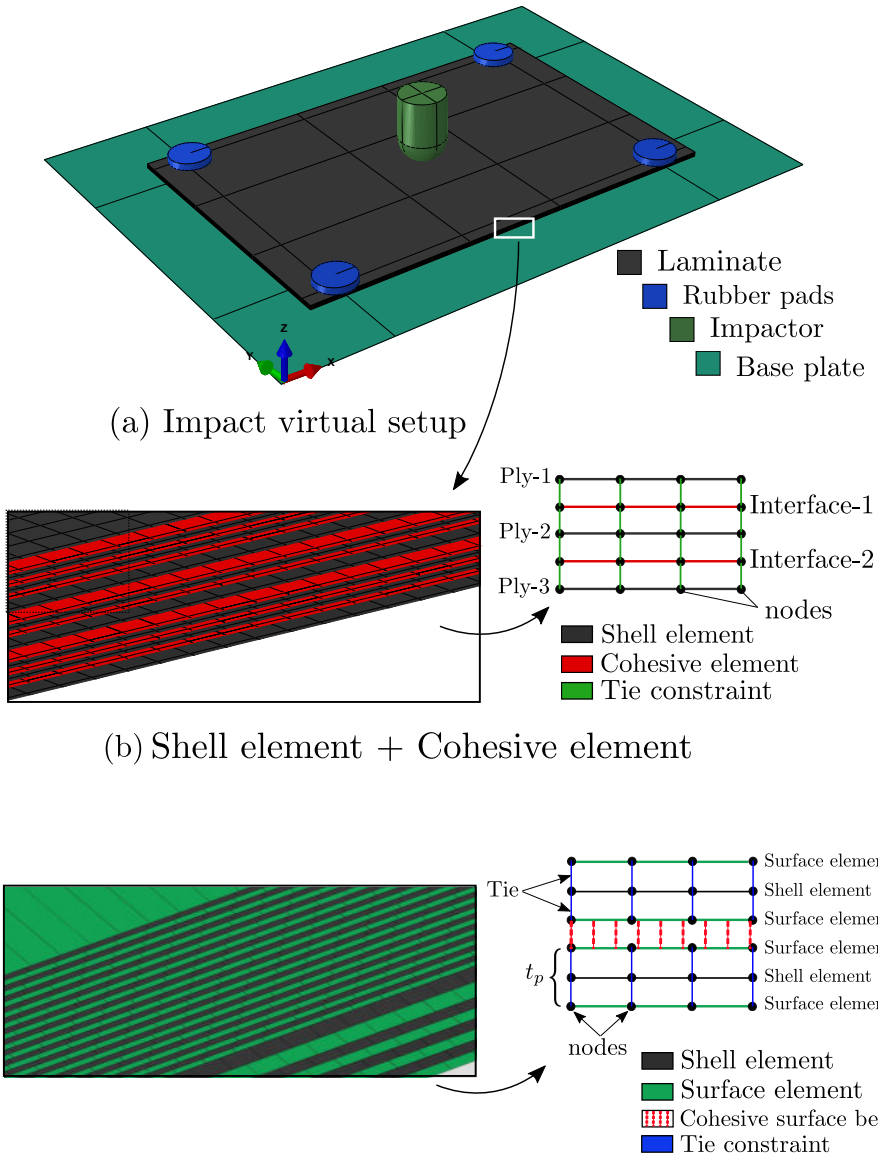

Fig. 3.12.: Sketch of the (a) impact virtual setup with two different modelling strategies explained in (b) and (c).

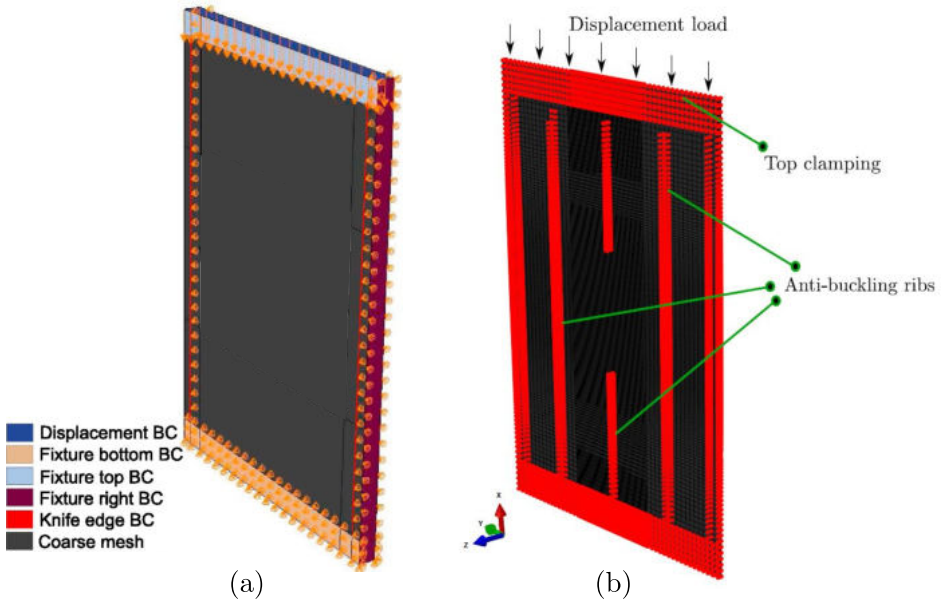

Fig. 3.13.: Sketch of the compression after impact virtual setup showing the boundary conditions applied in (a) thick standard laminates and (b) thin laminates. (Image adapted from [78]).

3.5.2 Modeling strategy

A meso-scale modelling strategy was used where the plies and interfaces are modelled differently to replicate the impact scenario. Conventional shell elements are used to model the plies mainly due to the following advantages: (a) they do not penalize the stable time increment (STI) (b) the plane stress conditions make the constitutive model much simpler than a 3D case (c) the additional rotational degrees of freedom with shell elements makes it equipped for bending problems. Two modelling strategies are used in this thesis as provided in Table 3.3. Shell elements along with zero-thickness cohesive elements are used in Paper F, where Fig. 3.12 (a) details the location of shells, cohesive elements and the tie constraints between them. In paper A, conventional shells are used along with cohesive surfaces (available in Abaqus), where additional surface elements are placed at the interface locations. They are linked to the shell elements by means of tie constraints to ensure correct kinematic description at the interfaces [90]. Fig. 3.12 (b) illustrates the above modelling strategy where surface based cohesive interaction is assigned between the surface elements. Contact is simulated by means of the general contact algorithm available in

Abaqus/Explicit. Friction is introduced between all the contacting surfaces through the Abaqus/Explicit built-in Coulomb friction model. A friction co-efficient of 0.3 is used between the plies. Accounting for the in-situ effect, the transverse tensile and in-plane shear strength values were calculated according to the ply thickness and the ply type (outer or embedded). To avoid excessive element distortion, an element was deleted when the fibre damage variable (d1) reached 1, and the transverse and shear damage variable was assigned a maximum value of 0.99 but without deleting the element.

Tab. 3.3.: Modeling strategies used in the thesis

Case	FE type	Interaction type	Strategy	Paper
S4R-CON	Conventional shell (S4R) with surface elements (SFM)	Cohesive surfaces	Fig. 3.12 (c)	A
S4R-COH	Conventional shell (S4R)	Zero-thickness cohesive elements (COH3D8)	Fig. 3.12 (b)	F

3.5.3 Constitutive modeling

We used a meso-scale continuum damage model (CDM) proposed by Maimí et al. [91, 92] to simulate the onset and propagation of intralaminar damage. The model considers plane-stress conditions and includes three in-plane damage variables associated with three failure modes: longitudinal d1, transverse d2 and in-plane shear d6. The damage activation functions are based on the LARC04 failure criteria. The CDM model ensures an objective response regardless of the mesh size by regularizing the dissipated energy for each damage mode with the element size in accordance with the crack-band model [93]. Besides, the constitutive models takes into account the in-situ effect of thin plies. The predictive capability of the model is already demonstrated by different researchers under different loading conditions such as impact, compression after impact [77, 78, 94] and open-hole tension [95].

In paper A, the interlaminar damage was modelled using the ABAQUS Explicit in-built surface based cohesive behaviour, where a contact based interaction is used to model the traction between the contact surfaces to simulate delamination. The delamination initiation is governed by a quadratic stress-based criterion implemented in ABAQUS, whereas delamination evolution is characterised by the mixed mode energy-based propagation criteria proposed by Benzeggagh and Kenane [96]. In paper F, the interlaminar damage is modelled using Abaqus zero-thickness cohesive

elements and the cohesize constitutive model proposed by González et al. [97]. The model ensures a correct energy dissipation under variable mixed-mode conditions. Both the intra- and inter laminar models are implemented in a VUMAT user-written subroutine for Abaqus/Explicit.

In conclusion, Table 3.4 provides an overview of the different experimental tests, damage inspection techniques and the numerical simulations performed in each paper(Note that PC refers to plain compression test).

Tab. 3.4.: Details of the experimental tests, damage inspections and numerical testing performed in each paper.

Paper	Experimental tests				Damage inspection		Numerical
	LVI	PC	QSI	CAI	C-scan	X-ray tomo.	
A	✓		✓		✓		✓
B	✓	✓		✓	✓	✓	
C	✓	✓		✓	✓		
D	✓	✓	✓	✓	✓		
E	✓	✓	✓	✓	✓		
F							✓

3.6 Theory of laminate unsymmetry and coupling responses

Classical lamination theory provides the relation between the laminate mid-plane strains (ϵ) and curvatures (κ) in terms of normal forces (N) and moments (M) as [98, 99]:

$$\begin{bmatrix} N \\ M \end{bmatrix} = \begin{bmatrix} A & B \\ B & D \end{bmatrix} \begin{bmatrix} \epsilon^o \\ \kappa \end{bmatrix}$$

where the ABD matrix corresponds to the extensional, extensional-bending coupling and coupling stiffnesses, respectively. Fig. 3.14 demonstrates the effects of various stiffness terms on the laminate deformation. The extensional stiffness matrix ([A]) equate the in-plane forces to the in-plane strains and the bending stiffness matrix ([D]) relates the bending moments to the laminate curvatures. The coupling stiffness matrix ([B]) couples the extension and bending as in with a non-zero B matrix, a normal in plane force induces curvature and twisting (as shown in Fig. 3.14) in the laminate.

Laminate mid-plane symmetry is a conventional and non-challenged constraint in the laminate design, as a symmetric laminate leads to a null B matrix. An laminate with non-zero B matrix induces coupling deformation responses. One important example is the undesired laminate warpage after curing process, where the thermal gradient induced load results in a curved laminate, due to the presence of non-zero B matrix terms.

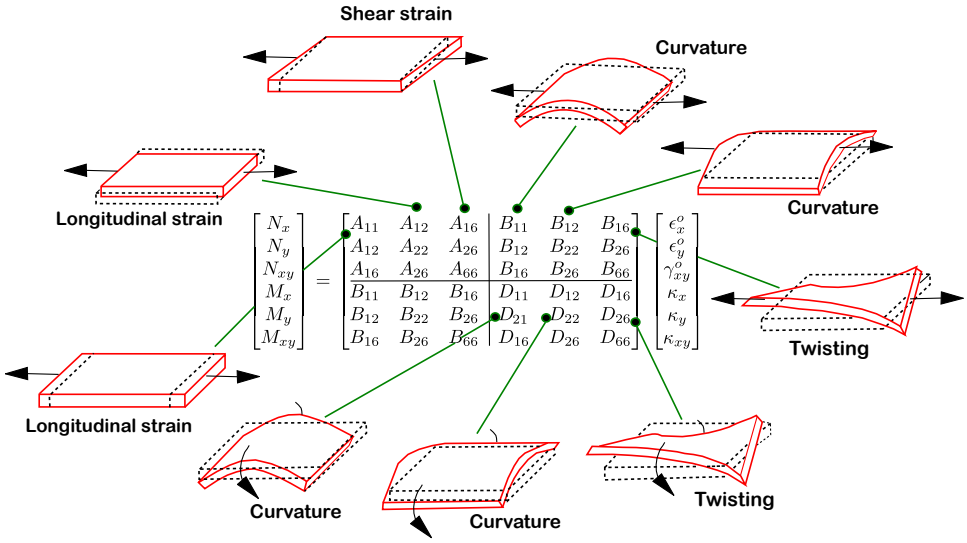

Fig. 3.14.: Effect of the different stiffness matrix elements on the deformation of the laminate (Image concept from [100]).

4

Paper A:

Unsymmetrical stacking sequences as a novel approach to tailor damage resistance under out-of-plane loading

A. Sasikumar[a,*], J. Costa[a,*], D. Trias[a,1], E. V. González[a], S. M. García-Rodríguez[a], P. Maimí[a]

[a] AMADE, Polytechnic School, Universitat de Girona, Campus Montilivi s/n, E-17003 Girona, Spain

[*] Corresponding author

[1] Serra Hunter Fellow

The paper has been published in *Composites Science and Technology* 173 (2019) 125–135.

Motivation & Synopsis

Laminate mid-plane symmetry has been followed on as a strict rule in the laminate design to avoid the undesired coupling responses induced by an unsymmetrical laminate. An impact event induces different damage modes in the laminate that are different in the top and bottom sub-laminates. At this instance, the main motivation behind this paper was to look for possibilities to challenge the conventional symmetry constraint and to question: why not propose unsymmetrical laminates with zero coupling responses and experimentally test their feasibility under impact loads? This paper proposes unsymmetrical stacking sequences with zero coupling responses and demonstrates that impact damage can be tailored to happen at pre-determined locations through judicious designing of the laminate.

Composites Science and Technology 173 (2019) 125–135

Contents lists available at ScienceDirect

Composites Science and Technology

journal homepage: www.elsevier.com/locate/compscitech

Unsymmetrical stacking sequences as a novel approach to tailor damage resistance under out-of-plane impact loading

A. Sasikumar*, J. Costa**, D. Trias[1], E.V. González, S.M. García-Rodríguez, P. Maimí

AMADE, Polytechnic School, Universitat de Girona, Campus Montilivi s/n, 17073 Girona, Spain

Abstract

In current composite design, stacking sequence symmetry around the laminate mid-plane is an unarguable constraint to avoid warpage during manufacturing. However, several load cases induce unevenly distributed stresses through the laminate thickness, such that symmetric laminates may not be the optimal solution. In this paper, we explore the damage resistance to out-of-plane low velocity impact loading of an unsymmetrical laminate with zero extension-bending coupling matrix ([B]), thereby assuring no undesired coupling deformations during mechanical or thermal loads. Using impact and quasi-static indentation tests, C-scan inspection and numerical modelling, we compare the damage pattern between an unsymmetrical laminate with ply clustering at the impacted face and a laminate with ply clustering at the non-impacted face (produced by flipping the former laminate upside down). The laminate with clusters at the impacted side exhibits better damage resistance for lower impact energies. More importantly, the location of the damage events obeys the predictions assumed when the laminate was designed, demonstrating the room for improvement by tailoring unsymmetrical laminates to particular load cases.

Keywords: Impact behaviour, Delamination, Damage mechanics, Finite element analysis (FEA), Unsymmetrical laminates

4.1 Introduction

Impact loading and the threat it poses to composite structures is a matter of concern for aircraft engineers and researchers. The severity of the impact induced damage

and its propagation during in-flight loads is the key research question to be answered as impact damage can reduce the residual strength of a structure by up to 60% [66]. In an effort to improve damage resistance, researchers have gone one step further in laminate design and have proposed non-conventional laminates using dispersed angles [11, 44, 45], varying mismatch angle at interfaces [11, 13] or selective ply clustering [9]. Despite the novelty in laminate designing, symmetry around the mid plane of the laminate remains an unquestioned constraint, mainly to avoid warpage during manufacturing and coupling responses under loading [99].

Impact loading is a complex loading case because of the interaction of different damage mechanisms, mainly in terms of matrix cracks and delamination, followed by fibre failure at higher impact energies. The damage scenario is unsymmetrical in the through-the-thickness direction [5, 6]: high contact compressive stresses cause matrix cracks by shear at the vicinity of the impactor (impacted face of the laminate), whereas tensile stresses cause transverse matrix cracking at the non-impacted face of the laminate. These cracks grow into the interfaces and initiate delamination oriented in the direction of the lower plies [5]. Acknowledging that the impacted and non-impacted laminate sides experience different damage mechanisms during impact, the constraint of laminate symmetry needs to be challenged.

Recently, quasi-static indentation (QSI) tests are considered as an alternative to the low velocity impact tests, due to the similarity in the loading responses and the damage characteristics [82–84]. In LVI loading, the impact contact time is long enough to allow the impact waves to get reflected multiple times from the specimen boundaries and hence the resulting impact response is considered purely static loading [42, 85, 86].

In this paper, we propose an unsymmetrical laminate with ply clustering at the impacted face of the laminate. As reported in [42], a clustered ply block induces high interlaminar shear stresses thereby triggering delamination at the corresponding ply interface. Here we attempt to use localized ply clusters in the laminate to foster delamination at pre-determined regions. Thanks to the unsymmetrical design, the same laminate, when flipped upside down, produces another stacking sequence with ply clustering at the non-impacted face. Low velocity impact (LVI) and quasi-static indentation responses of these two unsymmetrical laminates are studied in

order to shed light on how the initiation and propagation of the delaminations differ when imposed at different locations. Further, numerical results from an in-house finite element model featuring inter and intralaminar damage are compared with the experimental results, followed by an in-depth energy dissipation analysis for each ply and interface of both laminates. To the authors' knowledge, this is the first report on an experimental impact study on an unsymmetrical laminate.

4.2 Unsymmetrical laminate design

The unsymmetrical laminate was obtained by means of an optimization algorithm (genetic algorithm embedded in the MATLAB optimization toolbox [89]). The objective function was a minimum summation of the terms of the B matrix, with the intention of finding solutions with a null B matrix. A null B matrix assures that there is no extension-bending coupling response [98, 101] and as a result there will be no undesired deformation couplings such as warpage during manufacturing.

In addition to the objective function, the following constraints were also imposed: i) the laminate had to be in-plane quasi-isotropic and balanced with 24 plies; ii) as ply clustering induces delamination at the interfaces of the blocked plies [18, 42], four clusters (one cluster for each orientation, 0°, $\pm$45° and 90°) were imposed at the impacted side of the unsymmetrical laminate to trigger delamination at these locations; it was also made sure that not more than three plies of the same orientation were stacked together; iii) the surface ply was fixed to be either $45°$ or $-45°$ in order to tackle the shear loads [44]; and iv) a constant mismatch angle of $45°$ was used at the interfaces, thereby avoiding the effect of varied mismatch angled interfaces [11, 13].

The solution, with a zero B matrix was: [-45_2/90_2/45_2/0_3/45/90/-45/0/45/90/-45/0/45/90/-45/0/45/90/-45].

4.3 Methodology

4.3.1 Experimental

The unsymmetrical panel was manufactured using Hexcel IM7/8552 uni-directional prepreg tapes and was cured in an autoclave. Despite being unsymmetrical, the panel

had zero warpage after curing; as expected from the design study of the stacking sequence.

Impact specimens of standard 150 x 100 mm dimensions were cut out of the panel with 0° plies aligned in the longer direction. The 24-ply laminate had a cured thickness of 4.36 mm and a ply thickness of 0.182 mm. The specimens cut out were flipped upside down in order to obtain specimens with the same ply clustering at the non-impacted side. The laminate with ply clustering at the impacted side is hereafter called LPCI, and the laminate with ply clustering at the non-impacted side as LPCN (Fig. 4.1). It is to be noted that flipping a laminate upside down only interchanges the -45° plies with 45° plies, thus both laminates have the same in-plane stiffness in all directions and the same bending stiffnesses in the 0° and 90° directions.

As in [32, 42], impact tests were performed on 150 x 100 mm specimens in accordance with the ASTM D7136/D7136M-15 standards [64] using a CEAST Fractovis Plus instrumented drop-weight tower. The impactor featured a 16 mm in diameter hemispherical tip and the impactor mass was adjusted to 5 kg for the entire study. As the study aims to analyse the low velocity impact response (energy levels that create lesser damage than the barely visible impact damage (BVID) threshold) of the laminates, two LVI energies, 12 J and 18 J, were explored.

QSI tests were performed using an MTS INSIGHT 50 testing machine with a 50 kN load cell, replicating the same boundary conditions as the impact test. Specimens were placed on a base support with an open window of 125 x 75 mm and clamped at the edges using four rubber pads. Displacement controlled indentation was performed on the specimens at a rate of 1 mm/min using the same indenter configuration as for impact loading. Further details of the test setup are provided in [12].

QSI loading was interrupted for C-scan damage inspection followed by further indentation to the next indenter displacement level, thereby the same specimen was subjected to more than one indentation. A total of 8 indenter displacements (from d= 1.17 mm to 5.4 mm) were investigated, thus obtaining the complete damage evolution starting from the initiation of matrix cracks to complete delamination propagation. The indenter displacements were defined on the go: the indentation was stopped when a load drop or a change in stiffness of the force-displacement response, or an

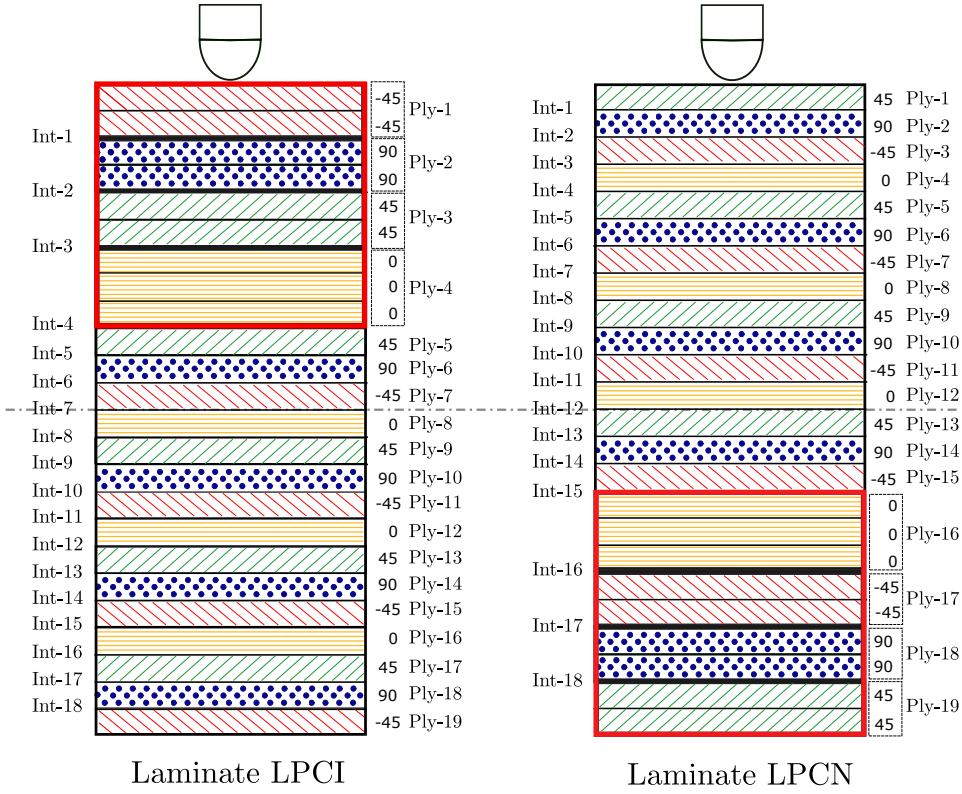

Fig. 4.1.: Unsymmetrical laminate LPCI with ply clustering at the impacted side (left) and laminate LPCN with ply clustering at the non-impacted side (right), which is produced by flipping the laminate LPCI upside down. Flipping upside down only interchanges the 45s by -45s plies, i.e., it does not alter the in-plane and bending stiffness in the $0°$ and $90°$ directions.

acoustic emission, was noticed.

Pulse-echo mode ultrasonic C-scan inspection was performed on all the QSI specimens after each displacement level and on all the impacted specimens using an OLYMPUS OMNI MX system employing a 5 MHz piezoelectric probe. As C-scan inspection has the drawback of larger delaminations masking the underlying ones, C-scan was performed from both sides of the specimens, and the results presented are the inspections providing the most information.

4.3.2 Numerical modelling

User-defined constitutive models from Maimí et al. [91, 92] were used to simulate the onset and propagation of intralaminar damage. Apart from the main highlights such as crack closure effects, incorporating in-situ effects [58, 102], and the inclusion of crack band model formulation, the complete description can be found in [90]. The model was implemented as an Abaqus/Explicit VUMAT user-written sub-routine. The interlaminar damage was modelled using the ABAQUS Explicit in-built surface based cohesive behaviour [103], where a contact based interaction is used to model the traction between the contact surfaces to simulate delamination. The delamination initiation is governed by a quadratic stress-based criterion implemented in ABAQUS, whereas delamination evolution is characterised by the mixed mode energy-based propagation criteria proposed by Benzeggagh and Kenane [96]. Formulations of the initiation and propagation criteria are not detailed here but can be found in the work of Tan et al. [104].

This study follows a novel FE modelling approach from González et al. [90]. Interested readers are referred to their work for a more detailed description. Each ply is modelled using a conventional shell element which is sandwiched by surface elements on the top and bottom faces of the ply. The surface elements are tied to the shell elements with rigid tie connectors, thereby transferring the kinematics from the shells to the surface elements. Delamination between two plies is modelled by assigning cohesive surface-based interaction between the bottom face of the surface elements of the top ply and the top face of the surface elements of the bottom ply, as seen in Fig. 4.2 for an illustrative two plies model.

Clustered plies were modelled as a single shell element layer, leading to a model consisting of 19 layers. S4R conventional shell elements were used for the plies and SFM3D4R for the surface elements. The mesh was finer under the impactor (a refined window of 75 by 75 mm, referenced from the impact centre, with element size, $l = 0.5$ mm) than elsewhere ($l = 4$ mm). Moreover, the in-situ effect is accounted for by considering the ply thickness and the ply type (outer and embedded). To avoid excessive element distortion, an element was deleted when the fibre damage variable (d_1) reached 1, whereas the transverse (d_2) and shear damage (d_6) variables were assigned a maximum value of 0.99, and no element deletion was considered.

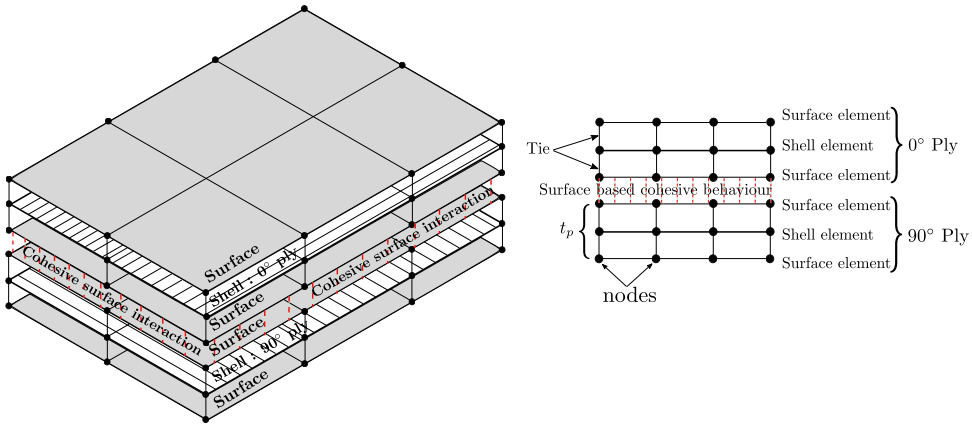

Fig. 4.2.: Schematic representation of the modelling strategy, where each ply is modelled using a shell element sandwiched between two surface elements using a tie interaction. Surface based cohesive interaction is assigned between the bottom surface of the top ply and the top surface of the bottom ply. t_p marks the thickness of the modelled ply, and there is no thickness defined between the surface elements.

A friction coefficient of μ=0.3 was assumed at the ply interfaces, as this property is not experimentally available. Further details about modelling (impactor, rubber clamps, base plate), contact algorithms, cohesive law shapes are explained in detail in [78, 90, 94]. The material data for IM7/8552 was obtained from [105].

4.4 Results

4.4.1 Experimental

The delamination threshold load, F_d, marked by the first clear load drop in the impact curves at 12 J and 18J (Fig. 4.3), is 30% higher for LPCI than LPCN, thereby LPCI clearly delays delamination onset compared to LPCN. After the delamination threshold load, a comparatively unstable response associated with intermittent load drops is seen with LPCI over LPCN. Maximum peak load, F_{max}, is approximately the same for both laminates at 12 J, whereas an increase of 12% is observed for LPCN over LPCI at 18 J. The energy dissipation of LPCI is 9% and 22% larger than LPCN for 12 J and 18 J, respectively. A compact quantitative overview of the various damage resistance parameters for both laminates and both impact energies is presented using a radar plot in Fig. 4.4.

Fig. 4.5 identifies the delaminated interfaces as well as the dominant delaminations

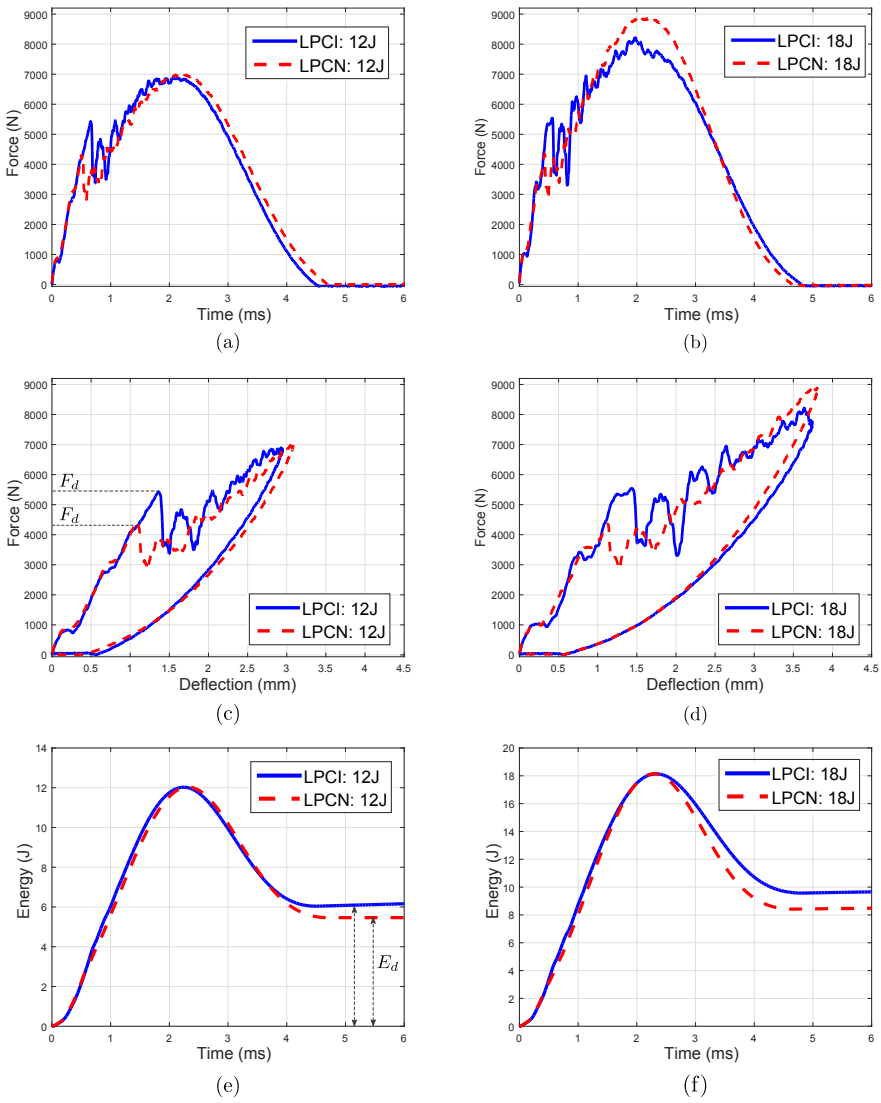

Fig. 4.3.: Force-time ((a),(b)), force-deflection ((c),(d)), and energy-time ((e),(f)) response curves for LPCI and LPCN for 12 J and 18 J impact energies.

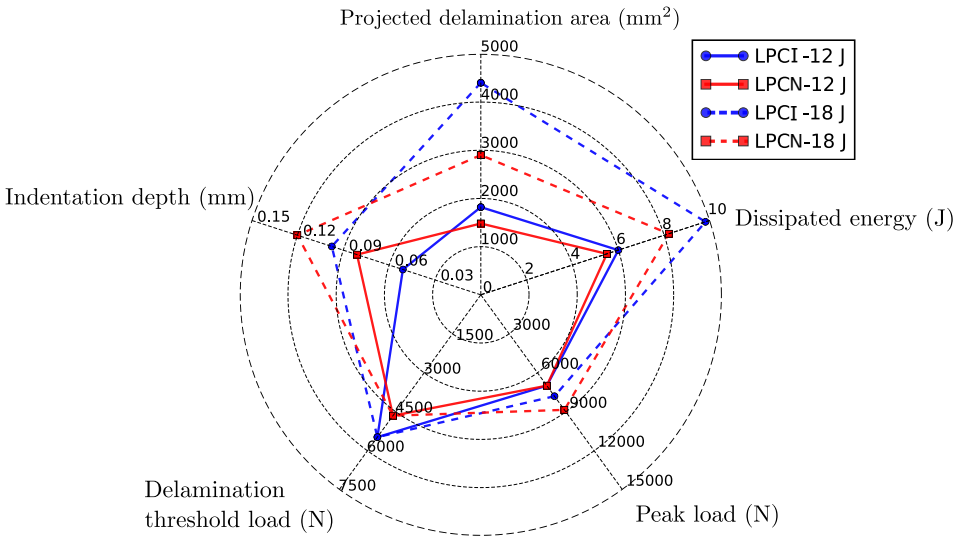

Fig. 4.4.: Quantitative overview of impact damage resistance parameters of LPCI and LPCN at both impact energies.

for both laminates. Dominant delaminations are those which govern the total delamination profile, thereby playing a major role in the damage tolerance of the structure [7, 12]. For LPCN, they appeared at all the interfaces within the clustered block (interfaces 15, 16, 17 and 18) and scaled up when moving from 12 J to 18 J. For LPCI, an unsymmetric delamination profile is observed for 12 J, with the dominant delaminations at interfaces within the clustered block at the impacted side (int. 3, 4) as well as just below the clustered block (int. 5, 6, 7). Moving on to the 18 J impact, a rapid growth in the projected delamination size is observed where the dominant delaminations are found outside the cluster block (int. 5, 6, 7), with the 90° oriented delamination (int. 5) almost reaching the impact window boundaries. When both laminates were compared, LPCI displayed a 20% reduced projected delamination area over LPCN for 12 J, whereas at 18 J it was 50% larger.

Unlike the impact tests, QSI tests interrupted for damage inspection provide information about the whole damage process. Fig. 8.10 shows the load displacement response of a pristine specimen up to the highest indenter displacement (d=5.4 mm) as well as the other indenter displacements (d_i), and the associated applied energies (E_a). The early delamination initiation of LPCN found in the impact test, is observed in the QSI results as well. After the delamination drop, the load deflection response

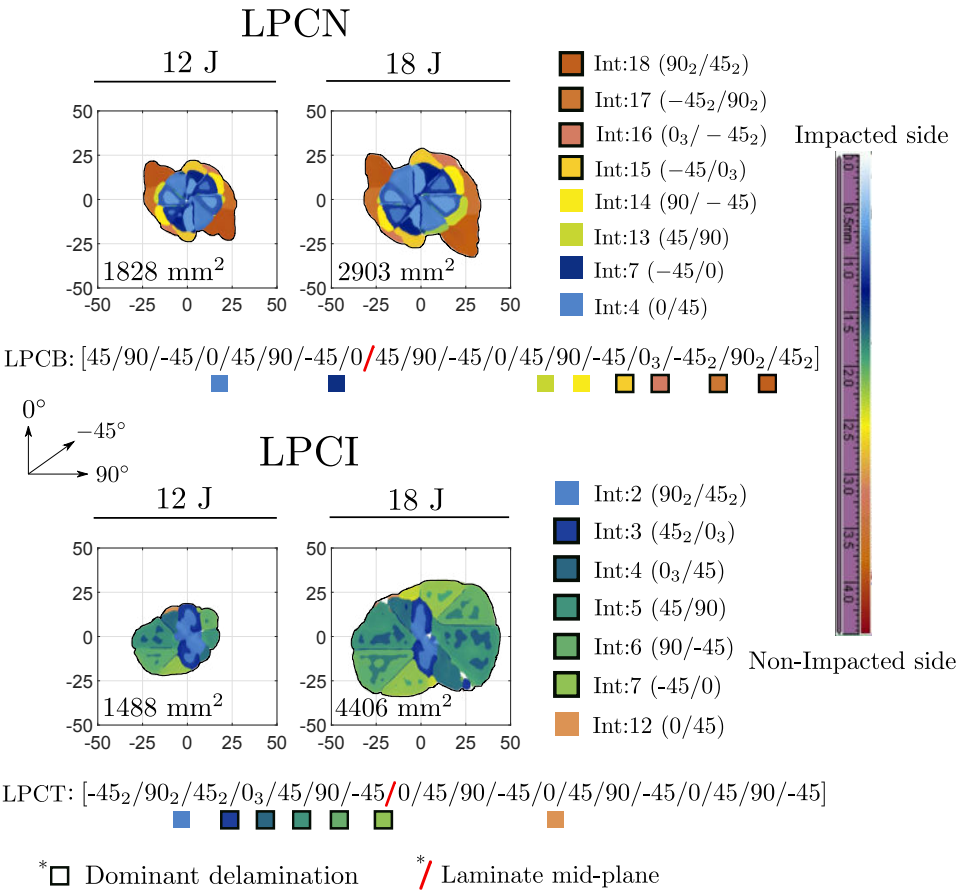

Fig. 4.5.: C-scan images of LPCN and LPCI inspected from the impacted face for 12 J and 18 J impact energies. Projected delamination area, identified delaminated interfaces and dominant delaminations are marked (The colour bar helps to identify the location of delamination in the thickness direction, and the axes are provided in millimetres).

for both LPCN and LPCI from indenter displacement d_3 to d_5 is similar. Beyond this, d_7 to d_8, LPCI shows a relative reduction in the stiffness followed by an increase.

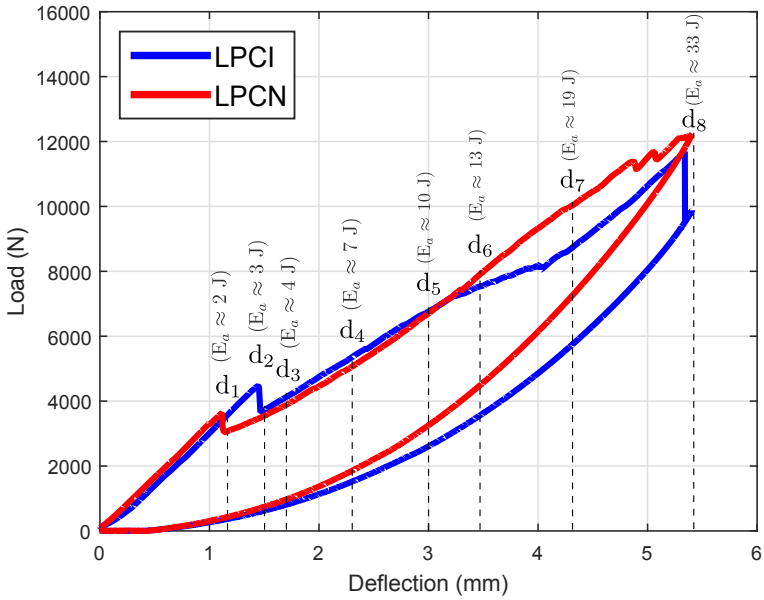

Fig. 4.6.: Load-deflection curve for the maximum indenter displacement d_8 = 5.4 mm for LPCN and LPCI, also showing the various other indenter displacements used in the study (The respective energy applied, E_a, is also marked for each indenter displacement).

Fig. 4.7(a) details the complete QSI delamination sequence obtained for both laminates using interrupted C-scan inspections, thus helping to relate each load drop or stiffness change (Fig. 8.10) to the corresponding delamination or its propagation. C-scan images of displacement d_1 (just after the first load drop of LPCN and before the load drop of LPCI) evidence the presence of delamination (initiated in the clustered block at the non-impacted side) in LPCN and yet there is no delamination initiation in LPCI. The first load drop is related to a simultaneous occurrence of matrix cracks and delamination initiation [6, 85]. Displacement d_2 (immediately after the load drop of LPCI) shows delamination initiation in the clustered block at the impacted side of LPCI and delamination extension at the interfaces of the non-impacted side for LPCN.

Through displacements d_3 to d_5, already formed delaminations propagate in both

laminates. The LPCI laminate exhibits dominant delamination mainly at the impacted side, whereas in LPCN delaminations at the interfaces of the non-impacted side dominate. The change in stiffness for LPCI (displacement d_6 in Fig. 8.10) corresponds to a rapid and unsymmetric growth of delaminations for LPCI within the interfaces 5, 6, 7 at the impacted side). At displacement d_7 (associated with the stiffness increase with LPCI), LPCI has its dominant delamination at interface 5 (oriented in 90°) develop into the supported region of the clamping (as seen with 18 J impact results), leading to stress redistribution and thereby an increase in stiffness, while LPCN showed further delamination extension. Ultimately, the last displacement resulted in further scaling up of delamination with LPCN, and delamination growing to the specimen edges for LPCI.

Fig. 4.7(b) depicts a quantitative evolution of the damage resistance parameters for all the indenter displacements. LPCI was seen to be more damage resistant than LPCN, in terms of projected damage area and dent depth, until the displacement of d_6, at which an overturn in the trend is noted. Comparing the impact results of 12 J with the QSI results for the same applied energy (corresponding to d_5), a good correlation is observed with the maximum peak force and the projected delamination area. Moving to 18 J, the QSI results (corresponding to d_7) slightly over-predict the above two parameters compared to the impact results (by 8% and 15%, respectively).

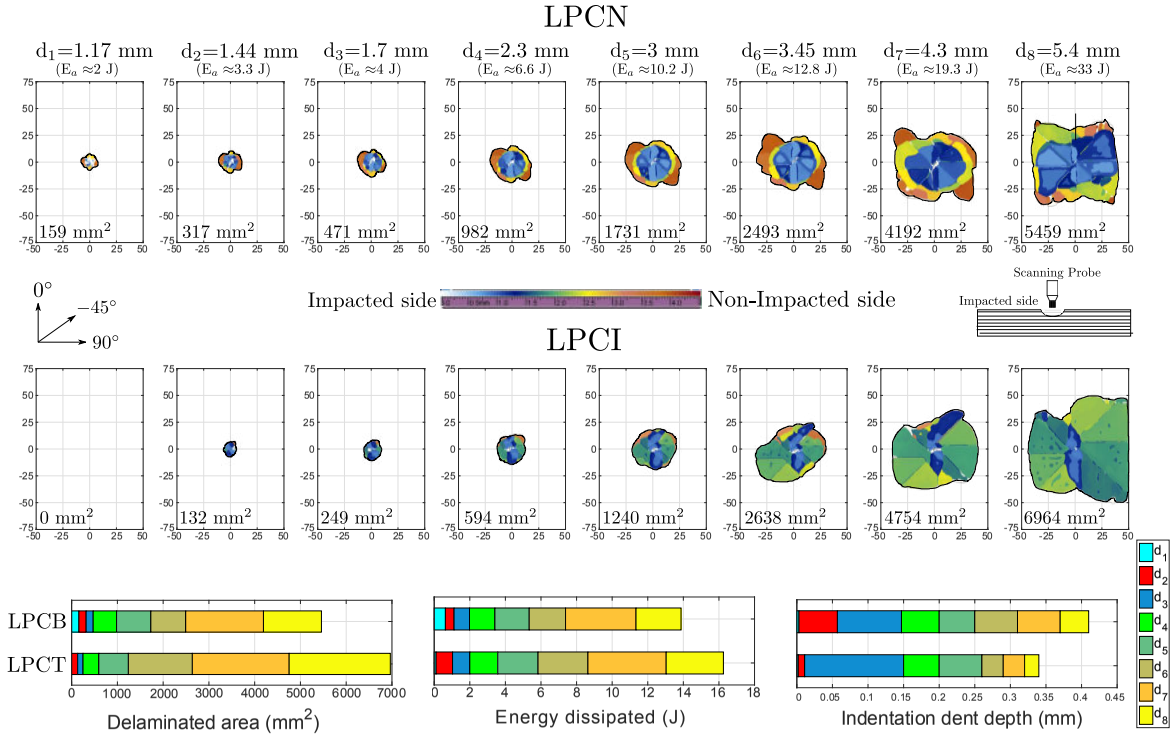

Fig. 4.7.: (a) Impacted face C-scan images revealing the delamination initiation and propagation for various indenter displacements (b) Quantitative evolution of damage resistance parameters for all indenter displacements for LPCN and LPCI.

4.4.2 Numerical

The numerical predictions of the impact response curves, namely the force-deflection and energy evolution curves (Fig. 4.8), are in excellent agreement with the experimental results, especially with the energy evolution for both laminates at both impact energies. Fig. 4.8 also depicts the impactor displacements chosen for the numerical analysis of the energy dissipated through intralaminar and interlaminar damage: marked by circles (A to E) for the force response and by dashed lines for the energy-time curves. This figure also distinguishes the energy dissipated through inter and intralaminar damage.

Moving away from the normal convention of comparing only the projected delamination contour or the area, we present a 'virtual C-scan', where along with the delamination profile and area, each delaminated interface is identified and presented as in a C-scan. Fig 4.9 shows the good agreement between the virtual and experimental C-scan, highlighting the potential of the numerical tools used. With LPCN laminates, the dominating delaminations and their extension is almost replicated in the prediction, although the projected damage area is slightly under-predicted by an average of 8%. For LPCI, dominant delaminated interfaces are correctly predicted, while the unsymmetric delamination extension for 12 J and the rapid growth of the close-to-mid-plane delaminations for 18 J are not, thus the projected damage area is underpredicted.

Fig. 4.10 illustrates the two laminates along with the amount of energy dissipated for each ply and each interface for both laminates. The figure quantitatively compares the inter- (delamination) and intra- (matrix cracks and fibre failure) laminar energy dissipated for all the plies and interfaces between LPCN and LPCI for 12 J. Note that the different colour codes in the figure represent the energy dissipated within the different displacement steps (A to E, as shown in Fig. 4.8) considered in the study. The figure also compares (at the bottom) the total energy dissipated (inter- and intralaminar) by the two laminates within the selected displacement steps.

With LPCN, as demonstrated by the experiment, the last four interfaces (15, 16, 17 and 18) dissipate the larger amount of energy through delaminations, whereas with LPCI the interfaces 3, 4 (within the cluster), 5, 6, and 14 dominate. The total energy dissipated by the dominant delaminations of LPCN over its other delaminated

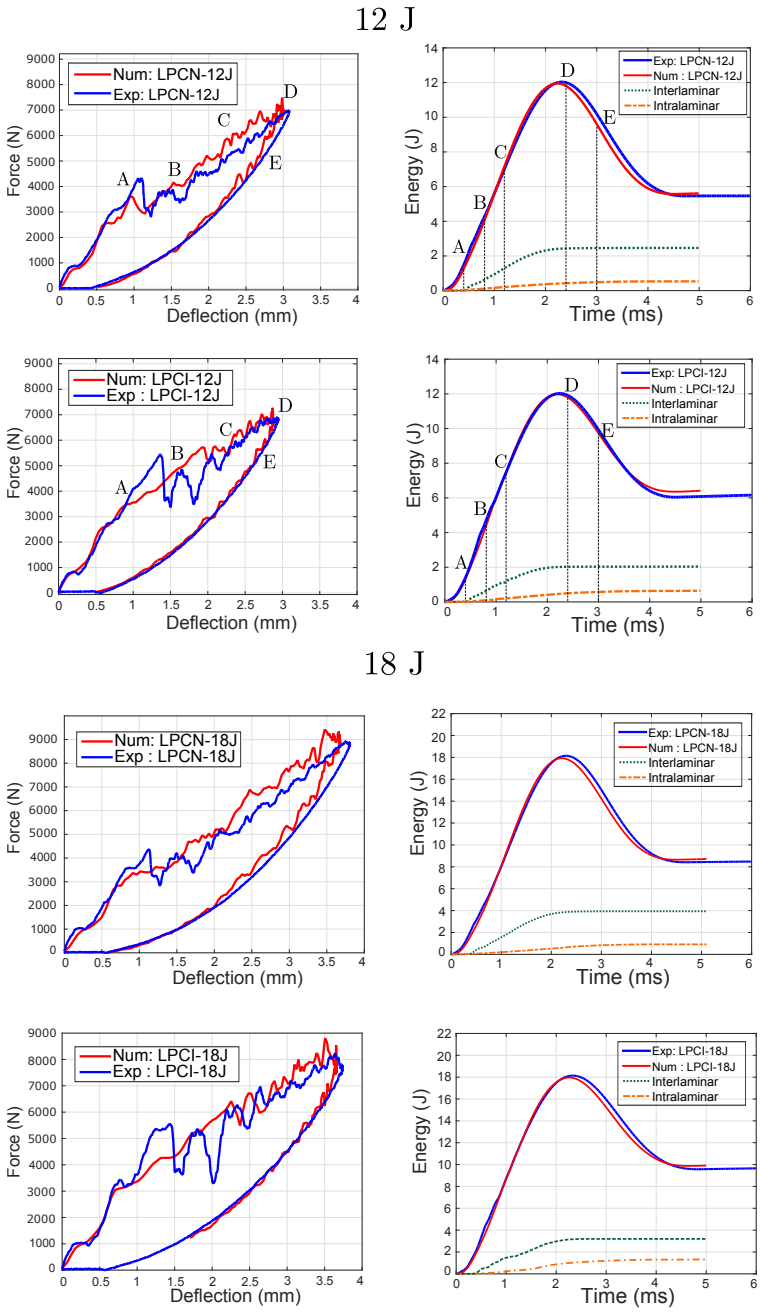

Fig. 4.8.: Numerical prediction of the impact response of LPCN and LPCI laminates compared with the experimental data for both 12 J and 18 J. Selected displacements (A to E) for energy dissipation study (in Fig. 4.10) are also marked for the 12 J energy case.

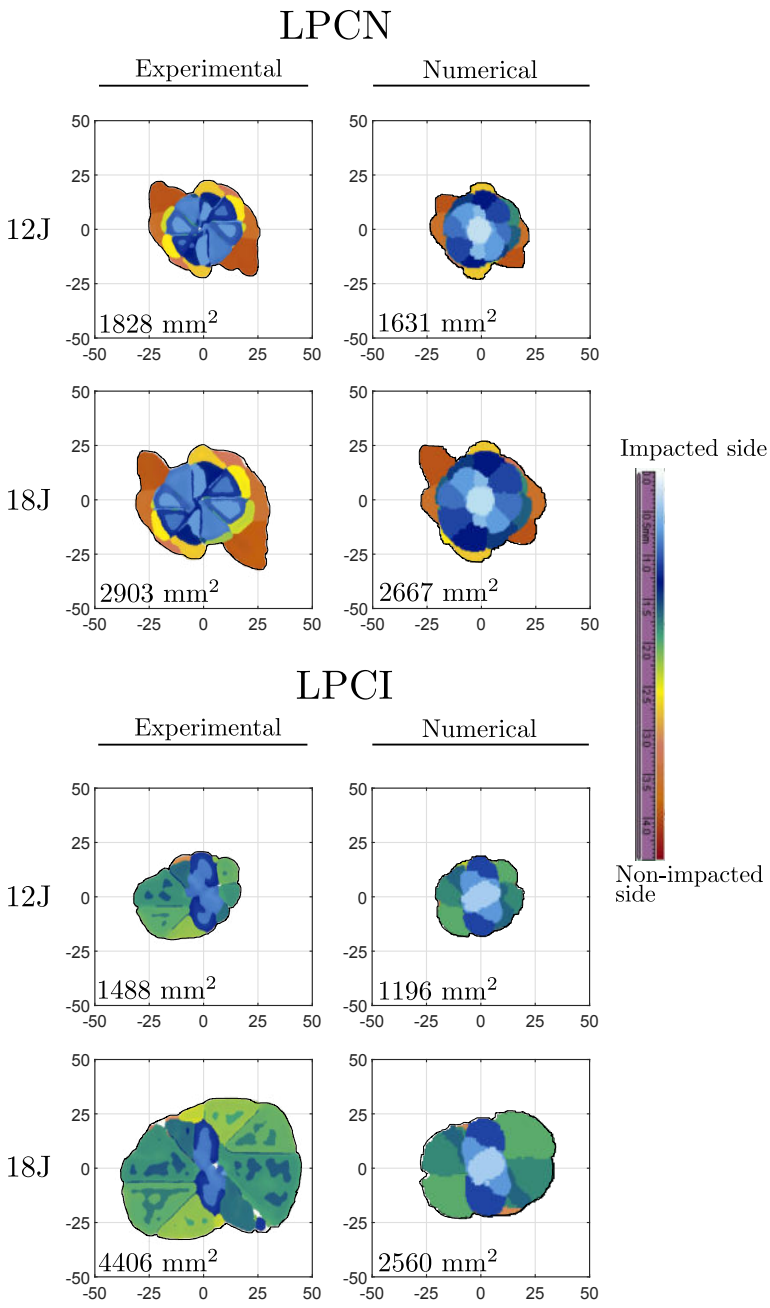

Fig. 4.9.: Comparison of the virtual C-scan from numerical study with the C-scan after impact testing for LPCN and LPCI for both 12 J and 18 J. Projected delamination area is provided in the bottom left corner of each box.

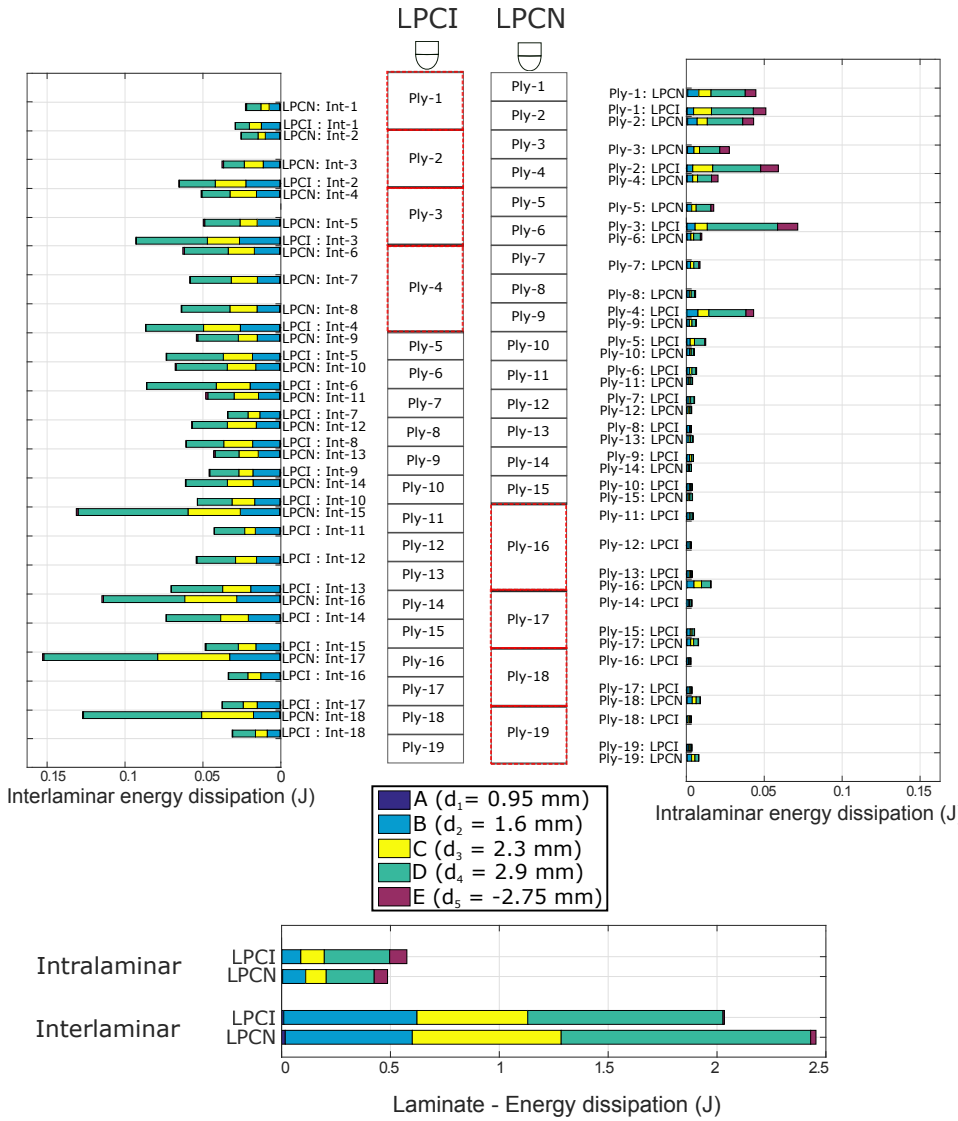

Fig. 4.10.: Illustration of the laminates and their plies along with the amount of inter and intralaminar energy dissipated for each ply and interface of both the laminates. Note that the clustered plies are considered as a single ply and hence, for example, interface 1 of LPCI is compared with the interface 2 of LPCN. The different colour codes represent the energy dissipated with the different displacement steps (A to E, as shown in Fig. 4.8). The total dissipated energies (inter- and intralaminar) by the laminates are also compared at the bottom.

interfaces is much higher (int. 15, 16, 17 and 18 account for 30% of the total interlaminar energy dissipated) than for LPCI. In the case of intralaminar damage, the first four plies of both laminates dissipated most of the energy, with LPCI being comparatively higher than LPCN, due to the clustered plies.

Displacement level A (chosen to be before the load drop for LPCN and before the stiffness change for LPCI in the numerical curve, as in Fig. 4.8) reveals no delamination for both laminates. Most of the delamination energy dissipation is observed at the final loading part, between the points C and D. The same occurs with the intralaminar damage, with local fibre failure being seen at the top two plies in the vicinity of the impactor. Fig. 4.10 compares the energy dissipation at the laminate level: the average energy dissipated through delaminations is approximately five times higher than that of the intralaminar damage, signifying the dominance of energy disspation through delamination within the energy levels explored. Comparing LPCI and LPCN for 12 J, LPCI dissipates 18% more energy through intralaminar damage, and 17% less through interlaminar damage.

4.5 Discussion

The experimental results revealed the different damage onset and evolution of the two laminates analysed. Delamination initiates earlier in the laminate with clustered plies at the non-impacted side (LPCN), which is related to the transverse cracks in the plies (at non-impacted side) induced by in-plane tensile loads from laminate bending. These cracks grow into the next available interface to initiate delamination. Clustered plies introduce high bending stiffness mismatch [18], leading to high interlaminar shear stresses at the adjacent interfaces. This triggers delamination and makes clustered plies a weak zone for delamination onset. Additionally, the reduced in-situ effect of the clustered plies favours transverse cracking when compared to the non-clustered plies [105]. When the transverse crack reaches the adjacent interface, the large energy release rate available acts as a catalyst for delamination. Substantial difference in damage mechanisms was observed when the clustered plies are on the impacted side (LPCI). Impact loading introduces high local out-of-plane compressive stresses at the vicinity of the impactor, which counteract the interlaminar shear stresses and lead to increased interlaminar friction [106]. This can be indirectly ascribed to the increase in mode II fracture toughness at regions close to the impactor,

as reported in [107, 108]. This constrains the delamination propagation, as observed in the first two interfaces within the clustered block of LPCI (see Fig. 4.5).

We also observed that the position of the larger delaminations varies from one laminate to the other. The idea of imposing delaminations at the non-impacted side in LPCN by tailoring clustered plies has paid off, with the dominant delaminations appearing at the interfaces within the clustered block (int. 15, 16, 17 and 18 in Fig. 4.5). In the case of LPCI, with the suppressed delaminations at the interfaces of the impacted side, the dominant delaminations were seen outside the cluster, due to the high interlaminar shear stresses at the laminate mid-plane. These high stresses trigger transverse shear cracks in the 45° and -45° plies (associated with the interfaces 5, 6 and 7 in Fig. 4.5) promoting delamination oriented in the 90° ply (which is placed in between the 45° and -45° plies as in Fig. 4.1). Finally, in terms of impact resistance, LPCI performed better at 12 J impact and earlier stages of indenter displacements (up to d_6). At higher energy levels, the rapid growth of close to mid-plane delaminations induced more damage than in LPCN.

The numerical study identified the local fibre failure caused by the impactor as the prime reason for the high intralaminar energy dissipation at the top plies (at impacted side) for both laminates. Owing to the cluster effect, LPCI showed higher values of intralaminar energy dissipation over LPCN for the top plies. While the same clustered plies of LPCN dissipated most of the energy through interlaminar damage, LPCI clustered plies dissipated it through intralaminar damage. This difference in behaviour signifies how the location in the laminate varies the damage mode and its evolution. The lack of accuracy of the numerical prediction of LPCI (as in Fig. 4.8 and Fig. 4.9), may be attributed to the inability of shell elements to capture the shear matrix cracks from the out-of-plane shear stresses close to the impactor. This could be tackled by incorporating a full three dimensional constitutive behaviour with solid elements [109] followed by a oriented mesh strategy (as demonstrated in [77]), but at the price of a higher computational time.

What is clear from the study, is that damage can be forced to occur at predetermined locations through judicious laminate designing, and thereby tailor the damage resistance. Unsymmetrical stacking designs can facilitate this task and raise the prospect of an improved impact damage resistance. Current numerical tools provide a detailed

physical representation of the damage mechanisms, so they can efficiently support this innovative design task. A continuation of this work will be to compare unsymmetrical laminates with symmetric quasi-isotropic laminates in terms of impact damage resistance and tolerance (Compression After Impact) to better assess the prospects of unsymmetrical laminates.

4.6 Conclusion

For the first time, unsymmetrical stacking sequences have been explored in an experimental low velocity impact framework. We designed an unsymmetrical laminate (with zero extension-bending coupling, and therefore warp-free) with tailored ply clustering at the impacted side, and flipped it upside down to yield a laminate with ply clustering at the non-impacted side. Both these laminates were tested under low velocity impact and quasi-static indentation loading to study their out-of-plane damage resistance. The experimental and numerical results revealed that clustering at the impacted side delayed the threshold load for delamination by 30% and reduced the projected delamination area by 20% for low impact energies. This improvement derived from a higher energy dissipation through intralaminar damage instead of delamination, the most important damage mechanism for the laminate with clusters at the non-impacted side. Damage patterns from both laminates were compared and, importantly, the dominant delaminations were observed at the locations predicted during the laminate design. This paper highlights the opportunity to move away from conventional symmetrical laminate design, thereby giving laminate designers the freedom to tailor the stacking sequence according to the expected stress states of given load cases.

5

Paper B:

On how unsymmetrical laminate designs with tailored ply clusters affect compression after impact strength compared to symmetric baseline

A. Sasikumar[a,*], S. M. García-Rodríguez[a], J.J. Arbeláez[a,b], D. Trias[a,1], J. Costa[a,*]

[a] AMADE, Polytechnic School, Universitat de Girona, Campus Montilivi s/n, E-17003 Girona, Spain

[b] Engineering Faculty, Instituto Tecnológico Metropolitano (ITM), C.73, No. 76-354, Medellín, Colombia

[*] Corresponding author

[1] Serra Hunter Fellow

The paper has been published in *Composite Structures* 238 (2020) 111958.

Motivation & Synopsis

Paper A has successfully demonstrated the possibility of unsymmetrical laminates with zero coupling responses, thanks to the optimization methods. The experimental results revealed that using stacking sequence designs, impact damage can be tailored to occur at pre-determined locations. Despite the interesting conclusions, the study lacked the vital impact damage tolerance results. In addition, to understand the complete feasibility of unsymmetrical laminates towards application in real life structures, they need to be compared with standard symmetric laminates. Hence, this paper is aimed to answer the open questions from Paper A. Along with the two unsymmetrical laminates from Paper A, an additional unsymmetrical laminate with ply clusters at middle is proposed here and the impact and compression after impact results are compared with a symmetric baseline laminate. Experimental results reveal that the unsymmetric laminate design improved the impact damage tolerance and hence demonstrating that symmetric laminates are not the optimal solution to impact load cases.

Composite Structures 238 (2020) 111958

Contents lists available at ScienceDirect

Composite Structures

journal homepage: www.elsevier.com/locate/compstruct

On how unsymmetrical laminate designs with tailored ply clusters affect compression after impact strength compared to symmetric baseline

A. Sasikumar[a,*], S.M. García-Rodríguez[a], J.J. Arbeláez[a,b], D. Trias[a,1], J. Costa[a,*]

[a] AMADE, Polytechnic School, University of Girona, Campus Montilivi s/n, 17073 Girona, Spain
[b] Engineering Faculty, Instituto Tecnológico Metropolitano (ITM), C.73, No. 76-354, Medellín, Colombia

Abstract

Out-of-plane loads induce unsymmetrical damage modes in the laminate thickness direction. Consequently, the authors have recently proposed overcoming the conventional laminate symmetry constraint by designing unsymmetrical laminates with zero coupling responses. While impact damage is able to be tailored with unsymmetrical laminates, comparing them to symmetric laminates and assessing their impact damage tolerances had yet to be addressed. In this paper, we study three unsymmetrical laminates with localized ply clusters positioned at different locations (at the impacted, at the middle and at the non-impacted sides), along with a standard symmetric laminate as a baseline. Using low-velocity impact, X-ray micro-computed tomography and compression after impact (CAI), we compared the impact and post-impact responses to understand the effect local ply clusters and the delamination location have on the CAI strength. Results revealed that the unsymmetrical laminate with the ply clusters in the middle, where the dominant delaminations also occured, improved the CAI strength by a maximum of 10% when compared to the symmetric baseline. Laminates with delaminations at the outer surfaces offered lesser resistance to buckling. While our study demonstrates that symmetric laminates are not the optimal damage tolerant solution for impact load cases, it also evidences the feasibility of unsymmetrical laminates.

Keywords: Delamination, Impact behaviour, Damage tolerance, Unsymmetrical laminates

5.1 Introduction

Low velocity impact loads continue to be one of the load case threats that aircraft can encounter in their life-cycles. Low velocity impact damage mainly consists of matrix cracks followed by delaminations at the ply interfaces. Impact damage below the detectability threshold (barely visible impact damage, BVID) formed within the laminate may propagate during aircraft flight cycles, leading to a major reduction in residual strength [5], especially the compression after impact (CAI) strength. During CAI loading, the formed delaminations tend to propagate and split the laminate into sub-laminates, and these thinner sub-laminates buckle easily, leading to final failure. In the case of standard thick laminates (4-5 mm), delamination induced buckling is the critical phenomenon causing structural collapse under compression, whereas in the case of thin laminates (1-2 mm), impact induced fibre failure triggers final laminate failure [110, 111].

In the quest to improve CAI strength, numerous researchers [12, 79, 112] initially tried to understand the relationship between impact damage and CAI strength. They studied the effect various damage parameters such as projected damage area [7], delamination threshold load [24] and impact dent depth [113] had on CAI strength. Because of unclear conclusions, researchers subsequently focussed on delamination parameters such as the through-the-thickness delamination position, orientation and size [114–117] and the associated laminate buckling modes [118] and how they affect CAI strength. Hu et al. [25] performed compressive numerical buckling analysis with one embedded delamination and reported that the buckling load increased significantly as the position of the delamination approached the laminate mid-plane due to the change in the buckling mode from a local to a global one. A similar conclusion was reported by Butler et al. [26] using an analytical model. They stated that deep sited delaminations were safe as they opened under compressive loading and would not grow to cause failure. Despite these interesting conclusions, in a real impact scenario the effect on CAI strength could be completely different due to the development of many more damage forms.

Apart from applying material reinforcement methods [32], researchers have also pushed the laminate design boundaries to propose non-conventional stacking sequences, such as varying mismatch angled interfaces [9, 11], complete [11, 42]

or localized ply clustering [13], or dispersed ply orientations [10, 51, 119] in an attempt to tailor the impact damage resistance and improve the CAI strength. Liv et al. [11] demonstrated that complete clustering of plies ($[90_3/-45_3/0_3/45_3]_s$) led to a decreased impact resistance and a 15% lower CAI strength compared to a non-clustered baseline ($[90/45/-0/-45]_{3s}$). This was mainly attributed to the wide extended delaminations adjacent to the ply clusters. However, Sebaey et al. [13] using dispersed ply orientations and localized clusters of 0° plies, reported an improvement in CAI strength over the baseline quasi-isotropic laminate.

Reviewing the damage morphology, low velocity impact induces damage modes that are unsymmetrical in the through-the-thickness direction of the laminate [5, 6]. Despite both the loading and the damage being unsymmetrical in the laminate, the conventional mid-plane symmetry constraint is still followed. In response, the authors [120] proposed warp-free unsymmetrical laminates (with the extensional-bending coupling matrix B=[0]) with localized ply clusters placed only on the impacted side of the laminate. The same laminate, when flipped upside down, led to another unsymmetrical laminate with clustered plies on the non-impacted side of the laminate. Experimental (low velocity impact and quasi-static indentation tests) and numerical studies on the two laminates concluded that (a) delaminations can be tailored to occur at pre-determined locations and (b) unsymmetrical stacking designs offer a promising prospect for unsymmetrical loading conditions. Despite demonstrating that impact damage can be tailored, the study lacked the crucial information of the resulting compressive strength (CAI) and a comparison with a symmetric baseline in terms of impact resistance and CAI strength.

Hence, in this paper we propose three unsymmetrical laminates, where local ply clusters are placed at the impacted side, the middle of the laminate and the non-impacted side, and a reference symmetric baseline laminate (with no ply clusters). Using low velocity impact, micro computed X-ray tomography inspections and CAI tests, we compare the impact resistance, damage evolution and CAI strengths of all four laminates. The objective of the study is twofold: (b) to understand the effect the local ply clusters, their location in the laminate, and the location of the dominant delaminations (imposed by the clusters) have on the CAI strength and (b) to compare the damage tolerance of the proposed non-conventional unsymmetrical laminates to that of the symmetric baseline laminate (as suggested in ASTM standards [64]) to

assess the prospects of the unsymmetrical laminate designs.

5.2 Laminate design

5.2.1 Optimization

Different laminates with local ply clusters at the impacted side, the middle of the laminate and the non-impacted side were designed. Because the clusters were placed only at particular locations in the laminate, this meant violating the conventional mid-plane symmetry constraint and therefore leading to unsymmetrical laminate solutions. Since unsymmetrical laminates can induce coupling responses under loading (due to the presence of non-zero extensional-bending coupling matrix ([B]) [121]), such as warping during the curing process, optimization methods were used to obtain unsymmetrical laminates with zero or close to zero B matrix terms.

Using a genetic algorithm from MATLAB [89], we obtained three unsymmetrical laminates (two that had already been proposed in the previous work [120]) with clustered ply blocks placed at the top, the middle or the bottom of the laminates. Note that top refers to the impacted side and bottom refers to the non-impacted side of the laminate. The objective function was set to minimize the summation of the B matrix terms to avoid undesired coupling responses. In addition, the following constraints were also included: (a) the laminate had to be quasi-isotropic and balanced with 24 plies in total, (b) four clustered ply blocks (one cluster for each ply orientation i.e., 0°, $\pm 45^\circ$ and 90°) were placed at the respective desired location (top/middle/bottom) to impose delamination damage at that location; (c) no more than three plies of the same orientation were placed together, (d) outer laminate plies were fixed to be either 45° or -45° to counteract the shear loads [10], and (e) the equivalent bending stiffness parameter D* of the proposed laminates were to match within 5% that of the baseline laminate (D* was proposed by Olsson [122, 123] to ensure proper comparisons between laminates, as was also implemented in [124]).

5.2.2 Laminates

The unsymmetrical laminate obtained with local ply clusters at the impacted side (top side) is referred to as LPCI, while the same flipped laminate with ply clusters at the non-impacted side (bottom side) is referred to as LPCN (as presented in [120]).

Finally, the unsymmetrical laminate with ply clusters at the middle of the laminate is hereafter referred to as LPCM. Note that LPCI and LPCN have null B matrices while LPCM has low but non-zero B matrix terms (with a maximum term of 2 kPa.m^2). In addition, we introduce a symmetric laminate (as recommended in the ASTM standard [64]) as the baseline comparison case. Table 9.1 details the stacking sequences and Fig. 5.1 provides an illustration of all four laminates and the through-the-thickness location of the ply clustered blocks. Fig. 5.2 (a) and (b) represent the polar plot of the in-plane and bending stiffness, respectively, of all the laminates. It is important to note that all the laminates are in-plane quasi-isotropic with equal ply counts in all the orientations. All the laminates have the same number of 0° plies, thus assuring a fair comparison for CAI strength which is measured at 0°. The equivalent bending stiffness values of LSYM, LPCI, LPCN and LPCM are 373.9, 372.2, 372.2 and 373.1 Nm, respectively, and the values of the proposed laminates fall within 1% of that of the baseline laminate. The bending stiffnesses of all three unsymmetrical laminates in the 0° and 90° directions are the same.

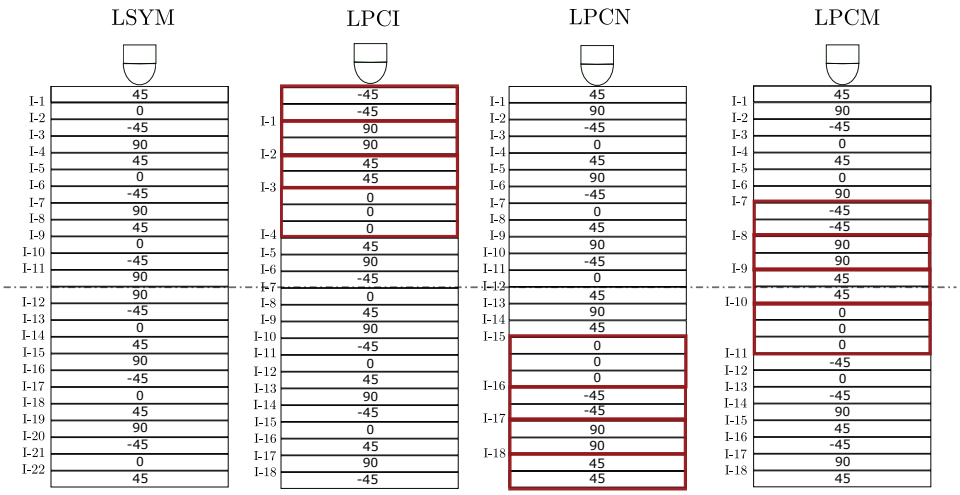

Fig. 5.1.: Illustration of all the laminates used for the study: LSYM, LPCI, LPCN and LPCM, where LPCN is obtained by flipping upside down LPCI. Note that T (top), B (bottom) and M (middle) refer to the location of the clustered block in the through-the-thickness direction of the laminate.

Tab. 5.1.: Laminates and their details

Laminate	Description	Stacking sequence (impacted side to non-impacted side)
LSYM	Symmetric baseline [64]	$[45/0/\text{-}45/90]_{3s}$
LPCI	Unsymmetric Clustered block at the top	$[\text{-}45_2/90_2/45_2/0_3/45/90/\text{-}45/0/45/90/\text{-}45/0/45/90/\text{-}45/0/45/90/\text{-}45]$
LPCN	Unsymmetric Clustered block at the bottom	$[45/90/\text{-}45/0/45/90/\text{-}45/0/45/90/\text{-}45/0/45/90/-45/0_3/\text{-}45_2/90_2/45_2]$
LPCM	Unsymmetric Clustered block at the middle	$[45/90/\text{-}45/0/45/0/90/\text{-}45_2/90_2/45_2/0_3/\text{-}45/0/\text{-}45/90/45/\text{-}45/90/45]$

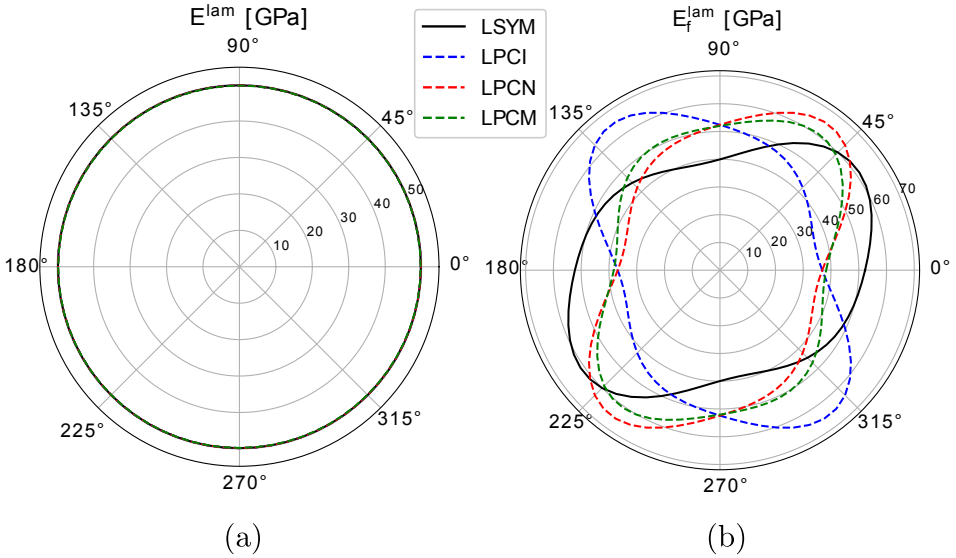

Fig. 5.2.: Polar plot representation of the (a) in-plane stiffnesses and (b) bending stiffness of all the laminates.

5.3 Experimental methods

The material used was IM7/M21 prepreg uni-directional tape, and the panels were cured in an autoclave. Impact specimens of 150 x 100 mm were cut out from the panel with 0° fibres aligned in the direction of the specimen length. The unsymmetrical laminates had no warping, with respect to the zero or low values of the B matrix. With a ply thickness of 0.184 mm and 24 plies, all the laminates resulted in a nominal thickness of 4.41 mm. The LPCI specimens were flipped upside down to obtain LPCN laminates. In accordance with ASTM D7136/D7136-M standards [64], impact tests were performed on the 150 x 100 mm specimens using a CEAST Fractovis Plus

instrumented drop-weight tower. A total of four impact energies were explored: 10, 16, 24, and 35 J, with three specimens per laminate tested for each impact energy. The range of impact energies was selected such that the lowest energy induces minimum damage in order to understand the damage initiation process, while the higher energies lead to barely visible impact damage and extended delaminations inside the laminate. A 16 mm in diameter hemispherical tip impactor, with a 5 kg impactor setup mass was used for all the tests in the study.

All the impacted specimens were subjected to compression using an MTS INSIGHT 300 machine with a 300 kN load cell, following the ASTM D7137/D7137-15 [88] in order to obtain the compression after impact strength. To measure the out-of-plane displacements and study the buckling modes, we placed two LVDT sensors, one each at the centre of the impacted and non-impacted sides of the impacted specimen. Furthermore, to evaluate the pristine compression strength, plain compression strength tests were performed in accordance with the ASTM D6641/D6641M-16 [125]. Five 140 x 13 mm specimens per laminate were tested under plain compression, and both compression tests above were performed with a cross head displacement of 0.5 mm/min.

The impact damage in all the laminates were inspected using a pulse-echo ultrasonic C-scan technique. We used an OLYMPUS OMNI MX system equipped with a 5 MHz piezoelectric probe. Furthermore, one of the 10 J impacted specimens per laminate was subjected to an X-ray micro-computed tomography (μCT) inspection. Before the inspection, the impact specimens were cut into 30 mm wide strips (with the impact point as the centre), making sure that all the impact damage was within this strip (determined by C-scan inspection). Using laminate strips instead of the whole impact specimen was done to minimize the unwanted X-ray absorption perpendicular to the axis of rotation as reported in [68]. The scanning parameters were: 50 kV, 175 μA, 1400 projections with three integrations per projection, an effective pixel size of 10 μm with a field of view of approximately 22 mm and the inspection time was two and a half hours per specimen. The μCT slices were post-processed using Matlab [89] and 3D rendered in Starviewer software [126], where we differentiated matrix cracks and delaminations in the final 3D image. For more details of the inspection equipment and the post-processing of the slices, the reader can refer to [68, 127]. All the above-mentioned tests and inspections were performed at the AMADE research

laboratory, which is NADCAP certified for non-metallic material testing, at the University of Girona.

5.4 Results

5.4.1 Impact responses

Figs. 5.3, 5.4 and 5.5 represent the force-time, force-deflection and energy-time responses of all the four laminates for all the impact energies, respectively. Due to the excellent repeatability in the impact responses, only one specimen data per impact energy per laminate is shown. The figures convey that the global impact responses of all four laminates are quite similar, mainly in terms of their maximum peak forces, impact response times and the energy evolution (in Figs. 5.3 and 5.4). Despite their similar responses, the delamination threshold loads (F_d) differ between the laminates. With LSYM as the baseline, laminate LPCN exhibited an early delamination initiation (13% reduction in the delamination threshold load), while LPCI and LPCM increased the threshold load by 7% and 5%, respectively, over LSYM (as in Fig. 5.3 (c)).

Figs. 5.6 (a) and (b) present the maximum peak loads and projected damage areas, respectively, for all the laminates. As previously mentioned, the peak loads are roughly the same for all the laminates throughout the entire range of energies, thus indicating the similar load carrying capability the four laminates have, despite the presence of clusters in the unsymmetrical laminates. However, this is not the case with the projected damage area. On comparing all four impact energies, the baseline LSYM exhibited the least damage area whereas LPCN exhibited the highest. For the lower impact energies (10 J and 16 J), LSYM and LPCM exhibited roughly the same damage areas. For higher energies, LPCM exhibited a 50% higher damage area, while LPCI showed a 60% more damage area than the baseline. Throughout all the impact energies, LPCN exhibited more than twice the damage area as that of LSYM.

Figs. 5.7 (a) and (b) show the dissipated energies and impact dent depths, respectively, of all the laminates for all impact energies. For the lowest energy, 10 J, all the laminates dissipated roughly the same amount of energy. In the cases of 16 J and 24 J, all three unsymmetrical laminates exhibited roughly the same dissipated energy

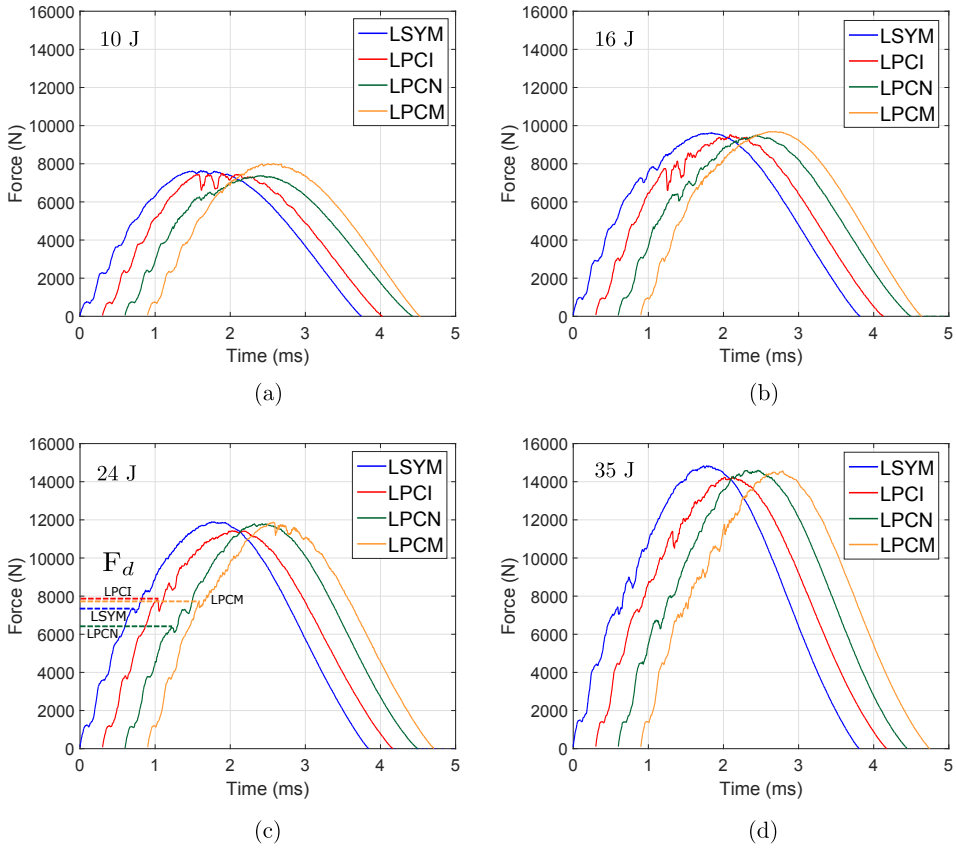

Fig. 5.3.: Impact force-time response curves of all laminates for all impact energies (Note that the responses of LPCI, LPCN and LPCM are offset by 0.3, 0.6 and 0.9 ms from LSYM, respectively, for proper comparison)

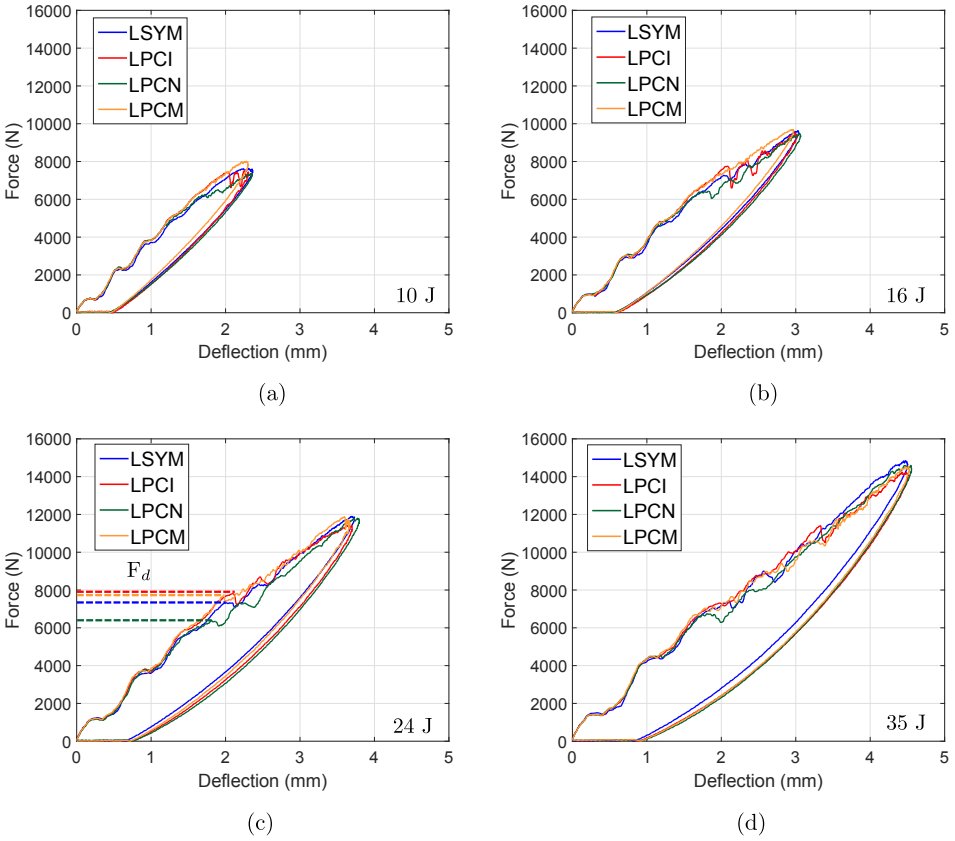

Fig. 5.4.: Impact force-deflection response curves of all laminates for all impact energies

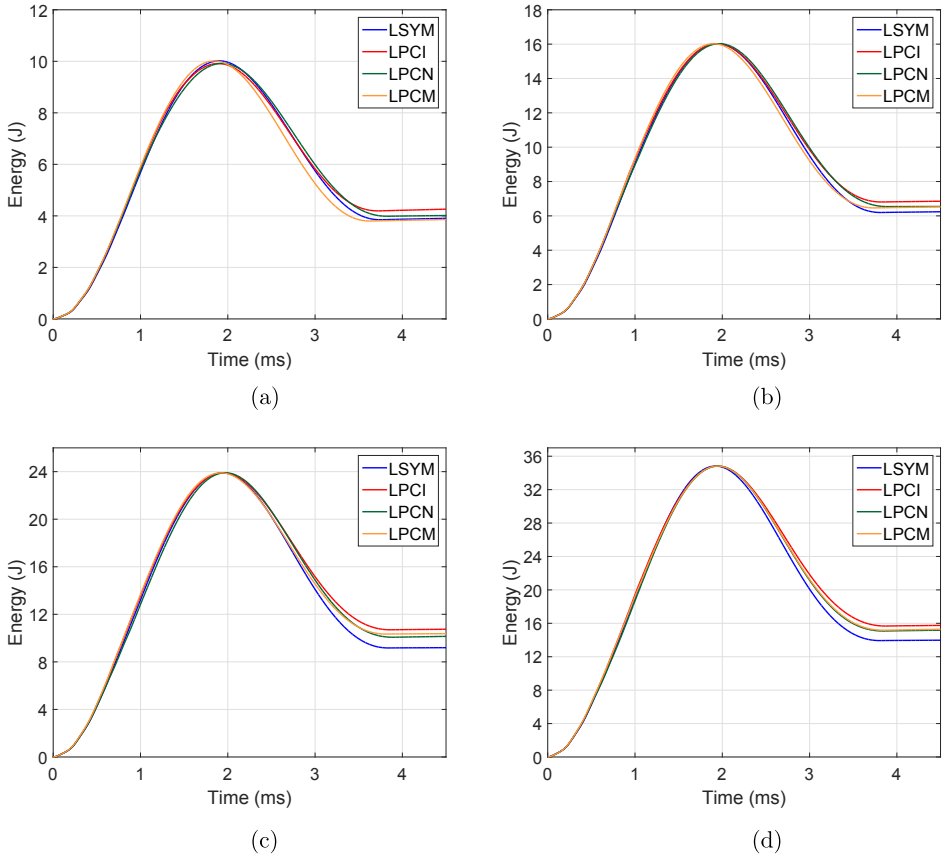

Fig. 5.5.: Impact energy-time response curves of all laminates for all impact energies

(around 10% higher than LSYM), whereas for the highest energy, 35 J, LSYM exhibited the least and LPCI dissipated the highest (18% higher than LSYM). Of the three unsymmetrical laminates, LPCM dissipated the least energy considering all the energies. In view of the impact dent depth, laminates LSYM and LPCI displayed similar dent depth values, whereas LPCN exhibited the highest for all the impact energies. For the highest impact energy, LPCM and LPCN displayed approximately 25% higher dent depth compared to the baseline LSYM.

5.4.2 Impact damage inspection

Fig. 5.8 presents the damage footprint (matrix cracks and delaminations) of all the laminates obtained from the post-processed μCT slices of the lowest impact energy (10 J). Using the same field of view for all the laminates, LPCN clearly exhibits a higher projected damage area, whereas LPCM displays the least. LSYM and LPCI exhibit similar projected damage contours with similar areas.

The projected damage presented above has been extruded in the laminate thickness direction to present a 3D view of the damage (Fig. 5.9) in order to: (a) identify whether the local ply clusters have induced delamination at their respective locations, and (b) understand and compare the different damage modes in the thickness direction between all the laminates. The laminates are presented as three sub-laminates where SL-1, SL-2 and SL-3 represent the top, middle and bottom sub-laminates. The clustered blocks, which consists of 9 plies, of the unsymmetrical laminates are grouped as one sub-laminate and are represented by a green box for easy comparison.

LSYM and LPCI displayed similar damage patterns when the three sub-laminates of both laminates are compared. Both laminates had their dominant delaminations in the sub-laminate closest to the non-impacted side (SL-3). Note that with LPCI, the clustered plies are in SL-1 and the dominant delaminations are found in SL-3, contrary to the prediction we made in the laminate design phase. As mentioned earlier, LPCN showed the highest projected damage and it is evident from the 3D view that all the damage is concentrated in the sub-laminate SL-3 (closest to non-impacted side), i.e., the sub-laminate where clustered plies were imposed. The delaminations within these interfaces (int. 15, 16, 17 and 18 as given in Fig. 5.1) have extended to the boundaries of the inspected field of view; something not observed in any other laminate. Finally, the LPCM laminate was found to have the least amount of

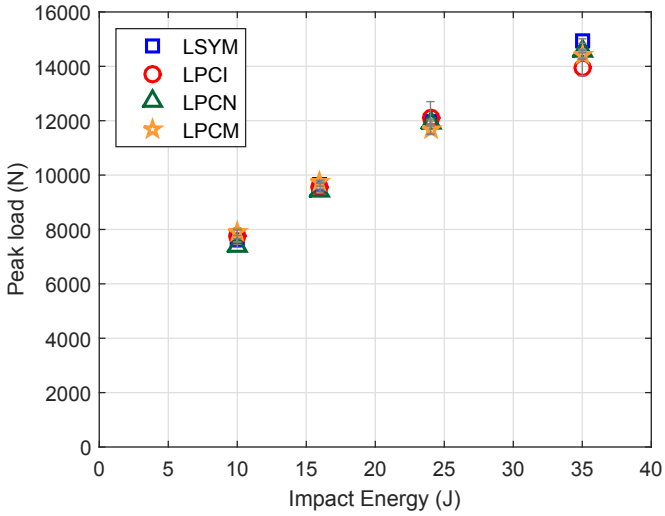

(a)

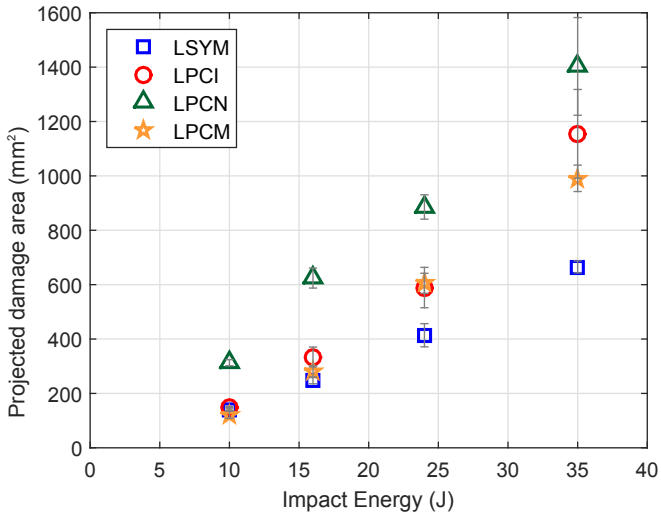

(b)

Fig. 5.6.: Impact damage resistance parameters (a) peak load and (b) projected damage area for all laminates for all impact energies

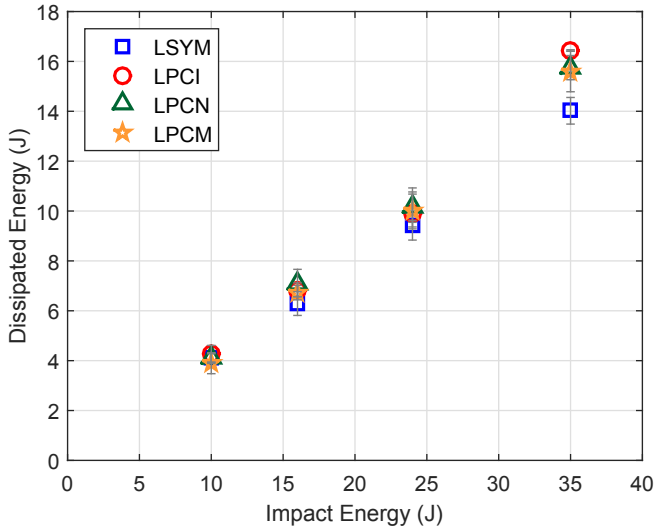

(a)

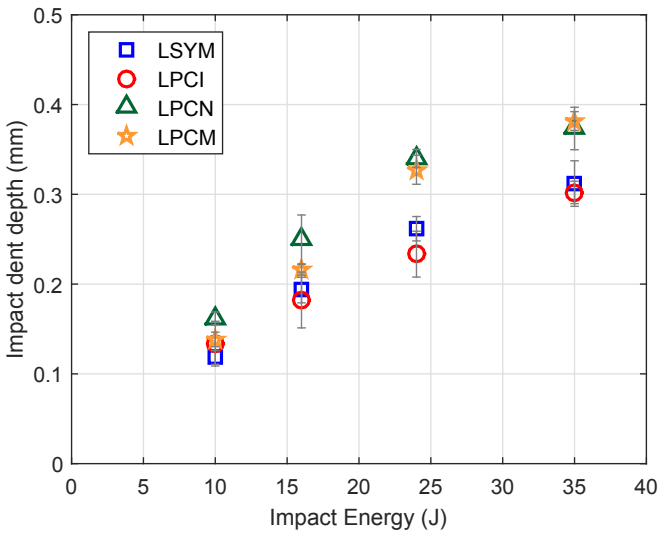

(b)

Fig. 5.7.: Impact damage resistance parameters (a) dissipated energy and (b) impact dent depth for all laminates for all impact energies

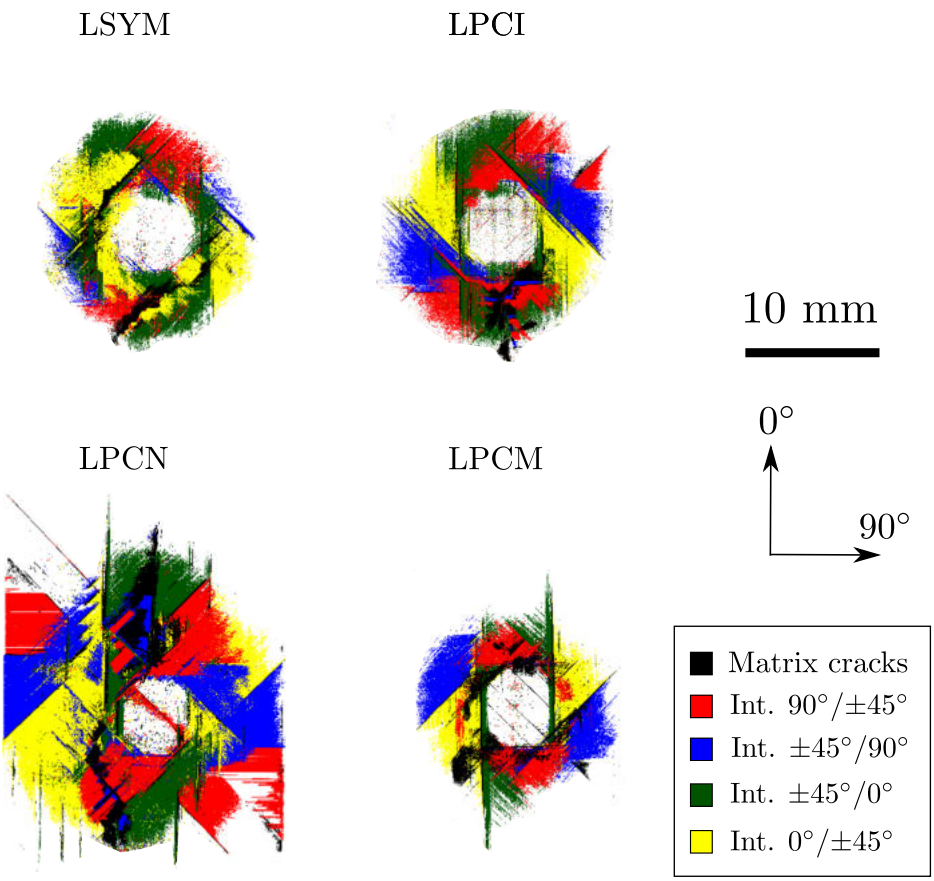

Fig. 5.8.: Projected damage footprint of all the laminates obtained from the post-processed μCT slices of the 10 J impact. Delaminations at different interfaces and matrix cracks are represented using colour codes as given in the legend and the represented field of view is 22 mm for all the laminates.

damage when compared with all the sub-laminates (SL-1, SL-2, and SL-3) of all four laminates. The dominant delamination was found in the clustered plies sub-laminate (SL-2), oriented in the 0° direction (int 10: (45/0), delamination marked by green). Note that all the laminates exhibited matrix cracks at the impacted surface (shown in black colour in the SL-1 sub-laminates) around the vicinity of the impactor.

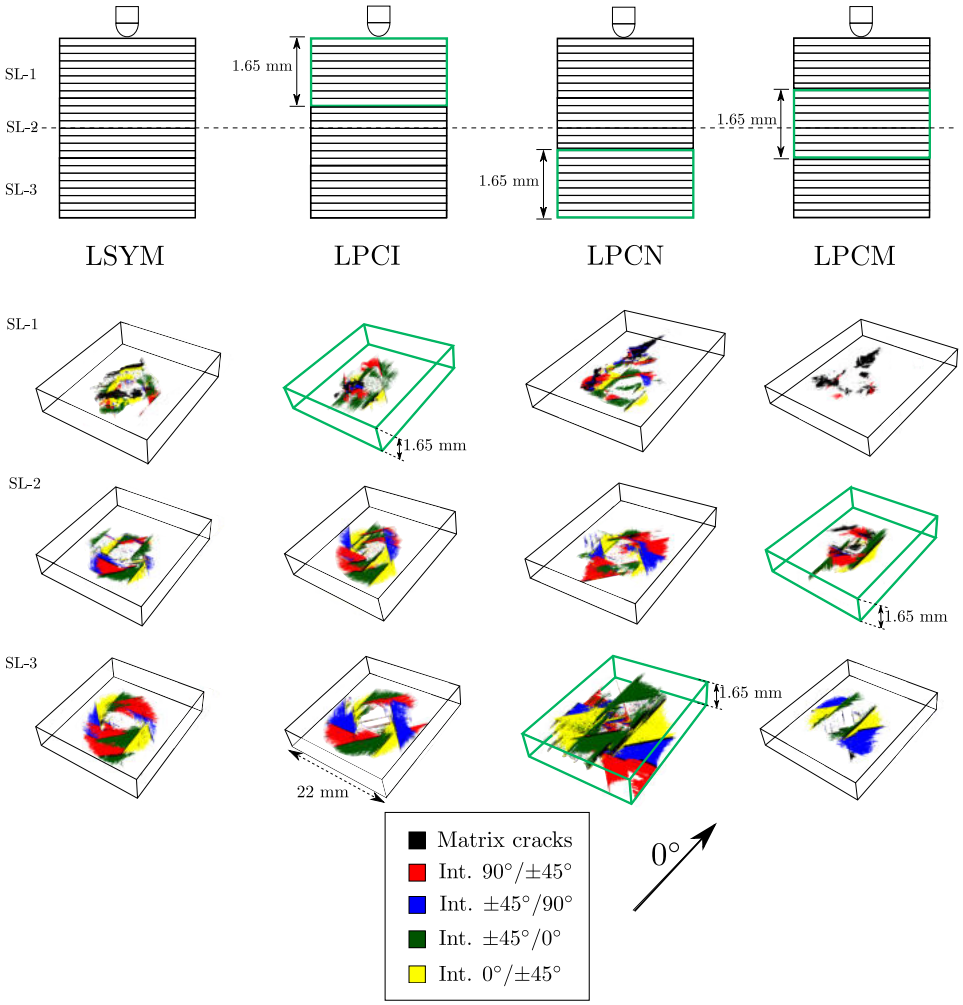

Fig. 5.9.: A 3D extruded illustration of the damage obtained from the post-processed μCT slices of the 10 J impact. Each laminate is divided into three sub-laminates and the sub-laminate containing the clustered plies of each unsymmetrical laminate is marked by a green box.

Moving to the higher impact energies, Fig. 5.10 presents the images of the C-scan

inspection (from the impacted face) of all the laminates for 16, 24 and 35 J impact energies. The dominant delaminations identified as well as the projected damage areas, are marked in the same figure. Compared to the proposed unsymmetrical laminates, the symmetric baseline laminate, LSYM, exhibited the least damage area for all the energies. Furthermore, due to the contribution of the different delaminations, it was difficult to pinpoint particular dominant delaminations. Moving to LPCI, lower energy 16 J produced a similar damage footprint as that of LSYM, but at higher energy levels the delamination at the clustered zone (Int 3: $(45_2/0_3)$, oriented in the 0° direction) became prominent. LPCN displayed the largest projected damage area compared to other laminates, and dominant delaminations were identified at the last three bottom interfaces (Int 16, 17 and 18), at the site of the clustered block. Out of the three unsymmetrical laminates, LPCM exhibited the lowest damage area, and from 24 J to 35 J, the dominant delaminations were found within the clustered zone (Int 10 $(-45_2/0_3)$) and below the cluster (Int 14 (-45/90)).

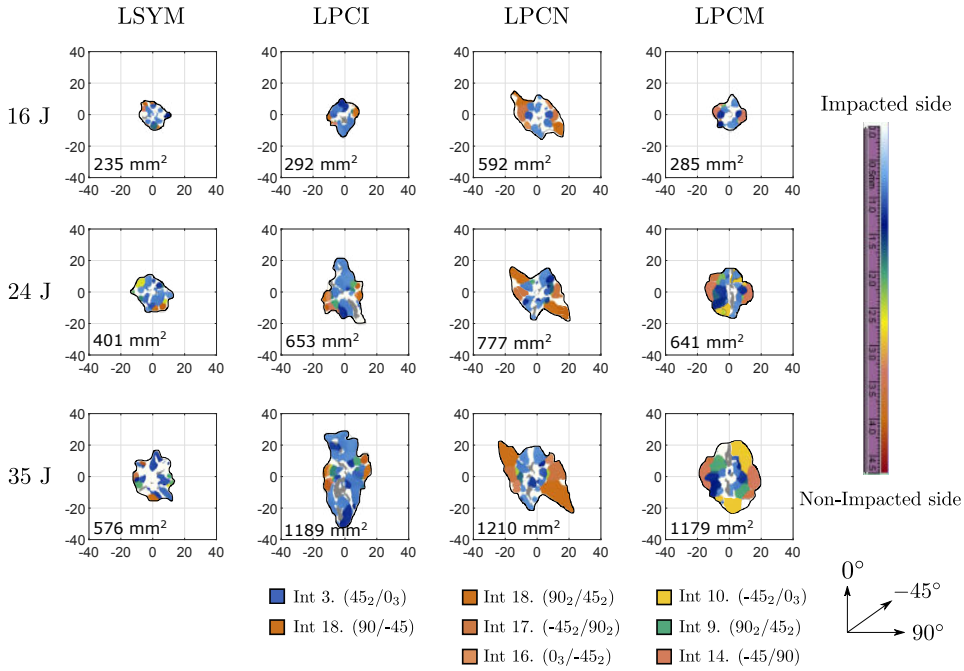

Fig. 5.10.: C-scan images of all four laminates inspected from the impacted side for the impact energies 16, 24 and 35 J. Projected delamination area is marked in the bottom left corner of each box and the field of view represented is 80 x 80 mm with the impact point as the centre.

5.4.3 Compression after impact

Fig. 5.11 (a) presents the pristine compression strengths along with the CAI strengths of all the laminates for increasing impact energies. Fig. 5.11 (b) depicts the compression strengths normalized with respect to the baseline LSYM. All three unsymmetrical laminates exhibited slightly higher plain compression strength over the baseline LSYM (LPCN and LPCI by 3% and LPCM by 7%). For the 10 J energy, LPCM exhibited the highest CAI strength out of all laminates (10% higher than the baseline LSYM), whereas LPCN exhibited the lowest (5% lower than LSYM). Moving to 16 J, LPCI showed a sudden drop in the CAI strength (from an increase of 5% for 10 J to an 8% reduction for 16 J, over the baseline LSYM). Both LPCI and LPCN showed reduced CAI strength over LSYM for the 16 J impact. Over the entire impact energy range, LPCM exhibited higher CAI strength than LSYM by an average of 8%. It should be noted that even though LPCN exhibited lower CAI strength for the first two impact energies, for the last two energies, LPCN showed the same CAI strengths as those of the baseline LSYM. On comparing the three unsymmetrical laminates, LPCM (laminate with the ply cluster in the middle) displayed higher CAI strength over the other two laminates (15% over LPCI and 10% over LPCN, considering the last three energy levels). Fig. 5.12 shows the normalized reduction (with respect to the pristine strength) in compression strength due to the impact damage for different impact energies. Almost similar strength reductions were observed with all the laminates, with LPCI exhibiting the highest reduction in residual strength, by around 60% for the higher impact energies.

Fig. 5.13 displays the macro photos of the failed CAI specimens' edge for all the laminates from the highest impact energy. The compression loading direction is represented in the figure and note that all the laminates are presented such that the impacted side of the specimen is at the top. In addition, the through-the-thickness location of the clustered block is marked by a yellow box for all unsymmetrical laminates. The dominant delaminations from the impact have propagated to the specimen edge and are seen in the figure. While in LPCI, the dominant delamination in the clustered block (at the top) is seen to have propagated and created a sub-laminate, the same is seen with the bottom delaminations of LPCN. In the case of LPCM, delamination close to the laminate mid-plane has reached the specimen edge. Hence, it is evident that the dominant delaminations (formed during impact damage)

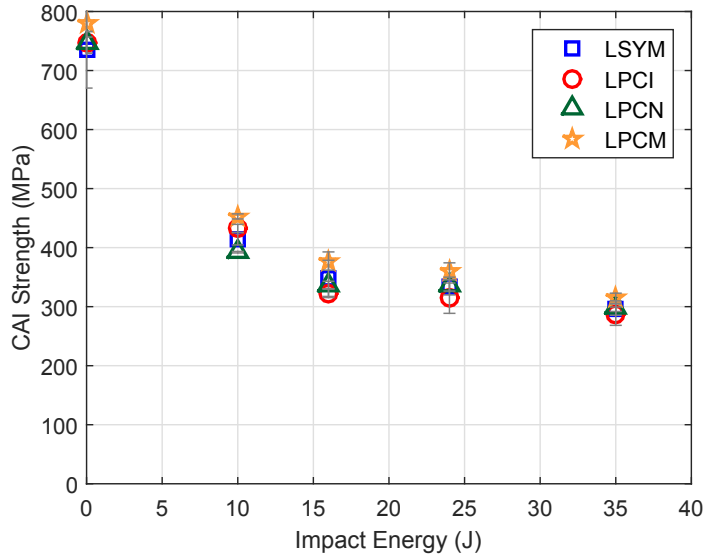

(a)

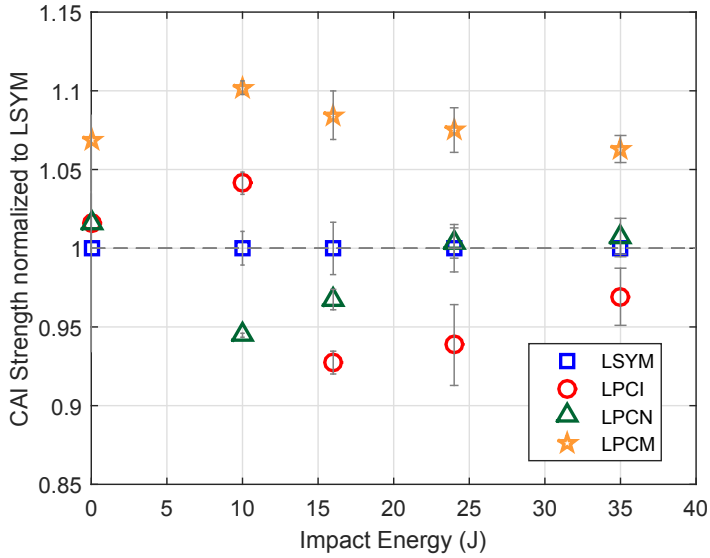

(b)

Fig. 5.11.: (a) Absolute and (b) Normalized (with respect to LSYM baseline) plain compression strengths and CAI strengths of all four laminates for all impact energies.

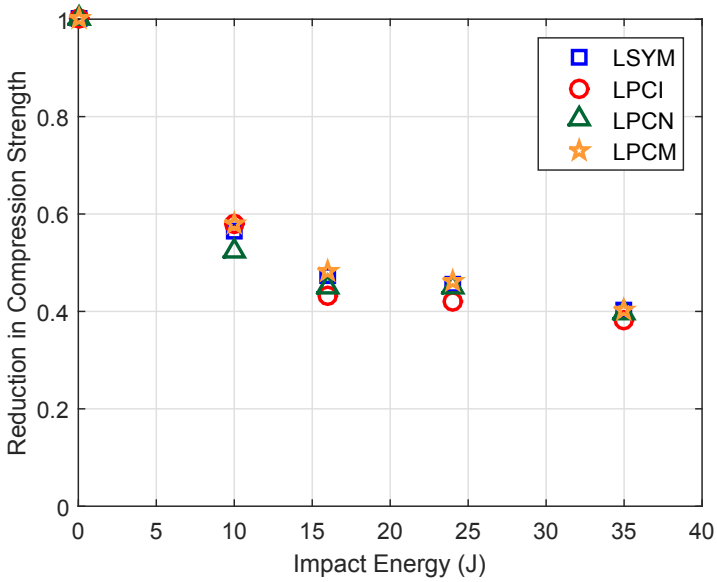

Fig. 5.12.: Normalized reduction in the compression strength due to the impact induced damage for all the impact energies.

located at the imposed clustered plies have propagated to the specimen edges to create sub-laminates during CAI loading (as reported in [12]).

Fig. 5.14 presents the evolution of the out-of-plane displacements of the LSYM and LPCM laminates obtained from LVDT-1 and LVDT-2 (placed at the centre of the impacted and non-impacted sides, respectively) during the CAI test of the 16 J impact. LVDT readings confirm that both laminates, LSYM and LPCM, buckled towards the non-impacted side during the CAI loading. LSYM buckled progressively towards the non-impacted side and finally led to the collapse of the laminate marking a maximum out-of-plane displacement of 0.2 mm. In the case of LPCM, at lower CAI loads (around 30 KN), there is a higher out-of-plane displacement compared to LSYM. But with increased loading, there is a saturation in the displacement value, evidence of the laminate resisting buckling. At the failure load, the out-of-displacement observed is roughly similar to the value seen at lower CAI loads. Furthermore, the final out-of-plane displacement value at the point of laminate failure is four times lesser for LPCM compared to LSYM. LPCI showed similar out-of-displacement values as LSYM but buckled globally towards the impacted side. LPCN behaved differently with respect to the impact energy levels. For the lower energy levels, LPCN showed

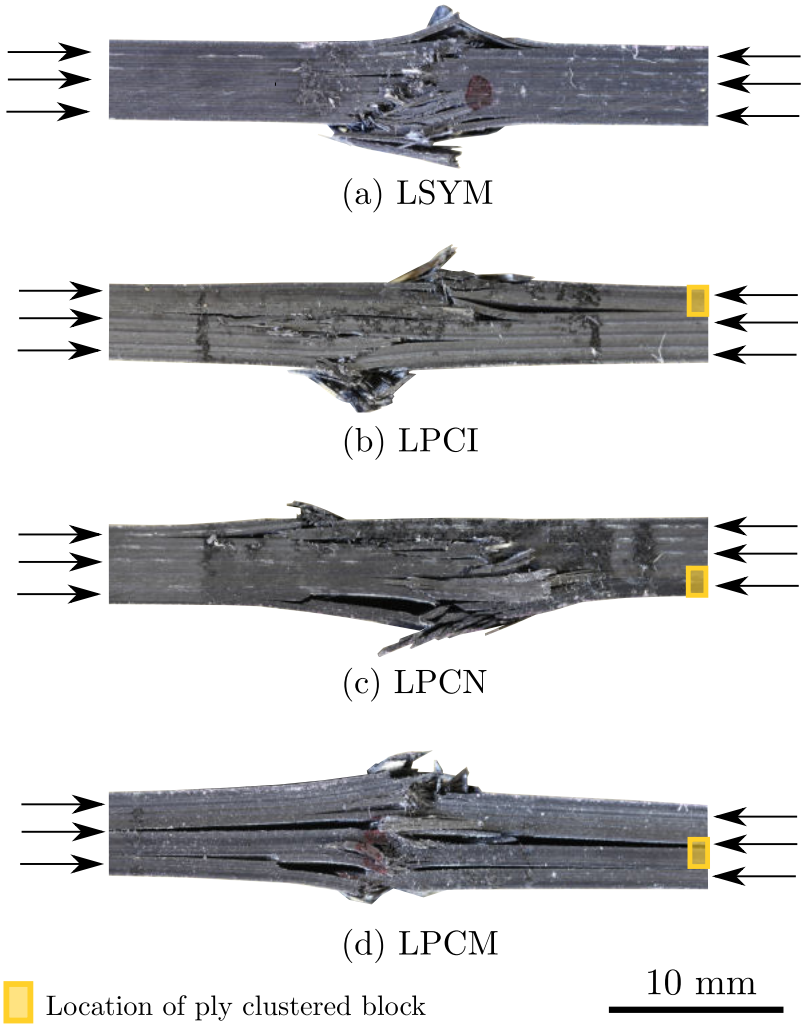

Fig. 5.13.: High resolution macro photos of the specimen edges showing the final CAI failure state of all four laminates (location of the clustered block is shown by the yellow box).

an open buckling mode where the impacted side and non-impacted side buckled towards the respective sides. Meanwhile for the higher energies it buckled as a whole towards the impacted side.

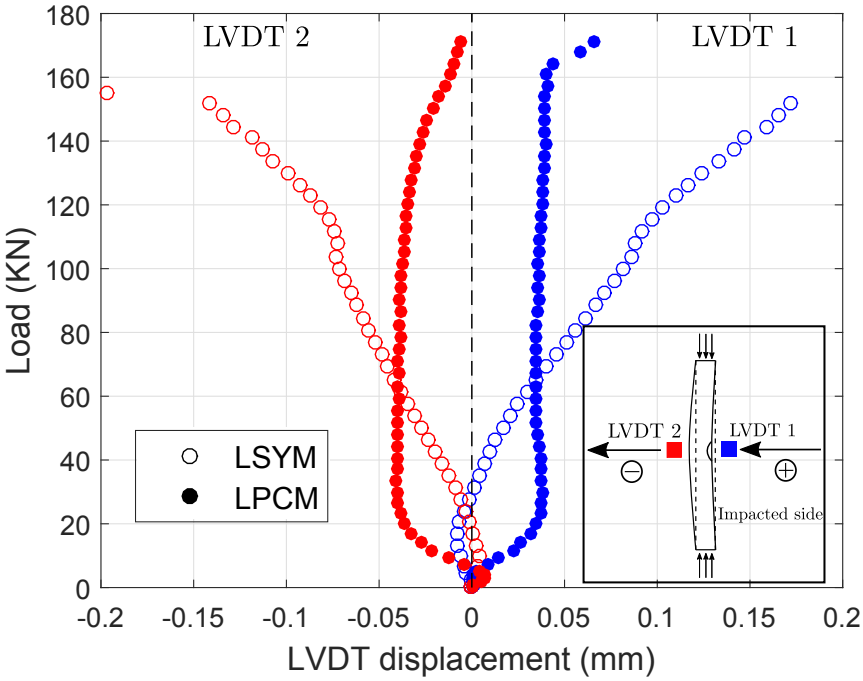

Fig. 5.14.: Out-of-plane displacements recorded by the LVDTs placed at the impacted and non-impacted face laminate centres during the CAI loading of a 16 J impact for LSYM and LPCM laminates (Note that blue indicates LVDT 1 placed at the impacted side and red indicates LVDT 2 placed at the non-impacted side. Outwards buckling (shown by the black arrows in the sub-figure) is indicated by positive values of LVDT 1 and negative values of LVDT 2).

5.5 Discussion

5.5.1 Impact damage analysis

During an impact, the laminate bends towards the non-impacted side which introduces in-plane tensile stresses in the bottom plies. The tensile loads induce transverse matrix cracks in the bottom plies, and, in addition, due to bending, the bottom interfaces are subjected to higher interlaminar shear stresses. The transverse tensile cracks and the shear cracks link up in the through-the-laminate thickness to induce delamination. Hence, in a conventional impact damage morphology, the laminate

exhibits a spiral stair-case delamination pattern (as reported in [5, 14]), where the delaminations are extended in the bottom interfaces and are reduced towards the impacted side. This is similar to what is seen in LSYM and LPCI for the 10 J impact case from the post-processed tomography images (Figs. 5.8 and 5.9). In addition, the existence of an undamaged cone under the impactor, as observed in [7], is evident in all the laminates studied (Fig. 5.9).

Further, when the similar oriented plies are clustered, they introduce a higher bending stiffness mismatch [18] and thereby higher interlaminar shear stresses at the adjacent interfaces compared to the non-clustered ply interfaces. Moreover, the transverse cracking is less constrained in the thicker plies (i.e., clustered) compared to the non-clustered, due to the in-situ effect [58]. Hence, as explained above, the bottom interfaces of the laminate are more prone to having extended delaminations compared to other locations, and clustering the plies at the bottom (as in laminate LPCN) serves as a catalyst to the already prone delaminations at the bottom. These bottom-clustered plies act as a source of early initiation of cracks and delamination and hence the delamination threshold load was seen to be the least for LPCN (as in Fig. 5.4). This also explains the reason behind the large extended delaminations found in the bottom sub-laminate for LPCN compared to the other laminates (Figs. 5.9 and 5.10).

In the case of LPCI (where the localised cluster is placed in the top sub-laminate), the lowest energy level 10 J failed to impose dominant delaminations at the top of the laminate (as was expected during the laminate design phase). Nevertheless, they were seen at the bottom sub-laminate similar to the case of LSYM. This is due to the effect of local through-the-thickness compressive stresses right under the impactor that delay the delamination by increasing interlaminar shear strength and mode II fracture toughness [107, 108, 120, 128]. However, for the higher impact energies, the C-scans inspections (Fig. 5.10) reveal that the dominant delaminations are formed at the location of the clustered plies, as the delaminations have extended outside the local compressive region thereby counterbalancing the effect of the local compressive stresses.

On the other hand, LPCM (where the cluster is in the middle of the laminate) also followed the predictions of the laminate design (delamination was observed at the middle sub-laminate, Fig. 5.9), even though smaller, but significant delaminations,

were found in the bottom sub-laminate too. The delaminations induced by the clusters in the mid-plane have significantly reduced or even avoided the delaminations at the top and bottom sub-laminates, when compared to the other three laminates. At higher energies, the delaminations within the clustered zone were prevalent, as evidenced by the C-scan images. Hence, the idea of forcing delamination to occur at desired places through laminate design techniques is demonstrated.

Despite the similar impact response curves by all the laminates for all the impact energies, the increased projected damage area for the unsymmetrical laminates over the symmetric baseline laminate is a result of the effect local clustered plies have. The effect the through-the-thickness delamination location has on impact resistance is evidenced by LPCM's reduced damage area and dissipated energy.

5.5.2 Effect of local ply clusters and delamination location on CAI strength

The small improvement in the plain compression strength of the unsymmetrical laminates over the baseline (Fig. 5.11) signifies that the thicker plies (or clustered plies), mainly the 0° plies, help in effectively carrying the compressive load. Further, the effect of the position of the local cluster is also significant as the laminate with the cluster at the middle showed higher compression strength over the ones with the clustered blocks placed at the specimen surfaces (top or bottom as in LPCI and LPCN, respectively). LPCM improved the CAI strength over LSYM due to the effect of clustered plies (mainly 0° plies) and the mid-plane location of the dominant delaminations it imposed. The lower CAI strength of LPCN and LPCI over LPCM shows that delaminations closer to the mid-plane resist buckling compared to the surface delaminations under compression loading. This is in line with the conclusions from the numerical studies in [12, 25], which reported that near surface delaminations induced buckling at lower loads.

The LPCN laminate exhibited different buckling modes depending on the impact energies. For lower energies, the dominant delaminations of LPCN at the bottom split the bottom sub-laminate from the rest of the laminate, and the plies within this sub-laminate easily buckled outwards to the non-impacted side. But for higher energies, the same bottom sub-laminate buckled inwards to the impacted side where the intact top sub-laminate helps resist and delay the final failure. This could be the

reason behind the lesser reduction in the CAI strength of LPCN (almost the same CAI strength as LSYM at 24 and 35 J) when moving from lower to higher energies.

Similarly with LPCI, the dominant delaminations split the laminate where the clustered block at the top can easily buckle outwards due to the reduced stiffness of the sub-laminate. In the case of LPCM, the out-of plane displacements suggest that there was initial global buckling towards the non-impacted side, but that the delamination propagation split the laminate into sub-laminates with the intact clustered block taking the compression load (Fig. 5.13). In addition, this cluster of plies (especially the 0° plies) resisted buckling (as also reported in [129]) because of the surrounding plies at the top and bottom. This is in agreement with the results reported in [13, 129], where clustered plies improved the damage tolerance through reduced buckling. Hence, it was the compressive failure of the main load-bearing plies that triggered the final CAI collapse (as evidenced in Fig. 5.14). This alternative failure mechanism of compressive fibre fracture because of the buckled plies was also reported in [22]. It is worth remarking that even though complete clustering of a laminate was reported to impair the impact resistance and damage tolerance [11, 42], clustering plies locally is observed as being advantageous in this study (as also reported by Sebaey et al. [13]).

5.5.3 Damage resistance parameters v/s CAI strength

The similar impact response curves of the different laminates elucidate the effectiveness of the laminate design study where the laminates were designed to have similar in-plane and bending responses for fair comparison. Since all four laminates have similar impact responses, it holds this as a fair platform from which the correlation of different impact resistance parameters on CAI strength can be studied. Aircraft manufacturers still use projected damage area to correlate CAI strength, where a higher area denotes less CAI strength. From this study, it is clear that projected damage area is a very misguiding parameter to relate CAI strength to, as also observed in [110]. For the highest impact energy, LPCN showed 115% increased damage area compared to the baseline LSYM, but both laminates showed similar CAI strength values. Similarly, the unsymmetrical laminate, LPCM, showed 7% higher CAI strength despite having 55% higher projected damage area over LSYM for the 35 J impact. A similar trend is seen for dissipated energy, where the lower dissipated

energy of LSYM did not proportionate to a higher CAI strength. Moreover, it is also observed that if a laminate has a higher resistance to the onset of delamination (LPCI in this case), this does not imply a higher CAI strength. LPCI delayed delamination onset and LPCN exhibited early delamination onset, but finally LPCN displayed higher CAI strength over LPCI. Hence, it is clear that CAI damage morphology is too complex to be predicted or correlated with the impact resistance parameters. The final failure is seen to depend more on the through-the-thickness position of the dominant delamination, the thickness of the sub-laminates formed during CAI loading and the buckling modes of the sub-laminates, rather than simply just the damage resistant parameters (as discussed above).

From an industrial point of view, the damage tolerance concept suggests that the structure should have enough strength to continue in service until the damage is detected by a scheduled inspection. A dent depth greater than 0.25 mm has greater probabilities of being detected during a visual inspection [130], and the corresponding energy level is termed as BVID energy level. Hence, in combining the laminate residual strength and the damage detectability, laminates LPCM and LPCN displayed higher dent depth (BVID energy level of 24 J) than LSYM and LPCI (BVID energy level of 36 J). Thus, despite having higher (as for LPCM) or equal (as for LPCN) CAI strengths compared to LSYM, the chances of detecting the damage in LPCM or LPCN are also greater compared to LSYM. The worst case is when the cluster is placed at the impacted side (as in LPCI), where the CAI strength and the chances of detecting the damage are the lowest, leading to a critical situation.

5.5.4 The prospects of unsymmetrical laminates

Using warp-free unsymmetrical stacking sequences, we have exhibited the capability to improve the damage tolerance compared to the standard ASTM baseline laminate. It should be kept in mind that even though the improvement is not dramatic, it was achieved economically by simply clustering some plies and through an unsymmetrical design (without reinforcing the material system or using dispersed ply orientations [10, 13]). That said and putting this improvement to one side, the different unsymmetrical laminates helped to obtain a clear understanding of the effect delamination position has on CAI strength, which until now had been missing, despite the conclusions reported from numerical and analytical studies [25, 26].

With the objective to investigating the CAI response of unsymmetrical laminates and their comparison with a symmetric baseline laminate) missing from the previous work [120], this study demonstrates that symmetric laminates are not the optimal damage tolerant solution to impact loading cases. A similar conclusion was reported by Baker et al. [49] supporting the idea of unsymmetric laminate design. In instances such as aircraft skins, unsymmetrical laminates may be a promising solution (e.g., for higher impact damage tolerance or higher electrical conductivity). Furthermore, unsymmetrical laminates can be looked upon as being an option to design hybrid laminates tailored for impact loads (as performed by the authors with thin laminates [124]), where the plies on the impacted side can be designed with thick plies and the non-impacted side with thin plies, thereby mitigating the critical delamination damage at the non-impacted side using thin plies.

5.6 Conclusion

This study extends the findings of a previous work [120] on unsymmetrical laminates tailored for impact resistance by evaluating the compression after impact strength and providing a comparison with a symmetric baseline laminate. In this paper, we designed three warp-free unsymmetrical laminates to have local ply clusters placed at the impacted side, middle and non-impacted side of the respective laminates, with the aim of imposing delaminations at these particular through-the-thickness locations. By means of low velocity impacts, X-ray tomography and ultrasonic C-scan inspection of the impacted specimens and compression after impact tests, we compared the impact responses, damage and the compression after impact strengths to that of a symmetric baseline laminate. The site of dominant delaminations at the location of clustered plies in the unsymmetrical laminates supports the concept that damage can be imposed at desired locations through laminate design. Despite the reduced impact resistance (50% increased damage area and 10% higher energy dissipated) over the baseline laminate, the unsymmetrical laminate with ply clusters at the middle improved CAI strength by 10%. The same laminate with delamination in the middle buckled the least under CAI (four times lesser out-of-plane displacements compared to symmetric baseline laminate) and increased the failure load (by 15%) over the other unsymmetrical laminates with delamination at the outer surfaces. We demonstrated that unsymmetrical over symmetrical laminates can offer improved

CAI strengths and can be an optimal solution for application in structures such as aircraft skins.

6

Paper C: Effect of ply thickness and ply level hybridization on the compression after impact strength of thin laminates

A. Sasikumar[a,*], D. Trias[a,1], J. Costa[a,*], N. Blanco[a], J. Orr[b], P. Linde[c,d]

[a] AMADE, Polytechnic School, Universitat de Girona, Campus Montilivi s/n, E-17003 Girona, Spain

[b] University of Dayton Research Institute, 300 College Park, Dayton, OH, USA

[c] Airbus Operations GmbH, Kreetslag 10, 21129 Hamburg, Germany

[d] Department of Industrial and Materials Science, Chalmers University of Technology, S-41296 Gothenburg, Sweden

[*] Corresponding author

[1] Serra Hunter Fellow

The paper has been published in *Composites Part A: Applied Science and Manufacturing* 121 (2019) 232–243.

Motivation & Synopsis

The previous two papers pointed out the fact that symmetric laminates are not the optimal impact damage tolerant solutions and opened up the possibility to consider novel unsymmetrical designs. At this instance, the manufacturer's shifted their interest from thick to thin laminates, due to the usage of thinner structures in aircrafts. Despite the extensive impact studies performed on thick laminates, clear understanding of the response of thin laminates towards impact loads was yet questionable. In addition, how ply thickness affects the compression after impact (CAI) strength of thin laminates was missing. Hence as a part of the Airnet project with Airbus, this paper is built to answer the above questions. Thick, intermediate and thin ply thin laminates are experimentally tested under impact and CAI, and in addition two hybrid laminates, where different ply grades are mixed, are proposed and tested. Experimental results revealed that thin laminates made of thin plies exhibit extensive fibre damage leading to a reduced CAI strength. The idea of ply level hybridization shows promising results with a significant improvement in the CAI strength.

Composites Part A 121 (2019) 232–243

Contents lists available at ScienceDirect

Composites Part A

journal homepage: www.elsevier.com/locate/compositesa

Effect of ply thickness and ply level hybridization on the compression after impact strength of thin laminates

A. Sasikumar[a,*], D. Trias[a,*,1], J. Costa[a], N. Blanco[a], J. Orr[b], P. Linde[c,d]

[a] AMADE, Polytechnic School, Universitat de Girona, Campus Montilivi s/n, 17073 Girona, Spain
[b] University of Dayton Research Institute, 300 College Park, Dayton, OH, USA
[c] Airbus Operations GmbH, Kreetslag 10, 21129 Hamburg, Germany
[d] Department of Industrial and Materials Science, Chalmers University of Technology, S-41296 Gothenburg, Sweden

Abstract

There is a lack of research available on how thin laminates respond to impact and post impact loads, even though thin structures are used in present-day aircrafts. This experimental paper employs thick, standard and thin uni-directional plies to investigate the effect ply thickness has on thin laminates on their impact and compression after impact (CAI) response. Further, we propose two hybrid laminates where thick or standard plies are mixed with thin plies, respectively, in an effort to improve the CAI strength of thin laminates. Results reveal that, contrary to thick laminates, thin laminates made of only thin plies exhibit extensive fibre failure, leading to a considerably reduced CAI strength. Moreover, the hybrid laminate where thick 0° plies are mixed with thin plies improves the CAI strength by 40% over the thin ply baseline laminate. Thus, hybridization with thin laminates appears to be an economic prospective in terms of improving damage tolerance.

Keywords: Impact behaviour, Compression after impact, Damage mechanics, Damage tolerance, Ply hybridization

6.1 Introduction

One of the aeronautic industry's main concerns is the impact behaviour of thin structures (< 2 mm), such as fuselages and wing skins, because low velocity impact can drastically reduce their residual structural strength [5]. However, many studies are

devoted to investigating the impact and compression after impact (CAI) response of "standard"thickness laminates ($\approx$ 4 mm, as recommended in ASTM D7136/D7136M-15 [64]), along with the effect ply thickness has on CAI strength [55, 61, 62].

Previous studies have shown the improved performance of thin plies over standard and thick plies in terms of first ply failure and delay of damage onset [60, 63, 131]. In the framework of impact and post impact response, research investigations [61, 62] reported an average improvement of 20% in CAI strength with thin plies for laminates with thicknesses ranging between 3.6 to 4.4 mm. Thin-ply laminates showcased quasi-brittle failure instead of extended cracking and delaminations as observed in thicker plies. Reviewing thinner laminates, Garcia et al. [32] recently studied the effect of ply thickness on CAI strength with 2.15 mm thick non-crimp fabric laminates. Standard plies showed similar and 27% higher CAI strength when compared to thin plies at 10 and 14 J impact energies, respectively. Hardly any work related to CAI response is reported for laminates with thicknesses less than 2 mm, albeit with the exception of Sanchez et al. [66], who compared CAI strength between quasi isotropic, cross ply, and woven fabrics made out of thick plies for laminates ranging from 1.6 to 2.2 mm in thickness.

Laminate design [9, 11, 44, 120] and material system reinforcement [32, 132, 133] are two approaches used to improve impact damage resistance and more specifically CAI strength. Laminate design, understood as tailoring the stacking sequence, is considered more economically feasible than material reinforcement. For instance, ply level hybridization consists of mixing plies of different thicknesses in an attempt to enhance a targeted response. Sihn et al. [55] suggested this approach for future work to improve the impact damage resistance of composite structures without increasing the layup costs. Furtado et al. [46] performed selective ply hybridization with different types of fabric architectures by mixing thin and intermediate fabric layers, which eventually resulted in an improved notched response. Arteiro et al. [47] demonstrated that blocking 0° fabric layers improves the structural behaviour of aerospace graded thin ply laminates. Sebaey et al. [48] studied the effect mixing thin and thick fabric layers has on damage tolerance using thick laminates, and when compared to the baseline thin ply, reported an increase of 15% in CAI strength for a configuration of thick plies surrounded by thin plies.

This study is the result of an industrial investigation headed by Airbus, in collaboration with the AMADE research group (University of Girona), INEGI (University of Porto) and the University of Dayton Research Institute, USA. The study investigates the effect of ply thickness on impact damage resistance and CAI strength through impact and CAI experimental tests for thin laminates ranging between 1.5 and 1.8 mm. Thick (268 gsm), standard (134 gsm), and thin (75 gsm) uni-directional (UD) plies are selected for the ply thickness study. Additionally, we study two hybrid laminates, the first of which is a mix of standard 0° plies and thin plies, while the second contains thick 0° plies along with thin plies. Results show that thin plies within thin laminates exhibit extensive fibre breakage and lead to the lowest CAI strength. Ply thickness hybridization alleviated the amount of fibre failure with increased delamination damage, and improved the CAI strength remarkably over the baseline thin ply.

6.2 Experimental methods

6.2.1 Material and Layup

Uni-directional prepreg tapes of T700/M21 carbon-epoxy supplied by Hexcel were used to prepare the panels required for the study. We used three ply grades, namely thick (268 gsm), standard (134 gsm) and thin (75 gsm) and hereafter the corresponding laminates prepared from them are referred to as H-268, H-134 and H-75, respectively. Furthermore, two hybrid laminates were proposed and are referred to as H-75-H1 and H-75-H2, where thin 0° plies are substituted by standard and thick 0° plies, respectively. Only 0° plies (thick and standard) were considered to be mixed with thin plies for ply hybridization, as they are the main load bearing plies during CAI loading. Fig. 6.1 illustrates the five different laminates and Table 6.1 describes the laminates, their stacking sequences and the ply and laminate thicknesses. Despite the fact that laminates consisted of different ply grades, the stacking sequences were designed to have the closest possible equivalent bending stiffness (D*, proposed by Olsson [123]) to guarantee a fair comparison. The D* values of the laminates are 27.5 (H-268), 22.1 (H-134), 17.6 (H-75), 18.3 (H-75-H1) and 20.4 Nm (H-75-H2). Additionally, note that all the laminates are centre-symmetric (denoted by $ in Table 6.1), which means that the axis of symmetry runs through the middle of the centre ply, so they are not in-plane quasi-isotropic.

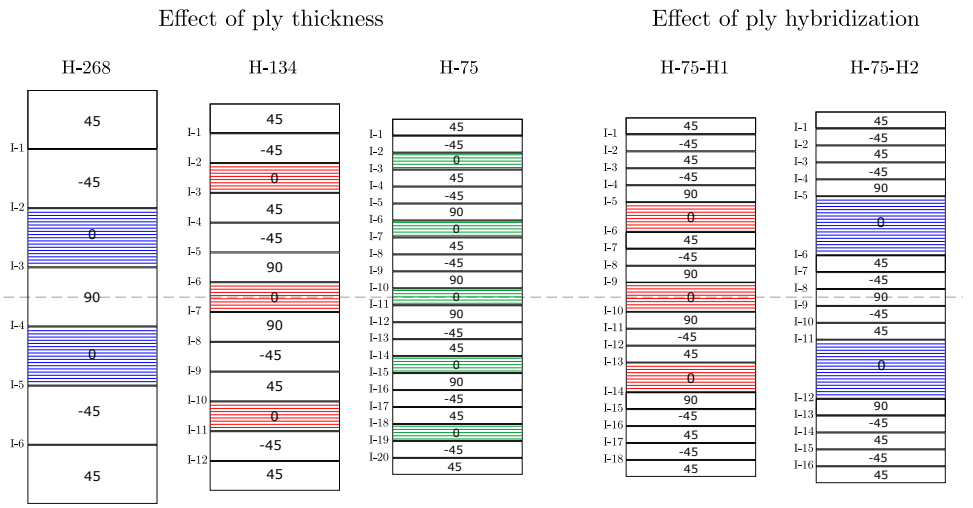

Fig. 6.1.: Illustration of all the laminates used to study the effect of ply thickness and ply hybridization on damage tolerance (corresponding laminate interfaces are also marked). Note that all the laminates are centre symmetric, which means that the axis of symmetry runs through the middle of the centre ply.

Tab. 6.1.: Laminates and their details

Laminate	Description	Stacking sequence	Ply thickness (mm)	Nominal laminate thickness (mm)
H-268	Thick plies	$[45/\text{-}45/0/90]_{\text{“\$”}}$	0.262	1.83
H-134	Standard plies	$[45/\text{-}45/0/45/\text{-}45/90/0]_{\text{“\$”}}$	0.131	1.70
H-75	Thin plies	$[45/\text{-}45/0/45/-45/90/0/45/\text{-}45/90/0]_{\text{“\$”}}$	0.075	1.58
H-75-H1	Thin & Standard plies	$[45/\text{-}45/45/\text{-}45/90/0_{134}/45/-45/90/0_{134}]_{\text{“\$”}}$	0.075 & 0.131	1.59
H-75-H2	Thin & Thick plies	$[45/\text{-}45/45/\text{-}45/90/0_{268}/45/-45/90]_{\text{“\$”}}$	0.075 & 0.262	1.65

* $ represents centre symmetry, which signifies that the axis of symmetry is along the middle of the centre ply.

6.2.2 Impact energy definition

As seen in the Table 6.1, using different ply grades raises the issue of having different laminate thicknesses. A significant 20% difference in measured thickness was noted between the thickest (H-268) and thinnest (H-75) laminate. Instead of impacting all the laminates with a same absolute energy, we introduced impact energies normalized to the measured laminate thickness in order to reduce the biasing on thicker laminates. In fact, ASTM D7136/D7136M-15 [64] also recommends defining impact energies normalized to the specimen thickness, as thicker laminates have an advantage over thin ones when impacted at the same absolute energy. Hence, we defined a total of four impact energies for the impact study: two absolute impact energies irrespective of the laminate thickness and two impact energies normalized with respect to the laminate thickness. Therefore, 5 J and 10.5 J were defined as the two absolute energies and will be referred to as IE_1 and IE_4, respectively. While the lowest impact energy 5 J was chosen to study the initiation of damage, the highest impact energy of 10.5 J was supposed to create barely visible damage according to the recommendations of ASTM D7136/D7136M-15 standards [64]. The two normalized energies were defined as 4.1 J/mm and 5.2 J/mm, and will be referred to as IE_2 and IE_3, respectively. The normalized energies 4.1 J/mm and 5.2 J/mm were determined such that their corresponding absolute energies were spaced evenly between the least (5 J) and highest (10.5 J) impact energies for all the laminates, whereas the highest energy value of 10.5 J was chosen with the aim of creating a barely visible impact damage (BVID) in the laminate. Table 6.2 displays the four impact energies defined for all the laminates.

Tab. 6.2.: Laminates and the defined impact energies

Laminate	Measured laminate thickness (mm)	Impact Energy 1: IE_1		Impact Energy 2: IE_2		Impact Energy 3: IE_3		Impact Energy 4: IE_4	
		Abs (J)	Norm (J/mm)	Abs (J)	Norm (J/mm)	Abs (J)	Norm (J/mm)	Abs (J)	Norm (J/mm)
H-268	1.85	5	2.7	7.6	4.1	9.6	5.2	10.5	5.7
H-134	1.70	5	2.9	7	4.1	8.9	5.2	10.5	6.2
H-75	1.56	5	3.2	6.4	4.1	8.2	5.2	10.5	6.7
H-75-H1	1.54	5	3.2	6.3	4.1	8	5.2	10.5	6.8
H-75-H2	1.65	5	3	6.8	4.1	8.6	5.2	10.5	6.4

6.2.3 Experimental tests

6.2.3.1 Impact and damage inspection

Impact tests were performed according to the ASTM D7136/D7136M-15 standards [64] using a CEAST Fractovis Plus instrumented drop-weight tower on impact specimens of dimensions 150 x 100 mm (with 0° fibres aligned with the specimen length). A 16 mm in diameter steel hemispherical impactor was used, and the total impactor setup was 3 kg. We tested a total of 12 specimens for each laminate, using 3 specimens for each impact energy level to validate the repeatability. The reader is referred to [42] for further details of the impact setup. Pulse-echo ultrasonic C-scan inspection was performed on all the impacted specimens using an OLYMPUS OMNI MX system. An automated robotic arm scanned the specimen placed inside a pool of water with a 5 MHz piezoelectric probe.

6.2.3.2 Plain compression and compression after impact (CAI)

To evaluate the reduction in the compression strength due to the impact damage, the compressive strength of the pristine specimens was first obtained. Instead of using pristine standard impact specimens, plain strength compression tests were performed following the ASTM standards D6484/D6484M-14 [87]. These tests were performed at the INEGI research laboratory at the University of Porto for all the five laminates defined above. Three specimens of dimensions 305 mm by 30 mm for each laminate were tested. Detailed information about the test setup is given in [131]. In addition, CAI tests were performed using an MTS INSIGHT300 machine with a 300 kN load cell, complying with the ASTM standards D7137/D7137M-15 [88]. All three impacted specimens per energy level were subjected to CAI test, to provide evidence of the scattering of the results. Both the above-mentioned compression tests were performed at a cross head displacement loading rate of 0.5 mm/min. To account for the thin laminates, we used an additional non-standard anti-buckling CAI device proposed by Remacha et al. [67]. Apart from the standard CAI device, this fixture utilizes a support structure with a set of vertical ribs that helps to avoid the premature buckling of such thin laminates, thus increasing their global buckling load. These extra supporting plates are clamped onto the CAI test setup with a pre-defined torque value of 5 Nmm. A rectangular window of 52 x 42 mm at the impacted site is left free from vertical ribs to allow for the impact damage to propagate and cause final

failure. This modified CAI fixture claims that the specimen fails by compression at the impacted region and not due to global buckling of the thin laminate. Further details about this anti-buckling device can be found in [67]. All the above-mentioned tests, except plain strength compression, were performed at the AMADE research laboratory in Girona, which is NADCAP certified for non-metallic-materials testing.

6.3 Experimental results

6.3.1 Impact response & damage assessment

The impact response of all the laminates is presented in terms of impactor force-time, impactor force-displacement, and energy evolution response curves in Figures 7.4, 7.5, and 7.6, respectively. Despite testing three specimens for each energy level, due to the good repeatability of the results, only one specimen data curve per energy level is presented.

The delamination load drop observed for the thick laminates, termed as delamination threshold load F_d, is not observed for the thin laminates [32, 65] (Fig 7.4 and 7.5). Most laminates exhibited a load drop close to or at maximum peak load, with H-134, H-75, H-75-H1 showcasing a high load drop at IE_4 due to fibre failure. H-75 laminate exhibited extended response in impact time and higher displacement for all the impact energies. Fig. 7.6 shows that H-75 has comparatively higher energy dissipation than the other laminates at all the impact energies, whereas H-75-H2 dissipated the least amount of energy at higher impact energies. At IE_4, laminates comprising thick plies (H-268 and H-75-H2) showed much less energy dissipation compared to the laminates comprising thin and standard plies (H-134, H-75, H-75-H1).

Fig. 6.5 displays the projected damage profile and the area enclosed from the C-scan inspection of all the laminates at all energies. H-268 displayed the highest projected damage area, with an extended delamination at the last interface -45°/45° oriented in the 45° (Note that the interfaces are numbered starting from the impacted side, with the last interface denoting the one closest to the non-impacted face, as in Fig. 6.1). H-134 exhibited the least damage area out of all the laminates for all impact energies, with the dominant delamination seen below the mid-plane (interface no.9: (-45°/45°) as in Fig. 6.1). H-75 and hybrid laminate H-75-H1 displayed similar damage profiles

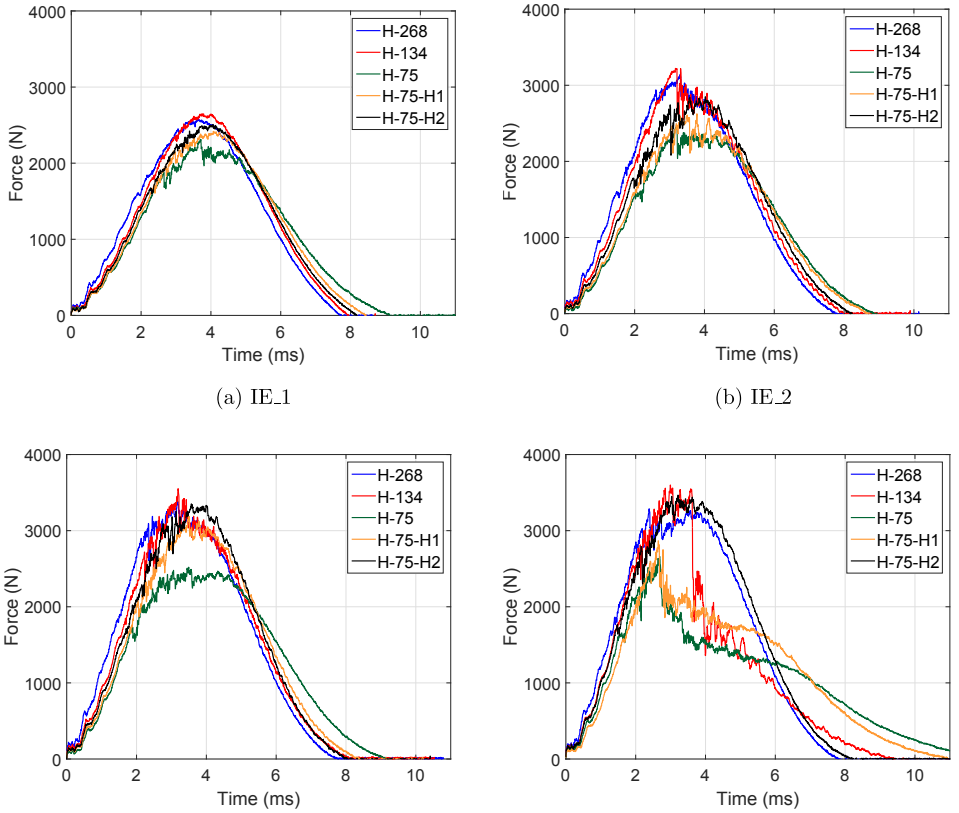

(a) IE_1 (b) IE_2

(c) IE_3 (d) IE_4

Fig. 6.2.: Force-time response of all the laminates for all the impact energies.

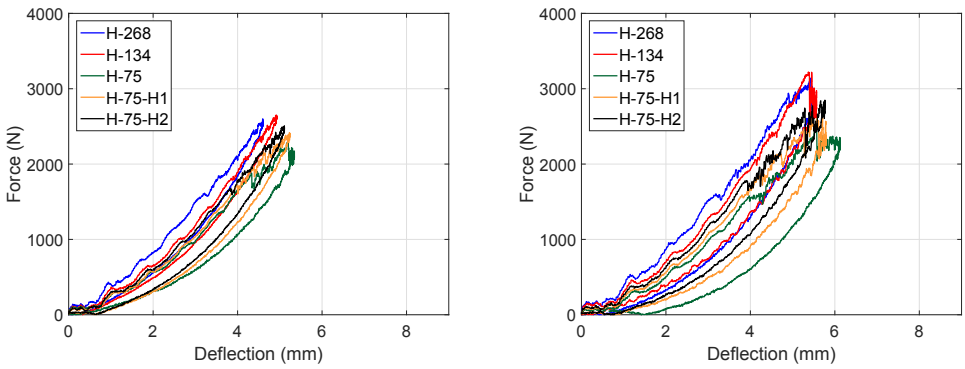

(a) IE_1 (b) IE_2

(c) IE_3 (d) IE_4

Fig. 6.3.: Force-deflection response of all the laminates for all the impact energies.

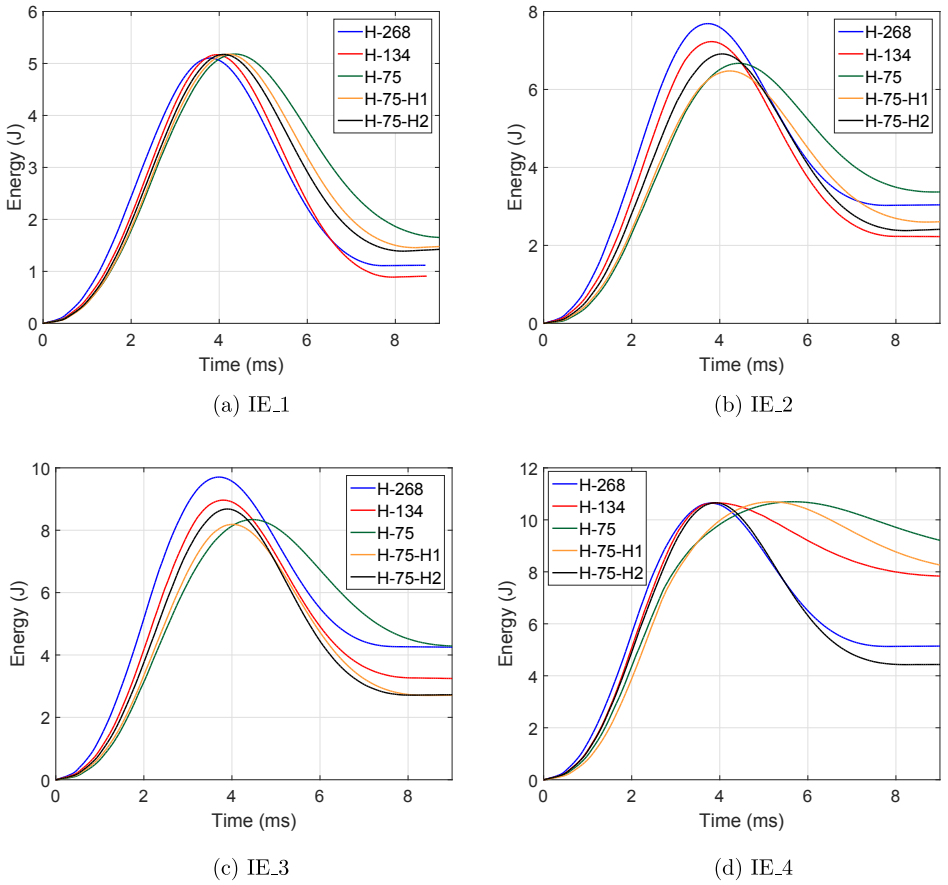

(a) IE_1 (b) IE_2

(c) IE_3 (d) IE_4

Fig. 6.4.: Energy evolution response of all the laminates for all the impact energies.

and areas, with a large increase in the projected damage area for the last impact energy of 10.5 J. C-scan inspection also provides an account of the high dent depth left by the impactor for H-75 and H-75-1 at IE_4. Hybrid laminate H-75-H2 showed dominant delamination at the last interface for lower energies, whereas in moving to higher energies it is shifted to the interface of the inserted thick 0° ply, (interface no.11: $(45°/0°_{268})$), oriented in the 0° direction.

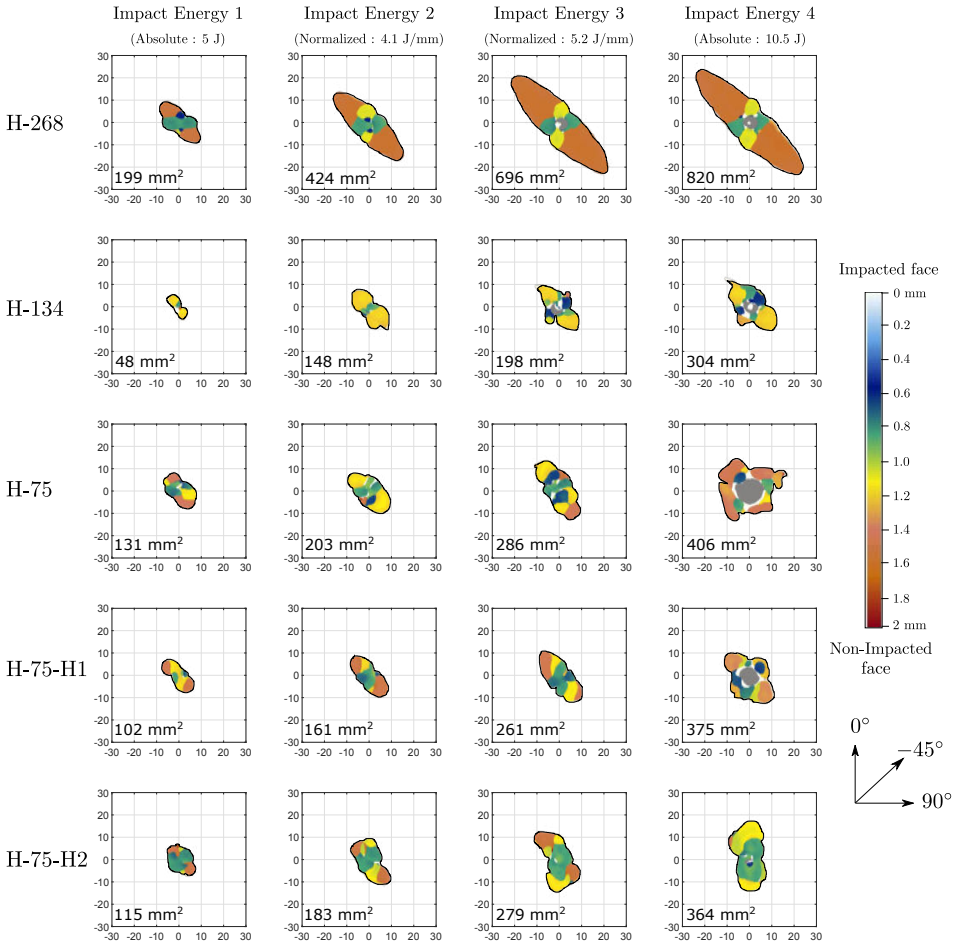

Fig. 6.5.: Projected damage profile obtained from C-scan inspection for all laminates at all impact energies (Average projected damage area presented along with the through-the-thickness colour bar, and the field of inspection represented is 60 x 60 mm^2).

Fig. 6.6 presents the impacted and non-impacted face photos of all the laminates

for the highest impact energy IE_4. A visual comparison was made between the laminates for the permanent indentation left by impactor and also the magnitude of back fibre splitting at the non-impacted face of the specimen. Thin plies were found to exhibit higher dent depth and extensive back fibre splitting, with the impactor nearly penetrating the laminate. This is evidenced as we visually compare the laminate photos from H-268 to H-75 (left to right in Fig. 6.6), where the dent depth and back fibre splits are found to increase. Furthermore, the inclusion of thick plies to thin plies was noticed to alleviate the same: as evidenced by comparing H-75 to H-75-H2 in Fig. 6.6. In addition, the presence of cracks due to fibre failure on both sides of the laminates can be observed.

Fig. 6.7 presents the average peak load and projected damage area, whereas Fig 6.8 displays the dissipated energy and permanent dent depth of all the laminates. H-75 exhibited the least load carrying capacity; as evidenced by the least peak load. In terms of projected damage area, the thick plies H-268 exhibited almost twice the damage area for all the impact energies compared to other laminates. From Fig. 6.8, the thin and standard ply laminates (H-134, H-75 and H-75-H1) are observed to have higher dent depth and dissipated energy at the highest impact energies, compared to laminates containing thicker plies (H-268 and H-75-H2). It is interesting to remark that H-75 dissipated close to 90% of the applied impact energy for IE_4, accompanied by an impact dent depth of almost twice its laminate thickness at IE_4, resulting in near impactor penetration.

6.3.2 Compression after impact

Along with the plain compression strength values, Fig. 6.9 (a) and (b) also present the CAI strength of all the laminates with respect to the absolute and normalized energies, respectively. Along with the CAI strength values, it is important to review the CAI failure mode as, despite using the anti-buckling fixture, some laminates still failed by structural local buckling at the specimen top rather than at the impacted zone. The same figure also depicts the CAI values and the corresponding laminates which exhibited invalid CAI failure mode (represented by a * coloured the same as the corresponding marker in Fig. 6.9). This was mainly observed for lower impact energies, as the higher impact energies induced enough damage to force a compressive failure at the specimen centre. It is worth remarking that thick ply H-268

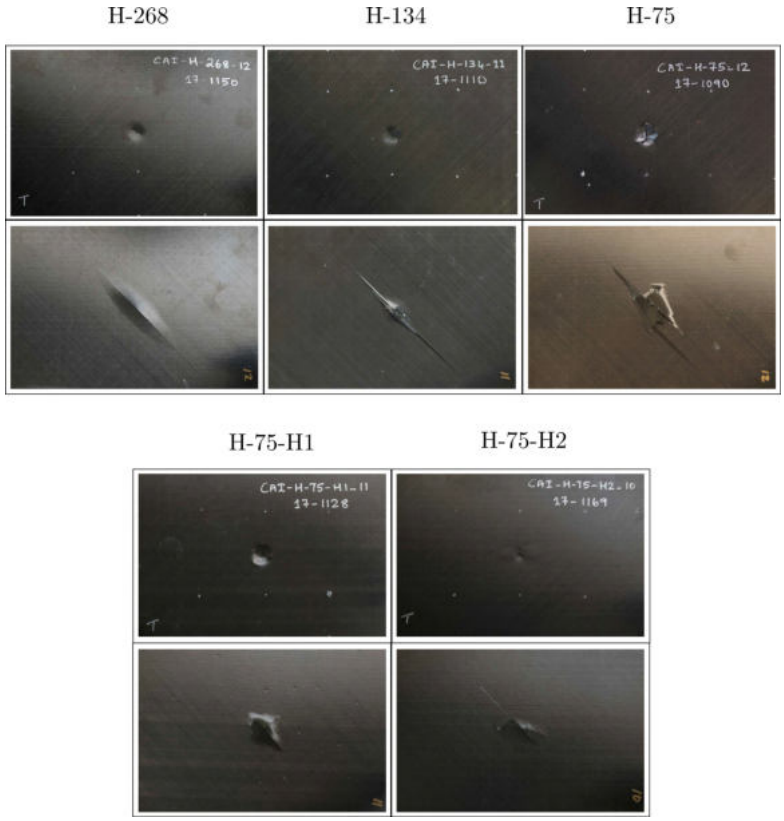

Fig. 6.6.: Post impact photos of the impacted (top) and non-impacted face (bottom) of all the laminates from 10.5 J impact (Each image represents the whole impact specimen of dimensions 150 x 100 mm).

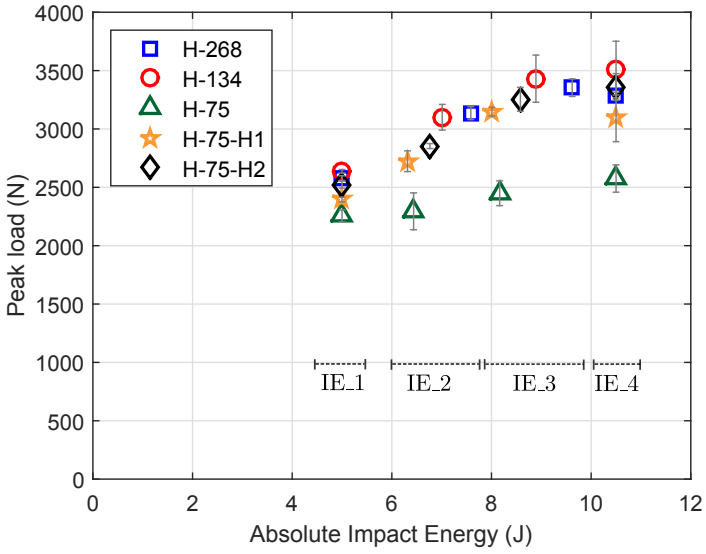

(a)

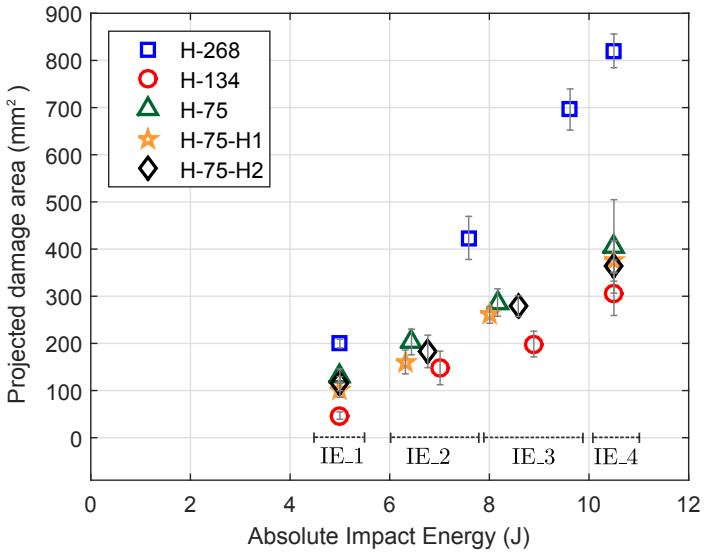

(b)

Fig. 6.7.: (a) Peak load and (b) projected damage area compared between all the laminates for all absolute impact energies (Average value is presented along with the standard deviation indicated by vertical markers).

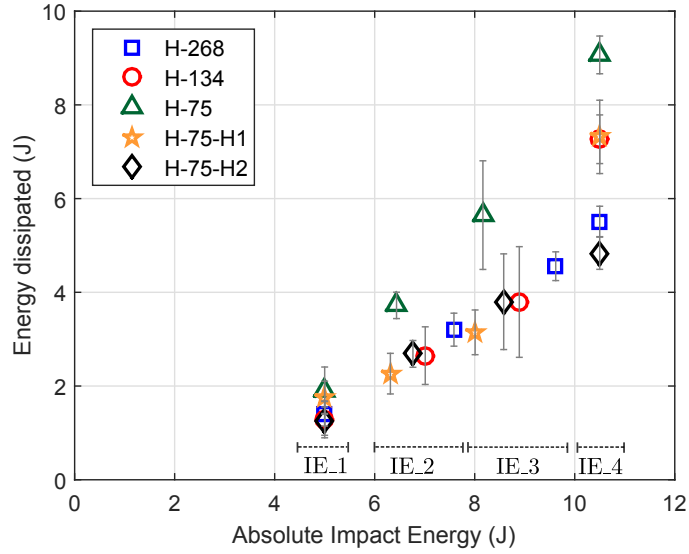

(a)

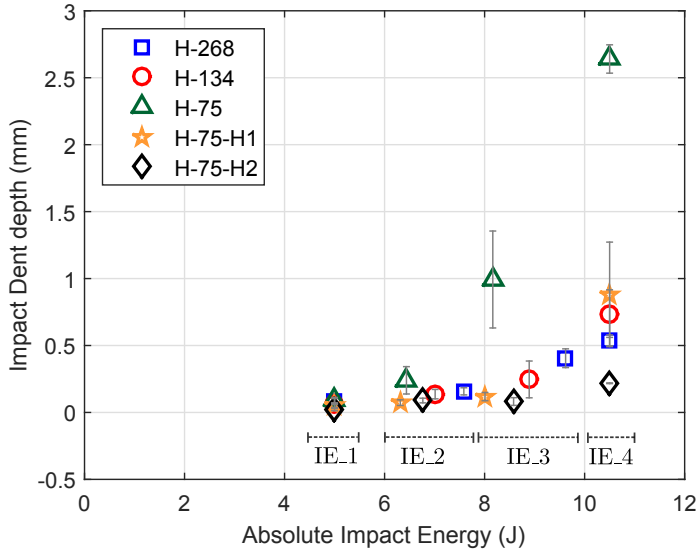

(b)

Fig. 6.8.: (a) Dissipated energy and (b) impact dent depth values compared between all the laminates for all absolute impact energies. Fitted linear and exponential curves are also presented. (Average value is presented along with the standard deviation indicated by vertical markers).

and thin ply H-75 showcased proper CAI failure for all the impact energies. Fig. 6.10 (a) illustrates the schematic representation of the CAI fixture, clearly differentiating the clamped region, anti-buckling ribs, the ribs-free area and the unsupported window at the top of the specimen. Fig 6.10 (b) displays the invalid CAI failure mode where the laminate fails due to the local buckling of the unsupported window (marked in red). Fig. 6.10 (c) presents the proper CAI failure observed at the centre of the specimen due to the evolution of the impact damage.

H-134 showed proper CAI failure for the last three energies, whereas H-75-H2 exhibited the same for the last two energies. H-75-H1 failed at the specimen top for all energies except for the highest impact energy. Within the three grades of ply thickness, thin plies exhibited the highest plain compression strength, approximately 23% higher than the thick plies and 4% higher than the standard plies, as seen in Fig. 6.9. H-75-H2 has the highest pristine compression strength out of all the laminates, at approximately 10% higher than the thin plies. Since the invalid CAI failure mode provides critical buckling values which are lower than the real CAI strength value, only the valid CAI failure mode values are accounted for during comparison studies. Fig. 6.11 compares the CAI strength normalized with respect to thin plies (H-75), which help to obtain a better outlook on the CAI strength comparison in terms of ply thickness and ply hybridization study.

Within the ply thickness study, the last three impact energy results reveal that H-268 and H-134 showed almost the same CAI strength (accounting for the average of last three energy results), whereas H-75 provides the least CAI strength. Reviewing IE_2 and IE_3, thick plies and standard plies exhibit an average increase of 18% and 20%, respectively, over the thin plies H-75. Commenting on the hybrid laminates, H-75-H2 provides the maximum CAI strength over all the laminates, when considering the last two impact energies. In terms of CAI strength improvement, H-75-H2 shows an average increase of 40% and 20% over its baselines H-75 and H-268. Accounting for the CAI strength of H-75-H1 at the highest energy IE_4 (as the other impact energies gave improper failure mode), it shows an average increase of 25% over the its baseline H-75. It is to be noted that both hybrid laminates showed an increased CAI strength over their individual baseline constituents, when considering the valid CAI failure mode values. H-75-H1 and H-75-H2 can be compared with their baseline H-75 for all the four impact energies, acknowledging that the difference between

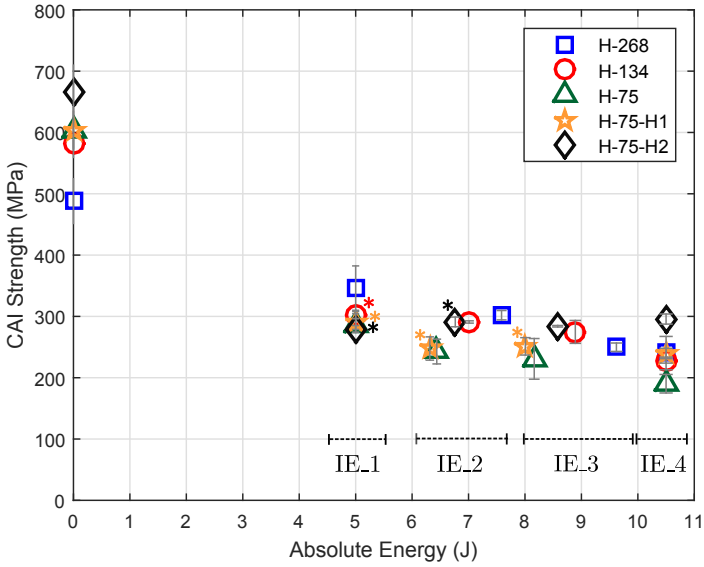

(a)

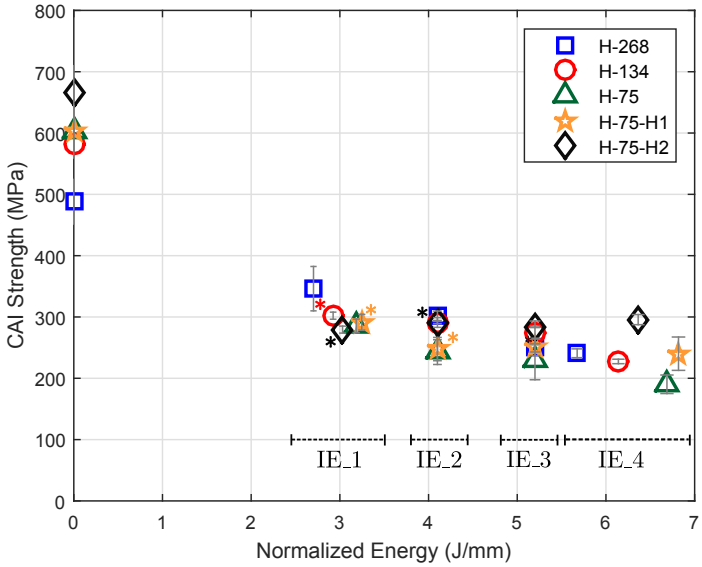

(b)

*CAI failure at the specimen top due to local buckling

Fig. 6.9.: Plain compression strength and CAI strength of all the laminates presented against (a) absolute energies and (b) normalized energies. Average value is presented along with the standard deviation indicated by grey vertical markers.

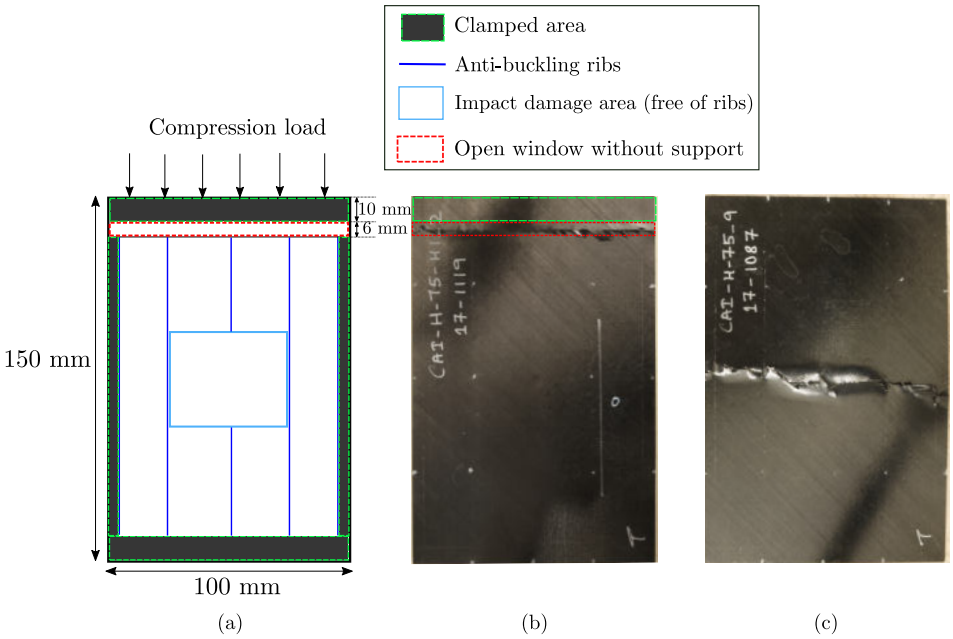

Fig. 6.10.: (a) Schematic illustration of the CAI fixture with anti-buckling ribs; (b) Invalid CAI failure at the centre of the unconstrained window at the top of the specimen; (c) Valid CAI failure at the specimen centre at the impacted site.

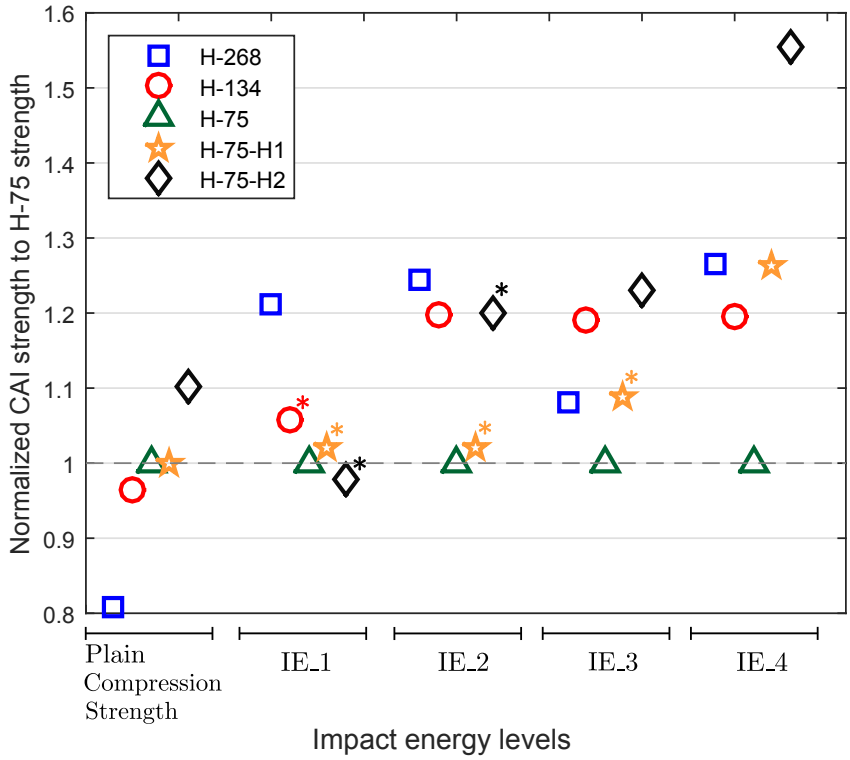

*CAI failure at the specimen top due to local buckling

Fig. 6.11.: Comparison of CAI strengths normalized with thin plies (H-75) as baseline. The plain compression strengths are also normalized with respect to the baseline H-75. (Note that in the horizontal axis, the different compression values are grouped into impact energy levels, and hence the horizontal axis does not have any quantitative significance).

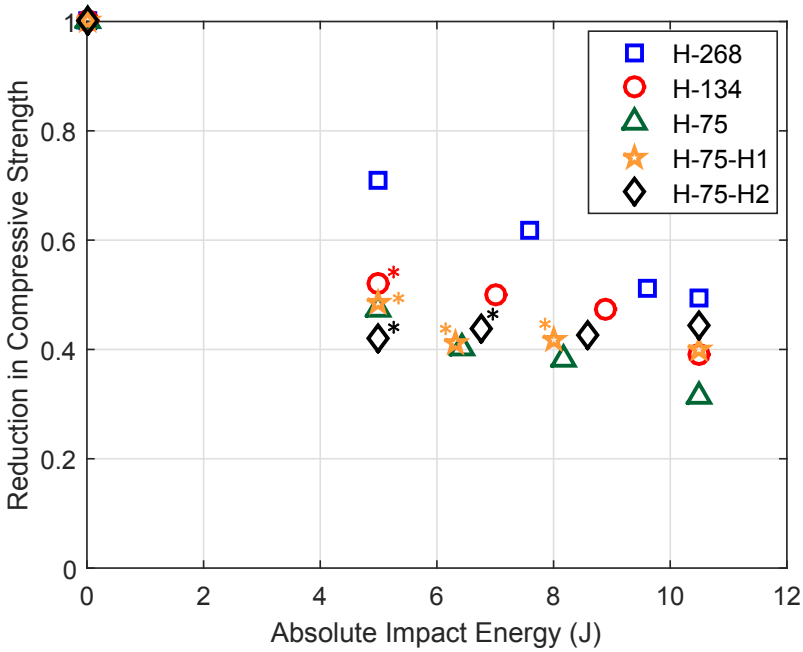

*CAI failure at the specimen top due to local buckling

Fig. 6.12.: Normalized reduction in the compressive strength due to the impact damage of all the laminates.

their laminate thickness is very little. Fig. 6.12 presents the average reduction in the compressive strength of all the laminates, with H-268 and H-75 having the least and highest reduction in compressive strength, respectively. At the highest energy, while H-268 displayed a reduction of 50% of its residual compressive strength, H-75 exhibited 70% reduction in the compressive strength due to the impact damage.

6.4 Discussion

6.4.1 Effect of ply thickness

Matrix cracking and delamination are the main forms of damage associated with low velocity impact loads in standard thick laminates as reported in [6]. For thick laminates, the thin plies helped to delay matrix cracking and delamination in the early stages [63], and were reported to have increased CAI strength over the other ply grades [61, 62]. As for the thin laminates, due to reduced bending stiffness, they underwent considerable amount of bending during impact which led to high in-plane tensile stresses at the non-impacted laminate face. This resulted in back fibre splitting, as seen in Fig. 6.6, for all the laminates. The magnitude of the fibre splitting was understood to depend on the ply thickness and thick ply H-268 was observed to exhibit the least when compared to thin plies. This is due to the energy dissipated by thick plies through matrix cracking and delamination, which means less energy is available for dissipation through fibre splitting. On the other hand, thin plies suppressed the initial damage of delamination, but at the cost of dissipating most of the energy through fibre breakage.

The brittle characteristic nature of thin plies is evidenced by high increase in dent depth and dissipated energy (for thin (H-75, H-75-H1) and standard ply (H-134) laminates in Fig. 6.8), at higher impact energies. In contrast, the laminates containing thick plies (H-268 and H-75-H2) exhibited progressive damage evidenced in the dent depth and dissipated energy with increasing impact energies, as seen in the same figure. For the projected damage area, despite H-268 showing more than twice the value of H-75 at IE_4, H-75 dissipated about 40% percentage more energy than H-268. In addition, for the highest impact energy, a threshold effect is seen with H-75 when the thin-ply laminate starts to be penetrated by the impactor. The other laminates did not reach this threshold under the impact energies explored.

Within the framework of CAI loading, the final collapse of a laminate has been reported to be complex and is generally associated with the following phenomena: sub-laminate buckling, growth of the existing delamination across the specimen width and compressive fibre failure in the 0° load bearing plies [79]. Compared to other laminates, H-268 exhibited larger delaminations and thin plies H-75 showed extensive fibre breakage. Hence, both laminates exhibited enough damage in one form or the other to induce compressive failure at the specimen centre during CAI testing for all impact energies.

As reported in [61, 63], the homogeneous distribution of the micro-structure and the higher in-situ strength associated to thin plies are the prime causes of the higher plain compression strength over the other ply grades. Despite H-75 having higher pristine compression strength over thick plies, the considerable decrease in CAI strength for the thin plies shows the greater influence fibre damage has over delaminations on this property. H-134 showcased an intermediate response, with reduced delamination when compared to H-268 and reduced fibre splitting as compared to H-75, thereby providing a balance in between the two damage modes.

6.4.2 Effect of ply hybridization

As discussed above, fibre failure is clearly linked to the loss of CAI strength. Thicker 0° plies were inserted among thin plies in an attempt to alleviate the amount of fibre damage by dissipating impact energy through matrix cracks and delamination. As expected, a balance between delamination and fibre damage was seen in the results of hybrid laminates,(Fig. 6.5 and 6.6).

The disposition of thin plies surrounding the thick 0° plies improved the CAI strength of the hybrid laminate H-75-H2. The thick 0° plies act as the main load bearing plies during the compression loading [47], and the surrounding thin plies help to constrain the buckling of the thick plies [48]. In addition, thin plies perform better than standard and thick plies under compression loading [63]. The hybridization has helped to reduce the fibre breakage associated with the thin plies by introducing thicker plies in the laminate.

Apart from the thick plies helping to reduce the magnitude of fibre damage, they also impose a dominant delamination at their adjacent interfaces, as seen for IE_3

and IE_4 in H-75-H2 (interface no. 11: $(45°/0°_{268})$). The thick ply introduces higher bending stiffness mismatch within the laminate which leads to high interlaminar shear stresses at the interface of the inserted thick ply [42]. Delaminations close to mid plane are reported to be more resistant to compressive loading compared to the surface delaminations [12, 134] due to the higher stiffness provided by the close-to-equally split sub-laminates. Further, the longitudinal orientation of the dominant delamination is also a reason for the increased CAI strength of H-75-H2 [135].

6.4.3 Compression after impact: Failure mode issues

As CAI strength is one of the decisive parameters in choosing one laminate over another, the issue of invalid CAI failure mode associated with thin laminates (as also reported in [136]) needs to be discussed. At low impact energies, many laminates failed due to local buckling at the open window of the anti-buckling fixture (see Fig. 6.10) [67], providing a critical buckling strength of the thin laminate, which is lower than the real laminate CAI strength for that particular impact energy. We evidenced no sign of extension in the impact damage in the post CAI C-scan inspection for those laminates which failed at the top. In this aspect, the CAI strength values obtained from the invalid failure modes are independent of impact energy and impact damage, as evidenced in Fig. 6.9. Within the framework of thin structures, it is evident that at low impact energies, local buckling is critical and more prone to cause final collapse than impact damage does. In the long run, research on thin laminates needs to resolve the issue of not being able to extract the real CAI strength. Furthermore, as a future work, it can be meaningful to access the residual strength reduction through tension after impact (TAI) tests for thin laminates where fibre failure is the dominant damage mode.

6.4.4 Effect of laminate thickness on damage mode

With a decrease in laminate thickness, a change in dominant damage mode from delamination to fibre failure was observed. Thin structures undergo large bending when impacted, which leads to high in-plane tensile stresses at the non-impacted side. This is the source of back fibre splitting; as found for all the laminates. This extensive fibre failure adversely affected both damage resistance and tolerance; as displayed by the thin plies in this study. In contrast to the thick laminates where delamination

damage is critical, with the thin laminates delamination indirectly helped to reduce the magnitude of fibre failure as evidenced with the hybrid laminates.

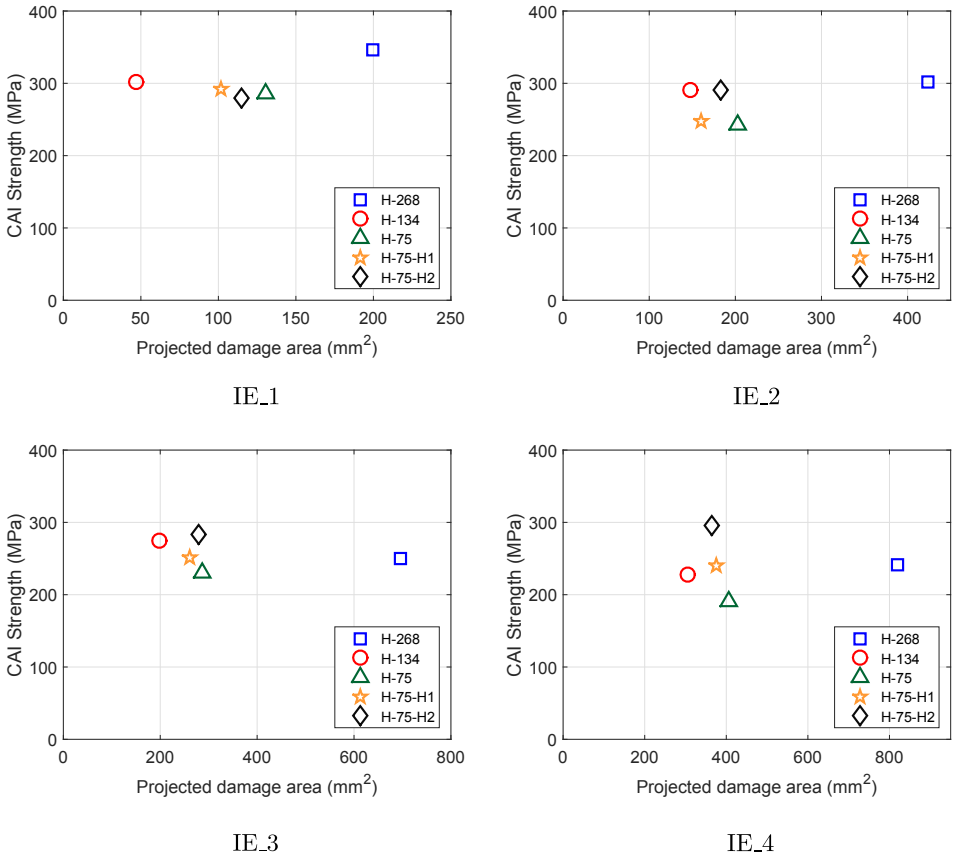

Fig. 6.13.: Comparing the relation between CAI strength and the projected damage area of all laminates for all the impact energies.

In the laminates of standard thickness, the projected damage area is considered to correlate well the damage resistance with the damage tolerance of a specimen [137]. Fig. 6.13 compares the relation between the projected damage area obtained from the C-scan inspection and the CAI strength. Even though H-268 showed twice the projected damage area compared to the other laminates for all impact energies, it exhibited better CAI strength than most of the other laminates (Fig. 6.13). This differs from the trend reported by [137] for thick laminates, where an increase in the damage area linearly reduced the CAI strength. It is clear that with the thin laminates, the damage area can be a misguiding parameter with which to assess

damage resistance and damage tolerance.

The damage tolerance design approach aims to assure that the structure has enough strength to continue in service until the damage is detected by a scheduled inspection. There is a high probability that a permanent indentation of 0.25 to 0.5 mm can be detected during the inspections [111]. In the current study, thin ply laminate H-75 exhibited dent depth higher than 0.25 mm from IE_2, whereas for the other laminates the BVID threshold was between IE_3 and IE_4. It is to be noted that, for the impact energy IE_3, the laminates failed at 50% of its pristine strength despite showing no signs of BVID damage (except H-75). This reduction in compressive strength not accompanied with detectable damage is a troubling fact in terms of the damage tolerance concept.

6.5 Conclusion

We performed an experimental campaign to study the effect of ply thickness on the impact and post impact responses of thin laminates (thicknesses ranging from 1.5 to 1.8 mm). Additionally, we proposed and tested two hybrid laminates where thick or standard 0° plies were mixed with thin plies. Unlike research reports for thick laminates, where thin plies provided higher CAI strength, thin laminates made with thin plies showcased the least CAI strength compared to other ply grades. Thin plies exhibited extensive fibre breakage accompanied by large dent depth and dissipated energy. The idea of ply hybridization, in an attempt to obtain a balance between the delamination damage and fibre failure by mixing thick and thin plies, provided an average increase in CAI strength of 40% over the baseline thin ply laminate. Further issues of thin laminates with improper failure modes during CAI testing were discussed. The non-dependence of the projected damage area on the CAI strength of the thin laminates was also observed. Finally, ply hybridization appears to be a promising economic prospective in the quest to improve the CAI strength of thin laminates.

7

Paper D:
Impact and compression after impact response in thin laminates of spread-tow woven and non-crimp fabrics

A. Sasikumar[a,*], D. Trias[a,1], J. Costa[a,*], N. Blanco[a], J. Orr[b], P. Linde[c,d]

[a] AMADE, Polytechnic School, Universitat de Girona, Campus Montilivi s/n, E-17003 Girona, Spain

[b] University of Dayton Research Institute, 300 College Park, Dayton, OH, USA

[c] Airbus Operations GmbH, Kreetslag 10, 21129 Hamburg, Germany

[d] Department of Industrial and Materials Science, Chalmers University of Technology, S-41296 Gothenburg, Sweden

[*] Corresponding author

[1] Serra Hunter Fellow

The paper has been published in *Composite Structures* 215 (2019) 432–445.

Motivation & Synopsis

As a part of the Airnet project, the previous paper studied the effect ply thickness and ply level hybridization have on the compression after impact of thin laminates using uni-directional (UD) tapes. In addition to UD tapes, textile fabrics have gained the interest of the manufacturers due to the reduced manufacturing costs associated with them over the UD. Hence, as a part of the same project, textile fabrics namely woven fabrics and non-crimp fabrics are also included in the experimental campaign to assess their impact resistance and tolerance in the framework of thin laminates. While in woven fabrics, two UD layers are woven together, in non-crimp fabrics, two UD layers are stitched together using a yarn. Both the fabrics studied in this paper as well as the UD tapes in the last paper were processed with the same fibre resin system. With different ply grades used for woven and non-crimp fabrics, the paper's aim is to study the effect of fabric architecture (woven v/s stitching) and ply thickness on the compression after impact response using thin laminates. Experimental results revealed that while woven fabrics offer higher impact damage resistance, non-crimp fabrics offer improved impact damage tolerance.

Composite Structures 215 (2019) 432–445

Contents lists available at ScienceDirect

Composite Structures

journal homepage: www.elsevier.com/locate/compstruct

Impact and compression after impact response in thin laminates of spread-tow woven and non-crimp fabrics

A. Sasikumar[a,*], D. Trias[a,1], J. Costa[a,*], N. Blanco[a], J. Orr[b], P. Linde[c,d]

[a] AMADE, Polytechnic School, University of Girona, Campus Montilivi s/n, 17073 Girona, Spain
[b] University of Dayton Research Institute, 300 College Park, Dayton, OH, USA
[c] Airbus Operations GmbH, Kreetslag 10, 21129 Hamburg, Germany
[d] Department of Industrial and Materials Science, Chalmers University of Technology, S-41296 Gothenburg, Sweden

Abstract

Recent research has been devoted to thin laminates as a result of aeronautic industries shifting to thinner and lighter structures. In an attempt to improve the out-of-plane response and reduce manufacturing costs considerably, airplane manufacturers are exploring (apart from unidirectional tapes) textile fabrics of different fabric architectures. Within the framework of thin laminates, this paper investigates the impact and compression after impact (CAI) of two types of aerospace graded spread-tow fabrics, namely non-crimp fabrics and woven fabrics, where stitching and weaving, respectively, govern the architecture. The study also comprises two different ply thicknesses (thin and intermediate ply grades) for both fabrics. Experimental results reveal that while woven fabrics display higher damage resistance, non-crimp fabrics ensure higher damage tolerance. The intermediate ply grade performed better than thin plies in terms of damage resistance and CAI strength for both fabrics, as thin ply non-crimp fabric laminates exhibited early and extensive fibre damage.

Keywords: Non-crimp fabrics, Woven fabrics, Impact behaviour, Damage tolerance, Thin laminates

7.1 Introduction

In an attempt to go even lighter, aircraft industries are now considering how to reduce the thickness of many aircraft parts, such as wing and fuselage skins, to less than 2 mm. The threat posed by low velocity impact loads on these thin structures,

accompanied by the change in the stress states and damage modes could be critical when compared to standard thick laminates [5, 110].

In the quest to improve the out-of-plane response, many concepts such as laminate design [9, 11, 120], interleaving [32], ply hybridization [48, 110], and the use of textile fabric composites have been explored [69]. Textile fabrics differ from uni-directional (UD) tapes in that the fibre tows are either woven, knitted, braided or stitched together in an attempt to enhance the mechanical performance and/or economic feasibility. Along with the efforts to reduce the structural weight of aircraft, the aeronautic industry is also working on cutting back manufacturing costs and, as such, fabric composites have been an excellent substitute for UD tapes, thanks to their faster deposition rates and reduced labour time [70].

Out of the different reinforcement architectures, non-crimp fabrics (where UD layers are stitched) and woven fabrics (where UD tows are woven) have gained increasing attention in aerospace industries, mainly due to the improvement they offer over UD tapes in terms of higher interlaminar strength, better out-of-plane response and a considerable reduction in manufacturing costs [70, 71]. As textile composites have evolved, standard ply grade woven fabrics provided a substitute for UD prepreg tapes, with their main advantage being the increased toughness from the woven architecture and the reduced manufacturing costs related to the faster lay-up. Nevertheless, these same fabrics caused a reduction in in-plane properties as a result of their wavy fibres [138], thus non-crimp fabrics provided the solution. In non-crimp fabrics, the UD layers are stitched, therefore not only eliminating the problem of waviness, but also offering the economic feasibility of faster lay-up. Despite this, non-crimp fabrics exhibited local resin rich areas and fibre waviness around the stitch that impaired the compressive properties [139]. Another step forward was to employ thin plies (using spread tow technology) with woven fabrics which reduce considerably waviness and the magnitude of resin rich areas [140]. Despite the advances in textile composites, not many studies report on the effect the architecture of the fabric has on impact and post-impact responses, especially when used with thin laminates.

Vallons et al. [72] compared the interlaminar fracture toughness and impact damage resistance of carbon non-crimp fabrics and twill weave composite fabrics. The study employed different ply grade thicknesses (270 gsm for non-crimp fabrics and

190 gsm for woven) with (on average) 2.1 mm thick laminates. The woven fabrics exhibited higher fracture toughness and higher damage resistance compared to the non-crimp fabrics. Sanchez et al. [66] worked with thin laminates and compared the compression after impact (CAI) strength of woven fabrics with that of quasi-isotropic UD plies (both made out of thick plies) for laminate thicknesses ranging between 1.6 to 2.2 mm. Results evidenced that, compared to UD tapes, woven fabrics have a higher CAI strength, resulting from the increased interlaminar fracture toughness of woven fabrics. It is worth noting that both of these studies used non-standard specimen dimensions.

In the case of out-of-plane loading, thin plies have exhibited higher damage resistance and CAI strength, when used with thick laminates [55, 61]. Arteiro et al. [140] conducted an extensive experimental campaign to study the effect of spread tow fabric thickness on various structural properties. Thin woven fabrics, when compared with thick woven fabrics, exhibited a higher unnotched compression strength, an improved in-plane shear response and exhibited higher compressive resistance in off-axis compression tests. Similarly [46, 47, 141] with non-crimp fabrics, studies demonstrated the higher damage capability thin fabric plies have over thick ones in terms of structural performance. Meanwhile, Garcia et al. [68] studied the effect fabric thickness has on impact and CAI strength using non-crimp fabrics and demonstrating the sequence of failure events. Thin and standard ply grades were used with 2.15 mm laminates, and thin plies were reported to exhibit lower load carrying capability and lower CAI strength for a 14 J maximum impact energy level.

This paper is the result of a research project led by Airbus, in collaboration with the research centres INEGI (University of Porto, Portugal), UDRI (University of Dayton Research Institute, USA) and AMADE (University of Girona, Spain). We performed an experimental campaign on thin laminates using two types of aerospace grade fabrics, namely woven fabrics and non-crimp fabrics. In order to determine only the effect of the reinforcement architecture, both fabrics used in the study were made using the same fibre-resin material system. Additionally, for each fabric type we considered two different ply grades: thin and intermediate. Hence, this study reports the effects fabric architecture and ply thickness have on the impact and CAI response of thin composite laminates. The experimental campaign included impact and CAI tests to evaluate damage resistance and tolerance. Quasi-static indentation tests

followed by C-scan damage inspection were also performed to study and compare the sequence of damage events.

7.2 Experimental methods

7.2.1 Material, fabric architecture and laminates

Two types of fabrics, namely spread-tow woven fabrics (WF) and spread-tow non-crimp fabrics (NCF), were processed at the University of Dayton Research Institute (UDRI) using carbon fibre T700 pre-impregnated with HexPly M21 resin. Note that, to provide a proper comparison between the two types of fabrics, both fabrics were made using the same fibre-resin material system. WF are produced using a plain weave textile process where the weft fibre tows go over and under the warp tows, resulting in an interlaced woven fabric. Plain weave represents the weaving pattern where the weft tows cross over the warp tows continuously. While WF use weaving as the form of fabric architecture, NCF utilize a secondary stitching yarn that holds the fibre tows of different orientations together, forming a blanket. A bi-angle NCF is used in this study where two differently oriented fibre tows are stacked together like UD plies, and stitched together using a polyester yarn. Note that the sole purpose of the stitch is to permit a faster layup and is not intended to take structural loads.

Fig. 7.1 presents a schematic projected representation of both types of fabrics and also the macro photos of the fabric laminates used in this study. We used NCF bi-axial layers of [0°/45°] and [0°/-45°] whereas the WF comes in [0°/90°] fabric layers. Other fabric layer orientations can be obtained through rotation and flipping. Note that the mismatch angle within the fabric layer is 45° and 90° for NCF and WF, respectively.

In regards to the ply thickness study, two different areal weights per fabric layer were used. For NCF these were 268 gsm and 134 gsm and for WF 240 gsm and 160 gsm. As both fabrics are bi-axial, the ply thickness corresponds to half of the fabric tow thickness, namely 0.134 and 0.067 mm for NCF and 0.12 mm and 0.08 mm for WF, accounting for the intermediate and thin ply grades, respectively. From here on, the four laminates used throughout the study will be referred to as NCF-Int, NCF-Thin, WF-Int and WF-Thin. The laminates and their stacking sequences are illustrated in Fig. 7.2, while Table 7.1 details the laminates, their

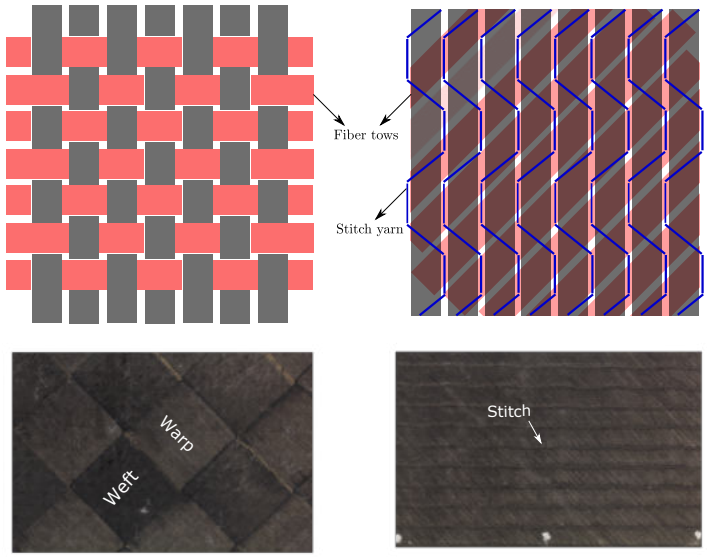

Fig. 7.1.: 2D planar illustration of the fabrics and their architecture (a) Woven fabrics (WF) with plain weave (b) Non-crimp fabrics (NCF) with plies stitched together using a polyester yarn.

stacking sequences, ply and laminate thicknesses. All four laminates are not quasi-isotropic, and NCF-Int utilises non-conventional [22.5°/-22.5°] NCF fabric blankets obtained by rotating the standard blanket layer. Since the study utilizes different fabric materials and different ply thicknesses, the approach followed to obtain similar in-plane and flexural responses in the different laminates consists on pursuing the closest equivalent bending stiffness parameter (D*, proposed by Olsson [123], which is a function of the bending stiffness matrix coefficients) as possible. The D* values of NCF-Int, NCF-Thin, WF-Int and WF-Thin are 18.6, 18.9, 21.5 and 25.9 respectively. (Note that the nominal laminate thickness of woven fabrics is higher than the non-crimp fabrics which resulted in the higher D* values for the woven fabrics.) Figs. 7.3(a) and (b) present the polar plot of the in-plane and bending stiffness, respectively, for all four laminates.

7.2.2 Impact energy definition

While both NCF laminates have the same laminate thicknesses, WF-Thin laminates displayed a higher measured laminate thickness compared to WF-Int (1.82 mm

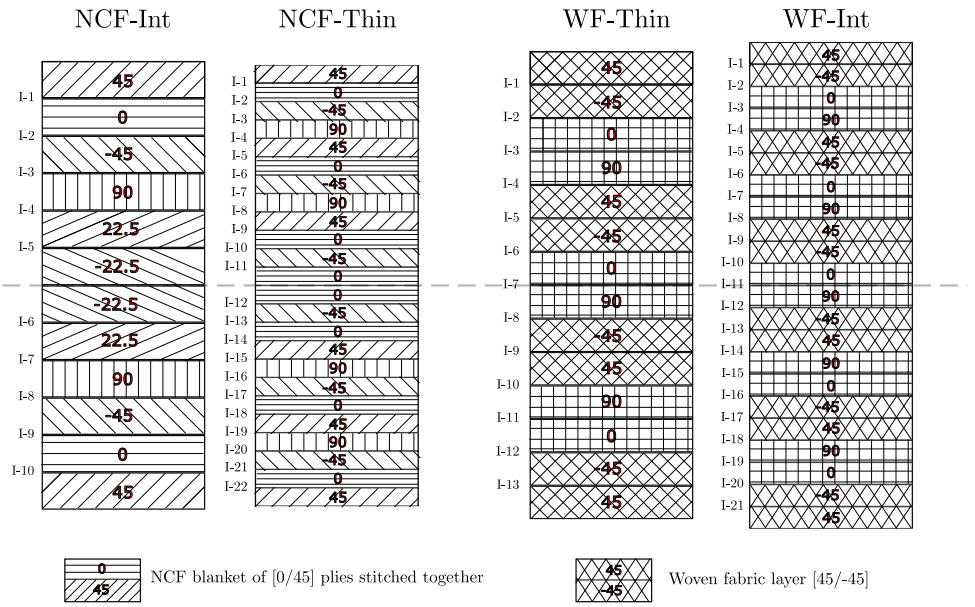

Fig. 7.2.: Schematic illustration of the laminates and their stacking sequences: Non-crimp fabrics (NCF) and Woven fabrics (WF).

Tab. 7.1.: Laminates and their details

Laminate	Description	Stacking sequence	Fabric grade (g/m^2)	Ply thickness (mm)	Nominal laminate thickness (mm)
NCF-Int	Intermediate plies	$[(45/0)/(-45/90)/(22.5/-22.5)]_S$	268	0.134	1.61
NCF-Thin	Thin plies	$[(45/0)/(-45/90)/(45/0)/(-45/90)/(45/0)/(-45/0)]_S$	134	0.067	1.61
WF-Int	Intermediate plies	$[(45/-45)/(0/90)/(45/-45)/(0/90)]_s$	240	0.12	1.68
WF-Thin	Thin plies	$[((45/-45)/(0/90))_2/(45/-45)/(0/90)]_s$	160	0.08	1.76

over 1.66 mm). However, when impacted at the same absolute impact energy, this might lead to misleading conclusions as a thicker laminate has an advantage over a thinner laminate. To avoid this bias, we defined two absolute and two normalized impact energies, where the normalization was performed with respect to the laminate thickness (as also suggested in ASTM D7136/D7136M-15 standards [64]). The authors are aware that this normalization will not guarantee 100% fair comparison, but still provides a fairer comparison. In total, four impact energies were explored, two absolute energies: 5 J and 10.5 J (referred to as IE_1 and IE_4, respectively) and two normalized energies: 4.1 J/mm and 5.2 J/mm (referred to as IE_2 and IE_3, respectively). Table 7.2 details the measured laminate thicknesses and the defined absolute and normalized impact energies for all laminates.

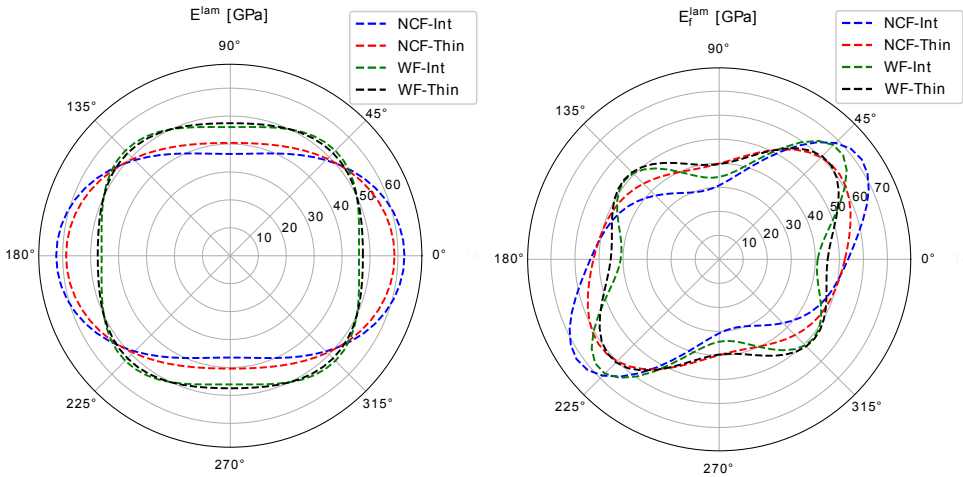

Fig. 7.3.: Polar plot representation of the (a) in-plane stiffness and (b) bending stiffness for all the laminates.

Tab. 7.2.: Laminates and the defined impact energies

Laminate	Measured laminate thickness (mm)	Impact Energy 1: IE_1		Impact Energy 2: IE_2		Impact Energy 3: IE_3		Impact Energy 4: IE_4	
		Abs (J)	Norm (J/mm)	Abs (J)	Norm (J/mm)	Abs (J)	Norm (J/mm)	Abs (J)	Norm (J/mm)
NCF-Int	1.57	5	3.2	6.4	4.1	8.2	5.2	10.5	6.7
NCF-Thin	1.58	5	3.2	6.5	4.1	8.3	5.2	10.5	6.6
WF-Int	1.66	5	3	6.8	4.1	8.7	5.2	10.5	6.3
WF-Thin	1.82	5	2.7	7.5	4.1	9.5	5.2	10.5	5.8

7.2.3 Experimental tests

7.2.3.1 Impact, quasi-static indentation and damage assessment

In accordance with the ASTM D7136/D7136M-15 standards [64], impact tests were performed on 150 x 100 mm specimens using a CEAST Fractovis Plus instrumented drop-weight tower. The specimens were cut with the 0° fibres aligned with the specimen length. A 16 mm in diameter steel hemispherical indenter was used, and the total mass of the impactor setup was 3 kg. We impacted 12 specimens per laminate, with three specimens for each impact energy in order to assess repeatability. Further details of the experimental impact setup can be found in [42].

Quasi-static indentation (QSI) tests were performed with an MTS INSIGHT 50

testing machine with a 50 kN load cell and displacement controlled loading of the indenter. The test setup replicates the impact test, where rubber clamps are placed at the four edges supporting the specimen. A 150 x 100 mm specimen was placed on a base plate, with an open window of 125 x 75 mm. A constant indenter displacement rate of 1 mm/min was used throughout the study. When a load drop or acoustic sound emission was noticed, tests were interrupted for C-scan damage inspection, followed by further indentation on the same specimen.

The main objective of QSI tests is to understand the onset and progression of the damage. As NCF-Int and NCF-Thin laminates have the same measured laminate thicknesses, they were tested under the same indenter displacement levels: d=3, 3.5, 3.95, 4.4, 4.7, 4.9, 5.3 and 6 mm. Initially the displacement levels for NCF-Int were decided arbitrarily, and then the same values were used for NCF-Thin in order to compare the damage sequence. Meanwhile, because of the differences in laminate thicknesses of the WF laminates, different indenter displacement levels were used. While WF-Int was indented at displacements d=2, 2.5, 3, 4.1, 5.6, 6.4 and 7 mm, WF-Thin was indented at d=2.5, 3.1, 4.1, 4.6, 5.1, 5.9 and 6.25 mm. Pulse-echo ultrasonic C-scan was used to inspect the damage from the impact and QSI tests. All the impacted and indented specimens after each indenter loading were inspected. C-scan inspection featured an OLYMPUS OMNI MX system and the specimens were placed in a pool of water while an automated robotic arm scanned them with a 5 MHz piezoelectric probe.

7.2.3.2 Plain strength compression and compression after impact

Prior to compression after impact, plain compression strength of all the laminates was determined following the ASTM D6484/D6484M-14 standard [87]. Plain compression tests were performed on three 305 mm x 30 mm specimens for each laminate at the INEGI research facility at the University of Porto.The interested reader can refer to [131] for more detailed information of the test setup.

Further, CAI tests were performed using an MTS INSIGHT300 machine with a 300 kN load cell, following ASTM D7317/D7137M-15 [88]. As thin laminates were reported to fail under structural global buckling rather than a compressive failure [136], we used a non-standard anti-buckling CAI device as proposed by Remacha

et al. [67]. This fixture ensures a proper compressive failure at the specimen centre induced by the existing impact damage. All the above-mentioned tests, except plain strength compression, were performed at the AMADE research laboratory at the University of Girona, which is NADCAP certified for non-metallic materials testing.

7.3 Experimental Results

7.3.1 Impact response

Figs. 7.4, 7.5 and 7.6 present the force-time, force-deflection, and energy-time impact curves, respectively, for all the laminates. While three specimens for each laminate and for each impact energy level were tested, because of the good repeatability in the responses, only one specimen per laminate has been presented in the impact curves. As the impact energies increase, NCF laminates lost their load carrying capacity compared to WF laminates, as evidenced by the reduced peak load (Figs. 7.4 and 7.5).

Both NCF laminates exhibited significant load drops at the peak loads, which was more pronounced in NCF-Thin, associated to fibre failure. Unlike the other three laminates, NCF-Thin displayed longer response times (Fig. 7.4) and larger laminate bending (Fig. 7.5). Both WF laminates exhibited similar impact responses, except that WF-Thin displayed slight load drops for higher impact energies compared to WF-Int, which are associated with the initiation of fibre failure. NCF-Int performed better than NCF-Thin in terms of the peak load. In view of these comparisons, it is important to keep in mind that the in-plane and bending responses of the laminates are not exactly the same, owing to the different stacking sequence designs. Of all the laminates, NCF-Thin and WF-Int exhibited the highest and lowest energy dissipation, respectively (see Fig 7.6). For all the impact energies, WF laminates dissipated much less energy compared to NCF laminates. For both types of fabrics, intermediate ply grades exhibited better damage resistance than thin plies (more pronounced for the NCF laminates), in terms of reduced energy dissipation and increased load carrying capability.

Fig 7.7 shows the projected impact damage profile of all the laminates for all the impact energies obtained from the C-scan inspection. For all the impact energies except IE_1, NCF-Int exhibited a reduced projected damage area compared to its

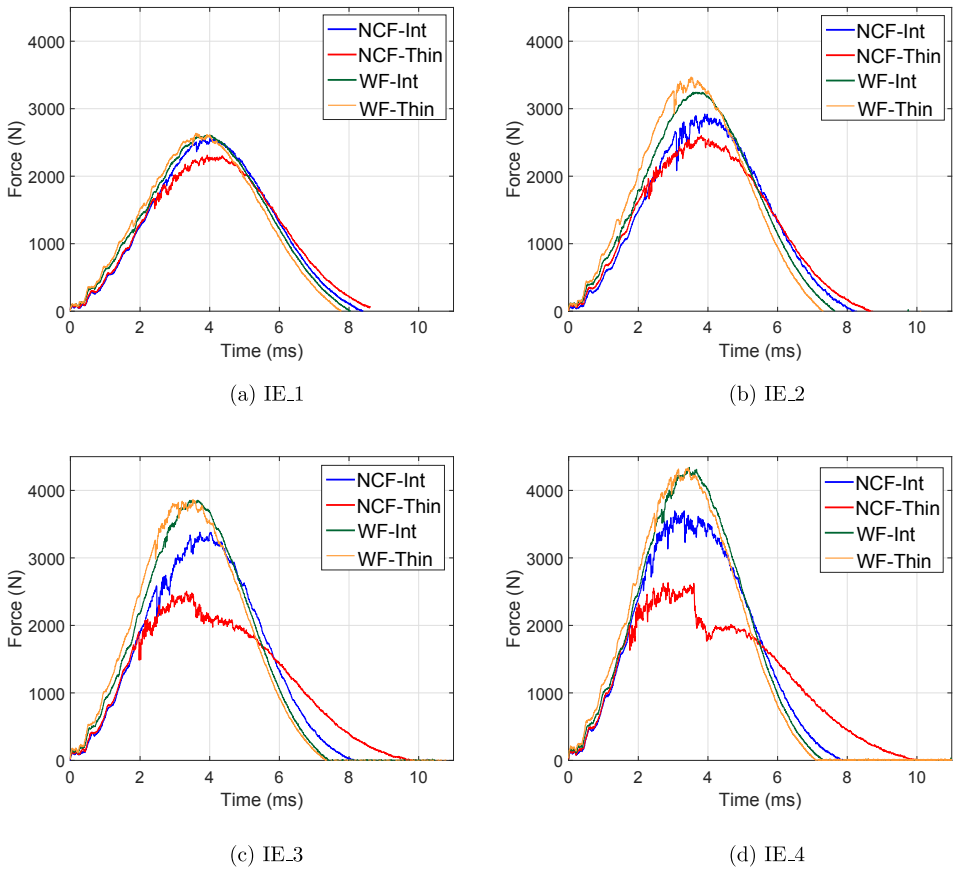

(a) IE_1 (b) IE_2

(c) IE_3 (d) IE_4

Fig. 7.4.: Force-time responses of all the laminates for all the impact energies.

thin ply counterpart NCF-Thin. Dominant delaminations were identified for NCF-Int at interface 6 (-22.5°/22.5°, oriented in the 22.5° direction) and at the last interface (int 10: 0°/45°, oriented in the 45° direction). Note that the interfaces are numbered from the impacted surface with the last interface denoting the interface closest to the non-impacted side, as shown in Fig 7.2. For NCF-Thin, a dominant delamination oriented in the 0° direction was identified at interface 10 (-45°/0°) just above the mid-plane. Additionally for higher impact energies, C-scan images of NCF-Thin exhibited permanent indentation, which was not observed in other laminates.

Both WF laminates exhibited a close-to-circular projected delamination profile, as also observed in [78, 90] for plain woven fabrics. They showed similar projected damage profiles and areas for the chosen impact energies. WF-Int showed a dominant

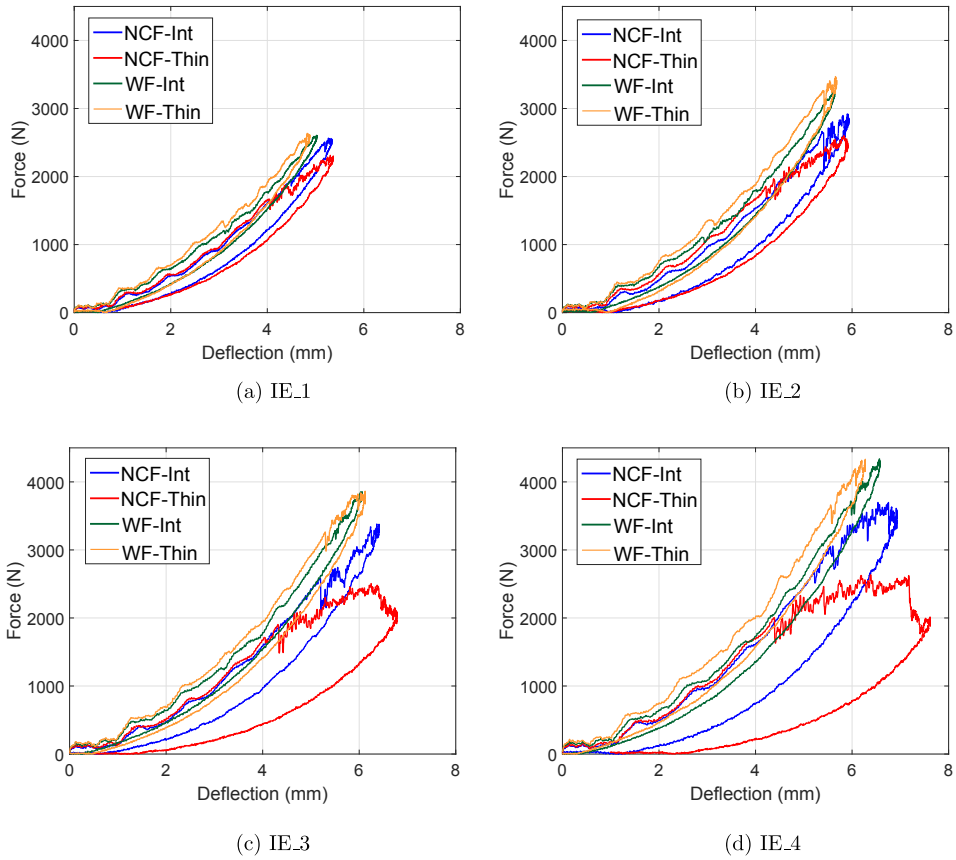

(a) IE_1 (b) IE_2

(c) IE_3 (d) IE_4

Fig. 7.5.: Force-displacement responses of all the laminates for all the impact energies.

delamination at interface 9 (-45°/45°) oriented in 45°, whereas WF-Thin exhibited delaminations at various interfaces, making it difficult to pinpoint the dominant ones. Comparatively, WF displayed a much smaller damage area than NCF, and furthermore, while the delamination profile of NCF was controlled by one or two dominant delaminations, WF had several delaminated interfaces contributing to the overall contour.

Fig. 7.8 displays the photos of the impacted and non-impacted specimen faces from the 10.5 J impact (IE_4). NCF-Thin showed higher permanent dent depth and extensive back fibre splitting compared to intermediate ply grade NCF-Int. By contrast, the WF laminates displayed very little or negligible visible damage as compared to NCF laminates, neither was much visual difference in dent depth and

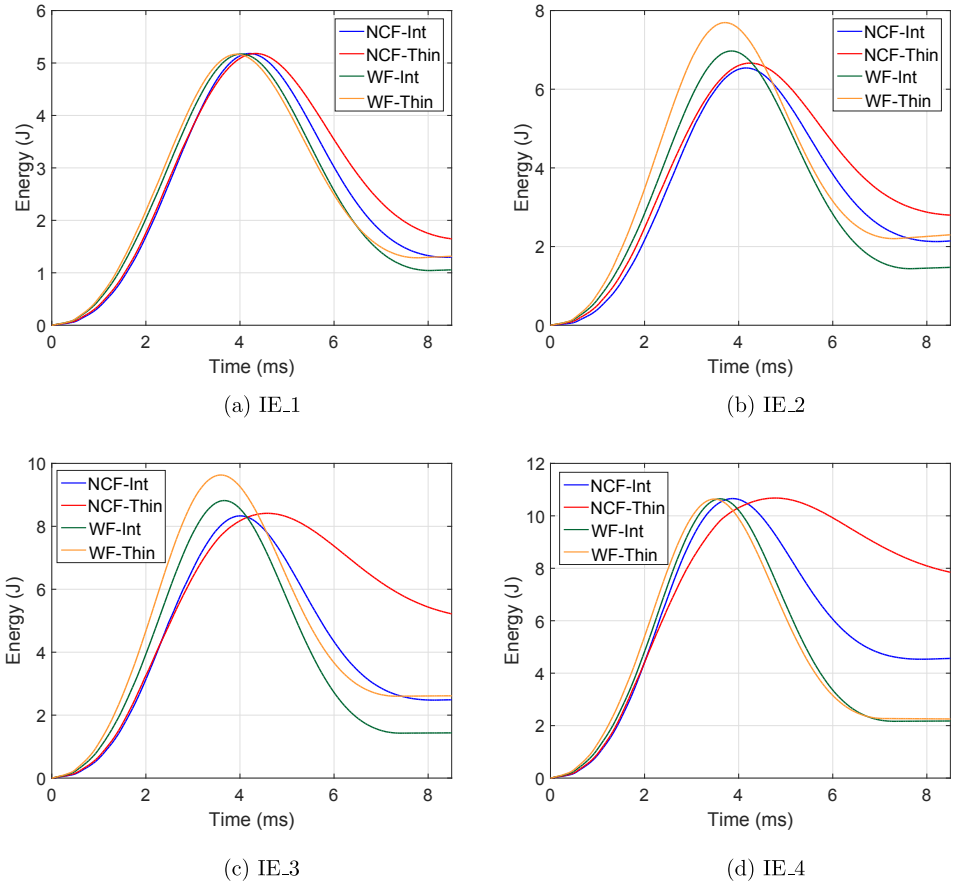

(a) IE_1 (b) IE_2

(c) IE_3 (d) IE_4

Fig. 7.6.: Impact energy evolution of all the laminates for all the impact energies.

back face splitting observed between the WF laminates.

Figs. 7.9 (a) and (b) present the evolution of the peak load and projected damage area, respectively, for the increasing absolute impact energies of all the laminates. When compared with NCF-Int, NCF-Thin showed a reduced load carrying capacity, a 13% reduction in peak load for IE_1 and IE_2 and 27% for IE_3 and IE_4. Similarly, NCF-Thin exhibited a 30% increase in the projected impact damage area over NCF-Int for the higher impact energies. WF-Int and WF-Thin roughly exhibited the same peak load and projected damage area, showing the negligible effect that ply thickness has on these damage resistance parameters. Within the two fabric types, WF displayed higher damage resistance over NCF, evidenced by the higher peak load for all impact energies and reduced damage area, especially at the higher impact energies.

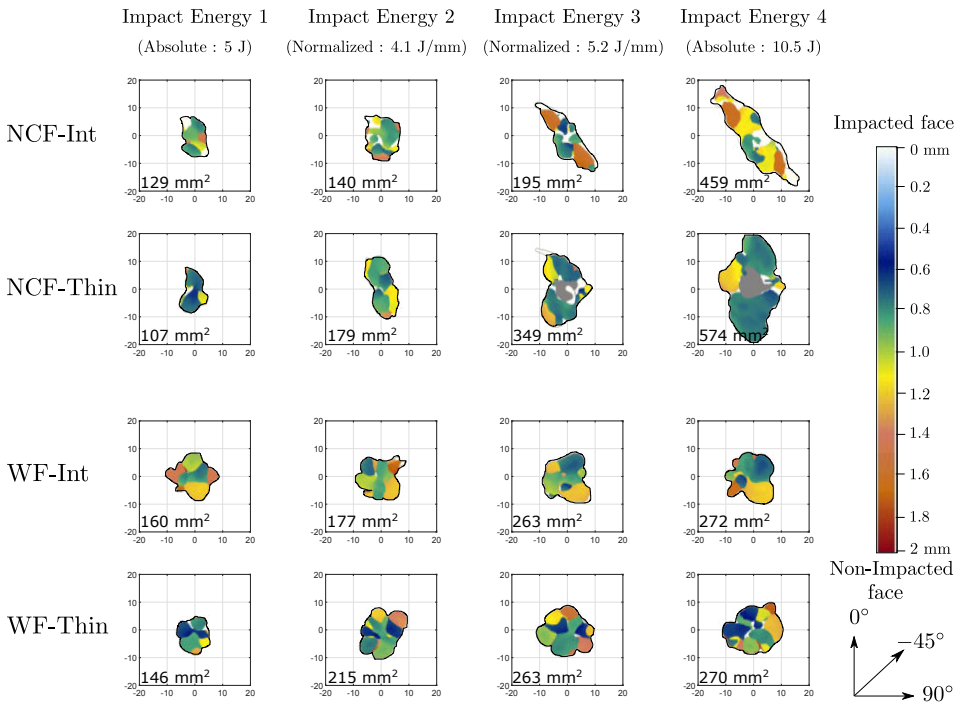

Fig. 7.7.: Projected damage contours and areas obtained from the C-scan damage assessment of all laminates for all impact energies (The average projected damage area is presented with the through-the-thickness colour bar. The field of inspection presented is 40 x 40 mm^2).

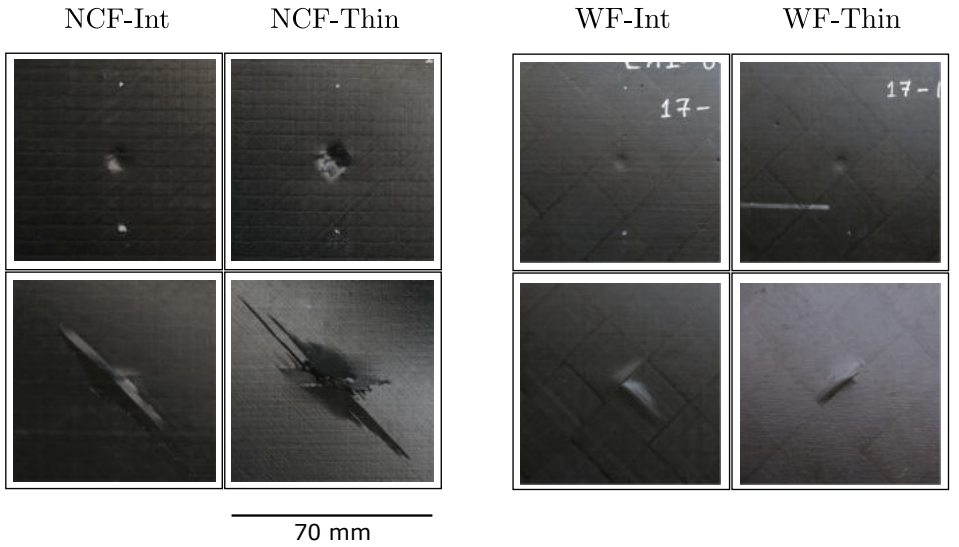

Fig. 7.8.: Photos of the impacted (top) and non-impacted (bottom) faces of NCF and WF laminates from the 10.5 J impact test (Each image represents a square window of 70 x 70 mm referenced from the impact centre).

Figs. 7.10 (a) and (b) display the dissipated energy and the impact dent depth, respectively, for all the absolute impact energies. At lower impact energies, both NCF laminates exhibited roughly the same dent depth, whereas for higher energies NCF-thin showed twice the dent depth compared to NCF-Int (as can also be seen in Fig. 7.8). The WF laminates displayed similar dent depth values, and when NCF and WF were compared, woven fabrics clearly exhibited lower dent depth. Both thin-ply fabrics (NCF-Thin and WF-Thin) showed higher energy dissipation compared to their intermediate-ply counterparts. As observed for other parameters, WF laminates exhibit better damage resistance by dissipating less energy than NCF laminates do.

7.3.2 Quasi-static indentation

Fig. 7.11 compares the force-deflection response of the maximum applied indenter displacement (d_8= 6 mm) of both NCF laminates. The other displacement levels studied, along with the respective energies applied (E_a), are also marked on the same figure. As observed with the impact results, QSI tests also showed reduced peak load and intermittent load drops with NCF-Thin, where the first visible load drop was observed at d_3= 4 mm, when compared to the delayed first load drop at d_7= 5.5 mm with NCF-Int. The projected damage contours obtained from the interrupted

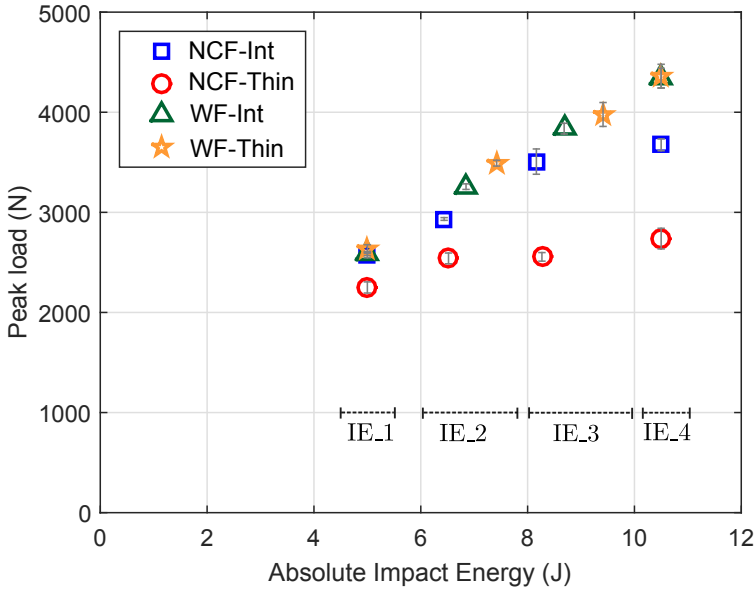

(a)

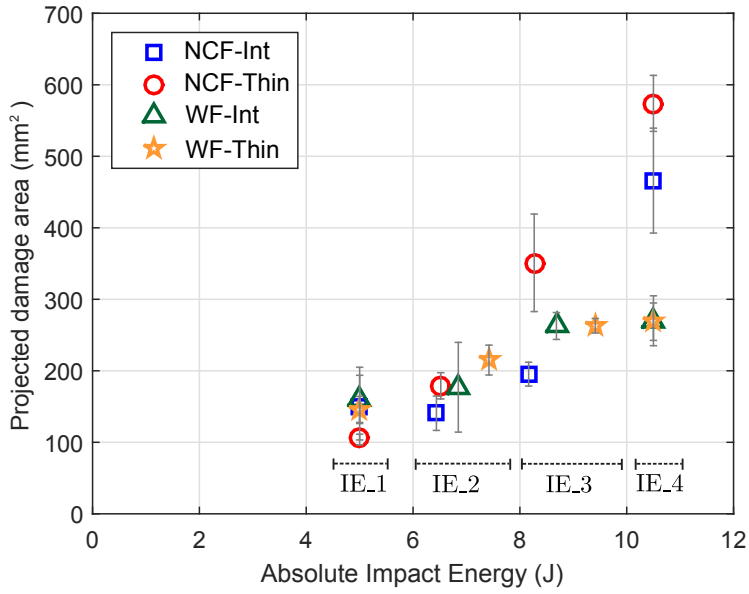

(b)

Fig. 7.9.: Impact damage resistance parameters (a) peak load and (b) projected damage area compared between all the laminates for all absolute impact energies (Average value presented along with the standard deviation indicated by the vertical markers).

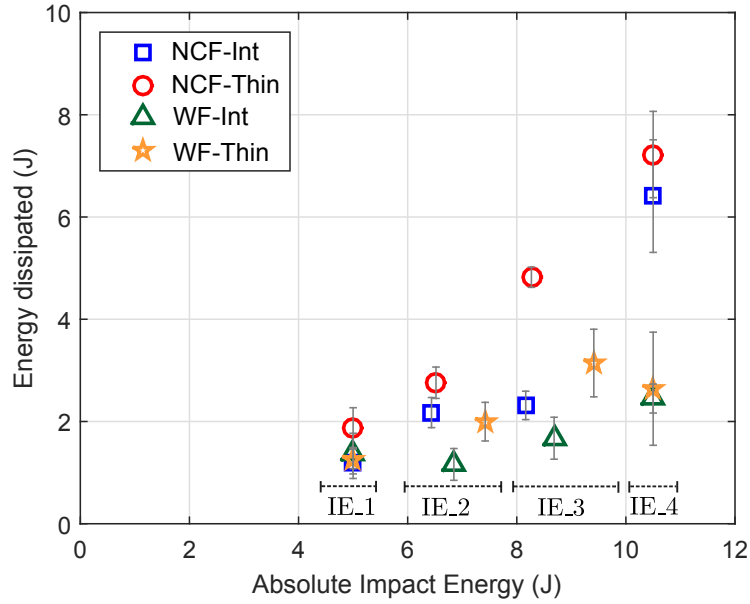

(a)

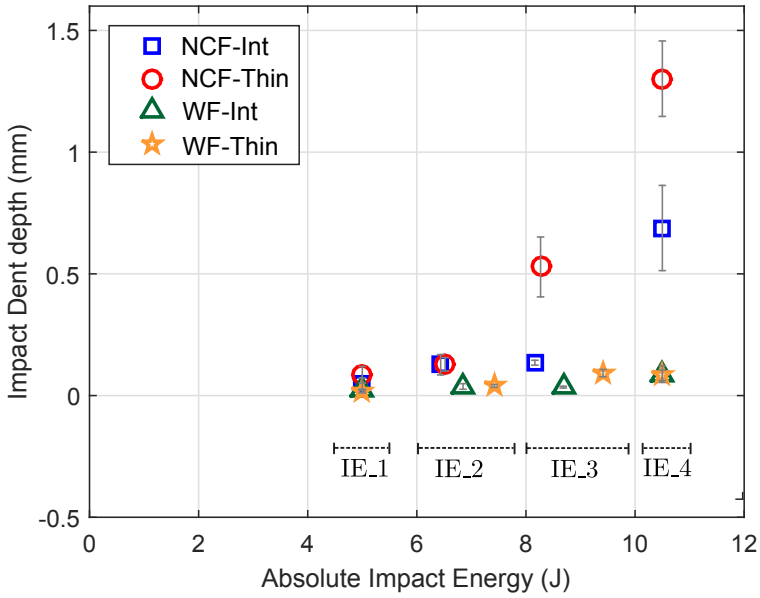

(b)

Fig. 7.10.: Impact damage resistance parameters (a) dissipated energy and (b) impact dent depth compared between all the laminates for all absolute impact energies (Average value presented along with the standard deviation indicated by the vertical markers).

C-scan damage inspection for all the indenter displacement levels of NCF laminates are compared in Fig. 7.12.

NCF-Thin exhibited delayed damage onset over NCF-Int (as in Fig. 7.12), where displacement d_1 results exhibited the initiation of delamination damage in NCF-Int (evidenced below the mid-plane at interface 7: -22.5°/22.5°), but there was no presence of damage in NCF-Thin. Displacement level d_2 provided an increase in the delamination area for NCF-Int, with new delaminated interfaces at the top (interface 5: 22.5°/-22.5°), meanwhile displacement d_3 marked the onset of delamination damage in NCF-Thin at the last interface (0°/45°). Mild intermittent cracking sounds were heard from NCF-Int in the loading stages starting from d_1, whereas the first acoustic emission for NCF-Thin was noticed at d_3, and was associated with the fibre splitting observed on the back face of the laminate and the first load drop. From displacements d_4 to d_6, the delamination profile scaled up with NCF-Int, and a dominant delamination oriented in the 0° direction, just above the mid-plane (interface 11; -45°/0°), was observed for NCF-Thin. Displacement d_7 resulted in the back fibre splitting of NCF-Int, evidenced by a load drop, whereas NCF-Thin underwent further fibre failure which induced a higher delamination area when compared to NCF-Int.

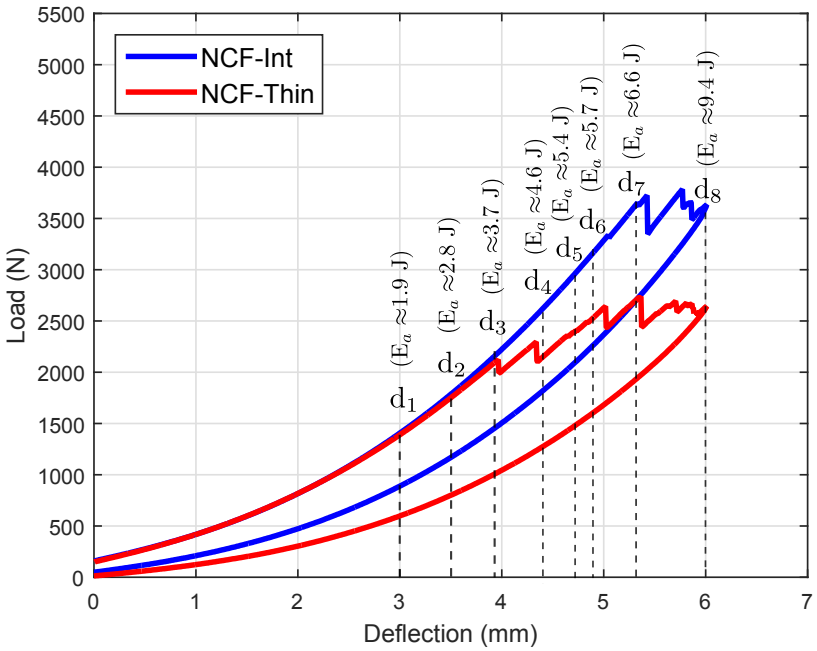

Fig. 7.11.: Load-indenter displacement QSI curve for NCF-Int and NCF-Thin for d=6 mm (the other displacement levels used in the study are also marked).

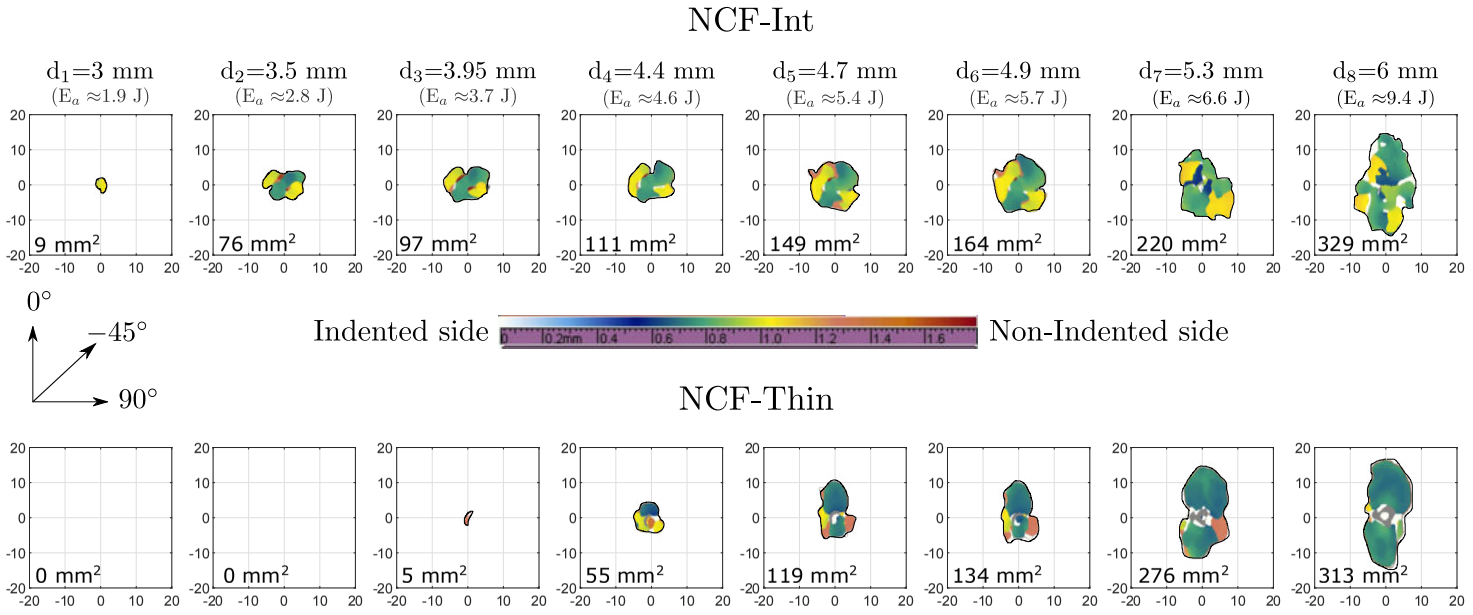

Fig. 7.12.: C-scan images comparing the evolution of damage in the NCF laminates for all the indenter displacement levels.

Moving on to woven fabrics, Figs. 7.13 (a) and (b) present the force-deflection response of WF-Int and WF-Thin, respectively, for their maximum applied indenter displacement ($d = 7$ mm for WF-Int and $d = 6.25$ mm for WF-Thin). Note that, unlike the NCF laminates, the WF laminates were indented at different displacement levels, due to their different laminate thicknesses, and hence the sole aim is to study the damage evolution rather than make comparisons. Fig. 7.13 also presents the other indenter displacements studied and their corresponding applied energies. C-scan inspection images of both WF laminates are presented in Fig. 7.14 aligned along the different deflection levels in the horizontal axis.

WF-Int displayed no load drop in the force response curve during the loading stages, and the first load drop was seen at the maximum load (between d_6 and d_7). In Fig. 7.14, no damage was observed for the d_1 displacement, whereas damage initiation was noticed at d_2 in the C-scan images. Delamination initiation was identified at interfaces 5 (45°/-45°), 9 (-45°/45°), 13 (-45°/45°) and all these interfaces correspond to interfaces within the fabric blanket. This could possibly be due to the higher mismatch angle within the fabric blanket. Despite no sign of load drop in the force-displacement curve, C-scan inspection showed that sufficient damage was formed in the laminate. With continued loading, the delamination contour enlarged and new delaminated interfaces appeared. We observed traces of back fibre splitting between displacements d_6 and d_7. The higher capability of standard ply grade woven fabrics to delay or suppress fibre failure is illustrated here, as the first sign of failure was observed at an applied energy, E_a, of 14 J.

In the case of WF-Thin, the first load drop was observed before the maximum load (between d_5 and d_6), and a further larger drop at the maximum peak load. As with NCF-Thin, back fibre splitting was observed at the point of the first load drop. The first sign of delamination (Fig. 7.14) was observed at displacement d_2, where interfaces 12 (45°/-45°) and 14 (45°/90°), both below the mid-plane, were found to be delaminated. Even though it is not open for direct comparison, it can be seen that WF-Thin delayed the onset of damage and accelerated the onset of fibre failure; something also observed with NCF-Thin. With further loading, new interfaces amounted to the existing delaminations, and the projected damage contours were roughly the same as for WF-Int. Additionally, a good coherence was seen between the results of the impact and QSI tests in terms of projected delamination profile,

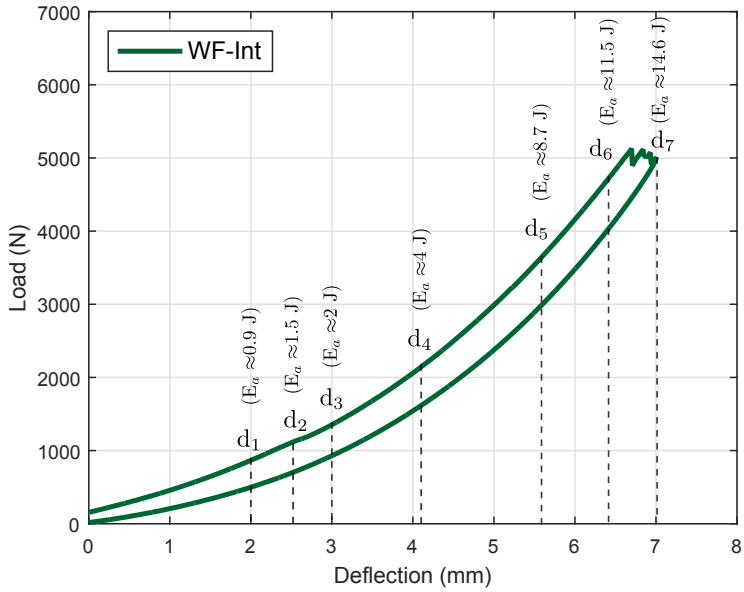

(a)

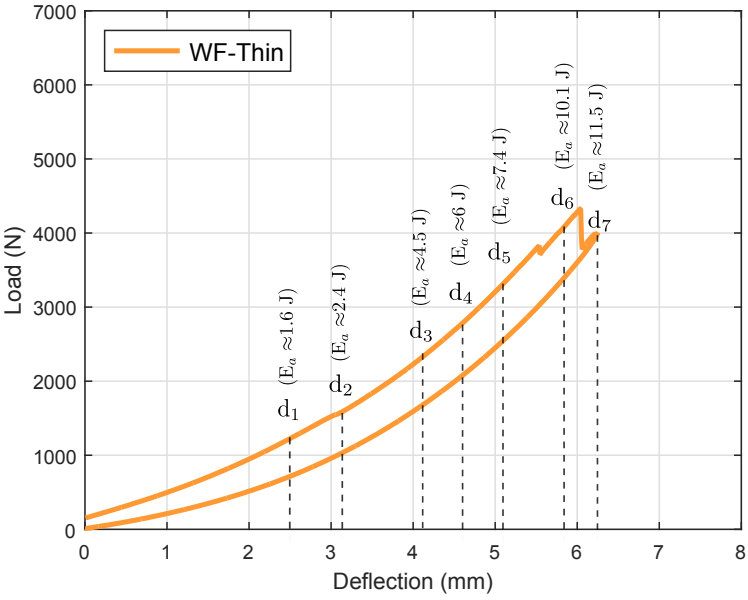

(b)

Fig. 7.13.: Load-indenter displacement QSI curve for WF-Int and WF-Thin for d=7 mm and d=6.25 mm, respectively (the other displacement levels used in the study are also marked).

area and the force level of fibre failure initiation for both types of fabrics.

7.3.3 Plain compression and compression after impact

Figs. 7.15 (a) and (b) present both pristine compression and compression after impact strength values for all laminates for absolute and normalized impact energies, respectively. The thin plies displayed a better plain compression strength than the intermediate plies: NCF-Thin and WF-Thin displayed 10% and 7% increase over their intermediate grade counterparts. An average increase of 15% in plain compression strength was observed for non-crimp fabrics when compared to woven fabrics (as in Fig 7.15).

Despite the use of an anti-buckling device, improper CAI failure at the specimen top (local buckling at the open top window of the fixture, instead of being at the impacted zone) was observed for laminates impacted at lower impact energies (as also reported in [110, 136] for thin laminates). All the laminates impacted at IE_1 and all the laminates impacted at IE_2, except NCF-Int, exhibited CAI failure at the top of the specimen due to local buckling. The laminates and the CAI values corresponding to improper CAI failure are also indicated in Fig. 7.15.

Plain compression and CAI strength values of all the laminates normalized with respect to NCF-Thin and WF-Thin values are presented in Figs. 7.16 (a) and (b), respectively. Intermediate grade plies showed higher CAI strength than thinner plies did and this was more pronounced for the NCF laminates. NCF-Int showed on average a 20% higher CAI strength than NCF-Thin (see IE_3 and IE_4 in Fig. 7.16 (a)), while WF-Int exhibited slightly higher CAI strength (9% for IE_3) over WF-Thin (Fig. 7.16 (b)).

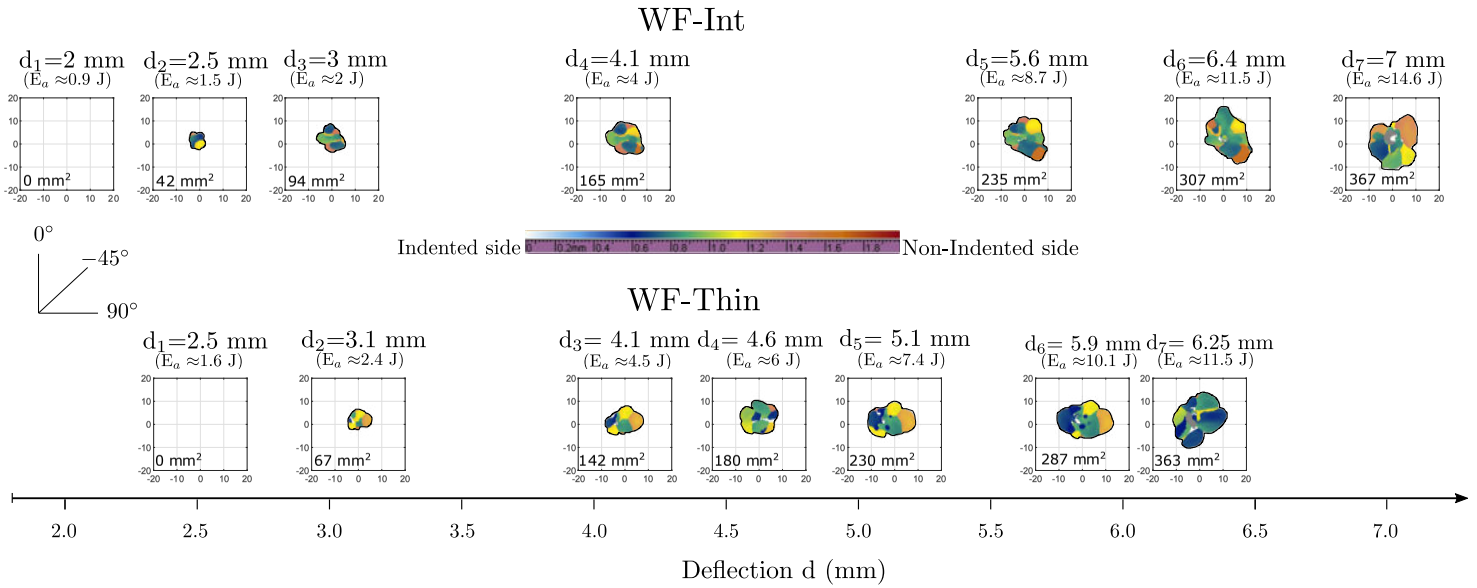

Fig. 7.14.: C-scan images showing the damage evolution in WF-Int (top) and WF-Thin (bottom) for all indenter displacement levels. Note that the scans are presented along an indenter deflection on the horizontal axis.

In a more detailed overview from all of the laminates, NCF-Int exhibited improved CAI strength (considering valid CAI values from IE_3 and IE_4 energies). Reviewing IE_3, NCF-Int displayed 20% higher CAI strength than NCF-Thin and WF-Int, and close to 30% higher than WF-Thin. Moving to IE_4, both WF-Int and WF-Thin showed better CAI strength than NCF-Thin, by 10% and 7%, respectively, whereas NCF-Int showed 16% higher CAI strength over its thin ply NCF. In terms of strength retention, NCF-Thin displayed the highest reduction (65%) in residual compression strength induced by the extensive fibre damage from impact (Fig. 7.17), whereas the WF laminates exhibited a reduction of approximately 50% in compression strength.

7.4 Discussion

7.4.1 Impact damage resistance

As evidenced by the experimental results, the woven fabrics exhibited better impact damage resistance than non-crimp fabrics did. The significant load drops reported for the NCF laminates are related to the initiation of fibre failure (see Fig. 7.5), as was also evidenced in the QSI results. At the same time, the absence of such load drops in the WF laminates suggests the reduced and delayed presence of fibre failure. The significant increase of the impact damage related parameters (Figs. 7.9 and 7.10) for NCF over WF also supports the escalation of fibre breakage in NCF at higher impact energy levels. It is important to keep in mind that the thin ply of NCF (67 gsm) is thinner than its WF counterpart (80 gsm), so the effect of the reduced ply thickness is more pronounced.

The higher damage resistance of woven fabrics is associated with their increased interlaminar fracture toughness. As a result of the woven architecture, the fibre tows have undulations/waviness and both the weft and warp tows are present in the same interface. Therefore, as a crack propagates at an interface, it follows a wavy path due to the waviness of the fibre tows, and further, as the crack encounters a different oriented fibre tow, the crack front jumps to follow this direction. All this results in an increased effective crack length and an excess energy dissipation, thereby an increased fracture toughness [71, 72]. On the other hand, NCF fibre tows are rather straight like UD tapes, except for the fact that two UD plies are stitched together. They are reported to have a reduced interlaminar fracture toughness compared to woven

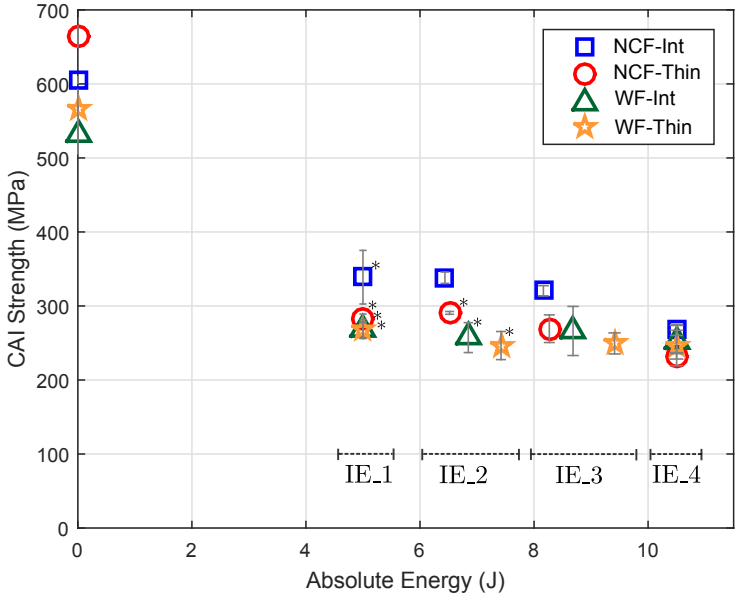

(a)

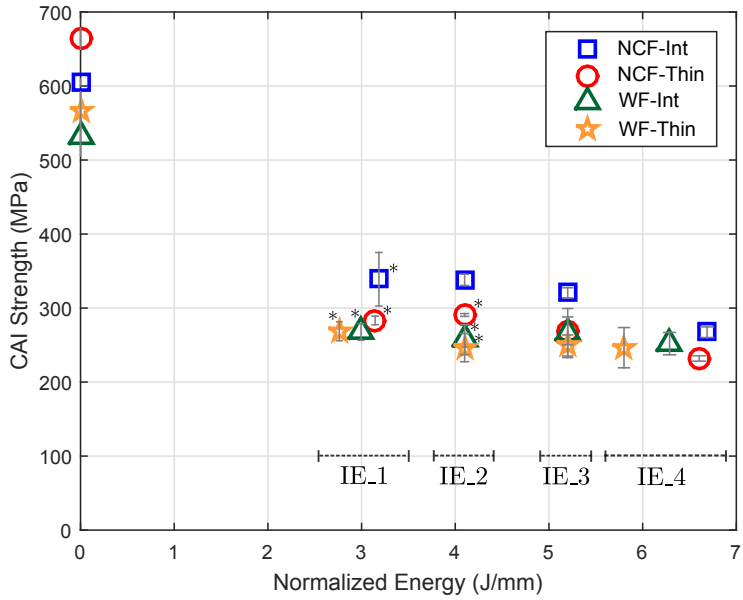

(b)

*CAI failure at the specimen top due to local buckling

Fig. 7.15.: Plain compression strength and compression after impact strength values against (a) absolute impact energies and (b) normalized impact energies for all the laminates.

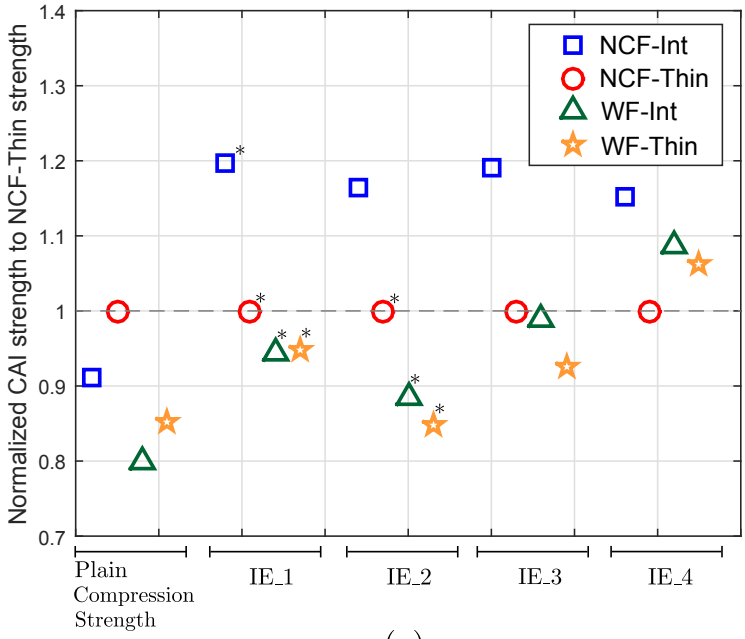

(a)

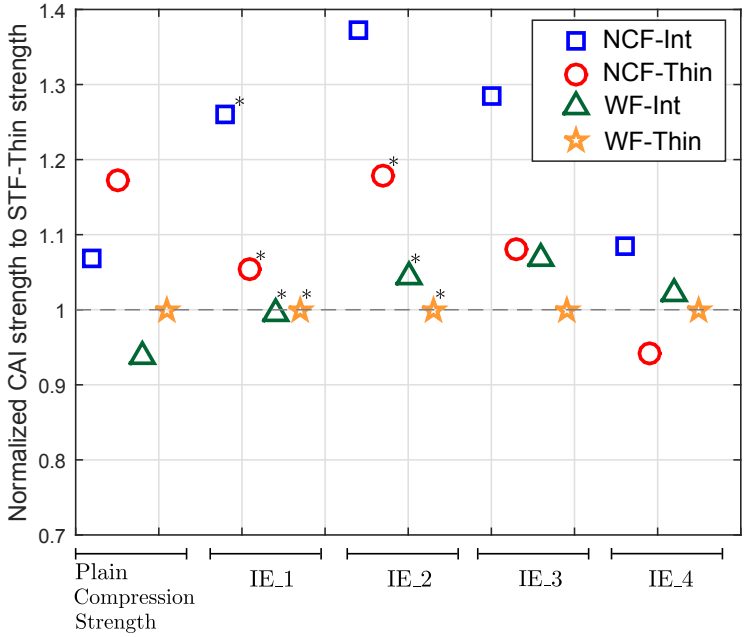

(b)

*CAI failure at the specimen top due to local buckling

Fig. 7.16.: Comparison of CAI strength normalized with (a) NCF-Thin as baseline and (b) WF-Thin as baseline. The plain compression strength is also normalized according to the respective baselines.

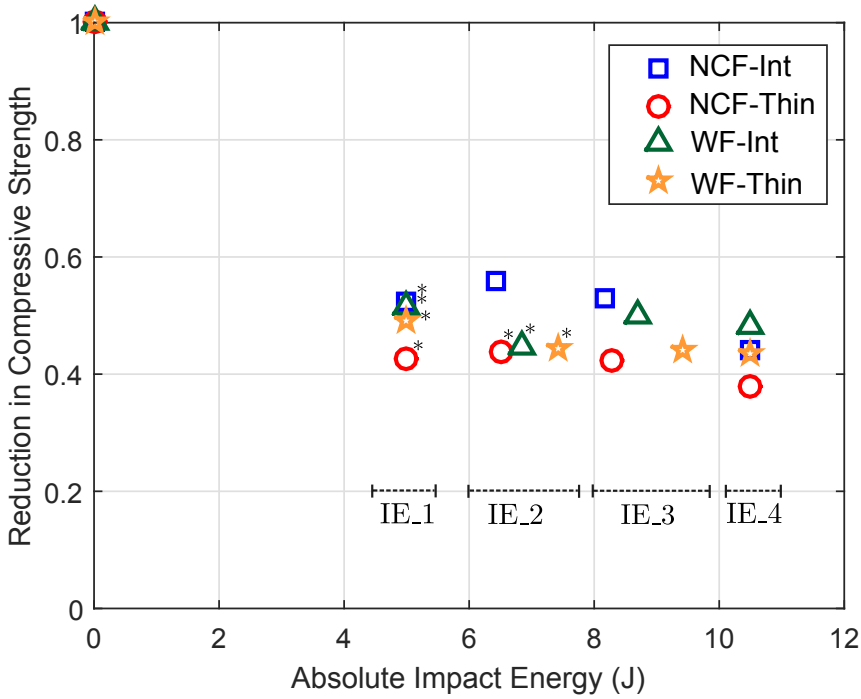

*CAI failure at the specimen top due to local buckling

Fig. 7.17.: Normalized reduction in the compressive strength due to the impact damage of all laminates.

fabrics [72], thereby demonstrating the effect of woven reinforcement architecture.

WF laminates exhibited more delaminated interfaces and a reduced projected area compared to NCF. QSI results revealed that most delaminations were formed within the WF fabric blanket, which can be due to the higher mismatch angle of 90° within the fabrics that favours delamination [9]. The reduced projected damage area of WF is reasoned to be either the higher number of delaminated interfaces or the delamination propagation being suppressed by the increased mode II fracture toughness of the woven fabrics, where the delamination cannot extend easily as it is forced to change its plane following the weft and warp. Further, the magnitude of fibre failure is far smaller in WF laminates compared to NCF. The delamination onset for WF laminates happens before delamination onset for NCF laminates (as in Figs. 7.12 and 7.14), and this could probably delay the fibre damage onset. In addition, the interwoven fabric architecture may help to suppress the escalation of

fibre damage. When a fibre bundle of a weft tow fails, the warp tows may help to re-distribute the stresses. Micro X-ray tomography investigations could help to obtain a proper understanding and can be employed in future work.

In analysing the ply thickness effect, thin laminates, due to the reduced bending stiffness, underwent significant bending during impact loads which led to high tensile stresses at the non-impacted laminate face. Because of the inherent in-situ effect of thin plies and lower interlaminar stresses, NCF-Thin delayed the onset of matrix cracking and consequently delaminations. However, with the delayed damage onset, early fibre failure was evidenced in NCF-Thin, as seen through the significant load drops in the impact response curves and also the early fibre splitting at the laminate back face evidenced in QSI results (Fig. 7.11 and Fig. 7.12). Even though delamination onset was suppressed, extensive delamination was observed after fibre failure in thin ply laminates (as reported in [62]), thus NCF-thin exhibited a higher projected damage area over NCF-Int at higher energies. On the other hand, early matrix cracking and delaminations in NCF-Int delayed and reduced the intensity of fibre failure by having less energy available for the fibre damage process.

The same explanation is valid for the greater damage resistance of WF-Int over WF-Thin, even though the improvement is marginal when compared with the NCF laminates. The roughly similar damage resistance response of the WF laminates may be due to the ply grades chosen for the study, as the difference between the thin ply grade (80 gsm) and standard ply grade (120 gsm) was not as significant as in the case of NCF laminates (67 vs 134 gsm). Delamination initiation and its location were evidenced in the QSI results, which otherwise would not have been able to be detected from the impact results. NCF-Int exhibited delaminations above and below the mid-plane cluster ply formed due to symmetry axis, and this cluster introduces high bending stiffness mismatch between the adjacent interfaces, leading to high interlaminar shear stresses. The same can be seen with NCF-Thin just below the mid-plane.

7.4.2 Impact damage tolerance

An average 15% lower plain compression strength was observed on woven fabrics when compared to non-crimp fabrics. With the same fibre-resin material system for both types of fabrics, the reduction in the in-plane compressive strength is related

to the fibre tow waviness of the woven fabrics [138]. It should also be kept in mind that the ply ratio along each orientation is not the same for NCF and WF laminates. Despite this, the waviness is greatly reduced in spread-tow woven fabrics compared to conventional ones [140, 142, 143]. The minimal waviness causes the in-plane properties of woven fabrics to be extremely close to that of the UD tapes. However, the minimal but inevitable waviness induces fibre kinking under compressive loading that impairs the compressive strength. Therefore, the same woven fibre architecture which helped to increase the damage resistance and fracture toughness, counteracted this with reduced CAI strength.

On the ply thickness effect, thin plies demonstrated an increased plain compression strength (10% for NCF and 7% for WF) over their intermediate ply counterparts. Thin plies possess increased longitudinal compression strength mainly attributed to the uniform micro-structure of the thin spread-tow, less waviness associated with thin plies, thus leading to fewer resin rich areas [63, 140]. In the framework of compression after impact, as discussed in the previous section, the behaviour thin plies possess characterised by early and extensive fibre failure (because of delayed matrix cracks and delamination) has resulted in the reduced CAI strength thin ply laminates demonstrate (also reported in [110]). Contrary to the thick or standard laminates, where thin plies improved the CAI strength over thicker plies [55], thin plies used with thin laminates have led to increased fibre failure leading to reduced CAI strength. As explained earlier, thin plies dissipated most of their energy through fibre failure, whereas the intermediate plies do this through delamination. The final collapse of the specimen during CAI loading is mainly driven by the impact induced fibre damage than by the delamination, as is seen in the case of thin laminates.

7.4.3 Thin laminates and masked delamination load drops

Contrary to the thick or standard laminates, the thin laminates exhibited no signs of load drop in the initial stages of loading, where the initiation and propagation of delaminations are literally hidden in the force response curves. This is clearly seen from the QSI results for both NCF and WF laminates, where a delamination observed in the C-scan inspection is not represented by any load drop in the force response curve. As reported in [65], this is explained as an effect of the reduced laminate thickness. The force-deflection response curve of a laminate is the sum of the bending

and membrane-stretching stiffnesses of the laminate. At higher deflections, where the membrane-stretching is dominant, the delaminations and their associated load drop have little influence on membrane behaviour. Hence, the significant load drops encountered in the force responses of the thin laminates is related to fibre damage, where the in-plane membrane stiffness drops due to the damaged fibres. Therefore, unlike the thick laminates, the force responses of the thin laminates does not signal the initiation or development of matrix and delamination damage through load drops, as these are only detected through damage inspections.

7.4.4 Damage tolerance in terms of damage detectability

One of the ultimate goals of the research community is to improve the damage tolerance of a structure. That is, the ability of the structure to have enough residual strength to carry post-impact service loads until the impact damage has been detected. It is also equally important for impact damage to be detected during service inspections so that it can be repaired and a final structural collapse avoided [19, 81]. Impact damage is normally detected through the permanent impact dent depth formed on the impacted surface. It has been reported that a dent depth between 0.25 to 0.5 mm deep is highly likely to be detected [17]. When comparing NCF and WF laminates in this framework, WF laminates exhibited less than 0.1 mm dent depth even at the highest impact energy, while NCF showed three or four times higher dent depth, thereby increasing their chances of being detected (as in Fig. 7.8). Moreover,WF laminates displayed a reduced residual strength which leads to a worse scenario as the damage can be left undetected, and at the same time they do not have a higher residual strength to withstand the loads. NCF outperform WF laminates in this, because the chances of detecting the damage is greater and also they have higher residual strength.

In a recent work by the authors [110], we carried out a similar study with UD tapes (using the same fibre-resin material as in this paper) considering different ply thicknesses. Comparing the impact and post-impact performance of fabrics with UD tapes (note that the UD baseline considered here is the intermediate ply grade of 134 gsm), the damage resistance of UD tapes and non-crimp fabrics is very similar, whereas the woven fabrics exhibit a superior performance compared to both UD and NCF. Meanwhile, non-crimp fabrics, NCF-Int exhibit considerably higher impact

tolerance values (about 15%) than UD and there were similar CAI values between the UD and the woven fabric WF-Int.

7.4.5 Textile fabrics: prospects and further work

The study concludes that woven fabrics have good damage resistance, while NCF have a higher residual strength for post-impact loads and also favour impact damage detectability. Hence, these fabrics can be customized according to particular aircraft structures and the type of loads encountered. As a further improvement, laminates can be designed with hybrid designs at the ply level, where the standard and the thin ply grades can be mixed in the same laminate, as was done by the authors with UD plies [110]. The standard plies help to reduce the magnitude of fibre failure by dissipating energy through delaminations, while the thin plies and their improved compressive strength help in post-impact compressive loads. For woven fabrics, the means of improvement is to have the least reduction in the in-plane compressive properties when compared to UD plies, which is a key factor in improving post-impact residual strength. Since the woven fabric architecture helps to improve the fracture toughness and at the same time reduces the in-plane compressive properties, a balance between these two features should be made. One of the options is to substitute 0° fabric layers with UD 0° plies, where the undistorted 0° plies provide the residual strength during the in-plane compressive loading of CAI [144].

7.5 Conclusion

We carried out an experimental campaign to study the effect of fabric reinforcement architecture and tow thickness on the impact and compression after impact response of thin laminates (1.6 - 1.8 mm). We used two types of aerospace graded fabrics, namely non-crimp fabrics and woven fabrics, where two UD layers/tows were stitched and weaved together, respectively. In addition, two different tow thicknesses (standard and thin ply grade) were used for each fabric. Impact results revealed that woven fabrics undoubtedly exhibited a superior impact damage resistance, evidenced by the 50% less dissipated energy, reduced dent depth and projected damage area over the non-crimp fabrics. In terms of ply thickness effect, thin plies with thin laminates delayed the onset of cracks and delamination, but displayed early fibre failure, especially with non-crimp fabrics. This was demonstrated through quasi-

static indentation tests, where the entire sequence of damage evolution was compared. The intermediate ply grade exhibited improved damage resistance (50% and 45% less energy dissipated for NCF and WF, respectively) over thin plies. Despite a lower impact damage resistance, non-crimp fabrics displayed an average 20% higher CAI strength over the woven fabrics. In addition, intermediate ply grade exhibited higher post-impact residual strength (20% and 10% higher CAI strength for NCF and WF, respectively) over their thin ply counterparts. With textile fabrics being a good economic prospect, future work can be dedicated to mixing plies of different thicknesses in the same laminate, thereby aiming to improve the damage tolerance.

8

Paper E:

Mitigating the weak impact response of thin-ply based thin laminates through an unsymmetrical laminate design incorporating intermediate grade plies

A. Sasikumar[a,*], D. Trias[a,1], J. Costa[a,*], V. Singery[b], P. Linde[c,d]

[a] AMADE, Polytechnic School, Universitat de Girona, Campus Montilivi s/n, E-17003 Girona, Spain

[b] Chomarat, 39 Avenue de Chabannes, 07160 Le Cheylard, France

[c] Airbus Operations GmbH, Kreetslag 10, 21129 Hamburg, Germany

[d] Department of Industrial and Materials Science, Chalmers University of Technology, S-41296 Gothenburg, Sweden

[*] Corresponding author

[1] Serra Hunter Fellow

The paper has been published in ***Composite Structures*** 220 (2019) 93–104.

Motivation & Synopsis

Paper D revealed the weak impact response of thin plies based non-crimp fabrics when used with thin laminate. The thin ply laminate exhibited extensive fibre failure and resulted in reduced CAI strength. Understanding that thin plies when used along with thin laminates result in critical fibre damage, the next immediate step is to improve the impact response of thin ply with thin laminates. While ply hybridization (from paper C) and unsymmetrical designs (from paper A) offered promising results, the idea of combining both the concepts in a laminate was the main foundation of this paper. An unsymmetrical hybrid laminate is proposed with intermediate plies placed at the non-impacted side of a thin laminate. The main idea is to demonstrate the feasibility of unsymmetrical designs, in this case with thin laminates, and ply hybridization towards mitigating fibre damage and improving CAI strength. The proposed unsymmetrical hybrid laminate substantially delayed and reduced the fibre damage, which in turn resulted in a 30% improved CAI strength over the baseline.

Composite Structures 220 (2019) 93–104

Contents lists available at ScienceDirect

Composite Structures

journal homepage: www.elsevier.com/locate/compstruct

Mitigating the weak impact response of thin-ply based thin laminates through an unsymmetrical laminate design incorporating intermediate grade plies

A. Sasikumar[a,*], D. Trias[a,1], J. Costa[a,*], V. Singery[b], P. Linde[c,d]

[a] AMADE, Polytechnic School, University of Girona, Campus Montilivi s/n, 17073 Girona, Spain
[b] Chomarat, 39 Avenue de Chabannes, 07160 Le Cheylard, France
[c] Airbus Operations GmbH, Kreetslag 10, 21129 Hamburg, Germany
[d] Department of Industrial and Materials Science, Chalmers University of Technology, S-41296 Gothenburg, Sweden

Abstract

With aeronautic industries focussing on thinner structures and reducing manufacturing costs, recent research has been dedicated to the impact and post impact response of thin laminates (< 2 mm) made of textile fabric composites. A recent study revealed that thin laminates based on thin plies exhibit extensive fibre failure and reduced compression after impact strength. To mitigate this weakness, we propose a novel laminate concept based on combining plies of different thicknesses in an unsymmetrical configuration (intermediate grade plies are located only at the bottom of the laminate, i.e., the non-impacted face). C-scan inspection on impacted and quasi-statically indented specimens, allowed the damage sequence of the proposed unsymmetrical hybrid laminate to be compared with that of the thin-ply baseline. The hybrid laminate with intermediate plies at the bottom, delayed and reduced the fibre damage, decreased the projected delamination area and led to a 30% increase in the compression after impact strength in contrast to the thin-ply baseline laminate.

Keywords: Hybrid laminates, Non-crimp fabrics, Impact behaviour, Damage tolerance, Unsymmetrical laminates

8.1 Introduction

In the quest to reduce structural weight, aircraft manufacturers are considering using thin structures, especially for the fuselage and wing skins. One of the main

difficulties with these thin structures (< 2 mm) is their increased vulnerability to out-of-plane loads, coupled with a high reduction in the residual strength during the post-impact service cycles of the aircraft [5]. Recent research has reported that a low velocity impact (enough to create a barely visible impact damage on the laminate) has caused a 60-70% reduction in the compressive strength of thin laminates [110, 111]. This alarming reduction has led aircraft manufacturers to consider non-conventional laminate designs, not only as an economic way to reduce the severity of impact damage but also to improve the compression after impact (CAI) strength.

Despite the vast amount of impact studies performed on thick laminates [11, 55, 61, 62, 145, 146] (4-5 mm, as suggested in the ASTM standard [88]), very few studies have been dedicated towards thin laminates and their response to impact and CAI loads. Recently, Garcia et al. [68] discussed the effect ply thickness has on the out-of-plane response of 2.15 mm laminates made of non-crimp fabrics using tomographic investigations. The current authors [111] compared the effect fabric architecture and ply thickness have on impact and CAI strength of thin laminates (1.6 - 1.8 mm), where two types of fabrics, namely woven and non-crimp fabrics, were studied. Results revealed that, unlike thick laminates [61, 147], thin laminates made of thin plies resulted in extensive fibre damage which led to reduced CAI strength. Meanwhile, intermediate ply grades, even though they exhibited early damage onset in terms of delamination, had comparably lesser fibre damage, and led to greater CAI strength than thin plies had [68, 111].

Concerning non-conventional laminate designs, in a recent work [110], the authors proposed mixing uni-directional (UD) plies of different thickness grades to produce hybrid thin laminates. One of the hybrid designs (where thick 0° plies were added close to the laminate mid-plane symmetry along with thin plies) demonstrated a significant improvement in CAI strength (40%) when compared to the thin-ply baseline laminate. This study promised that by using a hybrid laminate the potential benefits of the different ply grades can be exploited through ply level hybridization, as is also demonstrated in [46–48]. Despite the novelty of hybridization, the laminate mid-plane symmetry constraint found in the studies and which restricts the laminate to having the same top sub-laminate layup mirrored below the symmetry plane, was still adhered. Because damage from an impact induces unsymmetrical damage modes in the laminate thickness direction, it is necessary to move away from the conventional

symmetry designs and also to enlarge the stacking sequence design space. In a preliminary study with thick laminates and using plies of same thicknesses [120], the authors demonstrated that the mid-plane symmetry can be challenged without the worry of warping and from this the laminate can be tailored towards impact loads by having different top and bottom sub-laminates.

These two concepts (unsymmetry and ply hybridization) could be combined into a laminate design where thick plies can be mixed with thin plies to form a hybrid laminate. At the same time, the thicker plies can be placed at a desired location without having to worry about placing equivalent thick plies on the other side of the laminate's mid-plane symmetry line. By employing this design idea, an attempt is made to tailor the damage in an impact scenario which, will in turn, could help to improve the CAI strength. According to the authors' knowledge, this is the first work reporting on the impact and CAI response of such novel laminate designs. In this paper, we designed a hybrid and unsymmetrical laminate (with zero warp) using non-crimp fabrics where intermediate plies had been added to thin plies to form a hybrid laminate. Within the framework of thin laminates (1.6 mm), we carried out an experimental study to investigate the impact and CAI response of this novel laminate design. In addition, we also compared the results with those of the baseline laminates (symmetric and non-hybrid), where one laminate was made only of intermediate plies and the other with only thin plies (baseline results presented by the authors in [111]). We also performed quasi-static indentation tests interrupted for C-scan inspection, to compare the damage initiation and evolution between the hybrid and the baseline laminates. Experimental results reveal that the proposed novel laminate design could tailor the impact damage with less fibre breakage and thereby considerably improve the CAI strength over the thin-ply baseline laminate.

8.2 Laminate design

8.2.1 Material

We used bi-axial non-crimp fabrics (NCF), where two differently oriented fibre tows are stitched together using a polyester yarn. The double axis layup of the NCF blankets reduces the manufacturing costs significantly [148]. The material system used is a carbon fibre T700 pre-impregnated with HexPly M21 resin. Bi-axial prepreg

blankets of [0°/45°] and [0°/-45°] which can also lead to other orientations through flipping and/or rotation, were used. We employed two different fabric thickness grades: 268 and 134 gsm, so the UD ply thickness corresponds to 0.134 and 0.067 mm, and, in this paper, referred to as intermediate and thin ply grade, respectively.

8.2.2 Rationale behind the laminate design

From the experimental results reported in [110, 111], the thin laminates, unlike the thick laminates, underwent considerable bending under impact loads and the high in-plane tensile loads led to fibre splitting at the back face of the laminate. The thin laminates made of thin plies, delayed delamination but exhibited extensive back fibre splitting, while the intermediate ply grades displayed an early delamination onset, but with a reduced fibre damage. Hence, to exploit the potential of both ply grades (i.e., the ability of intermediate plies to reduce fibre damage by dissipating energy through delaminations and thin plies to delay damage onset, along with higher plain compression strength they possess [111]), we propose a hybrid laminate design, where intermediate plies are added to a thin-ply NCF laminate.

Furthermore, it is equally important to decide in which through-the-thickness location in the laminate, the intermediate plies have to be added. As the non-impacted face of the laminate is prone to extensive fibre splitting when used with thin plies, our intention was to add intermediate plies at the non-impacted laminate face, in an attempt to reduce fibre breakage by promoting delamination. Hence, this demands an unsymmetrical laminate design with a minimum bending stretching coupling matrix ([B]) to avoid warpage during manufacturing [99].

8.2.3 Unsymmetrical hybrid laminate design: Optimization

We used an optimization algorithm (a genetic algorithm embedded in the MATLAB optimization toolbox [89]) to search for unsymmetrical laminate designs with a minimum or null B value. The objective function was to minimize the sum of B matrix terms, and the constraints were as given below:

- Balanced and quasi-isotropic laminate.
- Four plies (two NCF blankets) of intermediate ply grade as bottom plies (at the non-impacted face of the laminate)

- As the outer plies are affected by impactor indentation (impacted face) and fibre splitting (non-impacted face), they were fixed to be 90° as they are comparatively the least influential on the CAI strength. For the same reason, the 0° plies were restricted from being placed in the outer NCF blankets.

- The equivalent bending stiffness parameter (D*, proposed by Olsson [123] and applied as an optimization constraint in [9]) is made to match within 1% of the value of the baseline laminates to have a proper comparison.

A solution (an unsymmetrical-hybrid laminate with null B matrix) satisfying all the constraints was obtained and is provided along with details in the following section.

8.2.4 Laminates and stacking sequences

The unsymmetrical-hybrid laminate (with zero B matrix) obtained is provided in Table 8.1, and hereafter will be referred to as NCF-UHB, denoting 'Unsymmetrical Hybrid laminate with intermediate plies at Bottom' (non-impacted side). The same laminate is flipped upside down to have an 'Unsymmetrical Hybrid laminate with the intermediate plies at the Top' (impacted side), and will be referred to as NCF-UHT. The objective of introducing the NCF-UHT laminate is to understand the effect the location (at impacted or non-impacted side) of the added intermediate plies has on the impact and CAI response. To study the effect of hybridization, the two unsymmetrical hybrid laminates are compared to baseline laminates, namely NCF-Int and NCF-Thin (results published by the authors in a recent work [111]). NCF-Int and NCF-Thin are symmetrical laminates made using only one ply grade, namely intermediate and thin ply grades, respectively. It is also important to recall that NCF-UHB and NCF-UHT are thin-ply dominant (comprising of 67% thin plies and 33% intermediate grade plies for the laminate thickness) hybrid laminates. All four laminates and their stacking sequences are illustrated in Fig. 8.1 and Table 8.1 provides further laminate details.

Figs. 8.2 (a) and (b) present the polar plots of the in-plane and bending stiffnesses, respectively, of all the laminates. Note that the baseline laminates are in-plane non-quasi isotropic, while the proposed unsymmetrical laminates are in-plane quasi-isotropic. The maximum deviation of the equivalent bending stiffnesses (D*) between the proposed and the baseline laminates is less than 0.2%,hence the difference is

negligible in terms of the practical application of these laminates.

Tab. 8.1.: Laminates and their details

Laminate	Description	Stacking sequence	Ply thickness (mm)	Laminate thickness (mm)	D* (Nm)
NCF-Int	Intermediate plies	$[(45/0)/(-45/90)/(22.5/-22.5)]_S$	0.134	1.61	18.6
NCF-Thin	Thin plies	$[(45/0)/(-45/90)/(45/0)/(-45/90)/(45/0)/(-45/0)]_S$	0.067	1.61	18.9
NCF-UHB	Hybrid (Int. and thin plies)	$[(90/-45)/(0/45)/(90/-45)/(0/45)/(90/-45)/(0/45)/(90/-45)/(0/45)/(45/0)_{268}/(-45/90)_{268}]$	0.134 & 0.067	1.61	18.8
NCF-UHT	Hybrid (Int. and thin plies)	$[(90/45)_{268}/(0/-45)_{268}/(-45/0)/(45/90)/(-45/0)/(45/90)/(-45/0)/(45/90)/(-45/0)/(45/90)]$	0.134 & 0.067	1.61	18.8

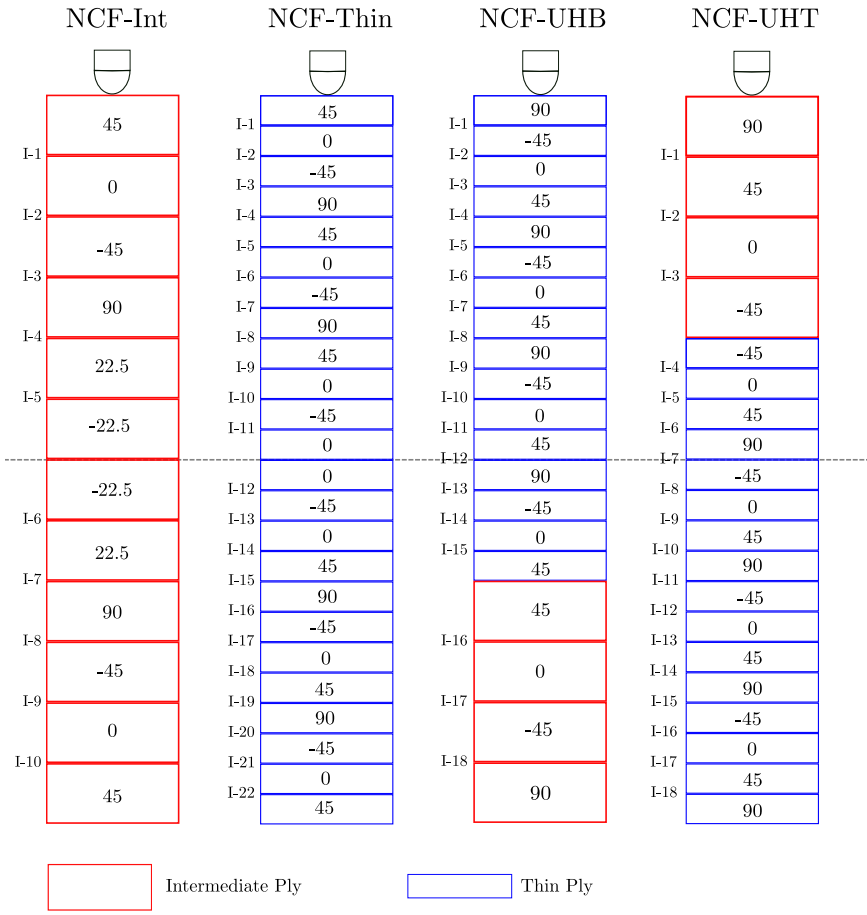

Fig. 8.1.: Illustration of all the laminates used for the study: NCF-Int, NCF-Thin, NCF-UHB and NCF-UHT, where NCF-UHT is obtained by flipping NCF-UHB upside down. Note that U refers to unsymmetry, H to hybrid design, T and B to top and bottom (location of intermediate grade plies).

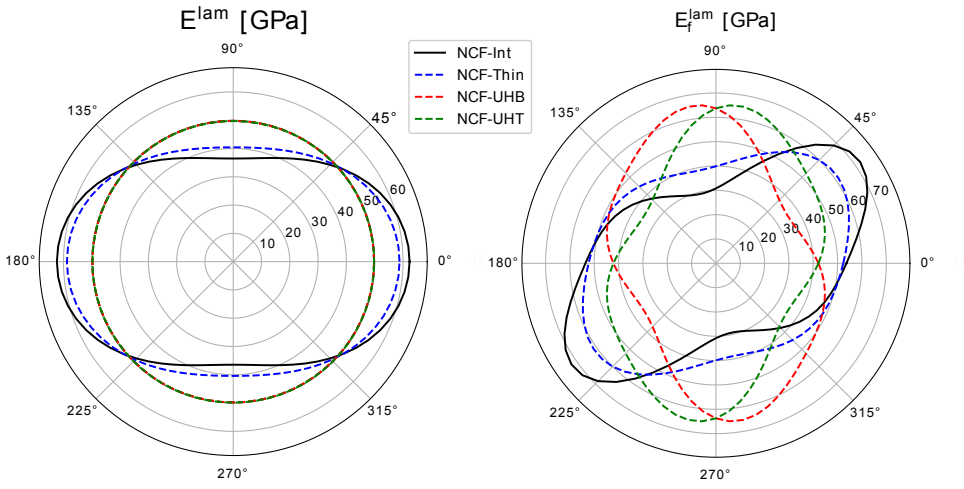

(a) (b)

Fig. 8.2.: Polar plot representation of the (a) in-plane stiffness and (b) bending stiffness of all the laminates.

8.3 Experimental methods

Impact specimens of dimensions 150 x 100 mm were cut from the panels with 0° plies aligned with the specimen length. NCF-UHB specimens were flipped upside down to obtain NCF-UHT specimens, i.e., the one with the intermediate plies at the top. Note that flipping a laminate upside down only interchanges the 45° plies by -45° and vice-versa. We performed the impact tests in accordance with the ASTM D7136/D7136-15 standard [64], using a CEAST Fractovis Plus instrumented drop-weight tower. A 16 mm steel hemispherical indenter was used and the total mass of the impactor setup was set to 3 kg.

Three impact energies, 6.4 J, 8.2 J and 10.5 J, (the same energies as used in [111] for the baseline laminates NCF-Int and NCF-Thin) were explored, and hereafter will be referred to as IE_1, IE_2 and IE_3, respectively. We impacted nine specimens per laminate, with three specimens for each impact energy, to assess the repeatability. Further details of the experimental impact setup can be found in [42].

We performed quasi-static indentation (QSI) tests with an MTS INSIGHT 50 testing machine with a 50 kN load cell and displacement controlled loading of the indenter. 150 x 100 mm specimens were placed on a base plate, which has an open window of

125 x 75 mm. Four rubber clamps were used to fasten the specimen to the base plate. A constant indenter displacement of 1 mm/min was used. We explored a total of seven indenter displacements, the same as in [111], for comparison purposes. A total of three specimens per laminate were used for the QSI tests, where a same specimen was loaded and then interrupted for C-scan damage inspection and then followed by a higher indenter displacement loading. The damage was inspected after impact and after each QSI loading level using a pulse-echo ultrasonic C-scan technique. The C-scan setup featured an OLYMPUS OMNI MX system along with a 5 MHz piezoelectric probe.

To evaluate the post-impact compressive strength, CAI tests were performed on the impacted specimens using an MTS INSIGHT300 machine with a 300 kN load cell, following the ASTM D7317/D7137M-15 [88]. To account for the reduced laminate thickness, we used an additional anti-buckling device (proposed by Remacha et al. [67]) along with the CAI fixture. The additional fixture ensured the specimen was refrained from global buckling, thus ensuring a proper compressive failure at the specimen's impacted site. Furthermore, to evaluate the pristine compression strength, plain compression strength tests were performed in accordance with the ASTM D6484/D6484M-14 standard [87]. Three 305 x 30 mm specimens were tested with a cross head displacement of 1 mm/min for the plain compression strength at the INEGI research facility at the University of Porto. All the above tests, except plain compression strength, were performed at the AMADE research laboratory (NADCAP certified for non-metallic material testing) at the University of Girona.

8.4 Results

8.4.1 Impact

Figs. 8.3, 8.4 and 8.5 present the impact force-time, impact force-deflection and impact energy-time curves, respectively, of all four laminates. Note that, due to good repeatability, only one specimen data per laminate per energy level is presented. Inspecting the curves in Figs. 8.3 and 8.4, a clear difference in the impact response is seen between NCF-UHB and NCF-UHT, indicating the effect the location of the added intermediate plies has on the impact response.

For the lowest energy level IE_1, no load drop was observed with NCF-UHB, which

also exhibited the maximum peak force (3200 N) compared to all other laminates. To the contrary, NCF-UHT exhibited its first significant load drop close to 2200 N, followed by further load drops, thereby leading to a suppressed load carrying capability compared to NCF-UHB. Moving on to the higher energies (IE_2 and IE_3), NCF-UHB displayed first significant load drop close to the peak load (3500 N) followed by successive drops. In reviewing the impact curves in Figs. 8.3 and 8.4, the laminates can be grouped in terms of their similar responses, for instance, NCF-Int and NCF-UHB in one group, and NCF-Thin and NCF-UHT in the other. Similar behaviour was observed with the energy evolution curves (Fig. 8.5) where NCF-UHB dissipated significantly less energy than NCF-UHT for all impact energies explored. While NCF-UHB had the least dissipated energy for IE_1, at higher energies it dissipated more energy than NCF-Int, but still significantly less than NCF-Thin and NCF-UHT.

Fig. 8.6 compares the projected impact damage profile for the four laminates obtained from C-scan inspection. The projected damage area, the dominant delaminations and their corresponding interfaces are also marked in the same figure. The thin-ply laminate NCF-Thin exhibited the highest projected damage area while the hybrid NCF-UHB displayed the least. It is important to note that both the hybrid laminates considerably reduced the damage area compared to their baselines. While NCF-Int had dominant delaminations at interface 10 (bottom interface) and 6 (interface just below the mid-plane) oriented at 45° and 22.5°, respectively, NCF-Thin exhibited a dominant delamination at interface 12 (just below the mid-plane ply cluster), as reported in [111].

With the hybrid designs, NCF-UHB displayed a dominant delamination at the last interface (int. 18 (-45°/90°), at the site of the intermediate grade plies added at the laminate bottom) oriented at 90°, as predicted during the laminate design phase. At the highest impact energy, the total projected damage area is governed by this single last interface delamination, where the other delaminations are found to be comparatively negligible (see Fig. 8.6). For NCF-UHT, interfaces 5 (0°/45°) and 10 (45°/90°) exhibited dominant delaminations, with orientations at 45° and 90°, respectively. Contrary to NCF-UHB, many interfaces contributed towards the total projected damage area of NCF-UHT. While NCF-UHB had dominant delamination at the non-impacted site where the intermediate plies were added, NCF-UHT exhibited

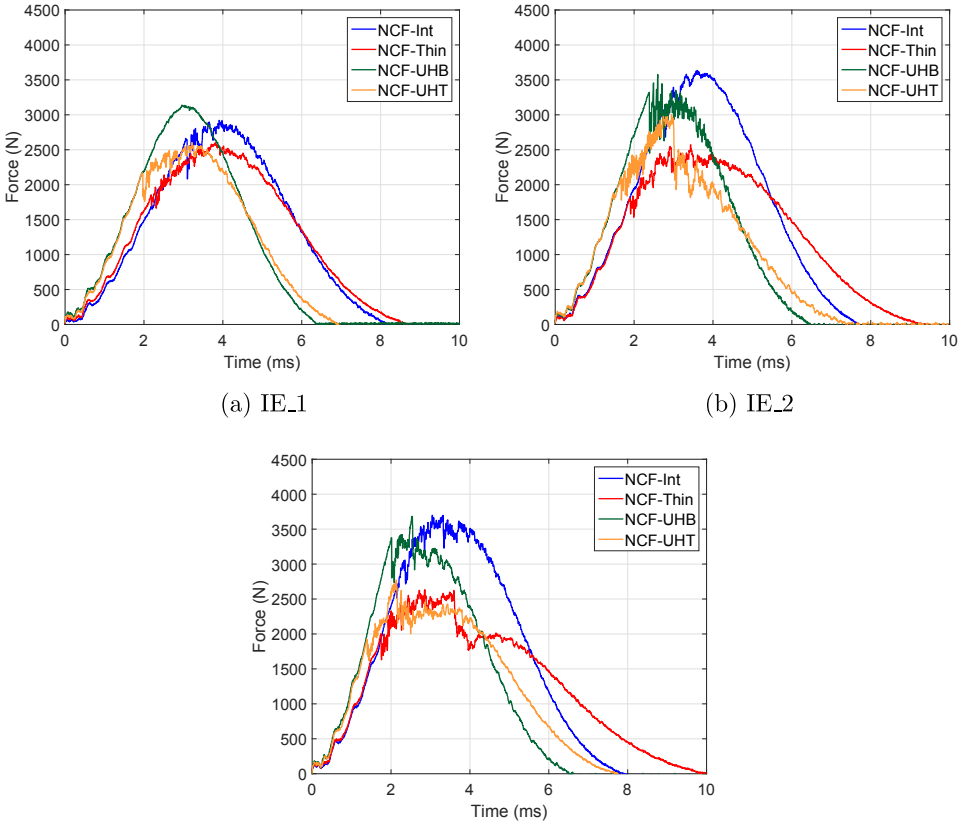

(a) IE_1

(b) IE_2

(c) IE_3

Fig. 8.3.: Impact force-time response curves of all laminates for all three impact energies.

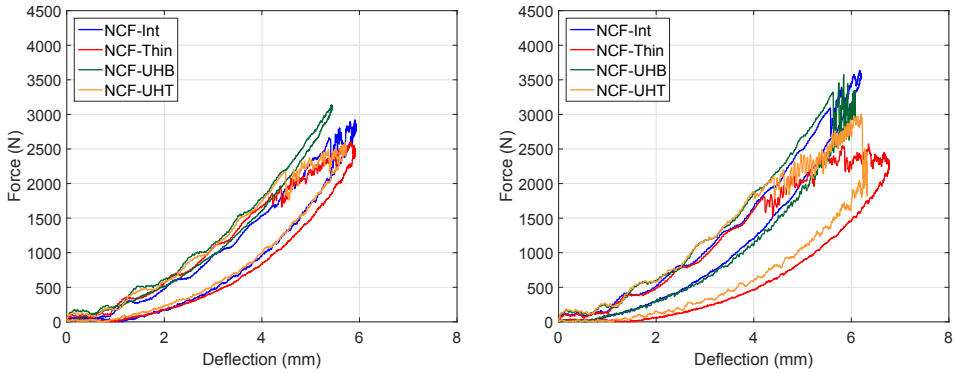

(a) IE_1

(b) IE_2

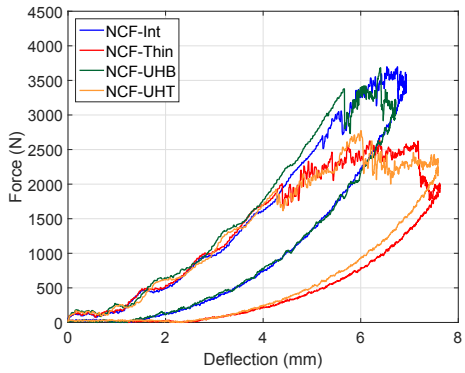

(c) IE_3

Fig. 8.4.: Impact force-deflection response curves of all laminates for all three impact energies.

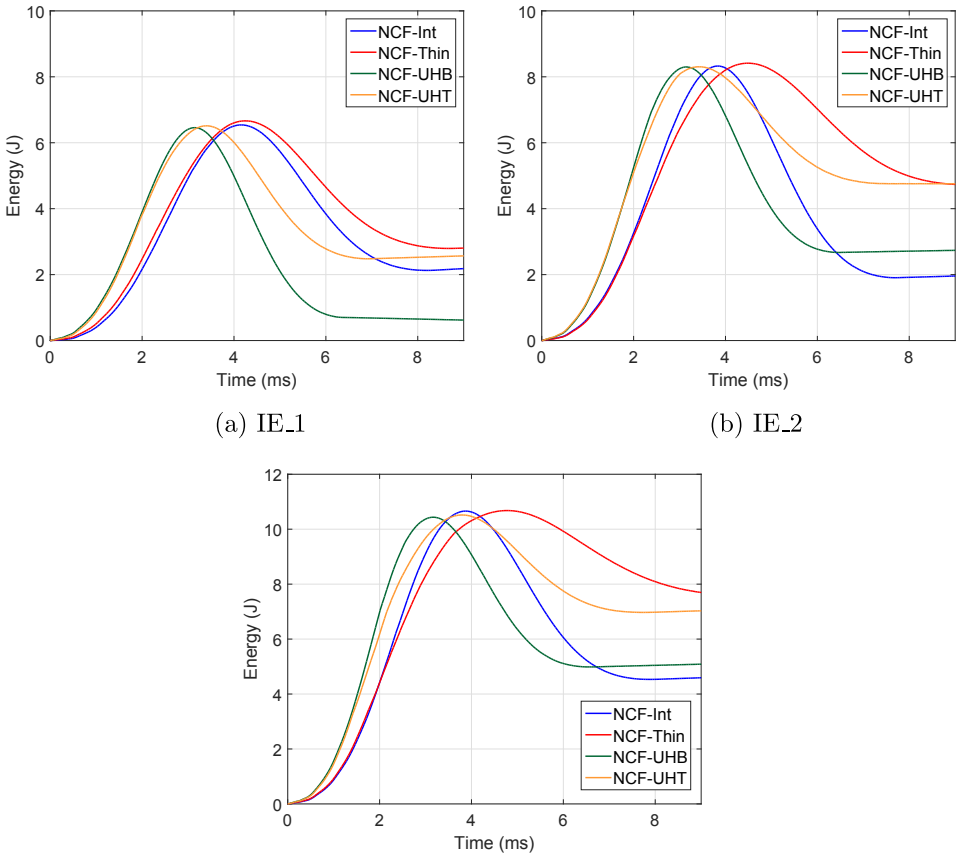

(a) IE_1

(b) IE_2

(c) IE_3

Fig. 8.5.: Impact energy evolution curves of all laminates for all three impact energies.

dominant delaminations just below the added intermediate plies (at and just below the mid-plane).

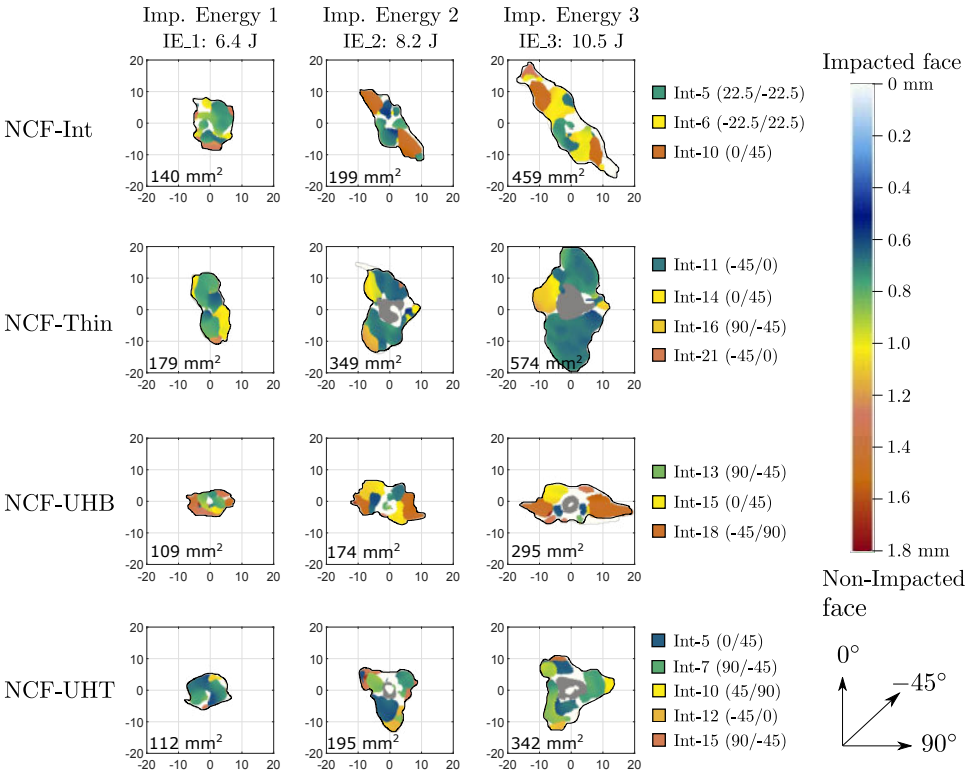

Fig. 8.6.: C-scan inspection images of all laminates along with the projected damage areas and the dominant delaminations identified (the field of inspection presented is a 40 x 40 mm square window with impacted site as the centre).

Fig. 8.7 presents the photos of the impacted and non-impacted faces of all the laminates from the 10.5 J impact. The impact dent depth at the impacted face and the fibre splitting (in the orientation of the last ply) at the non-impacted face can be visually compared between the four laminates. While the thin ply NCF-Thin exhibited the highest magnitude of impact dent depth and extensive fibre splitting, the intermediate-ply laminate NCF-Int comparatively suppressed both these parameters, as reported in [111]. The hybrid laminates, despite being a thin-ply dominant laminate, exhibited reduced back fibre splitting compared to its baseline NCF-Thin due to the inclusion of the intermediate plies.

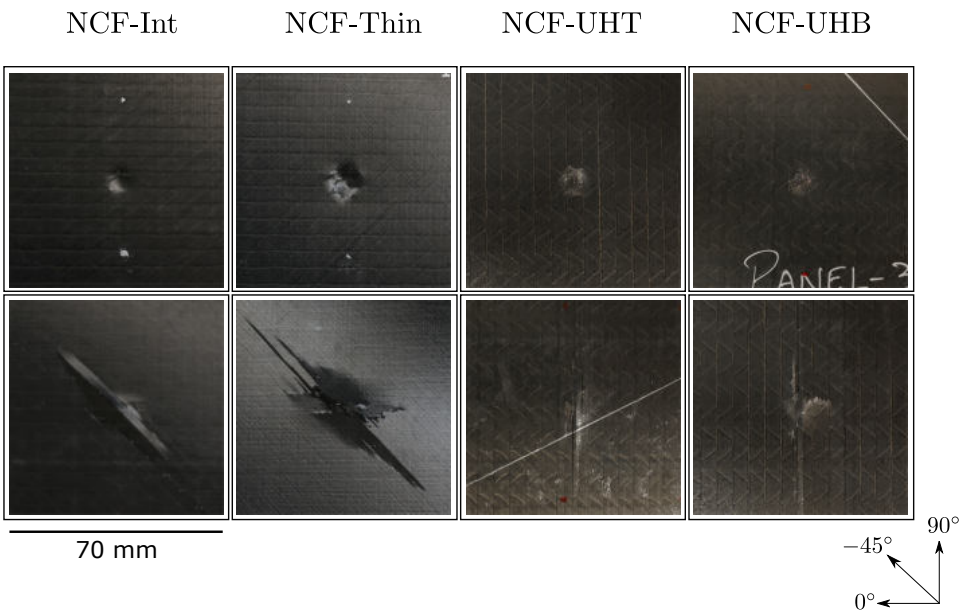

Fig. 8.7.: Impact (top) and non-impacted (bottom) laminate face photos of all laminates after the 10.5 J impact (represented field of view is a 70 x 70 mm square window with the impacted site as the centre).

Figs. 8.8(a) and (b) represent the evolution of the peak load and projected damage area, respectively, for increasing impact energies, while Figs. 8.9 (a) and (b) present the dissipated energy and impact dent depth against the impact energies, respectively. Out of all the laminates, NCF-Thin possessed the least load carrying capability, as evidenced by the least peak load (Fig. 8.8(a)). NCF-UHB and NCF-Int displayed similar values, despite NCF-UHB having slightly higher values for the first two energies. Compared to the baseline NCF-Thin, NCF-UHB exhibited a 30% higher peak force considering all the impact energies. In terms of the projected damage area, both hybrid laminates exhibited less area compared to the baselines, whereas NCF-Thin displayed the greatest damage area. NCF-UHB laminate showed the smallest damage area, with a significant reduction of 50% and 20% over the thin ply baseline NCF-Thin and the intermediate ply baseline NCF-Int, respectively (Fig. 8.8(b)).

NCF-Int and NCF-UHB exhibited the least dissipated energy, while NCF-Thin and NCF-UHT dissipated the highest. NCF-UHB exhibited a 30% reduction in the dissipated energy over NCF-Thin. We observed similar responses with the impact dent depth, where the thin-ply laminate NCF-Thin exhibited the highest dent depth followed by the hybrid laminate NCF-UHT. NCF-Int and NCF-UHB suppressed the impact dent depth compared to the other two laminates, where NCF-UHB displayed a 50% reduced dent depth compared to the thin ply baseline NCF-Thin.

8.4.2 Quasi-static indentation

Fig. 8.10 compares the force-deflection responses of the two hybrid laminates along with that of the baselines for the highest indenter deflection of d_7= 6 mm. Other indenter deflections studied (d_1 to d_6) are also marked on the same figure. As already reported in [111], NCF-Int exhibited the first load drop at around 3500 N, close to the maximum peak load. To the contrary, NCF-Thin exhibited an early load drop, at around 2000 N, followed by successive load drops leading to a reduced maximum load (as also observed in the impact results). With the hybrid laminates, NCF-UHT behaved similar to NCF-Thin, with early and intermittent load drops, whereas NCF-UHB displayed a similar response to that of NCF-Int with the first load drop occurring at the peak load. Compared to thin-ply baseline NCF-Thin, interestingly, both hybrid laminates delayed the first load drop. NCF-UHB and

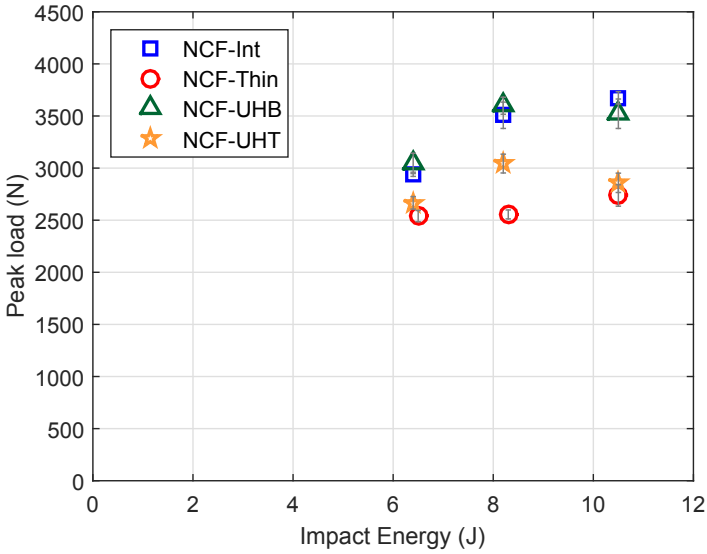

(a)

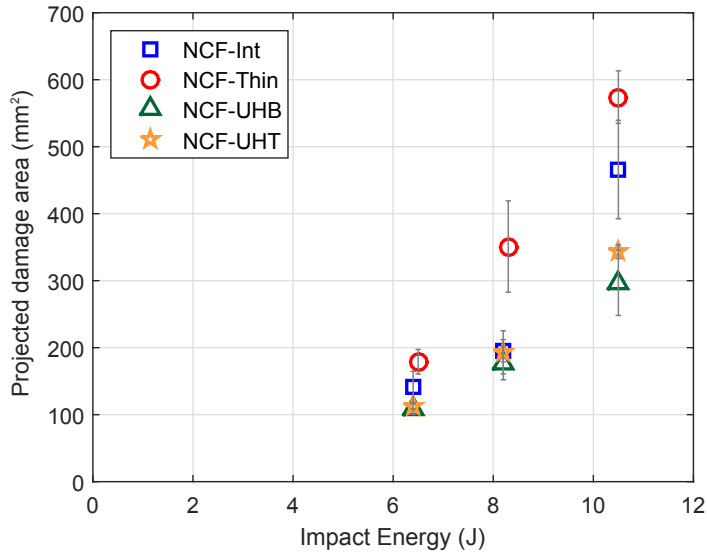

(b)

Fig. 8.8.: Impact damage resistance parameters (a) peak load and (b) projected damage area compared between all the laminates for all the impact energies (average value is presented along with the standard deviation indicated by the vertical markers).

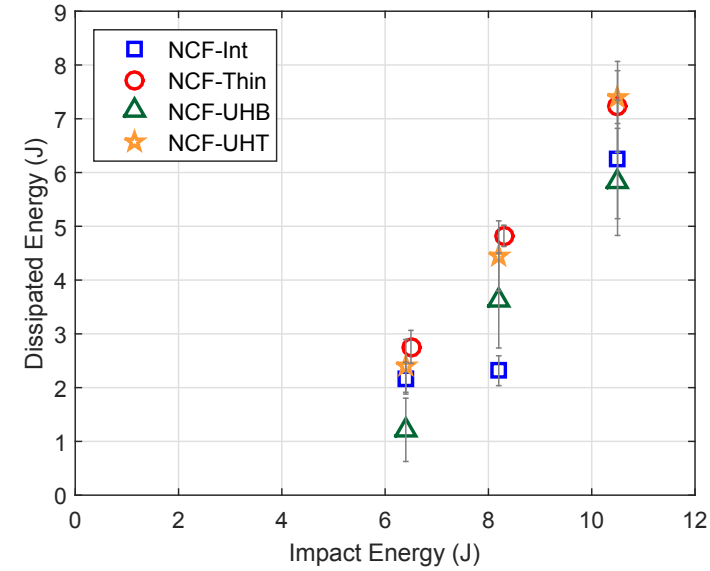

(a)

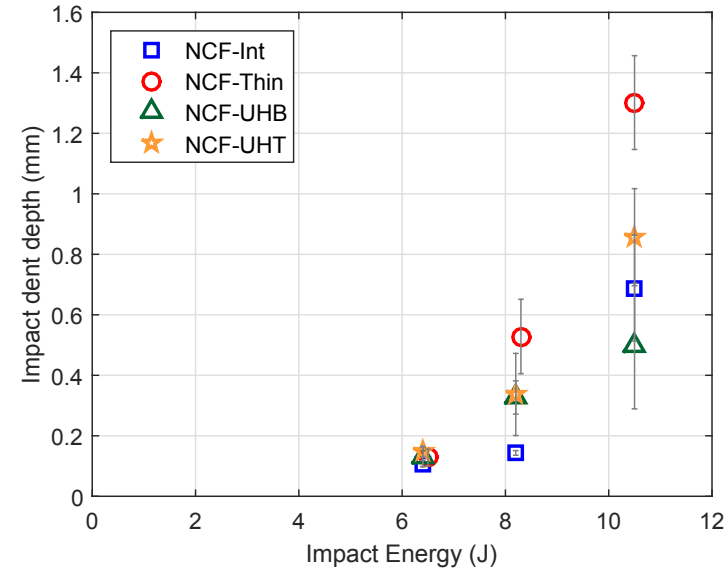

(b)

Fig. 8.9.: Impact damage resistance parameters (a) dissipated energy and (b) impact dent depth compared between all the laminates for all absolute impact energies (average value is presented along with the standard deviation indicated by the vertical markers).

NCF-UHT, respectively, exhibited a 55% (3300 N) and 15% (2400 N) increase in the force value at which the first load drop was observed (attributed to fibre damage initiation), when compared to NCF-Thin.

Fig. 8.11 presents the C-scan images of the damage profile for all the indenter displacement levels for all the laminates. The figure also presents the applied energy and projected damage area for each displacement, identified delaminated interfaces and the initiation of fibre splitting (marked by 'FS' denoting fibre split in Fig. 8.11), observed by visual inspection of the non-impacted surface. It is evident that intermediate plies (NCF-Int) displayed early delamination at d_1, even though no associated load drop was seen in the force-deflection response. There was no sign of damage in the other three laminates at d_1. At d_2, NCF-UHB showed the first instance of delamination, identified at the last interface (int 18: (-45°/90°)). NCF-Thin and NCF-UHT delayed the onset of damage, the first instance of which was observed at d_3, whereas damage had already been propagated in NCF-Int and NCF-UHB. Delamination onset was identified in NCF-UHT at the top sub-laminate (just below the added intermediate plies) at interface 5 (0°/45°). Moving on to d_4, NCF-Thin exhibited back fibre splitting associated with the load drop (see Fig. 8.10) between d_3 and d_4. On further loading, the dominant delamination was identifed in NCF-UHB at the last interface (at the bottom, within the added intermediate plies) and at the mid-plane (int 7: (90°/-45°)) for NCF-UHT. With continued loading, NCF-UHT displayed fibre splits associated with the load drop between d_5 and d_6. The highest indenter displacement d_7 marked the onset of fibre splits on NCF-Int and NCF-UHB, also indicated by the high load drops seen in their respective curves. It is interesting to note that both hybrid laminates exhibited 50% reduced damage area compared to the thin-ply baseline NCF-Thin. The QSI results (mainly the force-deflection curves, the damage profile and the first load drop) are coherent with the impact results. While the initiation of delamination is hidden in the force response curves of these thin laminates [111], the load drops correspond to the initiation and extension of fibre damage.

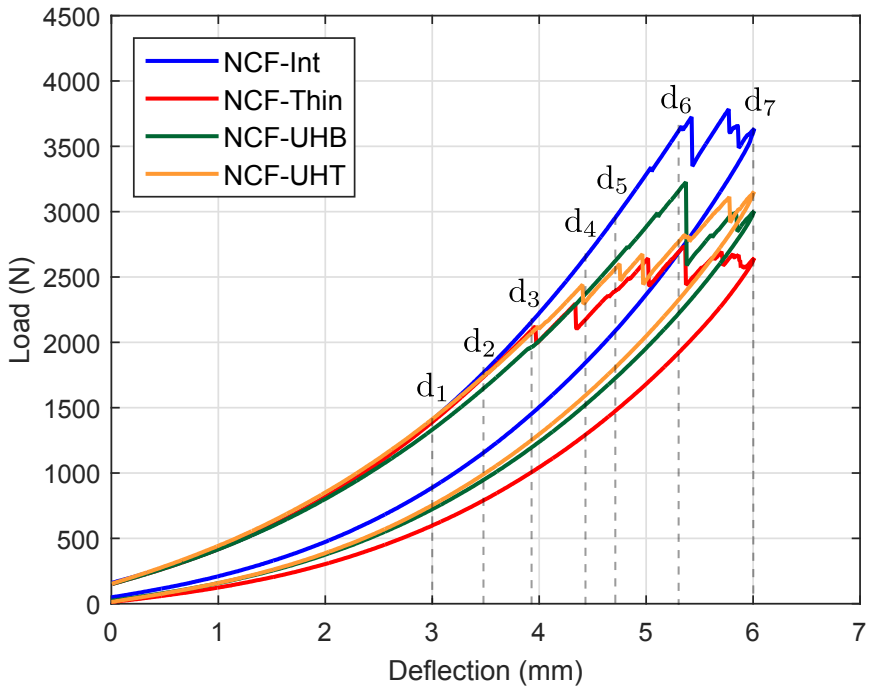

Fig. 8.10.: QSI load deflection responses of all laminates for the highest deflection d_7=6 mm, and the other indenter deflections studied (d_1 to d_6) are also marked.

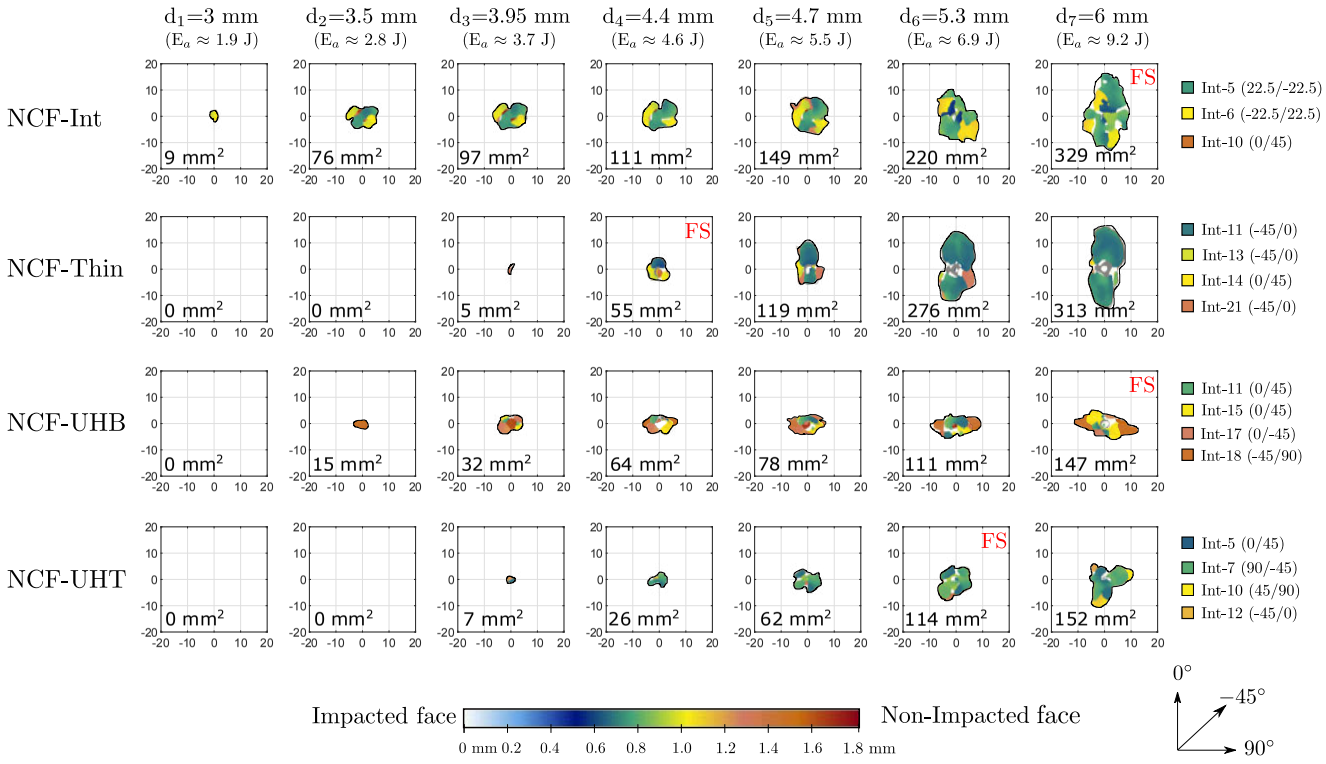

Fig. 8.11.: C-scan inspection images for all laminates for all the indenter deflections from d_1 to d_7. Projected damage profile and area are presented, furthermore the initiation of back fibre splitting is also identified and marked by 'FS'.

Fig. 8.12 presents the evolution of the dissipated energies (E_d) against the applied energies (E_a) for the different QSI deflection levels. The applied energies are calculated by integrating the area under the whole loading part of the respective QSI curves, while the dissipated energy is the area of the enclosed curve obtained. Until the applied energy of 4 J, NCF-Thin dissipated the least energy while for energies higher than 4 J, the same laminate dissipated the highest energy. At higher applied energies (above E_a of 5 J), both NCF-UHB and NCF-Int exhibited lower dissipated energies compared to NCF-Thin and NCF-UHT. NCF-UHB dissipated 50% and 60% less energy, respectively, when compared to its counterparts NCF-UHT and NCF-Thin.

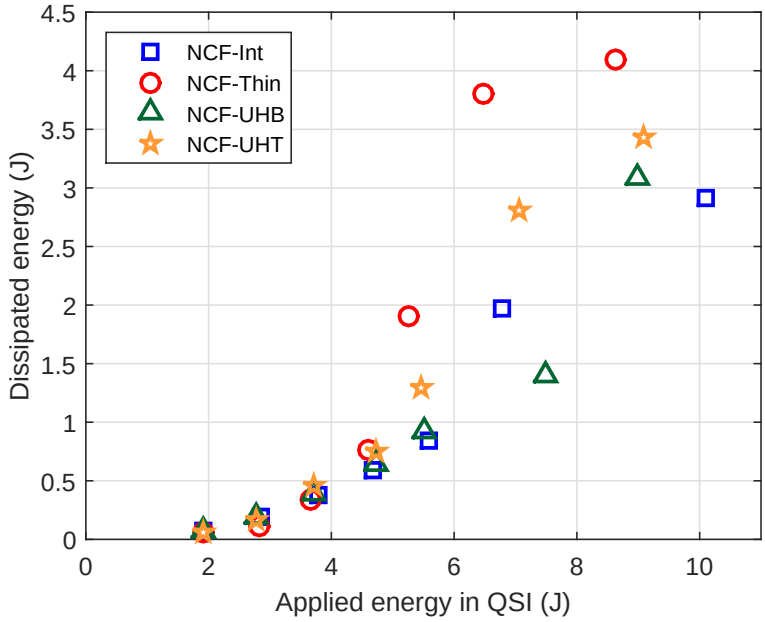

Fig. 8.12.: The evolution of dissipated energy (E_d) plotted against the applied energies (E_a) for all seven QSI deflection levels for all laminates

8.4.3 Compression after impact

Fig. 8.13 presents the pristine compression and CAI strength of all the laminates for all the impact energies. With intermediate and thin plies mixed in the same laminate, the hybrid laminate exhibited a plain compression strength value in between that of NCF-Int and NCF-Thin. NCF-UHT and NCF-UHB displayed a 5% lower plain

compression strength than the thin-ply laminate and a 5% higher value than NCF-Int. As reported in [110, 111], thin plies have a higher pristine compression strength (10% increase) over the intermediate plies. Note that the thin-ply laminate NCF-Thin at IE_1 exhibited invalid CAI failure mode (caused by local buckling at the top of the specimen as reported in [111]) despite using the anti-buckling ribs.

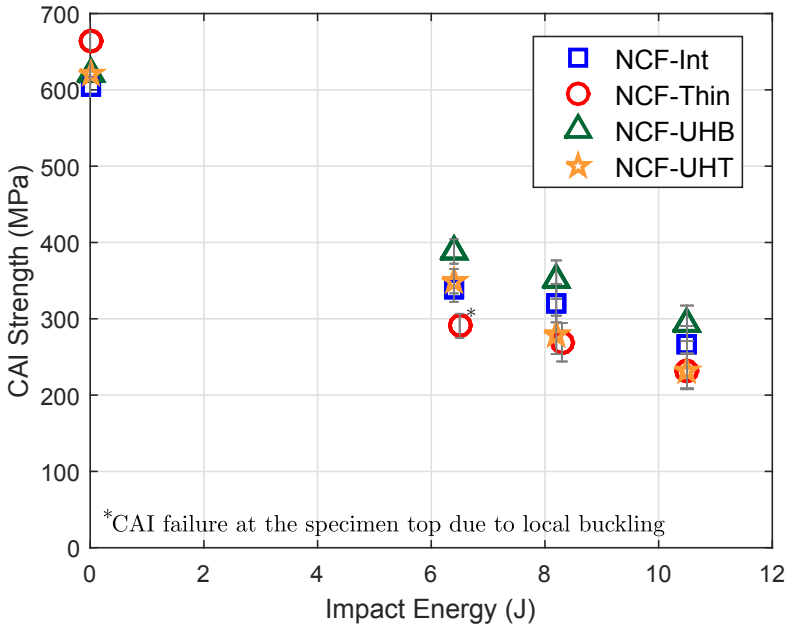

Fig. 8.13.: Plain compression strengths and CAI strengths of all laminates for all impact energies

Out of all the laminates and all the energies, the hybrid laminate NCF-UHB exhibited the highest CAI strength. Figs. 8.14 (a) and (b) present the plain compression and CAI strengths of the hybrid laminates normalized with respect to the baselines NCF-Int and NCF-Thin, respectively. On comparing NCF-UHB laminate to the baselines when reviewing all the impact energies, NCF-UHB exhibited 12% and 30% higher CAI strength over NCF-Int and NCF-Thin, respectively. Between the two hybrid laminates, NCF-UHB displayed 20% more CAI strength than NCF-UHT, indicating the importance the location of the added intermediate plies has on the post-impact response. NCF-UHT exhibited higher CAI strength that the baselines for IE_1, but at higher impact energies (IE_2 and IE_3) the CAI strength dropped

drastically and exhibited similar values to those of NCF-Thin. Fig. 8.15 shows the reduction in the residual compression strength caused by the impact damage for all laminates. NCF-Thin displayed the highest reduction (60%) in the compression strength, while NCF-UHB showed the lowest (40%).

8.5 Discussion

Thin laminates undergo severe bending during impact loading due to their reduced bending stiffness [110, 111]. Bending induces high in-plane tensile stresses at the non-impacted face of the laminate that leads to fibre splits or breakage in the bottom plies (Fig. 8.7). In addition, high bending creates shear stresses between the plies that trigger delamination at the interfaces closest to the bottom of the laminate. Studies on thin laminates [32, 110] reveal that the bottom interfaces (close to the non-impacted face) exhibit extensive delamination. Hence, the non-impacted face is the most critical or damage prone region in a thin laminate under low velocity impact loads, as evidenced by the delamination and fibre damage at this location.

As reported in [111], irrespective of the ply grade of non-crimp fabrics used, low velocity impact loads induce both delamination and fibre damage in thin laminates. However, the extent of the dominance of these damage modes depends significantly on the ply grade used. Thin laminates made of thin plies exhibited delayed delamination onset (associated to their in-situ effect [58, 105]), but with early and extended fibre damage. To the contrary, thicker plies dissipated energy through matrix cracks and delaminations, resulting in delayed and subdued fibre damage. Increased fibre damage with thin plies resulted in poor impact response (reduced peak loads and high energy dissipation) and a reduced CAI strength (as in NCF-Thin).

Unlike thin plies, intermediate plies (or a cluster of two thin plies) introduce higher interlaminar shear stresses at their adjacent interfaces (resulting from the high bending stiffness mismatch between the interfaces [18]) triggering delamination [42]. C-scan images of NCF-UHB revealed the dominant delamination at the last laminate interface, within the site of the added intermediate plies, thereby following the hypothesis formulated during the laminate design phase. On the other hand, impact loading induces high out-of-plane compressive stresses at the impactor vicinity and these stresses counteract the interlaminar shear stresses to increase the local interlam-

inar fracture toughness [107]. This explains the absence of dominant delaminations within the region of the added intermediate plies (at the top) in NCF-UHT.

The addition of the intermediate plies to the bottom of the laminate (critical region) resulted in suppressing/delaying the fibre damage by promoting early delamination. This is evidenced in the QSI results by the 55% increase in the force value over NCF-Thin at which the first load drop was observed (associated with the initiation of fibre damage). Meanwhile, the addition of intermediate plies to the top of the laminate helped to delay the initiation of fibre damage compared to NCF-Thin (as in Fig. 8.10) but with the critical bottom part of the laminate comprised of thin plies, fibre damage was dominant (evidenced by the successive load drops in Figs. 8.4 and 8.10).

CAI strength of a thin laminate depends on the extent of delamination and fibre damage in the laminate, with fibre damage being more critical and clearly linked to the drastic reduction in the CAI strength [110, 136]. On one hand, the already formed delaminations split the laminate into sub-laminates, and one of the sub-laminates buckles to result in a final collapse. On the other hand, a high magnitude of fibre failure in the laminate, especially the load sustaining 0° plies, promotes compressive fibre failure that leads to CAI failure. In NCF-UHB, the C-scan inspection reveals that entire damage area is significantly lower than that of the baselines and also governed by a single delamination at the last interface, oriented in the 90° direction. Hence, under CAI loads, the laminate will split with a thicker sub-laminate at the top (entire laminate except the last ply) and a thinner one at the bottom (last ply, 90°) which is not carrying a high load. The thicker sub-laminate sustains higher compressive loads leading to a higher CAI strength [149]. In addition to this, the reduced fibre failure, as a result of hybridization, is also a reason for the increased CAI strength. Meanwhile, the increased fibre damage in NCF-UHT laminate led to its reduced CAI strength, compared to its flipped counterpart.

While thin plies have been a remarkable asset to the composite community with their numerous advantages (delamination resistance [60], associated in-situ strength), their vulnerability towards impact and post impact loads is their Achilles heel. In this study, we have exhibited that the addition of some thicker plies could substantially mitigate the out-of-plane threats to a thin-ply laminate, evidenced in the form of

reduced fibre failure, delamination area and higher CAI strength. The results show that hybridization can be used to exploit the potential of different ply grades and help in tailoring the damage to occur at predetermined locations. Apart from the unsymmetrical design helping to understand the importance the location of added plies has, they can be the optimal solution for several load cases. When compared to the expensive alternatives of modifying the material system or using interface toughening agents to improve the out-of-plane response of thin plies, we have demonstrated the full potential laminate design has to come up with novel laminates promising remarkable improvements, and also economic feasibility. While in this study we proposed the idea of a novel laminate as a rule of thumb, the next immediate step is to explore all the laminates within a particular design space to find an optimum damage-tolerant laminate using numerical finite element tools.

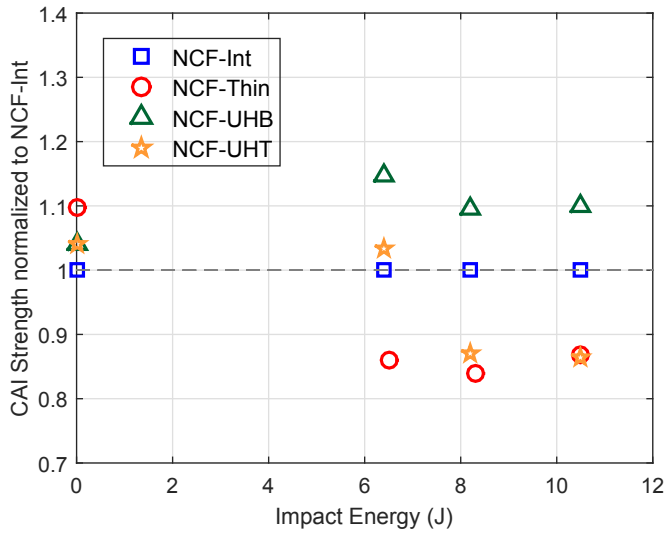

(a)

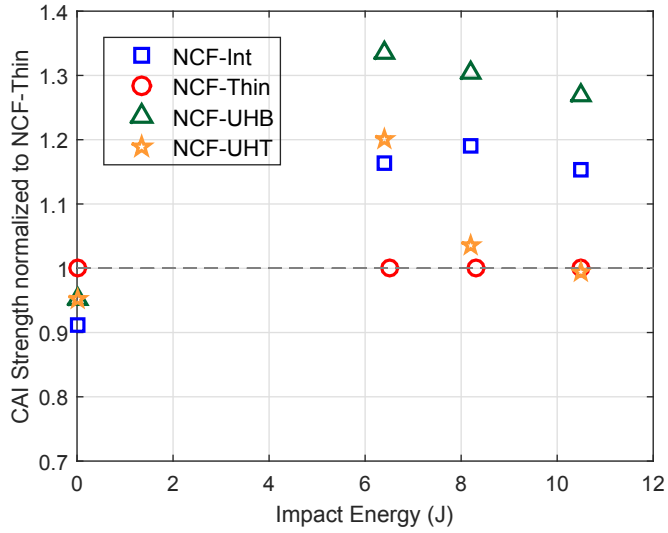

(b)

Fig. 8.14.: Comparison of CAI strengths normalised with (a) intermediate plies (NCF-Int) as baseline and (b) thin plies (NCF-Thin) as baseline. The plain compression strengths are also normalized according to the respective baselines.

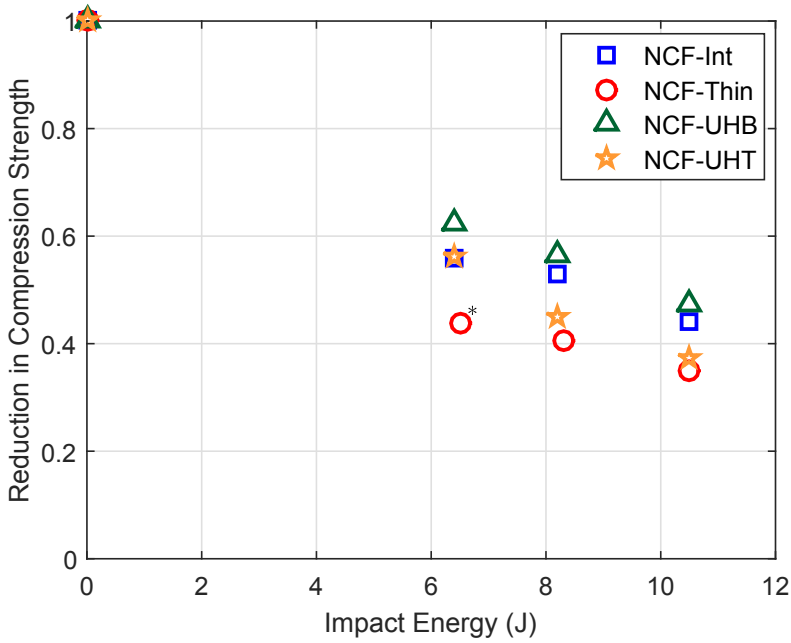

*CAI failure at the specimen top due to local buckling

Fig. 8.15.: Normalized reduction in the compressive strength due to the impact damage of all laminates.

8.6 Conclusion

Impact loads pose a great threat to thin laminates made of thin plies because of the extensive fibre failure and reduced CAI strength. To alleviate this vulnerability thin plies have towards out-of-plane responses, we have made a first attempt to design a novel laminate which combines ply hybridization and laminate mid-plane unsymmetry. We designed a hybrid laminate (made of non-crimp fabrics) which comprises both thin and intermediate plies, where the intermediate plies are placed only on the non-impacted side of the laminate (NCF-UHB). We carried out an experimental campaign using impact, compression after impact and quasi-static indentation tests and compared the responses of the proposed laminate to those of the symmetric and non-hybrid baseline laminates. We also included in the comparison the hybrid laminate flipped upside down (NCF-UHT, intermediate plies at the top) to illustrate how crucial is the location of the intermediate plies. The hybrid laminate NCF-UHB substantially delayed the fibre breakage onset (by 55%) and reduced the extent of fibre damage when compared to the thin-ply baseline NCF-Thin. The proposed laminate exhibited a 50% and 30% reduction in damage area and dissipated energy, respectively, over the thin-ply baseline laminate, thus providing a higher impact resistance. As a result of the improved impact response, the unsymmetrical-hybrid laminate increased the CAI strength by 30% (over the thin-ply baseline).In view of a practical application of the proposed novel design, for the baseline laminate to match the same residual strength as of the proposed laminate, additional plies have to be added to the baseline laminate, which in turn results in added mass and increased material costs. Finally, we have demonstrated the prospects of this novel laminate design (combining hybridization and unsymmetry) as an efficient and economic tool to mitigate the weakness of thin plies towards impact and post impact loads.

9

Paper F:

A virtual testing based search for optimum compression after impact strength in thin laminates using ply-thickness hybridization and unsymmetrical designs

A. Sasikumar[a,*], J. Costa[a,*], D. Trias[a,1], J. Llobet[a], I.R. Cozár, A. Turon[a], P. Linde[b,c]

[a] AMADE, Polytechnic School, Universitat de Girona, Campus Montilivi s/n, E-17003 Girona, Spain

[b] Airbus Operations GmbH, Kreetslag 10, 21129 Hamburg, Germany

[c] Department of Industrial and Materials Science, Chalmers University of Technology, S-41296 Gothenburg, Sweden

[*] Corresponding author

[1] Serra Hunter Fellow

The paper has been published in *Composites Science and Technology* 196 (2020) 108188.

Motivation & Synopsis

Last papers demonstrated the prospect of laminate designs in improving the compression after impact response of thin laminates in a cost-effective manner, where ply hybridization and unsymmetry have been the two key design concepts. Despite the improvement offered, the nonconventional laminates proposed in Paper C and Paper E were designed as a rule of thumb and lacked the exploration of the whole design space for the optimum laminate. With virtual testing tools gaining appreciation due to the accurate predictions and the cost-effectiveness, we decided to use virtual impact and CAI simulations to explore a design space of hybrid laminates made of thick and intermediate plies. Prior to this, the numerical model was validated with the experimental results from Paper C. Further, the proposed laminates are virtually tested under impact and CAI to obtain improved impact damage tolerant designs.

Composites Science and Technology 196 (2020) 108188

Contents lists available at ScienceDirect

Composites Science and Technology

journal homepage: http://www.elsevier.com/locate/compscitech

A virtual testing based search for optimum compression after impact strength in thin laminates using ply-thickness hybridization and unsymmetrical designs

A. Sasikumar [a,*], J. Costa [a,**], D. Trias [a,1], J. Llobet [a], I.R. Cózar [a], A. Turon [a], P. Linde [b,c]

[a] AMADE, Polytechnic School, Universitat de Girona, Campus Montilivi s/n, 17073 Girona, Spain
[b] Airbus Operations GmbH, Kreetslag 10, 21129, Hamburg, Germany
[c] Department of Industrial and Materials Science, Chalmers University of Technology, S-41296, Gothenburg, Sweden

Abstract

In the quest to improve the compression after impact (CAI) strength of thin laminates, ply-hybrid laminates (where plies of different thicknesses are mixed) have been used in a previous study to mitigate the fibre failure and, consequently, improve the CAI strength. In the same study, hybrid laminates were proposed following qualitative design rules. In this paper, we systematically look for hybrid stacking sequences with improved damage tolerance by virtually testing all the laminates in a defined design space. While the laminates in the design space are made of intermediate and thick ply grades, the baseline laminate has only intermediate grade plies. Using an in-house numerical model, we virtually tested, (impact and CAI at two impact energies), all the candidate stacking sequences. The best hybrid laminates considerably improved the CAI strength over the baseline (31% and 40% improvement for the symmetric and unsymmetrical hybrid laminates, respectively). One of the best hybrid laminates was then manufactured and tested experimentally to validate the approach. Through virtual testing, this study demonstrates the benefits of using ply thickness hybrid laminates and the feasibility of optimizing the stacking sequence for impact damage tolerance.

Keywords: Impact behaviour, Finite element analysis (FEA), Damage tolerance, Ply-thickness hybridization

9.1 Introduction

Low velocity impacts result in an alarming reduction in the residual strength of composite structures [5]. This fact is the reason for the search for optimum damage tolerant designs. Few studies [66, 150–152], however, have been devoted to understanding the impact and compression after impact (CAI) response of thin laminates (< 2 mm), like those found in fuselage skins and in some other surfaces in current aircraft structures. Studies into the effect ply thickness has on thin laminates concluded that thin uni-directional plies (75 gsm) resulted in extensive fibre damage and reduced CAI strength compared to intermediate (134 gsm) and thick (268 gsm) plies. A reduced CAI strength with thin plies was also reported with other material systems, such as woven [151] and non-crimp fabrics (NCF) [68, 151].

To enhance the thin ply structural response, attention can be turned to the design of the stacking sequence [153, 154]. Furtado et al. [46] and Arteiro et al. [47] performed selective ply level hybridization (combining different ply grades in the laminate) to improve the notched strength over a thin ply baseline. Sebaey et al. [48] designed a hybrid thick laminate (around 4.1 mm) where each thick fabric layer (320 gsm) was surrounded by a thin fabric layer (80 gsm) and improved the CAI strength by 15% over a baseline laminate made of only thick woven layers. We proposed an unsymmetrical and hybrid (intermediate and thin ply grades) thin laminate made of NCF to mitigate the fibre damage in thin plies and the CAI strength improved by 30% [155]. We followed a similar ply hybridization approach in [150] by adding thick 0° plies (268 gsm) to thin uni-directional plies, which resulted in a 40% improvement in the CAI strength. In these two previous studies [150, 155] the stacking sequences were designed following qualitative arguments which were unable to anticipate the attained improvement [150, 151]. In addition, such a design procedure ignored other possible laminates within the same design space. In spite of the usefulness of these approaches to illustrate the potential improvement of damage tolerance through laminate design, they did not constitute true optimization exercises.

Optimizing the impact and CAI response within a large design space of stacking sequences by experimental testing is infeasible. Therefore, researchers moved to virtual tests based on finite element methods to evaluate the CAI strength. Hongkarnjanakul et al. [43] studied twelve laminates to understand the effect stacking sequences have

on the low velocity impact response using a discrete 3D numerical model presented in [19]. Meanwhile, Dubary et al. [80] attempted to optimize damage tolerance with numerical tools [81].

In this paper, we take, as a baseline, a thin laminate (1.7 mm) made of aerospace grade intermediate plies (introduced in [150]) and attempt to find a stacking sequence with optimal damage tolerance. The design space comprehends symmetric and unsymmetric stacking sequences with combinations of thick and intermediate ply grades. An in-house constitutive model featuring inter- and intralaminar damage [91, 92, 97] and numerical modelling methodologies [78, 90, 94]) developed by the AMADE research group are used to perform virtual impact and CAI tests. The results revealed that symmetric hybrid laminates improved CAI strength by 30% over the baseline and that the improvement is even further enhanced for unsymmetrical laminates, by 40%. Finally, an experimental impact and CAI test carried out on one of the optimal hybrid stacking sequences validates the virtual approach. In addition, using the exhaustive numerical results, a correlation analysis pointed out impact dissipated energy and delamination area as the strongest and the weakest parameters, respectively, to correlate with CAI strength.

9.2 Methodology

9.2.1 Numerical modelling

We used the same numerical approach as that of Soto et al. [94], where Abaqus/Explicit conventional shell elements with reduced integration (S4R) were used to model the plies and zero thickness cohesive elements (COH3D8) to model the interfaces between the plies. Progressive intraply damage was accounted for with the continuum damage model (CDM) proposed by Maimí et al. [91, 92]. The damage activation functions are based on the LARC04 failure criteria [156] and the model, formulated in plane-stress, incorporates the crack band formulation [93]. The predictive capability of the model has been demonstrated under different loading conditions such as impact, compression after impact [77, 90, 119, 120] and open-hole tension [105, 109]. The cohesive constitutive model for the interfaces is that proposed by González et al. [97]. Both the intra- and inter laminar models are implemented in a VUMAT user-written subroutine.

The conventional shell elements were placed at the mid-ply location and were tied to the cohesive elements at the interfaces (Fig. 9.1). A finer structured mesh (oriented in the ply direction) with elements of 0.4 mm was defined for a 35 x 35 mm window under the impactor, whereas the remaining region had a coarse mesh (3 mm). The transverse tensile and in-plane shear strength values were calculated according to the ply thickness and the ply type (outer or embedded) to account for the in-situ strength [58]. To avoid excessive element distortion, an element was deleted when the fibre damage variable (d_1) reached 1, and the transverse and shear damage variables were limited to a maximum value of 0.99 but without deleting the element. Further details of the virtual approach are explained in [78, 94].

The CAI simulation was performed using the `RESTART` command in Abaqus/Explicit, where the impact assembly and results are imported. The rigid parts (impactor, base plate and rubber clamps) were removed before starting the CAI simulation. In addition to the standard CAI fixture, a non-standard anti-buckling fixture (recommended by [67] and used by [150, 151, 155, 157]) was accounted for in the simulations.

9.2.2 Laminate design space and optimization approach

The material system studied here is T700/M21 carbon-epoxy. The baseline laminate (Table 9.1) is made of 13 intermediate grade plies of 134 gsm (1.7 mm total thickness) and is centre-symmetric (i.e., the mid-plane axis runs through the centre of the mid-ply). It was named H-134 in [150], and was selected as the baseline as it offered the highest CAI strength when compared to that of the thick and thin ply grade laminates in [150].

Primarily, the laminate design space for the optimization exercise embraced hybrid symmetric thin laminates made up of intermediate (134 gsm) and thick (268 gsm) grade plies (NB: This combination of ply grades was not explored in the previous study by the authors [150]). Thin plies (75 gsm) were intentionally discarded because of the extensive fibre damage caused by LVI that impairs the CAI strength [150].

Thick plies (0.262 mm) were considered as a cluster of two intermediate plies (0.131 mm). The laminates had to obey the following constraints: (a) Symmetric and balanced with the same laminate thickness as that of the baseline (1.71 mm); (b) Surface plies are fixed to be $\pm 45^{\circ}$; (c) No clusters of more than three plies allowed;

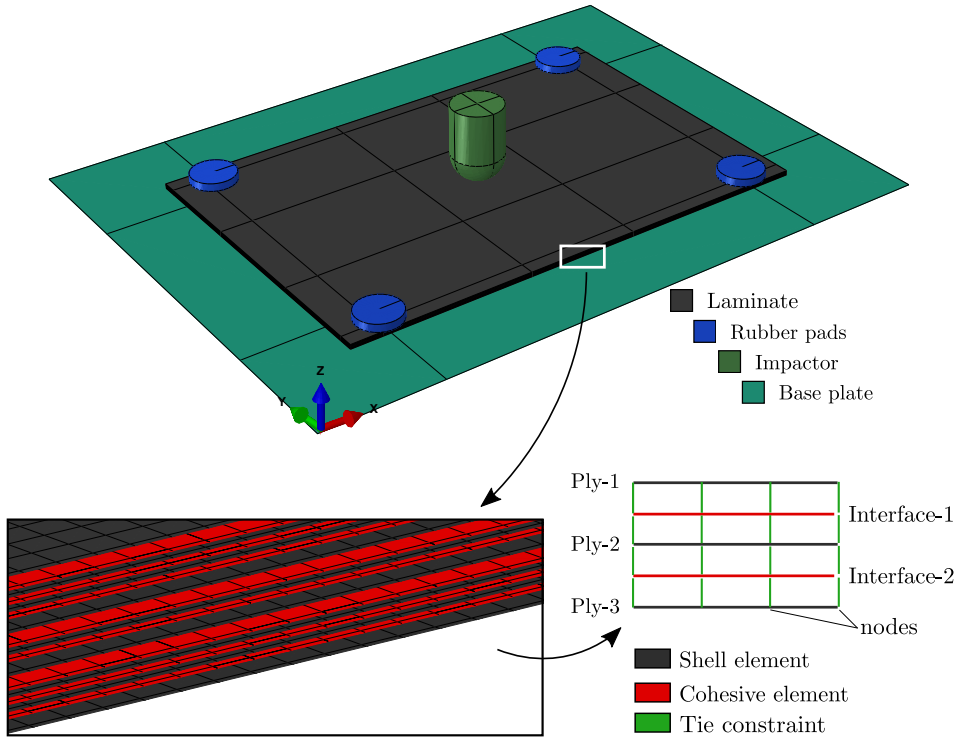

Fig. 9.1.: The virtual impact test setup followed by the modelling strategy with conventional shell elements linked with zero-thickness cohesive elements using tie constraints.

(d) Thick plies oriented in 0°, ±45° or 90° (not just limited to 0°, as in [150]); (e) % of 0° plies higher than the % of 90° (as in the baseline laminate); (f) A minimum of 10% of the total number of plies should be oriented in each of the four directions (0°, ±45° and 90°); (g) The number of 0° plies is set to be 3 (as in the baseline laminate) or 5 (to reach a larger design space); (h) The equivalent bending stiffness parameter (D*, proposed by Olsson [123]) within 5% tolerance of the baseline laminate (to have a proper comparison). No constraint was imposed on the mismatch angle between plies.

A total of 29 laminates obeyed the above constraints (Table 9.1). The maximum deviation in the D* values from the baseline was 4%. We grouped the laminates according to the total number of plies, G1 (7 plies), G2 (9 plies) and G3 (13 plies). The percentage of clustered plies (ratio of the thickness of all clustered plies to the total thickness) varied accordingly: 85% for G1, 54% and 62% for G2, 23% and

31% for G3. Hence, groups G1 and G2 can be referred to as the thick ply dominant groups (more than 50%) and group G3 as an intermediate ply dominant group (less than 30%).

The design space of unsymmetrical laminates obeyed the constraints given above except for the symmetry constraint, which was replaced by a null extensional-bending matrix (B=0) to avoid coupling responses [99, 158]), and led to 84 laminates. To reduce the computational cost, only 7 representative laminates with 8 to 11 plies were included in the virtual test study (Table 9.2).

Tab. 9.1.: Baseline laminate and all the symmetric hybrid laminates studied.

Group	Laminate	Stacking sequence	No. of plies	Ply % $[0/\pm 45/90]$	D* (Nm)
REF	H-134 (Baseline)	[45/-45/0/45/-45/90/0/90/-45/45/0/-45/45]	13	[23/31/15]	22.08
G1	L1	$[45_2/-45_2/90/0_3/90/-45_2/45_2]$	7	[23/31/15]	22.12
	L2	$[45_2/90/-45_2/0_3/-45_2/90/45_2]$	7	[23/31/15]	22.09
G2	L3	$[45_2/-45/90/-45/0_3/-45/90/-45/45_2]$	9	[23/31/15]	22.17
	L4	$[45/-45_2/45/90/0_3/90/45/-45_2/45]$	9	[23/31/15]	22.72
	L5	$[45/-45_2/90/45/0_3/45/90/-45_2/45]$	9	[23/31/15]	21.78
	L6	$[45/-45/0_2/90_2/0/90_2/0_2/-45/45]$	9	[38/15/31]	22.12
	L7	$[45/-45/0/90_2/0_3/90_2/0/-45/45]$	9	[38/15/31]	22.17
	L8	$[45/0_2/-45/90_2/0/90_2/-45/0_2/45]$	9	[38/15/31]	22.12
	L9	$[45/0/-45/90_2/0_3/90_2/-45/0/45]$	9	[38/15/31]	22.17
	L10	$[45/0_2/90_2/-45/0/-45/90_2/0_2/45]$	9	[38/15/31]	22.75
	L11	$[45/0/90_2/-45/0_3/-45/90_2/0/45]$	9	[38/15/31]	21.74
	L12	$[45/90/45/-45_2/0_3/-45_2/45/90/45]$	9	[23/31/15]	21.74
	L13	$[45/90/-45_2/45/0_3/45/-45_2/90/45]$	9	[23/31/15]	22.09
	L14	$[45/90_2/0_2/-45/0/-45/0_2/90_2/45]$	9	[38/15/31]	22.65
	L15	$[45/90_2/0/-45/0_3/-45/0/90_2/45]$	9	[38/15/31]	21.74
G3	L16	$[45/-45/45/-45/90/0_3/-45/45/-45/45]$	11	[23/31/15]	22.52
	L17	$[45/-45/45/90/-45/0_3/-45/90/45/-45/45]$	11	[23/31/15]	22.09
	L18	$[45/-45/90/45/-45/0_3/-45/45/90/-45/45]$	11	[23/31/15]	22.65
	L19	$[45/-45/90/0_2/90/0/90/0_2/90/-45/45]$	11	[38/15/31]	22.53
	L20	$[45/-45/90/0/90/0_3/90/0/90/-45/45]$	11	[38/15/31]	22.26
	L21	$[45/0_2/90/-45/90/0/90/-45/90/0_2/45]$	11	[38/15/31]	21.04
	L22	$[45/0/90/-45/90/0_3/90/-45/90/0/45]$	11	[38/15/31]	22.75
	L23	$[45/90/-45/45/-45/0_3/-45/45/-45/90/45]$	11	[23/31/15]	22.58
	L24	$[45/90/-45/0_2/90/0/90/0_2/-45/90/45]$	11	[38/15/31]	22.71
	L25	$[45/90/-45/0/90/0_3/90/0/-45/90/45]$	11	[38/15/31]	22.40
	L26	$[45/90/0_2/-45/90/0/90/-45/0_2/90/45]$	11	[38/15/31]	21.78
	L27	$[45/90/0/-45/90/0_3/90/-45/0/90/45]$	11	[38/15/31]	21.55
	L28	$[45/90/0_2/90/-45/0/-45/90/0_2/90/45]$	11	[38/15/31]	22.52
	L29	$[45/90/0/90/-45/0_3/-45/90/0/90/45]$	11	[38/15/31]	21.54

9.3 Results

Tab. 9.2.: Selected unsymmetric hybrid laminates

Group	Laminate	Stacking sequence	No. of plies	Ply % $[0/\pm 45/90]$	D* (Nm)
REF	H-134 (Baseline)	[45/-45/0/45/-45/90/0/90/-45/45/0/-45/45]	13	[23/31/15]	22.08
UNSYM	UL1	$[45_2/90/-45/0_2/-45_3/0/90/45_2]$	8	[23/31/15]	22.45
	UL2	$[45_2/90/0/-45_3/0_2/-45/90/45_2]$	8	[23/31/15]	22.45
	UL3	$[45/-45/0_3/90/45/90/-45_2/0_2/45]$	8	[38/23/15]	21.05
	UL4	$[45/0_2/-45/90_2/45/-45/90/0_2/45]$	9	[31/23/23]	21.26
	UL5	$[45/-45/0/90/0_2/90_3/0_2/-45/45]$	9	[38/23/15]	22.31
	UL6	$[45/90/-45/0_3/90/0/90_2/-45/0/45]$	10	[38/23/15]	22.74
	UL7	$[45/0/-45/90/0/-45/45/90_2/0_2/-45/45]$	11	[31/23/23]	22.14

9.3.1 Validation of the numerical model

Prior to the optimization procedure, we checked the capability of the numerical model to reproduce the experimental tests for impact and the CAI of the baseline laminate [150]. The validation was performed only for the 8.9 and 10.5 J impact energies. The agreement was good (Fig. 9.2), especially for the 10.5 J impact, where the load drop (associated with the onset of fibre failure) and dissipated energy were accurately predicted. The analysis of the numerical results indicated that the load drop at the peak load initiated due to fibre damage at the bottom ply, which then propagated to the upper plies.

Fig. 9.3 compares numerical and experimental impact damage resistance parameters (maximum peak force, projected delamination area, energy dissipated) and the CAI strengths. Predictions deviate from the experimental values by 5% (peak load), 9% (projected delamination area), 15% (dissipated energy) and 5% (CAI strength). The virtual test properly captured the impact induced back fibre splitting oriented in the 45° (last ply) and the compressive failure initiating from the edge of the fibre split towards the edge of the specimens (Fig. 9.4).

9.3.2 Optimization

All 29 symmetric laminates (Table 9.1) were virtually impacted at 8.9 J before the CAI virtual test. Fifteen hybrid laminates improved the CAI strength over the baseline, with the highest improvement reaching 13% (Fig. 9.5). The number of plies clearly influenced the CAI strength as almost all the G1 and G2 laminates improved that of the baseline, while those in the G3 group reduced it.

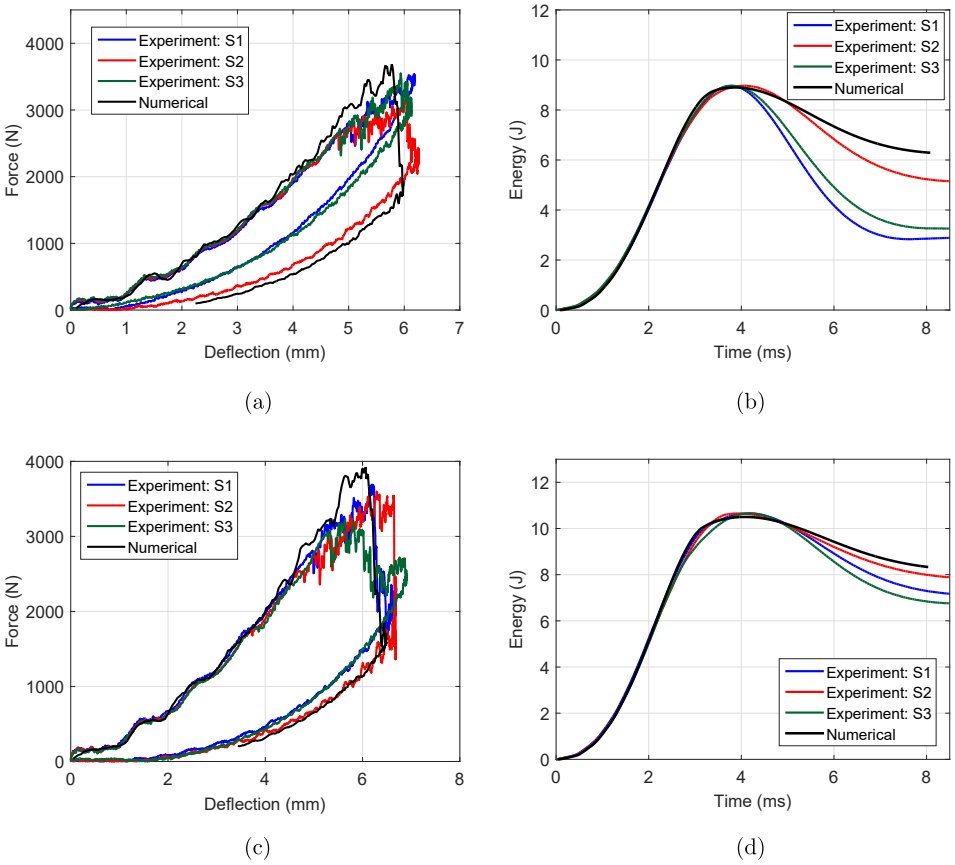

Fig. 9.2.: Comparison of experimental and numerical force-deflection and energy-time responses of the baseline H-134 for the 8.9 J ((a) and (b)) and 10.5 J ((c) and (d)) impacts.

Despite the use of anti-buckling ribs to delay the pre-mature buckling of the thin laminates, some hybrid laminates (all belonging to group G3) still exhibited failure at the top zone, where the specimen is unconstrained, due to local buckling. The corresponding laminates' CAI values are marked with an * in Fig. 9.5. A similar CAI failure mode was experimentally reported by the authors for the hybrid laminate referred to as H-75-H1 in [150]. The fidelity of the numerical model is further demonstrated by its capability to reproduce this failure (Fig. 9.7 for laminate L20).

Hybrid laminates exhibiting an improvement in CAI strength above 5% over the baseline for the 8.9 J impact were then virtually impacted at 10.5 J. Those 11

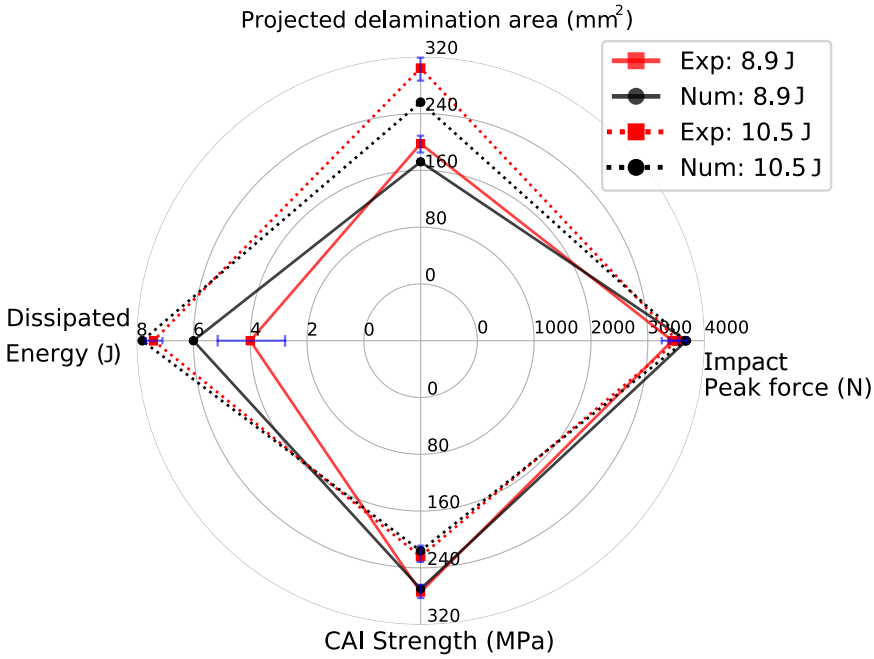

Fig. 9.3.: Comparing the impact damage resistance parameters and the CAI strengths between experimental and numerical analysis for 8.9 and 10.5 J. (Note that the blue lines denote the standard deviation in the experimental results from three specimens).

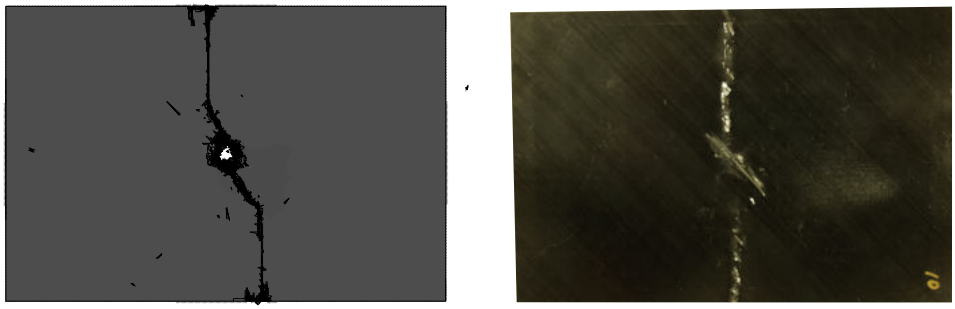

Fig. 9.4.: Comparison of the failed CAI specimens (non-impacted side view) from the 10.5 J impact energy from the virtual (left) and experimental test (right).

laminates (from G1 and G2) significantly improved the CAI strength over the baseline (up to 31% for L8) as in Fig. 9.6. The virtual impact force-deflection responses of the three symmetric laminates with better damage tolerance (L1, L8 and L9) were compared to that of the baseline(Fig. 9.8). This figure shows the damage status for

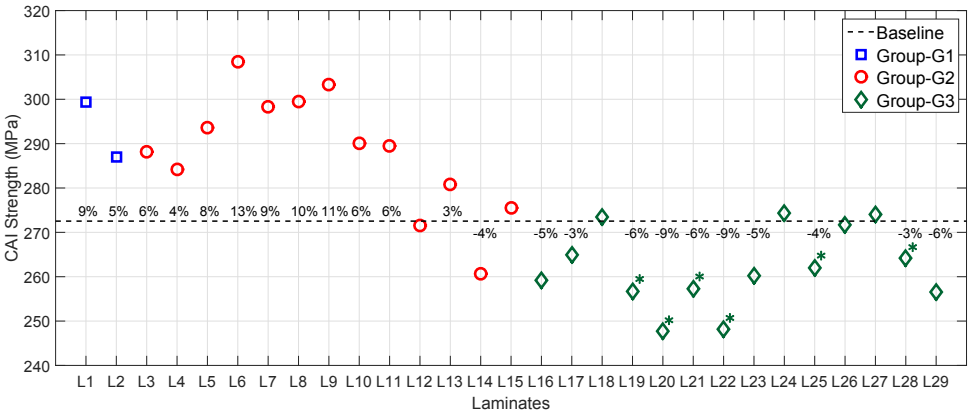

Fig. 9.5.: Comparison of the virtual CAI strengths between the hybrid laminates and the baseline from the 8.9 J impact (Note that the CAI values marked with an * denote invalid CAI failure mode at the top of the specimen as addressed in [150]).

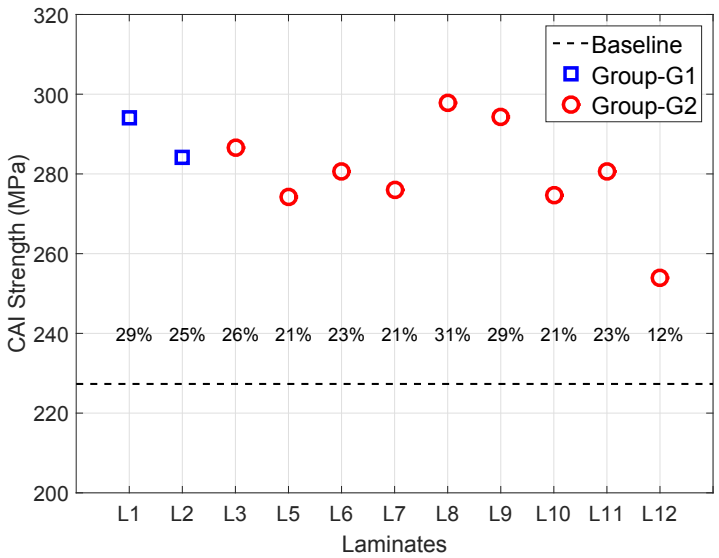

Fig. 9.6.: Comparison of the virtual CAI strengths between the selected hybrid laminates and the baseline from the 10.5 J impact.

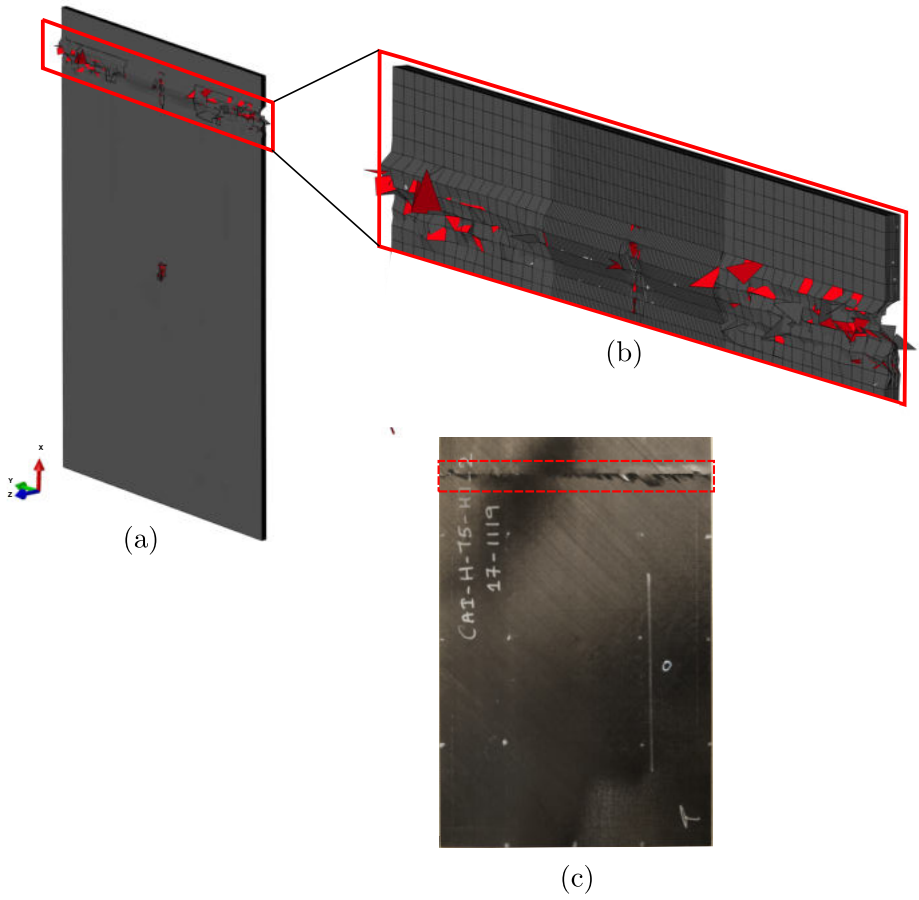

Fig. 9.7.: Invalid CAI failure mode obtained at the top of the laminate and compared with the similar failure mode obtained experimentally in [150].

the same deflection level (just after the load drop of the baseline, as indicated in the figure). The baseline laminate exhibited fibre damage locally under the impactor in all the plies (Fig. 9.8 (a)) whereas the hybrid laminates mitigated the load drop and constrained the fibre damage to the last ply.

All the 7 unsymmetrical hybrid laminates chosen, improved the CAI strength over the baseline laminates (Fig. 9.9); UL3 by 41% and UL5 37%. Note that laminate UL7 displayed CAI failure at the top due to the local buckling. Finally, Fig. 9.10 illustrates the stacking sequence of the best symmetric and unsymmetrical hybrid laminates obtained from the virtual testing campaign. The computational time for the LVI and CAI models run in a standard computer (12 cpus and 32 GB RAM per cpu) ranged from 25 to 121 hours, and 5 to 16 hours, respectively, depending on the laminate, the number of plies modeled and the impact energy. The higher the impact energy the higher the computational cost due to the higher element distortion that penalizes the stable time increment.

9.3.3 Experimental validation

Out of the different laminates, the symmetric hybrid laminate L1 was selected to validate experimentally the virtual approach described above. Hybrid laminate L1 has equal percentage of plies in the different orientations as that of the baseline (see Table 9.1), and hence was selected for the experimental validation. Impact (8.9 and 10.5 J) and CAI experimental tests followed the ASTM D7136/D7136M-15 and D7137/D7137M-15 standards, respectively. We tested three specimens per impact energy. Details of the experimental setup are described in [150]. The experimental and numerical impact responses of L1 are shown in Fig. 9.11, while Fig. 9.12 compares the CAI strengths of the hybrid laminate L1 (numerical and experimental) and baseline (experimental) for the 8.9 J and 10.5 J impacts.

9.4 Discussion

According to the virtual and experimental results, ply thickness hybridization (combination of thick and intermediate grade plies) in thin laminates improves the damage tolerance around 30% to 40% over a baseline of intermediate grade plies. This improvement is caused by the fact that, during impact, thick plies promote damage mechanisms other than fibre breakage (fibre breakage is behind the consequent im-

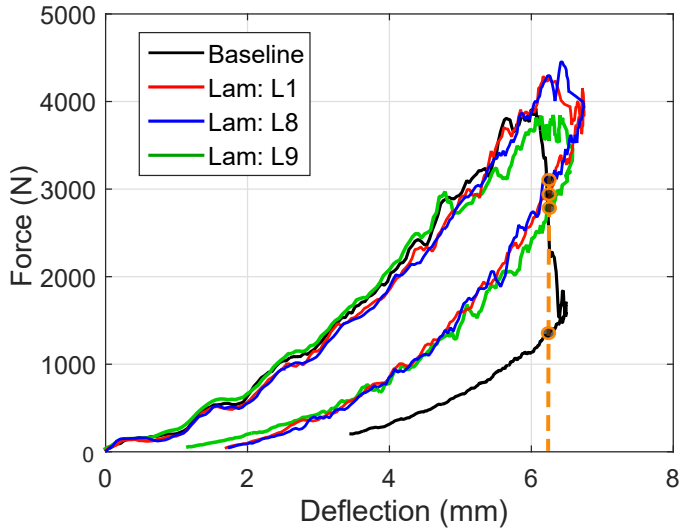

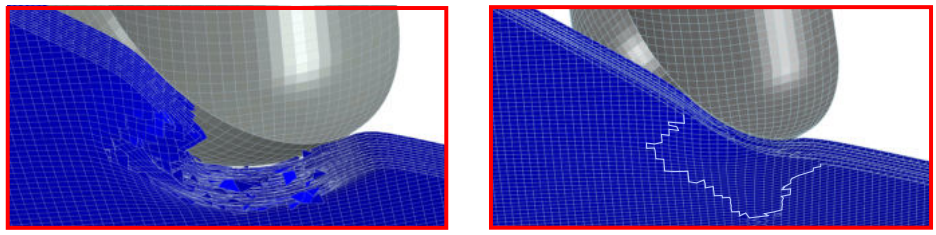

(a) Baseline (b) Laminate: L1

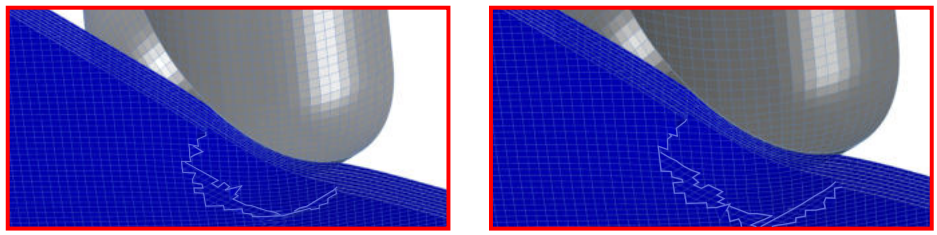

(c) Laminate: L8 (d) Laminate: L9

Fig. 9.8.: Comparison of the force-deflection response and the fibre damage from the 10.5 J impact for the baseline and the proposed optimum hybrid laminates for a selected deflection level. (Note that blue contour represents those elements with the fiber damage variable $d_1 < 1$ and the deleted elements are those with $d_1 = 1.0$)

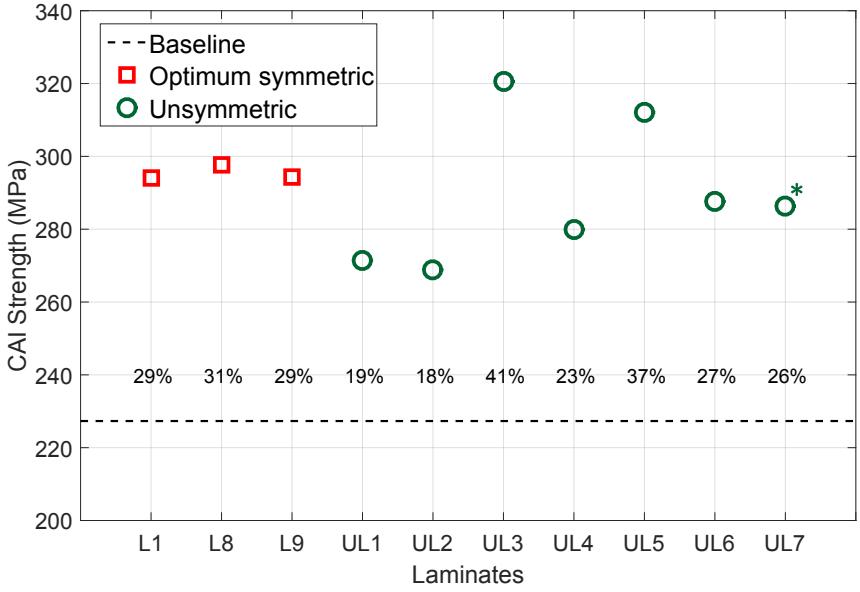

Fig. 9.9.: Comparison of the CAI strengths of all the selected unsymmetrical hybrid laminates with the optimum symmetric hybrid and the baseline laminate for the 10.5 J impact.

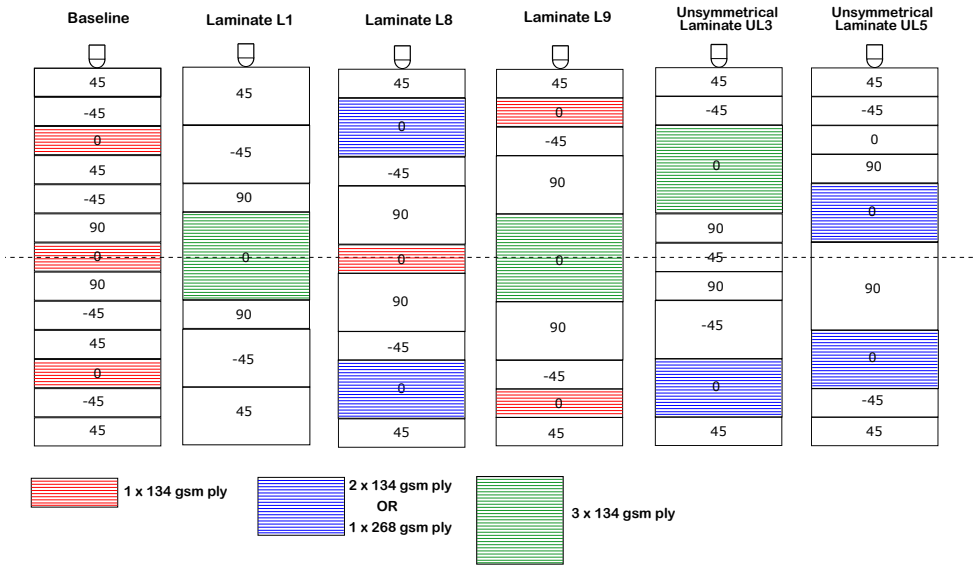

Fig. 9.10.: Illustration of the baseline along with the optimum symmetrical and unsymmetrical impact damage tolerant hybrid thin laminates (Note that the load bearing 0° plies are colored with respect to their ply thicknesses).

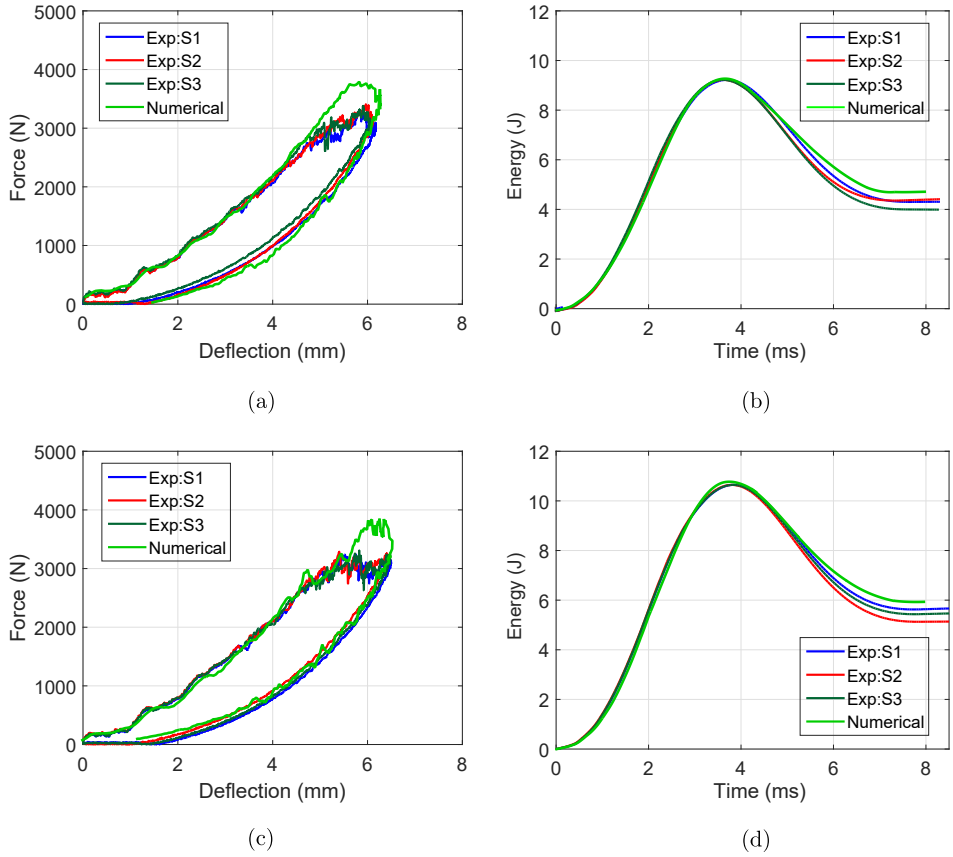

Fig. 9.11.: Comparison of the impact response curves from the numerical virtual tests and the experimental tests for 8.9 J ((a) and (b) and 10.5 J ((c) and (d)) of the hybrid laminate L1.

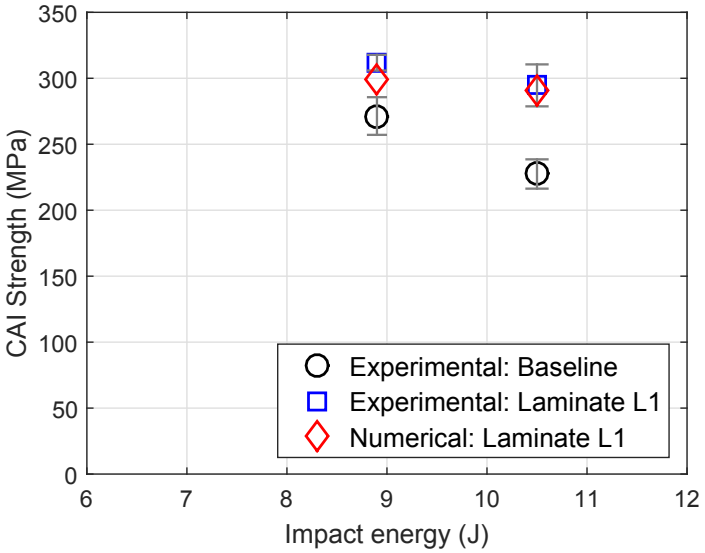

Fig. 9.12.: Comparing the CAI strengths of hybrid laminate L1 obtained from experimental and numerical tests for both 8.9 and 10.5 J impact energies. Experimental CAI strengths of the baseline H-134 are also presented.

pairment of compressive strength). Indeed, due to a reduced bending stiffness, thin laminates undergo considerable bending. While thicker plies are prone to early matrix cracking and delamination at adjacent interfaces (due to the higher interlaminar shear stresses and lower in-situ transverse strength for matrix cracking [58]), thin plies suppress/delay both of these damage mechanisms and lead to fibre splitting due to the high tensile stresses at the non-impacted side.

In the ply-hybrid laminates, the thicker plies reduce the amount of fibre damage by dissipating energy through early delaminations, while the thinner plies have a higher plain compression strength which enhances CAI strength. This is evidenced by the fact that the CAI strength decreases with the number of intermediate plies (compare the CAI strength for groups G1, thick ply dominant, to G3, intermediate ply dominant). It is also important to note that while ply thickness hybridization improves the damage tolerance, it is expected to impair the benefits of pure thin-ply laminates such as the delay of the onset of transverse cracking and fatigue damage.

We compared the evolution of the energy dissipated through intra-laminar (matrix cracks and fibre damage) and inter-laminar (delaminations) damage modes between

the baseline (intermediate plies) and laminate L1 (thick ply dominant hybrid laminate) as in Fig. 9.13. Both laminates have the same percentage distribution of ply orientations. In the early loading stage, we observed higher energy dissipation through delamination in L1. At the point of load drop for the baseline (Fig. 9.8), the baseline laminate underwent fibre splitting (intralaminar energy dissipation) and triggered delamination. Hence, intermediate plies (baseline) comparatively delayed the occurrence of delaminations. However, the earlier onset of extensive fibre damage induced delaminations (as explained in [159]), eventually led to a threefold higher interlaminar energy dissipation of baseline over L1.

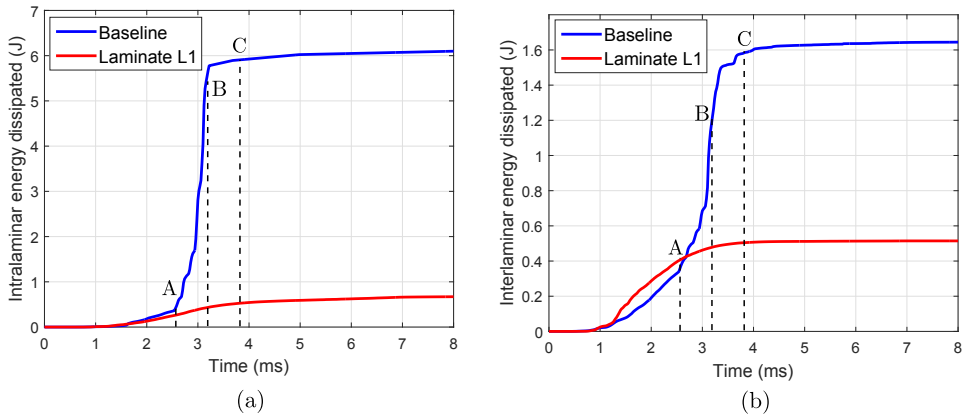

Fig. 9.13.: Comparison of the evolution of (a) intra- and (b) inter-laminar energy dissipated between the baseline and the optimum hybrid laminate L1 for the 10.5 J virtual impact test.

The results indicate that it is beneficial to group the 0° plies together rather than distributing them equally in the through-the-thickness direction (as in the baseline laminate in Fig. 9.10.) Further, this cluster of 0° plies is safeguarded by keeping it close to the mid-plane, away from the fibre damage prone locations.

Some of the hybrid laminates with improved CAI strength have a higher percentage of 0° plies compared to the baseline, which can provide an unfair comparison. Despite this, laminates L1, UL1 (that have the exact equal ply counts in all directions as the baseline) still justifies the importance of ply hybridization and unsymmetrical designs. To further demonstrate the potential of hybrid laminates, when compared to a thick ply laminate (laminate H-268 in [150]), the hybrid laminate L1 improved the CAI strength by around 20% for different impact energies.

The optimization of stacking sequences in a large design space (i.e., plies of different thicknesses) can only be accomplished with reliable virtual tools. This work demonstrates both the feasibility of optimizing the stacking sequence for impact damage tolerance by means of virtual testing and the benefits of using ply thickness hybrid laminates. It should be noted that while the study of symmetric laminates is a true optimization procedure (all candidates in the domain are explored to find the best one), only less than 10% of total unsymmetrical hybrid laminates were virtually tested.

Taking advantage of the high number of thin laminates virtually tested, we performed a correlation analysis to study the influence of several damage resistant parameters on the CAI strength for the 8.9 J impact case. The Pareto chart (Fig. 9.14) shows that the dissipated energy (factor B) is the most correlated parameter to the CAI strength, followed by the fibre damage area (factor C). The easiest parameter to measure experimentally and the most used for thicker laminates, the projected delamination area (factor D), is the least influencing parameter, and hence should not be taken as an indicator of the CAI strength in thin laminates. The same observation was experimentally concluded by the authors in [150] for thin laminates.

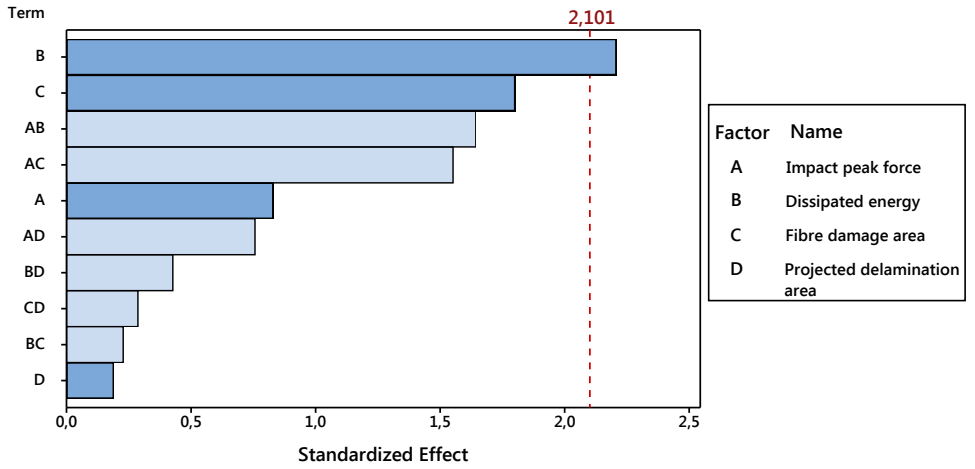

Fig. 9.14.: Pareto chart presenting the standardized effects of different damage resistance parameters on the CAI strength.

9.5 Conclusion

Ply level hybridization, i.e., mixing plies of different thicknesses within a laminate, is a promising and cost effective method to improve the compression after impact strength. In this paper, we concentrated on thin laminates and looked for optimum impact damage tolerant hybrid laminates made of intermediate and thick grade plies. An in-house finite element model was first validated with the already presented impact and CAI experimental results of the baseline (all intermediate plies) and then used for the optimization exercise over symmetric ply hybrid laminates. All symmetric laminates fulfilling the design constraints were virtually tested under impact (8.9 J and 10.5 J impact energies) and CAI. Optimum laminates improved the CAI strength by 31% over the baseline. The improvement was enhanced even further in unsymmetrical laminates (40% over the baseline and 10% over the optimum symmetric hybrid laminate), although only 10% of the much larger design space was preliminarily explored. One of the optimum symmetric hybrid laminates was experimentally tested to discern the same improvement in the CAI strength as predicted by the virtual tests. The benefit of ply hybrid laminates relies on the contribution of thick plies to dissipate energy in mechanisms different from fibre breakage and of thinner plies to resist compression. Finally, it is demonstrated that the projected delamination area for thin laminates does not correlate with the CAI strength, while the dissipated energy and the fibre damage area have a strong correlation on the CAI strength.

10 Discussion

This chapter discusses the whole thesis in line with its main objective of the thesis, proceeding through the different sub-objectives. The discussion is segmented into three sections corresponding to the three sub-objectives formulated in the introduction, followed by a final global discussion focussed on the prime objective of the thesis: to exploit the potential of laminate design to improve the impact damage tolerance of thick and thin laminates.

10.1 Unsymmetrical laminates to improve the impact behaviour compared to symmetric laminates

In an impact scenario, the laminate is subjected to different stress states in the thickness direction, that induces different damage modes in the top and bottom sub-laminates. Consequently, Papers A and B challenged the laminate mid-plane constraint that forces to mirror the same plies at top sub-laminate to the bottom sub-laminate. The three unsymmetrical laminates designed with zero or low extensional-bending coupling matrix ([B]), revealed the possibility to move away from the unnecessary symmetry constraint without the worry of coupling responses such as warpage during manufacturing. The experimental and the supporting numerical results (from Paper A and B) revealed that impact damage, mainly delamination in the case of thick laminates, can be pre-determined to occur at desired locations using ply clustering technique. The clustered ply blocks placed at the impacted side (LPCI), middle (LPCM) and the non-impacted side (LPCN) successfully imposed dominant delaminations at the corresponding locations of the clustered plies. When similar oriented plies are clustered, they introduce higher bending stiffness mismatch and create higher interlaminar shear stresses at the adjacent interfaces. Similar theory was used by Liv et al. [11] using large mismatch angles at the interfaces to successfully induce delaminations.

The experimental results also supported the findings in the literature [14] of the through-the-thickness compressive stresses and its influence in suppressing delamination. C-scan results for the lower impact energies (Paper A: 12 J and 18 J, Paper B:

10 J and 16 J) revealed that the ply clusters imposed at the top sub-laminate (at the impacted side) for LPCI did not induce the dominant delaminations at this location (as in Fig. 4.5 in Paper A and Fig. 5.10 in Paper B). Impact load induces high out-of-plane compressive stresses under the impactor that locally increase both the interlaminar shear strength and fracture toughness [14, 107, 108, 160]. As reported, these compressive stresses can suppress delamination in terms of increased critical mode II fracture energy as seen in the case of LPCI for the lower energies. Despite the different resins used in the two papers (IM7/8552 for Paper A and IM7/M21 for Paper B), both results favoured the suppression of the delamination. But at higher energies (24 J and 35 J in Paper B), the dominant delaminations were seen at the top sub-laminate (at the location of the clustered plies as per the predictions during the laminate design phase), evidencing a threshold energy level for the propagation of the delamination to overcome the compressive stresses.

On the other hand, laminate with the clustered block in the bottom sub-laminate (at the non-impacted side), LPCN, displayed substantial difference in the damage mechanisms compared to LPCI. The non-impacted side of the laminate is prone to bending under impact that initiates transverse tensile cracks (as presented in Fig. 2.1). These cracks propagate in the thickness direction and reach the adjacent interface to form a delamination. In the case of LPCN, the reduced in-situ effect of the clustered plies along with the high interlaminar shear stresses at the interfaces of the clustered plies acted as a catalyst for the extensive delaminations at the bottom. This made way for the highest projected delamination area for LPCN compared to other laminates for all energies. The same reason applies to the lowest delamination threshold value (F_d= 6200 N in paper B) of LPCN compared to other laminates.

In LPCM, the damage was concentrated within the clustered plies placed at the laminate middle. The damage imposed at the middle has alleviated the damage at the top and bottom sub-laminates of LPCM, when compared to the extension of the damage in LSYM (as in Fig. 10.1). Compared to LPCN, the extension of the dominant delamination was much smaller for LPCI and LPCM (around 20 to 40 % lower) as provided in Fig. 5.9. The numerical results, in Paper A, revealed that the same group of clustered plies dissipated most energy through intralaminar damage in LPCI and through interlaminar energy in LPCN, for the studied two impact energies. This evidences how the damage modes vary when the same clustered

block was moved from the top to the middle to the bottom of the laminate. The observed through-the-thickness location of the dominant delaminations demonstrated that laminate design can be used to pre-determine the location of the damage. In comparison to the unsymmetrical laminates, the symmetric baseline with no clusters exhibited conventional impact damage morphology of extended delaminations at the bottom that further linked transversely to the impact side like a spiral staircase pattern. All the different impact damage resistance parameters studied pointed to LSYM as the best in terms of damage resistance. This is due to the absence of clustered plies in the symmetrical laminate, as grouped plies favour the onset of delaminations as also reported in [9, 42].

The small improvement in plain compression strength of the unsymmetrical laminates over symmetric baseline is directly related to the clustered block of plies, especially the cluster of 0° plies, that help in effectively carrying the compression load. In a standard laminate, under CAI loading, the laminate splits into sub-laminates due to the presence of the impact induced delaminations and one of the typical final failure is the growth of the dominant delamination to the specimen edge. Inspection of the CAI specimens (using macro photos as shown in Fig. 5.13) evidenced the propagation of the dominant delaminations (formed during impact at the location of the clustered block) to the specimen edges. Delamination induced buckling was the reason for the CAI failure for all laminates except LPCM, where initial global buckling towards the non-impacted side was recorded similar to LSYM. But at higher loads, there was a saturation in the out-of-plane displacement values for LPCM with no further evidence of global buckling. This is due to the middle location of the clustered block which is constrained by other plies at the top and bottom. Hence, with no further buckling evidenced from the LVDT results, the final failure of LPCM is attributed to the compressive failure of the 0° clustered plies, similar to the conclusions from [8, 22]. This resulted in a 10% increase in the CAI strength of LPCM over the symmetric baseline, and around 10-15 % increase over the other unsymmetrical laminates with clusters at the laminate surfaces. Comparing the failure modes, the other unsymmetrical laminates exhibited buckling induced failure due to the location of the clustered plies at the laminate surfaces that offered less resistance to buckling, an observation reported in [25].

No impact damage resistant parameters correlated well with the CAI strength, leading

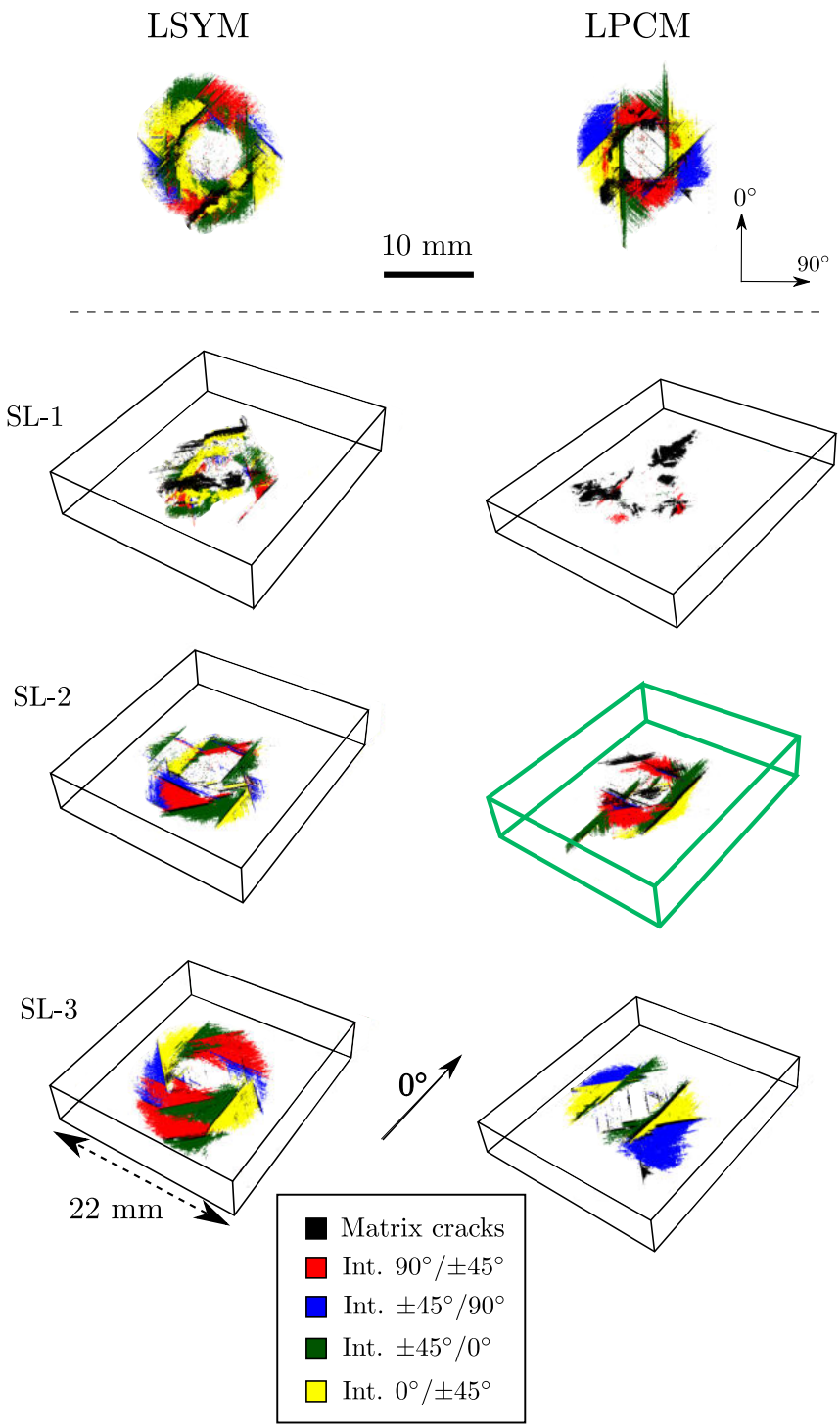

Fig. 10.1.: Comparison of the projected damage footprint (top) and the through-the-thickness 3D damage distribution (bottom) of LSYM and LPCM from the 10 J impact.

us to conclude that CAI damage morphology is too complex to be predicted by any impact damage parameter. Nevertheless, the final CAI failure for thick laminates was seen to depend more on the through-the-thickness delamination location, the thickness of the sub-laminates and the buckling modes than the usually considered impact resistance parameters.

Re-assessing the first sub-objective of the thesis, the papers answered the question regarding the feasibility to move away from the symmetry constraint to use unsymmetrical laminates towards out-of-plane loads. Using tailored clustered blocks, the location of the dominant delamination was controlled to happen at pre-determined locations. Assessing the CAI strengths, one of the unsymmetrical laminate improved impact damage tolerance, with respect to the symmetric baseline (recommended by the standard), hence raising the prospectives of this idea.

10.2 Thin-ply based thin laminates and their response to impact loads

Increased application of thin structures in aircrafts demanded manufacturers to move from thick to thin laminates. A reduction in the laminate thickness by more than 2.5 times (4.4 mm for the thick laminates studied in Papers A and B to 1.6 mm for the thin laminates in Papers C and D) resulted in a complete turnaround in the impact and CAI responses. The thin laminates underwent higher bending under impact due to the reduced bending stiffness compared to a thick laminate. Reviewing the force-deflection response of the thick (LSYM in Paper B) and thin laminates (H-134 in Paper C) for approximately 6.6 J/mm impact energy, the maximum laminate deflection read 4.5 mm and 6.5 mm for the thick and the thin laminates, respectively. This excessive bending (the thin laminate underwent 4 times the deflection as of its laminate thickness) induced high in-plane tensile stresses at the plies closest to the non-impacted face which in turn led to back fibre splitting. In the case of thick laminates, this damage phenomenon is reported only at high impact energies. All the thin laminates (irrespective of the ply thickness and the material system) exhibited fibre splitting at the laminate back face. However, the extent of this fibre damage substantially depended on the ply thickness and the material architecture.

Thin plies in the framework of thick laminates improved the CAI strength [55, 61, 62],

thanks to their in-situ effect [58] that suppresses matrix cracks and delaminations, the critical damage modes that impair the CAI strength. In the case of thin laminates, thin plies displayed extensive fibre splitting at the back face (refer to Fig. 6.6 in Paper C and Fig.7.8 in Paper D) compared to other ply grades. Thin plies suppressed initial damage of cracks and delamination, but at the cost of dissipating most of the energy through fibre breakage. In the case of thicker plies, impact energy was dissipated through matrix cracks and delamination which means less energy available for dissipation through fibre splitting. This behaviour of thin-ply based thin laminates was evident with all the different material architectures studied (UD, non-crimp and woven fabrics).

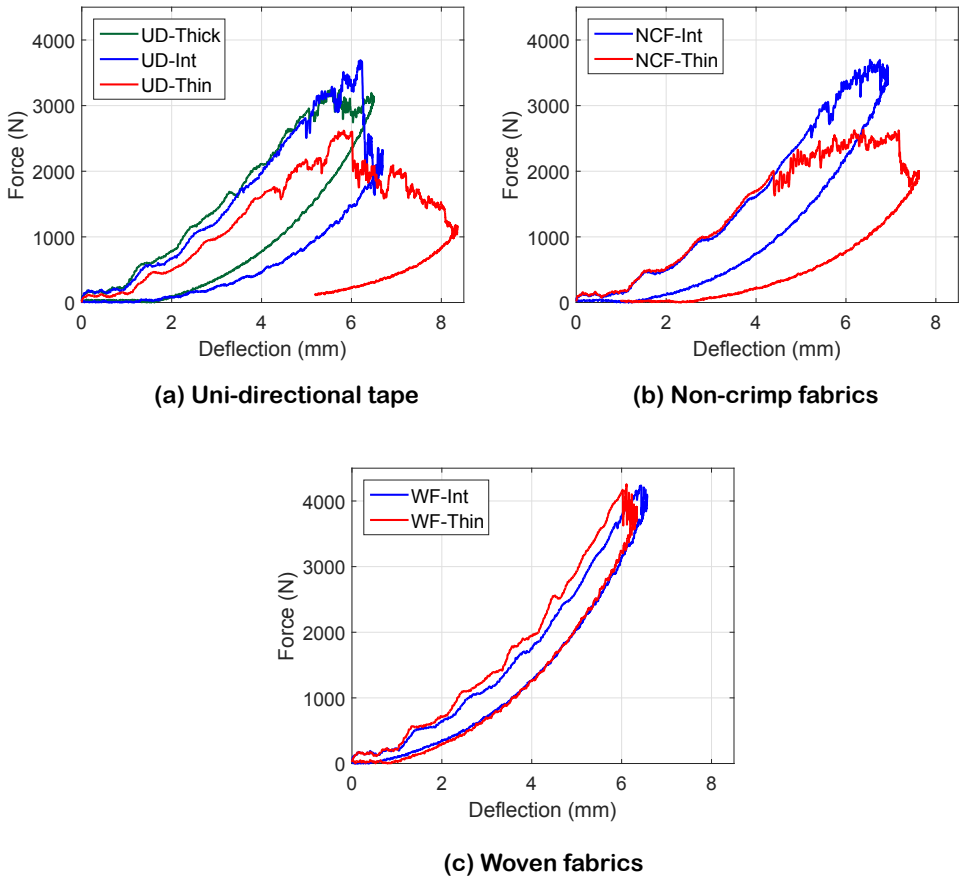

Fig. 10.2.: Understanding the ply thickness effect through the force-deflection responses for (a) UD tapes (b) non-crimp fabrics and (c) woven fabrics for the 10.5 J impact energy by comparing the thin ply grade with other ply grades.

The brittle characteristic nature of thin plies was evident in the force response curves presented in Fig. 10.2 from the 10.5 J impact case for all the material architectures. The load drops recorded with thin plies at the peak loads reduced the load carrying capacity. This load drop is ascribed to the initiation of back fibre splitting, evidenced in the QSI tests interrupted for damage inspection (Fig. 7.12 in Paper D).

Analysis of the various impact damage resistance parameters, especially dissipated energy, revealed the weak response of thin plies to impact loads. Thin plies dissipated around 30% (for UD), 20% (for NCF) and 5% (for woven fabrics) higher energy compared to the intermediate plies. Compared to UD and NCF, the thin and intermediate plies of woven fabrics did not show significant difference in the impact response (Fig. 10.2 (c)). This can be due to the thickness difference between the intermediate and thin ply for woven fabrics (120 vs 80 gsm, respectively,) in comparison to NCF (134 vs 67 gsm) and UD (134 gsm vs 75 gsm). Out of all the ply grades studied, the extended fibre damage associated with thin plies is responsible for the lowest CAI strength. With thin laminates, the final CAI failure is more influenced by the impact induced fibre damage than by delaminations as in the case of thick laminates. Thin plies showed an average reduction of 20% (for UD and NCF) and 10% (for WF) in CAI strength over the intermediate ply grades.

Discussing the effect of material architecture on low velocity impacts, Fig. 10.3 (a) and (b) compare the force-deflection curves of the three different material architectures based on the intermediate ply grade for impact energies IE-3 and IE-4, respectively (note that IE-3 (8-9 J) and IE-4 (10.5 J) are the highest impact energies studied, and please refer to the papers C and D for details). The UD tapes exhibited increased and early load drops (associated to the fibre failure) compared to NCF and WF. NCF behaved similar to UD, except for the reduced load drop for both the energies. On the contrary, woven fabrics WF-Int did not display any load drop that in turn led to a higher peak load.

We made the similar comparison for thin plies in Fig. 10.4. The improved damage resistance of woven fabrics is to be highlighted here, as both the thin grades of UD and NCF exhibited severe load drops, with the UD-Thin the most critical. The higher damage resistance of woven fabrics is associated with their increased interlaminar fracture toughness. In the woven architecture, the waviness of the fibre tows results

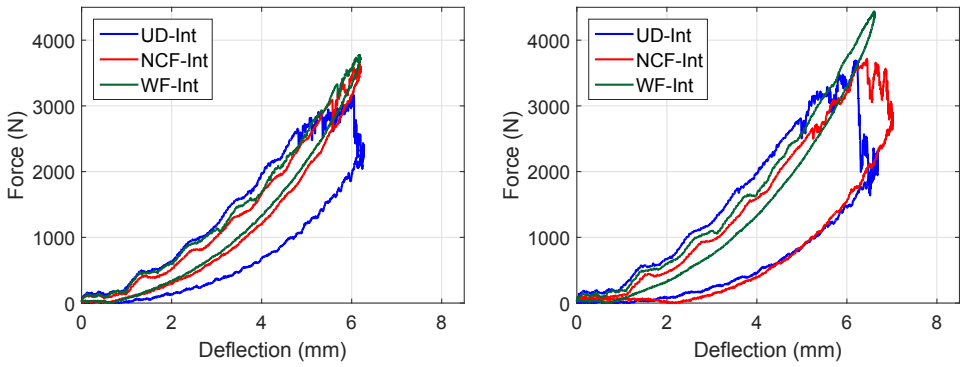

Fig. 10.3.: Comparing the force deflection responses between the intermediate ply grades of UD (134 gsm), non-crimp fabrics (134 gsm) and woven fabrics (120 gsm) for the impact energies (a) IE-3 and (b) IE-4.

in a crack front to jump from weft to warp directions thereby an increased energy dissipation and increased fracture toughness [71, 72]. On the other hand, non-crimp fabrics are rather straight like UD tapes, except that two UD plies are stitched together. The stitch yarn ensures a faster layup through binding layers but does not carry any structural loads, but does decrease the compression strength [161].

We compare various impact resistance parameters and CAI strength among the three different material architectures using a radar plot in Fig. 10.5 and 10.6 based on intermediate and thin plies, respectively. Note that in both the comparisons, the intermediate grade ply laminate is the baseline (referred to as H-134 in Paper C). On a global overview, woven fabrics exhibited the highest damage resistance followed by NCF and UD. Let's review the how the textile processes affect the laminate micro-structure in comparison to the UD. As discussed above, weaving introduces waviness to the fibres, and also induces resin rich areas at the local regions where the weft and warp tows cross each other. Similarly with NCFs, the stitching is reported to generate local waviness and resin areas at the local stitch regions (Fig. 10.7).

As explained before, the waviness is beneficial from the impact resistance point of view due to the increased interlaminar fracture toughness. In the case of NCF too, studies [139, 161] reported the improvement in the fracture toughness due to the local waviness of the fibres near the stitch regions. In addition, the resin rich areas introduced by the textile processes can act as the initiation points of matrix

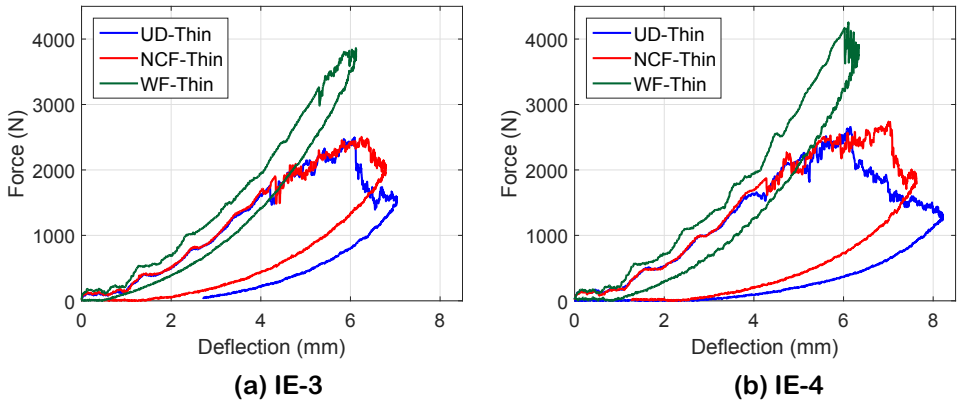

Fig. 10.4.: Comparing the force deflection responses between the thin ply grades of UD (75 gsm), non-crimp fabrics (67 gsm) and woven fabrics (80 gsm) for the impact energies (a) IE-3 and (b) IE-4.

cracks which can lead to delaminations, as reported in [68] through tomography investigations. In fact, this apparently can lead to extra energy dissipation during the early stages of loading which consequently reduces the energy available for damage through fibre failure. These may lead to the reason why UDs exhibited the least damage resistance with increased fibre damage (Fig. 10.5 and 10.6).

Moving to damage tolerance, NCFs displayed the highest CAI strength (around 20% over the UD and 10% over the woven fabrics) considering both the ply grades. The substantial improvement in the damage resistance of woven fabrics did not proportionate to the similar improvement in CAI strength. The same wavy architecture that increased the fracture toughness of woven fabrics compromised the in-plane properties, especially the compression ones. This is evidenced in the reduction of the plain compression strength (by around 10-15%) compared to UD. Still, thanks to the spread tow methodology, the reduction in the in-plane properties is very minimal due to the considerable reduction in the waviness compared to the conventional manufacturing methods. UD plies, that are rather straight compared to the fabrics, exhibited higher plain compression strengths over WFs. But the comparatively higher impact induced extensive fibre damage has impaired the CAI strength of UDs when compared to NCF and WF.

Re-visiting the second sub-objective of the thesis, the response of thin laminates towards impact loads is clearly elucidated. The extensive fibre damage associated

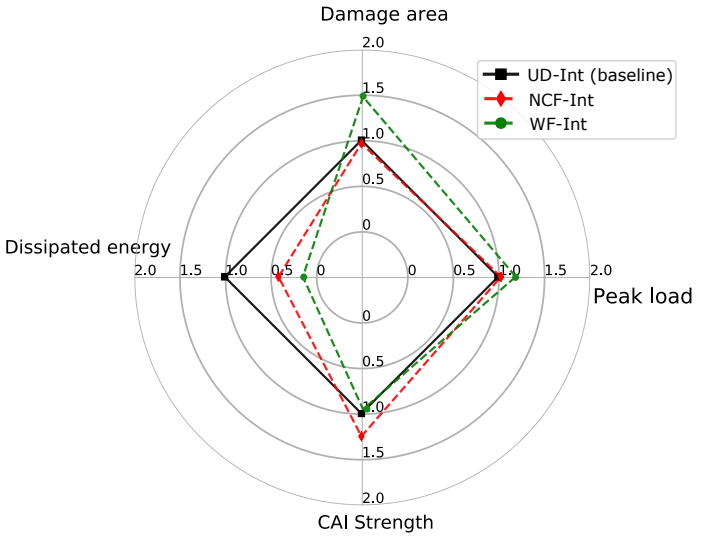

(a) IE-3

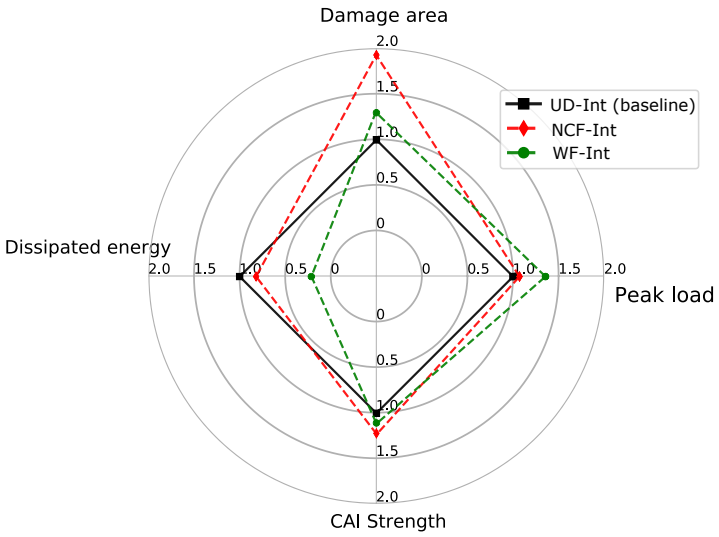

(b) IE-4

Fig. 10.5.: Comparison of the impact damage resistance parameters and CAI strength of intermediate ply grades of all the three material architectures for (a) IE-3 and (b) IE-4.

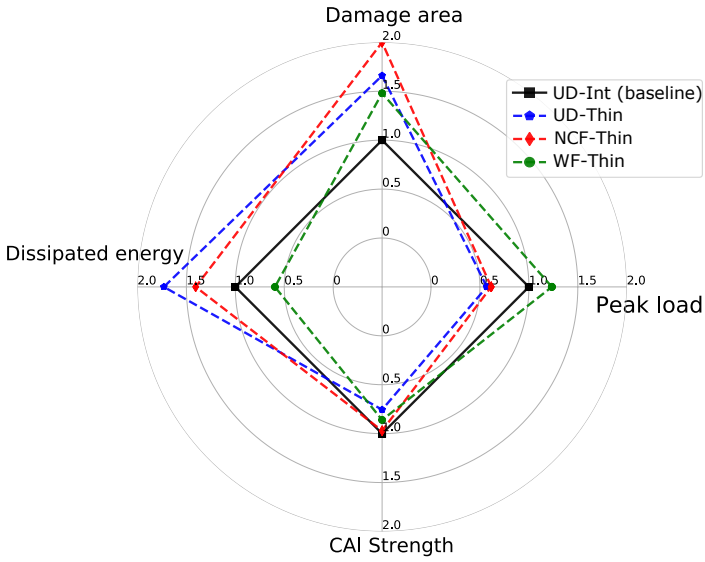

(a) IE-3

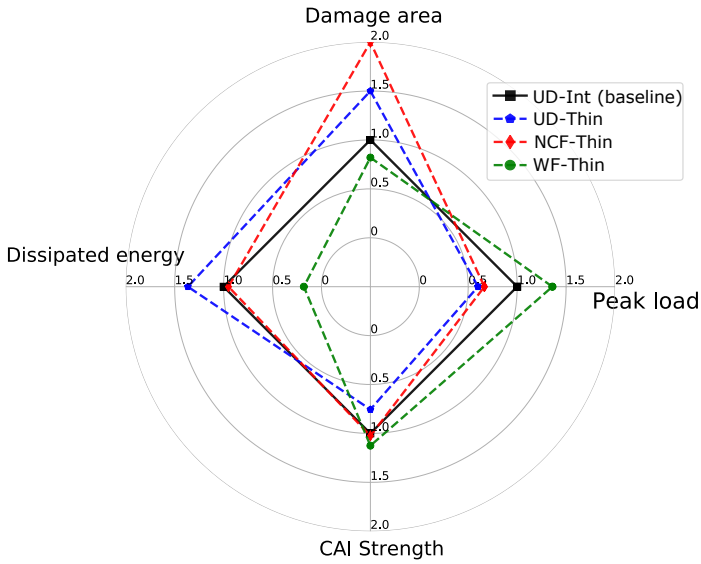

(b) IE-4

Fig. 10.6.: Comparison of the impact damage resistance parameters and CAI strength of thin ply grades of all the three material architectures for (a) IE-3 and (b) IE-4.

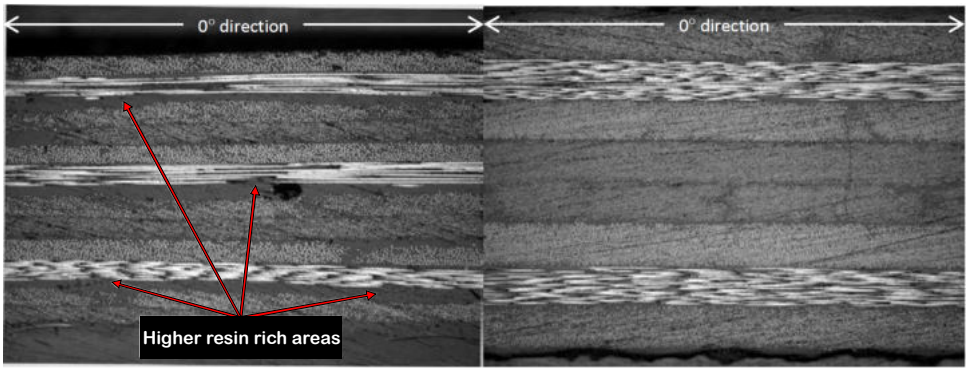

(a) Non-crimp fabrics (b) Uni-directional tape

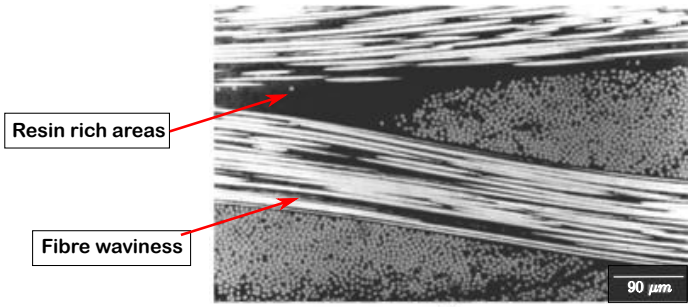

(c) Woven fabrics

Fig. 10.7.: Demonstrating the resin rich areas and fibre waviness in the textile fabrics when compared to the UD plies (Images adapted from [54, 162]).

with thin-ply based thin laminates is evidenced, and has a significant effect on the reduction of CAI strength. Contrary to the results from thick laminates, intermediate plies are better damage tolerant than thin plies. Furthermore, textile fabrics (NCFs and WFs) offered improved impact damage resistance and tolerance, and considering their cost effectiveness in manufacturing, they are a sure prospect to substitute the UD tapes.

10.3 Ply hybridization and unsymmetrical designs to improve the compression after impact strength

In the quest to improve the weak response of thin laminates, novel laminates designed by means of ply level hybridization and unsymmetrical designs remarkably reduced the extent of fibre failure to improve the CAI strength. The force response curves of the optimum hybrid laminates (UD from Paper C and NCF from Paper E) and their corresponding thin-ply baseline laminates are presented in Fig. 10.8 for the 10.5 J energy case.

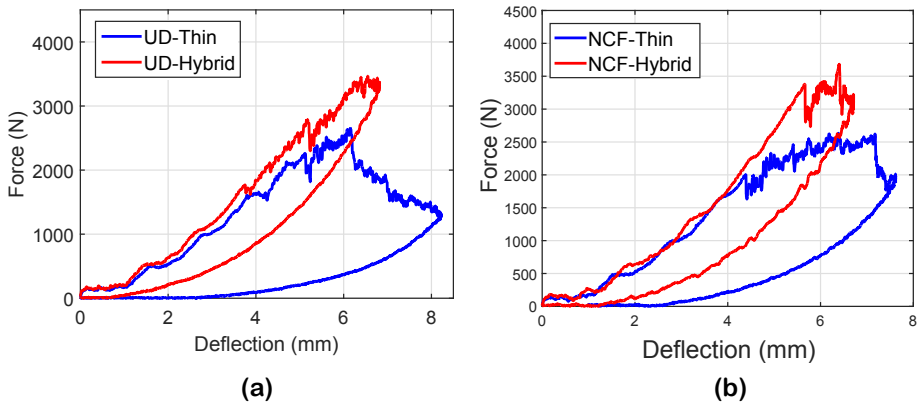

Fig. 10.8.: Comparing the force-deflection responses of the hybrid laminates with their corresponding thin-ply baseline laminates for (a)UD (Paper C) and (b) NCF (Paper E). (UD-Hybrid refers to H-75-H2 from Paper C and NCF-Hybrid refers to NCF-UHB from Paper-E).

As evidenced in Fig. 10.8 (a) and (b), the introduction of thicker plies has reduced and delayed the first load drop resulting in an increased peak load and reduced energy dissipated. The inserted thicker plies alleviated the amount of fibre damage by dissipating impact energy through matrix cracks and delamination. The delayed

initiation of fibre splitting was evidenced in the QSI tests (as in Fig 8.11 in Paper E). The main reason for the increased CAI strength is due to the added thicker plies that (a) mitigates the fibre damage and (b) effectively carry the compression after load, especially the load bearing 0° plies. The importance of locally clustered plies towards CAI improvement is in line with the results from Paper B with thick laminates. In addition, ply hybridization involves combining the potential benefits of thin plies (delay damage onset, along with higher plain compression strength due to the homogeneous micro-structure) and intermediate plies (the ability to reduce fibre damage by dissipating energy through delaminations).

Furthermore, the results from Paper E revealed that along with the addition of the thicker plies, it is of prime importance the through-the-thickness location where they are added. Addition of intermediate grade plies to the non-impacted side of the thin laminate mitigated the fibre damage and improved the CAI strength. The plies closest to the non-impacted side is identified as the critical weak region in the laminate where the fibre splitting is initiated. In addition, it is also vulnerable to delamination due to bending related interlaminar shear stresses. Hence, the substitution of thin plies by intermediate plies at the bottom of the laminate considerably promotes delamination and reduces the fibre damage. This is clearly evidenced in the C-scans of the laminate NCF-UHB, where there is a single dominant delamination at the interface closest to the non-impact side and followed by the reduced fibre damage (seen in photos and Fig. 10.8).

Fig. 10.9 presents the CAI strength and the impact damage parameters of five laminates namely: UD-Int as the baseline, UD-Thin and UD-Hybrid (all from Paper C), NCF-Thin and NCF-Hybrid (from Paper E). The hybrid laminates are compared with their respective thin ply baseline laminates to assess the potential of these novel designs. Both the hybrid laminates improved the CAI response substantially, with the unsymmetrical hybrid laminate (NCF-Hybrid) offering the highest improvement out of all.

The numerical results from Paper F strengthened the idea of ply level hybridization and unsymmetrical designs. Most of the proposed hybrid laminates (symmetrical and unsymmetrical) improved the CAI strength over the UD-Int baseline highlights the feasibility of such novel designs. Numerical results associated the steep load drop

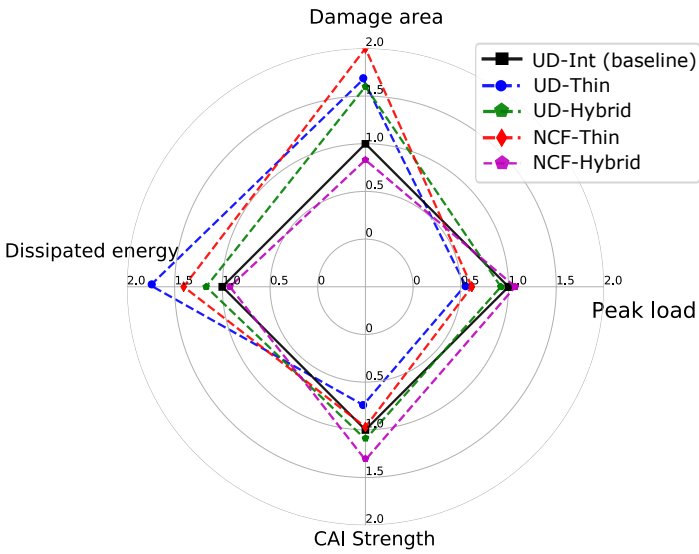

(a) IE-3

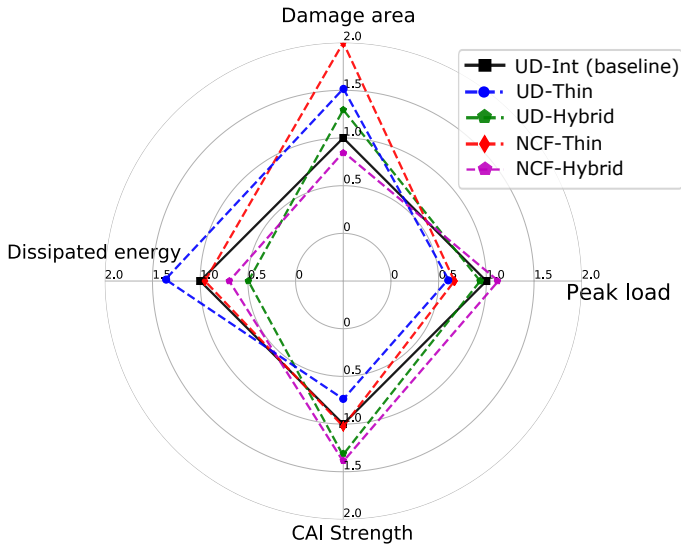

(b) IE-4

Fig. 10.9.: Comparison of the impact damage resistance parameters and CAI strength of hybrid laminates proposed and their corresponding thin-ply counterparts (a) IE-3 and (b) IE-4. Note that the intermediate ply grade from UD is considered as the baseline.

in the baseline laminate (Fig **??**) to the initiation of the fibre damage at the bottom ply and its propagation to the top of the laminate. In the case of the proposed hybrid plies, either no or reduced fibre damage was seen at the last ply and the addition of the thicker plies restricted the propagation to the other plies. Further in-depth analysis of the dissipated energy (Fig. 9.13 in Paper F) revealed that there was early delaminations in the hybrid laminates compared to the baseline. But the initiation of fibre damage in the baseline was accompanied by a steep increase in the interlaminar dissipated energy too, evidencing a 'fibre failure induced delamination'. All the studies (Paper C, D, E and F) pinpointed this fibre damage as the clear reason for the reduced CAI strength.

The flexibility to stack plies without the worry of symmetry constraint and the subsequent increased design space are the reasons for the increased CAI strength shown by the optimum unsymmetrical laminates over the best symmetric ones. A closer look at the optimum unsymmetrical stacking sequences conveys that a cluster of 0° plies or any other orientation can be placed just in the bottom sub-laminate or vice-versa without the need to mirror the same plies on to the other side of the laminate. Fig. 10.10 illustrates different hybrid laminates proposed in the thesis including both symmetrical and unsymmetrical laminates.

Hence, by means of experimental and numerical tests, the last sub-objective of the thesis was realised: exploring novel laminate design concepts incorporating unsymmetry and ply hybridization, we have demonstrated that fibre damage can be controlled by adding thicker plies at proper locations, which in turn can improve the CAI strength. Papers C, E and F provided a rather simple and effective solution to mitigate the critical fibre damage associated with thin plies. We highlighted the importance the stacking sequence design has in improving the CAI strength, one of the most important parameter looked upon by the aeronautic industries, in an economical and effective way.

10.4 Global laminate design guidelines for improved CAI strength

The CAI results from thick laminates were mainly influenced by delamination damage and its associated parameters such as the through-the-thickness location of

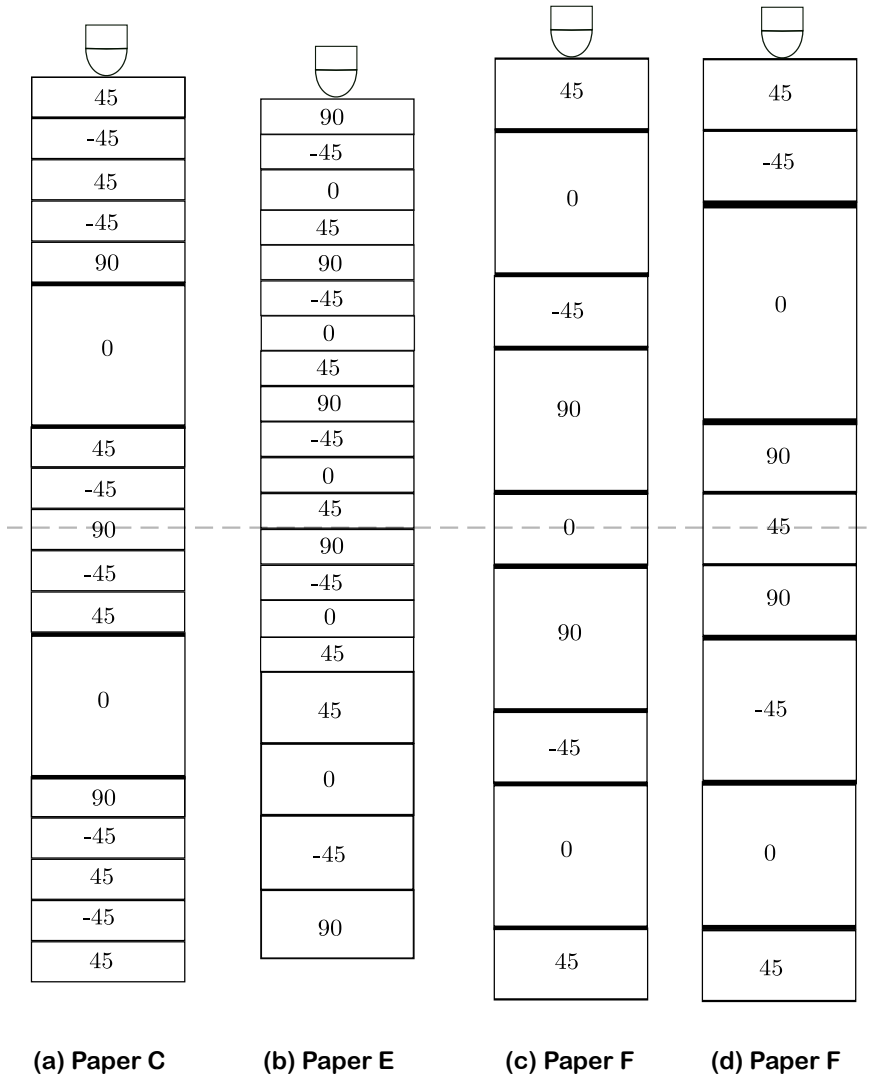

Fig. 10.10.: Illustration of the optimum hybrid laminates (both symmetric and unsymmetrical) proposed in the thesis.

the dominant delamination, the thickness of the split sub-laminates and the buckling modes. Tailoring of these parameters is the first attempt towards improving the CAI strength. In the case of thin laminates, fibre splitting is the critical damage mode that affects the CAI strength. Paper F validated the adverse effect of fibre damage area on the CAI strength. Compared to thick laminates, the idea behind improving the CAI strength is rather straight forward: reducing the amount of fibre damage. Departing from the understanding of the effect of different non-conventional laminate designs on improving CAI strength, we propose some stacking sequence guidelines that can be useful to improve the CAI strength.

- It is preferable to cluster the main load bearing plies (in this case 0° plies) than to disperse them within the laminate. When the laminate splits to form sub-laminates during CAI loading, the sub-laminate containing the intact clustered plies can effectively carry the load (inferred from Paper B)
- In-depth delaminations or delaminations close to the mid-plane offer higher buckling resistance under CAI loads. Hence, in combination with the above point, it is better to impose clustered plies near the laminate mid-plane (inferred from Paper B and also reported in [12, 25])
- With thin laminates, the sub-laminate at the non-impacted side is the critical damage prone region. Therefore, it is recommended to use thicker ply grades at this location than thin plies (inferred from Paper C and E)
- Safeguard the load bearing plies from the exterior surfaces of the laminate, where thin laminates undergo critical fibre splitting in the bottom plies and extensive indentation damage in the top plies (inferred from Paper E)

11 Conclusion

11.1 Concluding remarks

Using novel laminate designs, this thesis was dedicated to improving the compression after impact response of aerospace graded thick and thin laminates. Understanding the importance of a laminate stacking sequence on the loading response, the study primarily challenged the unnecessary conventional laminate mid-plane symmetry constraint, especially in terms of the unsymmetrical natured impact loads. The proposed unsymmetrical laminates with zero coupling responses clearly demonstrates the opportunity to move outside the symmetry box. Combining unsymmetrical designs with tailored ply clusters, impact damage was pre-determined to occur at desired through-the-thickness locations in the laminate. Furthermore, to assess the feasibility of unsymmetrical laminates in an industrial application, their impact damage tolerance was compared with standard symmetric baseline laminate. In addition to the improvement in CAI strength (by a maximum of 10%) over the symmetric baseline laminate, the unsymmetrical laminates provided insight into the effect delamination location has on the CAI strength.

Within the framework of thin laminates, the experimental study showed that thin plies do not offer the same improved damage tolerance as in the case with thick laminates. Thin-ply based thin laminates exhibited extensive fibre damage under low velocity impact loads that consequently led to a drastic reduction in the CAI strength. Compared to intermediate ply grades, a 20-30% increased energy dissipation followed by early and extensive back fibre splitting was observed with thin plies. This weak response of thin plies was also in line with the results of other material architectures (non-crimp and woven fabrics). In response to the extended fibre damage, thin plies reduced the CAI strength by an average of 20% over the intermediate grade plies. Out of all the material architectures, woven fabrics displayed superior impact damage resistance due to their woven fabric architecture. In terms of CAI strength, non-crimp fabrics provided the highest values followed by woven fabrics and UD tapes.

In the quest to improve this weak response that thin-ply based thin laminates have,

ply hybridization and unsymmetrical laminate designs were proposed. These designs substantially mitigated the weak impact response of thin plies, and improved the CAI strength. The thicker plies with thin plies helped to delay and reduce the fibre damage at the cost of dissipating energy through delaminations. The proposed novel designs improved the CAI strengths by 30-40% over the thin ply baseline; not to mention the cost effectiveness behind this laminate design approach. In addition, the study also provided insight into the importance of the through-the-thickness location in the laminate at which the thicker plies have to be added. Understanding that the non-impacted side is the critical damage-prone region in thin laminates, unsymmetrical laminates help to tailor thicker plies only at this location without the necessity to mirror them again. As a concluding study, the virtual CAI results of all the hybrid laminates from the proposed design space also pointed towards the effectiveness of ply hybridization and unsymmetry in improving the CAI strength. The virtually obtained optimum impact damage tolerant hybrid laminates (both symmetric and unsymmetric) dramatically improved the CAI strength (up to 40%) over the aerospace baseline laminate made of intermediate plies. An increased number of unsymmetrical laminate solutions and their improvement over the best symmetric hybrid laminate highlights the feasibility of considering unsymmetrical designs in the applications such as aircraft wing or fuselage skins.

Revisiting the main objective, we have pushed the boundaries of damage tolerant designs through novel stacking sequences dedicated to both thick and thin laminates. Multiples studies in the thesis confirm that symmetric laminates are not the optimal damage tolerant solution towards impact loads. It is time to re-consider the importance of laminate design which, if tailored judiciously, can substantially improve the impact and post-impact response without added manufacturing costs or changes to the micro-structure.

11.2 Perspectives & Future work

The potential of unsymmetrical laminates can be further extended with thick laminates, where thinner plies can be placed at the non-impacted side (the critical region for delamination) of the standard ply laminate. The inherent in-situ effect of thin plies can help to suppress the delaminations and these kind of laminates are promising for use in aircraft structures, such as wing or fuselage skins, to improve impact damage

tolerance. In this way, the plies at the surface of the skin can be tailored differently without the need to unnecessarily use the same plies at the other side of the surface.

Another immediate work is to experimentally test some of the optimum hybrid laminates found using virtual tests in the last part of the thesis. The experimental validation of these laminates will furthermore strengthen the idea of such novel laminate designs and the application of high fidelity numerical tools in laminate design studies. In addition, the whole design space of unsymmetrical laminates found in the last paper can be virtually tested to complete the study on unsymmetrical laminates, with the possibility of enhancing the already obtained 10% improvement over the best symmetric hybrid laminate.

Another interesting study would be to perform off-axis virtual CAI tests to understand how these hybrid laminates behave under loads applied in other directions apart from 0° (off-axis loads). A complete polar plot of the CAI strengths in different directions would be interesting from an aeronautic point of view too, as we are currently considering only the CAI strength in the 0° direction. From the knowledge gained during the course of the thesis, ply hybridization can be performed not just limited to 0° plies (load bearing during a longitudinal compression) but also to other orientations (as performed in Paper E and F). This is expected to provide improved damage tolerant designs even in off-axis loads.

Apart from impact loads, there are many cases where the loading stresses are not symmetric, for instance ply drop-off, bolted joints, skin-stiffened panels and a skin under bending. Unsymmetrical stacking sequences are worth exploring in such cases too. In addition, the unsymmetrical laminates can also be virtually tested under other loading conditions such as open hole tension and compression tests, to study their response over the symmetric laminates.

Compression after impact for thin laminates at low impact energies resulted in invalid failure mode. A future study would be to modify the current anti-buckling fixture to make sure that, even at lower impact energies, a proper CAI failure induced by the impact damage is obtained. Furthermore as a future study, it can be meaningful to access the residual strength reduction of thin laminates through tension after impact (TAI), instead of or in addition to CAI, as fibre failure is the dominant damage mode.

Bibliography

[1] J. Pinto, Economic comparison between materials in the aerospace industry, Master thesis, Tecnico Lisboa; 2017.

[2] T. Pringle, Preventing ramp and ground accidents, Transport Canada, 2010.

[3] M. Kaufmann, D. Zenkert, P. Wennhage, Integrated cost/weight optimization of aircraft structures, Structural and Multidisciplinary Optimization 41 (2009) 325–334.

[4] D. of access: 15-04-2019, Use of composites in aircraft construction, https://vandaair.com/2014/04/14/the-use-of-composites-in-aircraft-construction/.

[5] S. Abrate, Impact on Composite Structures, Cambridge University Press, 2005.

[6] A. Wagih, P. Maimí, N. Blanco, J. Costa, A quasi-static indentation test to elucidate the sequence of damage events in low velocity impacts on composite laminates, Composites Part A: Applied Science and Manufacturing 82 (2016) 180–189.

[7] D. Bull, S. Spearing, I. Sinclair, Observations of damage development from compression-after-impact experiments using ex situ micro-focus computed tomography, Composites Science and Technology 97 (2014) 106–114.

[8] C. Bouvet, Mechanics of Aeronautical Composite Materials, Wiley-ISTE, 2017.

[9] T. Sebaey, E. González, C. Lopes, N. Blanco, J. Costa, Damage resistance and damage tolerance of dispersed CFRP laminates: Effect of ply clustering, Composite Structures 106 (2013) 96–103.

[10] C. Lopes, O. Seresta, Y. Coquet, Z. Gürdal, P. Camanho, B. Thuis, Low-velocity impact damage on dispersed stacking sequence laminates. Part I: Experiments, Composites Science and Technology 69 (7-8) (2009) 926–936.

[11] Y. Liv, G. Guillamet, J. Costa, E. González, L. Marín, J. Mayugo, Experimental study into compression after impact strength of laminates with conventional and nonconventional ply orientations, Composites Part B: Engineering 126 (7) (2017) 133–142.

[12] Y. Liv, A contribution to the understanding of compression after impact of composite laminates, PhD thesis, University of Girona; 2017.

[13] T. Sebaey, E. González, C. Lopes, N. Blanco, P. Maimí, J. Costa, Damage resistance and damage tolerance of dispersed CFRP laminates: Effect of the mismatch angle between plies, Composite Structures 101 (2013) 255–264.

[14] M. Wisnom, The role of delamination in failure of fibre-reinforced composites, Philosophical Transactions of the Royal Society A: Mathematical, Physical and Engineering Sciences 370 (1965) (2012) 1850–1870.

[15] G. Davies, X. Zhang, G. Zhou, S. Watson, Numerical modelling of impact damage, Composites 25 (5) (1994) 342–350.

[16] D. Guedra-Degeorges, Recent advances to assess mono-and multi-delaminations behaviour of aerospace composites, Composites Science and Technology 66 (6) (2006) 796–806.

[17] N. Hongkarnjanakul, Modélisation numérique pour la tolérance aux dommages d'impact sur stratifié composite: de l'impact à la résistance résiduelle en compression, PhD thesis, ISAE, Toulouse.

[18] D. Liu, Impact-induced delamination—a view of bending stiffness mismatching, Journal of Composite Materials 22 (7) (1988) 674–692.

[19] C. Bouvet, S. Rivallant, J.-J. Barrau, Low velocity impact modeling in composite laminates capturing permanent indentation, Composites Science and Technology 72 (16) (2012) 1977–1988.

[20] T. Yokozeki, A. Kuroda, A. Yoshimura, T. Ogasawara, T. Aoki, Damage characterization in thin-ply composite laminates under out-of-plane transverse loadings, Composite structures 93 (1) (2010) 49–57.

[21] N. Uda, K. Ono, K. Kunoo, Compression fatigue failure of cfrp laminates with impact damage, Composites Science and Technology 69 (14) (2009) 2308–2314.

[22] C. Soutis, P. Curtis, Prediction of the post-impact compressive strength of cfrp laminated composites, Composites Science and Technology 56 (6) (1996) 677–684.

[23] S. Rivallant, C. Bouvet, E. A. Abdallah, B. Broll, J.-J. Barrau, Experimental analysis of cfrp laminates subjected to compression after impact: The role of impact-induced cracks in failure, Composite Structures 111 (2014) 147–157.

[24] D. Cartie, P. Irving, Effect of resin and fibre properties on impact and compression after impact performance of cfrp, Composites part A: applied science and manufacturing 33 (4) (2002) 483–493.

[25] N. Hu, H. Fukunaga, H. Sekine, K. M. Ali, Compressive buckling of laminates with an embedded delamination, Composites science and technology 59 (8) (1999) 1247–1260.

[26] R. Butler, D. P. Almond, G. Hunt, B. Hu, N. Gathercole, Compressive fatigue limit of impact damaged composite laminates, Composites Part A: applied science and manufacturing 38 (4) (2007) 1211–1215.

[27] M. Richardson, M. Wisheart, Review of low-velocity impact properties of composite materials, Composites Part A: Applied Science and Manufacturing 27 (12) (1996) 1123–1131.

[28] P. Hogg, Toughening of thermosetting composites with thermoplastic fibres, Materials Science and Engineering: A 412 (2005) 97–103.

[29] X. Xu, Z. Zhou, Y. Hei, B. Zhang, J. Bao, X. Chen, Improving compression-after-impact performance of carbon–fiber composites by CNTs/thermoplastic

hybrid film interlayer, Composites science and technology 95 (2014) 75–81.

[30] N. Nash, T. Young, P. McGrail, W. Stanley, An investigation of the damage tolerance of carbon/benzoxazine composites with a thermoplastic toughening interlayer, Composite Structures 147 (2016) 25–32.

[31] N. Nash, T. Young, P. McGrail, W. Stanley, Inclusion of a thermoplastic phase to improve impact and post-impact performances of carbon fibre reinforced thermosetting composites—a review, Materials & Design 85 (2015) 582–597.

[32] S. García-Rodríguez, J. Costa, V. Singery, I. Boada, J. Mayugo, The effect interleaving has on thin-ply non-crimp fabric laminate impact response: X-ray tomography investigation, Composites Part A: Applied Science and Manufacturing 107 (2018) 409–420.

[33] M. S. Sohn, X. Z. Hu, J. K. Kim, L. Walker, Impact damage characterisation of carbon fibre/epoxy composites with multi-layer reinforcement, Composites Part B: Engineering 31 (2000) 681–691.

[34] N. H. Nash, D. Ray, T. M. Young, W. F. Stanley, The influence of hydrothermal conditioning on the mode-i, thermal and flexural properties of carbon/benzoxazine composites with a thermoplastic toughening interlayer, Composites Part A: Applied Science and Manufacturing 76 (2015) 135–144.

[35] A. Mouritz, Review of z-pinned composite laminates, Composites Part A: applied science and manufacturing 38 (12) (2007) 2383–2397.

[36] L. Francesconi, F. Aymerich, Effect of z-pinning on the impact resistance of composite laminates with different layups, Composites Part A: Applied Science and Manufacturing 114 (2018) 136–148.

[37] M. Knaupp, F. Baudach, J. Franck, G. Scharr, Impact and post-impact properties of cfrp laminates reinforced with rectangular z-pins, Composites Science and Technology 87 (2013) 218–223.

[38] J. Teng, Z. Zhuang, B. Li, A study on low-velocity impact damage of z-pin reinforced laminates, Journal of mechanical science and technology 21 (2007)

2125–2132.

[39] G. Bullegas, J. Benoliel, P. Fenelli, S. Pinho, S. Pimenta, Towards quasi isotropic laminates with engineered fracture behaviour for industrial applications, Composites Science and Technology 165 (2018) 290–306.

[40] L. Mencattelli, J. Tang, Y. Swolfs, L. Gorbatikh, S. T. Pinho, Bio-inspired design for enhanced damage tolerance of self-reinforced polypropylene/carbon fibre polypropylene hybrid composites, Composites Part A: Applied Science and Manufacturing 121 (2019) 341–352.

[41] S. Hitchen, R. Kemp, The effect of stacking sequence on impact damage in a carbon fibre/epoxy composite, Composites 26 (1995) 207–214.

[42] E. González, P. Maimí, P. Camanho, C. Lopes, N. Blanco, Effects of ply clustering in laminated composite plates under low-velocity impact loading, Composites Science and Technology 71 (6) (2011) 805–817.

[43] N. Hongkarnjanakul, C. Bouvet, S. Rivallant, Validation of low velocity impact modelling on different stacking sequences of cfrp laminates and influence of fibre failure, Composite Structures 106 (2013) 549–559.

[44] C. Lopes, O. Seresta, Y. Coquet, Z. Gürdal, P. Camanho, B. Thuis, Low-velocity impact damage on dispersed stacking sequence laminates. Part I: Experiments, Composites Science and Technology 69 (7) (2009) 926–936.

[45] C. Lopes, P. Camanho, Z. Gürdal, P. Maimí, E. González, Low-velocity impact damage on dispersed stacking sequence laminates. Part II: Numerical simulations, Composites Science and Technology 69 (7-8) (2009) 937–947.

[46] C. Furtado, A. Arteiro, G. Catalanotti, J. Xavier, P. Camanho, Selective ply-level hybridisation for improved notched response of composite laminates, Composite Structures 145 (2016) 1–14.

[47] A. Arteiro, G. Catalanotti, J. Xavier, P. Linde, P. Camanho, A strategy to improve the structural performance of non-crimp fabric thin-ply laminates, Composite Structures 188 (2018) 438–449.

[48] T. Sebaey, E. Mahdi, Using thin-plies to improve the damage resistance and tolerance of aeronautical CFRP composites, Composites Part A: Applied Science and Manufacturing 86 (2016) 31–38.

[49] N. Baker, R. Butler, C. York, Damage tolerance of fully orthotropic laminates in compression, Composites Science and Technology 72 (2012) 1083–1089.

[50] F. Williams, D. Kennedy, M. Anderson, R. Butler, Viconopt-program for exact vibration and buckling analysis or design of prismatic plate assemblies, AIAA journal 29 (11) (1991) 1927–1928.

[51] A. Wagih, P. Maimí, N. Blanco, S. García-Rodríguez, G. Guillamet, R. Issac, A. Turon, J. Costa, Improving damage resistance and load capacity of thin-ply laminates using ply clustering and small mismatch angles, Composites Part A: Applied Science and Manufacturing 117 (2019) 76–91.

[52] F. Crossman, W. Warren, A. Wang, G. Law Jr, Initiation and growth of transverse cracks and edge delamination in composite laminates part 2. experimental correlation, Journal of Composite Materials 14 (1) (1980) 88–108.

[53] A. Wang, F. Crossman, Initiation and growth of transverse cracks and edge delamination in composite laminates part 1. an energy method, Journal of Composite Materials 14 (1) (1980) 71–87.

[54] A. J. C. Arteiro, Technology development and structural mechanics of composites built of spread tow thin-ply technology, PhD thesis, University of Porto.

[55] S. Sihn, R. Y. Kim, K. Kawabe, S. W. Tsai, Experimental studies of thin-ply laminated composites, Composites Science and Technology 67 (6) (2007) 996–1008.

[56] D. of access: 27-04-2019, North thin ply technology, www.thinplytechnology.com/technology/spread-tow-technology.

[57] P. P. Camanho, A. Arteiro, A. turon, J. Costa, G. Guillamet, E. Gonzalez, Structural integrity of thin-ply laminates, JEC composites (71) (2012) 91–92.

[58] P. P. Camanho, C. G. Dávila, S. T. Pinho, L. Iannucci, P. Robinson, Prediction of in situ strengths and matrix cracking in composites under transverse tension and in-plane shear, Composites Part A: Applied Science and Manufacturing 37 (2) (2006) 165–176.

[59] G. Guillamet, A. Turon, J. Costa, P. Linde, A quick procedure to predict free-edge delamination in thin-ply laminates under tension, Engineering Fracture Mechanics 168 (2016) 28–39.

[60] G. Guillamet, A. Turon, J. Costa, J. Renart, P. Linde, J. Mayugo, Damage occurrence at edges of non-crimp-fabric thin-ply laminates under off-axis uniaxial loading, Composites Science and Technology 98 (2014) 44–50.

[61] T. Yokozeki, Y. Aoki, T. Ogasawara, Experimental characterization of strength and damage resistance properties of thin-ply carbon fiber/toughened epoxy laminates, Composite Structures 82 (3) (2008) 382–389.

[62] H. Saito, M. Morita, K. Kawabe, M. Kanesaki, H. Takeuchi, M. Tanaka, I. Kimpara, Effect of ply-thickness on impact damage morphology in CFRP laminates, Journal of Reinforced Plastics and Composites 30 (13) (2011) 1097–1106.

[63] R. Amacher, J. Cugnoni, J. Botsis, L. Sorensen, W. Smith, C. Dransfeld, Thin ply composites: experimental characterization and modeling of size-effects, Composites Science and Technology 101 (2014) 121–132.

[64] ASTM D7136/D7136M-15, Standard test method for measuring the damage resistance of a fiber reinforced polymer matrix composite to a drop weight impact event, 2015.

[65] J. Lee, C. Soutis, Prediction of impact-induced fibre damage in circular composite plates, Applied Composite Materials 12 (2) (2005) 109–131.

[66] S. Sánchez-Sáez, E. Barbero, R. Zaera, C. Navarro, Compression after impact of thin composite laminates, Composites Science and Technology 65 (13) (2005) 1911–1919.

[67] M. Remacha, S. Sánchez-Sáez, B. López-Romano, E. Barbero, A new device for determining the compression after impact strength in thin laminates, Composite Structures 127 (2015) 99–107.

[68] S. García-Rodríguez, J. Costa, A. Bardera, V. Singery, D. Trias, A 3D tomographic investigation to elucidate the low-velocity impact resistance, tolerance and damage sequence of thin non-crimp fabric laminates: effect of ply-thickness, Composites Part A: Applied Science and Manufacturing 113 (2018) 53–65.

[69] G. Bibo, P. Hogg, The role of reinforcement architecture on impact damage mechanisms and post-impact compression behaviour, Journal of Materials Science 31 (5) (1996) 1115–1137.

[70] G. Bibo, P. Hogg, R. Backhouse, A. Mills, Carbon-fibre non-crimp fabric laminates for cost-effective damage-tolerant structures, Composites Science and Technology 58 (1) (1998) 129–143.

[71] J.-K. Kim, M.-L. Sham, Impact and delamination failure of woven-fabric composites, Composites Science and Technology 60 (5) (2000) 745–761.

[72] K. Vallons, A. Behaeghe, S. V. Lomov, I. Verpoest, Impact and post-impact properties of a carbon fibre non-crimp fabric and a twill weave composite, Composites Part A: Applied Science and Manufacturing 41 (8) (2010) 1019–1026.

[73] A. Petriccione, D. Annicchiarico, V. Antonucci, M. Giordano, A. Riccio, F. Scaramuzzino, M. Zarrelli, A stiffness volume averaging based approach to model non-crimp fabric reinforced composites, Composites Science and Technology 72 (2) (2012) 360–369.

[74] P. Sanial, How c-ply can change the way we design and manufacture, JEC composites.

[75] E. González, P. Maimí, P. Camanho, A. Turon, J. Mayugo, Simulation of drop-weight impact and compression after impact tests on composite laminates, Composite Structures 94 (11) (2012) 3364–3378.

[76] C. Bouvet, B. Castanié, M. Bizeul, J.-J. Barrau, Low velocity impact modelling in laminate composite panels with discrete interface elements, International Journal of Solids and Structures 46 (14-15) (2009) 2809–2821.

[77] C. Lopes, S. Sádaba, C. González, J. Llorca, P. Camanho, Physically-sound simulation of low-velocity impact on fiber reinforced laminates, International Journal of Impact Engineering 92 (2016) 3–17.

[78] A. Soto, E. González, P. Maimí, F. M. de la Escalera, J. S. de Aja, E. Alvarez, Low velocity impact and compression after impact simulation of thin ply laminates, Composites Part A: Applied Science and Manufacturing 109 (2018) 413–427.

[79] M. Abir, T. Tay, M. Ridha, H. Lee, On the relationship between failure mechanism and compression after impact (CAI) strength in composites, Composite Structures 182 (2017) 242–250.

[80] N. Dubary, C. Bouvet, S. Rivallant, L. Ratsifandrihana, Damage tolerance of an impacted composite laminate, Composite Structures 206 (2018) 261–271.

[81] S. Rivallant, C. Bouvet, N. Hongkarnjanakul, Failure analysis of cfrp laminates subjected to compression after impact: Fe simulation using discrete interface elements, Composites Part A: Applied Science and Manufacturing 55 (2013) 83–93.

[82] P. A. Lagace, J. E. Williamson, P. Wilson Tsang, E. Wolf, S. Thomas, A preliminary proposition for a test method to measure (impact) damage resistance, Journal of Reinforced Plastics and Composites 12 (5) (1993) 584–601.

[83] S. R. Swanson, Limits of quasi-static solutions in impact of composite structures, Composites Engineering 2 (4) (1992) 261–267.

[84] H. Kaczmarek, S. Maison, Comparative ultrasonic analysis of damage in cfrp under static indentation and low-velocity impact, Composites science and technology 51 (1) (1994) 11–26.

[85] E. Abisset, F. Daghia, X. Sun, M. R. Wisnom, S. R. Hallett, Interaction of

inter-and intralaminar damage in scaled quasi-static indentation tests: Part 1–experiments, Composite Structures 136 (2016) 712–726.

[86] D. Bull, S. Spearing, I. Sinclair, Investigation of the response to low velocity impact and quasi-static indentation loading of particle-toughened carbon-fibre composite materials, Composites Part A: Applied Science and Manufacturing 74 (2015) 38–46.

[87] ASTM D6484/D6484M-09, Standard test method for open-hole compressive strength of polymer matrix composite laminates, 2009.

[88] ASTM D7137/D7137-15, Standard Test Method for Compressive Residual Strength Properties of Damaged Polymer Matrix Composite Plates, 2015.

[89] MATLAB, version 8.5.0 (R2015a), The MathWorks Inc., Natick, Massachusetts, 2015.

[90] E. González, P. Maimí, E. Martín-Santos, A. Soto, P. Cruz, F. M. de la Escalera, J. S. de Aja, Simulating drop-weight impact and compression after impact tests on composite laminates using conventional shell finite elements, International Journal of Solids and Structures 144 (2018) 230–247.

[91] P. Maimí, P. P. Camanho, J. Mayugo, C. Dávila, A continuum damage model for composite laminates: Part I–Constitutive model, Mechanics of Materials 39 (10) (2007) 897–908.

[92] P. Maimí, P. P. Camanho, J. Mayugo, C. Dávila, A continuum damage model for composite laminates: Part II–Computational implementation and validation, Mechanics of Materials 39 (10) (2007) 909–919.

[93] Z. P. Bažant, B. H. Oh, Crack band theory for fracture of concrete, Matériaux et construction 16 (3) (1983) 155–177.

[94] A. Soto, E. González, P. Maimí, J. Mayugo, P. Pasquali, P. Camanho, A methodology to simulate low velocity impact and compression after impact in large composite stiffened panels, Composite Structures 204 (2018) 223–238.

[95] J. Llobet, P. Maimí, Y. Essa, F. Martin de la Escalera, A continuum damage

model for composite laminates: Part III - fatigue, Submitted to Mechanics of Materials.

[96] M. Benzeggagh, M. Kenane, Measurement of mixed-mode delamination fracture toughness of unidirectional glass/epoxy composites with mixed-mode bending apparatus, Composites Science and Technology 56 (4) (1996) 439–449.

[97] E. González, P. Maimí, A. Turon, P. Camanho, J. Renart, Simulation of delamination by means of cohesive elements using an explicit finite element code, Computers, Materials & Continua (CMC) 9 (1) (2009) 51.

[98] R. M. Jones, Mechanics of composite materials, CRC Press, 1998.

[99] C. T. Herakovich, Mechanics of fibrous composites, 1998.

[100] R. Cuntze, Classical Laminate Theory (CLT) for laminates composed of unidirectional (UD) laminae, analysis flow chart, and related topics, 2014.

[101] J. M. Whitney, Structural analysis of laminated anisotropic plates, CRC Press, 1987.

[102] P. P. Camanho, S. R. Hallett, Numerical modelling of failure in advanced composite materials, Woodhead Publishing, 2015.

[103] Abaqus, Inc, Abaqus version 6.12 user manual, Simulia, Providence, RI, USA.

[104] W. Tan, B. G. Falzon, L. N. Chiu, M. Price, Predicting low velocity impact damage and compression-after-impact (CAI) behaviour of composite laminates, Composites Part A: Applied Science and Manufacturing 71 (2015) 212–226.

[105] P. P. Camanho, P. Maimí, C. Dávila, Prediction of size effects in notched laminates using continuum damage mechanics, Composites Science and Technology 67 (13) (2007) 2715–2727.

[106] J. Zhang, X. Zhang, An efficient approach for predicting low-velocity impact force and damage in composite laminates, Composite Structures 130 (2015)

85–94.

[107] G. Catalanotti, C. Furtado, T. Scalici, G. Pitarresi, F. Van Der Meer, P. Camanho, The effect of through-thickness compressive stress on mode II interlaminar fracture toughness, Composite Structures 182 (2017) 153–163.

[108] X. Xu, M. R. Wisnom, X. Sun, S. R. Hallett, Experimental determination of through-thickness compression (TTC) enhancement factor for mode II fracture energy, Composites Science and Technology.

[109] A. Quintanas-Corominas, P. Maimí, E. Casoni, A. Turon, J. A. Mayugo, G. Guillamet, M. Vázquez, A 3d transversally isotropic constitutive model for advanced composites implemented in a high performance computing code, European Journal of Mechanics-A/Solids 71 (2018) 278–291.

[110] A. Sasikumar, D. Trias, J. Costa, N. Blanco, J. Orr, P. Linde, Effect of ply thickness and ply level hybridization on compression after impact strength of thin laminates, Composites Part A: Applied Science and Manufacturing 121 (2019) 232–243.

[111] A. Sasikumar, D. Trias, J. Costa, N. Blanco, J. Orr, P. Linde, Impact and compression after impact response in thin laminates of spread-tow woven and non-crimp fabrics, Composite Structures 215 (2019) 432–445.

[112] T. Sebaey, E. González, C. Lopes, N. Blanco, J. Costa, Damage resistance and damage tolerance of dispersed CFRP laminates: Design and optimization, Composite Structures 95 (2013) 569–576.

[113] S. Petit, C. Bouvet, A. Bergerot, J.-J. Barrau, Impact and compression after impact experimental study of a composite laminate with a cork thermal shield, Composites Science and Technology 67 (15-16) (2007) 3286–3299.

[114] M. A. Kouchakzadeh, H. Sekine, Compressive buckling analysis of rectangular composite laminates containing multiple delaminations, Composite Structures 50 (3) (2000) 249–255.

[115] A. T. Rhead, R. Butler, N. Baker, Analysis and compression testing of lami-

nates optimised for damage tolerance, Applied Composite Materials 18 (1) (2011) 85–100.

[116] S.-F. Hwang, S.-M. Huang, Postbuckling behavior of composite laminates with two delaminations under uniaxial compression, Composite Structures 68 (2) (2005) 157–165.

[117] V. Obdržálek, J. Vrbka, On buckling of a plate with multiple delaminations, Engineering mechanics 17 (1) (2010) 37–47.

[118] L. Reis, M. De Freitas, Damage growth analysis of low velocity impacted composite panels, Composite Structures 38 (1-4) (1997) 509–515.

[119] C. Lopes, P. Camanho, Z. Gürdal, P. Maimí, E. González, Low-velocity impact damage on dispersed stacking sequence laminates. Part II: Numerical simulations, Composites Science and Technology 69 (7-8) (2009) 937–947.

[120] A. Sasikumar, J. Costa, D. Trias, E. V. González, S. García-Rodríguez, P. Maimí, Unsymmetrical stacking sequences as a novel approach to tailor damage resistance under out-of-plane impact loading,, Composites Science and Technology 173 (2019) 125–135.

[121] R. M. Jones, C. Bert, Mechanics of composite materials (1975).

[122] R. Olsson, Mass criterion for wave controlled impact response of composite plates, Composites Part A: Applied Science and Manufacturing 31 (8) (2000) 879–887.

[123] R. Olsson, Closed form prediction of peak load and delamination onset under small mass impact, Composite Structures 59 (3) (2003) 341–349.

[124] A. Sasikumar, D. Trias, J. Costa, V. Singery, P. Linde, Mitigating the weak impact response of thin-ply based thin laminates through an unsymmetrical laminate design incorporating intermediate grade plies, Composite Structures 220 (2019) 93–104.

[125] ASTM D6641/D6641M-16, Standard test method for compressive properties of polymer matrix composite materials using a combined loading compression

(CLC) test fixture, 2016.

[126] Starviewer medical imaging software, http://starviewer.udg.edu.

[127] S. García-Rodríguez, J. Costa, P. Maimí, V. Singery, A. Sasikumar, On how matrix cracks induce delamination under out-of-plane shear and the associated in-situ effect, Submitted to Composites Science and Technology.

[128] X. Li, S. R. Hallett, M. R. Wisnom, Predicting the effect of through-thickness compressive stress on delamination using interface elements, Composites Part A: Applied Science and Manufacturing 39 (2) (2008) 218–230.

[129] M. Caminero, I. García-Moreno, G. Rodríguez, Experimental study of the influence of thickness and ply-stacking sequence on the compression after impact strength of carbon fibre reinforced epoxy laminates, Polymer Testing 66 (2018) 360–370.

[130] R. Talreja, N. Phan, Assessment of damage tolerance approaches for composite aircraft with focus on barely visible impact damage, Composite Structures 219 (2019) 1–7.

[131] A. Arteiro, G. Catalanotti, J. Xavier, P. Camanho, Notched response of non-crimp fabric thin-ply laminates, Composites Science and Technology 79 (2013) 97–114.

[132] D. Bull, A. Scott, S. Spearing, I. Sinclair, The influence of toughening-particles in cfrps on low velocity impact damage resistance performance, Composites Part A: Applied Science and Manufacturing 58 (2014) 47–55.

[133] D. W. Wong, H. Zhang, E. Bilotti, T. Peijs, Interlaminar toughening of woven fabric carbon/epoxy composite laminates using hybrid aramid/phenoxy interleaves, Composites Part A: Applied Science and Manufacturing 101 (2017) 151–159.

[134] Z. Aslan, F. Daricik, Effects of multiple delaminations on the compressive, tensile, flexural, and buckling behaviour of E-glass/epoxy composites, Composites Part B: Engineering 100 (2016) 186–196.

[135] M. Aktaş, R. Karakuzu, Y. Arman, Compression-after impact behavior of laminated composite plates subjected to low velocity impact in high temperatures, Composite Structures 89 (1) (2009) 77–82.

[136] D. Ghelli, G. Minak, Low velocity impact and compression after impact tests on thin carbon/epoxy laminates, Composites Part B: Engineering 42 (7) (2011) 2067–2079.

[137] X. Sun, S. Hallett, Failure mechanisms and damage evolution of laminated composites under compression after impact (CAI): Experimental and numerical study, Composites Part A: Applied Science and Manufacturing 104 (2018) 41–59.

[138] Y. Mahadik, S. Hallett, Effect of fabric compaction and yarn waviness on 3D woven composite compressive properties, Composites Part A: Applied Science and Manufacturing 42 (11) (2011) 1592–1600.

[139] S. V. Lomov, Non-crimp fabric composites: manufacturing, properties and applications, Elsevier, 2011.

[140] A. Arteiro, G. Catalanotti, J. Xavier, P. Linde, P. Camanho, Effect of tow thickness on the structural response of aerospace-grade spread-tow fabrics, Composite Structures 179 (2017) 208–223.

[141] A. Arteiro, G. Catalanotti, J. Xavier, P. Camanho, Large damage capability of non-crimp fabric thin-ply laminates, Composites Part A: Applied Science and Manufacturing 63 (2014) 110–122.

[142] H. M. EL-Dessouky, C. A. Lawrence, Ultra-lightweight carbon fibre/thermoplastic composite material using spread tow technology, Composites Part B: Engineering 50 (2013) 91–97.

[143] M. Shamsudin, C. York, Mechanically coupled laminates with balanced plain weave, Composite Structures 107 (2014) 416–428.

[144] P. Curtis, S. M. Bishop, An assessment of the potential of woven carbon fibre-reinforced plastics for high performance applications, Composites 15 (4)

(1984) 259–265.

[145] M. U. Saeed, Z. Chen, Z. Chen, B. Li, Compression behavior of laminated composites subjected to damage induced by low velocity impact and drilling, Composites Part B: Engineering 56 (2014) 815–820.

[146] F. Caputo, A. De Luca, R. Sepe, Numerical study of the structural behaviour of impacted composite laminates subjected to compression load, Composites Part B: Engineering 79 (2015) 456–465.

[147] J. Cugnoni, R. Amacher, S. Kohler, J. Brunner, E. Kramer, C. Dransfeld, W. Smith, K. Scobbie, L. Sorensen, J. Botsis, Towards aerospace grade thin-ply composites: Effect of ply thickness, fibre, matrix and interlayer toughening on strength and damage tolerance, Composites Science and Technology 168 (2018) 467–477.

[148] S. W. Tsai, M. Cognet, The amazing bi-angle thin-ply NCF, JEC composites (68) (2011) 51–52.

[149] S.-F. Hwang, G.-H. Liu, Buckling behavior of composite laminates with multiple delaminations under uniaxial compression, Composite structures 53 (2) (2001) 235–243.

[150] A. Sasikumar, D. Trias, J. Costa, J. Orr, P. Linde, Effect of ply thickness and ply level hybridization on compression after impact strength of thin laminates, Composites Part A: Applied Science and Manufacturing 121 (2019) 232–243.

[151] A. Sasikumar, D. Trias, J. Costa, N. Blanco, J. Orr, P. Linde, Impact and compression after impact response of thin laminates of spread-tow woven and non-crimp fabrics, Composite Structures 215 (2019) 432–445.

[152] A. Sasikumar, Improving compression after impact response of composite laminates through ply level hybridization with thin plies and unsymmetrical designs, PhD thesis, University of Girona; 2019.

[153] L. Mencattelli, S. T. Pinho, Realising bio-inspired impact damage-tolerant thin-ply CFRP bouligand structures via promoting diffused sub-critical helicoidal

damage, Composites Science and Technology (2019) 107684.

[154] C. Lopes, O. Seresta, Y. Coquet, Z. Gürdal, P. Camanho, B. Thuis, Low-velocity impact damage on dispersed stacking sequence laminates. part I: Experiments, Composites Science and Technology 69 (7-8) (2009) 926–936.

[155] A. Sasikumar, D. Trias, J. Costa, V. Singery, P. Linde, Mitigating the weak impact response of thin-ply based thin laminates through an unsymmetrical laminate design incorporating intermediate grade plies,, Composite Structures 220 (2019) 93–104.

[156] C. G. Davila, P. P. Camanho, C. A. Rose, Failure criteria for frp laminates, Journal of Composite Materials 39 (4) (2005) 323–345.

[157] S. García-Rodríguez, J. Costa, V. Singery, I. Boada, J. Mayugo, A 3D tomographic investigation to elucidate the low-velocity impact resistance and tolerance of thin non-crimp fabric laminates: effect of ply-thickness, Composites Part A: Applied Science and Manufacturing 113 (2018) 53–65.

[158] A. Sasikumar, S. García-Rodríguez, J. Arbeláez, D. Trias, J. Costa, On how unsymmetrical laminate designs with tailored ply clusters affect compression after impact strength compared to symmetric baseline, Composite Structures 238 (2020) 111958.

[159] R. Olsson, Analytical prediction of damage due to large mass impact on thin ply composites, Composites Part A: Applied Science and Manufacturing 72 (2015) 184–191.

[160] W. Cui, M. R. Wisnom, M. Jones, Effect of through thickness tensile and compressive stresses on delamination propagation fracture energy, Journal of Composites, Technology and Research 16 (4) (1994) 329–335.

[161] S. García-Rodríguez, J. Costa, K. Rankin, R. Boardman, V. Singery, J. Mayugo, Interleaving light veils to minimise the trade-off between mode-i interlaminar fracture toughness and in-plane properties, Submitted to Composites Part A: Applied Science and Manufacturing.

[162] H. Brian, G. Luther, Viewing Composite Specimens Using Reflected Light Microscopy, 2004.

Appendix. Published papers

A

A.1 Paper A

Unsymmetrical stacking sequences as a novel approach to tailor damage resistance under out-of-plane loading

A. Sasikumar[a,*], J. Costa[a,*], D. Trias[a,1], E. V. González[a], S. M. García-Rodríguez[a], P. Maimí[a]

[a]AMADE, Polytechnic School, Universitat de Girona, Campus Montilivi s/n, E-17003 Girona, Spain

[*] Corresponding author

[1] Serra Hunter Fellow

The paper has been published in *Composites Science and Technology* Vol. 173 (2019) 125–135.

Composites Science and Technology 173 (2019) 125–135

Contents lists available at ScienceDirect

Composites Science and Technology

journal homepage: www.elsevier.com/locate/compscitech

Unsymmetrical stacking sequences as a novel approach to tailor damage resistance under out-of-plane impact loading

A. Sasikumar*, J. Costa**, D. Trias[1], E.V. González, S.M. García-Rodríguez, P. Maimí

AMADE, Polytechnic School, Universitat de Girona, Campus Montilivi s/n, 17073 Girona, Spain

ARTICLE INFO

Keywords:
B. Impact behaviour
B. Delamination
C. Damage mechanics
C. Finite element analysis (FEA)
Unsymmetrical laminates

ABSTRACT

In current composite design, stacking sequence symmetry around the laminate mid-plane is an unarguable constraint to avoid warpage during manufacturing. However, several load cases induce unevenly distributed stresses through the laminate thickness, such that symmetric laminates may not be the optimal solution. In this paper, we explore the damage resistance to out-of-plane low velocity impact loading of an unsymmetrical laminate with zero extension-bending coupling matrix ([B]), thereby assuring no undesired coupling deformations during mechanical or thermal loads. Using impact and quasi-static indentation tests, C-scan inspection and numerical modelling, we compare the damage pattern between an unsymmetrical laminate with ply clustering at the impacted face and a laminate with ply clustering at the non-impacted face (produced by flipping the former laminate upside down). The laminate with clusters at the impacted side exhibits better damage resistance for lower impact energies. More importantly, the location of the damage events obeys the predictions assumed when the laminate was designed, demonstrating the room for improvement by tailoring unsymmetrical laminates to particular load cases.

1. Introduction

Impact loading and the threat it poses to composite structures is a matter of concern for aircraft engineers and researchers. The severity of the impact induced damage and its propagation during in-flight loads is the key research question to be answered as impact damage can reduce the residual strength of a structure by up to 60% [1]. In an effort to improve damage resistance, researchers have gone one step further in laminate design and have proposed non-conventional laminates using dispersed angles [2–4], varying mismatch angle at interfaces [4,5] or selective ply clustering [6]. Despite the novelty in laminate designing, symmetry around the mid plane of the laminate remains an unquestioned constraint, mainly to avoid warpage during manufacturing and coupling responses under loading [7].

Impact loading is a complex loading case because of the interaction of different damage mechanisms, mainly in terms of matrix cracks and delamination, followed by fibre failure at higher impact energies. The damage scenario is unsymmetrical in the through-the-thickness direction [8,9]: high contact compressive stresses cause matrix cracks by shear at the vicinity of the impactor (impacted face of the laminate), whereas tensile stresses cause transverse matrix cracking at the non-impacted face of the laminate. These cracks grow into the interfaces and initiate delamination oriented in the direction of the lower plies [8]. Acknowledging that the impacted and non-impacted laminate sides experience different damage mechanisms during impact, the constraint of laminate symmetry needs to be challenged.

Recently, quasi-static indentation (QSI) tests are considered as an alternative to the low velocity impact tests, due to the similarity in the loading responses and the damage characteristics [10–12]. In LVI loading, the impact contact time is long enough to allow the impact waves to get reflected multiple times from the specimen boundaries and hence the resulting impact response is considered purely static loading [13–15].

In this paper, we propose an unsymmetrical laminate with ply clustering at the impacted face of the laminate. As reported in Ref. [13], a clustered ply block induces high interlaminar shear stresses thereby triggering delamination at the corresponding ply interface. Here we attempt to use localized ply clusters in the laminate to foster delamination at pre-determined regions. Thanks to the unsymmetrical design, the same laminate, when flipped upside down, produces another stacking sequence with ply clustering at the non-impacted face. Low velocity impact (LVI) and quasi-static indentation responses of these

* Corresponding author.
** Corresponding author.
E-mail addresses: aravind.sasikumar@udg.edu (A. Sasikumar), josep.costa@udg.edu (J. Costa).
[1] Serra Hunter Fellow.

https://doi.org/10.1016/j.compscitech.2019.02.002
Received 17 July 2018; Received in revised form 1 February 2019; Accepted 2 February 2019
Available online 11 February 2019
0266-3538/

two unsymmetrical laminates are studied in order to shed light on how the initiation and propagation of the delaminations differ when imposed at different locations. Further, numerical results from an in-house finite element model featuring inter and intralaminar damage are compared with the experimental results, followed by an in-depth energy dissipation analysis for each ply and interface of both laminates. To the authors' knowledge, this is the first report on an experimental impact study on an unsymmetrical laminate.

2. Unsymmetrical laminate design

The unsymmetrical laminate was obtained by means of an optimization algorithm (genetic algorithm embedded in the MATLAB optimization toolbox [16]). The objective function was a minimum summation of the terms of the B matrix, with the intention of finding solutions with a null B matrix. A null B matrix assures that there is no extension-bending coupling response [17,18] and as a result there will be no undesired deformation couplings such as warpage during manufacturing.

In addition to the objective function, the following constraints were also imposed: i) the laminate had to be in-plane quasi-isotropic and balanced with 24 plies; ii) as ply clustering induces delamination at the interfaces of the blocked plies [13,19], four clusters (one cluster for each orientation, 0°, ±45° and 90°) were imposed at the impacted side of the unsymmetrical laminate to trigger delamination at these locations; it was also made sure that not more than three plies of the same orientation were stacked together; iii) the surface ply was fixed to be either 45° or − 45° in order to tackle the shear loads [2]; and iv) a constant mismatch angle of 45° was used at the interfaces, thereby avoiding the effect of varied mismatch angled interfaces [4,5].

The solution, with a zero B matrix was: $[-45_2/90_2/45_2/0_3/45/90/-45/0/45/90/-45/0/45/90/-45/0/45/90/-45]$.

3. Methodology

3.1. Experimental

The unsymmetrical panel was manufactured using Hexcel® IM7/8552 uni-directional prepreg tapes and was cured in an autoclave. Despite being unsymmetrical, the panel had zero warpage after curing; as expected from the design study of the stacking sequence.

Impact specimens of standard 150 × 100 mm dimensions were cut out of the panel with 0° plies aligned in the longer direction. The 24-ply laminate had a cured thickness of 4.36 mm and a ply thickness of 0.182 mm. The specimens cut out were flipped upside down in order to obtain specimens with the same ply clustering at the non-impacted side. The laminate with ply clustering at the impacted side is hereafter called LPCI, and the laminate with ply clustering at the non-impacted side as LPCN (Fig. 1). It is to be noted that flipping a laminate upside down only interchanges the − 45° plies with 45° plies, thus both laminates have the same in-plane stiffness in all directions and the same bending stiffnesses in the 0° and 90° directions.

As in Refs. [13,20], impact tests were performed on 150 × 100 mm specimens in accordance with the ASTM D7136/D7136M-15 standards [21] using a CEAST Fractovis Plus instrumented drop-weight tower. The impactor featured a 16 mm in diameter hemispherical tip and the impactor mass was adjusted to 5 kg for the entire study. As the study aims to analyse the low velocity impact response (energy levels that create lesser damage than the barely visible impact damage (BVID) threshold) of the laminates, two LVI energies, 12 J and 18 J, were explored.

QSI tests were performed using an MTS INSIGHT® 50 testing machine with a 50 kN load cell, replicating the same boundary conditions as the impact test. Specimens were placed on a base support with an open window of 125 × 75 mm and clamped at the edges using four rubber pads. Displacement controlled indentation was performed on the specimens at a rate of 1 mm/min using the same indenter configuration as for impact loading. Further details of the test setup are provided in Ref. [22].

QSI loading was interrupted for C-scan damage inspection followed by further indentation to the next indenter displacement level, thereby the same specimen was subjected to more than one indentation. A total of 8 indenter displacements (from d = 1.17 mm–5.4 mm) were investigated, thus obtaining the complete damage evolution starting from the initiation of matrix cracks to complete delamination propagation. The indenter displacements were defined on the go: the indentation was stopped when a load drop or a change in stiffness of the force-displacement response, or an acoustic emission, was noticed.

Pulse-echo mode ultrasonic C-scan inspection was performed on all the QSI specimens after each displacement level and on all the impacted specimens using an OLYMPUS OMNI MX system employing a 5 MHz piezoelectric probe. As C-scan inspection has the drawback of larger delaminations masking the underlying ones, C-scan was performed from both sides of the specimens, and the results presented are the inspections providing the most information.

3.2. Numerical modelling

User-defined constitutive models from Maimí et al. [23,24] were used to simulate the onset and propagation of intralaminar damage. Apart from the main highlights such as crack closure effects, incorporating in-situ effects [25,26], and the inclusion of crack band model formulation, the complete description can be found in Ref. [27]. The model was implemented as an Abaqus/Explicit VUMAT user-written sub-routine. The interlaminar damage was modelled using the ABAQUS Explicit in-built surface based cohesive behaviour [28], where a contact based interaction is used to model the traction between the contact surfaces to simulate delamination. The delamination initiation is governed by a quadratic stress-based criterion implemented in ABAQUS, whereas delamination evolution is characterised by the mixed mode energy-based propagation criteria proposed by Benzeggagh and Kenane [29]. Formulations of the initiation and propagation criteria are not detailed here but can be found in the work of Tan et al. [30].

This study follows a novel FE modelling approach from González et al. [27]. Interested readers are referred to their work for a more detailed description. Each ply is modelled using a conventional shell element which is sandwiched by surface elements on the top and bottom faces of the ply. The surface elements are tied to the shell elements with rigid tie connectors, thereby transferring the kinematics from the shells to the surface elements. Delamination between two plies is modelled by assigning cohesive surface-based interaction between the bottom face of the surface elements of the top ply and the top face of the surface elements of the bottom ply, as seen in Fig. 2 for an illustrative two plies model.

Clustered plies were modelled as a single shell element layer, leading to a model consisting of 19 layers. S4R conventional shell elements were used for the plies and SFM3D4R for the surface elements. The mesh was finer under the impactor (a refined window of 75 by 75 mm, referenced from the impact centre, with element size, $l = 0.5$ mm) than elsewhere ($l = 4$ mm). Moreover, the in-situ effect is accounted for by considering the ply thickness and the ply type (outer and embedded). To avoid excessive element distortion, an element was deleted when the fibre damage variable (d_1) reached 1, whereas the transverse (d_2) and shear damage (d_6) variables were assigned a maximum value of 0.99, and no element deletion was considered. A friction coefficient of $\mu = 0.3$ was assumed at the ply interfaces, as this property is not experimentally available. Further details about modelling (impactor, rubber clamps, base plate), contact algorithms, cohesive law shapes are explained in detail in Refs. [27,31,32]. The material data for IM7/8552 was obtained from Ref. [33].

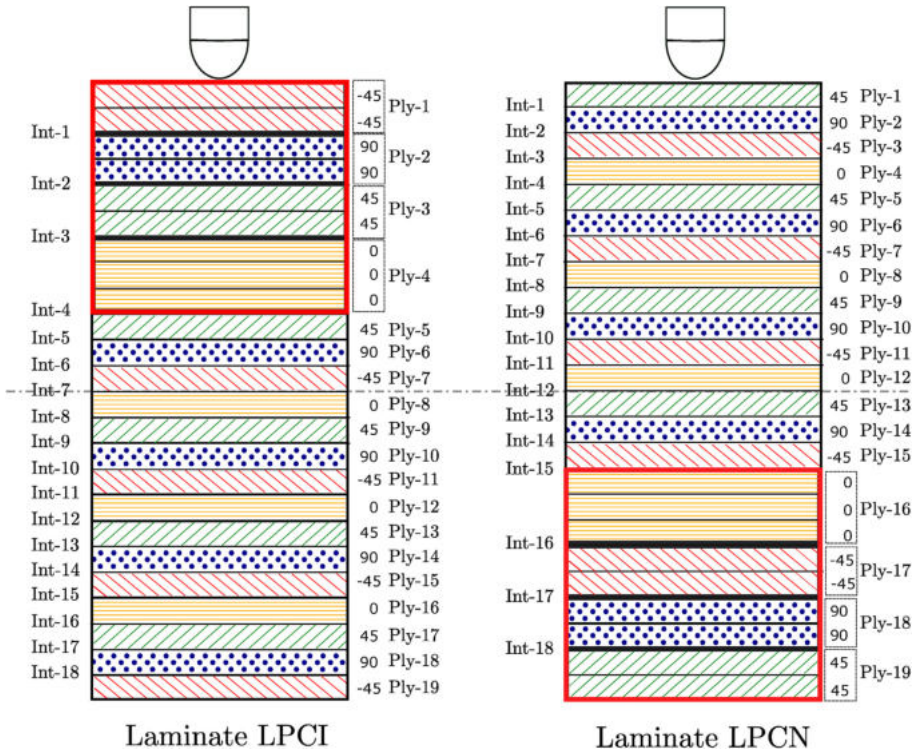

Fig. 1. Unsymmetrical laminate LPCI with ply clustering at the impacted side (left) and laminate LPCN with ply clustering at the non-impacted side (right), which is produced by flipping the laminate LPCI upside down. Flipping upside down only interchanges the 45s by − 45s plies, i.e., it does not alter the in-plane and bending stiffness in the 0° and 90° directions.

4. Results

4.1. Experimental

The delamination threshold load, F_d, marked by the first clear load drop in the impact curves at 12 J and 18 J (Fig. 3), is 30% higher for LPCI than LPCN, thereby LPCI clearly delays delamination onset compared to LPCN. After the delamination threshold load, a comparatively unstable response associated with intermittent load drops is seen with LPCI over LPCN. Maximum peak load, F_{max}, is approximately the same for both laminates at 12 J, whereas an increase of 12% is observed for LPCN over LPCI at 18 J. The energy dissipation of LPCI is 9% and 22% larger than LPCN for 12 J and 18 J, respectively. A compact quantitative overview of the various damage resistance parameters for

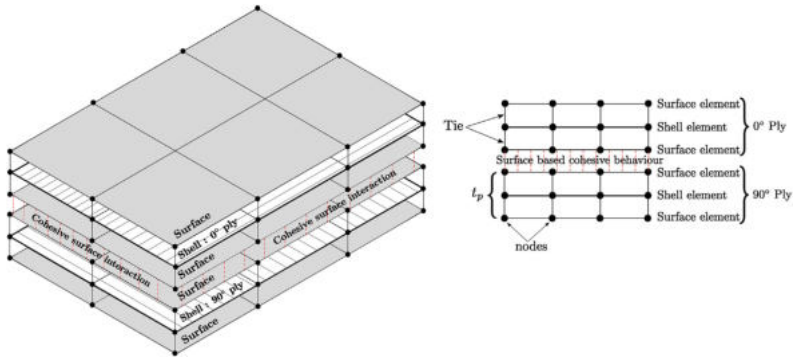

Fig. 2. Schematic representation of the modelling strategy, where each ply is modelled using a shell element sandwiched between two surface elements using a tie interaction. Surface based cohesive interaction is assigned between the bottom surface of the top ply and the top surface of the bottom ply. t_p marks the thickness of the modelled ply, and there is no thickness defined between the surface elements.

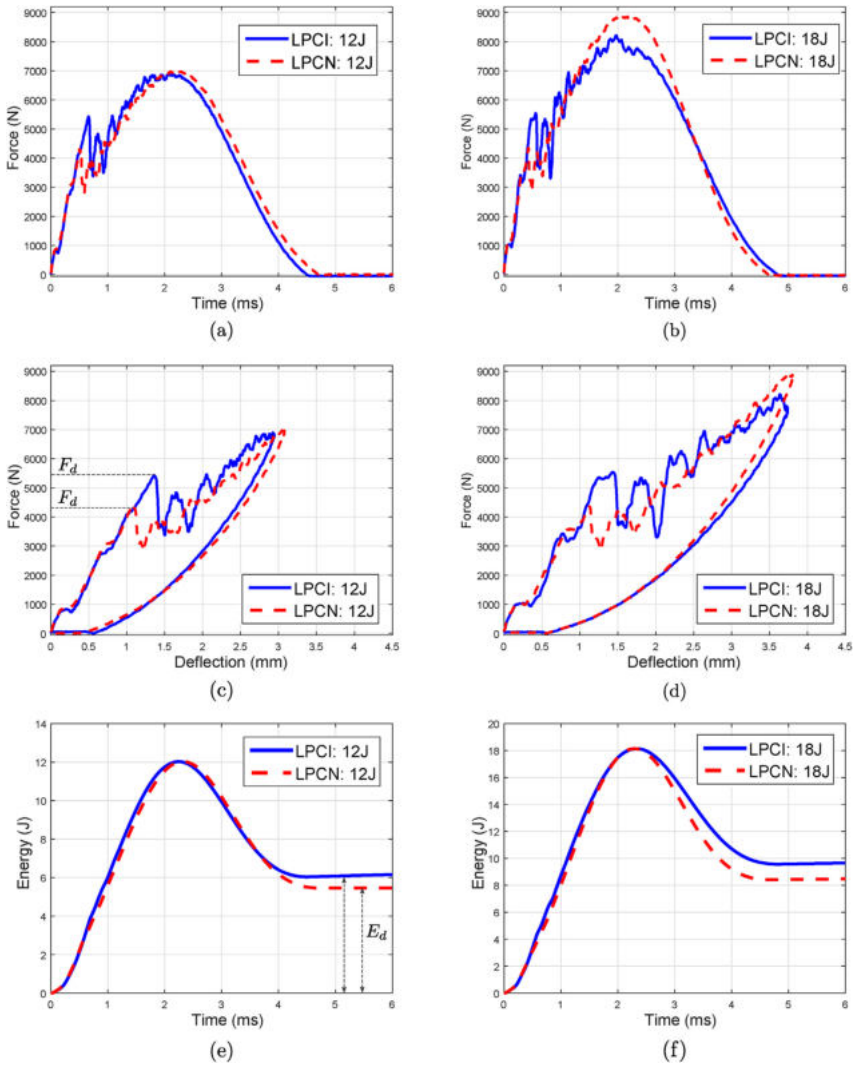

Fig. 3. Force-time ((a),(b)), force-deflection ((c),(d)), and energy-time ((e),(f)) response curves for LPCI and LPCN for 12 J and 18 J impact energies.

both laminates and both impact energies is presented using a radar plot in Fig. 4.

Fig. 5 identifies the delaminated interfaces as well as the dominant delaminations for both laminates. Dominant delaminations are those which govern the total delamination profile, thereby playing a major role in the damage tolerance of the structure [22,34]. For LPCN, they appeared at all the interfaces within the clustered block (interfaces 15, 16, 17 and 18) and scaled up when moving from 12 J to 18 J. For LPCI, an unsymmetric delamination profile is observed for 12 J, with the dominant delaminations at interfaces within the clustered block at the impacted side (int. 3, 4) as well as just below the clustered block (int. 5, 6, 7). Moving on to the 18 J impact, a rapid growth in the projected delamination size is observed where the dominant delaminations are found outside the cluster block (int. 5, 6, 7), with the 90° oriented delamination (int. 5) almost reaching the impact window boundaries. When both laminates were compared, LPCI displayed a 20% reduced projected delamination area over LPCN for 12 J, whereas at 18 J it was 50% larger.

Unlike the impact tests, QSI tests interrupted for damage inspection provide information about the whole damage process. Fig. 6 shows the load displacement response of a pristine specimen up to the highest indenter displacement (d = 5.4 mm) as well as the other indenter displacements (d_i), and the associated applied energies (E_a). The early delamination initiation of LPCN found in the impact test, is observed in the QSI results as well. After the delamination drop, the load deflection response for both LPCN and LPCI from indenter displacement d_3 to d_5 is similar. Beyond this, d_7 to d_8, LPCI shows a relative reduction in the stiffness followed by an increase.

Fig. 7 (a) details the complete QSI delamination sequence obtained for both laminates using interrupted C-scan inspections, thus helping to

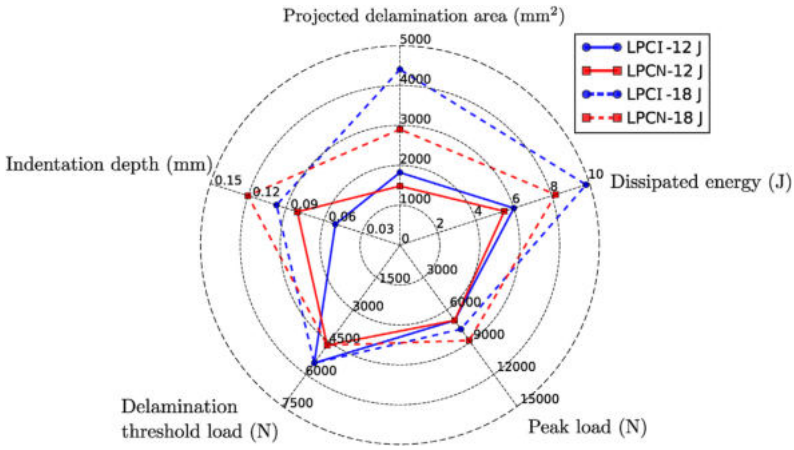

Fig. 4. Quantitative overview of impact damage resistance parameters of LPCI and LPCN at both impact energies.

relate each load drop or stiffness change (Fig. 6) to the corresponding delamination or its propagation. C-scan images of displacement d_1 (just after the first load drop of LPCN and before the load drop of LPCI) evidence the presence of delamination (initiated in the clustered block at the non-impacted side) in LPCN and yet there is no delamination initiation in LPCI. The first load drop is related to a simultaneous occurrence of matrix cracks and delamination initiation [9,14]. Displacement d_2 (immediately after the load drop of LPCI) shows delamination initiation in the clustered block at the impacted side of LPCI and delamination extension at the interfaces of the non-impacted side for LPCN.

Through displacements d_3 to d_5, already formed delaminations propagate in both laminates. The LPCI laminate exhibits dominant delamination mainly at the impacted side, whereas in LPCN delaminations at the interfaces of the non-impacted side dominate. The change in stiffness for LPCI (displacement d_6 in Fig. 6) corresponds to a rapid

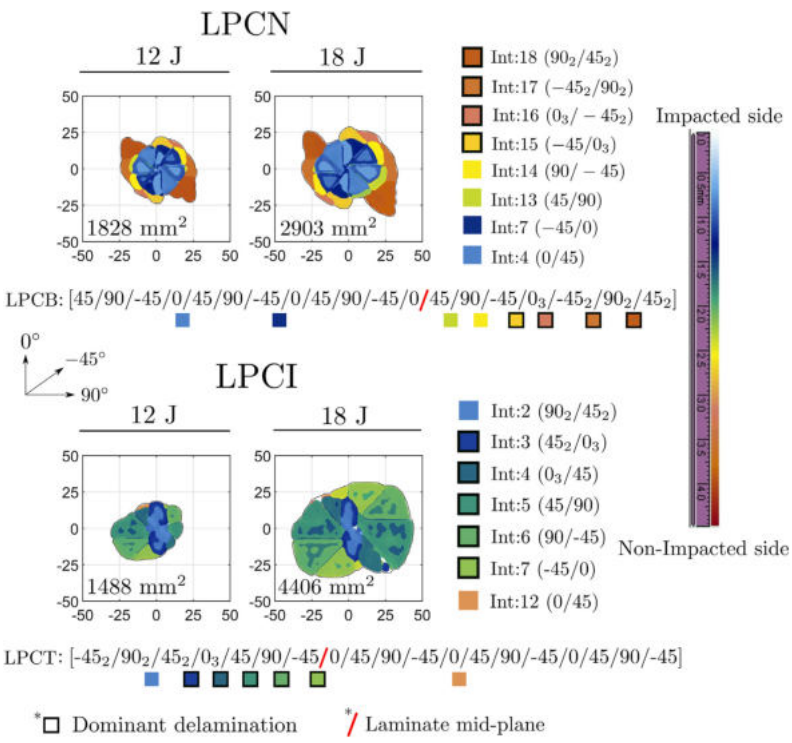

Fig. 5. C-scan images of LPCN and LPCI inspected from the impacted face for 12 J and 18 J impact energies. Projected delamination area, identified delaminated interfaces and dominant delaminations are marked (The colour bar helps to identify the location of delamination in the thickness direction, and the axes are provided in millimetres). (For interpretation of the references to colour in this figure legend, the reader is referred to the Web version of this article.)

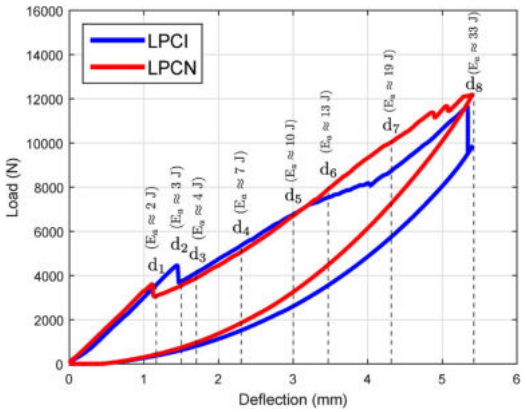

Fig. 6. Load-deflection curve for the maximum indenter displacement d_8 = 5.4 mm for LPCN and LPCI, also showing the various other indenter displacements used in the study (The respective energy applied, E_a, is also marked for each indenter displacement).

and unsymmetric growth of delaminations for LPCI within the interfaces 5, 6, 7 at the impacted side). At displacement d_7 (associated with the stiffness increase with LPCI), LPCI has its dominant delamination at interface 5 (oriented in 90˚) develop into the supported region of the clamping (as seen with 18 J impact results), leading to stress redistribution and thereby an increase in stiffness, while LPCN showed further delamination extension. Ultimately, the last displacement resulted in further scaling up of delamination with LPCN, and delamination growing to the specimen edges for LPCI.

Fig. 7(b) depicts a quantitative evolution of the damage resistance parameters for all the indenter displacements. LPCI was seen to be more damage resistant than LPCN, in terms of projected damage area and dent depth, until the displacement of d_6, at which an overturn in the trend is noted. Comparing the impact results of 12 J with the QSI results for the same applied energy (corresponding to d_5), a good correlation is observed with the maximum peak force and the projected delamination area. Moving to 18 J, the QSI results (corresponding to d_7) slightly over-predict the above two parameters compared to the impact results (by 8% and 15%, respectively).

4.2. Numerical

The numerical predictions of the impact response curves, namely the force-deflection and energy evolution curves (Fig. 8), are in excellent agreement with the experimental results, especially with the energy evolution for both laminates at both impact energies. Fig. 8 also depicts the impactor displacements chosen for the numerical analysis of the energy dissipated through intralaminar and interlaminar damage: marked by circles (A to E) for the force response and by dashed lines for the energy-time curves. This figure also distinguishes the energy dissipated through inter and intralaminar damage.

Moving away from the normal convention of comparing only the projected delamination contour or the area, we present a 'virtual C-scan', where along with the delamination profile and area, each delaminated interface is identified and presented as in a C-scan. Fig. 9 shows the good agreement between the virtual and experimental C-scan, highlighting the potential of the numerical tools used. With LPCN laminates, the dominating delaminations and their extension is almost replicated in the prediction, although the projected damage area is slightly under-predicted by an average of 8%. For LPCI, dominant

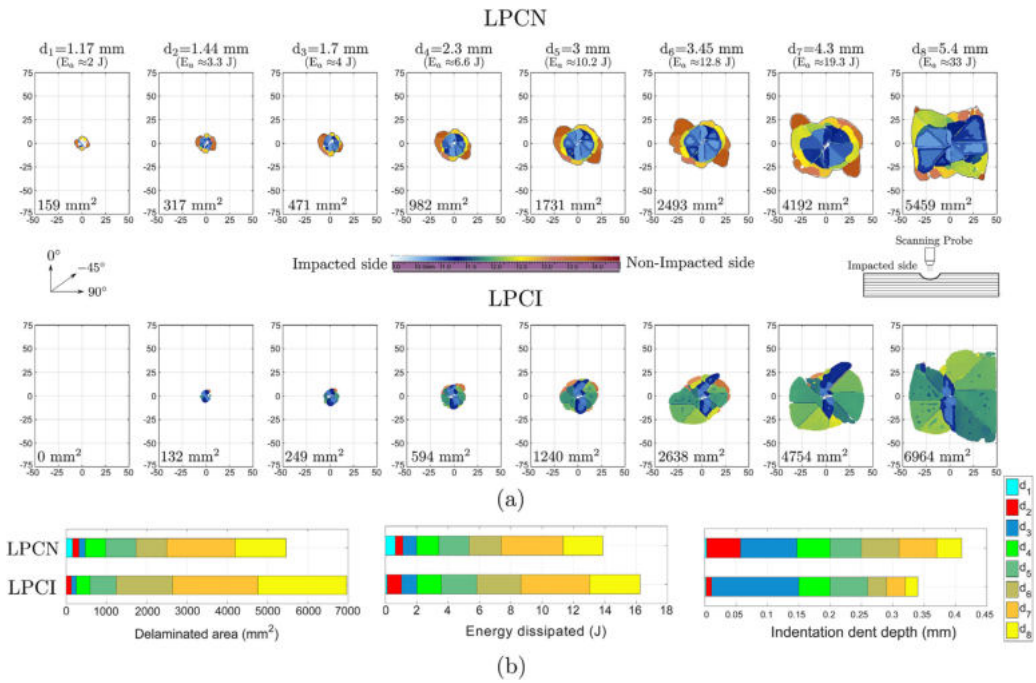

Fig. 7. (a) Impacted face C-scan images revealing the delamination initiation and propagation for various indenter displacements (b) Quantitative evolution of damage resistance parameters for all indenter displacements for LPCN and LPCI.

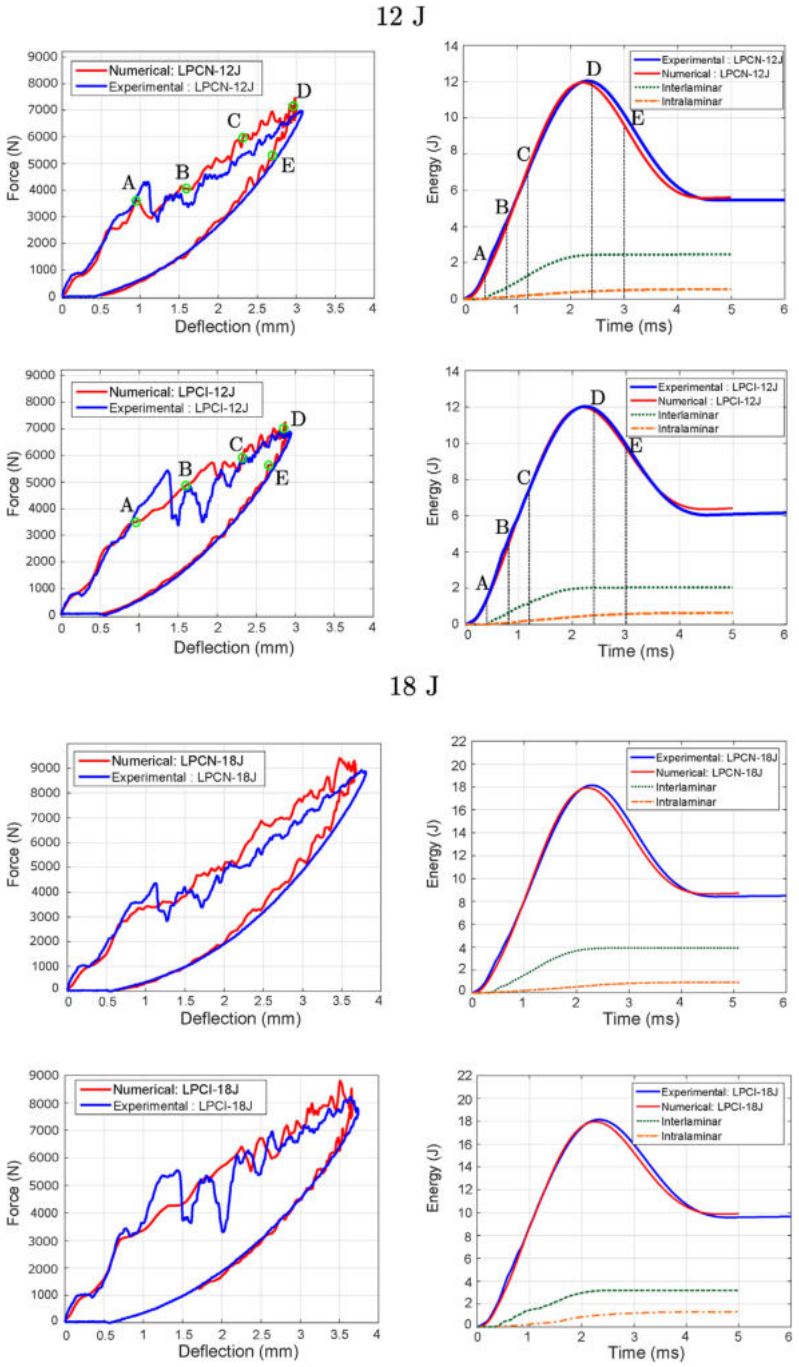

Fig. 8. Numerical prediction of the impact response of LPCN and LPCI laminates compared with the experimental data for both 12 J and 18 J. Selected displacements (A to E) for energy dissipation study (in Fig. 10) are also marked for the 12 J energy case.

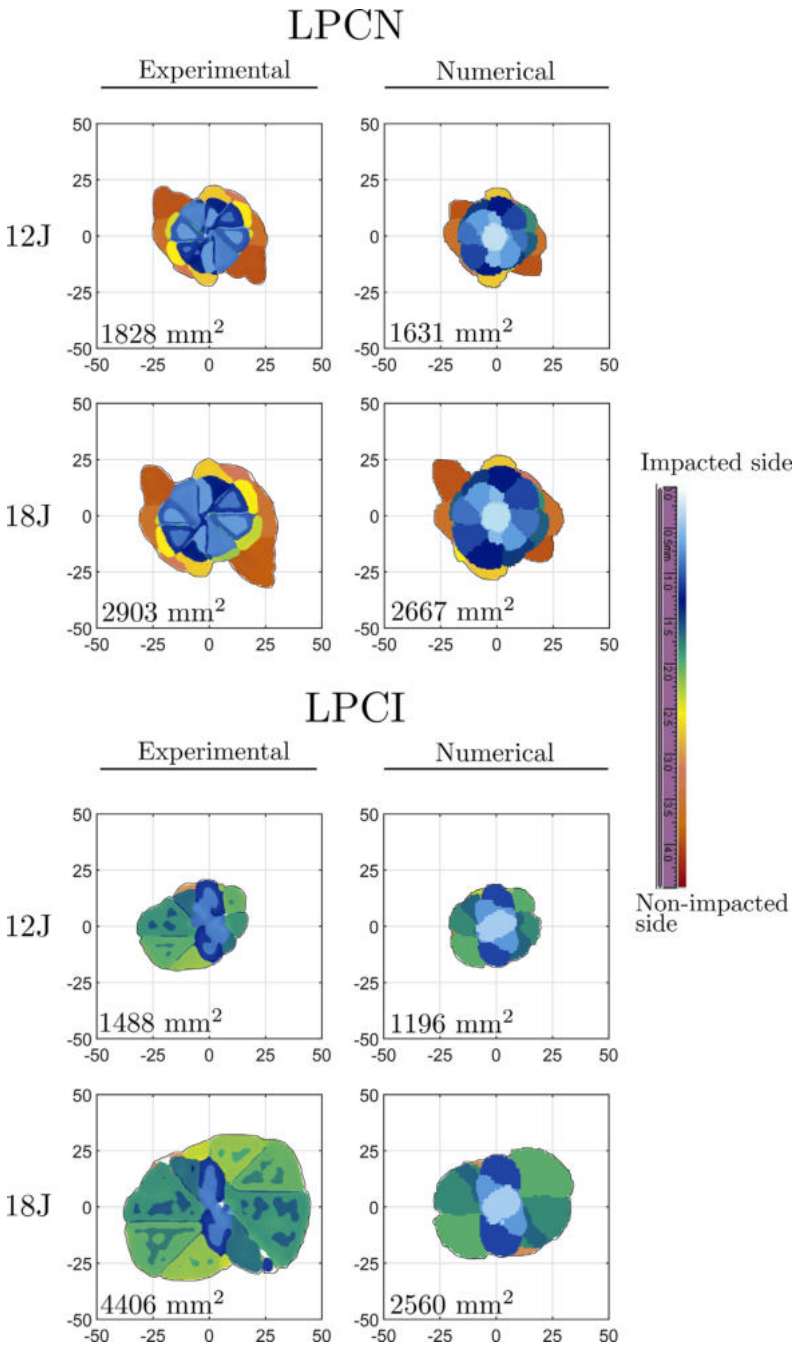

Fig. 9. Comparison of the virtual C-scan from numerical study with the C-scan after impact testing for LPCN and LPCI for both 12 J and 18 J. Projected delamination area is provided in the bottom left corner of each box.

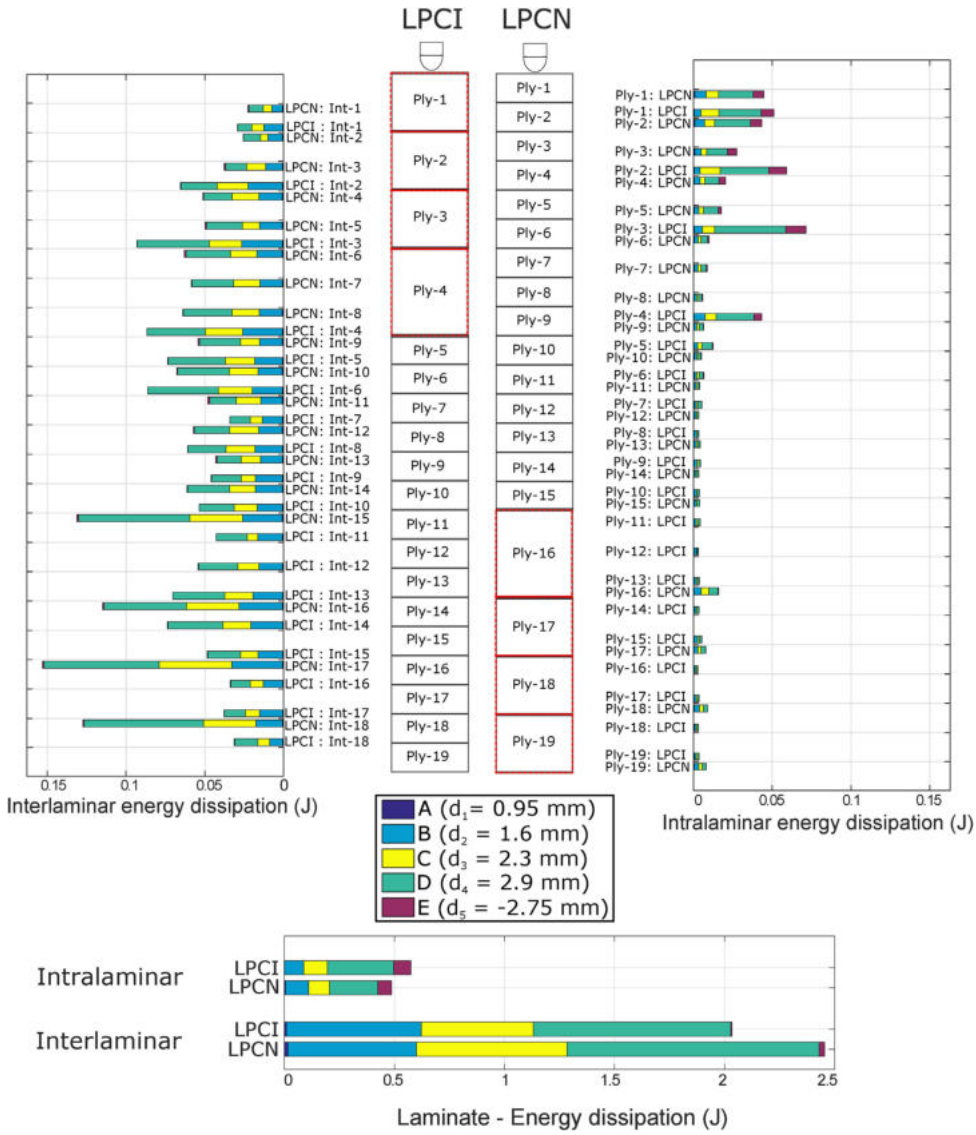

Fig. 10. Illustration of the laminates and their plies along with the amount of inter and intralaminar energy dissipated for each ply and interface of both the laminates. Note that the clustered plies are considered as a single ply and hence, for example, interface 1 of LPCI is compared with the interface 2 of LPCN. The different colour codes represent the energy dissipated with the different displacement steps (A to E, as shown in Fig. 8). The total dissipated energies (inter- and intralaminar) by the laminates are also compared at the bottom. (For interpretation of the references to colour in this figure legend, the reader is referred to the Web version of this article.)

delaminated interfaces are correctly predicted, while the unsymmetric delamination extension for 12 J and the rapid growth of the close-to-mid-plane delaminations for 18 J are not, thus the projected damage area is underpredicted.

Fig. 10 illustrates the two laminates along with the amount of energy dissipated for each ply and each interface for both laminates. The figure quantitatively compares the inter- (delamination) and intra- (matrix cracks and fibre failure) laminar energy dissipated for all the plies and interfaces between LPCN and LPCI for 12 J. Note that the different colour codes in the figure represent the energy dissipated within the different displacement steps (A to E, as shown in Fig. 8) considered in the study. The figure also compares (at the bottom) the total energy dissipated (inter- and intralaminar) by the two laminates within the selected displacement steps.

With LPCN, as demonstrated by the experiment, the last four interfaces (15, 16, 17 and 18) dissipate the larger amount of energy through delaminations, whereas with LPCI the interfaces 3, 4 (within the cluster), 5, 6, and 14 dominate. The total energy dissipated by the

dominant delaminations of LPCN over its other delaminated interfaces is much higher (int. 15, 16, 17 and 18 account for 30% of the total interlaminar energy dissipated) than for LPCI. In the case of intralaminar damage, the first four plies of both laminates dissipated most of the energy, with LPCI being comparatively higher than LPCN, due to the clustered plies.

Displacement level A (chosen to be before the load drop for LPCN and before the stiffness change for LPCI in the numerical curve, as in Fig. 8) reveals no delamination for both laminates. Most of the delamination energy dissipation is observed at the final loading part, between the points C and D. The same occurs with the intralaminar damage, with local fibre failure being seen at the top two plies in the vicinity of the impactor. Fig. 10 compares the energy dissipation at the laminate level: the average energy dissipated through delaminations is approximately five times higher than that of the intralaminar damage, signifying the dominance of energy dissipation through delamination within the energy levels explored. Comparing LPCI and LPCN for 12 J, LPCI dissipates 18% more energy through intralaminar damage, and 17% less through interlaminar damage.

5. Discussion

The experimental results revealed the different damage onset and evolution of the two laminates analysed. Delamination initiates earlier in the laminate with clustered plies at the non-impacted side (LPCN), which is related to the transverse cracks in the plies (at non-impacted side) induced by in-plane tensile loads from laminate bending. These cracks grow into the next available interface to initiate delamination. Clustered plies introduce high bending stiffness mismatch [19], leading to high interlaminar shear stresses at the adjacent interfaces. This triggers delamination and makes clustered plies a weak zone for delamination onset. Additionally, the reduced in-situ effect of the clustered plies favours transverse cracking when compared to the non-clustered plies [33]. When the transverse crack reaches the adjacent interface, the large energy release rate available acts as a catalyst for delamination. Substantial difference in damage mechanisms was observed when the clustered plies are on the impacted side (LPCI). Impact loading introduces high local out-of-plane compressive stresses at the vicinity of the impactor, which counteract the interlaminar shear stresses and lead to increased interlaminar friction [35]. This can be indirectly ascribed to the increase in mode II fracture toughness at regions close to the impactor, as reported in Refs. [36,37]. This constrains the delamination propagation, as observed in the first two interfaces within the clustered block of LPCI (see Fig. 5).

We also observed that the position of the larger delaminations varies from one laminate to the other. The idea of imposing delaminations at the non-impacted side in LPCN by tailoring clustered plies has paid off, with the dominant delaminations appearing at the interfaces within the clustered block (int. 15, 16, 17 and 18 in Fig. 5). In the case of LPCI, with the suppressed delaminations at the interfaces of the impacted side, the dominant delaminations were seen outside the cluster, due to the high interlaminar shear stresses at the laminate mid-plane. These high stresses trigger transverse shear cracks in the 45° and −45° plies (associated with the interfaces 5, 6 and 7 in Fig. 5) promoting delamination oriented in the 90° ply (which is placed in between the 45° and −45° plies as in Fig. 1). Finally, in terms of impact resistance, LPCI performed better at 12 J impact and earlier stages of indenter displacements (up to d_6). At higher energy levels, the rapid growth of close to mid-plane delaminations induced more damage than in LPCN.

The numerical study identified the local fibre failure caused by the impactor as the prime reason for the high intralaminar energy dissipation at the top plies (at impacted side) for both laminates. Owing to the cluster effect, LPCI showed higher values of intralaminar energy dissipation over LPCN for the top plies. While the same clustered plies of LPCN dissipated most of the energy through interlaminar damage, LPCI clustered plies dissipated it through intralaminar damage. This difference in behaviour signifies how the location in the laminate varies the damage mode and its evolution. The lack of accuracy of the numerical prediction of LPCI (as in Figs. 8 and 9), may be attributed to the inability of shell elements to capture the shear matrix cracks from the out-of-plane shear stresses close to the impactor. This could be tackled by incorporating a full three dimensional constitutive behaviour with solid elements [38] followed by an oriented mesh strategy (as demonstrated in Ref. [39]), but at the price of a higher computational time.

What is clear from the study, is that damage can be forced to occur at predetermined locations through judicious laminate designing, and thereby tailor the damage resistance. Unsymmetrical stacking designs can facilitate this task and raise the prospect of an improved impact damage resistance. Current numerical tools provide a detailed physical representation of the damage mechanisms, so they can efficiently support this innovative design task. A continuation of this work will be to compare unsymmetrical laminates with symmetric quasi-isotropic laminates in terms of impact damage resistance and tolerance (Compression After Impact) to better assess the prospects of unsymmetrical laminates.

6. Conclusion

For the first time, unsymmetrical stacking sequences have been explored in an experimental low velocity impact framework. We designed an unsymmetrical laminate (with zero extension-bending coupling, and therefore warp-free) with tailored ply clustering at the impacted side, and flipped it upside down to yield a laminate with ply clustering at the non-impacted side. Both these laminates were tested under low velocity impact and quasi-static indentation loading to study their out-of-plane damage resistance. The experimental and numerical results revealed that clustering at the impacted side delayed the threshold load for delamination by 30% and reduced the projected delamination area by 20% for low impact energies. This improvement derived from a higher energy dissipation through intralaminar damage instead of delamination, the most important damage mechanism for the laminate with clusters at the non-impacted side. Damage patterns from both laminates were compared and, importantly, the dominant delaminations were observed at the locations predicted during the laminate design. This paper highlights the opportunity to move away from conventional symmetrical laminate design, thereby giving laminate designers the freedom to tailor the stacking sequence according to the expected stress states of given load cases.

Acknowledgements

The first author would like to thank the Generalitat de Catalunya for the FI-DGR pre-doctoral grant (2017 FI-B1 00089). The authors would like to thank the Spanish Ministerio de Economía y Competitividad for the grant coded MAT2015-69491-C3-1-R and supported by FEDER/EU. The authors would also like to thank Airborne Composites SL, Girona, for manufacturing the specimens used in the study.

Appendix A. Supplementary data

Supplementary data to this article can be found online at https://doi.org/10.1016/j.compscitech.2019.02.002.

References

[1] S. Sánchez-Sáez, E. Barbero, R. Zaera, C. Navarro, Compression after impact of thin composite laminates, Compos. Sci. Technol. 65 (13) (2005) 1911–1919.
[2] C. Lopes, O. Seresta, Y. Coquet, Z. Gürdal, P. Camanho, B. Thuis, Low-velocity impact damage on dispersed stacking sequence laminates. part I: experiments, Compos. Sci. Technol. 69 (7) (2009) 926–936.
[3] C. Lopes, P. Camanho, Z. Gürdal, P. Maimí, E. González, Low-velocity impact damage on dispersed stacking sequence laminates. Part II: numerical simulations, Compos. Sci. Technol. 69 (7–8) (2009) 937–947.

[4] Y. Liv, G. Guillamet, J. Costa, E. González, L. Marín, J. Mayugo, Experimental study into compression after impact strength of laminates with conventional and non-conventional ply orientations, Compos. B Eng. 126 (7) (2017) 133–142.
[5] T. Sebaey, E. González, C. Lopes, N. Blanco, P. Maimí, J. Costa, Damage resistance and damage tolerance of dispersed CFRP laminates: effect of the mismatch angle between plies, Compos. Struct. 101 (2013) 255–264.
[6] T. Sebaey, E. González, C. Lopes, N. Blanco, J. Costa, Damage resistance and damage tolerance of dispersed CFRP laminates: effect of ply clustering, Compos. Struct. 106 (2013) 96–103.
[7] C.T. Herakovich, Mechanics of Fibrous Composites, (1998).
[8] S. Abrate, Impact on Composite Structures, Cambridge University Press, 2005.
[9] A. Wagih, P. Maimí, N. Blanco, J. Costa, A quasi-static indentation test to elucidate the sequence of damage events in low velocity impacts on composite laminates, Compos. Appl. Sci. Manuf. 82 (2016) 180–189.
[10] P.A. Lagace, J.E. Williamson, P. Wilson Tsang, E. Wolf, S. Thomas, A preliminary proposition for a test method to measure (impact) damage resistance, J. Reinforc. Plast. Compos. 12 (5) (1993) 584–601.
[11] S.R. Swanson, Limits of quasi-static solutions in impact of composite structures, Compos. Eng. 2 (4) (1992) 261–267.
[12] H. Kaczmarek, S. Maison, Comparative ultrasonic analysis of damage in cfrp under static indentation and low-velocity impact, Compos. Sci. Technol. 51 (1) (1994) 11–26.
[13] E. González, P. Maimí, P. Camanho, C. Lopes, N. Blanco, Effects of ply clustering in laminated composite plates under low-velocity impact loading, Compos. Sci. Technol. 71 (6) (2011) 805–817.
[14] E. Abisset, F. Daghia, X. Sun, M.R. Wisnom, S.R. Hallett, Interaction of inter-and intralaminar damage in scaled quasi-static indentation tests: Part 1–experiments, Compos. Struct. 136 (2016) 712–726.
[15] D. Bull, S. Spearing, I. Sinclair, Investigation of the response to low velocity impact and quasi-static indentation loading of particle-toughened carbon-fibre composite materials, Compos. Appl. Sci. Manuf. 74 (2015) 38–46.
[16] MATLAB, The MathWorks Inc., Natick, Massachusetts, 2015 (R2015a), version 8.5.0.
[17] R.M. Jones, Mechanics of Composite Materials, CRC Press, 1998.
[18] J.M. Whitney, Structural Analysis of Laminated Anisotropic Plates, CRC Press, 1987.
[19] D. Liu, Impact-induced delamination a view of bending stiffness mismatching, J. Compos. Mater. 22 (7) (1988) 674–692.
[20] S. García-Rodríguez, J. Costa, V. Singery, I. Boada, J. Mayugo, The effect interleaving has on thin-ply non-crimp fabric laminate impact response: X-ray tomography investigation, Compos. Appl. Sci. Manuf. 107 (2018) 409–420.
[21] ASTM D7136/D7136M-15, Standard Test Method for Measuring the Damage Resistance of a Fiber Reinforced Polymer Matrix Composite to a Drop Weight Impact Event, (2015).
[22] Y. Liv, A Contribution to the Understanding of Compression after Impact of Composite Laminates, PhD Thesis, University of Girona, 2017.
[23] P. Maimí, P.P. Camanho, J. Mayugo, C. Dávila, A continuum damage model for composite laminates: Part I–Constitutive model, Mech. Mater. 39 (10) (2007) 897–908.
[24] P. Maimí, P.P. Camanho, J. Mayugo, C. Dávila, A continuum damage model for composite laminates: Part II–Computational implementation and validation, Mech. Mater. 39 (10) (2007) 909–919.
[25] P.P. Camanho, C.G. Dávila, S.T. Pinho, L. Iannucci, P. Robinson, Prediction of in situ strengths and matrix cracking in composites under transverse tension and in-plane shear, Compos. Appl. Sci. Manuf. 37 (2) (2006) 165–176.
[26] P.P. Camanho, S.R. Hallett, Numerical Modelling of Failure in Advanced Composite Materials, Woodhead Publishing, 2015.
[27] E. González, P. Maimí, E. Martín-Santos, A. Soto, P. Cruz, F.M. de la Escalera, J.S. de Aja, Simulating drop-weight impact and compression after impact tests on composite laminates using conventional shell finite elements, Int. J. Solids Struct. 144 (2018) 230–247.
[28] Abaqus, Inc, Abaqus Version 6.12 User Manual, Simulia, Providence, RI, USA.
[29] M. Benzeggagh, M. Kenane, Measurement of mixed-mode delamination fracture toughness of unidirectional glass/epoxy composites with mixed-mode bending apparatus, Compos. Sci. Technol. 56 (4) (1996) 439–449.
[30] W. Tan, B.G. Falzon, L.N. Chiu, M. Price, Predicting low velocity impact damage and compression-after-impact (CAI) behaviour of composite laminates, Compos. Appl. Sci. Manuf. 71 (2015) 212–226.
[31] A. Soto, E. González, P. Maimí, F.M. de la Escalera, J.S. de Aja, E. Alvarez, Low velocity impact and compression after impact simulation of thin ply laminates, Compos. Appl. Sci. Manuf. 109 (2018) 413–427.
[32] A. Soto, E. González, P. Maimí, J. Mayugo, P. Pasquali, P. Camanho, A methodology to simulate low velocity impact and compression after impact in large composite stiffened panels, Compos. Struct. 204 (2018) 223–238.
[33] P.P. Camanho, P. Maimí, C. Dávila, Prediction of size effects in notched laminates using continuum damage mechanics, Compos. Sci. Technol. 67 (13) (2007) 2715–2727.
[34] D. Bull, S. Spearing, I. Sinclair, Observations of damage development from compression-after-impact experiments using ex situ micro-focus computed tomography, Compos. Sci. Technol. 97 (2014) 106–114.
[35] J. Zhang, X. Zhang, An efficient approach for predicting low-velocity impact force and damage in composite laminates, Compos. Struct. 130 (2015) 85–94.
[36] G. Catalanotti, C. Furtado, T. Scalici, G. Pitarresi, F. Van Der Meer, P. Camanho, The effect of through-thickness compressive stress on mode II interlaminar fracture toughness, Compos. Struct. 182 (2017) 153–163.
[37] X. Xu, M. R. Wisnom, X. Sun, S. R. Hallett, Experimental determination of through-thickness compression (TTC) enhancement factor for mode II fracture energy, Compos. Sci. Technol..
[38] A. Quintanas-Corominas, P. Maimí, E. Casoni, A. Turon, J.A. Mayugo, G. Guillamet, M. Vázquez, A 3d transversally isotropic constitutive model for advanced composites implemented in a high performance computing code, Eur. J. Mech. A Solid. 71 (2018) 278–291.
[39] C. Lopes, S. Sádaba, C. González, J. Llorca, P. Camanho, Physically-sound simulation of low-velocity impact on fiber reinforced laminates, Int. J. Impact Eng. 92 (2016) 3–17.

A.2 Paper B

On how unsymmetrical laminate designs with tailored ply clusters affect compression after impact strength compared to symmetric baseline

A. Sasikumar[a,*], S. M. García-Rodríguez[a], J.J. Arbeláez[a,b], D. Trias[a,1], J. Costa[a,*]

[a]AMADE, Polytechnic School, Universitat de Girona, Campus Montilivi s/n, E-17003 Girona, Spain

[b] Engineering Faculty, Instituto Tecnológico Metropolitano (ITM), C.73, No. 76-354, Medellín, Colombia

[*] Corresponding author

[1] Serra Hunter Fellow

The paper has been published in *Composite Structures* Vol. 238 (2020) 111958.

Composite Structures 238 (2020) 111958

Contents lists available at ScienceDirect

Composite Structures

journal homepage: www.elsevier.com/locate/compstruct

On how unsymmetrical laminate designs with tailored ply clusters affect compression after impact strength compared to symmetric baseline

A. Sasikumar[a,*], S.M. García-Rodríguez[a], J.J. Arbeláez[a,b], D. Trias[a,1], J. Costa[a,*]

[a] AMADE, Polytechnic School, University of Girona, Campus Montilivi s/n, 17073 Girona, Spain
[b] Engineering Faculty, Instituto Tecnológico Metropolitano (ITM), C.73, No. 76-354, Medellín, Colombia

ARTICLE INFO

Keywords:
Delamination
Impact behaviour
Damage tolerance
Unsymmetrical laminates

ABSTRACT

Out-of-plane loads induce unsymmetrical damage modes in the laminate thickness direction. Consequently, the authors have recently proposed overcoming the conventional laminate symmetry constraint by designing unsymmetrical laminates with zero coupling responses. While impact damage is able to be tailored with unsymmetrical laminates, comparing them to symmetric laminates and assessing their impact damage tolerances had yet to be addressed. In this paper, we study three unsymmetrical laminates with localized ply clusters positioned at different locations (at the impacted, at the middle and at the non-impacted sides), along with a standard symmetric laminate as a baseline. Using low-velocity impact, X-ray micro-computed tomography and compression after impact (CAI), we compared the impact and post-impact responses to understand the effect local ply clusters and the delamination location have on the CAI strength. Results revealed that the unsymmetrical laminate with the ply clusters in the middle, where the dominant delaminations also occured, improved the CAI strength by a maximum of 10% when compared to the symmetric baseline. Laminates with delaminations at the outer surfaces offered lesser resistance to buckling. While our study demonstrates that symmetric laminates are not the optimal damage tolerant solution for impact load cases, it also evidences the feasibility of unsymmetrical laminates.

1. Introduction

Low velocity impact loads continue to be one of the load case threats that aircraft can encounter in their life-cycles. Low velocity impact damage mainly consists of matrix cracks followed by delaminations at the ply interfaces. Impact damage below the detectability threshold (barely visible impact damage, BVID) formed within the laminate may propagate during aircraft flight cycles, leading to a major reduction in residual strength [1], especially the compression after impact (CAI) strength. During CAI loading, the formed delaminations tend to propagate and split the laminate into sub-laminates, and these thinner sub-laminates buckle easily, leading to final failure. In the case of standard thick laminates (4–5 mm), delamination induced buckling is the critical phenomenon causing structural collapse under compression, whereas in the case of thin laminates (1–2 mm), impact induced fibre failure triggers final laminate failure [2,3].

In the quest to improve CAI strength, numerous researchers [4–6] initially tried to understand the relationship between impact damage and CAI strength. They studied the effect various damage parameters such as projected damage area [7], delamination threshold load [8] and impact dent depth [9] had on CAI strength. Because of unclear conclusions, researchers subsequently focussed on delamination parameters such as the through-the-thickness delamination position, orientation and size [10–13] and the associated laminate buckling modes [14] and how they affect CAI strength. Hu et al. [15] performed compressive numerical buckling analysis with one embedded delamination and reported that the buckling load increased significantly as the position of the delamination approached the laminate mid-plane due to the change in the buckling mode from a local to a global one. A similar conclusion was reported by Butler et al. [16] using an analytical model. They stated that deep sited delaminations were safe as they opened under compressive loading and would not grow to cause failure. Despite these interesting conclusions, in a real impact scenario the effect on CAI strength could be completely different due to the development of many more damage forms.

Apart from applying material reinforcement methods [17], researchers have also pushed the laminate design boundaries to propose non-conventional stacking sequences, such as varying mismatch angled

* Corresponding authors.
E-mail addresses: aravind.sasikumar@udg.edu (A. Sasikumar), josep.costa@udg.edu (J. Costa).
[1] Serra Hunter Fellow.

https://doi.org/10.1016/j.compstruct.2020.111958
Received 8 May 2019; Received in revised form 11 December 2019; Accepted 17 January 2020
Available online 28 January 2020

interfaces [18,19], complete [20,19] or localized ply clustering [21], or dispersed ply orientations [22–24] in an attempt to tailor the impact damage resistance and improve the CAI strength. Liv et al. [19] demonstrated that complete clustering of plies ($[90_3/-45_3/0_3/45_3]_s$) led to a decreased impact resistance and a 15% lower CAI strength compared to a non-clustered baseline ($[90/45/-0/-45]_{3s}$). This was mainly attributed to the wide extended delaminations adjacent to the ply clusters. However, Sebaey et al. [21] using dispersed ply orientations and localized clusters of 0° plies, reported an improvement in CAI strength over the baseline quasi-isotropic laminate.

Reviewing the damage morphology, low velocity impact induces damage modes that are unsymmetrical in the through-the-thickness direction of the laminate [1,25]. Despite both the loading and the damage being unsymmetrical in the laminate, the conventional mid-plane symmetry constraint is still followed. In response, the authors [26] proposed warp-free unsymmetrical laminates (with the extensional-bending coupling matrix B = [0]) with localized ply clusters placed only on the impacted side of the laminate. The same laminate, when flipped upside down, led to another unsymmetrical laminate with clustered plies on the non-impacted side of the laminate. Experimental (low velocity impact and quasi-static indentation tests) and numerical studies on the two laminates concluded that (a) delaminations can be tailored to occur at pre-determined locations and (b) unsymmetrical stacking designs offer a promising prospect for unsymmetrical loading conditions. Despite demonstrating that impact damage can be tailored, the study lacked the crucial information of the resulting compressive strength (CAI) and a comparison with a symmetric baseline in terms of impact resistance and CAI strength.

Hence, in this paper we propose three unsymmetrical laminates, where local ply clusters are placed at the impacted side, the middle of the laminate and the non-impacted side, and a reference symmetric baseline laminate (with no ply clusters). Using low velocity impact, micro computed X-ray tomography inspections and CAI tests, we compare the impact resistance, damage evolution and CAI strengths of all four laminates. The objective of the study is twofold: (a) to understand the effect the local ply clusters, their location in the laminate, and the location of the dominant delaminations (imposed by the clusters) have on the CAI strength and (b) to compare the damage tolerance of the proposed non-conventional unsymmetrical laminates to that of the symmetric baseline laminate (as suggested in ASTM standards [27]) to assess the prospects of the unsymmetrical laminate designs. According to the authors' knowledge, this is the first report of a comparison between conventional symmetric laminate and nonconventional unsymmetrical laminates in the framework of impact damage and CAI strength.

2. Laminate design

2.1. Optimization

Different laminates with local ply clusters at the impacted side, the middle of the laminate and the non-impacted side were designed. Because the clusters were placed only at particular locations in the laminate, this meant violating the conventional mid-plane symmetry constraint and therefore leading to unsymmetrical laminate solutions. Since unsymmetrical laminates can induce coupling responses under loading (due to the presence of non-zero extensional-bending coupling matrix ([B]) [28]), such as warping during the curing process, optimization methods were used to obtain unsymmetrical laminates with zero or close to zero B matrix terms.

Using a genetic algorithm from MATLAB [29], we obtained three unsymmetrical laminates (two that had already been proposed in the previous work [26]) with clustered ply blocks placed at the top, the middle or the bottom of the laminates. Note that top refers to the impacted side and bottom refers to the non-impacted side of the laminate. The objective function was set to minimize the summation of the B matrix terms to avoid undesired coupling responses. In addition, the following constraints were also included: (a) the laminate had to be quasi-isotropic and balanced with 24 plies in total, (b) four clustered ply blocks (one cluster for each ply orientation i.e., 0°, ±45 ° and 90 °) were placed at the respective desired location (top/middle/bottom) to impose delamination damage at that location; (c) no more than three plies of the same orientation were placed together, (d) outer laminate plies were fixed to be either 45 ° or − 45 ° to counteract the shear loads [22], and (e) the equivalent bending stiffness parameter D* of the proposed laminates were to match within 5% that of the baseline laminate (D* was proposed by Olsson [30,31] to ensure proper comparisons between laminates, as was also implemented in [32]).

2.2. Laminates

The unsymmetrical laminate obtained with local ply clusters at the impacted side (top side) is referred to as LPCI, while the same flipped laminate with ply clusters at the non-impacted side (bottom side) is referred to as LPCN (as presented in [26]). Finally, the unsymmetrical laminate with ply clusters at the middle of the laminate is hereafter referred to as LPCM. Note that LPCI and LPCN have null B matrices while LPCM has low but non-zero B matrix terms (with a maximum term of 2 kPa.m^2). In addition, we introduce a symmetric laminate (as recommended in the ASTM standard [27]) as the baseline comparison case. Table 1 details the stacking sequences and Fig. 1 provides an illustration of all four laminates and the through-the-thickness location of the ply clustered blocks. Fig. 2 (a) and (b) represent the polar plot of the in-plane and bending stiffness, respectively, of all the laminates. It is important to note that all the laminates are in-plane quasi-isotropic with equal ply counts in all the orientations. All the laminates have the same number of 0 ° plies, thus assuring a fair comparison for CAI strength which is measured at 0 °. The equivalent bending stiffness values of LSYM, LPCI, LPCN and LPCM are 373.9, 372.2, 372.2 and 373.1 Nm, respectively, and the values of the proposed laminates fall within 1% of that of the baseline laminate. The bending stiffnesses of all three unsymmetrical laminates in the 0 ° and 90 ° directions are the same.

3. Experimental methods

The material used was IM7/M21 prepreg uni-directional tape, and the panels were cured in an autoclave. Impact specimens of 150 × 100 mm were cut out from the panel with 0 ° fibres aligned in the direction of the specimen length. The unsymmetrical laminates had no warping, with respect to the zero or low values of the B matrix. With a ply thickness of 0.184 mm and 24 plies, all the laminates resulted in a

Table 1
Laminates and their details.

Laminate	Description	Stacking sequence (impacted side to non-impacted side)
LSYM	Symmetric baseline [27]	$[45/0/-45/90]_{3s}$
LPCI	Unsymmetric, Clustered block at the top	$[-45_2/90_2/45_2/0_3/45/90/-45/0/45/90/-45/0/45/90/-45/0/45/90/-45]$
LPCN	Unsymmetric, Clustered block at the bottom	$[45/90/-45/0/45/90/-45/0/45/90/-45/0/45/90/-45/0_3/-45_2/90_2/45_2]$
LPCM	Unsymmetric, Clustered block at the middle	$[45/90/-45/0/45/0/90/-45_2/90_2/45_2/0_3/-45/0/-45/90/45/-45/90/45]$

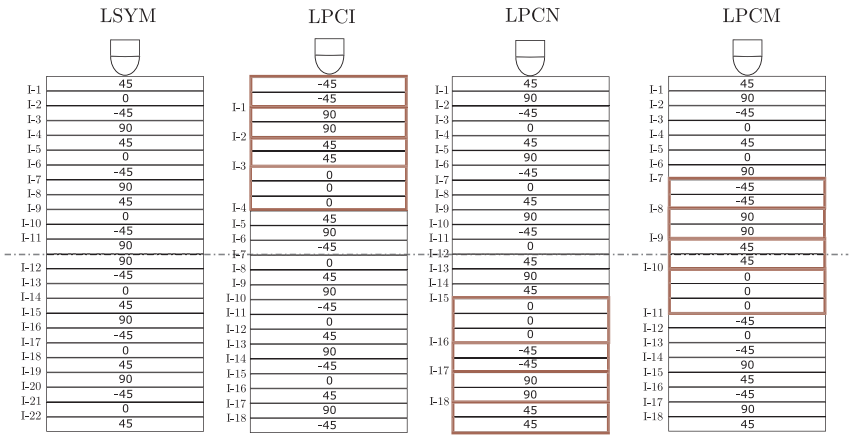

Fig. 1. Illustration of all the laminates used for the study: LSYM, LPCI, LPCN and LPCM, where LPCN is obtained by flipping upside down LPCI. Note that T (top), B (bottom) and M (middle) refer to the location of the clustered block in the through-the-thickness direction of the laminate.

nominal thickness of 4.41 mm. The LPCI specimens were flipped upside down to obtain LPCN laminates. In accordance with ASTMD7136/D7136-M standards [27], impact tests were performed on the 150 × 100 mm specimens using a CEAST Fractovis Plus instrumented drop-weight tower. A total of four impact energies were explored: 10, 16, 24, and 35 J, with three specimens per laminate tested for each impact energy. The range of impact energies was selected such that the lowest energy induces minimum damage in order to understand the damage initiation process, while the higher energies lead to barely visible impact damage and extended delaminations inside the laminate. Impact specimens were placed over a metallic fixture base with a rectangular cut out of 125 × 75 mm, and four rubber tipped clamps restrained the specimen during impact. A 16 mm in diameter hemispherical tip impactor, with a 5 kg impactor setup mass was used for all the tests in the study. For further details of the test setup, refer to [20,33].

All the impacted specimens were subjected to compression using an MTS INSIGHT 300 machine with a 300 kN load cell, following the ASTMD7137/D7137-15 [34] in order to obtain the compression after impact strength. The impacted specimen is placed between flat plates in the test fixture, and end-loaded under compression to obtain a compressive failure induced by the impact damage (refer to [33] for details of the test fixture). To measure the out-of-plane displacements and study the buckling modes, we placed two LVDT sensors, one each at the centre of the impacted and non-impacted sides of the impacted specimen. Furthermore, to evaluate the pristine compression strength, plain compression strength tests were performed in accordance with the ASTMD6641/D6641M-16 [35]. The compressive force is introduced into the specimen by combined end- and shear-loading and the specimens were tabbed leaving a 13 mm tab free region in the centre (refer to [33] for more details). Five 140 × 13 mm specimens per laminate were tested under plain compression, and both compression tests above were performed with a cross head displacement of 0.5 mm/min.

The impact damage in all the laminates were inspected using a pulse-echo ultrasonic C-scan technique. We used an OLYMPUS OMNI MX system equipped with a 5 MHz piezoelectric probe. The specimens were immersed in a water pool and the probe's movement was controlled by an automatized robotic arm (Refer to [33] for the details). Furthermore, one of the 10 J impacted specimens per laminate was subjected to an X-ray micro-computed tomography (μCT) inspection. Before the inspection, the impact specimens were cut into 30 mm wide strips (with the impact point as the centre), making sure that all the

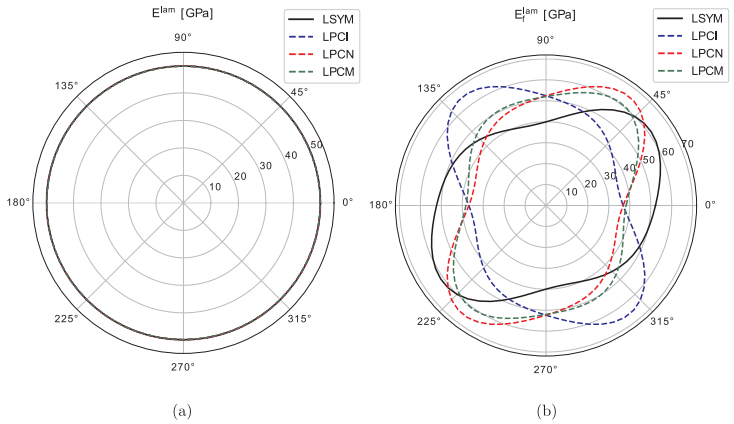

Fig. 2. Polar plot representation of the (a) in-plane stiffnesses and (b) bending stiffness of all the laminates.

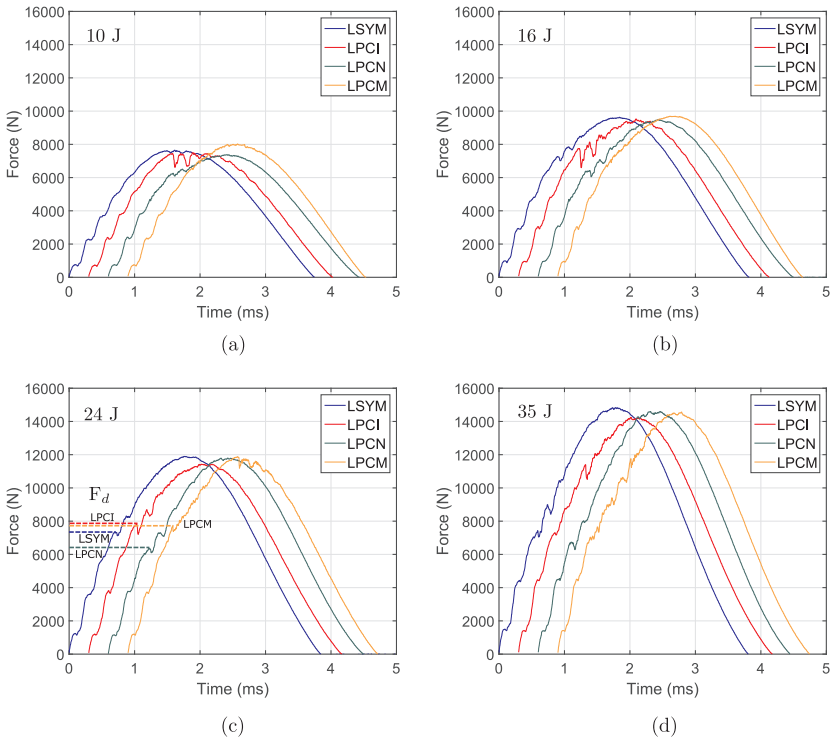

Fig. 3. Impact force-time response curves of all laminates for all impact energies (Note that the responses of LPCI, LPCN and LPCM are offset by 0.3, 0.6 and 0.9 ms from LSYM, respectively, for proper comparison).

impact damage was within this strip (determined by C-scan inspection). Using laminate strips instead of the whole impact specimen was done to minimize the unwanted X-ray absorption perpendicular to the axis of rotation as reported in [36]. The scanning parameters were: 50 kV, 175 μA, 1400 projections with three integrations per projection, an effective pixel size of 10 µm with a field of view of approximately 22 mm and the inspection time was two and a half hours per specimen. The μCT slices were post-processed using Matlab [29] and 3D rendered in Starviewer software [37], where we differentiated matrix cracks and delaminations in the final 3D image. For more details of the inspection equipment and the post-processing of the slices, the reader can refer to [36,38]. All the above-mentioned tests and inspections were performed at the AMADE research laboratory, which is NADCAP certified for non-metallic material testing, at the University of Girona.

4. Results

4.1. Impact responses

Figs. 3–5 represent the force-time, force-deflection and energy-time responses of all the four laminates for all the impact energies, respectively. Due to the excellent repeatability in the impact responses, only one specimen data per impact energy per laminate is shown. The figures convey that the global impact responses of all four laminates are quite similar, mainly in terms of their maximum peak forces, impact response times and the energy evolution (in Figs. 3 and 4). Despite their similar responses, the delamination threshold loads (F_d) differ between the laminates. With LSYM as the baseline, laminate LPCN exhibited an early delamination initiation (13% reduction in the delamination threshold load), while LPCI and LPCM increased the threshold load by 7% and 5%, respectively, over LSYM (as in Fig. 3 (c)).

Fig. 6(a) and (b) present the maximum peak loads and projected damage areas, respectively, for all the laminates. As previously mentioned, the peak loads are roughly the same for all the laminates throughout the entire range of energies, thus indicating the similar load carrying capability the four laminates have, despite the presence of clusters in the unsymmetrical laminates. However, this is not the case with the projected damage area. On comparing all four impact energies, the baseline LSYM exhibited the least damage area whereas LPCN exhibited the highest. For the lower impact energies (10 J and 16 J), LSYM and LPCM exhibited roughly the same damage areas. For higher energies, LPCM exhibited a 50% higher damage area, while LPCI showed a 60% more damage area than the baseline. Throughout all the impact energies, LPCN exhibited more than twice the damage area as that of LSYM.

Fig. 7(a) and (b) show the dissipated energies and impact dent depths, respectively, of all the laminates for all impact energies. For the lowest energy, 10 J, all the laminates dissipated roughly the same amount of energy. In the cases of 16 J and 24 J, all three unsymmetrical laminates exhibited roughly the same dissipated energy (around 10% higher than LSYM), whereas for the highest energy, 35 J, LSYM exhibited the least and LPCI dissipated the highest (18% higher than LSYM). Of the three unsymmetrical laminates, LPCM dissipated the least energy considering all the energies. In view of the impact dent depth, laminates LSYM and LPCI displayed similar dent depth values, whereas LPCN exhibited the highest for all the impact energies. For the

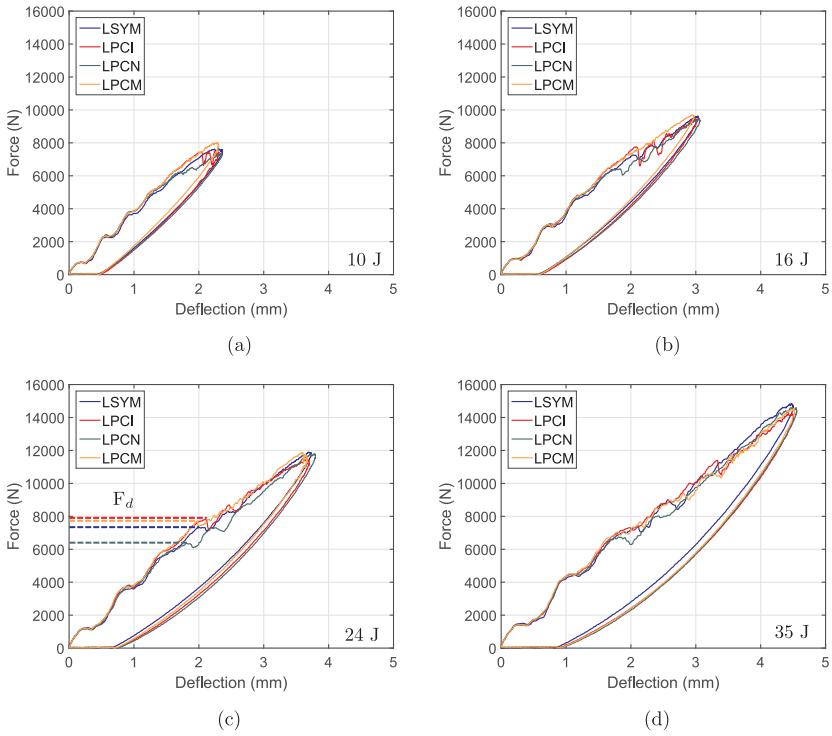

Fig. 4. Impact force-deflection response curves of all laminates for all impact energies.

highest impact energy, LPCM and LPCN displayed approximately 25% higher dent depth compared to the baseline LSYM.

4.2. Impact damage inspection

Fig. 8 presents the damage footprint (matrix cracks and delaminations) of all the laminates obtained from the post-processed μCT slices of the lowest impact energy (10 J). Using the same field of view for all the laminates, LPCN clearly exhibits a higher projected damage area, whereas LPCM displays the least. LSYM and LPCI exhibit similar projected damage contours with similar areas.

The projected damage presented above has been extruded in the laminate thickness direction to present a 3D view of the damage (Fig. 9) in order to: (a) identify whether the local ply clusters have induced delamination at their respective locations, and (b) understand and compare the different damage modes in the thickness direction between all the laminates. The laminates are presented as three sub-laminates where SL-1, SL-2 and SL-3 represent the top, middle and bottom sub-laminates. The clustered blocks, which consists of 9 plies, of the unsymmetrical laminates are grouped as one sub-laminate and are represented by a green box for easy comparison.

LSYM and LPCI displayed similar damage patterns when the three sub-laminates of both laminates are compared. Both laminates had their dominant delaminations in the sub-laminate closest to the non-impacted side (SL-3). Note that with LPCI, the clustered plies are in SL-1 and the dominant delaminations are found in SL-3, contrary to the prediction we made in the laminate design phase. As mentioned earlier, LPCN showed the highest projected damage and it is evident from the 3D view that all the damage is concentrated in the sub-laminate SL-3 (closest to non-impacted side), i.e., the sub-laminate where clustered plies were imposed. The delaminations within these interfaces (int. 15, 16, 17 and 18 as given in Fig. 1) have extended to the boundaries of the inspected field of view; something not observed in any other laminate. Finally, the LPCM laminate was found to have the least amount of damage when compared with all the sub-laminates (SL-1, SL-2, and SL-3) of all four laminates. The dominant delamination was found in the clustered plies sub-laminate (SL-2), oriented in the 0 ° direction (int 10: (45/0), delamination marked by green). Note that all the laminates exhibited matrix cracks at the impacted surface (shown in black colour in the SL-1 sub-laminates) around the vicinity of the impactor.

Moving to the higher impact energies, Fig. 10 presents the images of the C-scan inspection (from the impacted face) of all the laminates for 16, 24 and 35 J impact energies. The dominant delaminations identified as well as the projected damage areas, are marked in the same figure. Compared to the proposed unsymmetrical laminates, the symmetric baseline laminate, LSYM, exhibited the least damage area for all the energies. Furthermore, due to the contribution of the different delaminations, it was difficult to pinpoint particular dominant delaminations. Moving to LPCI, lower energy 16 J produced a similar damage footprint as that of LSYM, but at higher energy levels the delamination at the clustered zone (Int 3: $(45_2/0_3)$, oriented in the 0 ° direction) became prominent. LPCN displayed the largest projected damage area compared to other laminates, and dominant delaminations were identified at the last three bottom interfaces (Int 16, 17 and 18), at the site of the clustered block. Out of the three unsymmetrical laminates, LPCM exhibited the lowest damage area, and from 24 J to 35 J, the dominant delaminations were found within the clustered zone (Int 10 $(-45_2/0_3)$) and below the cluster (Int 14 (-45/90)).

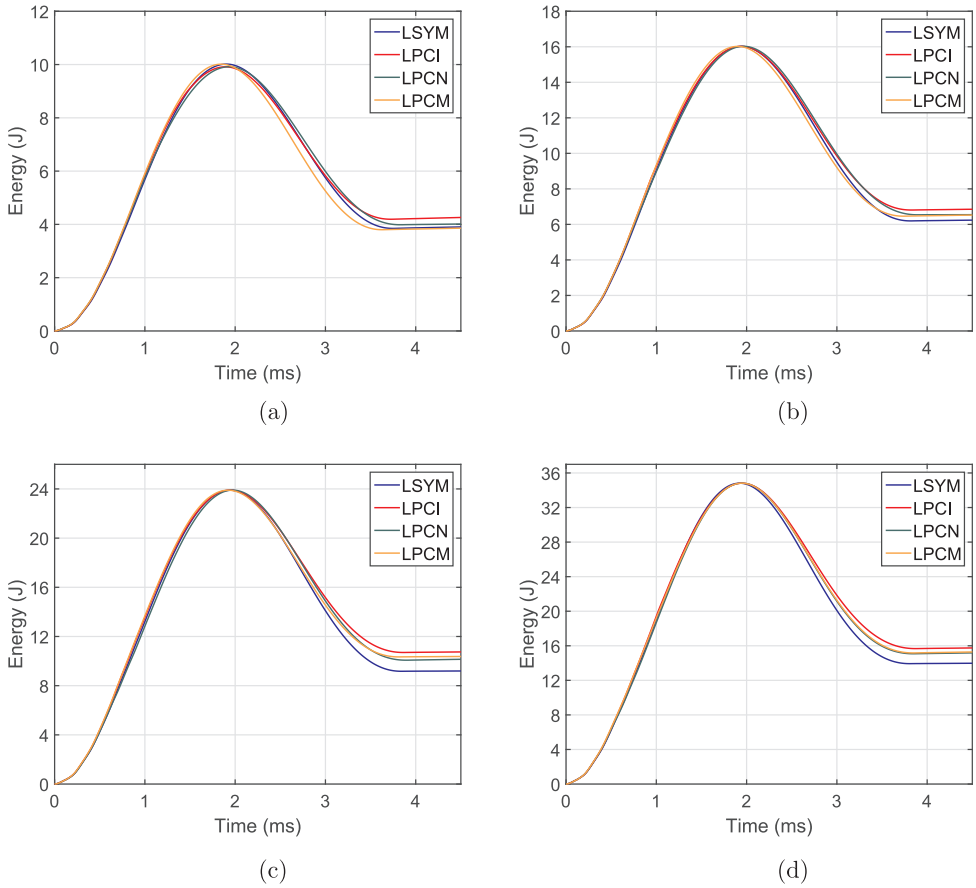

Fig. 5. Impact energy-time response curves of all laminates for all impact energies.

4.3. Compression after impact

Fig. 11 (a) presents the pristine compression strengths along with the CAI strengths of all the laminates for increasing impact energies. Fig. 11(b) depicts the compression strengths normalized with respect to the baseline LSYM. All three unsymmetrical laminates exhibited slightly higher plain compression strength over the baseline LSYM (LPCN and LPCI by 3% and LPCM by 7%). For the 10 J energy, LPCM exhibited the highest CAI strength out of all laminates (10% higher than the baseline LSYM), whereas LPCN exhibited the lowest (5% lower than LSYM). Moving to 16 J, LPCI showed a sudden drop in the CAI strength (from an increase of 5% for 10 J to an 8% reduction for 16 J, over the baseline LSYM). Both LPCI and LPCN showed reduced CAI strength over LSYM for the 16 J impact. Over the entire impact energy range, LPCM exhibited higher CAI strength than LSYM by an average of 8%. It should be noted that even though LPCN exhibited lower CAI strength for the first two impact energies, for the last two energies, LPCN showed the same CAI strengths as those of the baseline LSYM. On comparing the three unsymmetrical laminates, LPCM (laminate with the ply cluster in the middle) displayed higher CAI strength over the other two laminates (15% over LPCI and 10% over LPCN, considering the last three energy levels). Fig. 12 shows the normalized reduction (with respect to the pristine strength) in compression strength due to the impact damage for different impact energies. Almost similar strength reductions were observed with all the laminates, with LPCI exhibiting the highest reduction in residual strength, by around 60% for the higher impact energies.

Fig. 13 displays the macro photos of the failed CAI specimens' edge for all the laminates from the highest impact energy. The compression loading direction is represented in the figure and note that all the laminates are presented such that the impacted side of the specimen is at the top. In addition, the through-the-thickness location of the clustered block is marked by a yellow box for all unsymmetrical laminates. The dominant delaminations from the impact have propagated to the specimen edge and are seen in the figure. While in LPCI, the dominant delamination in the clustered block (at the top) is seen to have propagated and created a sub-laminate, the same is seen with the bottom delaminations of LPCN. In the case of LPCM, delamination close to the laminate mid-plane has reached the specimen edge. Hence, it is evident that the dominant delaminations (formed during impact damage) located at the imposed clustered plies have propagated to the specimen edges to create sub-laminates during CAI loading (as reported in [6]).

Fig. 14 presents the evolution of the out-of-plane displacements of the LSYM and LPCM laminates obtained from LVDT-1 and LVDT-2 (placed at the centre of the impacted and non-impacted sides, respectively) during the CAI test of the 16 J impact. LVDT readings confirm that both laminates, LSYM and LPCM, buckled towards the non-

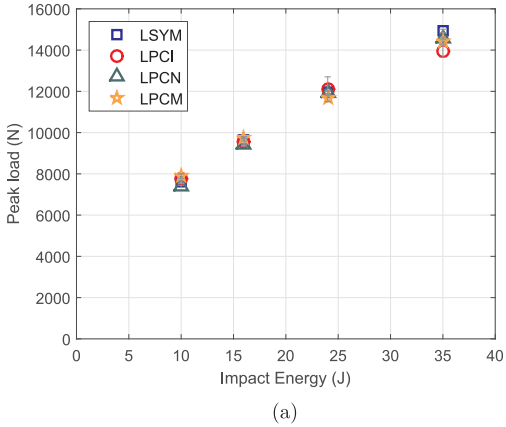

(a)

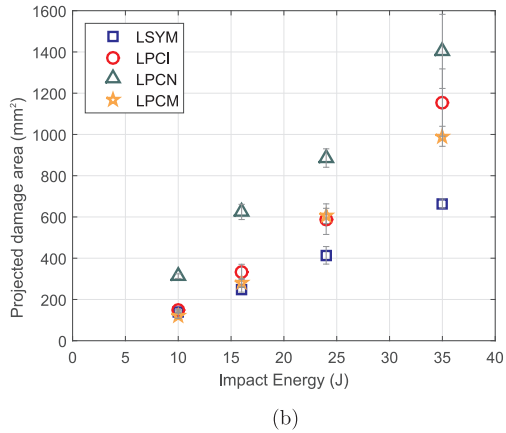

(b)

Fig. 6. Impact damage resistance parameters (a) peak load and (b) projected damage area for all laminates for all impact energies.

impacted side during the CAI loading. LSYM buckled progressively towards the non-impacted side and finally led to the collapse of the laminate marking a maximum out-of-plane displacement of 0.2 mm. In the case of LPCM, at lower CAI loads (around 30 KN), there is a higher out-of-plane displacement compared to LSYM. But with increased loading, there is a saturation in the displacement value, evidence of the laminate resisting buckling. At the failure load, the out-of-displacement observed is roughly similar to the value seen at lower CAI loads. Furthermore, the final out-of-plane displacement value at the point of laminate failure is four times lesser for LPCM compared to LSYM. LPCI showed similar out-of-displacement values as LSYM but buckled globally towards the impacted side. LPCN behaved differently with respect to the impact energy levels. For the lower energy levels, LPCN showed an open buckling mode where the impacted side and non-impacted side buckled towards the respective sides. Meanwhile for the higher energies it buckled as a whole towards the impacted side.

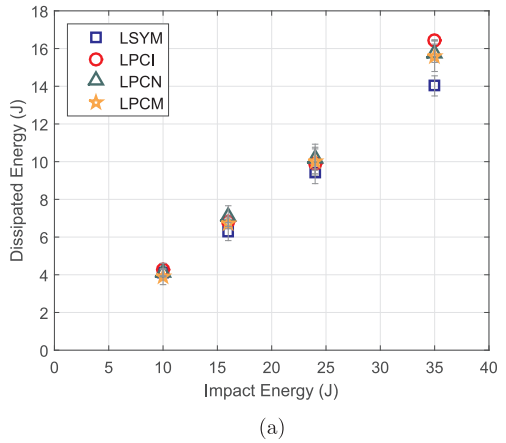

(a)

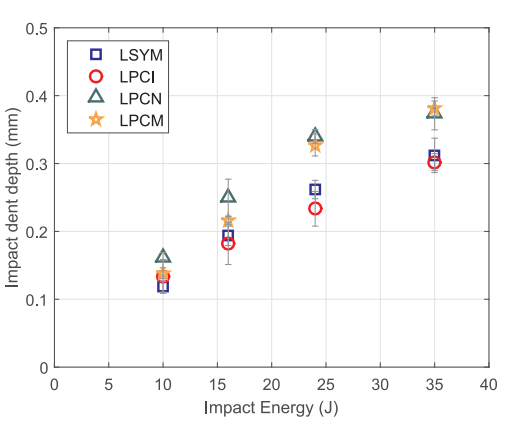

(b)

Fig. 7. Impact damage resistance parameters (a) dissipated energy and (b) impact dent depth for all laminates for all impact energies.

5. Discussion

5.1. Impact damage analysis

During an impact, the laminate bends towards the non-impacted side which introduces in-plane tensile stresses in the bottom plies. The tensile loads induce transverse matrix cracks in the bottom plies, and, in addition, due to bending, the bottom interfaces are subjected to higher interlaminar shear stresses. The transverse tensile cracks and the shear cracks link up in the through-the-laminate thickness to induce delamination. Hence, in a conventional impact damage morphology, the laminate exhibits a spiral stair-case delamination pattern (as reported in [1,39]), where the delaminations are extended in the bottom interfaces and are reduced towards the impacted side. This is similar to what is seen in LSYM and LPCI for the 10 J impact case from the post-processed tomography images (Figs. 8 and 9). In addition, the existence of an undamaged cone under the impactor, as observed in [7], is evident in all the laminates studied (Fig. 9).

Further, when the similar oriented plies are clustered, they introduce a higher bending stiffness mismatch [40] and thereby higher

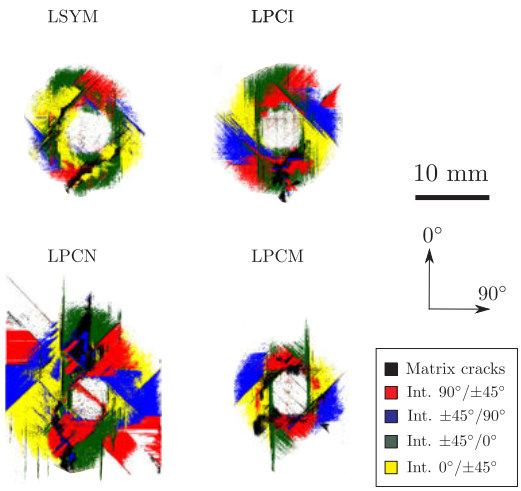

Fig. 8. Projected damage footprint of all the laminates obtained from the post-processed μCT slices of the 10 J impact. Delaminations at different interfaces and matrix cracks are represented using colour codes as given in the legend and the represented field of view is 22 mm for all the laminates.

interlaminar shear stresses at the adjacent interfaces compared to the non-clustered ply interfaces. Moreover, the transverse cracking is less constrained in the thicker plies (i.e., clustered) compared to the non-clustered, due to the in situ effect [41]. Hence, as explained above, the bottom interfaces of the laminate are more prone to having extended delaminations compared to other locations, and clustering the plies at the bottom (as in laminate LPCN) serves as a catalyst to the already prone delaminations at the bottom. These bottom-clustered plies act as a source of early initiation of cracks and delamination and hence the delamination threshold load was seen to be the least for LPCN (as in Fig. 4). This also explains the reason behind the large extended delaminations found in the bottom sub-laminate for LPCN compared to the other laminates (Figs. 9 and 10).

In the case of LPCI (where the localised cluster is placed in the top sub-laminate), the lowest energy level 10 J failed to impose dominant delaminations at the top of the laminate (as was expected during the laminate design phase). Nevertheless, they were seen at the bottom sub-laminate similar to the case of LSYM. This is due to the effect of local through-the-thickness compressive stresses right under the impactor that delay the delamination by increasing interlaminar shear strength and mode II fracture toughness [42–44,26]. However, for the higher impact energies, the C-scans inspections (Fig. 10) reveal that the dominant delaminations are formed at the location of the clustered plies, as the delaminations have extended outside the local compressive region thereby counterbalancing the effect of the local compressive stresses.

On the other hand, LPCM (where the cluster is in the middle of the laminate) also followed the predictions of the laminate design (delamination was observed at the middle sub-laminate, Fig. 9), even though smaller, but significant delaminations, were found in the bottom sub-laminate too. The delaminations induced by the clusters in the mid-plane have significantly reduced or even avoided the delaminations at the top and bottom sub-laminates, when compared to the other three laminates. At higher energies, the delaminations within the clustered zone were prevalent, as evidenced by the C-scan images. Hence, the idea of forcing delamination to occur at desired places through laminate design techniques is demonstrated. Similar observations of forcing delaminations were reported in [19,21] using laminate stacking sequence designs.

Despite the similar impact response curves by all the laminates for all the impact energies, the increased projected damage area for the unsymmetrical laminates over the symmetric baseline laminate is a result of the effect local clustered plies have. The effect the through-the-thickness delamination location has on impact resistance is evidenced by LPCM's reduced damage area and dissipated energy.

5.2. Effect of local ply clusters and delamination location on CAI strength

The small improvement in the plain compression strength of the unsymmetrical laminates over the baseline (Fig. 11) signifies that the thicker plies (or clustered plies), mainly the 0 ° plies, help in effectively carrying the compressive load. Further, the effect of the position of the local cluster is also significant as the laminate with the cluster at the middle showed higher compression strength over the ones with the clustered blocks placed at the specimen surfaces (top or bottom as in LPCI and LPCN, respectively). LPCM improved the CAI strength over LSYM due to the effect of clustered plies (mainly 0 ° plies) and the mid-plane location of the dominant delaminations it imposed. The lower CAI strength of LPCN and LPCI over LPCM shows that delaminations closer to the mid-plane resist buckling compared to the surface delaminations under compression loading. This is in line with the conclusions from the numerical studies in [6,15], which reported that near surface delaminations induced buckling at lower loads. Nevertheless it should be noted that despite understanding the significant effect of delamination location on the CAI strength, other factors such as the thickness and orientation of the other plies, laminate thickness, material system etc. play a significant role too, whose effect is not discussed in this study.

The LPCN laminate exhibited different buckling modes depending on the impact energies. For lower energies, the dominant delaminations of LPCN at the bottom split the bottom sub-laminate from the rest of the laminate, and the plies within this sub-laminate easily buckled outwards to the non-impacted side. But for higher energies, the same bottom sub-laminate buckled inwards to the impacted side where the intact top sub-laminate helps resist and delay the final failure. This could be the reason behind the lesser reduction in the CAI strength of LPCN (almost the same CAI strength as LSYM at 24 and 35 J) when moving from lower to higher energies.

Similarly with LPCI, the dominant delaminations split the laminate where the clustered block at the top can easily buckle outwards due to the reduced stiffness of the sub-laminate. In the case of LPCM, the out-of plane displacements suggest that there was initial global buckling towards the non-impacted side, but that the delamination propagation split the laminate into sub-laminates with the intact clustered block taking the compression load (Fig. 13). In addition, this cluster of plies (especially the 0 ° plies) resisted buckling (as also reported in [45]) because of the surrounding plies at the top and bottom. This is in agreement with the results reported in [45,21], where clustered plies improved the damage tolerance through reduced buckling. Hence, it was the compressive failure of the main load-bearing plies that triggered the final CAI collapse (as evidenced in Fig. 14). This alternative failure mechanism of compressive fibre fracture because of the buckled plies was also reported in [46]. It is worth remarking that even though complete clustering of a laminate was reported to impair the impact resistance and damage tolerance [19,20], clustering plies locally is observed as being advantageous in this study (as also reported by Sebaey et al. [21]).

5.3. Damage resistance parameters v/s CAI strength

The similar impact response curves of the different laminates elucidate the effectiveness of the laminate design study where the laminates were designed to have similar in-plane and bending responses for fair comparison. Since all four laminates have similar impact responses,

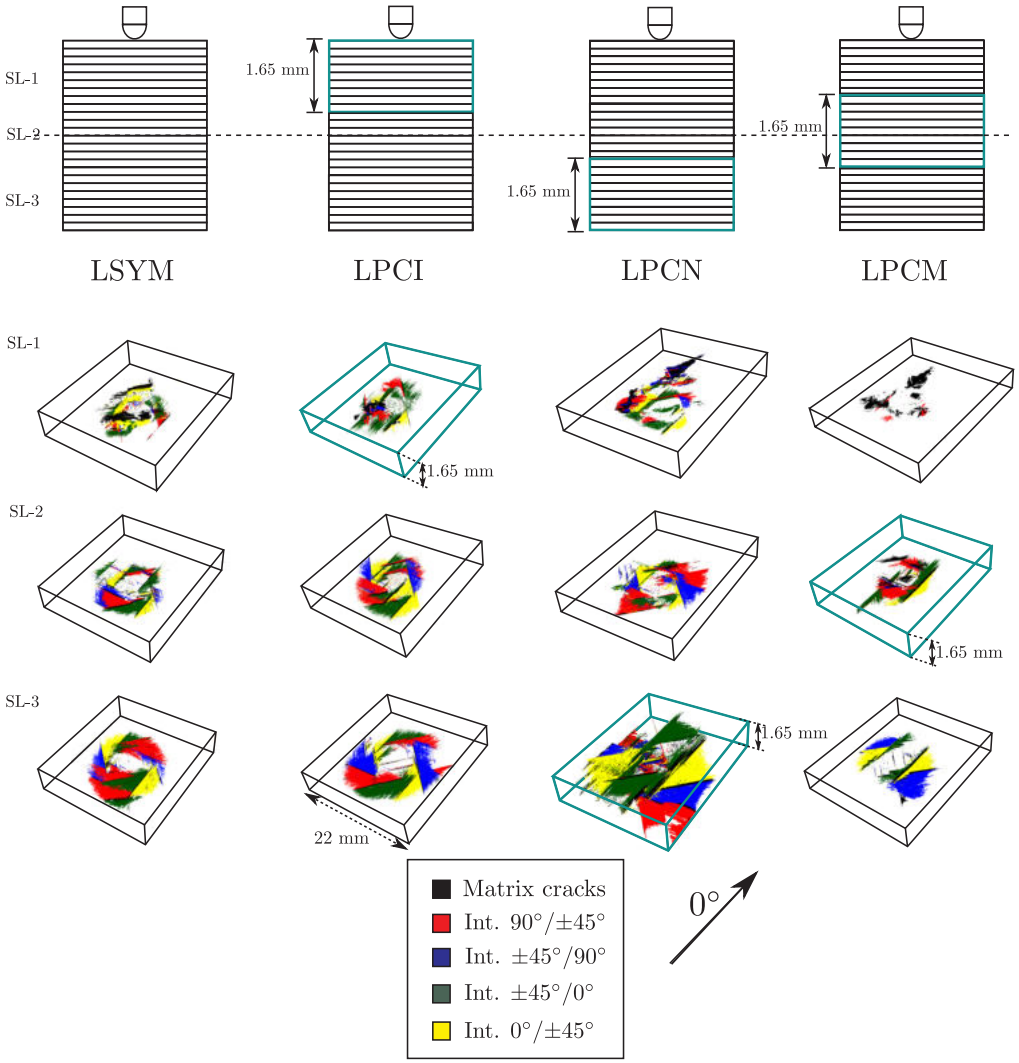

Fig. 9. A 3D extruded illustration of the damage obtained from the post-processed μCT slices of the 10 J impact. Each laminate is divided into three sub-laminates and the sub-laminate containing the clustered plies of each unsymmetrical laminate is marked by a green box.

it holds this as a fair platform from which the correlation of different impact resistance parameters on CAI strength can be studied. Aircraft manufacturers still use projected damage area to correlate CAI strength, where a higher area denotes less CAI strength. From this study, it is clear that projected damage area is a very misguiding parameter to relate CAI strength to, as also observed in [2]. For the highest impact energy, LPCN showed 115% increased damage area compared to the baseline LSYM, but both laminates showed similar CAI strength values. Similarly, the unsymmetrical laminate, LPCM, showed 7% higher CAI strength despite having 55% higher projected damage area over LSYM for the 35 J impact. A similar trend is seen for dissipated energy, where the lower dissipated energy of LSYM did not proportionate to a higher CAI strength. Moreover, it is also observed that if a laminate has a higher resistance to the onset of delamination (LPCI in this case), this does not imply a higher CAI strength. LPCI delayed delamination onset and LPCN exhibited early delamination onset, but finally LPCN displayed higher CAI strength over LPCI. Hence, it is clear that CAI damage morphology is too complex to be predicted or correlated with the impact resistance parameters. The final failure is seen to depend more on the through-the-thickness position of the dominant delamination, the thickness of the sub-laminates formed during CAI loading and the buckling modes of the sub-laminates, rather than simply just the damage resistant parameters (as discussed above).

From an industrial point of view, the damage tolerance concept suggests that the structure should have enough strength to continue in service until the damage is detected by a scheduled inspection. A dent depth greater than 0.25 mm has greater probabilities of being detected during a visual inspection [47], and the corresponding energy level is

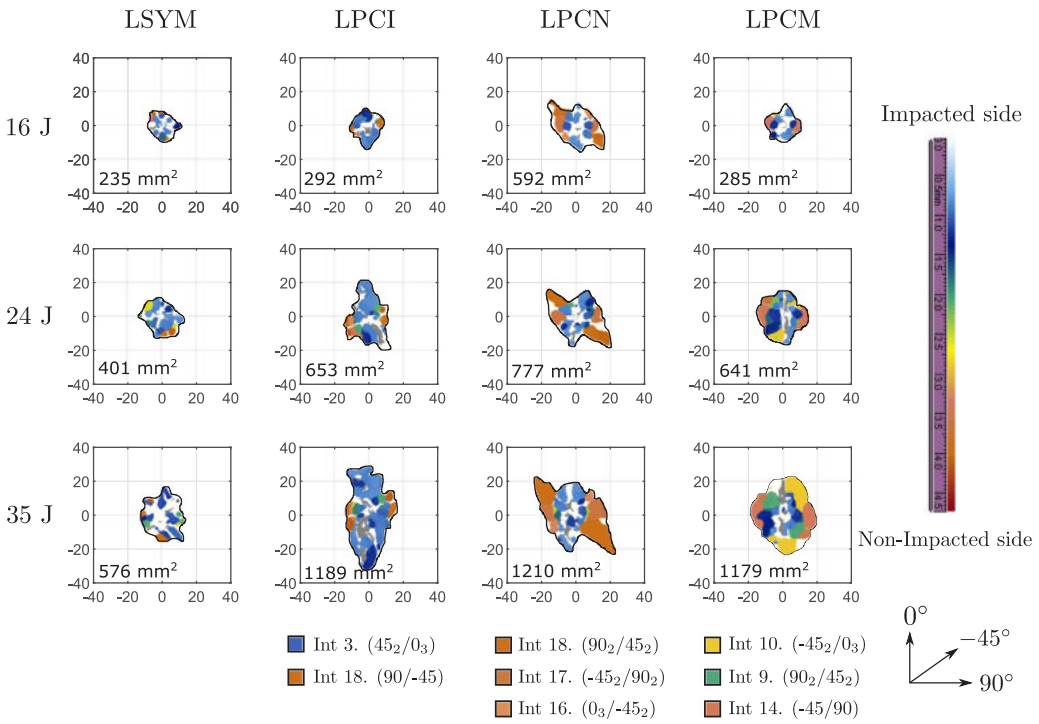

Fig. 10. C-scan images of all four laminates inspected from the impacted side for the impact energies 16, 24 and 35 J. Projected delamination area is marked in the bottom left corner of each box and the field of view represented is 80 × 80 mm with the impact point as the centre.

termed as BVID energy level. Hence, in combining the laminate residual strength and the damage detectability, laminates LPCM and LPCN displayed higher dent depth (BVID energy level of 24 J) than LSYM and LPCI (BVID energy level of 36 J). Thus, despite having higher (as for LPCM) or equal (as for LPCN) CAI strengths compared to LSYM, the chances of detecting the damage in LPCM or LPCN are also greater compared to LSYM. The worst case is when the cluster is placed at the impacted side (as in LPCI), where the CAI strength and the chances of detecting the damage are the lowest, leading to a critical situation.

5.4. The prospects of unsymmetrical laminates

Using warp-free unsymmetrical stacking sequences, we have exhibited the capability to improve the damage tolerance compared to the standard ASTM baseline laminate. It should be kept in mind that even though the improvement is not dramatic, it was achieved economically by simply clustering some plies and through an unsymmetrical design (without reinforcing the material system or using dispersed ply orientations [22,21]). That said and putting this improvement to one side, the different unsymmetrical laminates helped to obtain a clear understanding of the effect delamination position has on CAI strength, which until now had been missing, despite the conclusions reported from numerical and analytical studies [15,16].

With the objective to investigating the CAI response of unsymmetrical laminates and their comparison with a symmetric baseline laminate) missing from the previous work [26], this study demonstrates that symmetric laminates are not the optimal damage tolerant solution to impact loading cases. A similar conclusion was reported by Baker et al. [48] supporting the idea of unsymmetric laminate design.

In instances such as aircraft skins, unsymmetrical laminates may be a promising solution (e.g., for higher impact damage tolerance or higher electrical conductivity). Furthermore, unsymmetrical laminates can be looked upon as being an option to design hybrid laminates tailored for impact loads (as performed by the authors with thin laminates [32]), where the plies on the impacted side can be designed with thick plies and the non-impacted side with thin plies, thereby mitigating the critical delamination damage at the non-impacted side using thin plies.

6. Conclusion

This study extends the findings of a previous work [26] on unsymmetrical laminates tailored for impact resistance by evaluating the compression after impact strength and providing a comparison with a symmetric baseline laminate. In this paper, we designed three warp-free unsymmetrical laminates to have local ply clusters placed at the impacted side, middle and non-impacted side of the respective laminates, with the aim of imposing delaminations at these particular through-the-thickness locations. By means of low velocity impacts, X-ray tomography and ultrasonic C-scan inspection of the impacted specimens and compression after impact tests, we compared the impact responses, damage and the compression after impact strengths to that of a symmetric baseline laminate. The site of dominant delaminations at the location of clustered plies in the unsymmetrical laminates supports the concept that damage can be imposed at desired locations through laminate design. Despite the reduced impact resistance (50% increased damage area and 10% higher energy dissipated) over the baseline laminate, the unsymmetrical laminate with ply clusters at the middle improved CAI strength by 10%. The same laminate with delamination in the middle buckled the least under CAI (four times lesser out-of-plane displacements compared to symmetric baseline laminate) and increased

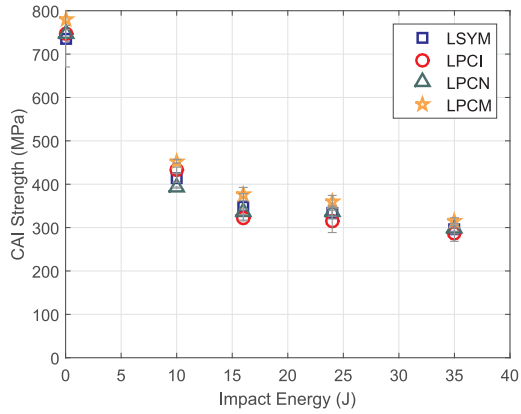

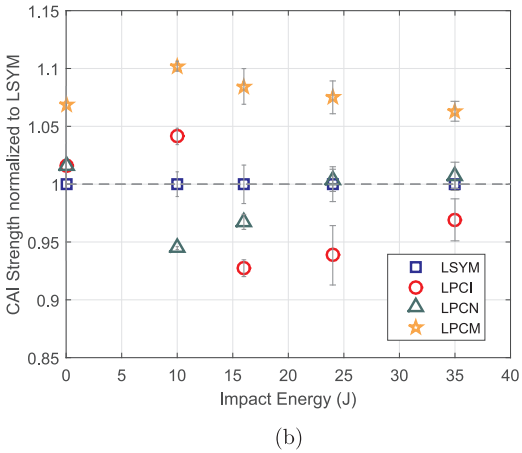

Fig. 11. (a) Absolute and (b) Normalized (with respect to LSYM baseline) plain compression strengths and CAI strengths of all four laminates for all impact energies.

the failure load (by 15%) over the other unsymmetrical laminates with delamination at the outer surfaces. We demonstrated that unsymmetrical over symmetrical laminates can offer improved CAI strengths and can be an optimal solution for application in structures such as aircraft skins.

CRediT authorship contribution statement

A. Sasikumar: Conceptualization, Methodology, Validation, Investigation, Formal analysis, Writing - original draft, Writing - review & editing, Visualization. **S.M. García-Rodríguez:** Software, Investigation, Formal analysis. **J.J. Arbeláez:** Formal analysis, Investigation. **D. Trias:** Conceptualization, Writing - review & editing, Supervision. **J. Costa:** Conceptualization, Writing - review & editing, Supervision, Project administration.

Declaration of Competing Interest

The authors declare that they have no known competing financial interests or personal relationships that could have appeared to influence the work reported in this paper.

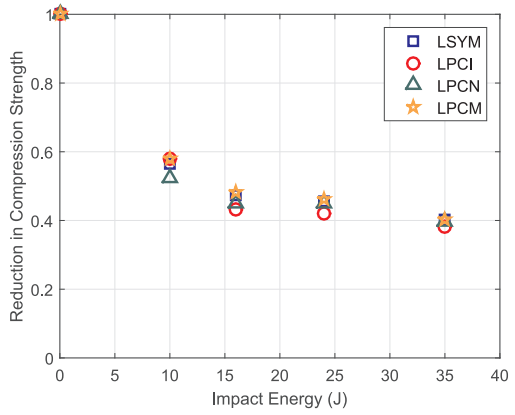

Fig. 12. Normalized reduction in the compression strength due to the impact induced damage for all the impact energies.

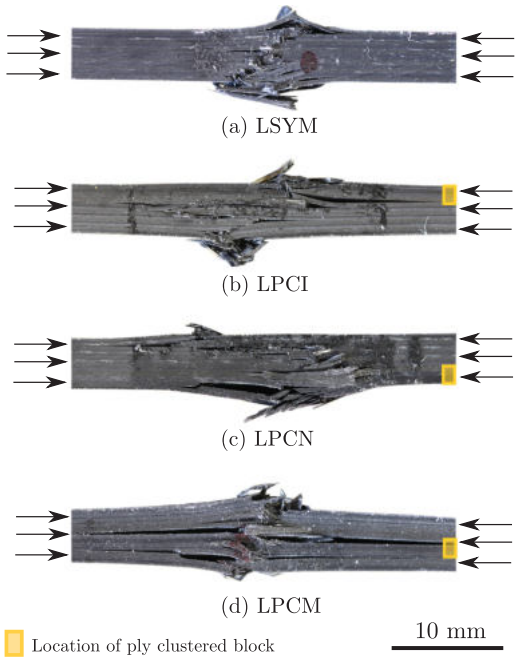

Fig. 13. High resolution macro photos of the specimen edges showing the final CAI failure state of all four laminates (location of the clustered block is shown by the yellow box).

Acknowledgements

The first author would like to thank the Generalitat de Catalunya for the FI-DGR pre-doctoral grant (2018 FI-B2 00118). The authors would like to thank the *Spanish Ministerio de Ciencia, Innovacíon y Universidades* for the grants coded RTI2018-097880-B-I00 and RTI2018-099373-B-I00. We would like to acknowledge Instituto Nacional de Técnica

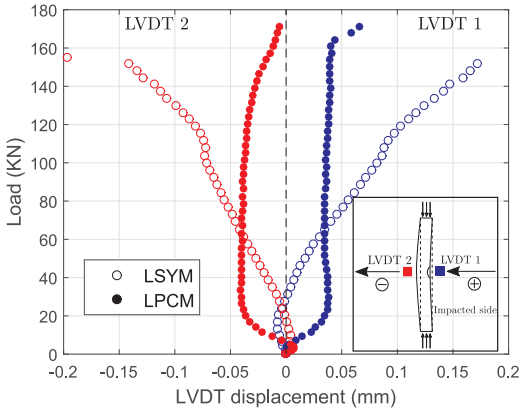

Fig. 14. Out-of-plane displacements recorded by the LVDTs placed at the impacted and non-impacted face laminate centres during the CAI loading of a 16 J impact for LSYM and LPCM laminates (Note that blue indicates LVDT 1 placed at the impacted side and red indicates LVDT 2 placed at the non-impacted side. Outwards buckling (shown by the black arrows in the sub-figure) is indicated by positive values of LVDT 1 and negative values of LVDT 2).

Aeroespacial (INTA), Madrid, Spain for manufacturing all the specimens used in this study. We also acknowledge the support of Dr. Imma Boada and her team (Graphics and Imaging Laboratory, University of Girona) for providing the Starviewer software that was used to 3D render the tomographic slices.

Appendix A. Supplementary data

Supplementary data associated with this article can be found, in the online version, athttps://doi.org/10.1016/j.compstruct.2020.111958.

References

[1] Abrate S. Impact on Composite Structures. Cambridge University Press; 2005.
[2] Sasikumar A, Trias D, Costa J, Orr J, Linde P. Effect of ply thickness and ply level hybridization on compression after impact strength of thin laminates. Compos Part A: Appl Sci Manuf 2019;121:232–43.
[3] Sasikumar A, Trias D, Costa J, Blanco N, Orr J, Linde P. Impact and compression after impact response of thin laminates of spread-tow woven and non-crimp fabrics. Compos Struct 2019;215:432–45.
[4] Abir M, Tay T, Ridha M, Lee H. On the relationship between failure mechanism and compression after impact (CAI) strength in composites. Compos Struct 2017;182:242–50.
[5] Sebaey T, González E, Lopes C, Blanco N, Costa J. Damage resistance and damage tolerance of dispersed CFRP laminates: design and optimization. Compos Struct 2013;95:569–76.
[6] Liv Y. A contribution to the understanding of compression after impact of composite laminates. University of Girona; 2017. [Ph.D. thesis].
[7] Bull D, Spearing S, Sinclair I. Observations of damage development from compression-after-impact experiments using ex-situ micro-focus computed tomography. Compos Sci Technol 2014;97:106–14.
[8] Cartie D, Irving P. Effect of resin and fibre properties on impact and compression after impact performance of CFRP. Compos Part A: Appl Sci Manuf 2002;33(4):483–93.
[9] Petit S, Bouvet C, Bergerot A, Barrau J-J. Impact and compression after impact experimental study of a composite laminate with a cork thermal shield. Compos Sci Technol 2007;67(15–16):3286–99.
[10] Kouchakzadeh MA, Sekine H. Compressive buckling analysis of rectangular composite laminates containing multiple delaminations. Compos Struct 2000;50(3):249–55.
[11] Rhead AT, Butler R, Baker N. Analysis and compression testing of laminates optimised for damage tolerance. Appl Compos Mater 2011;18(1):85–100.
[12] Hwang S-F, Huang S-M. Postbuckling behavior of composite laminates with two delaminations under uniaxial compression. Compos Struct 2005;68(2):157–65.
[13] Obdržálek V, Vrbka J. On buckling of a plate with multiple delaminations. Eng Mech 2010;17(1):37–47.
[14] Reis L, De Freitas M. Damage growth analysis of low velocity impacted composite panels. Compos Struct 1997;38(1–4):509–15.
[15] Hu N, Fukunaga H, Sekine H, Ali KM. Compressive buckling of laminates with an embedded delamination. Compos Sci Technol 1999;59(8):1247–60.
[16] Butler R, Almond DP, Hunt G, Hu B, Gathercole N. Compressive fatigue limit of impact damaged composite laminates. Compos Part A: Appl Sci Manuf 2007;38(4):1211–5.
[17] García-Rodríguez S, Costa J, Singery V, Boada I, Mayugo J. The effect interleaving has on thin-ply non-crimp fabric laminate impact response: X-ray tomography investigation. Compos Part A: Appl Sci Manuf 2018;107:409–20.
[18] Sebaey T, González E, Lopes C, Blanco N, Maimí P, Costa J. Damage resistance and damage tolerance of dispersed CFRP laminates: effect of the mismatch angle between plies. Compos Struct 2013;101:255–64.
[19] Liv Y, Guillamet G, Costa J, González E, Marín L, Mayugo J. Experimental study into compression after impact strength of laminates with conventional and non-conventional ply orientations. Compos Part B: Eng 2017;126:133–42.
[20] González E, Maimí P, Camanho P, Lopes C, Blanco N. Effects of ply clustering in laminated composite plates under low-velocity impact loading. Compos Sci Technol 2011;71(6):805–17.
[21] Sebaey T, González E, Lopes C, Blanco N, Costa J. Damage resistance and damage tolerance of dispersed CFRP laminates: effect of ply clustering. Compos Struct 2013;106:96–103.
[22] Lopes C, Seresta O, Coquet Y, Gürdal Z, Camanho P, Thuis B. Low-velocity impact damage on dispersed stacking sequence laminates. Part I: Experiments. Compos Sci Technol 2009;69(7–8):926–36.
[23] Lopes C, Camanho P, Gürdal Z, Maimí P, González E. Low-velocity impact damage on dispersed stacking sequence laminates. Part II: Numerical simulations. Compos Sci Technol 2009;69(7–8):937–47.
[24] Wagih A, Maimí P, Blanco N, García-Rodríguez S, Guillamet G, Issac R, Turon A, Costa J. Improving damage resistance and load capacity of thin-ply laminates using ply clustering and small mismatch angles. Compos Part A: Appl Sci Manuf 2019;117:76–91.
[25] Wagih A, Maimí P, Blanco N, Costa J. A quasi-static indentation test to elucidate the sequence of damage events in low velocity impacts on composite laminates. Compos Part A: Appl Sci Manuf 2016;82:180–9.
[26] Sasikumar A, Costa J, Trias D, González EV, García-Rodríguez S, Maimí P. Unsymmetrical stacking sequences as a novel approach to tailor damage resistance under out-of-plane impact loading. Compos Sci Technol 2019;173:125–35.
[27] ASTM D7136/D7136-15. Standard test method for measuring the damage resistance of a fiber reinforced polymer matrix composite to a drop weight impact event; 2015.
[28] Jones RM, Bert C. Mech Compos Mater 1975.
[29] MATLAB, version 8.5.0 (R2015a), The MathWorks Inc., Natick, Massachusetts; 2015.
[30] Olsson R. Mass criterion for wave controlled impact response of composite plates. Compos Part A: Appl Sci Manuf 2000;31(8):879–87.
[31] Olsson R. Closed form prediction of peak load and delamination onset under small mass impact. Compos Struct 2003;59(3):341–9.
[32] Sasikumar A, Trias D, Costa J, Singery V, Linde P. Mitigating the weak impact response of thin-ply based thin laminates through an unsymmetrical laminate design incorporating intermediate grade plies. Compos Struct 2019;220:93–104.
[33] Sasikumar A. Improving compression after impact response of composite laminates through ply level hybridization with thin plies and unsymmetrical designs. University of Girona; 2019. [Ph.D. thesis].
[34] ASTM D7137/D7137-15. Standard Test Method for Compressive Residual Strength Properties of Damaged Polymer Matrix Composite Plates; 2015.
[35] ASTM D6641/D6641M-16. Standard test method for compressive properties of polymer matrix composite materials using a combined loading compression (CLC) test fixture; 2016.
[36] García-Rodríguez S, Costa J, Bardera A, Singery V, Trias D. A 3d tomographic investigation to elucidate the low-velocity impact resistance, tolerance and damage sequence of thin non-crimp fabric laminates: effect of ply-thickness. Compos Part A: Appl Sci Manuf 2018;113:53–65.
[37] Starviewer medical imaging software,http://starviewer.udg.edu.
[38] García-Rodríguez S, Costa J, Maimí P, Singery V, Sasikumar A. On how matrix cracks induce delamination under out-of-plane shear and the associated in-situ effect, Submitted to Compos Sci Technol.
[39] Wisnom M. The role of delamination in failure of fibre-reinforced composites. Philos Trans R Soc A: Math, Phys and Eng Sci 2012;370(1965):1850–70.
[40] Liu D. Impact-induced delamination-a view of bending stiffness mismatching. J Compos Mater 1988;22(7):674–92.
[41] Camanho PP, Dávila CG, Pinho ST, Iannucci L, Robinson P. Prediction of in situ strengths and matrix cracking in composites under transverse tension and in-plane shear. Compos Part A: Appl Sci Manuf 2006;37(2):165–76.
[42] Li X, Hallett SR, Wisnom MR. Predicting the effect of through-thickness compressive stress on delamination using interface elements. Compos Part A: Appl Sci Manuf 2008;39(2):218–30.
[43] Catalanotti G, Furtado C, Scalici T, Pitarresi G, Van Der Meer F, Camanho P. The effect of through-thickness compressive stress on mode ii interlaminar fracture toughness. Compos Struct 2017;182:153–63.
[44] Xu X, Wisnom MR, Sun X, Hallett SR. Experimental determination of through-thickness compression (TTC) enhancement factor for mode ii fracture energy. Compos Sci Technol 2018;165:66–73.
[45] Caminero M, García-Moreno I, Rodríguez G. Experimental study of the influence of thickness and ply-stacking sequence on the compression after impact strength of carbon fibre reinforced epoxy laminates. Polym Testing 2018;66:360–70.
[46] Soutis C, Curtis P. Prediction of the post-impact compressive strength of CFRP laminated composites. Compos Sci Technol 1996;56(6):677–84.
[47] Talreja R, Phan N. Assessment of damage tolerance approaches for composite aircraft with focus on barely visible impact damage. Compos Struct 2019;219:1–7.
[48] Baker N, Butler R, York CB. Damage tolerance of fully orthotropic laminates in compression. Compos Sci Technol 2012;72(10):1083–9.

A.3 Paper C

Effect of ply thickness and ply level hybridization on the compression after impact strength of thin laminates

A. Sasikumar[a,*], D. Trias[a,1], J. Costa[a,*], N. Blanco[a], J. Orr[b], P. Linde[c,d]

[a] AMADE, Polytechnic School, Universitat de Girona, Campus Montilivi s/n, E-17003 Girona, Spain

[b] University of Dayton Research Institute, 300 College Park, Dayton, OH, USA

[c] Airbus Operations GmbH, Kreetslag 10, 21129 Hamburg, Germany

[d] Department of Industrial and Materials Science, Chalmers University of Technology, S-41296 Gothenburg, Sweden

[*] Corresponding author

[1] Serra Hunter Fellow

The paper has been published in *Composites Part A: Applied Science and Manufacturing* 121 (2019) 232–243.

Composites Part A 121 (2019) 232–243

Contents lists available at ScienceDirect

Composites Part A

journal homepage: www.elsevier.com/locate/compositesa

Effect of ply thickness and ply level hybridization on the compression after impact strength of thin laminates

A. Sasikumar[a,*], D. Trias[a,*,1], J. Costa[a], N. Blanco[a], J. Orr[b], P. Linde[c,d]

[a] AMADE, Polytechnic School, Universitat de Girona, Campus Montilivi s/n, 17073 Girona, Spain
[b] University of Dayton Research Institute, 300 College Park, Dayton, OH, USA
[c] Airbus Operations GmbH, Kreetslag 10, 21129 Hamburg, Germany
[d] Department of Industrial and Materials Science, Chalmers University of Technology, S-41296 Gothenburg, Sweden

ARTICLE INFO

Keywords:
B. Impact behaviour
B. Compression after impact
C. Damage mechanics
C. Damage tolerance
Ply hybridization

ABSTRACT

There is a lack of research available on how thin laminates respond to impact and post impact loads, even though thin structures are used in present-day aircrafts. This experimental paper employs thick, standard and thin unidirectional plies to investigate the effect ply thickness has on thin laminates on their impact and compression after impact (CAI) response. Further, we propose two hybrid laminates where thick or standard plies are mixed with thin plies, respectively, in an effort to improve the CAI strength of thin laminates. Results reveal that, contrary to thick laminates, thin laminates made of only thin plies exhibit extensive fibre failure, leading to a considerably reduced CAI strength. Moreover, the hybrid laminate where thick 0° plies are mixed with thin plies improves the CAI strength by 40% over the thin ply baseline laminate. Thus, hybridization with thin laminates appears to be an economic prospective in terms of improving damage tolerance.

1. Introduction

One of the aeronautic industry's main concerns is the impact behaviour of thin structures (<2 mm), such as fuselages and wing skins, because low velocity impact can drastically reduce their residual structural strength [1]. However, many studies are devoted to investigating the impact and compression after impact (CAI) response of "standard" thickness laminates (≈4 mm, as recommended in ASTM D7136/D7136M-15 [2]), along with the effect ply thickness has on CAI strength [3–5].

Previous studies have shown the improved performance of thin plies over standard and thick plies in terms of first ply failure and delay of damage onset [6–8]. In the framework of impact and post impact response, research investigations [3,5] reported an average improvement of 20% in CAI strength with thin plies for laminates with thicknesses ranging between 3.6 and 4.4 mm. Thin-ply laminates showcased quasi-brittle failure instead of extended cracking and delaminations as observed in thicker plies. Reviewing thinner laminates, Garcia et al. [9] recently studied the effect of ply thickness on CAI strength with 2.15 mm thick non-crimp fabric laminates. Standard plies showed similar and 27% higher CAI strength when compared to thin plies at 10 and 14 J impact energies, respectively. Hardly any work related to CAI response is reported for laminates with thicknesses less than 2 mm, albeit with the exception of Sanchez et al. [10], who compared CAI strength between quasi isotropic, cross ply, and woven fabrics made out of thick plies for laminates ranging from 1.6 to 2.2 mm in thickness.

Laminate design [11–14] and material system reinforcement [15–17] are two approaches used to improve impact damage resistance and more specifically CAI strength. Laminate design, understood as tailoring the stacking sequence, is considered more economically feasible than material reinforcement. For instance, ply level hybridization consists of mixing plies of different thicknesses in an attempt to enhance a targeted response. Sihn et al. [4] suggested this approach for future work to improve the impact damage resistance of composite structures without increasing the layup costs. Furtado et al. [18] performed selective ply hybridization with different types of fabric architectures by mixing thin and intermediate fabric layers, which eventually resulted in an improved notched response. Arteiro et al. [19] demonstrated that blocking 0° fabric layers improves the structural behaviour of aerospace graded thin ply laminates. Sebaey et al. [20] studied the effect mixing thin and thick fabric layers has on damage tolerance using thick laminates, and when compared to the baseline thin ply, reported an increase of 15% in CAI strength for a configuration of thick plies surrounded by thin plies.

* Corresponding authors.
E-mail addresses: aravind.sasikumar@udg.edu (A. Sasikumar), dani.trias@udg.edu (D. Trias).
[1] Serra Hunter Fellow.

https://doi.org/10.1016/j.compositesa.2019.03.022
Received 1 September 2018; Received in revised form 1 March 2019; Accepted 19 March 2019
Available online 25 March 2019
1359-835X/

This study is the result of an industrial investigation headed by Airbus, in collaboration with the AMADE research group (University of Girona), INEGI (University of Porto) and the University of Dayton Research Institute, USA. The study investigates the effect of ply thickness on impact damage resistance and CAI strength through impact and CAI experimental tests for thin laminates ranging between 1.5 and 1.8 mm. Thick (268 gsm), standard (134 gsm), and thin (75 gsm) unidirectional (UD) plies are selected for the ply thickness study. Additionally, we study two hybrid laminates, the first of which is a mix of standard 0° plies and thin plies, while the second contains thick 0° plies along with thin plies. Results show that thin plies within thin laminates exhibit extensive fibre breakage and lead to the lowest CAI strength. Ply thickness hybridization alleviated the amount of fibre failure with increased delamination damage, and improved the CAI strength remarkably over the baseline thin ply.

2. Experimental methods

2.1. Material and Layup

Uni-directional prepreg tapes of T700/M21 carbon-epoxy supplied by Hexcel® were used to prepare the panels required for the study. We used three ply grades, namely thick (268 gsm), standard (134 gsm) and thin (75 gsm) and hereafter the corresponding laminates prepared from them are referred to as H-268, H-134 and H-75, respectively. Furthermore, two hybrid laminates were proposed and are referred to as H-75-H1 and H-75-H2, where thin 0° plies are substituted by standard and thick 0° plies, respectively. Only 0° plies (thick and standard) were considered to be mixed with thin plies for ply hybridization, as they are the main load bearing plies during CAI loading. Fig. 1 illustrates the five different laminates and Table 1 describes the laminates, their stacking sequences and the ply and laminate thicknesses. Despite the fact that laminates consisted of different ply grades, the stacking sequences were designed to have the closest possible equivalent bending stiffness (D^*, proposed by Olsson [21]) to guarantee a fair comparison. The D^* values of the laminates are 27.5 (H-268), 22.1 (H-134), 17.6 (H-75), 18.3 (H-75-H1) and 20.4 Nm (H-75-H2). Additionally, note that all the laminates are centre-symmetric (denoted by $ in Table 1), which means that the axis of symmetry runs through the middle of the centre ply, so they are not in-plane quasi-isotropic.

2.2. Impact energy definition

As seen in the Table 1, using different ply grades raises the issue of having different laminate thicknesses. A significant 20% difference in measured thickness was noted between the thickest (H-268) and thinnest (H-75) laminate. Instead of impacting all the laminates with a same absolute energy, we introduced impact energies normalized to the measured laminate thickness in order to reduce the biasing on thicker laminates. In fact, ASTM D7136/D7136M-15 [2] also recommends defining impact energies normalized to the specimen thickness, as thicker laminates have an advantage over thin ones when impacted at the same absolute energy. Hence, we defined a total of four impact energies for the impact study: two absolute impact energies irrespective of the laminate thickness and two impact energies normalized with respect to the laminate thickness. Therefore, 5 J and 10.5 J were defined as the two absolute energies and will be referred to as IE_1 and IE_4, respectively. While the lowest impact energy 5 J was chosen to study the initiation of damage, the highest impact energy of 10.5 J was supposed to create barely visible damage according to the recommendations of ASTM D7136/D7136M-15 standards [2]. The two normalized energies were defined as 4.1 J/mm and 5.2 J/mm, and will be referred to as IE_2 and IE_3, respectively. The normalized energies 4.1 J/mm and 5.2 J/mm were determined such that their corresponding absolute energies were spaced evenly between the least (5 J) and highest (10.5 J) impact energies for all the laminates 10.5 J. Table 2 displays the four impact energies defined for all the laminates.

2.3. Experimental tests

2.3.1. Impact and damage inspection

Impact tests were performed according to the ASTM D7136/D7136M-15 standards [2] using a CEAST Fractovis Plus instrumented drop-weight tower on impact specimens of dimensions 150 × 100 mm (with 0° fibres aligned with the specimen length). A 16 mm in diameter steel hemispherical impactor was used, and the total impactor setup was 3 kg. We tested a total of 12 specimens for each laminate, using 3 specimens for each impact energy level to validate the repeatability.

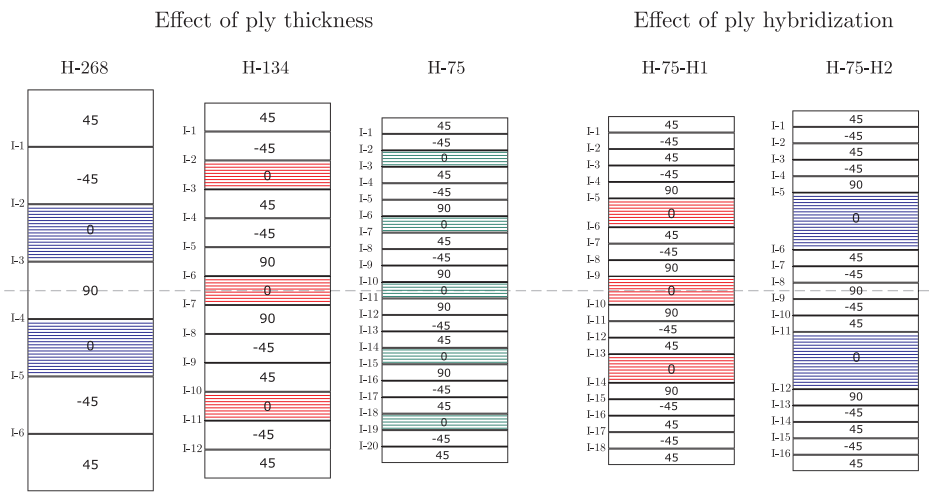

Fig. 1. Illustration of all the laminates used to study the effect of ply thickness and ply hybridization on damage tolerance (corresponding laminate interfaces are also marked). Note that all the laminates are centre symmetric, which means that the axis of symmetry runs through the middle of the centre ply. (For interpretation of the references to colour in this figure legend, the reader is referred to the web version of this article.)

Table 1
Laminates and their details.

Laminate	Description	Stacking sequence	Ply thickness (mm)	Nominal laminate thickness (mm)
H-268	Thick plies	$[45/-45/0/90]_{s}^{*}$	0.262	1.83
H-134	Standard plies	$[45/-45/0/45/-45/90/0]_{s}^{*}$	0.131	1.70
H-75	Thin plies	$[45/-45/0/45/-45/90/0/45/-45/90/0]_{s}^{*}$	0.075	1.58
H-75-H1	Thin & Standard plies	$[45/-45/45/-45/90/0_{134}/45/-45/90/0_{134}]_{s}^{*}$	0.075 & 0.131	1.59
H-75-H2	Thin & Thick plies	$[45/-45/45/-45/90/0_{268}/45/-45/90]_{s}^{*}$	0.075 & 0.262	1.65

* $ represents centre symmetry, which signifies that the axis of symmetry is along the middle of the centre ply.

Table 2
Laminates and the defined impact energies.

Laminate	Measured laminate thickness (mm)	Impact Energy 1: IE_1		Impact Energy 2: IE_2		Impact Energy 3: IE_3		Impact Energy 4: IE_4	
		Abs (J)	Norm (J/mm)	Abs (J)	Norm (J/mm)	Abs (J)	Norm (J/mm)	Abs (J)	Norm (J/mm)
H-268	1.85	5	2.7	7.6	4.1	9.6	5.2	10.5	5.7
H-134	1.70	5	2.9	7	4.1	8.9	5.2	10.5	6.2
H-75	1.56	5	3.2	6.4	4.1	8.2	5.2	10.5	6.7
H-75-H1	1.54	5	3.2	6.3	4.1	8	5.2	10.5	6.8
H-75-H2	1.65	5	3	6.8	4.1	8.6	5.2	10.5	6.4

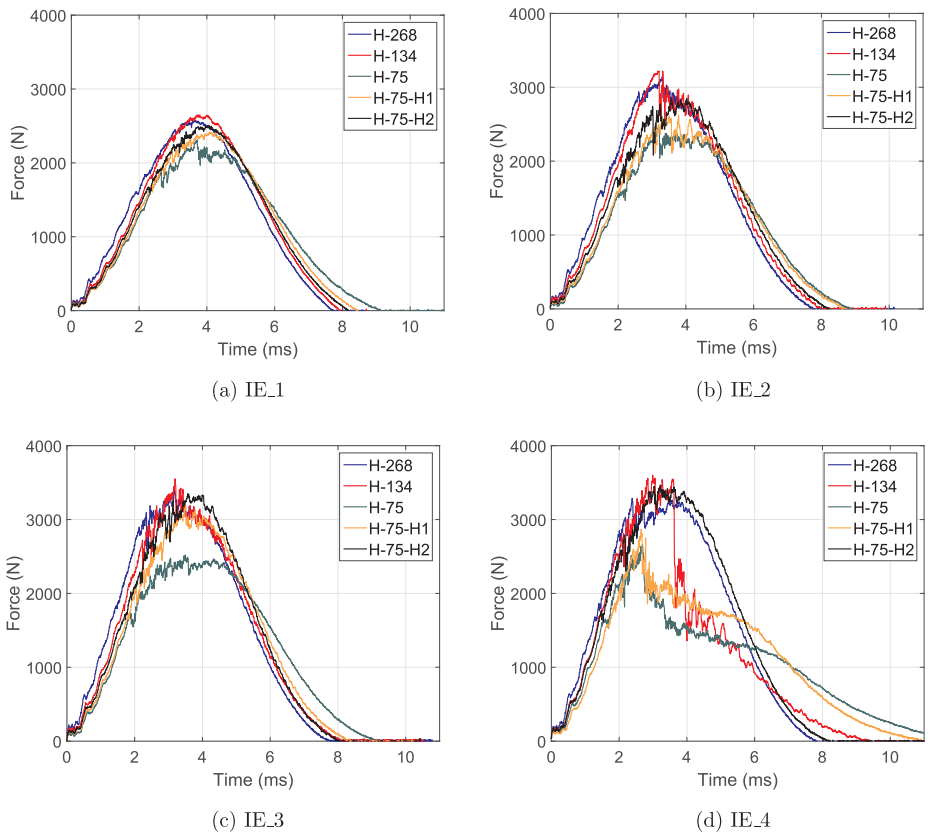

Fig. 2. Force-time response of all the laminates for all the impact energies. (For interpretation of the references to colour in this figure legend, the reader is referred to the web version of this article.)

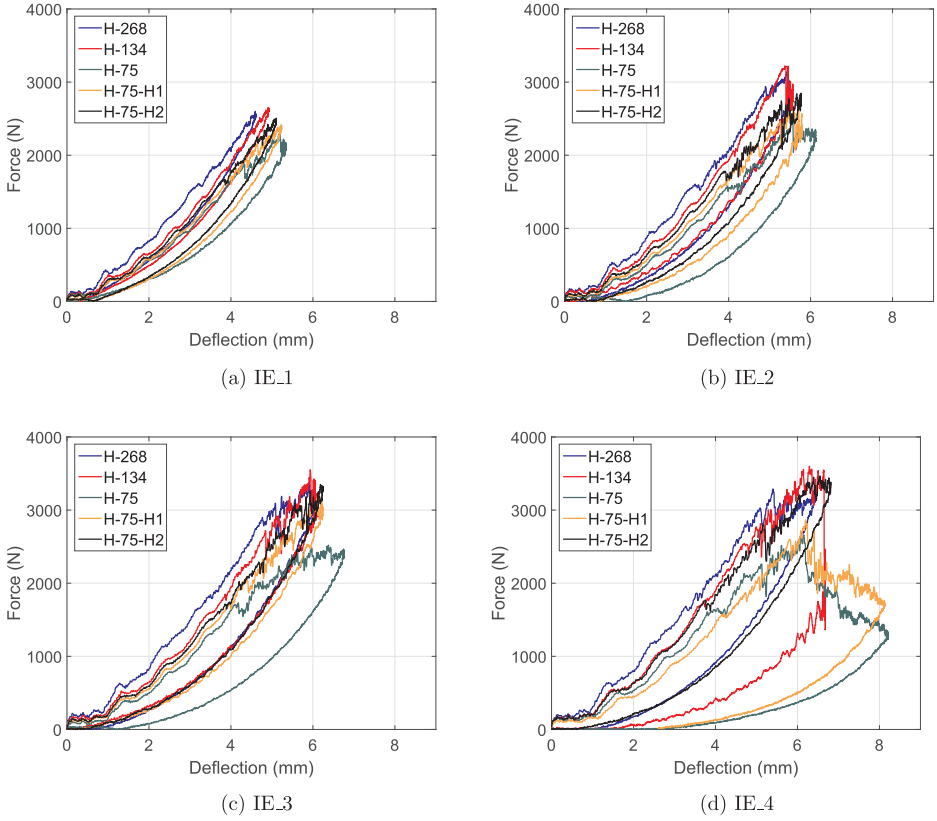

Fig. 3. Force-deflection response of all the laminates for all the impact energies. (For interpretation of the references to colour in this figure legend, the reader is referred to the web version of this article.)

The reader is referred to [22] for further details of the impact setup. Pulse-echo ultrasonic C-scan inspection was performed on all the impacted specimens using an OLYMPUS OMNI MX system. An automated robotic arm scanned the specimen placed inside a pool of water with a 5 MHz piezoelectric probe.

2.3.2. Plain compression and compression after impact (CAI)

To evaluate the reduction in the compression strength due to the impact damage, the compressive strength of the pristine specimens was first obtained. Instead of using pristine standard impact specimens, plain strength compression tests were performed following the ASTM standards D6484/D6484M-14 [23]. These tests were performed at the INEGI research laboratory at the University of Porto for all the five laminates defined above. Three specimens of dimensions 305 mm by 30 mm for each laminate were tested. Detailed information about the test setup is given in [8]. In addition, CAI tests were performed using an MTS INSIGHT*300 machine with a 300 kN load cell, complying with the ASTM standards D7137/D7137M-15 [24]. All three impacted specimens per energy level were subjected to CAI test, to provide evidence of the scattering of the results. Both the above-mentioned compression tests were performed at a cross head displacement loading rate of 0.5 mm/min. To account for the thin laminates, we used an additional non-standard anti-buckling CAI device proposed by Remacha et al. [25]. Apart from the standard CAI device, this fixture utilizes a support structure with a set of vertical ribs that helps to avoid the premature buckling of such thin laminates, thus increasing their global buckling load. These extra supporting plates are clamped onto the CAI test setup with a pre-defined torque value of 5 Nmm. A rectangular window of 52 × 42 mm at the impacted site is left free from vertical ribs to allow for the impact damage to propagate and cause final failure. This modified CAI fixture claims that the specimen fails by compression at the impacted region and not due to global buckling of the thin laminate. Further details about this anti-buckling device can be found in [25]. All the above-mentioned tests, except plain strength compression, were performed at the AMADE research laboratory in Girona, which is NADCAP certified for non-metallic-materials testing.

3. Experimental results

3.1. Impact response & damage assessment

The impact response of all the laminates is presented in terms of impactor force-time, impactor force-displacement, and energy evolution response curves in Figs. 2–4, respectively. Despite testing three specimens for each energy level, due to the good repeatability of the results, only one specimen data curve per energy level is presented.

The delamination load drop observed for the thick laminates, termed as delamination threshold load F_d, is not observed for the thin laminates [9,26] (Figs. 2 and 3). Most laminates exhibited a load drop close to or at maximum peak load, with H-134, H-75, H-75-H1

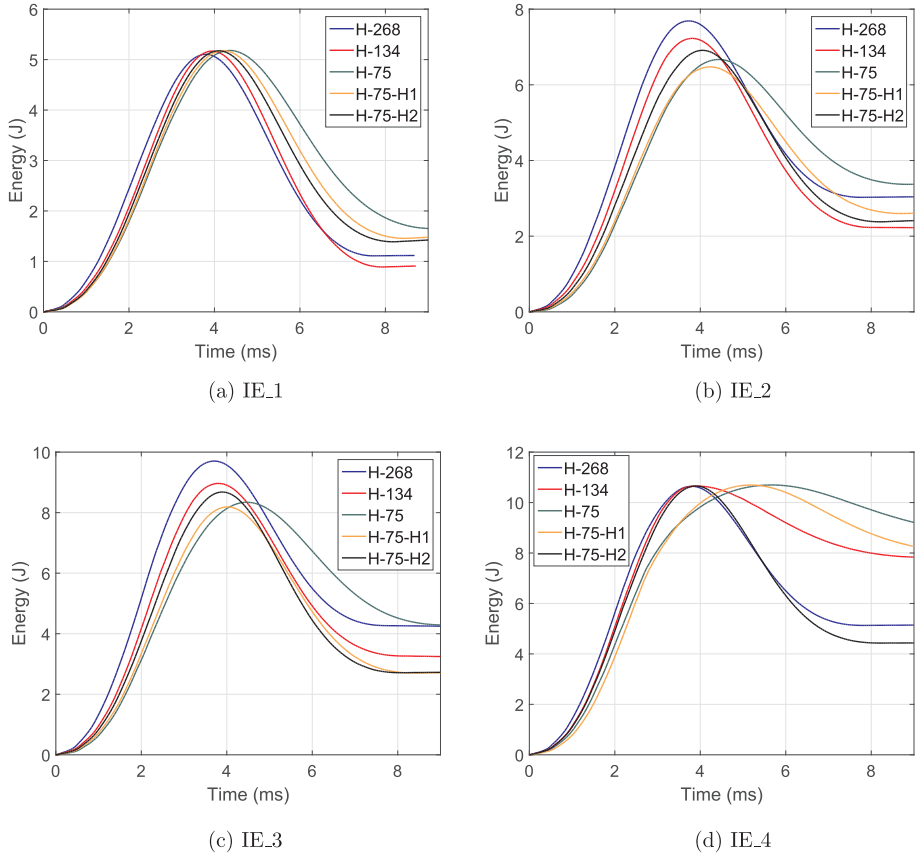

Fig. 4. Energy evolution response of all the laminates for all the impact energies. (For interpretation of the references to colour in this figure legend, the reader is referred to the web version of this article.)

showcasing a high load drop at IE_4 due to fibre failure. H-75 laminate exhibited extended response in impact time and higher displacement for all the impact energies. Fig. 4 shows that H-75 has comparatively higher energy dissipation than the other laminates at all the impact energies, whereas H-75-H2 dissipated the least amount of energy at higher impact energies. At IE_4, laminates comprising thick plies (H-268 and H-75-H2) showed much less energy dissipation compared to the laminates comprising thin and standard plies (H-134, H-75, H-75-H1).

Fig. 5 displays the projected damage profile and the area enclosed from the C-scan inspection of all the laminates at all energies. H-268 displayed the highest projected damage area, with an extended delamination at the last interface $-45^{\circ}/45^{\circ}$ oriented in the 45° (Note that the interfaces are numbered starting from the impacted side, with the last interface denoting the one closest to the non-impacted face, as in Fig. 1). H-134 exhibited the least damage area out of all the laminates for all impact energies, with the dominant delamination seen below the mid-plane (interface No.9: $(-45^{\circ}/45^{\circ})$ as in Fig. 1). H-75 and hybrid laminate H-75-H1 displayed similar damage profiles and areas, with a large increase in the projected damage area for the last impact energy of 10.5 J. C-scan inspection also provides an account of the high dent depth left by the impactor for H-75 and H-75-1 at IE_4. Hybrid laminate H-75-H2 showed dominant delamination at the last interface for lower energies, whereas in moving to higher energies it is shifted to the interface of the inserted thick 0° ply, (interface No.11: $(45^{\circ}/0^{\circ}_{268})$), oriented in the 0° direction.

Fig. 6 presents the impacted and non-impacted face photos of all the laminates for the highest impact energy IE_4. A visual comparison was made between the laminates for the permanent indentation left by impactor and also the magnitude of back fibre splitting at the non-impacted face of the specimen. Thin plies were found to exhibit higher dent depth and extensive back fibre splitting, with the impactor nearly penetrating the laminate. This is evidenced as we visually compare the laminate photos from H-268 to H-75 (left to right in Fig. 6), where the dent depth and back fibre splits are found to increase. Furthermore, the inclusion of thick plies to thin plies was noticed to alleviate the same: as evidenced by comparing H-75 to H-75-H2 in Fig. 6. In addition, the presence of cracks due to fibre failure on both sides of the laminates can be observed.

Fig. 7 presents the average peak load and projected damage area, whereas Fig. 8 displays the dissipated energy and permanent dent depth of all the laminates. H-75 exhibited the least load carrying capacity; as evidenced by the least peak load. In terms of projected damage area, the thick plies H-268 exhibited almost twice the damage area for all the impact energies compared to other laminates. From Fig. 8, the thin and standard ply laminates (H-134, H-75 and H-75-H1) are observed to have higher dent depth and dissipated energy at the highest impact energies, compared to laminates containing thicker plies (H-268 and H-

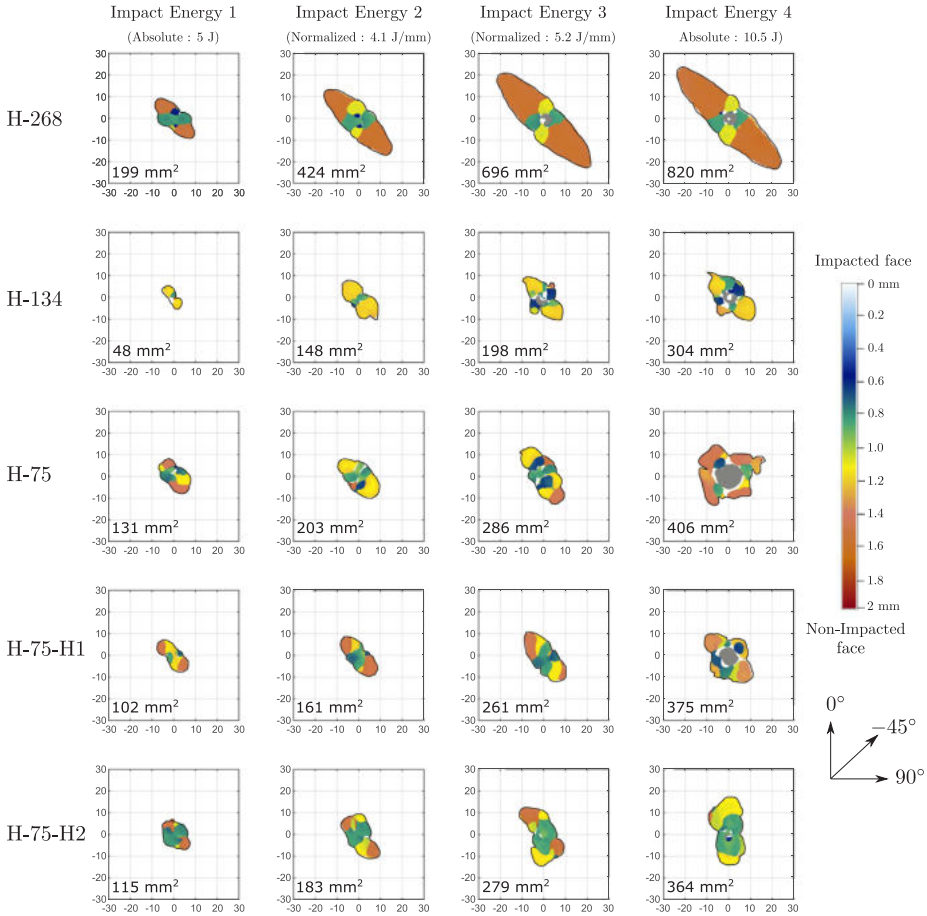

Fig. 5. Projected damage profile obtained from C-scan inspection for all laminates at all impact energies (Average projected damage area presented along with the through-the-thickness colour bar, and the field of inspection represented is 60 × 60 mm^2). (For interpretation of the references to colour in this figure legend, the reader is referred to the web version of this article.) (For interpretation of the references to colour in this figure legend, the reader is referred to the web version of this article.)

75-H2). It is interesting to remark that H-75 dissipated close to 90% of the applied impact energy for IE_4, accompanied by an impact dent depth of almost twice its laminate thickness at IE_4, resulting in near impactor penetration.

3.2. Compression after impact

Along with the plain compression strength values, Fig. 9(a) and (b) also present the CAI strength of all the laminates with respect to the absolute and normalized energies, respectively. Along with the CAI strength values, it is important to review the CAI failure mode as, despite using the anti-buckling fixture, some laminates still failed by structural local buckling at the specimen top rather than at the impacted zone. The same figure also depicts the CAI values and the corresponding laminates which exhibited invalid CAI failure mode (represented by a ∗ coloured the same as the corresponding marker in Fig. 9). This was mainly observed for lower impact energies, as the higher impact energies induced enough damage to force a compressive failure at the specimen centre. It is worth remarking that thick ply H-268 and thin ply H-75 showcased proper CAI failure for all the impact energies. Fig. 10(a) illustrates the schematic representation of the CAI fixture, clearly differentiating the clamped region, anti-buckling ribs, the ribs-free area and the unsupported window at the top of the specimen. Fig. 10 (b) displays the invalid CAI failure mode where the laminate fails due to the local buckling of the unsupported window (marked in red). Fig. 10 (c) presents the proper CAI failure observed at the centre of the specimen due to the evolution of the impact damage.

H-134 showed proper CAI failure for the last three energies, whereas H-75-H2 exhibited the same for the last two energies. H-75-H1 failed at the specimen top for all energies except for the highest impact energy. Within the three grades of ply thickness, thin plies exhibited the highest plain compression strength, approximately 23% higher than the thick plies and 4% higher than the standard plies, as seen in Fig. 9. H-75-H2 has the highest pristine compression strength out of all the laminates, at approximately 10% higher than the thin plies. Since the invalid CAI failure mode provides critical buckling values which are lower than the real CAI strength value, only the valid CAI failure mode values are accounted for during comparison studies. Fig. 11 compares

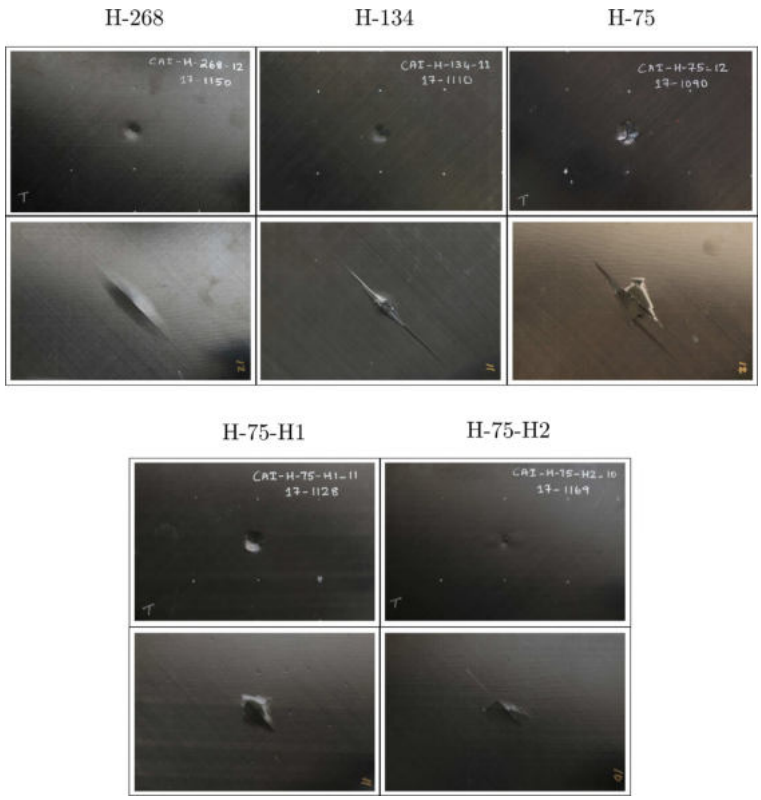

Fig. 6. Post impact photos of the impacted (top) and non-impacted face (bottom) of all the laminates from 10.5 J impact (Each image represents the whole impact specimen of dimensions 150 × 100 mm). (For interpretation of the references to colour in this figure legend, the reader is referred to the web version of this article.)

the CAI strength normalized with respect to thin plies (H-75), which help to obtain a better outlook on the CAI strength comparison in terms of ply thickness and ply hybridization study.

Within the ply thickness study, the last three impact energy results reveal that H-268 and H-134 showed almost the same CAI strength (accounting for the average of last three energy results), whereas H-75 provides the least CAI strength. Reviewing IE_2 and IE_3, thick plies and standard plies exhibit an average increase of 18% and 20%, respectively, over the thin plies H-75. Commenting on the hybrid laminates, H-75-H2 provides the maximum CAI strength over all the laminates, when considering the last two impact energies. In terms of CAI strength improvement, H-75-H2 shows an average increase of 40% and 20% over its baselines H-75 and H-268. Accounting for the CAI strength of H-75-H1 at the highest energy IE_4 (as the other impact energies gave improper failure mode), it shows an average increase of 25% over the its baseline H-75. It is to be noted that both hybrid laminates showed an increased CAI strength over their individual baseline constituents, when considering the valid CAI failure mode values. H-75-H1 and H-75-H2 can be compared with their baseline H-75 for all the four impact energies, acknowledging that the difference between their laminate thickness is very little. Fig. 12 presents the average reduction in the compressive strength of all the laminates, with H-268 and H-75 having the least and highest reduction in compressive strength, respectively. At the highest energy, while H-268 displayed a reduction of 50% of its residual compressive strength, H-75 exhibited 70% reduction in the compressive strength due to the impact damage.

4. Discussion

4.1. Effect of ply thickness

Matrix cracking and delamination are the main forms of damage associated with low velocity impact loads in standard thick laminates as reported in [27]. For thick laminates, the thin plies helped to delay matrix cracking and delamination in the early stages [7], and were reported to have increased CAI strength over the other ply grades [3,5]. As for the thin laminates, due to reduced bending stiffness, they underwent considerable amount of bending during impact which led to high in-plane tensile stresses at the non-impacted laminate face. This resulted in back fibre splitting, as seen in Fig. 6, for all the laminates. The magnitude of the fibre splitting was understood to depend on the ply thickness and thick ply H-268 was observed to exhibit the least when compared to thin plies. This is due to the energy dissipated by thick plies through matrix cracking and delamination, which means less energy is available for dissipation through fibre splitting. On the other hand, thin plies suppressed the initial damage of delamination, but at the cost of dissipating most of the energy through fibre breakage.

The brittle characteristic nature of thin plies is evidenced by high increase in dent depth and dissipated energy (for thin (H-75, H-75-H1) and standard ply (H-134) laminates in Fig. 8), at higher impact energies. In contrast, the laminates containing thick plies (H-268 and H-75-H2) exhibited progressive damage evidenced in the dent depth and dissipated energy with increasing impact energies, as seen in the same

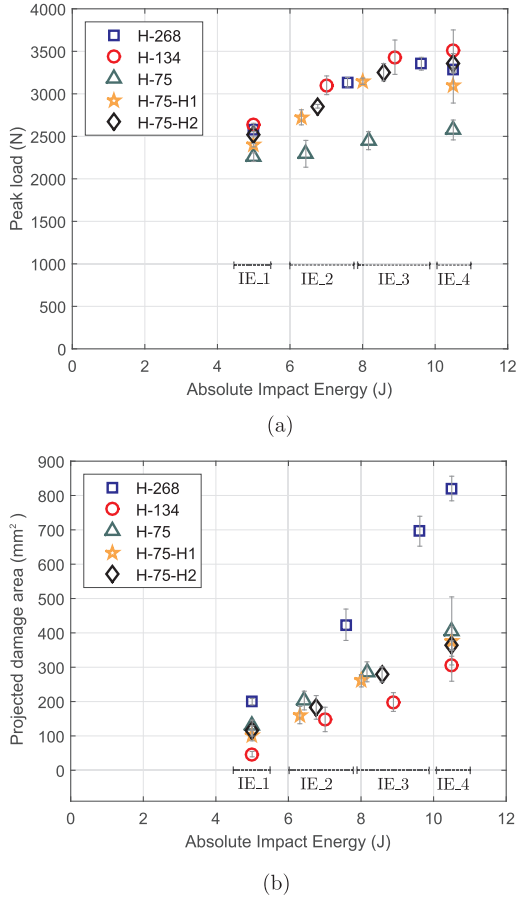

Fig. 7. (a) Peak load and (b) projected damage area compared between all the laminates for all absolute impact energies (Average value is presented along with the standard deviation indicated by vertical markers). (For interpretation of the references to colour in this figure legend, the reader is referred to the web version of this article.)

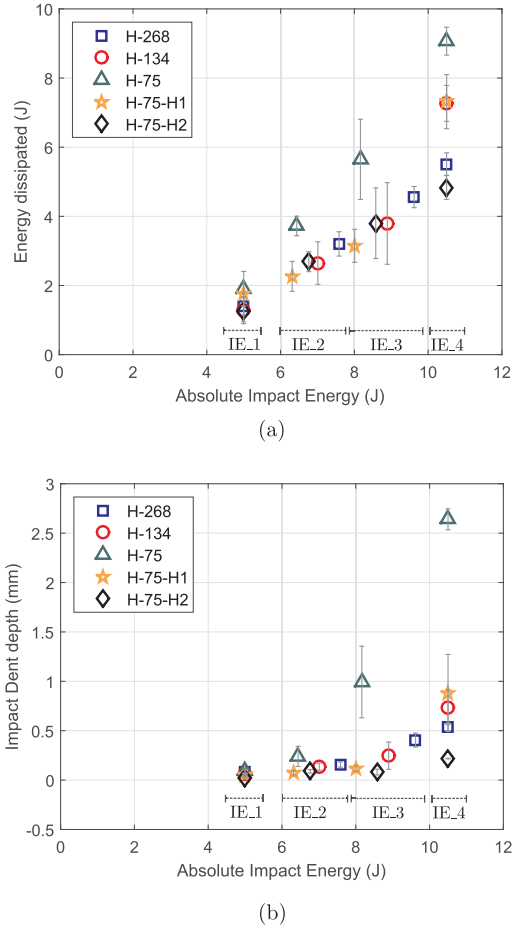

Fig. 8. (a) Dissipated energy and (b) impact dent depth values compared between all the laminates for all absolute impact energies. Fitted linear and exponential curves are also presented. (Average value is presented along with the standard deviation indicated by vertical markers). (For interpretation of the references to colour in this figure legend, the reader is referred to the web version of this article.)

figure. For the projected damage area, despite H-268 showing more than twice the value of H-75 at IE_4, H-75 dissipated about 40% more energy than H-268. In addition, for the highest impact energy, a threshold effect is seen with H-75 when the thin-ply laminate starts to be penetrated by the impactor. The other laminates did not reach this threshold under the impact energies explored.

Within the framework of CAI loading, the final collapse of a laminate has been reported to be complex and is generally associated with the following phenomena: sub-laminate buckling, growth of the existing delamination across the specimen width and compressive fibre failure in the 0° load bearing plies [28]. Compared to other laminates, H-268 exhibited larger delaminations and thin plies H-75 showed extensive fibre breakage. Hence, both laminates exhibited enough damage in one form or the other to induce compressive failure at the specimen centre during CAI testing for all impact energies.

As reported in [3,7], the homogeneous distribution of the microstructure and the higher in situ strength associated to thin plies are the prime causes of the higher plain compression strength over the other ply grades. Despite H-75 having higher pristine compression strength over thick plies, the considerable decrease in CAI strength for the thin plies shows the greater influence fibre damage has over delaminations on this property. H-134 showcased an intermediate response, with reduced delamination when compared to H-268 and reduced fibre splitting as compared to H-75, thereby providing a balance in between the two damage modes.

4.2. Effect of ply hybridization

As discussed above, fibre failure is clearly linked to the loss of CAI strength. Thicker 0° plies were inserted among thin plies in an attempt to alleviate the amount of fibre damage by dissipating impact energy through matrix cracks and delamination. As expected, a balance between delamination and fibre damage was seen in the results of hybrid laminates, (Figs. 5 and 6).

The disposition of thin plies surrounding the thick 0° plies improved the CAI strength of the hybrid laminate H-75-H2. The thick 0° plies act

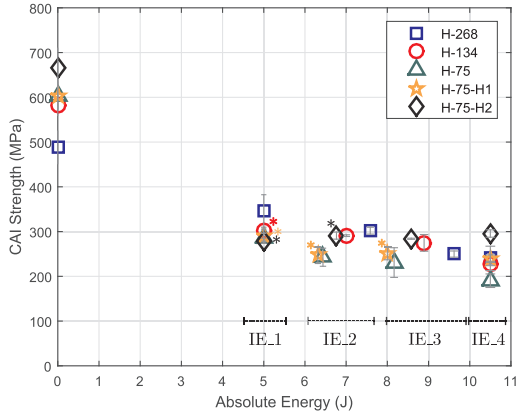

(a)

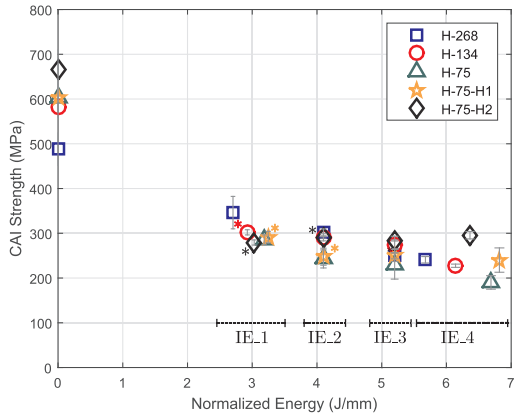

(b)

*CAI failure at the specimen top due to local buckling

Fig. 9. Plain compression strength and CAI strength of all the laminates presented against (a) absolute energies and (b) normalized energies. Average value is presented along with the standard deviation indicated by grey vertical markers. (For interpretation of the references to colour in this figure legend, the reader is referred to the web version of this article.)

as the main load bearing plies during the compression loading [19], and the surrounding thin plies help to constrain the buckling of the thick plies [20]. In addition, thin plies perform better than standard and thick plies under compression loading [7]. The hybridization has helped to reduce the fibre breakage associated with the thin plies by introducing thicker plies in the laminate.

Apart from the thick plies helping to reduce the magnitude of fibre damage, they also impose a dominant delamination at their adjacent interfaces, as seen for IE_3 and IE_4 in H-75-H2 (interface No. 11: $(45°/0°_{268})$). The thick ply introduces higher bending stiffness mismatch within the laminate which leads to high interlaminar shear stresses at the interface of the inserted thick ply [22]. Delaminations close to mid plane are reported to be more resistant to compressive loading compared to the surface delaminations [29,30] due to the higher stiffness provided by the close-to-equally split sub-laminates. Further, the longitudinal orientation of the dominant delamination is also a reason for the increased CAI strength of H-75-H2 [31].

4.3. Compression after impact: Failure mode issues

As CAI strength is one of the decisive parameters in choosing one laminate over another, the issue of invalid CAI failure mode associated with thin laminates (as also reported in [32]) needs to be discussed. At low impact energies, many laminates failed due to local buckling at the open window of the anti-buckling fixture (see Fig. 10) [25], providing a critical buckling strength of the thin laminate, which is lower than the real laminate CAI strength for that particular impact energy. We evidenced no sign of extension in the impact damage in the post CAI C-scan inspection for those laminates which failed at the top. In this aspect, the CAI strength values obtained from the invalid failure modes are independent of impact energy and impact damage, as evidenced in Fig. 9. Within the framework of thin structures, it is evident that at low impact energies, local buckling is critical and more prone to cause final collapse than impact damage does. In the long run, research on thin laminates needs to resolve the issue of not being able to extract the real CAI strength. Furthermore, as a future work, it can be meaningful to access the residual strength reduction through tension after impact (TAI) tests for thin laminates where fibre failure is the dominant damage mode.

4.4. Effect of laminate thickness on damage mode

With a decrease in laminate thickness, a change in dominant damage mode from delamination to fibre failure was observed. Thin structures undergo large bending when impacted, which leads to high in-plane tensile stresses at the non-impacted side. This is the source of back fibre splitting; as found for all the laminates. This extensive fibre failure adversely affected both damage resistance and tolerance; as displayed by the thin plies in this study. In contrast to the thick laminates where delamination damage is critical, with the thin laminates delamination indirectly helped to reduce the magnitude of fibre failure as evidenced with the hybrid laminates.

In the laminates of standard thickness, the projected damage area is considered to correlate well the damage resistance with the damage tolerance of a specimen [33]. Fig. 13 compares the relation between the projected damage area obtained from the C-scan inspection and the CAI strength. Even though H-268 showed twice the projected damage area compared to the other laminates for all impact energies, it exhibited better CAI strength than most of the other laminates (Fig. 13). This differs from the trend reported by [33] for thick laminates, where an increase in the damage area linearly reduced the CAI strength. It is clear that with the thin laminates, the damage area can be a misguiding parameter with which to assess damage resistance and damage tolerance.

The damage tolerance design approach aims to assure that the structure has enough strength to continue in service until the damage is detected by a scheduled inspection. There is a high probability that a permanent indentation of 0.25 to 0.5 mm can be detected during the inspections [34]. In the current study, thin ply laminate H-75 exhibited dent depth higher than 0.25 mm from IE_2, whereas for the other laminates the BVID threshold was between IE_3 and IE_4. It is to be noted that, for the impact energy IE_3, the laminates failed at 50% of its pristine strength despite showing no signs of BVID damage (except H-75). This reduction in compressive strength not accompanied with detectable damage is a troubling fact in terms of the damage tolerance concept.

5. Conclusion

We performed an experimental campaign to study the effect of ply thickness on the impact and post impact responses of thin laminates

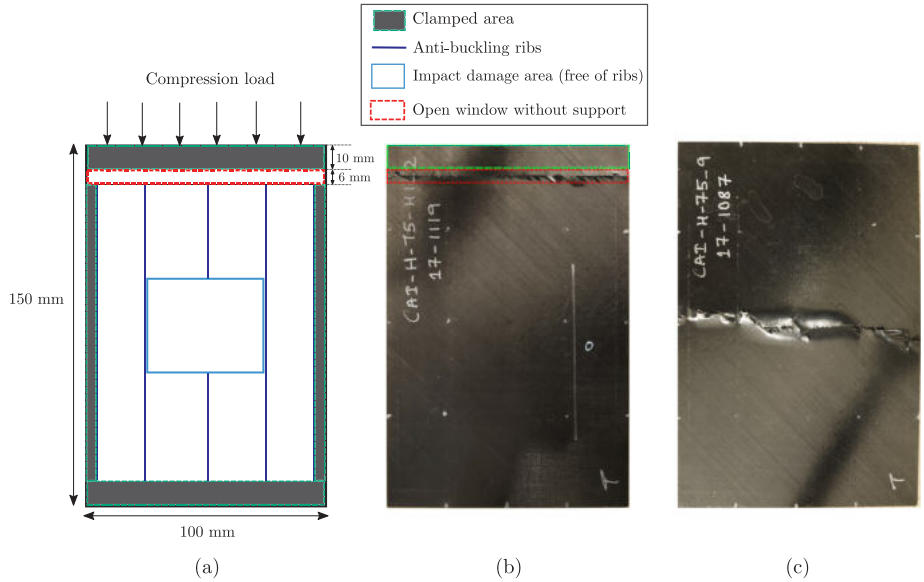

Fig. 10. (a) Schematic illustration of the CAI fixture with anti-buckling ribs; (b) Invalid CAI failure at the centre of the unconstrained window at the top of the specimen; (c) Valid CAI failure at the specimen centre at the impacted site. (For interpretation of the references to colour in this figure legend, the reader is referred to the web version of this article.)

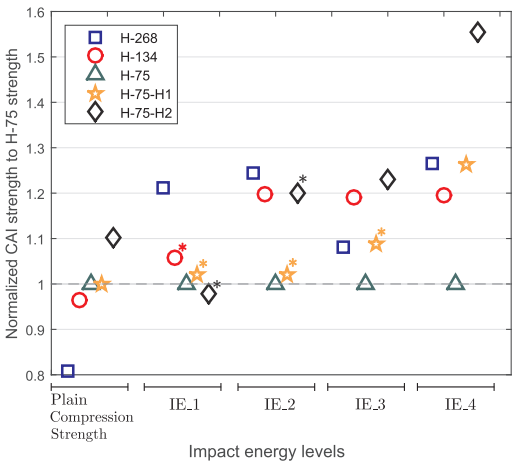

*CAI failure at the specimen top due to local buckling

Fig. 11. Comparison of CAI strengths normalized with thin plies (H-75) as baseline. The plain compression strengths are also normalized with respect to the baseline H-75. (Note that in the horizontal axis, the different compression values are grouped into impact energy levels, and hence the horizontal axis does not have any quantitative significance). (For interpretation of the references to colour in this figure legend, the reader is referred to the web version of this article.)

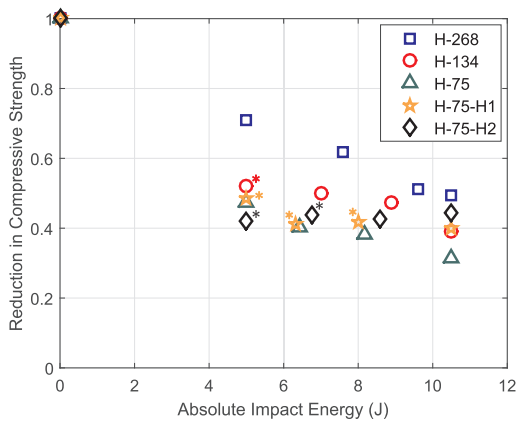

*CAI failure at the specimen top due to local buckling

Fig. 12. Normalized reduction in the compressive strength due to the impact damage of all the laminates. (For interpretation of the references to colour in this figure legend, the reader is referred to the web version of this article.)

(thicknesses ranging from 1.5 to 1.8 mm). Additionally, we proposed and tested two hybrid laminates where thick or standard 0° plies were mixed with thin plies. Unlike research reports for thick laminates, where thin plies provided higher CAI strength, thin laminates made with thin plies showcased the least CAI strength compared to other ply grades. Thin plies exhibited extensive fibre breakage accompanied by large dent depth and dissipated energy. The idea of ply hybridization, in an attempt to obtain a balance between the delamination damage and fibre failure by mixing thick and thin plies, provided an average increase in CAI strength of 40% over the baseline thin ply laminate. Further issues of thin laminates with improper failure modes during CAI testing were discussed. The non-dependence of the projected damage area on the CAI strength of the thin laminates was also observed. Finally, ply hybridization appears to be a promising economic prospective in the quest to improve the CAI strength of thin laminates.

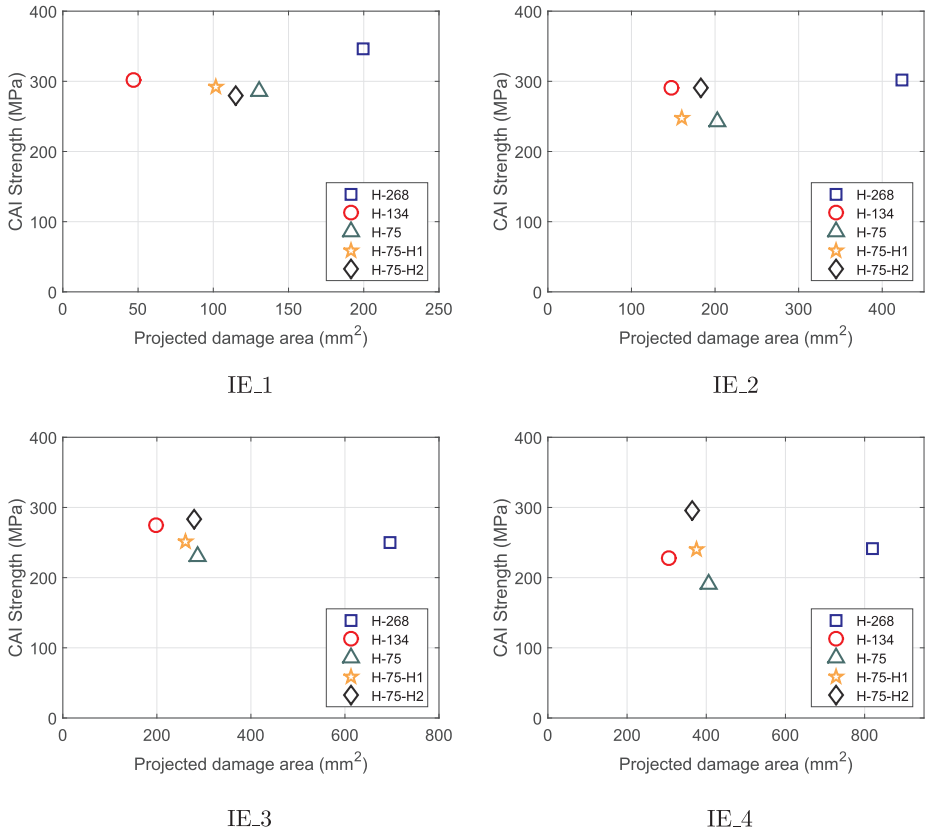

Fig. 13. Comparing the relation between CAI strength and the projected damage area of all laminates for all the impact energies. (For interpretation of the references to colour in this figure legend, the reader is referred to the web version of this article.)

Acknowledgements

The first author would like to thank the Generalitat de Catalunya for the FI-DGR pre-doctoral grant (2017 FI-B1 00089). The authors would like to thank the *Spanish Ministerio de Economía y Competitividad* for the grant coded MAT2015-69491-C3-1-R, supported by FEDER/EU. The study is a part of an extensive project funded by Airbus, partnered by the AMADE research laboratory (University of Girona), INEGI (University of Porto), and the University of Dayton Research Group. The authors would also like to thank Hexcel® for providing the material for the experimental campaign, and University of Dayton Research Institute (UDRI), USA, for manufacturing the specimens. Special thanks to Prof. Pedro Camanho and his team from the INEGI group for their research support and also for sharing the plain compression strength results.

Appendix A. Supplementary material

Supplementary data associated with this article can be found, in the online version, at https://doi.org/10.1016/j.compositesa.2019.03.022.

References

[1] Abrate S. Impact on composite structures. Cambridge University Press; 2005.
[2] ASTM D7136/D7136-15. Standard test method for measuring the damage resistance of a fiber reinforced polymer matrix composite to a drop weight impact event, 2015.
[3] Yokozeki T, Aoki Y, Ogasawara T. Experimental characterization of strength and damage resistance properties of thin-ply carbon fiber/toughened epoxy laminates. Compos Struct 2008;82(3):382–9.
[4] Sihn S, Kim RY, Kawabe K, Tsai SW. Experimental studies of thin-ply laminated composites. Compos Sci Technol 2007;67(6):996–1008.
[5] Saito H, Morita M, Kawabe K, Kanesaki M, Takeuchi H, Tanaka M, et al. Effect of ply-thickness on impact damage morphology in CFRP laminates. J Reinf Plast Compos 2011;30(13):1097–106.
[6] Guillamet G, Turon A, Costa J, Renart J, Linde P, Mayugo J. Damage occurrence at edges of non-crimp-fabric thin-ply laminates under off-axis uniaxial loading. Compos Sci Technol 2014;98:44–50.
[7] Amacher R, Cugnoni J, Botsis J, Sorensen L, Smith W, Dransfeld C. Thin ply composites: experimental characterization and modeling of size-effects. Compos Sci Technol 2014;101:121–32.
[8] Arteiro A, Catalanotti G, Xavier J, Camanho P. Notched response of non-crimp fabric thin-ply laminates. Compos Sci Technol 2013;79:97–114.
[9] García-Rodríguez S, Costa J, Singery V, Boada I, Mayugo J. A 3D tomographic investigation to elucidate the low-velocity impact resistance and tolerance of thin non-crimp fabric laminates: effect of ply-thickness. Compos Part A: Appl Sci Manuf 2018;113:53–65.
[10] Sánchez-Sáez S, Barbero E, Zaera R, Navarro C. Compression after impact of thin composite laminates. Compos Sci Technol 2005;65(13):1911–9.
[11] Sebaey T, González E, Lopes C, Blanco N, Costa J. Damage resistance and damage tolerance of dispersed CFRP laminates: Effect of ply clustering. Compos Struct 2013;106:96–103.
[12] Lopes C, Seresta O, Coquet Y, Gürdal Z, Camanho P, Thuis B. Low-velocity impact damage on dispersed stacking sequence laminates. Part I: Experiments. Compos Sci Technol 2009;69(7-8):926–36.
[13] Liv Y, Guillamet G, Costa J, González E, Marín L, Mayugo J. Experimental study into compression after impact strength of laminates with conventional and non-conventional ply orientations. Compos Part B: Eng 2017;126:133–42.

[14] Sasikumar A, Costa J, Trias D, González EV, García-Rodríguez S, Maimí P. Unsymmetrical stacking sequences as a novel approach to tailor damage resistance under out-of-plane impact loading. Compos Sci Technol 2019;173:125–35.
[15] Bull D, Scott A, Spearing S, Sinclair I. The influence of toughening-particles in CFRPS on low velocity impact damage resistance performance. Compos Part A: Appl Sci Manuf 2014;58:47–55.
[16] García-Rodríguez S, Costa J, Singery V, Boada I, Mayugo J. The effect interleaving has on thin-ply non-crimp fabric laminate impact response: X-ray tomography investigation. Compos Part A: Appl Sci Manuf 2018;107:409–20.
[17] Wong DW, Zhang H, Bilotti E, Peijs T. Interlaminar toughening of woven fabric carbon/epoxy composite laminates using hybrid aramid/phenoxy interleaves. Compos Part A: Appl Sci Manuf 2017;101:151–9.
[18] Furtado C, Arteiro A, Catalanotti G, Xavier J, Camanho P. Selective ply-level hybridisation for improved notched response of composite laminates. Compos Struct 2016;145:1–14.
[19] Arteiro A, Catalanotti G, Xavier J, Linde P, Camanho P. A strategy to improve the structural performance of non-crimp fabric thin-ply laminates. Compos Struct 2018;188:438–49.
[20] Sebaey T, Mahdi E. Using thin-plies to improve the damage resistance and tolerance of aeronautical CFRP composites. Compos Part A: Appl Sci Manuf 2016;86:31–8.
[21] Olsson R. Closed form prediction of peak load and delamination onset under small mass impact. Compos Struct 2003;59(3):341–9.
[22] González E, Maimí P, Camanho P, Lopes C, Blanco N. Effects of ply clustering in laminated composite plates under low-velocity impact loading. Compos Sci Technol 2011;71(6):805–17.
[23] ASTM D6484/D6484M-09. Standard test method for open-hole compressive strength of polymer matrix composite laminates, 2009.
[24] ASTM D7137/D7137-15. Standard test method for compressive residual strength properties of damaged polymer matrix composite plates, 2015.
[25] Remacha M, Sánchez-Sáez S, López-Romano B, Barbero E. A new device for determining the compression after impact strength in thin laminates. Compos Struct 2015;127:99–107.
[26] Lee J, Soutis C. Prediction of impact-induced fibre damage in circular composite plates. Appl Compos Mater 2005;12(2):109–31.
[27] Wagih A, Maimí P, Blanco N, Costa J. A quasi-static indentation test to elucidate the sequence of damage events in low velocity impacts on composite laminates. Compos Part A: Appl Sci Manuf 2016;82:180–9.
[28] Abir M, Tay T, Ridha M, Lee H. On the relationship between failure mechanism and compression after impact (CAI) strength in composites. Compos Struct 2017;182:242–50.
[29] Aslan Z, Daricik F. Effects of multiple delaminations on the compressive, tensile, flexural, and buckling behaviour of E-glass/epoxy composites. Compos Part B: Eng 2016;100:186–96.
[30] Liv Y. A contribution to the understanding of compression after impact of composite laminates, PhD thesis, University of Girona; 2017.
[31] Aktaş M, Karakuzu R, Arman Y. Compression-after impact behavior of laminated composite plates subjected to low velocity impact in high temperatures. Compos Struct 2009;89(1):77–82.
[32] Ghelli D, Minak G. Low velocity impact and compression after impact tests on thin carbon/epoxy laminates. Compos Part B: Eng 2011;42(7):2067–79.
[33] Sun X, Hallett S. Failure mechanisms and damage evolution of laminated composites under compression after impact (CAI): Experimental and numerical study. Compos Part A: Appl Sci Manuf 2018;104:41–59.
[34] Sasikumar A, Trias D, Costa J, Blanco N, Orr J, Linde P. Impact and compression after impact response in thin laminates of spread-tow woven and non-crimp fabrics. Compos Struct 2019;215:432–45.

A.4 Paper D

Impact and compression after impact response in thin laminates of spread-tow woven and non-crimp fabrics

A. Sasikumar[a,*], D. Trias[a,1], J. Costa[a,*], N. Blanco[a], J. Orr[b], P. Linde[c,d]

[a] AMADE, Polytechnic School, Universitat de Girona, Campus Montilivi s/n, E-17003 Girona, Spain

[b] University of Dayton Research Institute, 300 College Park, Dayton, OH, USA

[c] Airbus Operations GmbH, Kreetslag 10, 21129 Hamburg, Germany

[d] Department of Industrial and Materials Science, Chalmers University of Technology, S-41296 Gothenburg, Sweden

[*] Corresponding author

[1] Serra Hunter Fellow

The paper has been published in *Composite Structures* 215 (2019) 432–445.

Composite Structures 215 (2019) 432–445

Contents lists available at ScienceDirect

Composite Structures

journal homepage: www.elsevier.com/locate/compstruct

Impact and compression after impact response in thin laminates of spread-tow woven and non-crimp fabrics

A. Sasikumar[a,*], D. Trias[a,1], J. Costa[a,*], N. Blanco[a], J. Orr[b], P. Linde[c,d]

[a] AMADE, Polytechnic School, University of Girona, Campus Montilivi s/n, 17073 Girona, Spain
[b] University of Dayton Research Institute, 300 College Park, Dayton, OH, USA
[c] Airbus Operations GmbH, Kreetslag 10, 21129 Hamburg, Germany
[d] Department of Industrial and Materials Science, Chalmers University of Technology, S-41296 Gothenburg, Sweden

ARTICLE INFO

Keywords:
Non-crimp fabrics
Woven fabrics
Impact behaviour
Damage tolerance
Thin laminates

ABSTRACT

Recent research has been devoted to thin laminates as a result of aeronautic industries shifting to thinner and lighter structures. In an attempt to improve the out-of-plane response and reduce manufacturing costs considerably, airplane manufacturers are exploring (apart from unidirectional tapes) textile fabrics of different fabric architectures. Within the framework of thin laminates, this paper investigates the impact and compression after impact (CAI) of two types of aerospace graded spread-tow fabrics, namely non-crimp fabrics and woven fabrics, where stitching and weaving, respectively, govern the architecture. The study also comprises two different ply thicknesses (thin and intermediate ply grades) for both fabrics. Experimental results reveal that while woven fabrics display higher damage resistance, non-crimp fabrics ensure higher damage tolerance. The intermediate ply grade performed better than thin plies in terms of damage resistance and CAI strength for both fabrics, as thin ply non-crimp fabric laminates exhibited early and extensive fibre damage.

1. Introduction

In an attempt to go even lighter, aircraft industries are now considering how to reduce the thickness of many aircraft parts, such as wing and fuselage skins, to less than 2 mm. The threat posed by low velocity impact loads on these thin structures, accompanied by the change in the stress states and damage modes could be critical when compared to standard thick laminates [1,2].

In the quest to improve the out-of-plane response, many concepts such as laminate design [3–5], interleaving [6], ply hybridization [2,7], and the use of textile fabric composites have been explored [8]. Textile fabrics differ from uni-directional (UD) tapes in that the fibre tows are either woven, knitted, braided or stitched together in an attempt to enhance the mechanical performance and/or economic feasibility. Along with the efforts to reduce the structural weight of aircraft, the aeronautic industry is also working on cutting back manufacturing costs and, as such, fabric composites have been an excellent substitute for UD tapes, thanks to their faster deposition rates and reduced labour time [9].

Out of the different reinforcement architectures, non-crimp fabrics (where UD layers are stitched) and woven fabrics (where UD tows are woven) have gained increasing attention in aerospace industries, mainly due to the improvement they offer over UD tapes in terms of higher interlaminar strength, better out-of-plane response and a considerable reduction in manufacturing costs [9,10]. As textile composites have evolved, standard ply grade woven fabrics provided a substitute for UD prepreg tapes, with their main advantage being the increased toughness from the woven architecture and the reduced manufacturing costs related to the faster lay-up. Nevertheless, these same fabrics caused a reduction in in-plane properties as a result of their wavy fibres [11], thus non-crimp fabrics provided the solution. In non-crimp fabrics, the UD layers are stitched, therefore not only eliminating the problem of waviness, but also offering the economic feasibility of faster lay-up. Despite this, non-crimp fabrics exhibited local resin rich areas and fibre waviness around the stitch that impaired the compressive properties [12]. Another step forward was to employ thin plies (using spread tow technology) with woven fabrics which considerably reduces the waviness and the magnitude of resin rich areas [13]. Despite the advances in textile composites, not many studies report on the effect the architecture of the fabric has on impact and post-impact responses, especially when used with thin laminates.

Vallons et al. [14] compared the interlaminar fracture toughness

* Corresponding authors.
E-mail addresses: aravind.sasikumar@udg.edu (A. Sasikumar), josep.costa@udg.edu (J. Costa).
[1] Serra Hunter Fellow.

https://doi.org/10.1016/j.compstruct.2019.02.054
Received 16 November 2018; Received in revised form 16 January 2019; Accepted 15 February 2019
Available online 19 February 2019

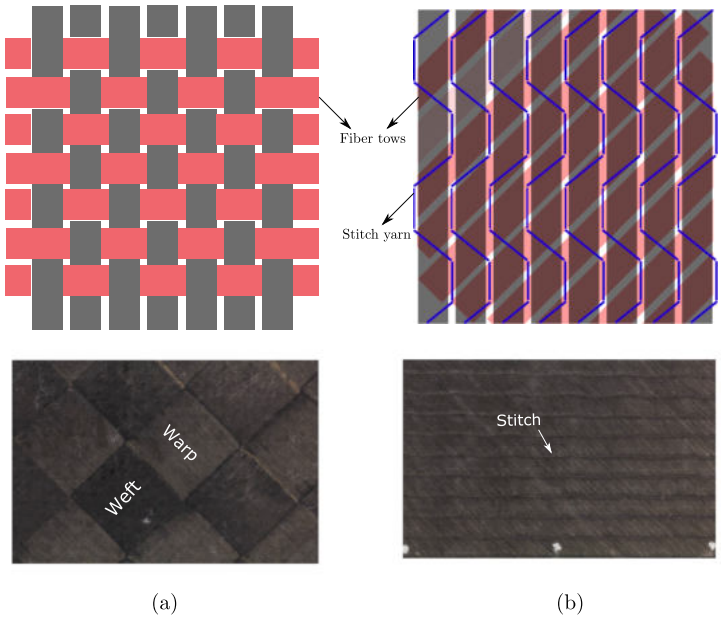

Fig. 1. 2D planar illustration of the fabrics and their architecture (a) Woven fabrics (WF) with plain weave (b) Non-crimp fabrics (NCF) with plies stitched together using a polyester yarn.

and impact damage resistance of carbon non-crimp fabrics and twill weave composite fabrics. The study employed different ply grade thicknesses (270 gsm for non-crimp fabrics and 190 gsm for woven) with (on average) 2.1 mm thick laminates. The woven fabrics exhibited higher fracture toughness and higher damage resistance compared to the non-crimp fabrics. Sanchez et al. [15] worked with thin laminates and compared the compression after impact (CAI) strength of woven fabrics with that of quasi-isotropic UD plies (both made out of thick plies) for laminate thicknesses ranging between 1.6 and 2.2 mm. Results evidenced that, compared to UD tapes, woven fabrics have a higher CAI strength, resulting from the increased interlaminar fracture toughness of woven fabrics. It is worth noting that both of these studies used non-standard specimen dimensions.

In the case of out-of-plane loading, thin plies have exhibited higher damage resistance and CAI strength, when used with thick laminates [16,17]. Arteiro et al. [13] conducted an extensive experimental campaign to study the effect of spread tow fabric thickness on various structural properties. Thin woven fabrics, when compared with thick woven fabrics, exhibited a higher unnotched compression strength, an improved in-plane shear response and exhibited higher compressive resistance in off-axis compression tests. Similarly [18–20] with non-crimp fabrics, studies demonstrated the higher damage capability thin fabric plies have over thick ones in terms of structural performance. Meanwhile, Garcia et al. [21] studied the effect fabric thickness has on impact and CAI strength using non-crimp fabrics and demonstrating the sequence of failure events. Thin and standard ply grades were used with 2.15 mm laminates, and thin plies were reported to exhibit lower load carrying capability and lower CAI strength for a 14 J maximum impact energy level.

This paper is the result of a research project led by Airbus, in collaboration with the research centres INEGI (University of Porto, Portugal), UDRI (University of Dayton Research Institute, USA) and AMADE (University of Girona, Spain). We performed an experimental campaign on thin laminates using two types of aerospace grade fabrics, namely woven fabrics and non-crimp fabrics. In order to determine only the effect of the reinforcement architecture, both fabrics used in the study were made using the same fibre-resin material system. Additionally, for each fabric type we considered two different ply grades: thin and intermediate. Hence, this study reports the effects fabric architecture and ply thickness have on the impact and CAI response of thin composite laminates. The experimental campaign included impact and CAI tests to evaluate damage resistance and tolerance. Quasi-static indentation tests followed by C-scan damage inspection were also performed to study and compare the sequence of damage events.

2. Experimental methods

2.1. Material, fabric architecture and laminates

Two types of fabrics, namely spread-tow woven fabrics (WF) and spread-tow non-crimp fabrics (NCF), were processed at the University of Dayton Research Institute (UDRI) using carbon fibre T700 pre-impregnated with HexPly® M21 resin. Note that, to provide a proper comparison between the two types of fabrics, both fabrics were made using the same fibre-resin material system. WF are produced using a plain weave textile process where the weft fibre tows go over and under the warp tows, resulting in an interlaced woven fabric. Plain weave represents the weaving pattern where the weft tows cross over the warp tows continuously. While WF use weaving as the form of fabric architecture, NCF utilize a secondary stitching yarn that holds the fibre tows of different orientations together, forming a blanket. A bi-angle NCF is used in this study where two differently oriented fibre tows are stacked together like UD plies, and stitched together using a polyester yarn. Note that the sole purpose of the stitch is to permit a faster layup and is not intended to take structural loads.

Fig. 1 presents a schematic projected representation of both types of fabrics and also the macro photos of the fabric laminates used in this

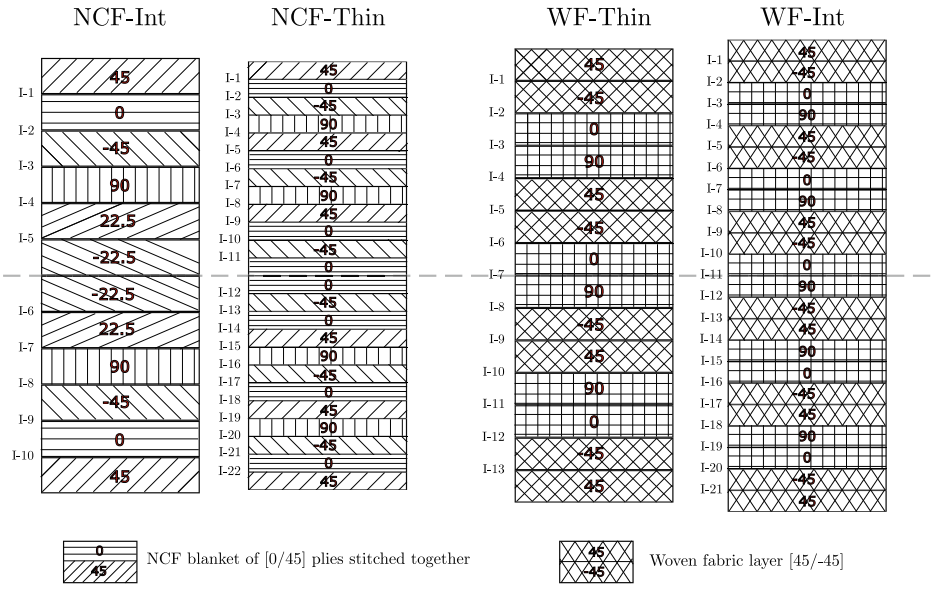

Fig. 2. Schematic illustration of the laminates and their stacking sequences: Non-crimp fabrics (NCF) and Woven fabrics (WF).

study. We used NCF bi-axial layers of [0°/45°] and [0°/-45°] whereas the WF comes in [0°/90°] fabric layers. Other fabric layer orientations can be obtained through rotation and flipping. Note that the mismatch angle within the fabric layer is 45° and 90° for NCF and WF, respectively.

In regards to the ply thickness study, two different areal weights per fabric layer were used. For NCF these were 268 gsm and 134 gsm and for WF 240 gsm and 160 gsm. As both fabrics are bi-axial, the ply thickness corresponds to half of the fabric tow thickness, namely 0.134 and 0.067 mm for NCF and 0.12 mm and 0.08 mm for WF, accounting for the intermediate and thin ply grades, respectively. From here on, the four laminates used throughout the study will be referred to as NCF-Int, NCF-Thin, WF-Int and WF-Thin. The laminates and their stacking sequences are illustrated in Fig. 2, while Table 1 details the laminates, their stacking sequences, ply and laminate thicknesses. All four laminates are not quasi-isotropic, and NCF-Int utilises non-conventional [22.5°/−22.5°] NCF fabric blankets obtained by rotating the standard blanket layer. Since the study utilizes different fabric materials and different ply thicknesses, the approach followed to obtain similar in-plane and flexural responses in the different laminates consists on pursuing the closest equivalent bending stiffness parameter (D*, proposed by Olsson [22], which is a function of the bending stiffness matrix coefficients) as possible. The D* values of NCF-Int, NCF-Thin, WF-Int and WF-Thin are 18.6, 18.9, 21.5 and 25.9 respectively. (Note that the nominal laminate thickness of woven fabrics is higher than the non-crimp fabrics which resulted in the higher D* values for the woven fabrics.) Fig. 3(a) and (b) present the polar plot of the in-plane and bending stiffness, respectively, for all four laminates.

2.2. Impact energy definition

While both NCF laminates have the same laminate thicknesses, WF-Thin laminates displayed a higher measured laminate thickness compared to WF-Int (1.82 mm over 1.66 mm). However, when impacted at the same absolute impact energy, this might lead to misleading conclusions as a thicker laminate has an advantage over a thinner laminate. To avoid this bias, we defined two absolute and two normalized impact energies, where the normalization was performed with respect to the laminate thickness (as also suggested in ASTMD7136/D7136M-15 standards [23]). The authors are aware that this normalization will not guarantee 100% fair comparison, but still provides a fairer comparison. In total, four impact energies were explored, two absolute energies: 5 J and 10.5 J (referred to as IE_1 and IE_4, respectively) and two normalized energies: 4.1 J/mm and 5.2 J/mm (referred to as IE_2 and IE_3, respectively). Table 2 details the measured laminate thicknesses and the defined absolute and normalized impact energies for all laminates.

2.3. Experimental tests

2.3.1. Impact, quasi-static indentation and damage assessment

In accordance with the ASTMD7136/D7136M-15 standards [23], impact tests were performed on 150 × 100 mm specimens using a CEAST Fractovis Plus instrumented drop-weight tower. The specimens were cut with the 0° fibres aligned with the specimen length. A 16 mm

Table 1
Laminates and their details.

Laminate	Description	Stacking sequence	Fabric grade (g/m^2)	Ply thickness (mm)	Nominal laminate thickness (mm)
NCF-Int	Intermediate plies	$[(45/0)/(-45/90)/(22.5/-22.5)]_S$	268	0.134	1.61
NCF-Thin	Thin plies	$[(45/0)/(-45/90)/(45/0)/(-45/90)/(45/0)/(-45/0)]_S$	134	0.067	1.61
WF-Int	Intermediate plies	$[(45/-45)/(0/90)/(45/-45)/(0/90)]_{S^*}$	240	0.12	1.68
WF-Thin	Thin plies	$[((45/-45)/(0/90))_2/(45/-45)/(0/90)]_{S^*}$	160	0.08	1.76

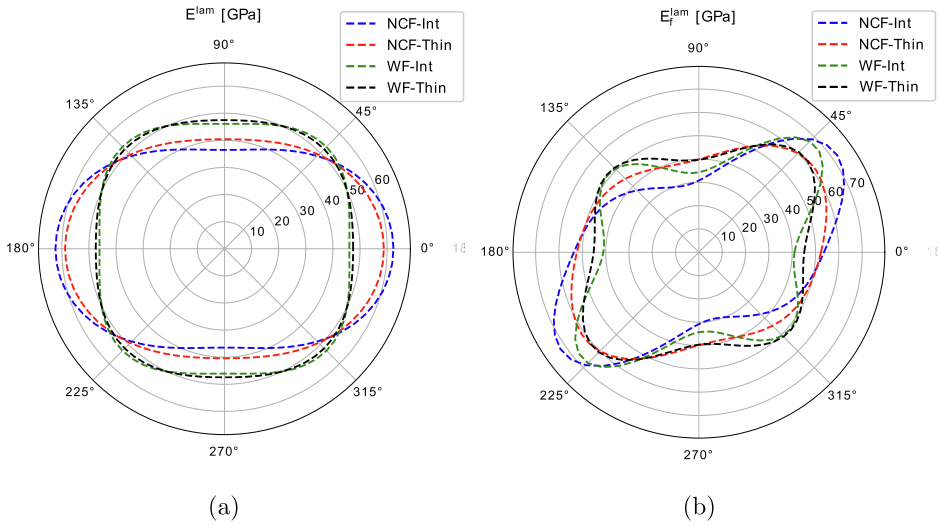

Fig. 3. Polar plot representation of the (a) in-plane stiffness and (b) bending stiffness for all the laminates.

in diameter steel hemispherical indenter was used, and the total mass of the impactor setup was 3 kg. We impacted 12 specimens per laminate, with three specimens for each impact energy in order to assess repeatability. Further details of the experimental impact setup can be found in [24].

Quasi-static indentation (QSI) tests were performed with an MTS INSIGHT® 50 testing machine with a 50 kN load cell and displacement controlled loading of the indenter. The test setup replicates the impact test, where rubber clamps are placed at the four edges supporting the specimen. A 150 × 100 mm specimen was placed on a base plate, with an open window of 125 × 75 mm. A constant indenter displacement rate of 1 mm/min was used throughout the study. When a load drop or acoustic sound emission was noticed, tests were interrupted for C-scan damage inspection, followed by further indentation on the same specimen.

The main objective of QSI tests is to understand the onset and progression of the damage. As NCF-Int and NCF-Thin laminates have the same measured laminate thicknesses, they were tested under the same indenter displacement levels: d = 3, 3.5, 3.95, 4.4, 4.7, 4.9, 5.3 and 6 mm. Initially the displacement levels for NCF-Int were decided arbitrarily, and then the same values were used for NCF-Thin in order to compare the damage sequence. Meanwhile, because of the differences in laminate thicknesses of the WF laminates, different indenter displacement levels were used. While WF-Int was indented at displacements d = 2, 2.5, 3, 4.1, 5.6, 6.4 and 7 mm, WF-Thin was indented at d = 2.5, 3.1, 4.1, 4.6, 5.1, 5.9 and 6.25 mm. Pulse-echo ultrasonic C-scan was used to inspect the damage from the impact and QSI tests. All the impacted and indented specimens after each indenter loading were inspected. C-scan inspection featured an OLYMPUS OMNI MX system and the specimens were placed in a pool of water while an automated robotic arm scanned them with a 5 MHz piezoelectric probe.

2.3.2. Plain strength compression and compression after impact

Prior to compression after impact, plain compression strength of all the laminates was determined following the ASTMD6484/D6484M-14 standard [25]. Plain compression tests were performed on three 305 mm × 30 mm specimens for each laminate at the INEGI research facility at the University of Porto. The interested reader can refer to [26] for more detailed information of the test setup.

Further, CAI tests were performed using an MTS INSIGHT®300 machine with a 300 kN load cell, following ASTMD7317/D7137M-15 [27]. As thin laminates were reported to fail under structural global buckling rather than a compressive failure [28], we used a non-standard anti-buckling CAI device as proposed by Remacha et al. [29]. This fixture ensures a proper compressive failure at the specimen centre induced by the existing impact damage. All the above-mentioned tests, except plain strength compression, were performed at the AMADE research laboratory at the University of Girona, which is NADCAP certified for non-metallic materials testing.

3. Experimental Results

3.1. Impact response

Figs. 4–6 present the force-time, force-deflection, and energy-time impact curves, respectively, for all the laminates. While three specimens for each laminate and for each impact energy level were tested, because of the good repeatability in the responses, only one specimen

Table 2
Laminates and the defined impact energies.

Laminate	Measured laminate thickness (mm)	Impact Energy 1: IE_1		Impact Energy 2: IE_2		Impact Energy 3: IE_3		Impact Energy 4: IE_4	
		Abs (J)	Norm (J/mm)	Abs (J)	Norm (J/mm)	Abs (J)	Norm (J/mm)	Abs (J)	Norm (J/mm)
NCF-Int	1.57	5	3.2	6.4	4.1	8.2	5.2	10.5	6.7
NCF-Thin	1.58	5	3.2	6.5	4.1	8.3	5.2	10.5	6.6
WF-Int	1.66	5	3	6.8	4.1	8.7	5.2	10.5	6.3
WF-Thin	1.82	5	2.7	7.5	4.1	9.5	5.2	10.5	5.8

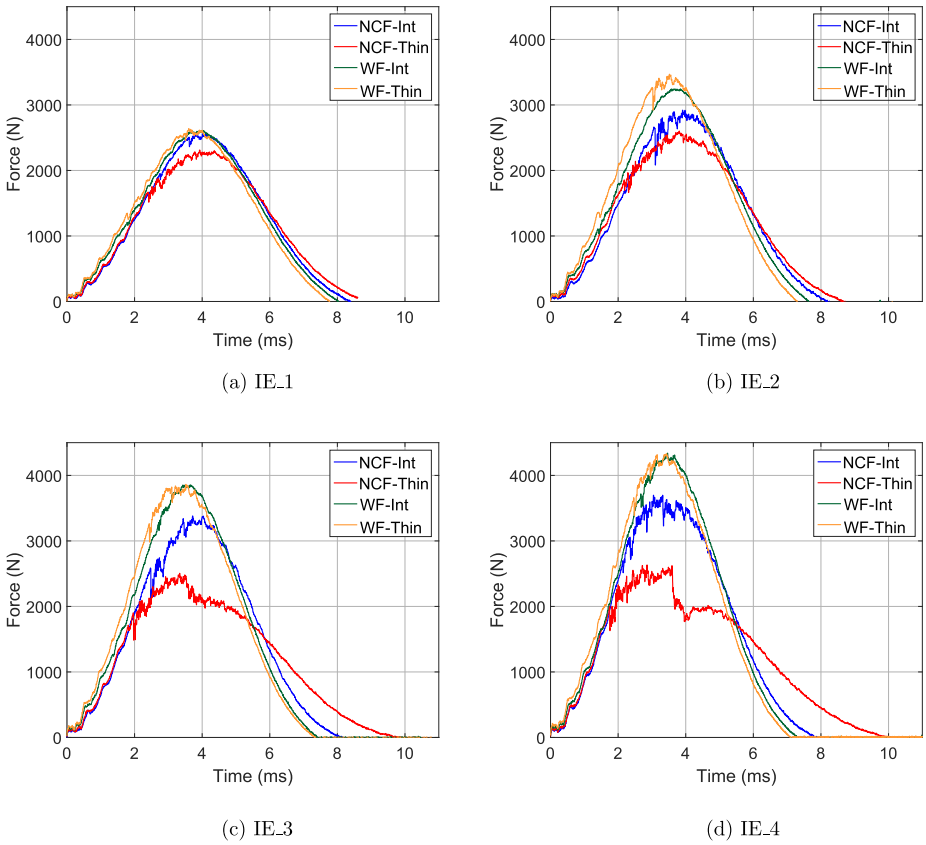

Fig. 4. Force-time responses of all the laminates for all the impact energies.

per laminate has been presented in the impact curves. As the impact energies increase, NCF laminates lost their load carrying capacity compared to WF laminates, as evidenced by the reduced peak load (Figs. 4 and 5). Both NCF laminates exhibited significant load drops at the peak loads, which was more pronounced in NCF-Thin, associated to fibre failure. Unlike the other three laminates, NCF-Thin displayed longer response times (Fig. 4) and larger laminate bending (Fig. 5). Both WF laminates exhibited similar impact responses, except that WF-Thin displayed slight load drops for higher impact energies compared to WF-Int, which are associated with the initiation of fibre failure. NCF-Int performed better than NCF-Thin in terms of the peak load. In view of these comparisons, it is important to keep in mind that the in-plane and bending responses of the laminates are not exactly the same, owing to the different stacking sequence designs. Of all the laminates, NCF-Thin and WF-Int exhibited the highest and lowest energy dissipation, respectively (see Fig. 6). For all the impact energies, WF laminates dissipated much less energy compared to NCF laminates. For both types of fabrics, intermediate ply grades exhibited better damage resistance than thin plies (more pronounced for the NCF laminates), in terms of reduced energy dissipation and increased load carrying capability.

Fig. 7 shows the projected impact damage profile of all the laminates for all the impact energies obtained from the C-scan inspection. For all the impact energies except IE_1, NCF-Int exhibited a reduced projected damage area compared to its thin ply counterpart NCF-Thin. Dominant delaminations were identified for NCF-Int at interface 6 (-22.5°/22.5°, oriented in the 22.5° direction) and at the last interface (int 10: 0°/45°, oriented in the 45° direction). Note that the interfaces are numbered from the impacted surface with the last interface denoting the interface closest to the non-impacted side, as shown in Fig. 2. For NCF-Thin, a dominant delamination oriented in the 0° direction was identified at interface 10 (−45°/0°) just above the mid-plane. Additionally for higher impact energies, C-scan images of NCF-Thin exhibited permanent indentation, which was not observed in other laminates.

Both WF laminates exhibited a close-to-circular projected delamination profile, as also observed in [30,31] for plain woven fabrics. They showed similar projected damage profiles and areas for the chosen impact energies. WF-Int showed a dominant delamination at interface 9 (−45°/45°) oriented in 45°, whereas WF-Thin exhibited delaminations at various interfaces, making it difficult to pinpoint the dominant ones. Comparatively, WF displayed a much smaller damage area than NCF, and furthermore, while the delamination profile of NCF was controlled by one or two dominant delaminations, WF had several delaminated interfaces contributing to the overall contour.

Fig. 8 displays the photos of the impacted and non-impacted specimen faces from the 10.5 J impact (IE_4). NCF-Thin showed higher permanent dent depth and extensive back fibre splitting compared to intermediate ply grade NCF-Int. By contrast, the WF laminates displayed very little or negligible visible damage as compared to NCF laminates, neither was much visual difference in dent depth and back face

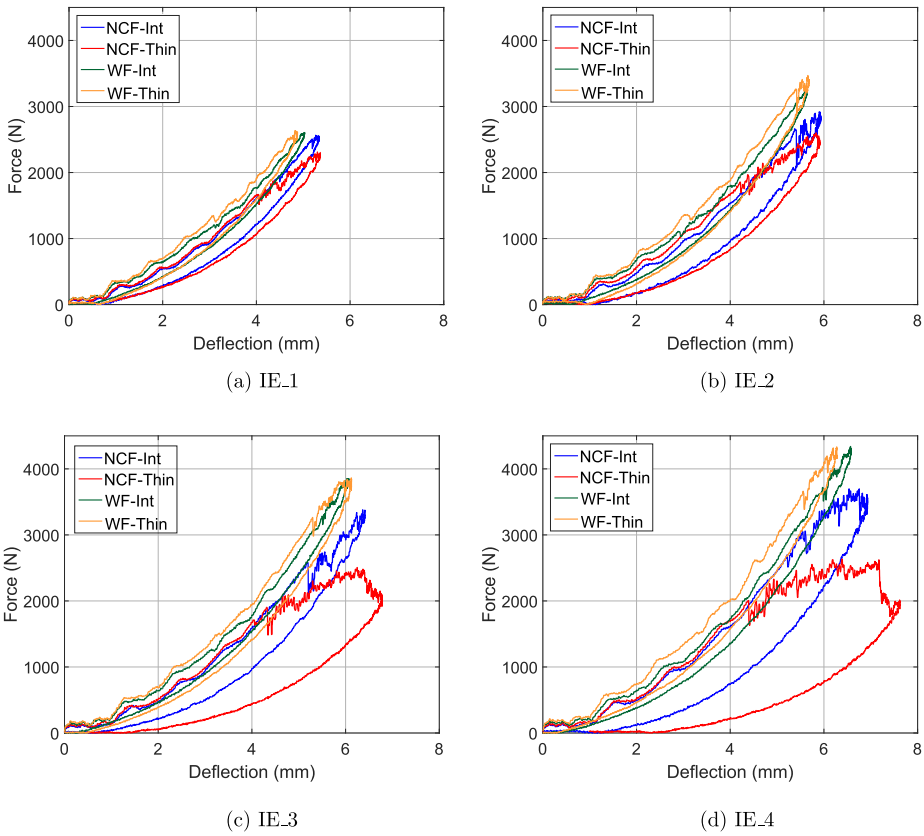

Fig. 5. Force-displacement responses of all the laminates for all the impact energies.

splitting observed between the WF laminates.

Fig. 9(a) and (b) present the evolution of the peak load and projected damage area, respectively, for the increasing absolute impact energies of all the laminates. When compared with NCF-Int, NCF-Thin showed a reduced load carrying capacity, a 13% reduction in peak load for IE_1 and IE_2 and 27% for IE_3 and IE_4. Similarly, NCF-Thin exhibited a 30% increase in the projected impact damage area over NCF-Int for the higher impact energies. WF-Int and WF-Thin roughly exhibited the same peak load and projected damage area, showing the negligible effect that ply thickness has on these damage resistance parameters. Within the two fabric types, WF displayed higher damage resistance over NCF, evidenced by the higher peak load for all impact energies and reduced damage area, especially at the higher impact energies.

Fig. 10(a) and (b) display the dissipated energy and the impact dent depth, respectively, for all the absolute impact energies. At lower impact energies, both NCF laminates exhibited roughly the same dent depth, whereas for higher energies NCF-thin showed twice the dent depth compared to NCF-Int (as can also be seen in Fig. 8). The WF laminates displayed similar dent depth values, and when NCF and WF were compared, woven fabrics clearly exhibited lower dent depth. Both thin-ply fabrics (NCF-Thin and WF-Thin) showed higher energy dissipation compared to their intermediate-ply counterparts. As observed for other parameters, WF laminates exhibit better damage resistance by dissipating less energy than NCF laminates do.

3.2. Quasi-static indentation

Fig. 11 compares the force-deflection response of the maximum applied indenter displacement ($d_8 = 6$ mm) of both NCF laminates. The other displacement levels studied, along with the respective energies applied (E_a), are also marked on the same figure. As observed with the impact results, QSI tests also showed reduced peak load and intermittent load drops with NCF-Thin, where the first visible load drop was observed at $d_3 = 4$ mm, when compared to the delayed first load drop at $d_7 = 5.5$ mm with NCF-Int. The projected damage contours obtained from the interrupted C-scan damage inspection for all the indenter displacement levels of NCF laminates are compared in Fig. 12.

NCF-Thin exhibited delayed damage onset over NCF-Int (as in Fig. 12), where displacement d_1 results exhibited the initiation of delamination damage in NCF-Int (evidenced below the mid-plane at interface 7: $-22.5^{\circ}/22.5^{\circ}$), but there was no presence of damage in NCF-Thin. Displacement level d_2 provided an increase in the delamination area for NCF-Int, with new delaminated interfaces at the top (interface 5: $22.5^{\circ}/-22.5^{\circ}$), meanwhile displacement d_3 marked the onset of delamination damage in NCF-Thin at the last interface ($0^{\circ}/45^{\circ}$). Mild intermittent cracking sounds were heard from NCF-Int in the loading stages starting from d_1, whereas the first acoustic emission for NCF-Thin was noticed at d_3, and was associated with the fibre splitting observed on the back face of the laminate and the first load drop. From displacements d_4 to d_6, the delamination profile scaled up with NCF-Int,

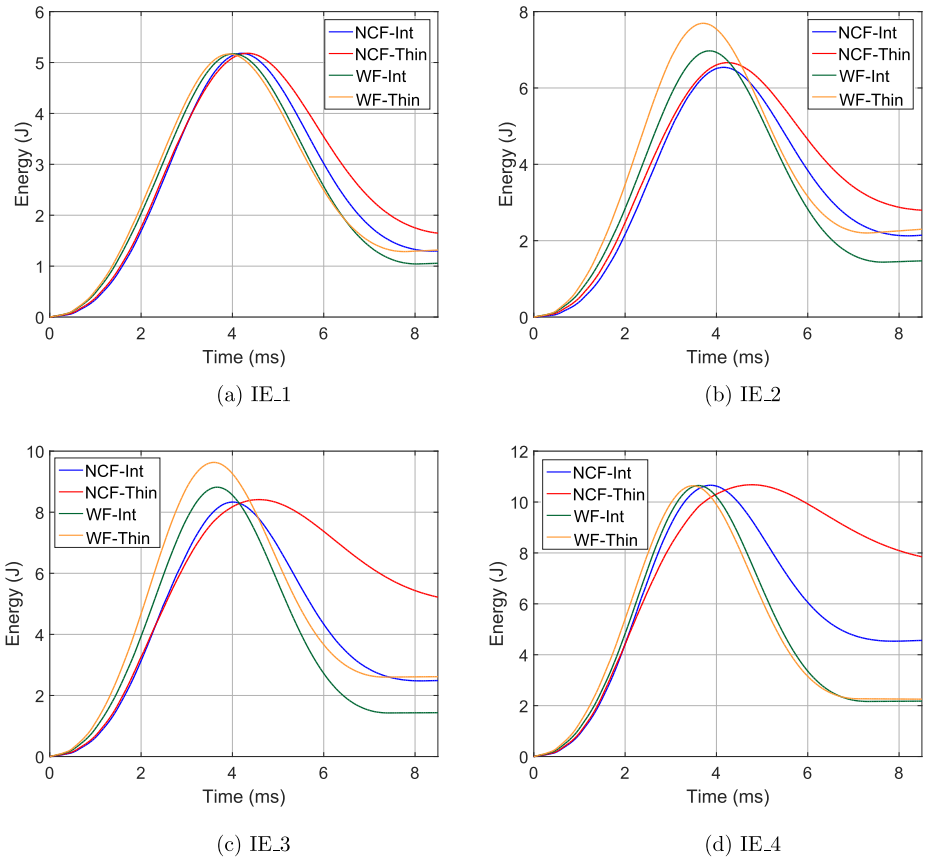

Fig. 6. Impact energy evolution of all the laminates for all the impact energies.

and a dominant delamination oriented in the 0° direction, just above the mid-plane (interface 11; −45°/0°), was observed for NCF-Thin. Displacement d_7 resulted in the back fibre splitting of NCF-Int, evidenced by a load drop, whereas NCF-Thin underwent further fibre failure which induced a higher delamination area when compared to NCF-Int.

Moving on to woven fabrics, Fig. 13 (a) and (b) present the force-deflection response of WF-Int and WF-Thin, respectively, for their maximum applied indenter displacement ($d = 7$ mm for WF-Int and $d = 6.25$ mm for WF-Thin). Note that, unlike the NCF laminates, the WF laminates were indented at different displacement levels, due to their different laminate thicknesses, and hence the sole aim is to study the damage evolution rather than make comparisons. Fig. 13 also presents the other indenter displacements studied and their corresponding applied energies. C-scan inspection images of both WF laminates are presented in Fig. 14 aligned along the different deflection levels in the horizontal axis.

WF-Int displayed no load drop in the force response curve during the loading stages, and the first load drop was seen at the maximum load (between d_6 and d_7). In Fig. 14, no damage was observed for the d_1 displacement, whereas damage initiation was noticed at d_2 in the C-scan images. Delamination initiation was identified at interfaces 5 (45°/−45°), 9 (−45°/45°), 13 (−45°/45°) and all these interfaces correspond to interfaces within the fabric blanket. This could possibly be due to the higher mismatch angle within the fabric blanket. Despite no sign of load drop in the force-displacement curve, C-scan inspection showed that sufficient damage was formed in the laminate. With continued loading, the delamination contour enlarged and new delaminated interfaces appeared. We observed traces of back fibre splitting between displacements d_6 and d_7. The higher capability of standard ply grade woven fabrics to delay or suppress fibre failure is illustrated here, as the first sign of failure was observed at an applied energy, E_a, of 14 J.

In the case of WF-Thin, the first load drop was observed before the maximum load (between d_5 and d_6), and a further larger drop at the maximum peak load. As with NCF-Thin, back fibre splitting was observed at the point of the first load drop. The first sign of delamination (Fig. 14) was observed at displacement d_2, where interfaces 12 (45°/−45°) and 14 (45°/90°), both below the mid-plane, were found to be delaminated. Even though it is not open for direct comparison, it can be seen that WF-Thin delayed the onset of damage and accelerated the onset of fibre failure; something also observed with NCF-Thin. With further loading, new interfaces amounted to the existing delaminations, and the projected damage contours were roughly the same as for WF-Int. Additionally, a good coherence was seen between the results of the impact and QSI tests in terms of projected delamination profile, area and the force level of fibre failure initiation for both types of fabrics.

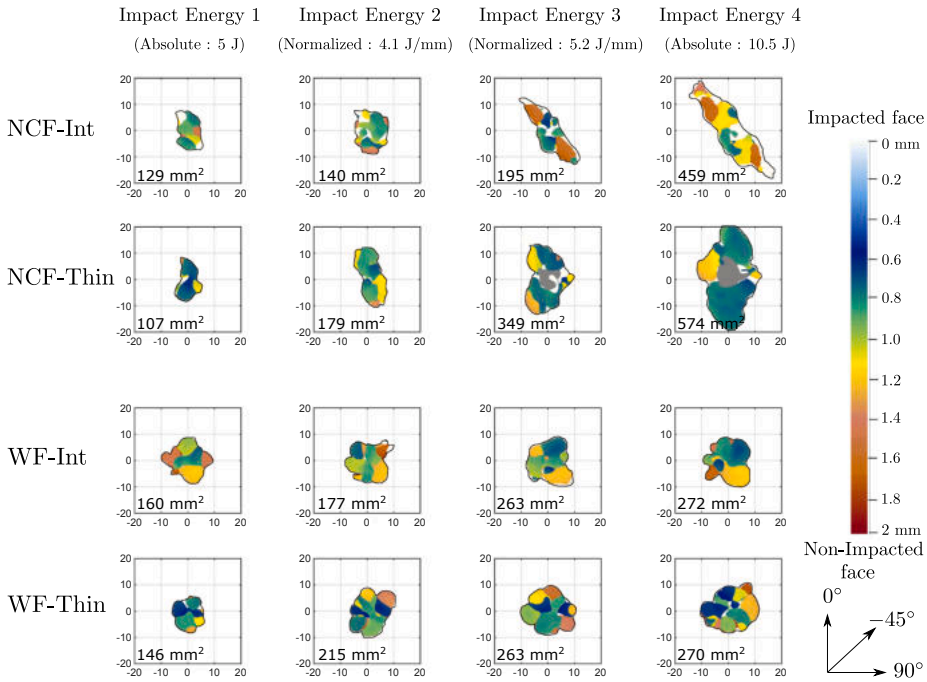

Fig. 7. Projected damage contours and areas obtained from the C-scan damage assessment of all laminates for all impact energies (The average projected damage area is presented with the through-the-thickness colour bar. The field of inspection presented is 40 × 40 mm²).

3.3. Plain compression and compression after impact

Fig. 15(a) and (b) present both pristine compression and compression after impact strength values for all laminates for absolute and normalized impact energies, respectively. The thin plies displayed a better plain compression strength than the intermediate plies: NCF-Thin and WF-Thin displayed 10% and 7% increase over their intermediate grade counterparts. An average increase of 15% in plain compression strength was observed for non-crimp fabrics when compared to woven fabrics (as in Fig. 15).

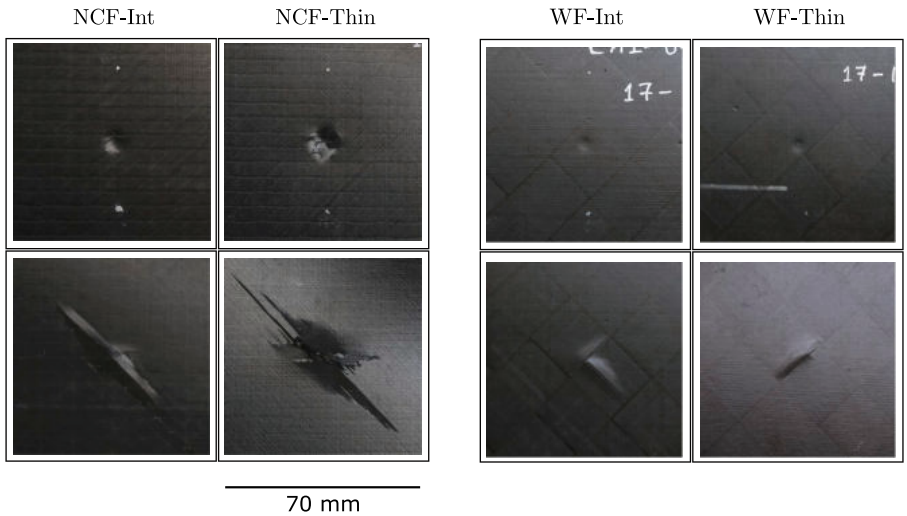

Fig. 8. Photos of the impacted (top) and non-impacted (bottom) faces of NCF and WF laminates from the 10.5 J impact test (Each image represents a square window of 70 × 70 mm referenced from the impact centre).

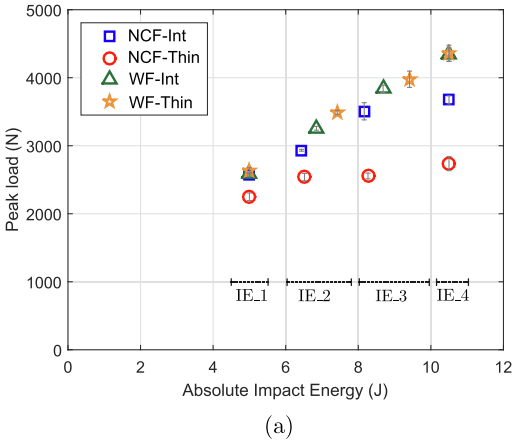

Fig. 9. Impact damage resistance parameters (a) peak load and (b) projected damage area compared between all the laminates for all absolute impact energies (Average value presented along with the standard deviation indicated by the vertical markers).

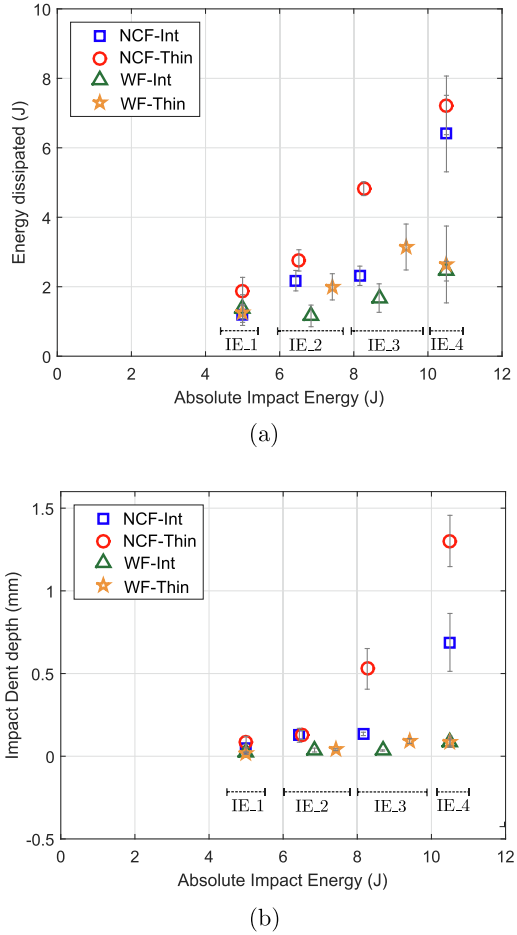

Fig. 10. Impact damage resistance parameters (a) dissipated energy and (b) impact dent depth compared between all the laminates for all absolute impact energies (Average value presented along with the standard deviation indicated by the vertical markers).

Despite the use of an anti-buckling device, improper CAI failure at the specimen top (local buckling at the open top window of the fixture, instead of being at the impacted zone) was observed for laminates impacted at lower impact energies (as also reported in [2,28] for thin laminates). All the laminates impacted at IE_1 and all the laminates impacted at IE_2, except NCF-Int, exhibited CAI failure at the top of the specimen due to local buckling. The laminates and the CAI values corresponding to improper CAI failure are also indicated in Fig. 15.

Plain compression and CAI strength values of all the laminates normalized with respect to NCF-Thin and WF-Thin values are presented in Fig. 16(a) and (b), respectively. Intermediate grade plies showed higher CAI strength than thinner plies did and this was more pronounced for the NCF laminates. NCF-Int showed on average a 20% higher CAI strength than NCF-Thin (see IE_3 and IE_4 in Fig. 16 (a)), while WF-Int exhibited slightly higher CAI strength (9% for IE_3) over WF-Thin (Fig. 16 (b)).

In a more detailed overview from all of the laminates, NCF-Int exhibited improved CAI strength (considering valid CAI values from IE_3 and IE_4 energies). Reviewing IE_3, NCF-Int displayed 20% higher CAI strength than NCF-Thin and WF-Int, and close to 30% higher than WF-Thin. Moving to IE_4, both WF-Int and WF-Thin showed better CAI strength than NCF-Thin, by 10% and 7%, respectively, whereas NCF-Int showed 16% higher CAI strength over its thin ply NCF. In terms of strength retention, NCF-Thin displayed the highest reduction (65%) in residual compression strength induced by the extensive fibre damage from impact (Fig. 17), whereas the WF laminates exhibited a reduction of approximately 50% in compression strength.

4. Discussion

4.1. Impact damage resistance

As evidenced by the experimental results, the woven fabrics exhibited better impact damage resistance than non-crimp fabrics did. The significant load drops reported for the NCF laminates are related to the initiation of fibre failure (see Fig. 5), as was also evidenced in the QSI results. At the same time, the absence of such load drops in the WF

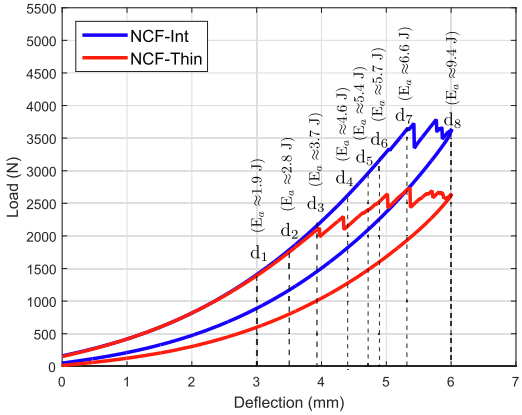

Fig. 11. Load-indenter displacement QSI curve for NCF-Int and NCF-Thin for d = 6 mm (the other displacement levels used in the study are also marked).

laminates suggests the reduced and delayed presence of fibre failure. The significant increase of the impact damage related parameters (Figs. 9 and 10) for NCF over WF also supports the escalation of fibre breakage in NCF at higher impact energy levels. It is important to keep in mind that the thin ply of NCF (67 gsm) is thinner than its WF counterpart (80 gsm), so the effect of the reduced ply thickness is more pronounced.

The higher damage resistance of woven fabrics is associated with their increased interlaminar fracture toughness. As a result of the woven architecture, the fibre tows have undulations/waviness and both the weft and warp tows are present in the same interface. Therefore, as a crack propagates at an interface, it follows a wavy path due to the waviness of the fibre tows, and further, as the crack encounters a different oriented fibre tow, the crack front jumps to follow this direction. All this results in an increased effective crack length and an excess energy dissipation, thereby an increased fracture toughness [10,14]. On the other hand, NCF fibre tows are rather straight like UD tapes, except for the fact that two UD plies are stitched together. They are reported to have a reduced interlaminar fracture toughness compared to woven fabrics [14], thereby demonstrating the effect of woven reinforcement architecture.

WF laminates exhibited more delaminated interfaces and a reduced projected area compared to NCF. QSI results revealed that most

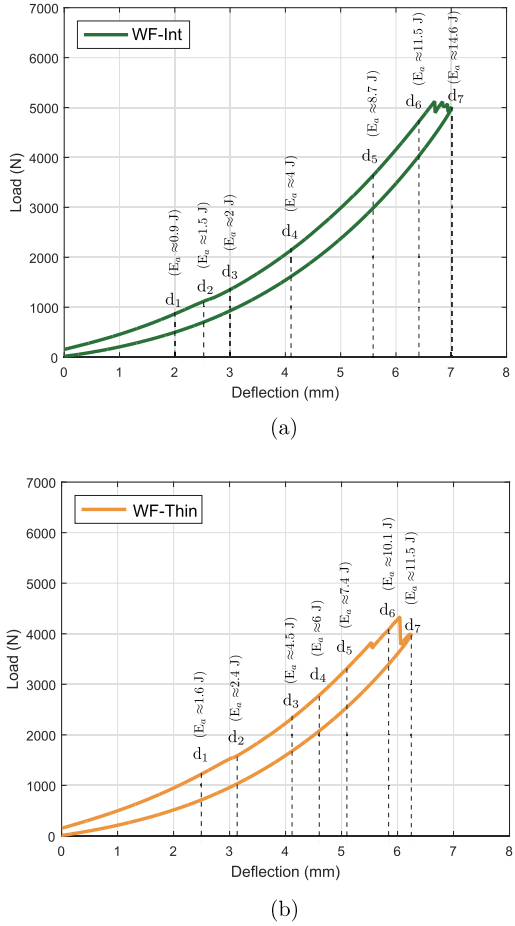

Fig. 13. Load-indenter displacement QSI curve for WF-Int and WF-Thin for d = 7 mm and d = 6.25 mm, respectively (the other displacement levels used in the study are also marked).

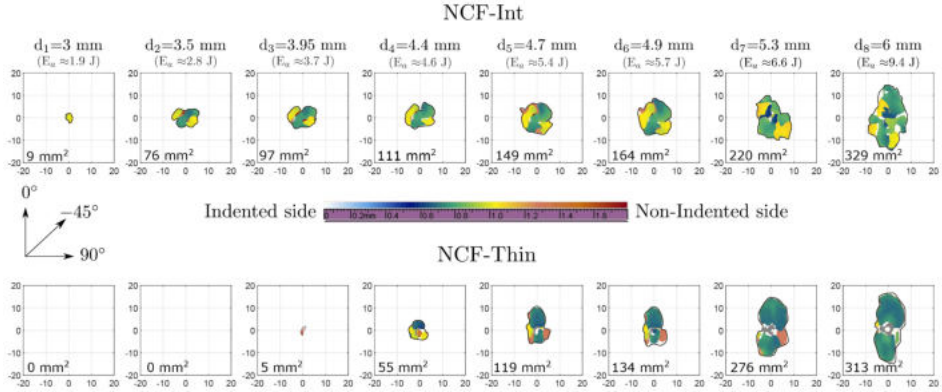

Fig. 12. C-scan images comparing the evolution of damage in the NCF laminates for all the indenter displacement levels.

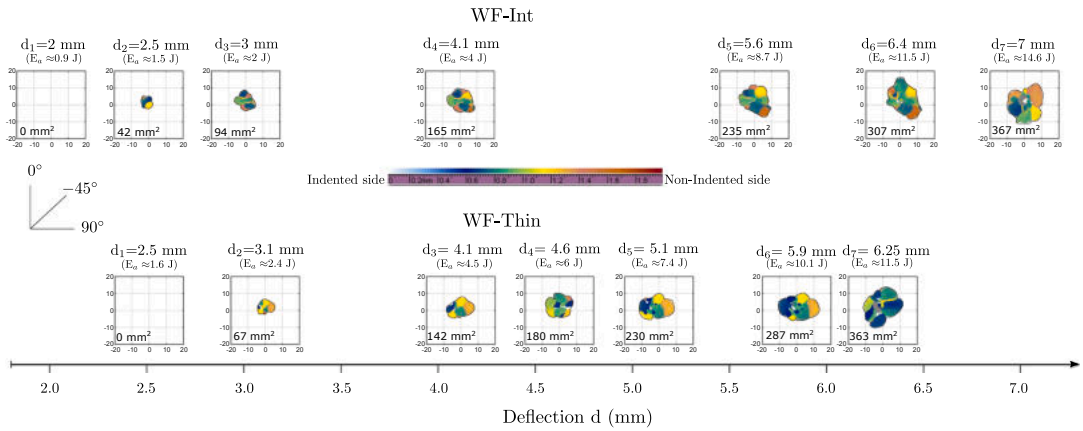

Fig. 14. C-scan images showing the damage evolution in WF-Int (top) and WF-Thin (bottom) for all indenter displacement levels. Note that the scans are presented along an indenter deflection on the horizontal axis.

delaminations were formed within the WF fabric blanket, which can be due to the higher mismatch angle of 90° within the fabrics that favours delamination [3]. The reduced projected damage area of WF is reasoned to be either the higher number of delaminated interfaces or the delamination propagation being suppressed by the increased mode II fracture toughness of the woven fabrics, where the delamination cannot extend easily as it is forced to change its plane following the weft and warp. Further, the magnitude of fibre failure is far smaller in WF laminates compared to NCF. The delamination onset for WF laminates happens before delamination onset for NCF laminates (as in Figs. 12 and 14), and this could probably delay the fibre damage onset. In addition, the interwoven fabric architecture may help to suppress the escalation of fibre damage. When a fibre bundle of a weft tow fails, the warp tows may help to re-distribute the stresses. Micro X-ray tomography investigations could help to obtain a proper understanding and can be employed in future work.

In analysing the ply thickness effect, thin laminates, due to the reduced bending stiffness, underwent significant bending during impact loads which led to high tensile stresses at the non-impacted laminate face. Because of the inherent in situ effect of thin plies and lower interlaminar stresses, NCF-Thin delayed the onset of matrix cracking and consequently delaminations. However, with the delayed damage onset, early fibre failure was evidenced in NCF-Thin, as seen through the significant load drops in the impact response curves and also the early fibre splitting at the laminate back face evidenced in QSI results (Fig. 11 and Fig. 12). Even though delamination onset was suppressed, extensive delamination was observed after fibre failure in thin ply laminates (as reported in [32]), thus NCF-thin exhibited a higher projected damage area over NCF-Int at higher energies. On the other hand, early matrix cracking and delaminations in NCF-Int delayed and reduced the intensity of fibre failure by having less energy available for the fibre damage process.

The same explanation is valid for the greater damage resistance of WF-Int over WF-Thin, even though the improvement is marginal when compared with the NCF laminates. The roughly similar damage resistance response of the WF laminates may be due to the ply grades chosen for the study, as the difference between the thin ply grade (80 gsm) and standard ply grade (120 gsm) was not as significant as in the case of NCF laminates (67 vs 134 gsm). Delamination initiation and its location were evidenced in the QSI results, which otherwise would not have been able to be detected from the impact results. NCF-Int exhibited delaminations above and below the mid-plane cluster ply formed due to symmetry axis, and this cluster introduces high bending stiffness mismatch between the adjacent interfaces, leading to high interlaminar shear stresses. The same can be seen with NCF-Thin just below the mid-plane.

4.2. Impact damage tolerance

An average 15% lower plain compression strength was observed on woven fabrics when compared to non-crimp fabrics. With the same fibre-resin material system for both types of fabrics, the reduction in the in-plane compressive strength is related to the fibre tow waviness of the woven fabrics [11]. It should also be kept in mind that the ply ratio along each orientation is not the same for NCF and WF laminates. Despite this, the waviness is greatly reduced in spread-tow woven fabrics compared to conventional ones [13,33,34]. The minimal waviness causes the in-plane properties of woven fabrics to be extremely close to that of the UD tapes. However, the minimal but inevitable waviness induces fibre kinking under compressive loading that impairs the compressive strength. Therefore, the same woven fibre architecture which helped to increase the damage resistance and fracture toughness, counteracted this with reduced CAI strength.

On the ply thickness effect, thin plies demonstrated an increased plain compression strength (10% for NCF and 7% for WF) over their intermediate ply counterparts. Thin plies possess increased longitudinal compression strength mainly attributed to the uniform micro-structure of the thin spread-tow, less waviness associated with thin plies, thus leading to fewer resin rich areas [13,35]. In the framework of compression after impact, as discussed in the previous section, the behaviour thin plies possess characterised by early and extensive fibre failure (because of delayed matrix cracks and delamination) has resulted in the reduced CAI strength thin ply laminates demonstrate (also reported in [2]). Contrary to the thick or standard laminates, where thin plies improved the CAI strength over thicker plies [16], thin plies used with thin laminates have led to increased fibre failure leading to reduced CAI strength. As explained earlier, thin plies dissipated most of their energy through fibre failure, whereas the intermediate plies do this through delamination. The final collapse of the specimen during CAI loading is mainly driven by the impact induced fibre damage than by the delamination, as is seen in the case of thin laminates.

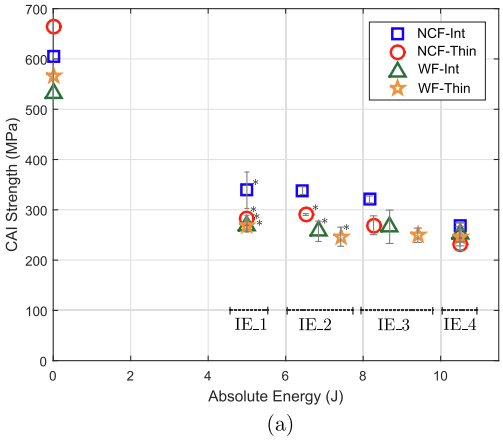

*CAI failure at the specimen top due to local buckling

Fig. 15. Plain compression strength and compression after impact strength values against (a) absolute impact energies and (b) normalized impact energies for all the laminates.

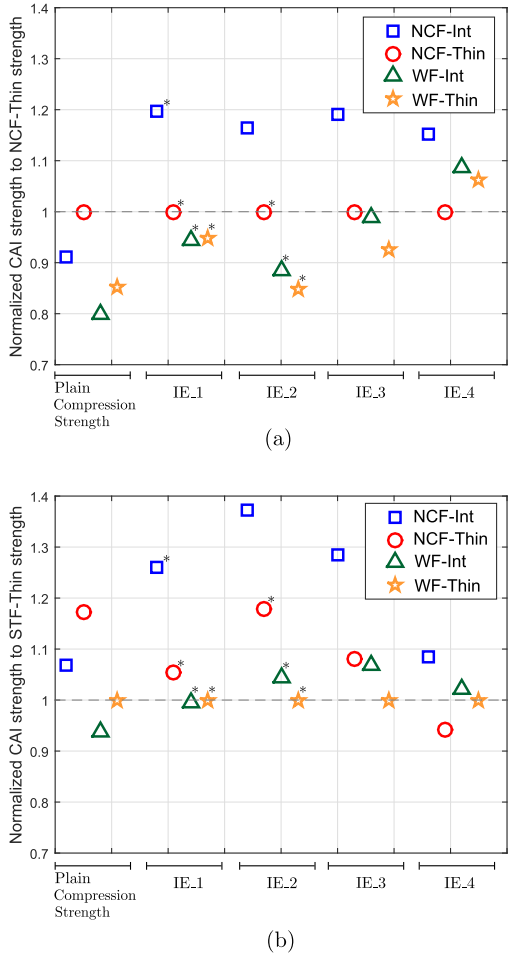

*CAI failure at the specimen top due to local buckling

Fig. 16. Comparison of CAI strength normalized with (a) NCF-Thin as baseline and (b) WF-Thin as baseline. The plain compression strength is also normalized according to the respective baselines.

4.3. Thin laminates and masked delamination load drops

Contrary to the thick or standard laminates, the thin laminates exhibited no signs of load drop in the initial stages of loading, where the initiation and propagation of delaminations are literally hidden in the force response curves. This is clearly seen from the QSI results for both NCF and WF laminates, where a delamination observed in the C-scan inspection is not represented by any load drop in the force response curve. As reported in [36], this is explained as an effect of the reduced laminate thickness. The force-deflection response curve of a laminate is the sum of the bending and membrane-stretching stiffnesses of the laminate. At higher deflections, where the membrane-stretching is dominant, the delaminations and their associated load drop have little influence on membrane behaviour. Hence, the significant load drops encountered in the force responses of the thin laminates is related to fibre damage, where the in-plane membrane stiffness drops due to the damaged fibres. Therefore, unlike the thick laminates, the force responses of the thin laminates does not signal the initiation or development of matrix and delamination damage through load drops, as these are only detected through damage inspections.

4.4. Damage tolerance in terms of damage detectability

One of the ultimate goals of the research community is to improve the damage tolerance of a structure. That is, the ability of the structure to have enough residual strength to carry post-impact service loads until the impact damage has been detected. It is also equally important for impact damage to be detected during service inspections so that it can be repaired and a final structural collapse is avoided [37,38]. Impact damage is normally detected through the permanent impact dent depth formed on the impacted surface. It has been reported that a dent depth between 0.25 and 0.5 mm deep is highly likely to be detected [39]. When comparing NCF and WF laminates in this framework, WF laminates exhibited less than 0.1 mm dent depth even at the highest impact energy, while NCF showed three or four times higher dent

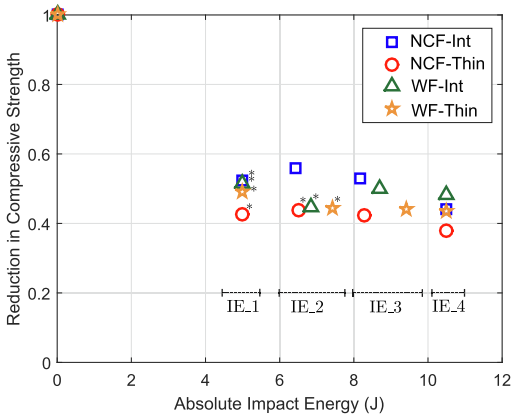

*CAI failure at the specimen top due to local buckling

Fig. 17. Normalized reduction in the compressive strength due to the impact damage of all laminates.

depth, thereby increasing their chances of being detected (as in Fig. 8). Moreover,WF laminates displayed a reduced residual strength which leads to a worse scenario as the damage can be left undetected, and at the same time they do not have a higher residual strength to withstand the loads. NCF outperform WF laminates in this, because the chances of detecting the damage is greater and also they have higher residual strength.

In a recent work by the authors [2], we carried out a similar study with UD tapes (using the same fibre-resin material as in this paper) considering different ply thicknesses. Comparing the impact and post-impact performance of fabrics with UD tapes (note that the UD baseline considered here is the intermediate ply grade of 134 gsm), the damage resistance of UD tapes and non-crimp fabrics is very similar, whereas the woven fabrics exhibit a superior performance compared to both UD and NCF. Meanwhile, non-crimp fabrics, NCF-Int exhibit considerably higher impact tolerance values (about 15%) than UD and there were similar CAI values between the UD and the woven fabric WF-Int.

4.5. Textile fabrics: prospects and further work

The study concludes that woven fabrics have good damage resistance, while NCF have a higher residual strength for post-impact loads and also favour impact damage detectability. Hence, these fabrics can be customized according to particular aircraft structures and the type of loads encountered. As a further improvement, laminates can be designed with hybrid designs at the ply level, where the standard and the thin ply grades can be mixed in the same laminate, as was done by the authors with UD plies [2]. The standard plies help to reduce the magnitude of fibre failure by dissipating energy through delaminations, while the thin plies and their improved compressive strength help in post-impact compressive loads. For woven fabrics, the means of improvement is to have the least reduction in the in-plane compressive properties when compared to UD plies, which is a key factor in improving post-impact residual strength. Since the woven fabric architecture helps to improve the fracture toughness and at the same time reduces the in-plane compressive properties, a balance between these two features should be made. One of the options is to substitute 0° fabric layers with UD 0° plies, where the undistorted 0° plies provide the residual strength during the in-plane compressive loading of CAI [40].

5. Conclusion

We carried out an experimental campaign to study the effect of fabric reinforcement architecture and tow thickness on the impact and compression after impact response of thin laminates (1.6–1.8 mm). We used two types of aerospace graded fabrics, namely non-crimp fabrics and woven fabrics, where two UD layers/tows were stitched and weaved together, respectively. In addition, two different tow thicknesses (standard and thin ply grade) were used for each fabric. Impact results revealed that woven fabrics undoubtedly exhibited a superior impact damage resistance, evidenced by the 50% less dissipated energy, reduced dent depth and projected damage area over the non-crimp fabrics. In terms of ply thickness effect, thin plies with thin laminates delayed the onset of cracks and delamination, but displayed early fibre failure, especially with non-crimp fabrics. This was demonstrated through quasi-static indentation tests, where the entire sequence of damage evolution was compared. The intermediate ply grade exhibited improved damage resistance (50% and 45% less energy dissipated for NCF and WF, respectively) over thin plies. Despite a lower impact damage resistance, non-crimp fabrics displayed an average 20% higher CAI strength over the woven fabrics. In addition, intermediate ply grade exhibited higher post-impact residual strength (20% and 10% higher CAI strength for NCF and WF, respectively) over their thin ply counterparts. With textile fabrics being a good economic prospect, future work can be dedicated to mixing plies of different thicknesses in the same laminate, thereby aiming to improve the damage tolerance.

Acknowledgements

The first author would like to thank the Generalitat de Catalunya for the FI-DGR pre-doctoral grant 2018 FI-B2 00118. The authors would like to thank the *Spanish Ministerio de Economía y Competitividad* for the grant coded MAT2015-69491-C3-1-R supported by FEDER/EU. The study is part of an extensive project funded by Airbus, partnered by the AMADE research laboratory (University of Girona), INEGI research group (University of Porto), and the University of Dayton Research Group. The authors would like to thank the University of Dayton Research Institute (UDRI) for manufacturing the specimens. Thanks to Prof. Pedro P. Camanho and the colleagues from the INEGI group for performing and sharing the plain compression strength results.

Data availability

The raw/processed data required to reproduce these findings cannot be shared at this time due to legal or ethical reasons.

Appendix A. Supplementary data

Supplementary data associated with this article can be found, in the online version, at https://doi.org/10.1016/j.compstruct.2019.02.054.

References

[1] Abrate S. Impact on composite structures. Cambridge University Press; 2005.
[2] Sasikumar A, Trias D, Costa J, Blanco N, Orr J, Linde P. Effect of ply thickness and ply level hybridization on compression after impact strength of thin laminates. Compos Part A: Appl Sci Manuf (Submitted).
[3] Sebaey T, González E, Lopes C, Blanco N, Maimí P, Costa J. Damage resistance and damage tolerance of dispersed CFRP laminates: effect of the mismatch angle between plies. Compos Struct 2013;101:255–64.
[4] Liv Y, Guillamet G, Costa J, González E, Marín L, Mayugo J. Experimental study into compression after impact strength of laminates with conventional and nonconventional ply orientations. Compos Part B: Eng 2017;126:133–42.
[5] Sasikumar A, Costa J, Trias D, González EV, García-Rodríguez S, Maimí P. Unsymmetrical stacking sequences as a novel approach to tailor damage resistance under out-of-plane impact loading. Compos Sci Technol 2019;173:125–35.
[6] García-Rodríguez S, Costa J, Singery V, Boada I, Mayugo J. The effect interleaving has on thin-ply non-crimp fabric laminate impact response: X-ray tomography investigation. Compos Part A: Appl Sci Manuf 2018;107:409–20.
[7] Sebaey T, Mahdi E. Using thin-plies to improve the damage resistance and tolerance

of aeronautical CFRP composites. Compos Part A: Appl Sci Manuf 2016;86:31–8.
[8] Bibo G, Hogg P. The role of reinforcement architecture on impact damage mechanisms and post-impact compression behaviour. J Mater Sci 1996;31(5):1115–37.
[9] Bibo G, Hogg P, Backhouse R, Mills A. Carbon-fibre non-crimp fabric laminates for cost-effective damage-tolerant structures. Compos Sci Technol 1998;58(1):129–43.
[10] Kim J-K, Sham M-L. Impact and delamination failure of woven-fabric composites. Compos Sci Technol 2000;60(5):745–61.
[11] Mahadik Y, Hallett S. Effect of fabric compaction and yarn waviness on 3D woven composite compressive properties. Compos Part A: Appl Sci Manuf 2011;42(11):1592–600.
[12] Lomov SV. Non-crimp fabric composites: manufacturing, properties and applications. Elsevier; 2011.
[13] Arteiro A, Catalanotti G, Xavier J, Linde P, Camanho P. Effect of tow thickness on the structural response of aerospace-grade spread-tow fabrics. Compos Struct 2017;179:208–23.
[14] Vallons K, Behaeghe A, Lomov SV, Verpoest I. Impact and post-impact properties of a carbon fibre non-crimp fabric and a twill weave composite. Compos Part A: Appl Sci Manuf 2010;41(8):1019–26.
[15] Sánchez-Sáez S, Barbero E, Zaera R, Navarro C. Compression after impact of thin composite laminates. Compos Sci Technol 2005;65(13):1911–9.
[16] Sihn S, Kim RY, Kawabe K, Tsai SW. Experimental studies of thin-ply laminated composites. Compos Sci Technol 2007;67(6):996–1008.
[17] Yokozeki T, Aoki Y, Ogasawara T. Experimental characterization of strength and damage resistance properties of thin-ply carbon fiber/toughened epoxy laminates. Compos Struct 2008;82(3):382–9.
[18] Furtado C, Arteiro A, Catalanotti G, Xavier J, Camanho P. Selective ply-level hybridisation for improved notched response of composite laminates. Compos Struct 2016;145:1–14.
[19] Arteiro A, Catalanotti G, Xavier J, Camanho P. Large damage capability of non-crimp fabric thin-ply laminates. Compos Part A: Appl Sci Manuf 2014;63:110–22.
[20] Arteiro A, Catalanotti G, Xavier J, Linde P, Camanho P. A strategy to improve the structural performance of non-crimp fabric thin-ply laminates. Compos Struct 2018;188:438–49.
[21] García-Rodríguez S, Costa J, Bardera A, Singery V, Trias D. A 3D tomographic investigation to elucidate the low-velocity impact resistance, tolerance and damage sequence of thin non-crimp fabric laminates: effect of ply-thickness. Compos Part A: Appl Sci Manuf 2018;113:53–65.
[22] Olsson R. Closed form prediction of peak load and delamination onset under small mass impact. Compos Struct 2003;59(3):341–9.
[23] ASTM D7136/D7136-15. Standard test method for measuring the damage resistance of a fiber reinforced polymer matrix composite to a drop weight impact event; 2015.
[24] González E, Maimí P, Camanho P, Lopes C, Blanco N. Effects of ply clustering in laminated composite plates under low-velocity impact loading. Compos Sci Technol 2011;71(6):805–17.
[25] ASTM D6484/D6484M-09. Standard test method for open-hole compressive strength of polymer matrix composite laminates; 2009.
[26] Arteiro A, Catalanotti G, Xavier J, Camanho P. Notched response of non-crimp fabric thin-ply laminates. Compos Sci Technol 2013;79:97–114.
[27] ASTM D7137/D7137-15. Standard Test Method for Compressive Residual Strength Properties of Damaged Polymer Matrix Composite Plates; 2015.
[28] Ghelli D, Minak G. Low velocity impact and compression after impact tests on thin carbon/epoxy laminates. Compos Part B: Eng 2011;42(7):2067–79.
[29] Remacha M, Sánchez-Sáez S, López-Romano B, Barbero E. A new device for determining the compression after impact strength in thin laminates. Compos Struct 2015;127:99–107.
[30] González E, Maimí P, Martín-Santos E, Soto A, Cruz P, de la Escalera FM, de Aja JS. Simulating drop-weight impact and compression after impact tests on composite laminates using conventional shell finite elements. Int J Solids Struct 2018;144:230–47.
[31] Soto A, González E, Maimí P, de la Escalera FM, de Aja JS, Alvarez E. Low velocity impact and compression after impact simulation of thin ply laminates. Compos Part A: Appl Sci Manuf 2018;109:413–27.
[32] Saito H, Morita M, Kawabe K, Kanesaki M, Takeuchi H, Tanaka M, Kimpara I. Effect of ply-thickness on impact damage morphology in CFRP laminates. J Reinf Plast Compos 2011;30(13):1097–106.
[33] EL-Dessouky HM, Lawrence CA. Ultra-lightweight carbon fibre/thermoplastic composite material using spread tow technology. Compos Part B: Eng 2013;50:91–7.
[34] Shamsudin M, York C. Mechanically coupled laminates with balanced plain weave. Compos Struct 2014;107:416–28.
[35] Amacher R, Cugnoni J, Botsis J, Sorensen L, Smith W, Dransfeld C. Thin ply composites: experimental characterization and modeling of size-effects. Compos Sci Technol 2014;101:121–32.
[36] Lee J, Soutis C. Prediction of impact-induced fibre damage in circular composite plates. Appl Compos Mater 2005;12(2):109–31.
[37] Bouvet C, Rivallant S, Barrau J-J. Low velocity impact modeling in composite laminates capturing permanent indentation. Compos Sci Technol 2012;72(16):1977–88.
[38] Rivallant S, Bouvet C, Hongkarnjanakul N. Failure analysis of CFRP laminates subjected to compression after impact: FE simulation using discrete interface elements. Compos Part A: Appl Sci Manuf 2013;55:83–93.
[39] Hongkarnjanakul N. Modélisation numérique pour la tolérance aux dommages d'impact sur stratifié composite: de l'impact à la résistance résiduelle en compression, ISAE, Toulouse (Ph.D. thesis).
[40] Curtis P, Bishop SM. An assessment of the potential of woven carbon fibre-reinforced plastics for high performance applications. Composites 1984;15(4):259–65.

A.5 Paper E

Mitigating the weak impact response of thin-ply based thin laminates through an unsymmetrical laminate design incorporating intermediate grade plies

A. Sasikumar[a,*], D. Trias[a,1], J. Costa[a,*], V. Singery[b], P. Linde[c,d]

[a] AMADE, Polytechnic School, Universitat de Girona, Campus Montilivi s/n, E-17003 Girona, Spain

[b] Chomarat, 39 Avenue de Chabannes, 07160 Le Cheylard, France

[c] Airbus Operations GmbH, Kreetslag 10, 21129 Hamburg, Germany

[d] Department of Industrial and Materials Science, Chalmers University of Technology, S-41296 Gothenburg, Sweden

[*] Corresponding author

[1] Serra Hunter Fellow

The paper has been published in *Composite Structures* 220 (2019) 93–104.

Composite Structures 220 (2019) 93–104

Contents lists available at ScienceDirect

Composite Structures

journal homepage: www.elsevier.com/locate/compstruct

Mitigating the weak impact response of thin-ply based thin laminates through an unsymmetrical laminate design incorporating intermediate grade plies

A. Sasikumar[a,*], D. Trias[a,1], J. Costa[a,*], V. Singery[b], P. Linde[c,d]

[a] AMADE, Polytechnic School, University of Girona, Campus Montilivi s/n, 17073 Girona, Spain
[b] Chomarat, 39 Avenue de Chabannes, 07160 Le Cheylard, France
[c] Airbus Operations GmbH, Kreetslag 10, 21129 Hamburg, Germany
[d] Department of Industrial and Materials Science, Chalmers University of Technology, S-41296 Gothenburg, Sweden

ARTICLE INFO

Keywords:
Hybrid laminates
Non-crimp fabrics
Impact behaviour
Damage tolerance
Unsymmetrical laminates

ABSTRACT

With aeronautic industries focussing on thinner structures and reducing manufacturing costs, recent research has been dedicated to the impact and post impact response of thin laminates (< 2 mm) made of textile fabric composites. A recent study revealed that thin laminates based on thin plies exhibit extensive fibre failure and a reduced compression after impact strength. To mitigate this weakness, we propose a novel laminate concept based on combining plies of different thicknesses in an unsymmetrical configuration (intermediate grade plies are located only at the bottom of the laminate, i.e., the non-impacted face). C-scan inspection on impacted and quasi-statically indented specimens, allowed the damage sequence of the proposed unsymmetrical hybrid laminate to be compared with that of the thin-ply baseline. The hybrid laminate with intermediate plies at the bottom, delayed and reduced the fibre damage, decreased the projected delamination area and led to a 30% increase in the compression after impact strength in contrast to the thin-ply baseline laminate.

1. Introduction

In the quest to reduce structural weight, aircraft manufacturers are considering using thin structures, especially for the fuselage and wing skins. One of the main difficulties with these thin structures (< 2 mm) is their increased vulnerability to out-of-plane loads, coupled with a high reduction in the residual strength during the post-impact service cycles of the aircraft [1]. Recent research has reported that a low velocity impact (enough to create a barely visible impact damage on the laminate) has caused a 60–70% reduction in the compressive strength of thin laminates [2,3]. This alarming reduction has led aircraft manufacturers to consider non-conventional laminate designs, not only as an economic way to reduce the severity of impact damage but also to improve the compression after impact (CAI) strength.

Despite the vast amount of impact studies performed on thick laminates [4–9] (4–5 mm, as suggested in the ASTM standard [10]), very few studies have been dedicated towards thin laminates and their response to impact and CAI loads. Recently, Garcia et al. [11] discussed the effect ply thickness has on the out-of-plane response of 2.15 mm laminates made of non-crimp fabrics using tomographic investigations. The current authors [3] compared the effect fabric architecture and ply thickness have on impact and CAI strength of thin laminates (1.6–1.8 mm), where two types of fabrics, namely woven and non-crimp fabrics, were studied. Results revealed that, unlike thick laminates [5,12], thin laminates made of thin plies resulted in extensive fibre damage which led to reduced CAI strength. Meanwhile, intermediate ply grades, even though they exhibited early damage onset in terms of delamination, had comparably lesser fibre damage, and led to greater CAI strength than thin plies had [3,11].

Concerning non-conventional laminate designs, in a recent work [2], the authors proposed mixing uni-directional (UD) plies of different thickness grades to produce hybrid thin laminates. One of the hybrid designs (where thick 0° plies were added close to the laminate mid-plane symmetry along with thin plies) demonstrated a significant improvement in CAI strength (40%) when compared to the thin-ply baseline laminate. This study promised that by using a hybrid laminate the potential benefits of the different ply grades can be exploited through ply level hybridization, as is also demonstrated in [13–15].

* Corresponding authors.
E-mail addresses: aravind.sasikumar@udg.edu (A. Sasikumar), josep.costa@udg.edu (J. Costa).
[1] Serra Hunter Fellow.

https://doi.org/10.1016/j.compstruct.2019.03.069
Received 21 December 2018; Received in revised form 27 February 2019; Accepted 21 March 2019
Available online 27 March 2019

Despite the novelty of hybridization, the laminate mid-plane symmetry constraint found in the studies and which restricts the laminate to having the same top sub-laminate layup mirrored below the symmetry plane, was still adhered. Because damage from an impact induces unsymmetrical damage modes in the laminate thickness direction, it is necessary to move away from the conventional symmetry designs and also to enlarge the stacking sequence design space. In a preliminary study with thick laminates and using plies of same thicknesses [16], the authors demonstrated that the mid-plane symmetry can be challenged without the worry of warping and from this the laminate can be tailored towards impact loads by having different top and bottom sub-laminates.

These two concepts (unsymmetry and ply hybridization) could be combined into a laminate design where thick plies can be mixed with thin plies to form a hybrid laminate. At the same time, the thicker plies can be placed at a desired location without having to worry about placing equivalent thick plies on the other side of the laminate's mid-plane symmetry line. By employing this design idea, an attempt is made to tailor the damage in an impact scenario which, will in turn, could help to improve the CAI strength. According to the authors' knowledge, this is the first work reporting on the impact and CAI response of such novel laminate designs. In this paper, we designed a hybrid and unsymmetrical laminate (with zero warp) using non-crimp fabrics where intermediate plies had been added to thin plies to form a hybrid laminate. Within the framework of thin laminates (1.6 mm), we carried out an experimental study to investigate the impact and CAI response of this novel laminate design. In addition, we also compared the results with those of the baseline laminates (symmetric and non-hybrid), where one laminate was made only of intermediate plies and the other with only thin plies (baseline results presented by the authors in [3]). We also performed quasi-static indentation tests interrupted for C-scan inspection, to compare the damage initiation and evolution between the hybrid and the baseline laminates. Experimental results reveal that the proposed novel laminate design could tailor the impact damage with less fibre breakage and thereby considerably improve the CAI strength over the thin-ply baseline laminate.

2. Laminate design

2.1. Material

We used bi-axial non-crimp fabrics (NCF), where two differently oriented fibre tows are stitched together using a polyester yarn. The double axis layup of the NCF blankets reduces the manufacturing costs significantly [17]. The material system used is a carbon fibre T700 pre-impregnated with HexPly® M21 resin. Bi-axial prepreg blankets of [0°/45°] and [0°/−45°] which can also lead to other orientations through flipping and/or rotation, were used. We employed two different fabric thickness grades: 268 and 134 gsm, so the UD ply thickness corresponds to 0.134 and 0.067 mm, and, in this paper, referred to as intermediate and thin ply grade, respectively.

2.2. Rationale behind the laminate design

From the experimental results reported in [2,3], the thin laminates, unlike the thick laminates, underwent considerable bending under impact loads and the high in-plane tensile loads led to fibre splitting at the back face of the laminate. The thin laminates made of thin plies, delayed delamination but exhibited extensive back fibre splitting, while the intermediate ply grades displayed an early delamination onset, but with a reduced fibre damage. Hence, to exploit the potential of both ply grades (i.e., the ability of intermediate plies to reduce fibre damage by dissipating energy through delaminations and thin plies to delay damage onset, along with higher plain compression strength they possess [3]), we propose a hybrid laminate design, where intermediate plies are added to a thin-ply NCF laminate.

Furthermore, it is equally important to decide in which through-the-thickness location in the laminate, the intermediate plies have to be added. As the non-impacted face of the laminate is prone to extensive fibre splitting when used with thin plies, our intention was to add intermediate plies at the non-impacted laminate face, in an attempt to reduce fibre breakage by promoting delamination. Hence, this demands an unsymmetrical laminate design with a minimum bending stretching coupling matrix ([B]) to avoid warpage during manufacturing [18].

2.3. Unsymmetrical hybrid laminate design: optimization

We used an optimization algorithm (a genetic algorithm embedded in the MATLAB optimization toolbox [19]) to search for unsymmetrical laminate designs with a minimum or null B value. The objective function was to minimize the sum of B matrix terms, and the constraints were as given below:

- Balanced and quasi-isotropic laminate.
- Four plies (two NCF blankets) of intermediate ply grade as bottom plies (at the non-impacted face of the laminate)
- As the outer plies are affected by impactor indentation (impacted face) and fibre splitting (non-impacted face), they were fixed to be 90° as they are comparatively the least influential on the CAI strength. For the same reason, the 0° plies were restricted from being placed in the outer NCF blankets.
- The equivalent bending stiffness parameter (D*, proposed by Olsson [20] and applied as an optimization constraint in [21]) is made to match within 1% of the value of the baseline laminates to have a proper comparison.

A solution (an unsymmetrical-hybrid laminate with null B matrix) satisfying all the constraints was obtained and is provided along with details in the following section.

2.4. Laminates and stacking sequences

The unsymmetrical-hybrid laminate (with zero B matrix) obtained is provided in Table 1, and hereafter will be referred to as NCF-UHB, denoting 'Unsymmetrical Hybrid laminate with intermediate plies at Bottom' (non-impacted side). The same laminate is flipped upside down to have an 'Unsymmetrical Hybrid laminate with the intermediate plies at the Top' (impacted side), and will be referred to as NCF-UHT. The objective of introducing the NCF-UHT laminate is to understand the

Table 1
Laminates and their details.

Laminate	Description	Stacking sequence	Ply thickness (mm)	Laminate thickness (mm)	D* (Nm)
NCF-Int	Intermediate plies	$[(45/0)/(-45/90)/(22.5/-22.5)]_S$	0.134	1.61	18.6
NCF-Thin	Thin plies	$[(45/0)/(-45/90)/(45/0)/(-45/90)/(45/0)/(-45/0)]_S$	0.067	1.61	18.9
NCF-UHB	Hybrid (Int. and thin plies)	$[(90/-45)/(0/45)/(90/-45)/(0/45)/(90/-45)/(0/45)/(90/-45)/(0/45)/(45/0)_{268}/(-45/90)_{268}]$	0.134 & 0.067	1.61	18.8
NCF-UHT	Hybrid (Int. and thin plies)	$[(90/45)_{268}/(0/-45)_{268}/(-45/0)/(45/90)/(-45/0)/(45/90)/(-45/0)/(45/90)/(-45/0)/(45/90)]$	0.134 & 0.067	1.61	18.8

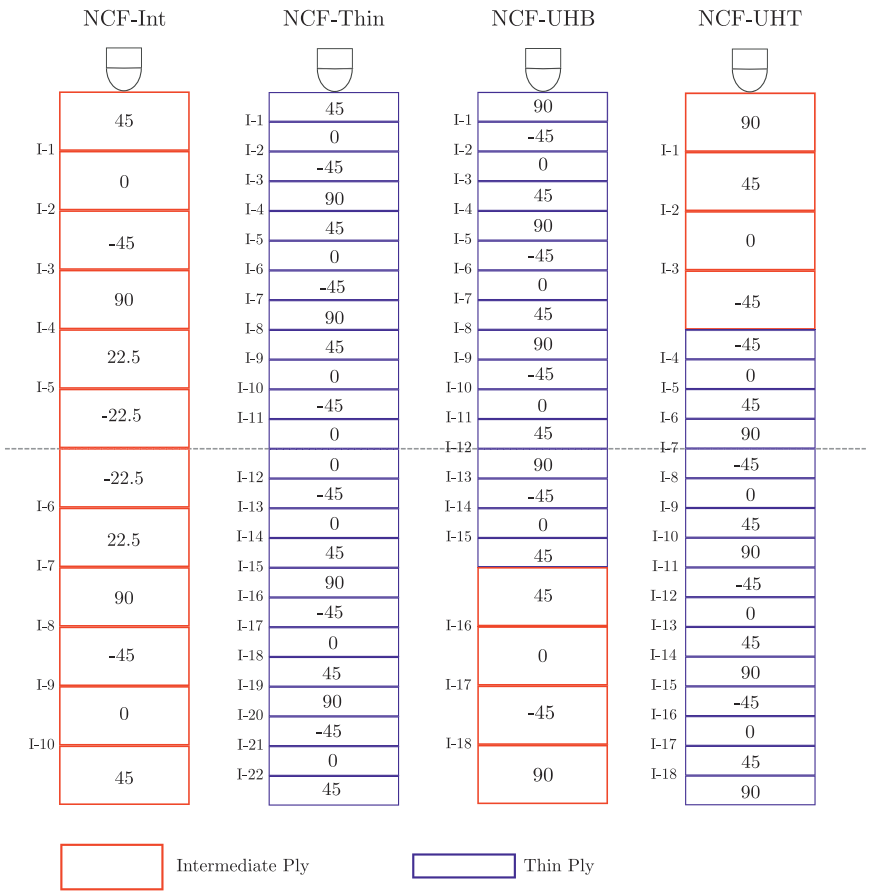

Fig. 1. Illustration of all the laminates used for the study: NCF-Int, NCF-Thin, NCF-UHB and NCF-UHT, where NCF-UHT is obtained by flipping NCF-UHB upside down. Note that U refers to unsymmetry, H to hybrid design, T and B to top and bottom (location of intermediate grade plies).

effect the location (at impacted or non-impacted side) of the added intermediate plies has on the impact and CAI response. To study the effect of hybridization, the two unsymmetrical hybrid laminates are compared to baseline laminates, namely NCF-Int and NCF-Thin (results published by the authors in a recent work [3]). NCF-Int and NCF-Thin are symmetrical laminates made using only one ply grade, namely intermediate and thin ply grades, respectively. It is also important to recall that NCF-UHB and NCF-UHT are thin-ply dominant (comprising of 67% thin plies and 33% intermediate grade plies for the laminate thickness) hybrid laminates. All four laminates and their stacking sequences are illustrated in Fig. 1 and Table 1 provides further laminate details.

Fig. 2(a) and (b) present the polar plots of the in-plane and bending stiffnesses, respectively, of all the laminates. Note that the baseline laminates are in-plane non-quasi isotropic, while the proposed unsymmetrical laminates are in-plane quasi-isotropic. The maximum deviation of the equivalent bending stiffnesses (D*) between the proposed and the baseline laminates is less than 0.2%, hence the difference is negligible in terms of the practical application of these laminates.

3. Experimental methods

Impact specimens of dimensions 150 × 100 mm were cut from the panels with 0° plies aligned with the specimen length. NCF-UHB specimens were flipped upside down to obtain NCF-UHT specimens, i.e., the one with the intermediate plies at the top. Note that flipping a laminate upside down only interchanges the 45° plies by −45° and vice versa. We performed the impact tests in accordance with the ASTMD7136/D7136-15 standard [22], using a CEAST Fractovis Plus instrumented drop-weight tower. A 16 mm steel hemispherical indenter was used and the total mass of the impactor setup was set to 3 kg.

Three impact energies, 6.4 J, 8.2 J and 10.5 J, (the same energies as used in [3] for the baseline laminates NCF-Int and NCF-Thin) were explored, and hereafter will be referred to as IE_1, IE_2 and IE_3, respectively. We impacted nine specimens per laminate, with three specimens for each impact energy, to assess the repeatability. Further details of the experimental impact setup can be found in [23].

We performed quasi-static indentation (QSI) tests with an MTS INSIGHT® 50 testing machine with a 50 kN load cell and displacement controlled loading of the indenter. 150 × 100 mm specimens were placed on a base plate, which has an open window of 125 × 75 mm. Four rubber clamps were used to fasten the specimen to the base plate.

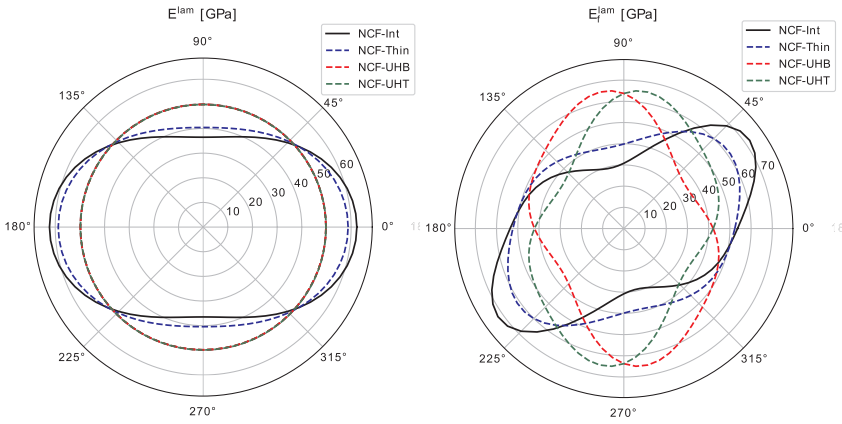

Fig. 2. Polar plot representation of the (a) in-plane stiffness and (b) bending stiffness of all the laminates.

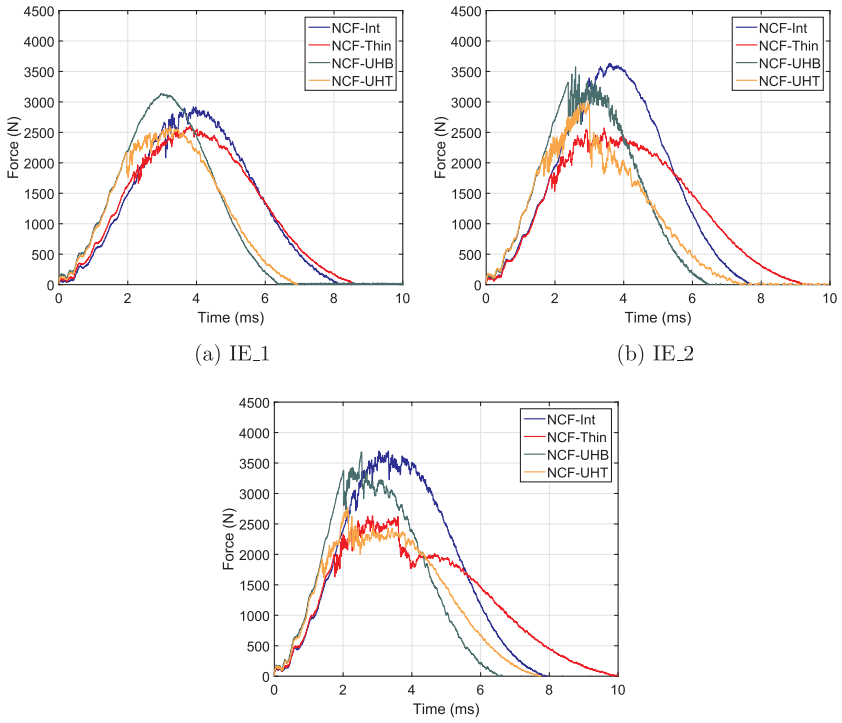

Fig. 3. Impact force-time response curves of all laminates for all three impact energies.

A constant indenter displacement of 1 mm/min was used. We explored a total of seven indenter displacements, the same as in [3], for comparison purposes. A total of three specimens per laminate were used for the QSI tests, where a same specimen was loaded and then interrupted for C-scan damage inspection and then followed by a higher indenter displacement loading. The damage was inspected after impact and after each QSI loading level using a pulse-echo ultrasonic C-scan technique. The C-scan setup featured an OLYMPUS OMNI MX system along with a

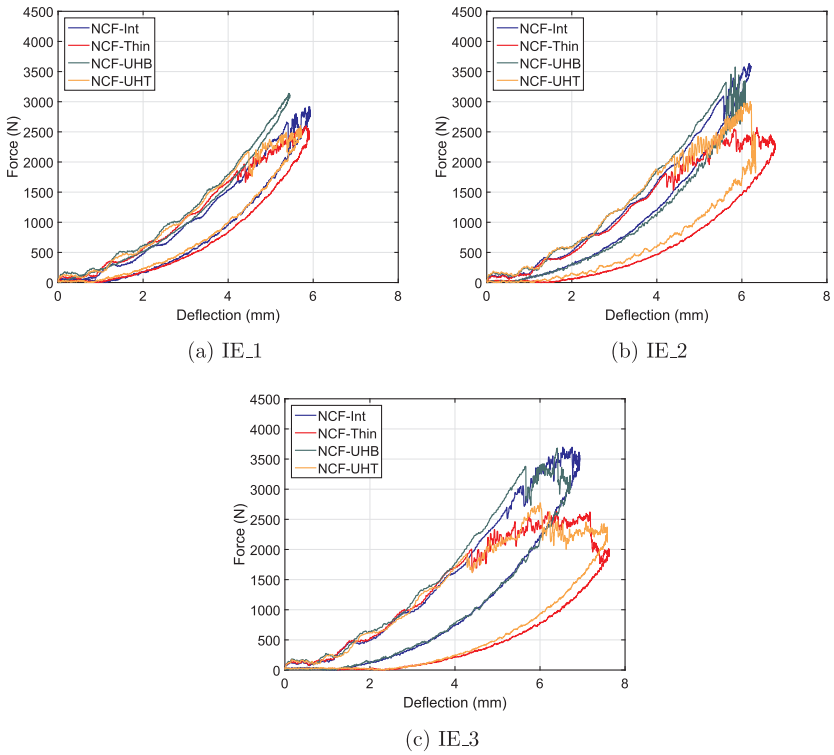

Fig. 4. Impact force-deflection response curves of all laminates for all three impact energies.

5 MHz piezoelectric probe.

To evaluate the post-impact compressive strength, CAI tests were performed on the impacted specimens using an MTS INSIGHT®300 machine with a 300 kN load cell, following the ASTMD7317/D7137M-15 [10]. To account for the reduced laminate thickness, we used an additional anti-buckling device (proposed by Remacha et al. [24]) along with the CAI fixture. The additional fixture ensured the specimen was refrained from global buckling, thus ensuring a proper compressive failure at the specimen's impacted site. Furthermore, to evaluate the pristine compression strength, plain compression strength tests were performed in accordance with the ASTMD6484/D6484M-14 standard [25]. Three 305 × 30 mm specimens were tested with a cross head displacement of 1 mm/min for the plain compression strength at the INEGI research facility at the University of Porto. All the above tests, except plain compression strength, were performed at the AMADE research laboratory (NADCAP certified for non-metallic material testing) at the University of Girona.

4. Results

4.1. Impact

Figs. 3–5 present the impact force-time, impact force-deflection and impact energy-time curves, respectively, of all four laminates. Note that, due to good repeatability, only one specimen data per laminate per energy level is presented. Inspecting the curves in Figs. 3 and 4, a clear difference in the impact response is seen between NCF-UHB and NCF-UHT, indicating the effect the location of the added intermediate plies has on the impact response.

For the lowest energy level IE_1, no load drop was observed with NCF-UHB, which also exhibited the maximum peak force (3200 N) compared to all other laminates. To the contrary, NCF-UHT exhibited its first significant load drop close to 2200 N, followed by further load drops, thereby leading to a suppressed load carrying capability compared to NCF-UHB. Moving on to the higher energies (IE_2 and IE_3), NCF-UHB displayed first significant load drop close to the peak load (3500 N) followed by successive drops. In reviewing the impact curves in Figs. 3 and 4, the laminates can be grouped in terms of their similar responses, for instance, NCF-Int and NCF-UHB in one group, and NCF-Thin and NCF-UHT in the other. Similar behaviour was observed with the energy evolution curves (Fig. 5) where NCF-UHB dissipated significantly less energy than NCF-UHT for all impact energies explored. While NCF-UHB had the least dissipated energy for IE_1, at higher energies it dissipated more energy than NCF-Int, but still significantly less than NCF-Thin and NCF-UHT.

Fig. 6 compares the projected impact damage profile for the four laminates obtained from C-scan inspection. The projected damage area, the dominant delaminations and their corresponding interfaces are also marked in the same figure. The thin-ply laminate NCF-Thin exhibited the highest projected damage area while the hybrid NCF-UHB displayed the least. It is important to note that both the hybrid laminates considerably reduced the damage area compared to their baselines. While NCF-Int had dominant delaminations at interface 10 (bottom interface) and 6 (interface just below the mid-plane) oriented at 45° and 22.5°, respectively, NCF-Thin exhibited a dominant delamination at interface 12 (just below the mid-plane ply cluster), as reported in [3].

With the hybrid designs, NCF-UHB displayed a dominant delamination at the last interface (int. 18 (−45°/90°), at the site of the

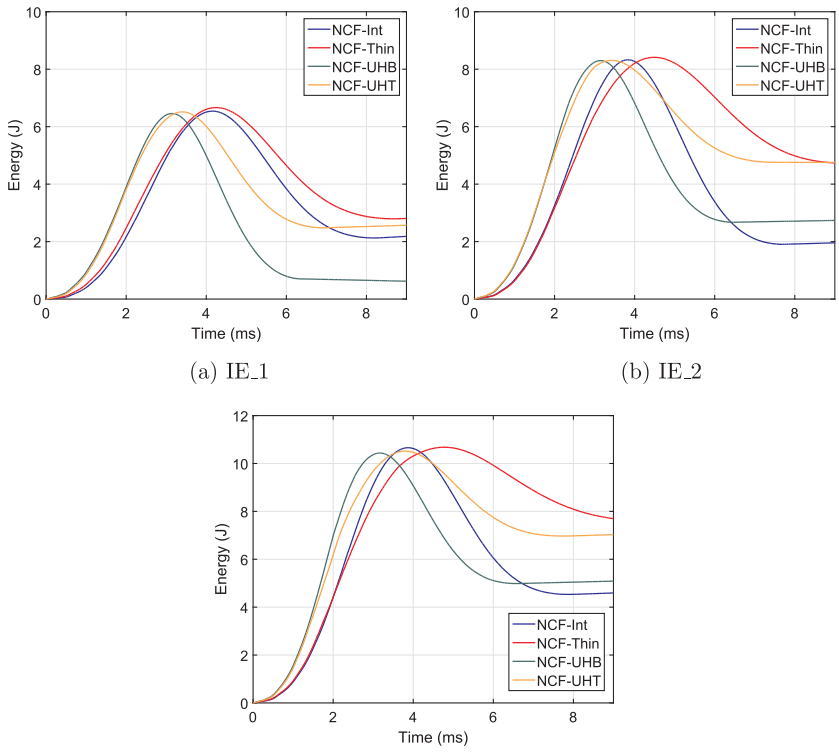

Fig. 5. Impact energy evolution curves of all laminates for all three impact energies.

intermediate grade plies added at the laminate bottom) oriented at 90°, as predicted during the laminate design phase. At the highest impact energy, the total projected damage area is governed by this single last interface delamination, where the other delaminations are found to be comparatively negligible (see Fig. 6). For NCF-UHT, interfaces 5 (0°/45°) and 10 (45°/90°) exhibited dominant delaminations, with orientations at 45° and 90°, respectively. Contrary to NCF-UHB, many interfaces contributed towards the total projected damage area of NCF-UHT. While NCF-UHB had dominant delamination at the non-impacted site where the intermediate plies were added, NCF-UHT exhibited dominant delaminations just below the added intermediate plies (at and just below the mid-plane).

Fig. 7 presents the photos of the impacted and non-impacted faces of all the laminates from the 10.5 J impact. The impact dent depth at the impacted face and the fibre splitting (in the orientation of the last ply) at the non-impacted face can be visually compared between the four laminates. While the thin ply NCF-Thin exhibited the highest magnitude of impact dent depth and extensive fibre splitting, the intermediate-ply laminate NCF-Int comparatively suppressed both these parameters, as reported in [3]. The hybrid laminates, despite being a thin-ply dominant laminate, exhibited reduced back fibre splitting compared to its baseline NCF-Thin due to the inclusion of the intermediate plies.

Fig. 8(a) and (b) represent the evolution of the peak load and projected damage area, respectively, for increasing impact energies, while Fig. 9(a) and (b) present the dissipated energy and impact dent depth against the impact energies, respectively. Out of all the laminates, NCF-Thin possessed the least load carrying capability, as evidenced by the least peak load (Fig. 8(a)). NCF-UHB and NCF-Int displayed similar values, despite NCF-UHB having slightly higher values for the first two energies. Compared to the baseline NCF-Thin, NCF-UHB exhibited a 30% higher peak force considering all the impact energies. In terms of the projected damage area, both hybrid laminates exhibited less area compared to the baselines, whereas NCF-Thin displayed the greatest damage area. NCF-UHB laminate showed the smallest damage area, with a significant reduction of 50% and 20% over the thin ply baseline NCF-Thin and the intermediate ply baseline NCF-Int, respectively (Fig. 8(b)).

NCF-Int and NCF-UHB exhibited the least dissipated energy, while NCF-Thin and NCF-UHT dissipated the highest. NCF-UHB exhibited a 30% reduction in the dissipated energy over NCF-Thin. We observed similar responses with the impact dent depth, where the thin-ply laminate NCF-Thin exhibited the highest dent depth followed by the hybrid laminate NCF-UHT. NCF-Int and NCF-UHB suppressed the impact dent depth compared to the other two laminates, where NCF-UHB displayed a 50% reduced dent depth compared to the thin ply baseline NCF-Thin.

4.2. Quasi-static indentation

Fig. 10 compares the force-deflection responses of the two hybrid laminates along with that of the baselines for the highest indenter

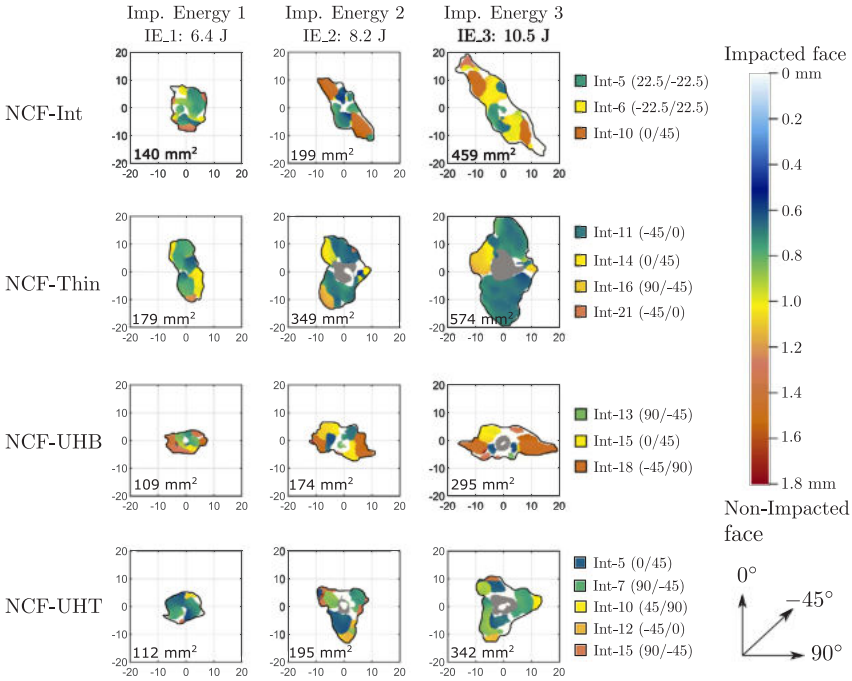

Fig. 6. C-scan inspection images of all the laminates along with the projected damage areas and the dominant delaminations identified (the field of inspection presented is a 40 × 40 mm square window with impacted site as the centre).

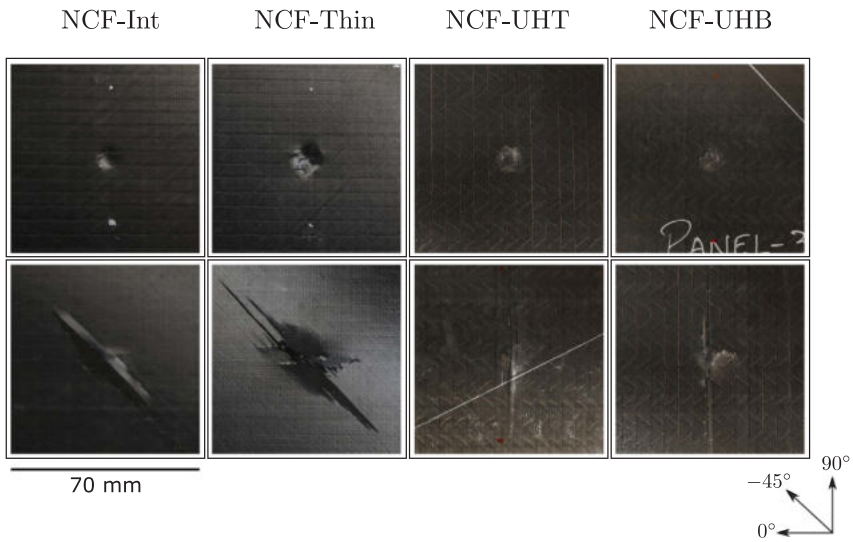

Fig. 7. Impact (top) and non-impacted (bottom) laminate face photos of all the laminates after the 10.5 J impact (represented field of view is a 70 × 70 mm square window with the impacted site as the centre).

deflection of d_7 = 6 mm. Other indenter deflections studied (d_1–d_6) are also marked on the same figure. As already reported in [3], NCF-Int exhibited the first load drop at around 3500 N, close to the maximum peak load. To the contrary, NCF-Thin exhibited an early load drop, at around 2000 N, followed by successive load drops leading to a reduced maximum load (as also observed in the impact results). With the hybrid laminates, NCF-UHT behaved similar to NCF-Thin, with early and intermittent load drops, whereas NCF-UHB displayed a similar response

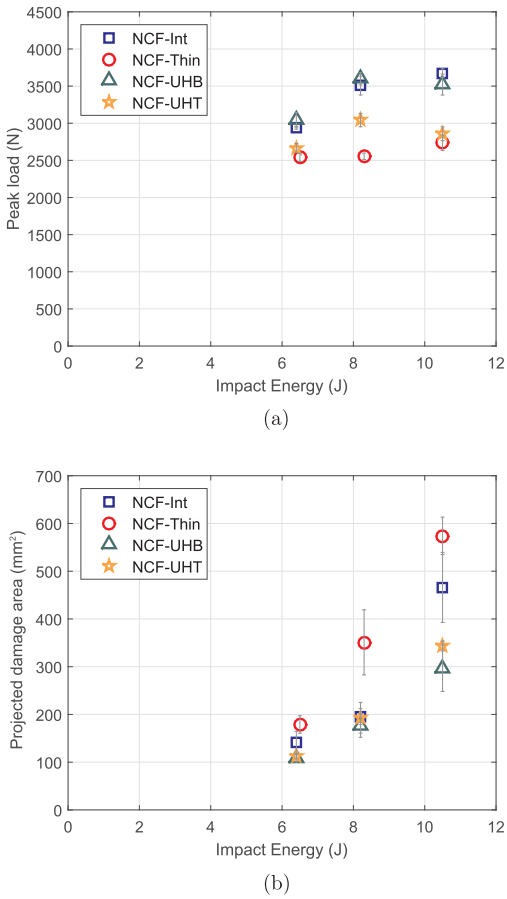

Fig. 8. Impact damage resistance parameters (a) peak load and (b) projected damage area compared between all the laminates for all the impact energies (average value is presented along with the standard deviation indicated by the vertical markers).

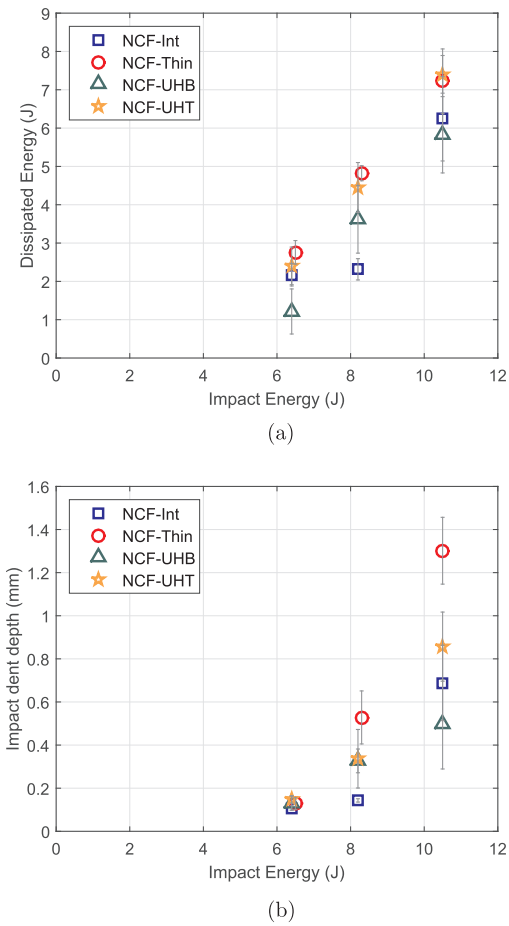

Fig. 9. Impact damage resistance parameters (a) dissipated energy and (b) impact dent depth compared between all the laminates for all absolute impact energies (average value is presented along with the standard deviation indicated by the vertical markers).

to that of NCF-Int with the first load drop occurring at the peak load. Compared to thin-ply baseline NCF-Thin, interestingly, both hybrid laminates delayed the first load drop. NCF-UHB and NCF-UHT, respectively, exhibited a 55% (3300 N) and 15% (2400 N) increase in the force value at which the first load drop was observed (attributed to fibre damage initiation), when compared to NCF-Thin.

Fig. 11 presents the C-scan images of the damage profile for all the indenter displacement levels for all the laminates. The figure also presents the applied energy and projected damage area for each displacement, identified delaminated interfaces and the initiation of fibre splitting (marked by 'FS' denoting fibre split in Fig. 11), observed by visual inspection of the non-impacted surface. It is evident that intermediate plies (NCF-Int) displayed early delamination at d_1, even though no associated load drop was seen in the force-deflection response. There was no sign of damage in the other three laminates at d_1. At d_2, NCF-UHB showed the first instance of delamination, identified at the last interface (int 18: (−45°/90°)). NCF-Thin and NCF-UHT delayed the onset of damage, the first instance of which was observed at d_3, whereas damage had already been propagated in NCF-Int and NCF-UHB. Delamination onset was identified in NCF-UHT at the top sub-laminate (just below the added intermediate plies) at interface 5 (0°/45°). Moving on to d_4, NCF-Thin exhibited back fibre splitting associated with the load drop (see Fig. 10) between d_3 and d_4. On further loading, the dominant delamination was identifed in NCF-UHB at the last interface (at the bottom, within the added intermediate plies) and at the mid-plane (int 7: (90°/−45°)) for NCF-UHT. With continued loading, NCF-UHT displayed fibre splits associated with the load drop between d_5 and d_6. The highest indenter displacement d_7 marked the onset of fibre splits on NCF-Int and NCF-UHB, also indicated by the high load drops seen in their respective curves. It is interesting to note that both hybrid laminates exhibited 50% reduced damage area compared to the thin-ply baseline NCF-Thin. The QSI results (mainly the force-deflection curves, the damage profile and the first load drop) are coherent with the impact results. While the initiation of delamination is hidden in the force response curves of these thin laminates [3], the load drops correspond to the initiation and extension of fibre damage.

Fig. 12 presents the evolution of the dissipated energies (E_d) against

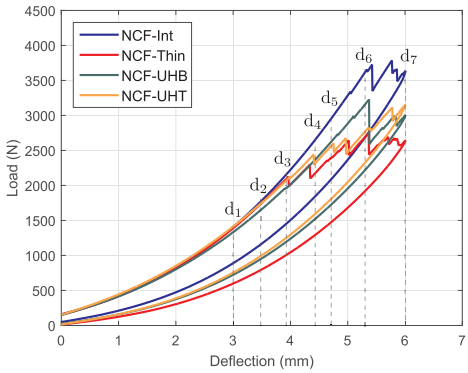

Fig. 10. QSI load deflection responses of all the laminates for the highest deflection d_7 = 6 mm, and the other indenter deflections studied (d_1 to d_6) are also marked.

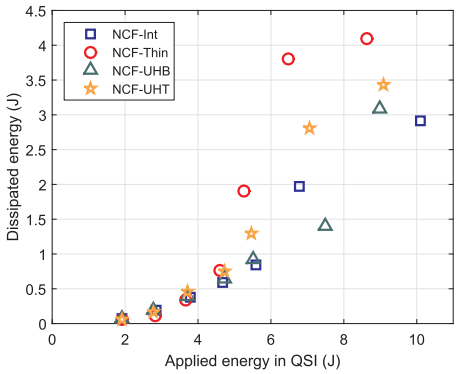

Fig. 12. The evolution of dissipated energy (E_d) plotted against the applied energies (E_a) for all seven QSI deflection levels for all laminates.

the applied energies (E_a) for the different QSI deflection levels. The applied energies are calculated by integrating the area under the whole loading part of the respective QSI curves, while the dissipated energy is the area of the enclosed curve obtained. Until the applied energy of 4 J, NCF-Thin dissipated the least energy while for energies higher than 4 J, the same laminate dissipated the highest energy. At higher applied energies (above E_a of 5 J), both NCF-UHB and NCF-Int exhibited lower dissipated energies compared to NCF-Thin and NCF-UHT. NCF-UHB dissipated 50% and 60% less energy, respectively, when compared to its counterparts NCF-UHT and NCF-Thin.

4.3. Compression after impact

Fig. 13 presents the pristine compression and CAI strength of all the laminates for all the impact energies. With intermediate and thin plies mixed in the same laminate, the hybrid laminate exhibited a plain compression strength value in between that of NCF-Int and NCF-Thin. NCF-UHT and NCF-UHB displayed a 5% lower plain compression strength than the thin-ply laminate and a 5% higher value than NCF-Int. As reported in [2,3], thin plies have a higher pristine compression strength (10% increase) over the intermediate plies. Note that the thin-ply laminate NCF-Thin at IE_1 exhibited invalid CAI failure mode (caused by local buckling at the top of the specimen as reported in [3])

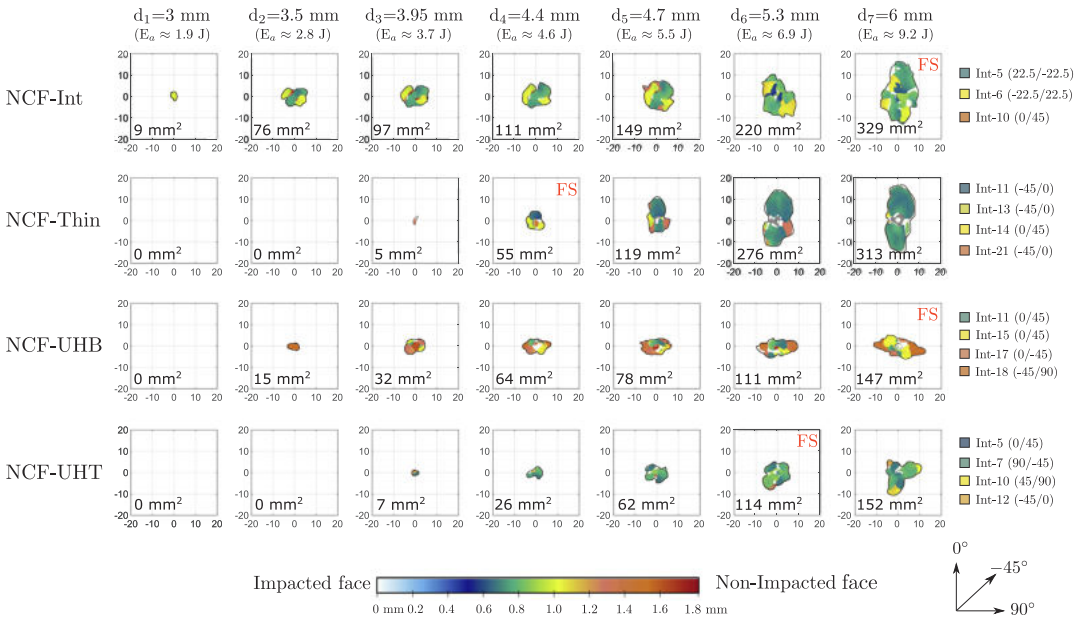

Fig. 11. C-scan inspection images for all the laminates for all the indenter deflections from d_1 to d_7. Projected damage profile and area are presented, furthermore the initiation of back fibre splitting is also identified and marked by 'FS'.

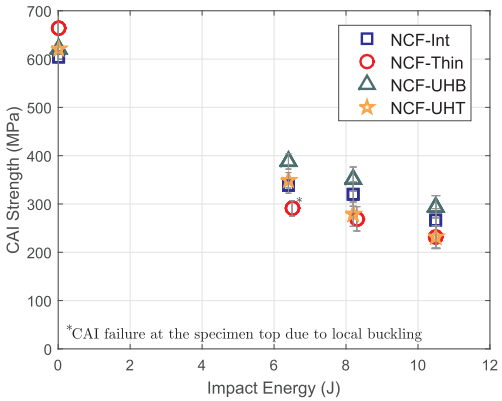

Fig. 13. Plain compression strengths and CAI strengths of all laminates for all impact energies.

despite using the anti-buckling ribs.

Out of all the laminates and all the energies, the hybrid laminate NCF-UHB exhibited the highest CAI strength. Fig. 14 (a) and (b) present the plain compression and CAI strengths of the hybrid laminates normalized with respect to the baselines NCF-Int and NCF-Thin, respectively. On comparing NCF-UHB laminate to the baselines when reviewing all the impact energies, NCF-UHB exhibited 12% and 30% higher CAI strength over NCF-Int and NCF-Thin, respectively. Between the two hybrid laminates, NCF-UHB displayed 20% more CAI strength than NCF-UHT, indicating the importance the location of the added intermediate plies has on the post-impact response. NCF-UHT exhibited higher CAI strength that the baselines for IE_1, but at higher impact energies (IE_2 and IE_3) the CAI strength dropped drastically and exhibited similar values to those of NCF-Thin. Fig. 15 shows the reduction in the residual compression strength caused by the impact damage for all laminates. NCF-Thin displayed the highest reduction (60%) in the compression strength, while NCF-UHB showed the lowest (40%).

5. Discussion

Thin laminates undergo severe bending during impact loading due to their reduced bending stiffness [2,3]. Bending induces high in-plane tensile stresses at the non-impacted face of the laminate that leads to fibre splits or breakage in the bottom plies (Fig. 7). In addition, high bending creates shear stresses between the plies that trigger delamination at the interfaces closest to the bottom of the laminate. Studies on thin laminates [2,26] reveal that the bottom interfaces (close to the non-impacted face) exhibit extensive delamination. Hence, the non-impacted face is the most critical or damage prone region in a thin laminate under low velocity impact loads, as evidenced by the delamination and fibre damage at this location.

As reported in [3], irrespective of the ply grade of non-crimp fabrics used, low velocity impact loads induce both delamination and fibre damage in thin laminates. However, the extent of the dominance of these damage modes depends significantly on the ply grade used. Thin laminates made of thin plies exhibited delayed delamination onset (associated to their in situ effect [27,28]), but with early and extended fibre damage. To the contrary, thicker plies dissipated energy through matrix cracks and delaminations, resulting in delayed and subdued fibre damage. Increased fibre damage with thin plies resulted in poor impact response (reduced peak loads and high energy dissipation) and a reduced CAI strength (as in NCF-Thin).

Unlike thin plies, intermediate plies (or a cluster of two thin plies)

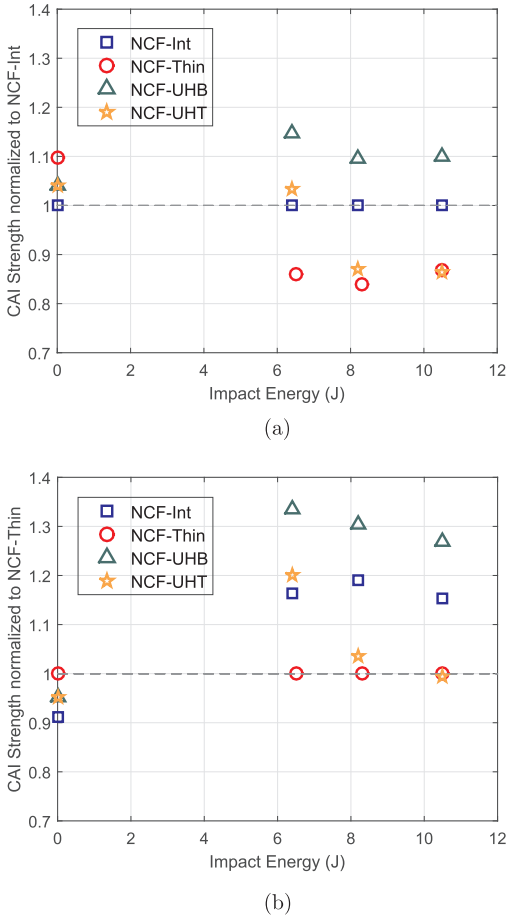

Fig. 14. Comparison of CAI strengths normalised with (a) intermediate plies (NCF-Int) as baseline and (b) thin plies (NCF-Thin) as baseline. The plain compression strengths are also normalized according to the respective baselines.

introduce higher interlaminar shear stresses at their adjacent interfaces (resulting from the high bending stiffness mismatch between the interfaces [29]) triggering delamination [23]. C-scan images of NCF-UHB revealed the dominant delamination at the last laminate interface, within the site of the added intermediate plies, thereby following the hypothesis formulated during the laminate design phase. On the other hand, impact loading induces high out-of-plane compressive stresses at the impactor vicinity and these stresses counteract the interlaminar shear stresses to increase the local interlaminar fracture toughness [30]. This explains the absence of dominant delaminations within the region of the added intermediate plies (at the top) in NCF-UHT.

The addition of the intermediate plies to the bottom of the laminate (critical region) resulted in suppressing/delaying the fibre damage by promoting early delamination. This is evidenced in the QSI results by the 55% increase in the force value over NCF-Thin at which the first load drop was observed (associated with the initiation of fibre damage). Meanwhile, the addition of intermediate plies to the top of the laminate helped to delay the initiation of fibre damage compared to NCF-Thin (as

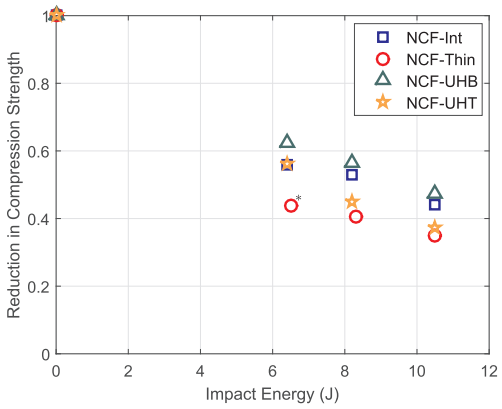

*CAI failure at the specimen top due to local buckling

Fig. 15. Normalized reduction in the compressive strength due to the impact damage of all the laminates.

in Fig. 10) but with the critical bottom part of the laminate comprised of thin plies, fibre damage was dominant (evidenced by the successive load drops in Figs. 4 and 10).

CAI strength of a thin laminate depends on the extent of delamination and fibre damage in the laminate, with fibre damage being more critical and clearly linked to the drastic reduction in the CAI strength [2,31]. On one hand, the already formed delaminations split the laminate into sub-laminates, and one of the sub-laminates buckles to result in a final collapse. On the other hand, a high magnitude of fibre failure in the laminate, especially the load sustaining 0° plies, promotes compressive fibre failure that leads to CAI failure. In NCF-UHB, the C-scan inspection reveals that entire damage area is significantly lower than that of the baselines and also governed by a single delamination at the last interface, oriented in the 90° direction. Hence, under CAI loads, the laminate will split with a thicker sub-laminate at the top (entire laminate except the last ply) and a thinner one at the bottom (last ply, 90°) which is not carrying a high load. The thicker sub-laminate sustains higher compressive loads leading to a higher CAI strength [32]. In addition to this, the reduced fibre failure, as a result of hybridization, is also a reason for the increased CAI strength. Meanwhile, the increased fibre damage in NCF-UHT laminate led to its reduced CAI strength, compared to its flipped counterpart.

While thin plies have been a remarkable asset to the composite community with their numerous advantages (delamination resistance [33], associated in situ strength), their vulnerability towards impact and post impact loads is their Achilles heel. In this study, we have exhibited that the addition of some thicker plies could substantially mitigate the out-of-plane threats to a thin-ply laminate, evidenced in the form of reduced fibre failure, delamination area and higher CAI strength. The results show that hybridization can be used to exploit the potential of different ply grades and help in tailoring the damage to occur at predetermined locations. Apart from the unsymmetrical design helping to understand the importance the location of added plies has, they can be the optimal solution for several load cases. When compared to the expensive alternatives of modifying the material system or using interface toughening agents to improve the out-of-plane response of thin plies, we have demonstrated the full potential laminate design has to come up with novel laminates promising remarkable improvements, and also economic feasibility. While in this study we proposed the idea of a novel laminate as a rule of thumb, the next immediate step is to explore all the laminates within a particular design space to find an optimum damage-tolerant laminate using numerical finite element tools.

6. Conclusion

Impact loads pose a great threat to thin laminates made of thin plies because of the extensive fibre failure and reduced CAI strength. To alleviate this vulnerability thin plies have towards out-of-plane responses, we have made a first attempt to design a novel laminate which combines ply hybridization and laminate mid-plane unsymmetry. We designed a hybrid laminate (made of non-crimp fabrics) which comprises both thin and intermediate plies, where the intermediate plies are placed only on the non-impacted side of the laminate (NCF-UHB). We carried out an experimental campaign using impact, compression after impact and quasi-static indentation tests and compared the responses of the proposed laminate to those of the symmetric and non-hybrid baseline laminates. We also included in the comparison the hybrid laminate flipped upside down (NCF-UHT, intermediate plies at the top) to illustrate how crucial is the location of the intermediate plies. The hybrid laminate NCF-UHB substantially delayed the fibre breakage onset (by 55%) and reduced the extent of fibre damage when compared to the thin-ply baseline NCF-Thin. The proposed laminate exhibited a 50% and 30% reduction in damage area and dissipated energy, respectively, over the thin-ply baseline laminate, thus providing a higher impact resistance. As a result of the improved impact response, the unsymmetrical-hybrid laminate increased the CAI strength by 30% (over the thin-ply baseline). In view of a practical application of the proposed novel design, for the baseline laminate to match the same residual strength as of the proposed laminate, additional plies have to be added to the baseline laminate, which in turn results in added mass and increased material costs. Finally, we have demonstrated the prospects of this novel laminate design (combining hybridization and unsymmetry) as an efficient and economic tool to mitigate the weakness of thin plies towards impact and post impact loads.

Data availability

The raw/processed data required to reproduce these findings cannot be shared at this time due to legal or ethical reasons.

Acknowledgements

The first author would like to thank the Generalitat de Catalunya for the FI-DGR pre-doctoral grant (2018 FI-B2 00118). The authors would like to thank Chomarat at Le Cheylard, France, for providing the materials used in this study. This work has been supported by the Spanish Ministerio de Economía y Competitividad through the grant coded MAT2015-69491-C3-1-R, supported by FEDER/EU. The baseline laminates for comparison purposes are from a research project led by Airbus, partnered with AMADE (University of Girona, Spain), INEGI (University of Porto, Portugal), and the University of Dayton Research Institute (UDRI, US). Thanks to Airborne Composites at Girona, Spain, for manufacturing the unsymmetrical laminates.

Appendix A. Supplementary data

Supplementary data associated with this article can be found, in the online version, at https://doi.org/10.1016/j.compstruct.2019.03.069.

References

[1] Abrate S. Impact on composite structures. Cambridge University Press; 2005.
[2] Sasikumar A, Trias D, Costa J, Orr J, Linde P. Effect of ply thickness and ply hybridization on compression after impact strength of thin composite laminates. Submitted to Composites Part A: Applied Science and Manufacturing.
[3] Sasikumar A, Trias D, Costa J, Blanco N, Orr J, Linde P. Impact and compression after impact response in thin laminates of spread-tow woven and non-crimp fabrics.

Compos Struct 2019;215:432–45.
[4] Saito H, Morita M, Kawabe K, Kanesaki M, Takeuchi H, Tanaka M, Kimpara I. Effect of ply-thickness on impact damage morphology in CFRP laminates. J Reinforced Plast Compos 2011;30(13):1097–106.
[5] Yokozeki T, Aoki Y, Ogasawara T. Experimental characterization of strength and damage resistance properties of thin-ply carbon fiber/toughened epoxy laminates. Compos Struct 2008;82(3):382–9.
[6] Saeed MU, Chen Z, Chen Z, Li B. Compression behavior of laminated composites subjected to damage induced by low velocity impact and drilling. Compos Part B: Eng 2014;56:815–20.
[7] Sihn S, Kim RY, Kawabe K, Tsai SW. Experimental studies of thin-ply laminated composites. Compos Sci Technol 2007;67(6):996–1008.
[8] Liv Y, Guillamet G, Costa J, González E, Marín L, Mayugo J. Experimental study into compression after impact strength of laminates with conventional and nonconventional ply orientations. Compos Part B: Eng 2017;126:133–42.
[9] Caputo F, De Luca A, Sepe R. Numerical study of the structural behaviour of impacted composite laminates subjected to compression load. Compos Part B: Eng 2015;79:456–65.
[10] ASTM D7137/D7137-15. Standard test method for compressive residual strength properties of damaged polymer matrix composite plates; 2015.
[11] García-Rodríguez S, Costa J, Bardera A, Singery V, Trias D. A 3D tomographic investigation to elucidate the low-velocity impact resistance, tolerance and damage sequence of thin non-crimp fabric laminates: effect of ply-thickness. Compos Part A: Appl Sci Manuf 2018;113:53–65.
[12] Cugnoni J, Amacher R, Kohler S, Brunner J, Kramer E, Dransfeld C, et al. Towards aerospace grade thin-ply composites: effect of ply thickness, fibre, matrix and interlayer toughening on strength and damage tolerance. Compos Sci Technol 2018;168:467–77.
[13] Sebaey T, Mahdi E. Using thin-plies to improve the damage resistance and tolerance of aeronautical CFRP composites. Compos Part A: Appl Sci Manuf 2016;86:31–8.
[14] Arteiro A, Catalanotti G, Xavier J, Linde P, Camanho P. A strategy to improve the structural performance of non-crimp fabric thin-ply laminates. Compos Struct 2018;188:438–49.
[15] Furtado C, Arteiro A, Catalanotti G, Xavier J, Camanho P. Selective ply-level hybridisation for improved notched response of composite laminates. Compos Struct 2016;145:1–14.
[16] Sasikumar A, Costa J, Trias D, González EV, García-Rodríguez S, Maimí P. Unsymmetrical stacking sequences as a novel approach to tailor damage resistance under out-of-plane impact loading. Compos Sci Technol 2019;173:125–35.
[17] Tsai SW, Cognet M. The amazing bi-angle thin-ply NCF. JEC Compos 2011(68):51–2.
[18] Herakovich CT. Mechanics of fibrous composites; 1998.
[19] MATLAB, version 8.5.0 (R2015a). The MathWorks Inc.: Natick, Massachusetts; 2015.
[20] Olsson R. Closed form prediction of peak load and delamination onset under small mass impact. Compos Struct 2003;59(3):341–9.
[21] Sebaey T, González E, Lopes C, Blanco N, Maimí P, Costa J. Damage resistance and damage tolerance of dispersed CFRP laminates: effect of the mismatch angle between plies. Compos Struct 2013;101:255–64.
[22] ASTM D7136/D7136-15. Standard test method for measuring the damage resistance of a fiber reinforced polymer matrix composite to a drop weight impact event; 2015.
[23] González E, Maimí P, Camanho P, Lopes C, Blanco N. Effects of ply clustering in laminated composite plates under low-velocity impact loading. Compos Sci Technol 2011;71(6):805–17.
[24] Remacha M, Sánchez-Sáez S, López-Romano B, Barbero E. A new device for determining the compression after impact strength in thin laminates. Compos Struct 2015;127:99–107.
[25] ASTM D6484/D6484M-09. Standard test method for open-hole compressive strength of polymer matrix composite laminates; 2009.
[26] García-Rodríguez S, Costa J, Singery V, Boada I, Mayugo J. The effect interleaving has on thin-ply non-crimp fabric laminate impact response: X-ray tomography investigation. Compos Part A: Appl Sci Manuf 2018;107:409–20.
[27] Camanho PP, Dávila CG, Pinho ST, Iannucci L, Robinson P. Prediction of in situ strengths and matrix cracking in composites under transverse tension and in-plane shear. Compos Part A: Appl Sci Manuf 2006;37(2):165–76.
[28] Camanho PP, Maimí P, Dávila C. Prediction of size effects in notched laminates using continuum damage mechanics. Compos Sci Technol 2007;67(13):2715–27.
[29] Liu D. Impact-induced delamination-a view of bending stiffness mismatching. J Compos Mater 1988;22(7):674–92.
[30] Catalanotti G, Furtado C, Scalici T, Pitarresi G, Van Der Meer F, Camanho P. The effect of through-thickness compressive stress on mode II interlaminar fracture toughness. Compos Struct 2017;182:153–63.
[31] Ghelli D, Minak G. Low velocity impact and compression after impact tests on thin carbon/epoxy laminates. Compos Part B: Eng 2011;42(7):2067–79.
[32] Hwang S-F, Liu G-H. Buckling behavior of composite laminates with multiple delaminations under uniaxial compression. Compos Struct 2001;53(2):235–43.
[33] Guillamet G, Turon A, Costa J, Renart J, Linde P, Mayugo J. Damage occurrence at edges of non-crimp-fabric thin-ply laminates under off-axis uniaxial loading. Compos Sci Technol 2014;98:44–50.

A.6 Paper F

A virtual testing based search for optimum compression after impact strength in thin laminates using ply-thickness hybridization and unsymmetrical designs

A. Sasikumar[a,*], J. Costa[a,*], D. Trias[a,1], J. Llobet[a], I. R. Cozár[a], A. Turon[a], P. Linde[b,c]

[a] AMADE, Polytechnic School, Universitat de Girona, Campus Montilivi s/n, E-17003 Girona, Spain

[b] Airbus Operations GmbH, Kreetslag 10, 21129 Hamburg, Germany

[c] Department of Industrial and Materials Science, Chalmers University of Technology, S-41296 Gothenburg, Sweden

[*] Corresponding author

[1] Serra Hunter Fellow

The paper has been published in *Composites Science and Technology* 196 (2020) 108188.

Composites Science and Technology 196 (2020) 108188

Contents lists available at ScienceDirect

Composites Science and Technology

journal homepage: http://www.elsevier.com/locate/compscitech

A virtual testing based search for optimum compression after impact strength in thin laminates using ply-thickness hybridization and unsymmetrical designs

A. Sasikumar [a,*], J. Costa [a,**], D. Trias [a,1], J. Llobet [a], I.R. Cózar [a], A. Turon [a], P. Linde [b,c]

[a] AMADE, Polytechnic School, Universitat de Girona, Campus Montilivi s/n, 17073 Girona, Spain
[b] Airbus Operations GmbH, Kreetslag 10, 21129, Hamburg, Germany
[c] Department of Industrial and Materials Science, Chalmers University of Technology, S-41296, Gothenburg, Sweden

ARTICLE INFO

Keywords:
B. impact behaviour
C. Finite element analysis (FEA)
C. Damage tolerance
Ply-thickness hybridization

ABSTRACT

In the quest to improve the compression after impact (CAI) strength of thin laminates, ply-hybrid laminates (where plies of different thicknesses are mixed) have been used in a previous study to mitigate the fibre failure and, consequently, improve the CAI strength. In the same study, hybrid laminates were proposed following qualitative design rules. In this paper, we systematically look for hybrid stacking sequences with improved damage tolerance by virtually testing all the laminates in a defined design space. While the laminates in the design space are made of intermediate and thick ply grades, the baseline laminate has only intermediate grade plies. Using an in-house numerical model, we virtually tested, (impact and CAI at two impact energies), all the candidate stacking sequences. The best hybrid laminates considerably improved the CAI strength over the baseline (31% and 40% improvement for the symmetric and unsymmetrical hybrid laminates, respectively). One of the best hybrid laminates was then manufactured and tested experimentally to validate the approach. Through virtual testing, this study demonstrates the benefits of using ply thickness hybrid laminates and the feasibility of optimizing the stacking sequence for impact damage tolerance.

1. Introduction

Low velocity impacts result in an alarming reduction in the residual strength of composite structures [1]. This fact is the reason for the search for optimum damage tolerant designs. Few studies [2–5], however, have been devoted to understanding the impact and compression after impact (CAI) response of thin laminates (< 2 mm), like those found in fuselage skins and in some other surfaces in current aircraft structures. Studies into the effect ply thickness has on thin laminates concluded that thin uni-directional plies (75 gsm) resulted in extensive fibre damage and reduced CAI strength compared to intermediate (134 gsm) and thick (268 gsm) plies. A reduced CAI strength with thin plies was also reported with other material systems, such as woven [4] and non-crimp fabrics (NCF) [4,6].

To enhance the thin ply structural response, attention can be turned to the design of the stacking sequence [7,8]. Furtado et al. [9] and Arteiro et al. [10] performed selective ply level hybridization (combining different ply grades in the laminate) to improve the notched strength over a thin ply baseline. Sebaey et al. [11] designed a hybrid thick laminate (around 4.1 mm) where each thick fabric layer (320 gsm) was surrounded by a thin fabric layer (80 gsm) and improved the CAI strength by 15% over a baseline laminate made of only thick woven layers. We proposed an unsymmetrical and hybrid (intermediate and thin ply grades) thin laminate made of NCF to mitigate the fibre damage in thin plies and the CAI strength improved by 30% [12]. We followed a similar ply hybridization approach in [3] by adding thick 0° plies (268 gsm) to thin uni-directional plies, which resulted in a 40% improvement in the CAI strength. In these two previous studies [3,12] the stacking sequences were designed following qualitative arguments which were unable to anticipate the attained improvement [3,4]. In addition, such a design procedure ignored other possible laminates within the same design space. In spite of the usefulness of these approaches to illustrate

* Corresponding author.
** Corresponding author.
E-mail addresses: aravind.sasikumar@udg.edu (A. Sasikumar), josep.costa@udg.edu (J. Costa).
[1] Serra Hunter Fellow.

https://doi.org/10.1016/j.compscitech.2020.108188
Received 5 December 2019; Received in revised form 2 March 2020; Accepted 8 April 2020
Available online 7 May 2020

the potential improvement of damage tolerance through laminate design, they did not constitute true optimization exercises.

Optimizing the impact and CAI response within a large design space of stacking sequences by experimental testing is infeasible. Therefore, researchers moved to virtual tests based on finite element methods to evaluate the CAI strength. Hongkarnjanakul et al. [13] studied twelve laminates to understand the effect stacking sequences have on the low velocity impact response using a discrete 3D numerical model presented in [14]. Meanwhile, Dubary et al. [15] attempted to optimize damage tolerance with numerical tools [16].

In this paper, we take, as a baseline, a thin laminate (1.7 mm) made of aerospace grade intermediate plies (introduced in Ref. [3]) and attempt to find a stacking sequence with optimal damage tolerance. The design space comprehends symmetric and unsymmetric stacking sequences with combinations of thick and intermediate ply grades. An in-house constitutive model featuring inter- and intralaminar damage [17–19] and numerical modelling methodologies [20–22]) developed by the AMADE research group are used to perform virtual impact and CAI tests. The results revealed that symmetric hybrid laminates improved CAI strength by 30% over the baseline and that the improvement is even further enhanced for unsymmetrical laminates, by 40%. Finally, an experimental impact and CAI test carried out on one of the optimal hybrid stacking sequences validates the virtual approach. In addition, using the exhaustive numerical results, a correlation analysis pointed out impact dissipated energy and delamination area as the strongest and the weakest parameters, respectively, to correlate with CAI strength.

2. Methodology

2.1. Numerical modelling

We used the same numerical approach as that of Soto et al. [21], where Abaqus/Explicit conventional shell elements with reduced integration (S4R) were used to model the plies and zero thickness cohesive elements (COH3D8) to model the interfaces between the plies. Progressive intraply damage was accounted for with the continuum damage model (CDM) proposed by Maimí et al. [17,18]. The damage activation functions are based on the LARC04 failure criteria [23] and the model, formulated in plane-stress, incorporates the crack band formulation [24]. The predictive capability of the model has been demonstrated under different loading conditions such as impact, compression after impact [22,25–27] and open-hole tension [28,29]. The cohesive constitutive model for the interfaces is that proposed by González et al. [19]. Both the intra- and inter laminar models are implemented in a VUMAT user-written subroutine.

The conventional shell elements were placed at the mid-ply location and were tied to the cohesive elements at the interfaces (Fig. 1). A finer structured mesh (oriented in the ply direction) with elements of 0.4 mm was defined for a 35 × 35 mm window under the impactor, whereas the remaining region had a coarse mesh (3 mm). The transverse tensile and in-plane shear strength values were calculated according to the ply thickness and the ply type (outer or embedded) to account for the in-situ strength [30]. To avoid excessive element distortion, an element was deleted when the fibre damage variable (d_1) reached 1, and the transverse and shear damage variables were limited to a maximum value of 0.99 but without deleting the element. Further details of the virtual approach are explained in Refs. [20,21].

The CAI simulation was performed using the RESTART command in Abaqus/Explicit, where the impact assembly and results are imported. The rigid parts (impactor, base plate and rubber clamps) were removed before starting the CAI simulation. In addition to the standard CAI fixture, a non-standard anti-buckling fixture (recommended by Refs. [31] and used by Refs. [3,4,12,32]) was accounted for in the simulations.

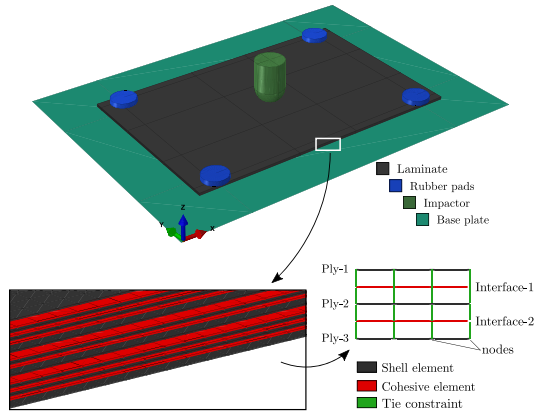

Fig. 1. The virtual impact test setup followed by the modelling strategy with conventional shell elements linked with zero-thickness cohesive elements using tie constraints.

2.2. Laminate design space and optimization approach

The material system studied here is T700/M21 carbon-epoxy. The baseline laminate (Table 1) is made of 13 intermediate grade plies of 134 gsm (1.7 mm total thickness) and is centre-symmetric (i.e., the mid-plane axis runs through the centre of the mid-ply). It was named H-134 in Ref. [3], and was selected as the baseline as it offered the highest CAI strength when compared to that of the thick and thin ply grade laminates in Ref. [3].

Primarily, the laminate design space for the optimization exercise embraced hybrid symmetric thin laminates made up of intermediate (134 gsm) and thick (268 gsm) grade plies (NB: This combination of ply grades was not explored in the previous study by the authors [3]). Thin plies (75 gsm) were intentionally discarded because of the extensive fibre damage caused by LVI that impairs the CAI strength [3].

Thick plies (0.262 mm) were considered as a cluster of two intermediate plies (0.131 mm). The laminates had to obey the following constraints: (a) Symmetric and balanced with the same laminate thickness as that of the baseline (1.71 mm); (b) Surface plies are fixed to be ±45°; (c) No clusters of more than three plies allowed; (d) Thick plies oriented in 0° , ±45° or 90° (not just limited to 0° , as in Ref. [3]); (e) % of 0° plies higher than the % of 90 (as in the baseline laminate); (f) A minimum of 10% of the total number of plies should be oriented in each of the four directions (0° , ±45° and 90°); (g) The number of 0° plies is set to be 3 (as in the baseline laminate) or 5 (to reach a larger design space); (h) The equivalent bending stiffness parameter (D*, proposed by Olsson [33]) within 5% tolerance of the baseline laminate (to have a proper comparison). No constraint was imposed on the mismatch angle between plies.

A total of 29 laminates obeyed the above constraints (Table 1). The maximum deviation in the D* values from the baseline was 4%. We grouped the laminates according to the total number of plies, G1 (7

Table 1
Baseline laminate and all the symmetric hybrid laminates studied.

Group	Laminate	Stacking sequence	No. of plies	Ply % [0/ ±45/90]	D* (Nm)
REF	H-134 (Baseline)	[45/-45/0/45/-45/90/0/90/-45/45/0/-45/45]	13	[23/31/15]	22.08
G1	L1	$[45_2/-45_2/90/0_3/90/-45_2/45_2]$	7	[23/31/15]	22.12
	L2	$[45_2/90/-45_2/0_3/-45_2/90/45_2]$	7	[23/31/15]	22.09
G2	L3	$[45_2/-45/90/-45/0_3/-45/90/-45/45_2]$	9	[23/31/15]	22.17
	L4	$[45/-45_2/45/90/0_3/90/45/-45_2/45]$	9	[23/31/15]	22.72
	L5	$[45/-45_2/90/45/0_3/45/90/-45_2/45]$	9	[23/31/15]	21.78
	L6	$[45/-45/0_2/90_2/0/90_2/0_2/-45/45]$	9	[38/15/31]	22.12
	L7	$[45/-45/0/90_2/0_3/90_2/0/-45/45]$	9	[38/15/31]	22.17
	L8	$[45/0_2/-45/90_2/0/90_2/-45/0_2/45]$	9	[38/15/31]	22.12
	L9	$[45/0/-45/90_2/0_3/90_2/-45/0/45]$	9	[38/15/31]	22.17
	L10	$[45/0_2/90_2/-45/0/-45/90_2/0_2/45]$	9	[38/15/31]	22.75
	L11	$[45/0/90_2/-45/0_3/-45/90_2/0/45]$	9	[38/15/31]	21.74
	L12	$[45/90/45/-45_2/0_3/-45_2/45/90/45]$	9	[23/31/15]	21.74
	L13	$[45/90/-45_2/45/0_3/45/-45_2/90/45]$	9	[23/31/15]	22.09
	L14	$[45/90_2/0_2/-45/0/-45/0_2/90_2/45]$	9	[38/15/31]	22.65
	L15	$[45/90_2/0/-45/0_3/-45/0/90_2/45]$	9	[38/15/31]	21.74
G3	L16	$[45/-45/45/-45/90/0_3/-45/45/-45/45]$	11	[23/31/15]	22.52
	L17	$[45/-45/45/90/-45/0_3/-45/90/45/-45/45]$	11	[23/31/15]	22.09
	L18	$[45/-45/90/45/-45/0_3/-45/45/90/-45/45]$	11	[23/31/15]	22.65
	L19	$[45/-45/90/0_2/90/0/90/0_2/90/-45/45]$	11	[38/15/31]	22.53
	L20	$[45/-45/90/0/90/0_3/90/0/90/-45/45]$	11	[38/15/31]	22.26
	L21	$[45/0_2/90/-45/90/0/90/-45/90/0_2/45]$	11	[38/15/31]	21.04
	L22	$[45/0/90/-45/90/0_3/90/-45/90/0/45]$	11	[38/15/31]	22.75
	L23	$[45/90/-45/45/-45/0_3/-45/45/-45/90/45]$	11	[23/31/15]	22.58
	L24	$[45/90/-45/0_2/90/0/90/0_2/-45/90/45]$	11	[38/15/31]	22.71
	L25	$[45/90/-45/0/90/0_3/90/0/-45/90/45]$	11	[38/15/31]	22.40
	L26	$[45/90/02/-45/90/0/90/-45/0_2/90/45]$	11	[38/15/31]	21.78
	L27	$[45/90/0/-45/90/0_3/90/-45/0/90/45]$	11	[38/15/31]	21.55
	L28	$[45/90/0_2/90/-45/0/-45/90/0_2/90/45]$	11	[38/15/31]	22.52
	L29	$[45/90/0/90/-45/0_3/-45/90/0/90/45]$	11	[38/15/31]	21.54

plies), G2 (9 plies) and G3 (13 plies). The percentage of clustered plies (ratio of the thickness of all clustered plies to the total thickness) varied accordingly: 85% for G1, 54% and 62% for G2, 23% and 31% for G3. Hence, groups G1 and G2 can be referred to as the thick ply dominant groups (more than 50%) and group G3 as an intermediate ply dominant group (less than 30%).

The design space of unsymmetrical laminates obeyed the constraints given above except for the symmetry constraint, which was replaced by a null extensional-bending matrix (B = 0) to avoid coupling responses [34,35]), and led to 84 laminates. To reduce the computational cost, only 7 representative laminates with 8–11 plies were included in the virtual test study (Table 2).

3. Results

3.1. Validation of the numerical model

Prior to the optimization procedure, we checked the capability of the numerical model to reproduce the experimental tests for impact and the CAI of the baseline laminate [3]. The validation was performed only for the 8.9 and 10.5 J impact energies. The agreement was good (Fig. 2), especially for the 10.5 J impact, where the load drop (associated with the onset of fibre failure) and dissipated energy were accurately predicted. The analysis of the numerical results indicated that the load drop at the peak load initiated due to fibre damage at the bottom ply, which

Table 2
Selected unsymmetric hybrid laminates.

Group	Laminate	Stacking sequence	No. of plies	Ply % [0/ ±45/90]	D* (Nm)
REF	H-134 (Baseline)	[45/-45/0/45/-45/90/0/90/-45/45/0/-45/45]	13	[23/31/15]	22.08
UNSYM	UL1	$[45_2/90/-45/0_2/-45_3/0/90/45_2]$	8	[23/31/15]	22.45
	UL2	$[45_2/90/0/-45_3/0_2/-45/90/45_2]$	8	[23/31/15]	22.45
	UL3	$[45/-45/0_3/90/45/90/-45_2/0_2/45]$	8	[38/23/15]	21.05
	UL4	$[45/0_2/-45/90_2/45/-45/90/0_2/45]$	9	[31/23/23]	21.26
	UL5	$[45/-45/0/90/0_2/90_3/0_2/-45/45]$	9	[38/23/15]	22.31
	UL6	$[45/90/-45/0_3/90/0/90_2/-45/0/45]$	10	[38/23/15]	22.74
	UL7	$[45/0/-45/90/0/-45/45/90_2/0_2/-45/45]$	11	[31/23/23]	22.14

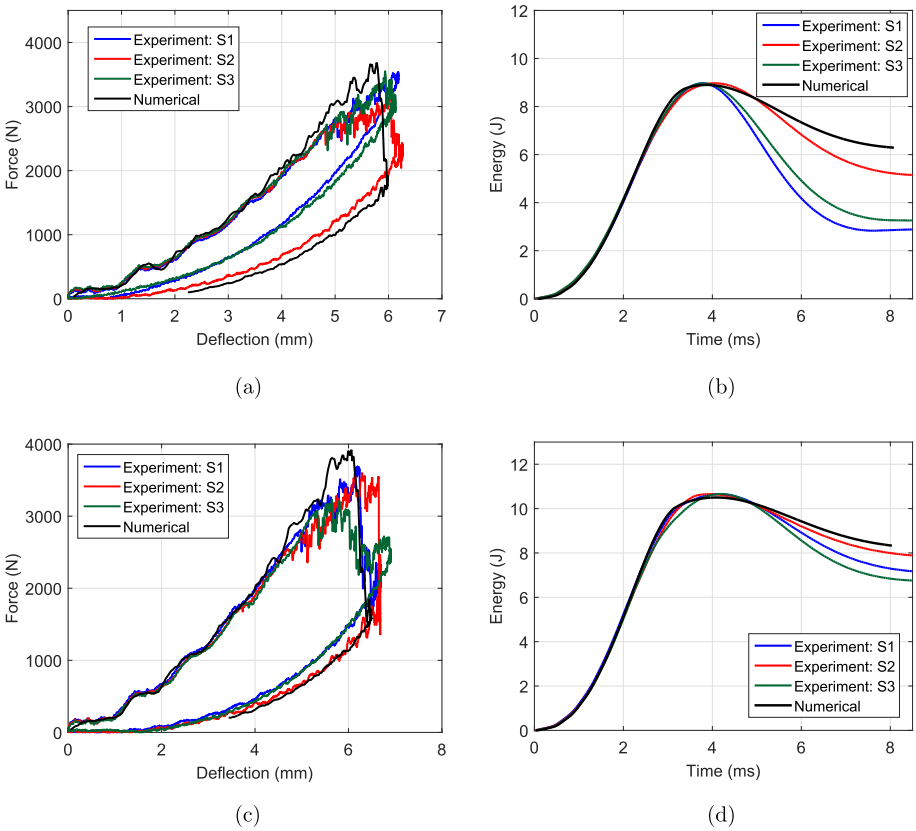

Fig. 2. Comparison of experimental and numerical force-deflection and energy-time responses of the baseline H-134 for the 8.9 J ((a) and (b)) and 10.5 J ((c) and (d)) impacts.

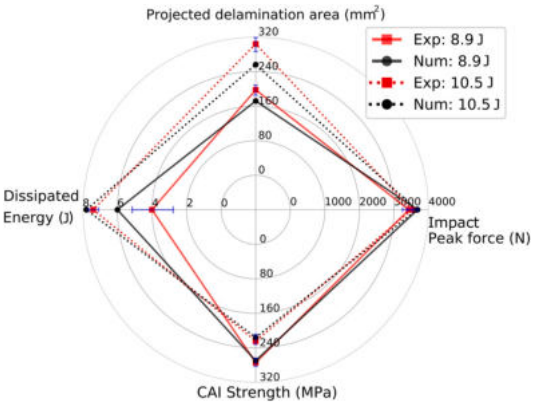

Fig. 3. Comparing the impact damage resistance parameters and the CAI strengths between experimental and numerical analysis for 8.9 and 10.5 J. (Note that the blue lines denote the standard deviation in the experimental results from three specimens). (For interpretation of the references to color in this figure legend, the reader is referred to the Web version of this article.)

then propagated to the upper plies.

Fig. 3 compares numerical and experimental impact damage resistance parameters (maximum peak force, projected delamination area, energy dissipated) and the CAI strengths. Predictions deviate from the experimental values by 5% (peak load), 9% (projected delamination area), 15% (dissipated energy) and 5% (CAI strength). The virtual test properly captured the impact induced back fibre splitting oriented in the 45° (last ply) and the compressive failure initiating from the edge of the fibre split towards the edge of the specimens (Fig. 4).

3.2. Optimization

All 29 symmetric laminates (Table 1) were virtually impacted at 8.9 J before the CAI virtual test. Fifteen hybrid laminates improved the CAI strength over the baseline, with the highest improvement reaching 13% (Fig. 5). The number of plies clearly influenced the CAI strength as almost all the G1 and G2 laminates improved that of the baseline, while those in the G3 group reduced it.

Despite the use of anti-buckling ribs to delay the pre-mature buckling of the thin laminates, some hybrid laminates (all belonging to group G3) still exhibited failure at the top zone, where the specimen is unconstrained, due to local buckling. The corresponding laminates' CAI values are marked with an * in Fig. 5. A similar CAI failure mode was experimentally reported by the authors for the hybrid laminate referred to as

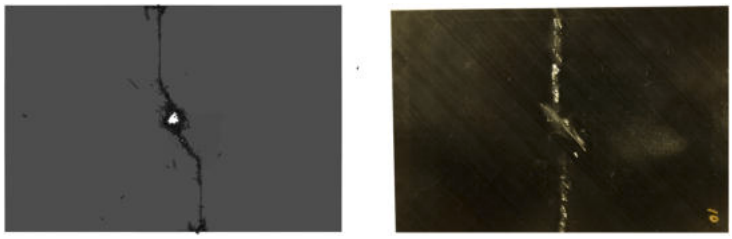

Fig. 4. Comparison of the failed CAI specimens (non-impacted side view) from the 10.5 J impact energy from the virtual (left) and experimental test (right).

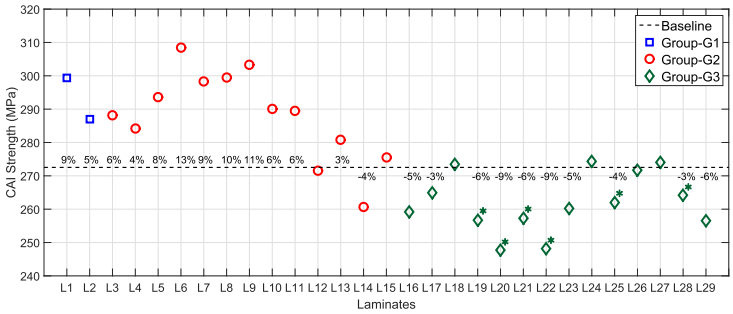

Fig. 5. Comparison of the virtual CAI strengths between the hybrid laminates and the baseline from the 8.9 J impact (Note that the CAI values marked with an * denote invalid CAI failure mode at the top of the specimen as addressed in Ref. [3]).

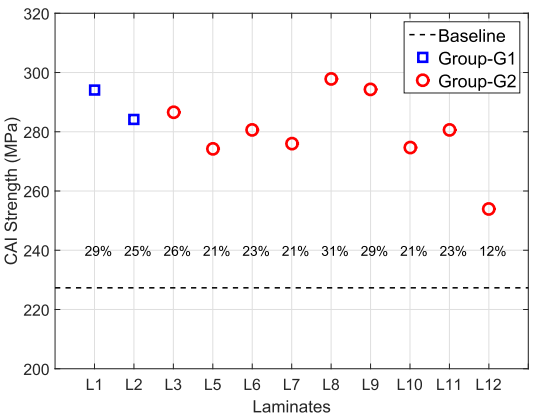

Fig. 6. Comparison of the virtual CAI strengths between the selected hybrid laminates and the baseline from the 10.5 J impact.

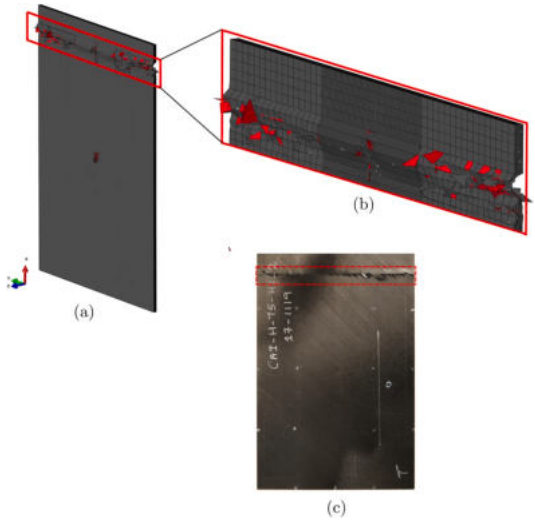

Fig. 7. Invalid CAI failure mode obtained at the top of the laminate and compared with the similar failure mode obtained experimentally in Ref. [3].

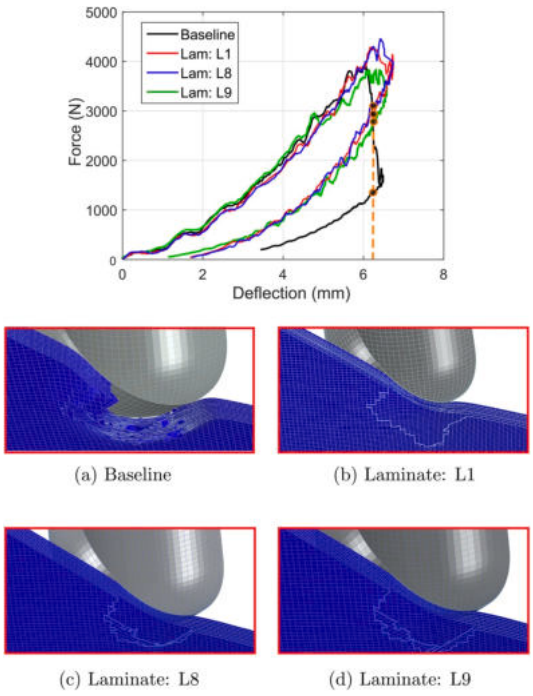

Fig. 8. Comparison of the force-deflection response and the fibre damage from the 10.5 J impact for the baseline and the proposed optimum hybrid laminates for a selected deflection level. (Note that blue contour represents those elements with the fiber damage variable $d_1 < 1$ and the deleted elements are those with $d_1 = 1.0$). (For interpretation of the references to color in this figure legend, the reader is referred to the Web version of this article.)

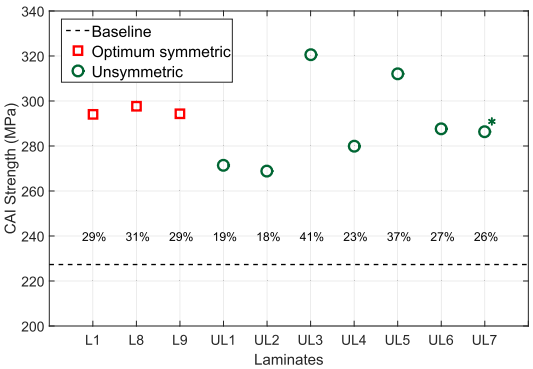

Fig. 9. Comparison of the CAI strengths of all the selected unsymmetrical hybrid laminates with the optimum symmetric hybrid and the baseline laminate for the 10.5 J impact.

H-75-H1 in Ref. [3]. The fidelity of the numerical model is further demonstrated by its capability to reproduce this failure (Fig. 7 for laminate L20).

Hybrid laminates exhibiting an improvement in CAI strength above 5% over the baseline for the 8.9 J impact were then virtually impacted at 10.5 J. Those 11 laminates (from G1 and G2) significantly improved the CAI strength over the baseline (up to 31% for L8) as in Fig. 6. The virtual impact force-deflection responses of the three symmetric laminates with better damage tolerance (L1, L8 and L9) were compared to that of the baseline(Fig. 8). This figure shows the damage status for the same deflection level (just after the load drop of the baseline, as indicated in the figure). The baseline laminate exhibited fibre damage locally under the impactor in all the plies (Fig. 8 (a)) whereas the hybrid laminates mitigated the load drop and constrained the fibre damage to the last ply.

All the 7 unsymmetrical hybrid laminates chosen, improved the CAI strength over the baseline laminates (Fig. 9); UL3 by 41% and UL5 37%. Note that laminate UL7 displayed CAI failure at the top due to the local buckling. Finally, Fig. 10 illustrates the stacking sequence of the best symmetric and unsymmetrical hybrid laminates obtained from the virtual testing campaign. The computational time for the LVI and CAI models run in a standard computer (12 cpus and 32 GB RAM per cpu) ranged from 25 to 121 h, and 5–16 h, respectively, depending on the laminate, the number of plies modeled and the impact energy. The higher the impact energy the higher the computational cost due to the higher element distortion that penalizes the stable time increment.

3.3. Experimental validation

Out of the different laminates, the symmetric hybrid laminate L1 was selected to validate experimentally the virtual approach described above. Hybrid laminate L1 has equal percentage of plies in the different orientations as that of the baseline (see Table 1), and hence was selected for the experimental validation. Impact (8.9 and 10.5 J) and CAI experimental tests followed the ASTM D7136/D7136M-15 and D7137/D7137M-15 standards, respectively. We tested three specimens per impact energy. Details of the experimental setup are described in Refs. [3]. The experimental and numerical impact responses of L1 are shown in Fig. 11, while Fig. 12 compares the CAI strengths of the hybrid laminate L1 (numerical and experimental) and baseline (experimental) for the 8.9 J and 10.5 J impacts.

4. Discussion

According to the virtual and experimental results, ply thickness hybridization (combination of thick and intermediate grade plies) in thin laminates improves the damage tolerance around 30% to 40% over a baseline of intermediate grade plies. This improvement is caused by the fact that, during impact, thick plies promote damage mechanisms other than fibre breakage (fibre breakage is behind the consequent impairment of compressive strength). Indeed, due to a reduced bending stiffness, thin laminates undergo considerable bending. While thicker plies are prone to early matrix cracking and delamination at adjacent interfaces (due to the higher interlaminar shear stresses and lower in-situ transverse strength for matrix cracking [30]), thin plies suppress/delay both of these damage mechanisms and lead to fibre splitting due to the high tensile stresses at the non-impacted side.

In the ply-hybrid laminates, the thicker plies reduce the amount of fibre damage by dissipating energy through early delaminations, while the thinner plies have a higher plain compression strength which enhances CAI strength. This is evidenced by the fact that the CAI strength

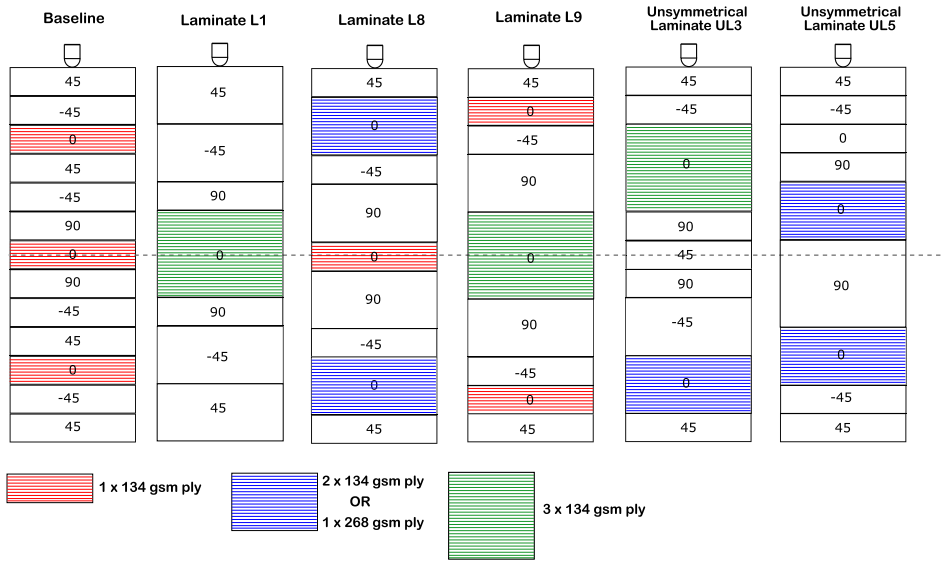

Fig. 10. Illustration of the baseline along with the optimum symmetrical and unsymmetrical impact damage tolerant hybrid thin laminates (Note that the load bearing 0° plies are colored with respect to their ply thicknesses).

decreases with the number of intermediate plies (compare the CAI strength for groups G1, thick ply dominant, to G3, intermediate ply dominant). It is also important to note that while ply thickness hybridization improves the damage tolerance, it is expected to impair the benefits of pure thin-ply laminates such as the delay of the onset of transverse cracking and fatigue damage.

We compared the evolution of the energy dissipated through intralaminar (matrix cracks and fibre damage) and inter-laminar (delaminations) damage modes between the baseline (intermediate plies) and laminate L1 (thick ply dominant hybrid laminate) as in Fig. 13. Both laminates have the same percentage distribution of ply orientations. In the early loading stage, we observed higher energy dissipation through delamination in L1. At the point of load drop for the baseline (Fig. 8), the baseline laminate underwent fibre splitting (intralaminar energy dissipation) and triggered delamination. Hence, intermediate plies (baseline) comparatively delayed the occurrence of delaminations. However, the earlier onset of extensive fibre damage induced delaminations (as explained in Ref. [36]), eventually led to a threefold higher interlaminar energy dissipation of baseline over L1.

The results indicate that it is beneficial to group the 0° plies together rather than distributing them equally in the through-the-thickness direction (as in the baseline laminate in Fig. 10.) Further, this cluster of 0° plies is safeguarded by keeping it close to the mid-plane, away from the fibre damage prone locations.

Some of the hybrid laminates with improved CAI strength have a higher percentage of 0° plies compared to the baseline, which can provide an unfair comparison. Despite this, laminates L1, UL1 (that have the exact equal ply counts in all directions as the baseline) still justifies the importance of ply hybridization and unsymmetrical designs. To further demonstrate the potential of hybrid laminates, when compared to a thick ply laminate (laminate H-268 in Refs. [3]), the hybrid laminate L1 improved the CAI strength by around 20% for different impact energies.

The optimization of stacking sequences in a large design space (i.e., plies of different thicknesses) can only be accomplished with reliable virtual tools. This work demonstrates both the feasibility of optimizing the stacking sequence for impact damage tolerance by means of virtual testing and the benefits of using ply thickness hybrid laminates. It should be noted that while the study of symmetric laminates is a true optimization procedure (all candidates in the domain are explored to find the best one), only less than 10% of total unsymmetrical hybrid laminates were virtually tested.

Taking advantage of the high number of thin laminates virtually tested, we performed a correlation analysis to study the influence of several damage resistant parameters on the CAI strength for the 8.9 J impact case. The Pareto chart (Fig. 14) shows that the dissipated energy (factor B) is the most correlated parameter to the CAI strength, followed by the fibre damage area (factor C). The easiest parameter to measure experimentally and the most used for thicker laminates, the projected delamination area (factor D), is the least influencing parameter, and hence should not be taken as an indicator of the CAI strength in thin laminates. The same observation was experimentally concluded by the authors in Ref. [3] for thin laminates.

5. Conclusion

Ply level hybridization, i.e., mixing plies of different thicknesses within a laminate, is a promising and cost effective method to improve the compression after impact strength. In this paper, we concentrated on

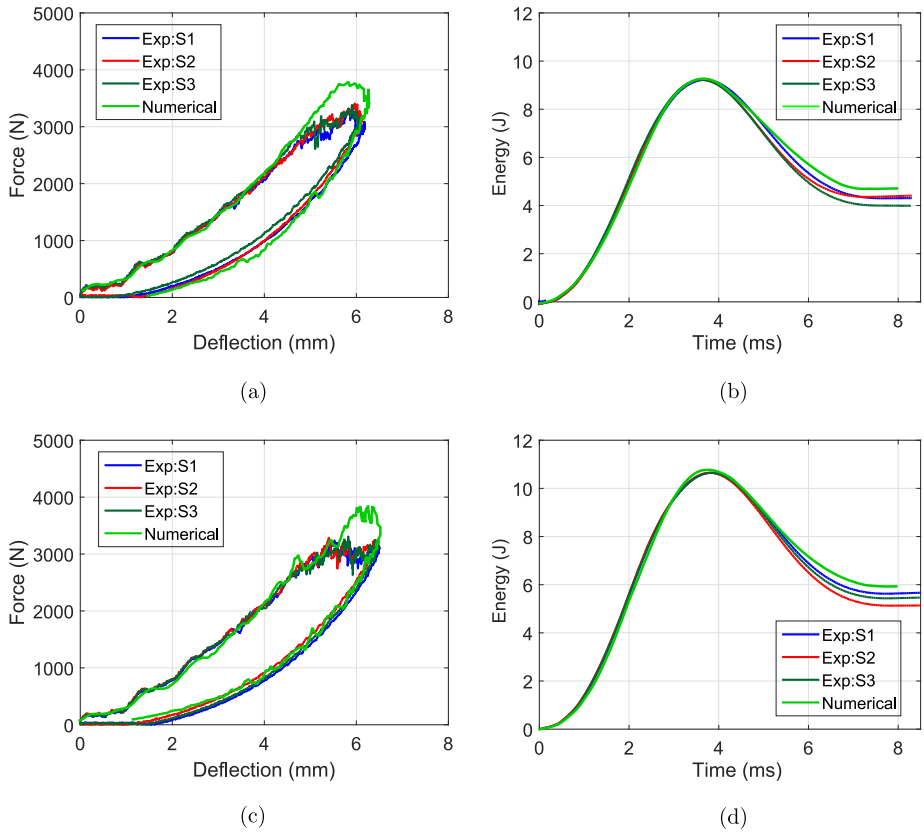

Fig. 11. Comparison of the impact response curves from the numerical virtual tests and the experimental tests for 8.9 J ((a) and (b) and 10.5 J ((c) and (d)) of the hybrid laminate L1.

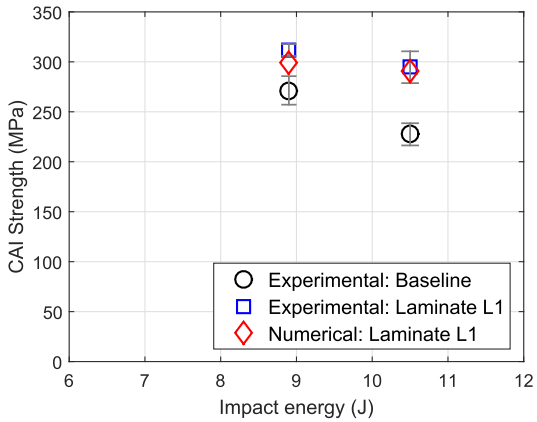

Fig. 12. Comparing the CAI strengths of hybrid laminate L1 obtained from experimental and numerical tests for both 8.9 and 10.5 J impact energies. Experimental CAI strengths of the baseline H-134 are also presented.

thin laminates and looked for optimum impact damage tolerant hybrid laminates made of intermediate and thick grade plies. An in-house finite element model was first validated with the already presented impact and CAI experimental results of the baseline (all intermediate plies) and then used for the optimization exercise over symmetric ply hybrid laminates. All symmetric laminates fulfilling the design constraints were virtually tested under impact (8.9 J and 10.5 J impact energies) and CAI. Optimum laminates improved the CAI strength by 31% over the baseline. The improvement was enhanced even further in unsymmetrical laminates (40% over the baseline and 10% over the optimum symmetric hybrid laminate), although only 10% of the much larger design space was preliminarily explored. One of the optimum symmetric hybrid laminates was experimentally tested to discern the same improvement in the CAI strength as predicted by the virtual tests. The benefit of ply hybrid laminates relies on the contribution of thick plies to dissipate energy in mechanisms different from fibre breakage and of thinner plies to resist compression. Finally, it is demonstrated that the projected delamination area for thin laminates does not correlate with the CAI strength, while the dissipated energy and the fibre damage area have a strong correlation on the CAI strength.

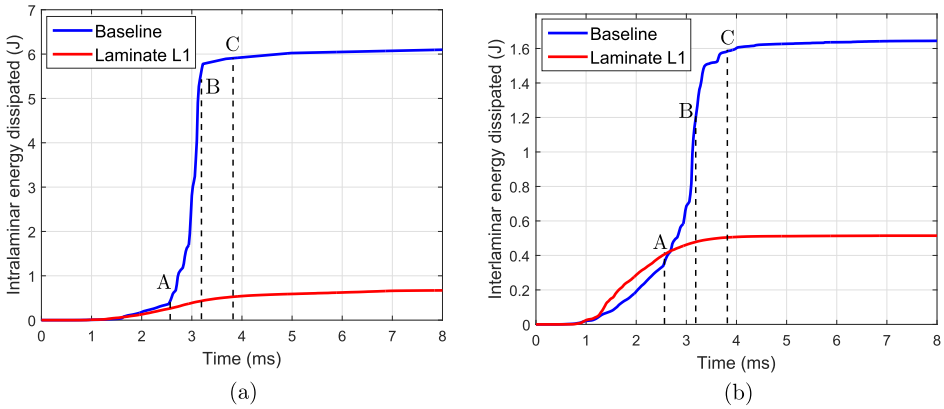

Fig. 13. Comparison of the evolution of (a) intra- and (b) inter-laminar energy dissipated between the baseline and the optimum hybrid laminate L1 for the 10.5 J virtual impact test.

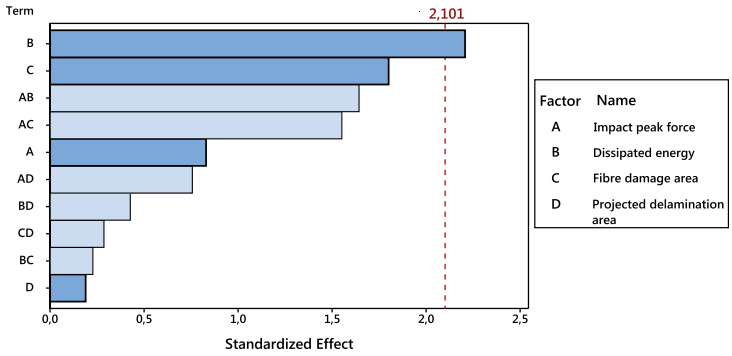

Fig. 14. Pareto chart presenting the standardized effects of different damage resistance parameters on the CAI strength.

Acknowledgements

The first author would like to thank the Generalitat de Catalunya for the FI-DGR pre-doctoral grant (2018 FI-B2 00118). The authors would like to thank the *Spanish Ministerio de Ciencia, Innovacíon y Universidades* for the grant coded RTI2018-097880-B-I00 and RTI2018-099373-B-I00. The authors acknowledge Hexcel® for the preparation of the test specimens dedicated for this study.

Appendix A. Supplementary data

Supplementary data to this article can be found online at https://doi.org/10.1016/j.compscitech.2020.108188.

References

[1] S. Abrate, Impact on Composite Structures, Cambridge University Press, 2005.
[2] S. Sánchez-Sáez, E. Barbero, R. Zaera, C. Navarro, Compression after impact of thin composite laminates, Compos. Sci. Technol. 65 (13) (2005) 1911–1919.
[3] A. Sasikumar, D. Trias, J. Costa, J. Orr, P. Linde, Effect of ply thickness and ply level hybridization on compression after impact strength of thin laminates, Compos. Appl. Sci. Manuf. 121 (2019) 232–243.
[4] A. Sasikumar, D. Trias, J. Costa, N. Blanco, J. Orr, P. Linde, Impact and compression after impact response of thin laminates of spread-tow woven and non-crimp fabrics, Compos. Struct. 215 (2019) 432–445.
[5] A. Sasikumar, Improving Compression after Impact Response of Composite Laminates through Ply Level Hybridization with Thin Plies and Unsymmetrical Designs, PhD Thesis, University of Girona, 2019.
[6] S. García-Rodríguez, J. Costa, A. Bardera, V. Singery, D. Trias, A 3D tomographic investigation to elucidate the low-velocity impact resistance, tolerance and damage sequence of thin non-crimp fabric laminates: effect of ply-thickness, Compos. Appl. Sci. Manuf. 113 (2018) 53–65.
[7] L. Mencattelli, S.T. Pinho, Realising bio-inspired impact damage-tolerant thin-ply CFRP bouligand structures via promoting diffused sub-critical helicoidal damage, Compos. Sci. Technol. (2019) 107684.
[8] C. Lopes, O. Seresta, Y. Coquet, Z. Gürdal, P. Camanho, B. Thuis, Low-velocity impact damage on dispersed stacking sequence laminates. Part I: Experiments, Compos. Sci. Technol. 69 (7–8) (2009) 926–936.
[9] C. Furtado, A. Arteiro, G. Catalanotti, J. Xavier, P. Camanho, Selective ply-level hybridisation for improved notched response of composite laminates, Compos. Struct. 145 (2016) 1–14.
[10] A. Arteiro, G. Catalanotti, J. Xavier, P. Linde, P. Camanho, A strategy to improve the structural performance of non-crimp fabric thin-ply laminates, Compos. Struct. 188 (2018) 438–449.
[11] T. Sebaey, E. Mahdi, Using thin-plies to improve the damage resistance and tolerance of aeronautical CFRP composites, Compos. Appl. Sci. Manuf. 86 (2016) 31–38.
[12] A. Sasikumar, D. Trias, J. Costa, V. Singery, P. Linde, Mitigating the weak impact response of thin-ply based thin laminates through an unsymmetrical laminate design incorporating intermediate grade plies, Compos. Struct. 220 (2019) 93–104.
[13] N. Hongkarnjanakul, C. Bouvet, S. Rivallant, Validation of low velocity impact modelling on different stacking sequences of CFRP laminates and influence of fibre failure, Compos. Struct. 106 (2013) 549–559.
[14] C. Bouvet, S. Rivallant, J.-J. Barrau, Low velocity impact modeling in composite laminates capturing permanent indentation, Compos. Sci. Technol. 72 (16) (2012) 1977–1988.
[15] N. Dubary, C. Bouvet, S. Rivallant, L. Ratsifandrihana, Damage Tolerance of an Impacted Composite Laminate, Composite Structures.
[16] S. Rivallant, C. Bouvet, N. Hongkarnjanakul, Failure analysis of CFRP laminates subjected to compression after impact: Fe simulation using discrete interface elements, Compos. Appl. Sci. Manuf. 55 (2013) 83–93.
[17] P. Maimí, P.P. Camanho, J. Mayugo, C. Dávila, A continuum damage model for composite laminates: Part I–Constitutive model, Mech. Mater. 39 (10) (2007) 897–908.
[18] P. Maimí, P.P. Camanho, J. Mayugo, C. Dávila, A continuum damage model for composite laminates: Part II–Computational implementation and validation, Mech. Mater. 39 (10) (2007) 909–919.
[19] E. González, P. Maimí, A. Turon, P. Camanho, J. Renart, Simulation of delamination by means of cohesive elements using an explicit finite element code, Comput. Mater. Continua (CMC) 9 (1) (2009) 51.
[20] A. Soto, E. González, P. Maimí, F.M. de la Escalera, J.S. de Aja, E. Alvarez, Low velocity impact and compression after impact simulation of thin ply laminates, Compos. Appl. Sci. Manuf. 109 (2018) 413–427.
[21] A. Soto, E. González, P. Maimí, J. Mayugo, P. Pasquali, P. Camanho, A methodology to simulate low velocity impact and compression after impact in large composite stiffened panels, Compos. Struct. 204 (2018) 223–238.
[22] E. González, P. Maimí, E. Martín-Santos, A. Soto, P. Cruz, F.M. de la Escalera, J. S. de Aja, Simulating drop-weight impact and compression after impact tests on composite laminates using conventional shell finite elements, Int. J. Solid Struct. 144 (2018) 230–247.
[23] C.G. Davila, P.P. Camanho, C.A. Rose, Failure criteria for FRP laminates, J. Compos. Mater. 39 (4) (2005) 323–345.
[24] Z.P. Bažant, B.H. Oh, Crack band theory for fracture of concrete, Matériaux et construction 16 (3) (1983) 155–177.
[25] C. Lopes, S. Sádaba, C. González, J. Llorca, P. Camanho, Physically-sound simulation of low-velocity impact on fiber reinforced laminates, Int. J. Impact Eng. 92 (2016) 3–17.
[26] C. Lopes, P. Camanho, Z. Gürdal, P. Maimí, E. González, Low-velocity impact damage on dispersed stacking sequence laminates. Part II: numerical simulations, Compos. Sci. Technol. 69 (7–8) (2009) 937–947.
[27] A. Sasikumar, J. Costa, D. Trias, E. González, S. García-Rodríguez, P. Maimí, Unsymmetrical stacking sequences as a novel approach to tailor damage resistance under out-of-plane impact loading, Compos. Sci. Technol. 173 (2019) 125–135.
[28] P.P. Camanho, P. Maimí, C. Dávila, Prediction of size effects in notched laminates using continuum damage mechanics, Compos. Sci. Technol. 67 (13) (2007) 2715–2727.
[29] A. Quintanas-Corominas, P. Maimí, E. Casoni, A. Turon, J.A. Mayugo, G. Guillamet, M. Vázquez, A 3D transversally isotropic constitutive model for advanced composites implemented in a high performance computing code, Eur. J. Mech. Solid. 71 (2018) 278–291.
[30] P.P. Camanho, C.G. Dávila, S.T. Pinho, L. Iannucci, P. Robinson, Prediction of in situ strengths and matrix cracking in composites under transverse tension and in-plane shear, Compos. Appl. Sci. Manuf. 37 (2) (2006) 165–176.
[31] M. Remacha, S. Sánchez-Sáez, B. López-Romano, E. Barbero, A new device for determining the compression after impact strength in thin laminates, Compos. Struct. 127 (2015) 99–107.
[32] S. García-Rodríguez, J. Costa, A. Bardera, V. Singery, D. Trias, A 3D tomographic investigation to elucidate the low-velocity impact resistance and tolerance of thin non-crimp fabric laminates: effect of ply-thickness, Compos. Appl. Sci. Manuf. 113 (2018) 53–65.
[33] R. Olsson, Closed form prediction of peak load and delamination onset under small mass impact, Compos. Struct. 59 (3) (2003) 341–349.
[34] C.T. Herakovich, Mechanics of Fibrous Composites, 1998.
[35] A. Sasikumar, S. García-Rodríguez, J. Arbeláez, D. Trias, J. Costa, On how unsymmetrical laminate designs with tailored ply clusters affect compression after impact strength compared to symmetric baseline, Compos. Struct. 238 (2020) 111958.
[36] R. Olsson, Analytical prediction of damage due to large mass impact on thin ply composites, Compos. Appl. Sci. Manuf. 72 (2015) 184–191.